



HAL
open science

Range-separated density-functional theory for molecular excitation energies

Elisa Rebolini

► **To cite this version:**

Elisa Rebolini. Range-separated density-functional theory for molecular excitation energies. Analytical chemistry. Université Pierre et Marie Curie - Paris VI, 2014. English. NNT : 2014PA066214 . tel-01027522

HAL Id: tel-01027522

<https://theses.hal.science/tel-01027522>

Submitted on 22 Jul 2014

HAL is a multi-disciplinary open access archive for the deposit and dissemination of scientific research documents, whether they are published or not. The documents may come from teaching and research institutions in France or abroad, or from public or private research centers.

L'archive ouverte pluridisciplinaire **HAL**, est destinée au dépôt et à la diffusion de documents scientifiques de niveau recherche, publiés ou non, émanant des établissements d'enseignement et de recherche français ou étrangers, des laboratoires publics ou privés.



Université Pierre et Marie Curie

Ecole Doctorale ED 388

Laboratoire de Chimie Théorique

Range-separated density-functional theory for molecular excitation energies

Théorie de la fonctionnelle de la densité à séparation de portée pour les énergies d'excitation moléculaires

Par Elisa REBOLINI

Thèse de doctorat de Chimie Analytique Physique et Théorique

Présentée et soutenue publiquement le 27 juin 2014 devant le jury composé de :

Dr. Christian BROUDER	CNRS & UPMC	(Président)
Prof. Andreas GÖRLING	Friedrich-Alexander Universität	(Rapporteur)
Dr. Lucia REINING	CNRS & Ecole Polytechnique	(Rapporteur)
Dr. Emmanuel FROMAGER	Université de Strasbourg	(Examineur)
Prof. Trygve HELGAKER	University of Oslo	(Examineur)
Prof. Thierry LEININGER	Université Paul Sabatier	(Examineur)
Dr. Julien TOULOUSE	UPMC	(Co-encadrant)
Dr. Andreas SAVIN	CNRS & UPMC	(Directeur)

À mes parents
À mes frères et sœurs
À Benoît

Acknowledgements

Il est toujours délicat d'écrire des remerciements et de n'oublier personne. Je m'excuse donc par avance auprès de ceux qui ne seront pas mentionnés, qu'ils veuillent bien me pardonner.

Je tiens tout d'abord à remercier les différents acteurs qui ont rendus cette thèse possible : le Laboratoire de Chimie Théorique, dirigé par Olivier Parisel, pour m'avoir accueillie pendant ces trois années et m'avoir procuré des conditions optimales pour réaliser cette thèse ; l'école doctorale 388, et en particulier Hélène et Koonna pour leur disponibilité ; et enfin mes deux encadrants, Andreas Savin et Julien Toulouse, d'avoir accepté d'entreprendre cette aventure avec moi. Andreas et Julien ont été pour moi des encadrants hors-norme. Je les remercie sincèrement pour leur gentillesse, leur patience et la qualité de l'encadrement dont ils ont fait preuve avec constance. Ils ont su m'accompagner aussi bien au niveau scientifique qu'au niveau personnel dans tous les développements de cette thèse en me laissant beaucoup de libertés et en étant toujours disponible pour répondre à mes nombreuses questions.

I would like to thank all the members of my PhD committee, Dr. Christian Brouder, Dr. Emmanuel Fromager, Prof. Trygve Helgaker, Prof. Thierry Leninger, and especially my two referees Dr. Lucia Reining and Prof. Andreas Görling for accepting to review my work and to attend to my defense.

Although one name only is written on the front page, this work was the result of numerous interactions, first with my advisers, but also with the other members of the lab, in conferences or workshops... I thank all the people who got interested in this work and contributed in a way or another during these discussions. I especially want to thank Trygve Helgaker and the Center for Computational and Theoretical Chemistry for inviting me to spend a month in Oslo and Andy Teale for his developments on the DALTON code which made part of this work possible. Finally, I want to thank Lucia Reining and her group for our Bethe-Salpeter meetings where chemists and physicists tried to understand each other.

Concernant l'aspect informatique de cette thèse, je tiens à remercier François Colonna, Romain Bardou, la promotion d'informatique ENS-09 et bien sûr Benoît pour leurs conseils en matière de programmation. Je remercie aussi Marie-France et Antoine de m'avoir assuré des conditions de travail optimales et d'avoir réparé mes bêtises.

Un grand merci à tous les membres du Laboratoire de Chimie Théorique pour les

discussions scientifiques ou non et pour tous les moments que nous avons partagés. Merci à Olga, Lauréline, Zeineb, Abdou, Neus, Yi-Shuai, Sehr, Aixiao, Christophe, Odile, Samira, Stéphanie, Inès, Leo, Julia, Roberto, Etienne, Marcos, Morgane, Slavko, Simon, d'avoir partagé le bureau 407 avec moi, et à leurs encadrants pour avoir respecté plus ou moins l'ambiance très studieuse qui y régnait... Grazie Leo per i nostri caffè italiani, per il tuo lavoro sul Bethe-Salpeter e per avere fatto da mediatore. Merci à Amélie, Eléonore, Aude, Marie-Laure et tant d'autres pour avoir contribué à la vie étudiante du laboratoire.

Enfin merci à ma famille et mes amis de m'avoir entourée et supportée pendant ces trois années. Je remercie tout particulièrement mes parents pour avoir cru en moi, pour m'avoir donné le goût du travail bien fait, éveillé ma curiosité et pour tout le reste. Je ne pensais pas le dire un jour mais merci Philippe de m'avoir cassé les pieds pendant des années pour que je ne devienne pas prof. C'est un peu grâce à toi que je suis arrivée jusqu'ici. Enfin merci Benoît pour tout ton amour et pour avoir tout supporté...

Paris, le 28 avril 2014

Contents

General introduction	3
I Excitation energies from time-independent DFT	9
1 Background on DFT	11
1.1 Introduction	11
1.2 Schrödinger equation for a N -electron system	12
1.3 Electron density and pair density	16
1.4 Theoretical foundation of density-functional theory	18
1.5 Kohn-Sham approach	21
1.6 Local density approximation	25
1.7 Range separation of the two-electron interaction	27
1.8 Conclusion	32
2 Excitation energies along a range-separated AC	33
2.1 Introduction	34
2.2 Range-separated density-functional theory	35
2.3 Taylor expansions of the excitation energies	37
2.4 Computational details	41
2.5 Results and discussion	42
2.6 Conclusion	49
3 Perturbation theory along the AC	51
3.1 Introduction	51
3.2 Excited states from perturbation theory	53
3.3 Results and discussion	58
3.4 Conclusion	64
4 Extrapolation along the AC	65
4.1 Introduction	66
4.2 Energy extrapolation	67
4.3 Results and discussion	69
4.4 Conclusion	78

II	Excitation energies from linear-response TDDFT	89
5	Background on TDDFT	91
5.1	Introduction	91
5.2	Time-dependent framework	92
5.3	TDDFT Formalism	94
5.4	Linear-response TDDFT	97
5.5	Resolution for a finite molecular system	101
5.6	Usual approximations	104
5.7	Known deficiencies and remedies	106
5.8	Conclusion	108
6	Excitation energies from TDRSH	111
6.1	Introduction	112
6.2	Linear-response range-separated hybrid scheme	113
6.3	Short-range adiabatic exchange-correlation kernels	116
6.4	Computational details	120
6.5	Results and discussion	122
6.6	Conclusion	127
III	Excitation energies from Green’s function methods	141
7	Background on Green’s function	143
7.1	Introduction	143
7.2	One-particle Green’s function	144
7.3	Two-particle Green’s function	146
7.4	Dyson equation	148
7.5	Bethe-Salpeter Equation	152
7.6	Hedin’s equations	152
7.7	Conclusion	154
8	Static GW-BSE kernel in a finite orbital basis	157
8.1	Introduction	157
8.2	Static GW approximation	159
8.3	Expressions in a finite orbital basis	160
8.4	Example of H ₂ in a minimal basis	164
8.5	Conclusion	178
9	Second-order static BSE kernel	181
9.1	Introduction	181
9.2	Second-order self-energy	183
9.3	Second-order Bethe-Salpeter kernel	186
9.4	Application to H ₂ in a minimal basis	193

9.5	Conclusion	198
10	Dynamical RSH-BSE2 kernel	199
10.1	Introduction	200
10.2	Dynamical second-order Bethe-Salpeter kernel	201
10.3	Resolution of the Bethe-Salpeter equation	208
10.4	Application to H ₂ in a minimal basis	210
10.5	Computational details	214
10.6	Results and discussion	215
10.7	Conclusion	217
	General conclusion and perspectives	231
	List of publications	235
	Appendices	237
A	Mathematical tools	239
A.1	Functionals	239
A.2	Fourier transform and complex analysis	241
A.3	Spherical mean	243
B	Taylor expansions of the RS energies	245
B.1	Taylor expansions around the KS system	245
B.2	Taylor expansions near the real system	250
C	Fit of the energies along the AC	255
C.1	Form of the fit	255
C.2	Fitted parameters	256
D	Double adiabatic connection	259
E	Range-separated kernels	263
E.1	Spin-adapted kernels	263
E.2	Short-range LDA exchange-correlation functional	264
F	Fourier transform of χ_0	269
F.1	Non-interacting polarizability	269
F.2	Particle-hole or hole-particle propagator	270
F.3	Particle-particle or hole-hole propagator	272
F.4	Summary	273
G	Second-order self-energy and static BSE kernel	275
G.1	Correlation self-energy	275

G.2	Correlation kernel	277
G.3	Spin-adaptation of the correlation kernel	281
G.4	Summary	283
H	Dynamic BSE	285
H.1	Fourier transform of the Bethe-Salpeter Equation	285
H.2	Matrix elements of the effective kernel	288
H.3	Summary	292
I	MolExc manual	295
I.1	Presentation	295
I.2	MolExc input syntax	296
I.3	Molpro input syntax	297
	Résumé en français	303

General introduction

The ability to understand the phenomena induced by the interaction between light and matter constitutes a key step to the global understanding of our immediate environment. Light is constituted of photons which carry quanta of energy. The interaction between a photon and matter is complex and involves processes such as absorption, emission or scattering. In fact, at the scale of a molecule, classical physics does not apply anymore and a quantum description of matter with discrete energy levels is required. Assuming a system in its ground state (the state of minimal energy), the absorption of a photon induces the excitation of the system to a state of higher energy. Once in this excited state, several processes can occur:

- The system can return to its ground state (or a lower excited state) by a non-radiative transition where no light is emitted (internal conversion, intersystem crossing or vibrational relaxation) or by a radiative transition with the emission of a photon (fluorescence or phosphorescence) as summarized in the Perrin-Jablonski diagram in Figure 1. In these processes, the system conserves its “integrity” as no chemical bonds are broken. This defines therefore photophysical phenomena. They are extremely interesting as they are responsible for instance for the light emission of stars, for the color of the objects surrounding us and are involved in the design of photovoltaic cells where a material (often a semiconductor) absorbs photons in sunlight to create a difference of potential. Photophysical processes are also widely used as analytic tools in spectroscopy experiments to extract useful information on a system as they provide a “probe” to study the ground and excited states. Depending on the experimental set-up (energy range, direction of observation), different kinds of information can be extracted as for instance the energy levels of the electronic states (bold lines in Figure 1) which describe the electronic configuration of the system, or in the case of a molecule in gas phase, of the ro-vibrational ones (thin lines) which characterize its rotations and its vibrations.
- In some cases, when the system gets excited by absorption of a photon, it does not go back to its original ground state and uses this extra energy to initiate a chemical reaction either by itself (photoisomerization) or involving other reactants (photoactivation). Photochemistry is the branch of chemistry which studies such phenomena. The most famous example of a photochemical reaction is probably given by the photosynthesis but in fact many processes requires a photoactivation such as the degradation of plastics or the formation of vitamin D with sunlight. A wide research area is also interested in using light to control a reaction in order to promote a particular product. This can improve the reaction yields so that less reactants are needed and less waste is produced. This approach is therefore of particular interest for a “green” chemistry.

In all these phenomena, the number of electrons in the system remains constant. However, if the energy of the excitation is strong enough, an electron can be ejected from

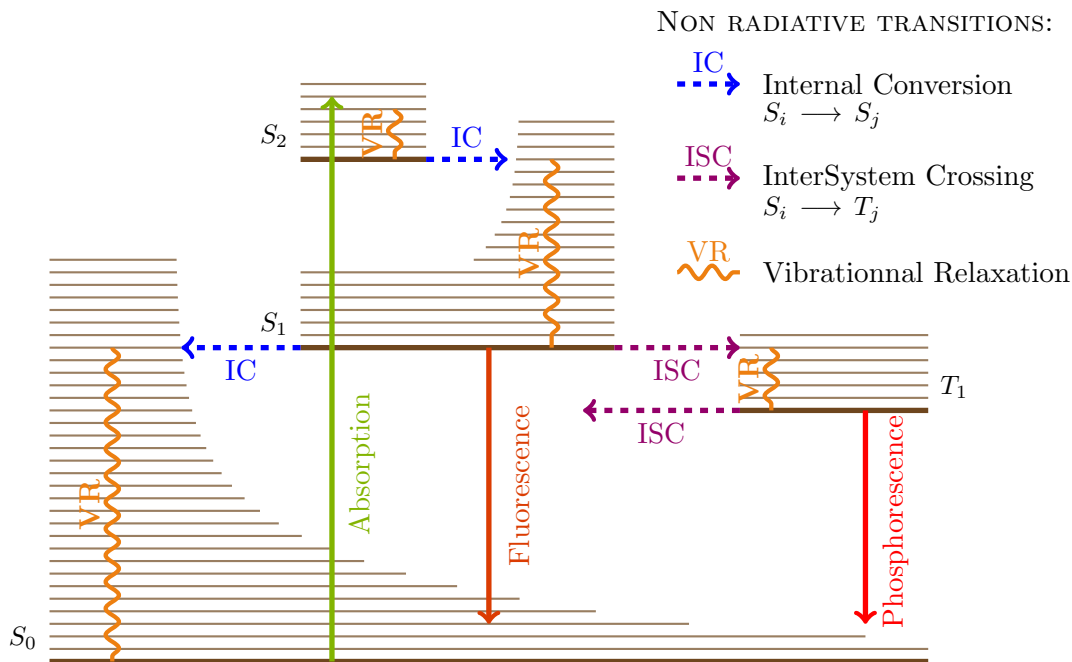


Figure 1 – Perrin-Jablonski diagram. The bold lines represent the electronic singlet ground state S_0 , the first singlet (S_1 and S_2) and triplet (T_1) excited states. The thin lines are the vibrational states. The possible radiative (with emission or absorption of light) and non-radiative transitions between these states are represented by different arrows.

the system as in photoemission spectroscopy experiments which provide other kinds of information such as electron affinities. However, such processes will not be considered in the framework of this thesis and we will focus only on electronic excitation energies in a molecular system. The energy range of these excitations is usually in the visible or ultraviolet part of the spectrum and they are experimentally studied by UV-vis spectroscopy.

The prediction or the analysis of experimental electronic spectra by computer simulation is nowadays an active area of research either to help with the interpretation of some experiments, to design new compounds with interesting biological or structural properties or to study hostile environments where experiments are difficult or impossible to perform as for instance in space, in extreme temperature or pressure conditions or in strong magnetic fields. In order to get quantitative results, computational chemists need reliable methods with a low computational cost in order to be able to treat relatively large systems. In order to compute an electronic excitation spectrum, two kinds of information are required: the excitation energies and the probability of the transition which is given by the *oscillator strengths*. The transition probabilities can vary a lot over a small range of excitation energies and therefore can affect significantly the final spectrum. This is related to the concept of forbidden or allowed transitions.

In practice, the calculation of the excitation energies of a system is often a two-step

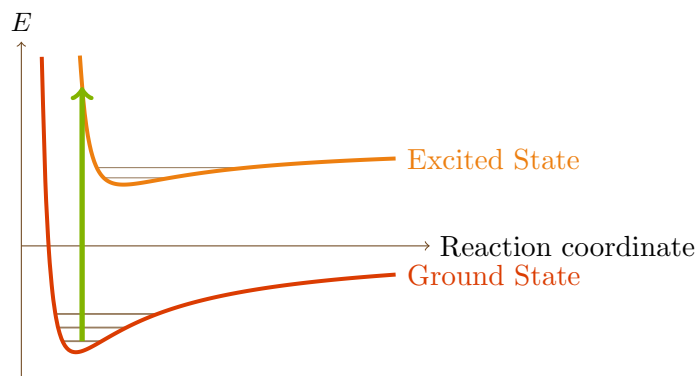


Figure 2 – Representation of a vertical transition. At the time scale of the nuclear motion, an electronic excitation can be considered instantaneous. It is thus vertical with respect to the reaction coordinate (which describe the positions of the nuclei). The transition between the electronic ground and excited states (bold line) is then represented by a vertical arrow.

procedure. First, the system is calculated in its ground state, then vertical excitation energies are calculated at the same geometry assuming that these excitations are instantaneous in comparison with the time scale of nuclear motion. However, when in an excited state, the geometry of the system may relaxes as shown in Figure 2 such that in principle, a potential energy surface is required to grasp the whole physics of the system. Moreover, in order to get as close as possible to a real spectrum the rovibronics effects and the broadening should be taken into account. However in this thesis, we will focus only on the determination of electronic excitation energies and of oscillator strengths of a molecule in gas phase, at zero temperature and fixed geometry.

The whole complexity of quantum calculations consists in the description of the correlated motion of the electrons, due to their electrostatic interaction and to their intrinsic quantum nature. Historically, quantum chemists have used methods based on wave functions by refining more and more the well-known Hartree-Fock (HF) method where the correlation is completely absent. Post-HF (multi-reference) methods reintroduce (part of) this correlation and have the undeniable advantage that they can systematically be improved and can give very accurate results. However, they are usually computationally expensive as they depend on the coordinates of all the electrons of the system. Therefore, they scale pretty badly with the size of the system and become often impractical for calculations on medium and big systems such as solids or compounds of biological interest. Nevertheless active research is undergoing in order to reduce the computational cost of such methods using for instance the density-fitting scheme or exploiting the localization of the orbitals.

Another kind of approach is provided by density-functional theory (DFT) which is based on the electron density of the system in its ground state instead of the electronic wave function. The electron density can be seen as the average number of electron

by volume element. It therefore depends only on one (spin)-space coordinate whatever the number of electrons of the system is. Such an approach decreases dramatically the computational cost. However, the price to pay is that the whole complexity of the calculation is now hidden in an unknown object, the energy functional. Within the approach proposed by Kohn and Sham, the calculation uses a fictitious system of non-interacting electrons having the same ground-state density. The idea is to calculate exactly the maximum of things so that the remaining unknown part will be as small as possible and in principle easier to approximate. To reproduce the physical system, what is missing is the effects coming from the electron-electron interaction which is then taken into account by the Hartree-exchange-correlation functional which needs to be approximated. A wide variety of approximate functionals such as local density (LDA) or generalized gradient (GGA) approximations has been developed in the past decades and usually allows DFT to provide results with a reasonable accuracy. Its good ratio cost/accuracy has thus made DFT very popular for complex systems.

In its original time-independent formulation, DFT provides only the ground-state electron density and energy. However, in their famous theorems, Hohenberg and Kohn also showed that the ground-state electron density contains in fact all the information on the system, and in particular the excitation energies. With the introduction of time dependence, it is possible to extract these excitation energies from the density for instance with linear-response theory. In this approach, the response of the electron density of the system to a small oscillatory time-dependent perturbation is studied. If the frequency of the perturbation corresponds to an energy difference between the ground state and an excited state, the system changes state so the change in density will be important while otherwise it remains very small. In linear-response time-dependent density-functional theory (TDDFT), one can then detect the excitation energies as the frequencies where the change of density is large.

Similarly to the time-independent case, this method requires a functional, called the Hartree-exchange-correlation kernel, to treat the effects coming from the electron-electron interaction. Rigorously, the kernel cannot be determined from the ground-state energy functional and in practice an adiabatic approximation is performed for the kernel on top on the approximations which have already been made for the energy functionals. In this approximation, the kernel becomes independent of the frequency of the considered perturbation which leads to several shortcomings. However, within the usual adiabatic LDA or GGA approximations, the excitation energies are nevertheless generally well reproduced for low-lying states (valence states), but are underestimated for high-lying states (Rydberg states). A second problem is the reproduction of the charge-transfer excitation energies and a third one occurs when multiple excitations are involved.

The first two problems are mostly due to the poor behavior of the approximate functionals at long electron-electron distance, while the third one is directly related to the adiabatic approximation. For an isolated system in its equilibrium geometry, double (or higher-order) excitations are not so common in the lowest part of the excitation

spectra. They are for instance present for linear polyenes but do not play an important role in most systems. However, when one is interested in chemical reactivity and reaction paths, things get more complicated. In fact, along a reaction path, the excited states of a system are subject to crossings and/or conical intersection in the vicinity of which multiple excitations are more likely to occur as several states are close to each other. It is then crucial to be able to describe this region properly as it is usually a critical region to understand the reaction mechanism. TDDFT within the usual approximations is not able to account for these multiple excitations and can produce poor quality results in this case.

One possible strategy to cope with these issues is to divide the electron-electron interaction into a short-range part where the electrons are close to each other and a long-range part when they are faraway. Within the usual approximations, DFT is able to describe the short-range part of the electron-electron interaction with a good accuracy but fails for the long-range one. This part can then be treated by wave-function methods or many-body perturbation theory. The range of the separation can then be adjusted by a range-separation parameter. This range-separation technique has successfully been applied to ground-state calculations but is still being explored for excited-state ones. When applied to the exchange part of the kernel with the introduction of a long-range HF exchange kernel, range separation improves the description of the Rydberg and charge-transfer excitation energies as it allows to recover the correct asymptotic behavior of the potential at large electron-electron distance.

In this thesis, we want to explore the effects of range separation on the description of excitation energies both in a time-independent and a time-dependent formulation. In particular, we want to apply range separation on the TDDFT correlation kernel in order to improve the description of excitation energies involving contributions from double excitations by introducing a long-range frequency-dependent kernel. In order to do so, this work has been divided in three main parts.

In the first part of this thesis, the effects of range separation on the excitation energies of a system are studied in the time-independent framework. This is done by following the evolution of the excited states of a partially interacting system where only the long-range part of the electron-electron interaction has been introduced along an adiabatic connection where the ground-state density is kept constant by Lieb optimization of the potential. This study is first done analytically by expanding the energies around the two limit cases where no interaction or all the interaction is included. It is then applied on the helium and beryllium atoms and on the dihydrogen molecule without any approximations except for the finite basis set one, in order to be able to attribute our observations to the range separation only. Starting from the obtained energies, we then explore two possibilities to improve the description of the excitation energies of the physical system from the ones of the partially interacting system: first-order perturbation theory is tested and an energy extrapolation scheme is also studied.

In the second part of this thesis, we apply range separation on both the exchange and

correlation TDDFT kernels within a single determinant approximation. This defines the time-dependent extension of the range-separated hybrid (RSH) method used for ground-state calculations. Within this approximation, the long-range part of the exchange kernel is treated at the Hartree-Fock level while the long-range correlation kernel is absent. This would thus allow for the perturbative addition of a frequency-dependent long-range correlation kernel in a second step. In practice, this implies that the long-range part has to be removed from the usual correlation kernel and is done within the local-density approximation in the closed-shell case. The time-dependent range-separated hybrid (TDRSH) method is then applied on a set of five small molecules and on a charge-transfer dimer in order to study the impact of the removal of the long-range correlation on their first excitation energies.

In the last part, we design a long-range frequency-dependent correlation kernel and add it to the TDRSH one. In order to do so, we use many-body perturbation-theory techniques which are based on one-particle Green's functions used in the condensed-matter physics community. In this approach, the excitation energies of the system are obtained by solving the Bethe-Salpeter equation which structure is very close to the TDDFT equations, but is however more general. Our motivation to go to this more complicated formalism is that it allows one to get an explicit frequency-dependent kernel and to circumvent the problematic adiabatic approximation encountered in TDDFT. As finite molecular systems are concerned, some reformulation is required and the applicability of the usual approximations made for solids needs to be questioned. In this part, we derive a dynamical second-order correlation kernel with respect to the electron-electron interaction which we illustrate on the model system of the dihydrogen molecule in a minimal basis at each step of the derivation. This kernel is derived algebraically but most of the technical details are given in the appendices so that only the main steps and their Feynman diagram interpretations are given in the main text. Finally, this kernel is applied in a perturbative manner on four small molecules within the range-separation framework.

Part I

Excitation energies from time-independent density-functional theory

Chapter 1

Theoretical background on density-functional theory

In this chapter, a brief review of the many-body problem is given. This problem is encountered by both quantum chemists and physicists, either on finite systems such as atoms, molecules or supramolecular systems, or on solids. Starting from the Schrödinger equation in the time-independent non-relativistic case, emphasis is placed on one of the possible approaches which can be used to solve this equation: density-functional theory (DFT). As this method lies at the heart of this thesis, particular care is taken to define all the quantities used throughout this manuscript. The theoretical and pragmatic aspects of DFT are reviewed together with some of its possible extensions. In particular, the range-separated DFT scheme is described in its initial context, namely ground-state calculations.

1.1 Introduction

When calculations are performed on a quantum system composed of several nuclei and electrons, an extremely complex many-body problem arises from the interactions between the different constituents of the system. Although the equation governing the behavior of these particles is known and, in the case of a non-relativistic system, is given by the Schrödinger equation, no analytic solutions are available in the general case.

In this chapter, first, the many-body problem is recalled in the second quantization formalism in Section 1.2. Then, the electron density and pair density are introduced in Section 1.3 as they are the key quantities involved in DFT. The formal foundations of DFT provided by Hohenberg and Kohn are given in Section 1.4 and the Kohn-Sham approach is explained in Section 1.5. The local-density approximation with its successes and its limitations is discussed in Section 1.6. Finally, the extension of the Kohn-Sham approach by range separation of the electronic interaction is described in Section 1.7. This method allows one to cope with some of the limitations of DFT within the usual

approximations. More mathematical details can be found in Appendix A. For a more exhaustive review, some articles [1–5] and books [6–11] provide a good introduction on the subject.

1.2 Schrödinger equation for a N -electron system

1.2.1 Non-relativistic time-independent Schrödinger equation

Our system of interest consists of N non-relativistic electrons and M nuclei interacting with one another in absence of any time-dependent external field. Each nucleus (A) is characterized by its atomic number Z_A , its mass M_A and its position \mathbf{R}_A , while the electrons (i) have a mass $m_e = 9.11 \times 10^{-31}$ kg and an elementary charge $q_e = -e = -1.60 \times 10^{-19}$ C and are described by their spin-space coordinates $\mathbf{x}_i = (\mathbf{r}_i, \sigma_i)$ where $\sigma_i = \alpha, \beta$ is the spin and \mathbf{r}_i the spatial coordinates. SI units are not well suited for quantum systems. It is convenient to work with atomic units which are defined such that

$$\hbar = m_e = e^2/(4\pi\epsilon_0) = 1. \quad (1.1)$$

This unit system will be used hereinafter.

The way the particles behave and interact with each other is described by the Hamiltonian of the system H_{tot} , which depends in principle on all nuclear and electronic coordinates ($\{\mathbf{x}_N\}, \{\mathbf{R}_M\}$). This Hamiltonian splits into two kinds of contributions:

- kinetic terms coming from the motion of both the nuclei and the electrons;
- potential terms due to the nucleus-nucleus and electron-electron repulsion and the nucleus-electron attraction.

The total Hamiltonian of the system in atomic units in absence of any extra external field is then

$$\begin{aligned} H_{\text{tot}}(\{\mathbf{x}_N\}, \{\mathbf{R}_M\}) = & - \sum_{A=1}^M \frac{\nabla_A^2}{2M_A} - \sum_{i=1}^N \frac{\nabla_i^2}{2} + \sum_{A=1}^M \sum_{B>A}^M \frac{Z_A Z_B}{|\mathbf{R}_A - \mathbf{R}_B|} \\ & - \sum_{i=1}^N \sum_{A=1}^M \frac{Z_A}{|\mathbf{R}_A - \mathbf{r}_i|} + \sum_{i=1}^N \sum_{j>i}^N \frac{1}{|\mathbf{r}_i - \mathbf{r}_j|}, \end{aligned} \quad (1.2)$$

where ∇_A^2 and ∇_i^2 are the Laplacians with respect to the spatial nuclear coordinates \mathbf{R}_A and electronic coordinates \mathbf{r}_i , respectively. The stationary quantum states of the system are then obtained by solving the *Time-Independent Non-Relativistic Schrödinger Equation*:

$$H_{\text{tot}}(\{\mathbf{x}_N\}, \{\mathbf{R}_M\})\Psi_{i,\text{tot}}(\{\mathbf{x}_N\}, \{\mathbf{R}_M\}) = E_{i,\text{tot}}\Psi_{i,\text{tot}}(\{\mathbf{x}_N\}, \{\mathbf{R}_M\}), \quad (1.3)$$

which is an eigenvalue equation. This equation states that if the system is in a stationary

state of energy $E_{i,\text{tot}}$ then its wave function $\Psi_{i,\text{tot}}$ is an eigenvector of the total Hamiltonian and is associated with the eigenvalue $E_{i,\text{tot}}$. In practice, except for some very simple systems, it is not possible to solve this equation exactly and one has to design some efficient approximated resolution schemes.

The first approximation which is usually done concerns the coupling between the motions of the electrons and the nuclei. The mass of a nucleon is around 1800 times the mass of an electron. Hence, the coupling between the nuclear and electronic parts of the Hamiltonian can be neglected as a first approximation such that an electronic Hamiltonian H_e can be constructed in which the positions of the nuclei enter only as parameters,

$$H_e(\{\mathbf{x}_N\}; \{\mathbf{R}_M\}) = - \sum_{i=1}^N \frac{\nabla_i^2}{2} + - \sum_{i=1}^N \sum_{A=1}^M \frac{Z_A}{|\mathbf{R}_A - \mathbf{r}_i|} + \sum_{i=1}^N \sum_{j>i}^N \frac{1}{|\mathbf{r}_i - \mathbf{r}_j|}. \quad (1.4)$$

This means that the electrons still feel the Coulomb interaction coming from the nuclei but see them fixed. This defines the so-called the *Born-Oppenheimer approximation*. Within this approximation, the total wave function of the system can be factorized into a nuclear part Ψ_n and an electronic part Ψ_e in which the nuclear positions are only parameters:

$$\Psi_{i,\text{tot}}(\{\mathbf{x}_N\}, \{\mathbf{R}_M\}) = \Psi_{i,e}(\{\mathbf{x}_N\}; \{\mathbf{R}_M\}) \Psi_{i,n}(\{\mathbf{R}_M\}). \quad (1.5)$$

The *electronic Schrödinger equation*

$$H_e(\{\mathbf{x}_N\}; \{\mathbf{R}_M\}) \Psi_{i,e}(\{\mathbf{x}_N\}; \{\mathbf{R}_M\}) = E_{i,e}(\{\mathbf{R}_M\}) \Psi_{i,e}(\{\mathbf{x}_N\}; \{\mathbf{R}_M\}) \quad (1.6)$$

is then solved in a first step. The nuclear kinetic term corresponding to the first term of the r.h.s. of Equation (1.2) and the nucleus-nucleus potential, are then added back in a second step so that the Schrödinger equation for the nuclear motion can be solved

$$[T_n(\{\mathbf{R}_M\}) + V_{nn}(\{\mathbf{R}_M\}) + E_{i,e}(\{\mathbf{R}_M\})] \Psi_{i,n}(\{\mathbf{R}_M\}) = E_{i,\text{tot}} \Psi_{i,n}(\{\mathbf{R}_M\}). \quad (1.7)$$

The electronic wave function $\Psi_e(\mathbf{x}_1, \dots, \mathbf{x}_N)$ is a complex-valued function which defines a probability amplitude. The quantity $|\Psi_e(\mathbf{x}_1, \dots, \mathbf{x}_N)|^2 d\mathbf{x}_1 d\mathbf{x}_2 \cdots d\mathbf{x}_N$ is then the probability of finding simultaneously electron 1 in the volume element $d\mathbf{x}_1$ around \mathbf{x}_1 , electron 2 in $d\mathbf{x}_2$ around \mathbf{x}_2 , etc. As a probability, it must integrate to 1 which leads to the *normalization condition*

$$\int |\Psi_e(\mathbf{x}_1, \dots, \mathbf{x}_N)|^2 d\mathbf{x}_1 d\mathbf{x}_2 \cdots d\mathbf{x}_N = 1. \quad (1.8)$$

Moreover, as electrons are fermions, the *Pauli principle* states that the electronic wave function must be antisymmetric with respect to the exchange of any two electrons,

$$\Psi_e(\mathbf{x}_1 \cdots \mathbf{x}_i \cdots \mathbf{x}_j \cdots \mathbf{x}_N) = -\Psi_e(\mathbf{x}_1 \cdots \mathbf{x}_j \cdots \mathbf{x}_i \cdots \mathbf{x}_N). \quad (1.9)$$

In this thesis, we will focus only on the resolution of the electronic Schrödinger equation (1.6) within the Born-Oppenheimer and non-relativistic frameworks. For the sake of conciseness, the subscript “e” will therefore be dropped hereinafter.

1.2.2 Electronic Hamiltonian in second quantization

Up to this point, all the quantities were expressed in the first quantization formalism. An alternative powerful framework is given by second quantization as it provides a convenient, compact formalism for the study of the electronic problem. It relies on creation and annihilation field operators $\hat{\Psi}_\sigma^\dagger(\mathbf{r})$ and $\hat{\Psi}_\sigma(\mathbf{r})$ which respectively creates or destroys an electron of spin σ at the position \mathbf{r} . In order to enforce the Pauli principle, these operators fulfill the following anticommutation relations:

$$\begin{aligned} \left[\hat{\Psi}_\sigma(\mathbf{r}), \hat{\Psi}_{\sigma'}(\mathbf{r}') \right]_+ &= 0, \\ \left[\hat{\Psi}_\sigma^\dagger(\mathbf{r}), \hat{\Psi}_{\sigma'}^\dagger(\mathbf{r}') \right]_+ &= 0, \\ \left[\hat{\Psi}_\sigma(\mathbf{r}), \hat{\Psi}_{\sigma'}^\dagger(\mathbf{r}') \right]_+ &= \delta_{\sigma,\sigma'} \delta(\mathbf{r} - \mathbf{r}'). \end{aligned} \quad (1.10)$$

Using this formalism, the electronic Hamiltonian can be expressed as:

$$\hat{H} = \hat{T} + \hat{V}_{\text{ne}} + \hat{W}_{\text{ee}}, \quad (1.11)$$

where \hat{T} is the kinetic energy operator

$$\hat{T} = -\frac{1}{2} \sum_{\sigma} \int \hat{\Psi}_\sigma^\dagger(\mathbf{r}) \nabla^2 \hat{\Psi}_\sigma(\mathbf{r}) d\mathbf{r}, \quad (1.12)$$

\hat{V}_{ne} is the electron-nuclei interaction operator

$$\hat{V}_{\text{ne}} = \sum_{\sigma} \int \hat{\Psi}_\sigma^\dagger(\mathbf{r}) v_{\text{ne}}(\mathbf{r}) \hat{\Psi}_\sigma(\mathbf{r}) d\mathbf{r} \quad (1.13)$$

with the one-electron nuclei-electron potential $v_{\text{ne}}(\mathbf{r}) = -\sum_A Z_A / |\mathbf{R}_A - \mathbf{r}|$, and \hat{W}_{ee} is the electron-electron operator

$$\hat{W}_{\text{ee}} = \frac{1}{2} \sum_{\sigma,\sigma'} \iint \hat{\Psi}_\sigma^\dagger(\mathbf{r}) \hat{\Psi}_{\sigma'}^\dagger(\mathbf{r}') w_{\text{ee}}(\mathbf{r}, \mathbf{r}') \hat{\Psi}_{\sigma'}(\mathbf{r}') \hat{\Psi}_\sigma(\mathbf{r}) d\mathbf{r} d\mathbf{r}'. \quad (1.14)$$

with the two-electron interaction $w_{\text{ee}}(\mathbf{r}, \mathbf{r}') = w_{\text{ee}}(|\mathbf{r} - \mathbf{r}'|) = 1/|\mathbf{r} - \mathbf{r}'|$.

For the electrons, the field created by the nuclei is external. However, the Coulomb potential is only one example of an external potential v able to bind N electrons. These external potentials define a set \mathcal{V}_N such that the corresponding Hamiltonians have a N -electron ground state [12]:

$$\mathcal{V}_N = \{v \mid \hat{H}[v] \text{ has a } N\text{-electron ground state}\}. \quad (1.15)$$

In this expression, the square bracket notation in $\hat{H}[v]$ denotes a *functional* dependence of the Hamiltonian \hat{H} on the potential v . More details on functional calculus are given in Appendix A.1 or can be found in [6] for instance.

1.2.3 Variational principle

The first step of a quantum calculation is often the determination of the ground state of the system, i.e., the state with the lowest energy. As its energy is minimal, the Rayleigh-Ritz variational principle [13] can be used. It means in particular that for any trial N -electron wave function Ψ_{trial} satisfying the normalization condition (1.8), the expectation value of the Hamiltonian over this wave function is higher than the ground-state energy E_0 ,

$$E[\Psi_{\text{trial}}] = \langle \Psi_{\text{trial}} | \hat{H} | \Psi_{\text{trial}} \rangle \geq \langle \Psi_0 | \hat{H} | \Psi_0 \rangle = E_0. \quad (1.16)$$

This inequality sharpens into an equality only for a ground-state wave function $\Psi_{\text{trial}} = \Psi_0$. Minimizing the energy over all the N -electron normalized wave functions provides thus a strategy to find the ground-state wave function. In order to perform the minimization under the normalization constraint, it is convenient to introduce a Lagrange multiplier E , and then solve the equation

$$\delta \left[\langle \Psi | \hat{H} | \Psi \rangle - E \langle \Psi | \Psi \rangle \right] = 0 \quad (1.17)$$

without constraints, where the optimized value of the Lagrange multiplier is the energy of the state $|\Psi\rangle$. Unfortunately, it is usually not possible in practice to perform the minimization over all the possible wave functions and only a subset is considered. Consequently, the calculated ground-state energy is only an upper bound to the true wave function.

For the past decades, quantum chemists and physicists have designed a multitude of methods to approach the ground-state wave function. The simplest one is the *Hartree-Fock method* in which the considered subset of wave functions is the set of single *Slater determinants*, i.e., antisymmetrized products of N one-electron wave functions $\phi(\mathbf{x})$. These one-electron wave functions are called *spin-orbitals* and can be decomposed into a spatial orbital $\varphi(\mathbf{r})$ and a spin function $\chi(\sigma)$ such that $\phi(\mathbf{x}) = \varphi(\mathbf{r})\chi(\sigma)$. The Hartree-Fock reference wave function can then be refined by extending the search subset or by using perturbation methods.

1.3 Electron density and pair density

The N -electron wave function is a complicated object which depends on all electronic coordinates. It was soon pointed out that this level of complexity may not be required to describe the system and that simpler quantities could be used instead of the full wave function. One of these quantities is the electron density $n(\mathbf{r})$ which was first suggested by Thomas and Fermi in 1927 [14, 15].

1.3.1 Electron density

Given a normalized N -electron wave function $\Psi(\mathbf{x}_1, \dots, \mathbf{x}_N)$, we have already mentioned that its square modulus $|\Psi(\mathbf{x}_1, \dots, \mathbf{x}_N)|^2 d\mathbf{x}_1 d\mathbf{x}_2 \cdots d\mathbf{x}_N$ is the probability of finding simultaneously electron 1 in the volume element $d\mathbf{x}_1$ around \mathbf{x}_1 , electron 2 in $d\mathbf{x}_2$ around \mathbf{x}_2 , etc. As the electrons are indistinguishable, this leads to the definition of the *electron density* $n(\mathbf{r})$ by integrating over all the spin variables and all but one of the spatial variables

$$n(\mathbf{r}) = N \int |\Psi(\mathbf{x}, \mathbf{x}_2, \dots, \mathbf{x}_N)|^2 d\sigma d\mathbf{x}_2 \cdots d\mathbf{x}_N, \quad (1.18)$$

where the N prefactor accounts for the indistinguishability of the electrons. The quantity $n(\mathbf{r})d\mathbf{r}$ can therefore be interpreted as the average number of electrons with arbitrary spin in the volume element $d\mathbf{r}$ around \mathbf{r} . The electron density is considerably simpler than the electronic wave function as it depends only on the space coordinates of one electron instead of the spin-space coordinates of all electrons. Moreover, it is an observable of the system and can be measured experimentally, for instance by X-ray diffraction. It is to be related to the *density operator*

$$\hat{n}(\mathbf{r}) = \sum_{\sigma} \hat{\Psi}_{\sigma}^{\dagger}(\mathbf{r}) \hat{\Psi}_{\sigma}(\mathbf{r}), \quad (1.19)$$

as it can be obtained by taking the expectation value of this operator over the wave function $n(\mathbf{r}) = \langle \Psi | \hat{n}(\mathbf{r}) | \Psi \rangle$.

Using the definition of the density operator, the nuclei-electron potential can be rewritten as

$$\hat{V}_{\text{ne}} = \int v_{\text{ne}}(\mathbf{r}) \hat{n}(\mathbf{r}) d\mathbf{r}. \quad (1.20)$$

The ground-state density is a function from \mathbb{R}^3 to \mathbb{R} which satisfies several properties:

1. It is a non-negative function, $n(\mathbf{r}) \geq 0$.
2. It integrates to the total number of electrons, $\int n(\mathbf{r}) d\mathbf{r} = N$.
3. It fulfills the Kato cusp condition [16]: when an electron is on-top of a nucleus A , the electron-nuclei potential diverges. This divergence is compensated by a cusp in the electron density, such that in terms of the spherically averaged density $\tilde{n}(r_A)$,

where r_A is the distance between the electron and the nucleus,

$$\left. \frac{\partial \tilde{n}(r_A)}{\partial r_A} \right|_{r_A \rightarrow 0} = -2Z_A \tilde{n}(0). \quad (1.21)$$

Hence, in the vicinity of the nucleus A , the electron density behaves like

$$\tilde{n}(r) \sim e^{-2Z_A r}. \quad (1.22)$$

4. Its long-range asymptotic behavior is fixed by the ionization energy [17]: at large r , the electron density decays exponentially and this decay is governed by the ionization energy \mathcal{E}_I of the system $n(r) \sim e^{-2\sqrt{2\mathcal{E}_I}r}$.

The densities coming from an N -electron ground-state wave function define the set

$$\mathcal{A}_N = \{n \mid n \text{ comes from an } N\text{-electron ground-state wave function}\}. \quad (1.23)$$

Spin density and spin polarization

The electron density does not differentiate electrons with respect to their spin. However, in particular for open-shell systems, this differentiation can become useful. The probability density of finding an electron with a specific spin σ is given by its *spin density* $n(\mathbf{x})$ or $n_\sigma(\mathbf{r})$. The sum of the α and β spin densities gives back the total density, while their difference defines the *spin polarization* (or spin magnetization) density

$$m(\mathbf{r}) = n_\alpha(\mathbf{r}) - n_\beta(\mathbf{r}). \quad (1.24)$$

1.3.2 Pair density

In the electronic Hamiltonian, two-electron interactions are also involved. To describe them, one needs to know the position of two electrons simultaneously. It is thus convenient to have access to the average number of electron pairs with arbitrary spins around two positions \mathbf{r} and \mathbf{r}' . This information is given by the *pair density*

$$n_2(\mathbf{r}, \mathbf{r}') = N(N-1) \int |\Psi(\mathbf{x}, \mathbf{x}', \mathbf{x}_3, \dots, \mathbf{x}_N)|^2 d\sigma d\sigma' d\mathbf{x}_3 \cdots d\mathbf{x}_N, \quad (1.25)$$

up to a normalization factor, where the factor $N(N-1)$ accounts for the fact that electrons are indistinguishable. The *pair density operator*

$$\begin{aligned} \hat{n}_2(\mathbf{r}, \mathbf{r}') &= \sum_{\sigma, \sigma'} \hat{\Psi}_\sigma^\dagger(\mathbf{r}) \hat{\Psi}_{\sigma'}^\dagger(\mathbf{r}') \hat{\Psi}_{\sigma'}(\mathbf{r}') \hat{\Psi}_\sigma(\mathbf{r}) \\ &= \hat{n}(\mathbf{r}) \hat{n}(\mathbf{r}') - \hat{n}(\mathbf{r}) \delta(\mathbf{r} - \mathbf{r}') \end{aligned} \quad (1.26)$$

is directly related to the pair density as the latter is its expectation value $n_2(\mathbf{r}, \mathbf{r}') = \langle \Psi | \hat{n}_2(\mathbf{r}, \mathbf{r}') | \Psi \rangle$. It can be used to reformulate the expression of the electron-electron operator

$$\hat{W}_{ee} = \frac{1}{2} \iint \hat{n}_2(\mathbf{r}, \mathbf{r}') w_{ee}(\mathbf{r}, \mathbf{r}') d\mathbf{r} d\mathbf{r}'. \quad (1.27)$$

Due to their fermionic nature and the electron-electron interaction, electrons have correlated motions. Therefore, the pair density is not simply the product of the two electron densities: an additional term, the exchange-correlation pair density, $n_{2,xc}$, enters its expression to take these effects into account:

$$\begin{aligned} n_2(\mathbf{r}, \mathbf{r}') &= n(\mathbf{r})n(\mathbf{r}') + n_{2,xc}(\mathbf{r}, \mathbf{r}') \\ &= n(\mathbf{r})n(\mathbf{r}') + n(\mathbf{r})h_{xc}(\mathbf{r}, \mathbf{r}'). \end{aligned} \quad (1.28)$$

where h_{xc} is the exchange-correlation hole. The pair density has some interesting properties worth mentioning:

1. It is a non-negative function: $n_2(\mathbf{r}, \mathbf{r}') \geq 0$.
2. It is symmetric with respect to the interchange of its arguments: $n_2(\mathbf{r}, \mathbf{r}') = n_2(\mathbf{r}', \mathbf{r})$.
3. It integrates to the number of pairs: $\iint n_2(\mathbf{r}, \mathbf{r}') d\mathbf{r} d\mathbf{r}' = N(N - 1)$.
The exchange-correlation hole normalization is then: $\int h_{xc}(\mathbf{r}, \mathbf{r}') d\mathbf{r}' = -1$.
4. When the electrons are on-top of each other, the pair density reduces to the *on-top pair density* $n_2(\mathbf{r}, \mathbf{r})$. In this point, the Hamiltonian diverges but the energy of the system remains finite. This divergence has thus to be counterbalanced by the derivative of the pair density and defines the electron-electron cusp condition [18].

1.4 Theoretical foundation of density-functional theory

The motivation at the root of density-functional theory is to replace the variational principle (1.17) where the minimization is done with respect to the wave function, by a minimization over the electron density. The first mathematical justification for this approach was given by Kohn and Hohenberg in their famous theorems [19]. Their theory was later extended by Levy [20] and Lieb [21] in order to minimize over an explicitly known set and to ensure the existence of an unique solution. A brief overview of these formal justifications is sketched in the following section. More details can be found for instance in [6–9, 22, 23]

1.4.1 Hohenberg-Kohn theorems

In order to construct the electronic Hamiltonian of a system, very few information is really needed. The number of electrons N is all what is required to write down the

kinetic operator and the electronic interaction, and the external potential v allows the construction of \hat{V}_{ne} . The Hamiltonian is therefore a functional of both N and v , $\hat{H}[v, N]$.

The first Hohenberg-Kohn (HK) theorem states that the ground-state density is in fact sufficient and can be used instead of v and N to construct the Hamiltonian of the system.

Theorem 1 (First HK theorem). Each N -electron density is the ground-state density of at most one Hamiltonian $\hat{H}[v, N]$ where the external potential v is determined up to an additive constant c

$$n(\mathbf{r}) = n'(\mathbf{r}) \quad \Rightarrow \quad v(\mathbf{r}) = v'(\mathbf{r}) + c. \quad (1.29)$$

The proof of this theorem is surprisingly simple and uses a *reductio ad absurdum* argument [19]. This theorem states that the ground-state density n_0 contains by itself all the information to construct the Hamiltonian of the system $\hat{H}[v, N]$. Therefore, one should be able to extract the number of electrons and the external potential from the ground-state density. The first is trivial as the density integrates to the number of particles N . For the latter, it is easy to get an insight in the case of the Coulombic potential although the HK theorem is more general. In fact, as mentioned in Equation (1.21), the density presents a cusp at the position of each nucleus \mathbf{R}_A which size is proportional to the atomic number of the given nucleus Z_A . The density contains therefore all the information needed to construct the electron-nuclei potential so that the Hamiltonian can be completely determined. This can be summarized as $n \Rightarrow [v, N] \Rightarrow \hat{H}$. The consequence of this theorem is that all the properties of the system, and in particular, the ground-state energy, are functionals of the density. As the dependence in N of the Hamiltonian is trivial, it is dropped in the following.

Although the physical interpretation of this theorem can seem straightforward, all its subtlety lies in the “at most”. It means that only *some* ground-state densities arise from an external potential, those which satisfy this condition are said to be *v-representable*. It means that there exist some “reasonable” N -electron densities, i.e., which are positive and L^1 -integrable, which do not correspond to any physical potential. Actually, in order to have a ground-state density, the ground state should exist, which means that the potential should be able to bind N electrons. The first HK theorem therefore defines a mapping between the set of densities \mathcal{A}_N which comes from an N -electron ground-state wave function and the set of potentials \mathcal{V}_N which are able to bind N electrons.

Given an Hamiltonian $\hat{H}[v]$, with $v \in \mathcal{V}_N$, and $\Psi[n]$ its ground-state wave function associated to the density $n \in \mathcal{A}_N$, the ground-state energy is

$$\begin{aligned} E[v] &= \langle \Psi[n] | \hat{T} + \hat{W}_{ee} + \hat{V} | \Psi[n] \rangle \\ &= \langle \Psi[n] | \hat{T} + \hat{W}_{ee} | \Psi[n] \rangle + \int v(\mathbf{r})n(\mathbf{r})d\mathbf{r}. \end{aligned} \quad (1.30)$$

In this expression, the part $\langle \Psi[n] | \hat{T} + \hat{W}_{\text{ee}} | \Psi[n] \rangle = F_{\text{HK}}[n]$ does not depend explicitly on the external potential. It is called the *HK functional* and can be seen as an *universal functional* as it is system-independent.

The second HK theorem states that the variational principle holds for this universal functional $F_{\text{HK}}[n]$.

Theorem 2 (Second HK theorem). For any positive integer N and potential $v \in \mathcal{V}_N$, it exists a density functional $F_{\text{HK}}[n]$ such that $F_{\text{HK}}[n] + \int v(\mathbf{r})n(\mathbf{r})d\mathbf{r}$ reaches its minimal value at the ground-state density of a system composed of N electrons in the potential $v(\mathbf{r})$. This minimum is then the ground-state energy of this system $E[v]$.

This theorem can be formulated in terms of two equivalent variation principles

$$E[v] = \min_{n \in \mathcal{A}_N} \left\{ F[n] + \int v(\mathbf{r})n(\mathbf{r})d\mathbf{r} \right\}, \quad v \in \mathcal{V}_N, \quad (1.31a)$$

$$F[n] = \max_{v \in \mathcal{V}_N} \left\{ E[v] - \int v(\mathbf{r})n(\mathbf{r})d\mathbf{r} \right\}, \quad n \in \mathcal{A}_N. \quad (1.31b)$$

These two theorems lay the formal justification for density functional theory. Unfortunately, neither the form of the HK functional nor the two sets \mathcal{V}_N and \mathcal{A}_N are known. In order to have explicitly known sets, Levy and Lieb defined weaker conditions on the potentials and densities which lead first to the Levy-Lieb constrained-search and then to the Lieb convex-conjugate formulation of DFT.

1.4.2 Levy-Lieb formulation

A generalization of the HK theorem which does not require the density to be v -representable was proposed, by Levy [20] and Lieb [21] and is usually known as the Levy or Levy-Lieb constrained-search formulation. Their idea was to extend the set of potentials from the potentials which give an N -electron ground state to the potentials which give a finite energy, $\mathcal{U} = L^\infty + L^{3/2} \supset \mathcal{V}_N$. For such potentials, as they may not come anymore from an Hamiltonian which has a ground state, the minimizing wave function may not exist and the minimum therefore becomes an infimum in the Rayleigh-Ritz variational principle.

The minimization can be performed into two steps, an outer minimization over n and an inner minimization over all the wave functions which give the same density n . The constraint over the density is weaker than in the original HK scheme as it only needs to be N -representable:

$$\begin{aligned} E[v] &= \inf_{\Psi} \langle \Psi | H[v] | \Psi \rangle \quad v \in \mathcal{U} \\ &= \inf_{n \in \mathcal{I}_N} \left\{ \inf_{\Psi \rightarrow n} \langle \Psi | \hat{T} + \hat{W}_{\text{ee}} | \Psi \rangle + \int v(\mathbf{r})n(\mathbf{r})d\mathbf{r} \right\}. \end{aligned} \quad (1.32)$$

The set of N -representable densities is

$$\begin{aligned} \mathcal{I}_N &= \{n \mid n \text{ comes from some } N\text{-electron wave function } \Psi\} \\ &= \{n \mid \forall \mathbf{r}, n(\mathbf{r}) \geq 0, \int n(\mathbf{r}) d\mathbf{r} = N, \int |\nabla \sqrt{n(\mathbf{r})}|^2 d\mathbf{r} < \infty\}. \end{aligned} \quad (1.33)$$

The Levy-Lieb functional is then

$$\tilde{F}[n] = \inf_{\Psi \rightarrow n} \langle \Psi | \hat{T} + \hat{W}_{ee} | \Psi \rangle, \quad n \in \mathcal{I}_N. \quad (1.34)$$

The set of N -representable densities is explicitly known and $\tilde{F}[n] = F_{\text{HK}}[n]$ if $n \in \mathcal{A}_N$. However this functional is still not convex as pointed out by Lieb in [21]. In order to have an unique solution, Lieb then proposed a convex-conjugate functional, $F[n]$, which also has an explicitly known domain and can guarantee an unique solution due to its convexity

$$F[n] = \sup_{v \in X^*} \left\{ E[v] - \int v(\mathbf{r}) n(\mathbf{r}) d\mathbf{r} \right\}, \quad n \in X. \quad (1.35)$$

This functional is the convex-envelope of the Levy-Lieb functional and is obtained by convex-conjugation (or Legendre-Fenchel transform) of the energy [12, 21]. The density and potential spaces X and X^* are then conjugated Banach spaces given by $X = L^3 \cap L^1$ and $X^* = L^{3/2} + L^\infty = \mathcal{U}$ and are explicitly known. The HK, Levy-Lieb and Lieb functionals give the same results for ground-state densities.

1.5 Kohn-Sham approach

The HK theorems provide the formal framework for DFT, but in practice, to be able to perform calculations, a pragmatic way to construct the universal functional is still required. To achieve this, in 1965, just one year after the HK theorems, Kohn and Sham proposed to partition the universal functional, using an auxiliary fictitious system of non-interacting electrons [24].

1.5.1 Kohn-Sham system

The approach proposed by Kohn and Sham consists in replacing the real system of N interacting electrons by a much simpler system of N non-interacting electrons. In the auxiliary system, the electrons move in an effective potential such that its ground-state density is the one of the real system. A schematic representation of the Kohn-Sham and real systems is given in Figure 1.1. As the ground-state density contains all the information thanks to the HK theorems, it is therefore possible in principle to calculate all the properties of the real system using the auxiliary system, as they have the same ground-state density.

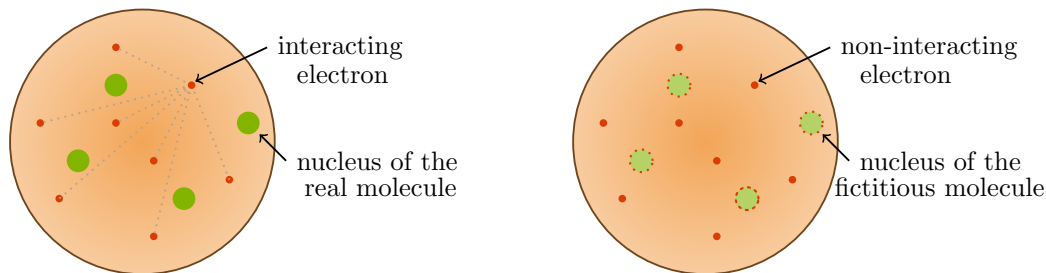


Figure 1.1 – Schematic representation of the Kohn-Sham approach. On the left, the real system of N interacting electrons moving in the field of the nuclei is represented. On the right, the fictitious system of N non-interacting electrons is shown. These electrons move in a modified potential such that both the real and the fictitious system have the same ground-state density.

The universal functional of the Kohn-Sham (KS) system is explicitly known (though the dependence in the density is implicit) and reduces to the kinetic contribution of the non-interacting electrons. In the Levy-Lieb formulation, the KS functional is then defined as

$$F^{\text{KS}}[n] = \inf_{\Psi \rightarrow n} \langle \Psi | \hat{T} | \Psi \rangle = T_{\text{S}}[n]. \quad (1.36)$$

As the electrons do not interact with each other, the minimizing wave function can be represented by a single Slater determinant Φ_0 constructed on the KS orbital basis set $\{\varphi_k\}$ such that

$$\Phi_0(\mathbf{x}_1, \mathbf{x}_2, \dots, \mathbf{x}_N) = \frac{1}{\sqrt{N!}} \det\{\varphi_i(\mathbf{x}_j)\}, \quad (1.37)$$

and its density is then given by

$$n(\mathbf{r}) = \sum_i |\varphi_i(\mathbf{r})|^2 \quad (1.38)$$

where the index i runs over the occupied orbitals. The non-interacting kinetic functional $T_{\text{S}}[n]$ can be calculated exactly and when expressed in terms of orbitals, is given by

$$T_{\text{S}}[n] = -\frac{1}{2} \sum_i \langle \varphi_i | \nabla^2 | \varphi_i \rangle. \quad (1.39)$$

In this expression, the density dependence of T_{S} is implicit and is built in through the orbitals by Equation (1.38).

As the ground-state energy is a functional of the density, it should be the same whether it is calculated with the real system or the fictitious one. This means that the KS potential must therefore take care of all the effects coming from the electron-electron interaction which are not taken into account in the KS functional. With respect to the external potential v of the real system, the KS potential v^{KS} needs thus an additional contribution to describe the interaction. This extra term is called the Hartree-exchange-correlation potential v_{Hxc} such that $v^{\text{KS}}(\mathbf{r}) = v(\mathbf{r}) + v_{\text{Hxc}}(\mathbf{r})$. It can be split into its classical

contribution, the Hartree potential

$$v_{\text{H}}[n](\mathbf{r}) = \int \frac{n(\mathbf{r}')}{|\mathbf{r} - \mathbf{r}'|} d\mathbf{r}' \quad (1.40)$$

which describes the Coulomb interaction, and the exchange and correlation potentials, whose explicit forms are unknown and which must describe all the non-classical effects. The ground-state energy can then be expressed equivalently using the real system or the KS system as

$$E_0 = \min_{\{\varphi_i\}} \left\{ F[n] + \int n(\mathbf{r})v(\mathbf{r})d\mathbf{r} \right\}, \quad (1.41a)$$

$$= \min_{\{\varphi_i\}} \left\{ T_{\text{S}}[n] + E_{\text{Hxc}}[n] + \int n(\mathbf{r})v(\mathbf{r})d\mathbf{r} \right\}. \quad (1.41b)$$

where the density is obtained in terms of the KS orbitals by Equation (1.38) and, where the term $E_{\text{Hxc}}[n]$ is the Hartree-exchange-correlation energy functional and is related to the corresponding potential by functional differentiation

$$v_{\text{Hxc}}[n](\mathbf{r}) = \frac{\delta E_{\text{Hxc}}[n]}{\delta n(\mathbf{r})}. \quad (1.42)$$

1.5.2 KS Hamiltonian

The resolution of Equation (1.41b) under the orthonormality constraint: $\langle \varphi_i | \varphi_j \rangle = \delta_{ij}$ on the KS orbitals leads to the resolution of the set of one-electron KS equations

$$\left[-\frac{1}{2}\nabla^2 + v^{\text{KS}}(\mathbf{r}) \right] \varphi_i(\mathbf{r}) = \varepsilon_i \varphi_i(\mathbf{r}), \quad (1.43)$$

where the eigenvalues ε_i are the KS orbital energies associated to the KS orbitals φ_i . This is equivalent to the equation

$$\hat{H}^{\text{KS}}[n]|\Phi\rangle = \left(\hat{T} + \hat{V}^{\text{KS}}[n] \right) |\Phi\rangle = \mathcal{E}^{\text{KS}}[n]|\Phi\rangle \quad (1.44)$$

where $\hat{H}^{\text{KS}}[n]$ is the KS Hamiltonian, $\hat{V}^{\text{KS}}[n] = \int v^{\text{KS}}[n](\mathbf{r})\hat{n}(\mathbf{r})d\mathbf{r}$ is the KS potential operator and $\mathcal{E}^{\text{KS}}[n]$ are the KS eigenvalues. This equation has to be solved iteratively as the KS potential depends on the orbitals. When convergence is reached, the minimizing wave function is the KS ground-state wave function and gives back the exact ground-state density of the real system.

Meaning of the KS wave function and orbital energies

Although it reproduces the exact ground-state density, the KS ground-state wave function is not the exact ground-state wave function. Similarly the energies of the KS orbital are not *a priori* related to the excited-state energies of the real system. However, the energy of the highest occupied molecular orbital (HOMO) can be interpreted from the

extension of Koopmans' theorem [25, 26], as the opposite of the ionization energy of the N -electron system and the opposite of the electronic affinity of the $(N - 1)$ -electron system.

Asymptotic behavior of the KS potential

The nuclear potential of a neutral N -electron system behaves as $-N/r$ when $r \rightarrow \infty$ and the Hartree potential goes asymptotically as N/r . Therefore, they cancel each other in this limit. When an electron is very far away from the rest of the system, it should feel the electrostatic attraction due to the remaining positive ion. Thus, the asymptotic behavior of the exchange-correlation potential must be

$$v_{xc}(\mathbf{r}) \xrightarrow{r \rightarrow \infty} -\frac{1}{r}. \quad (1.45)$$

This illustrates the fact that there is no self-interaction in the exact Kohn-Sham formalism as for an 1-electron system, the Hartree and exchange potentials cancel exactly.

1.5.3 Hartree, exchange and correlation functionals

All the difficulty in the KS scheme lies into the determination of the Hartree-exchange-correlation functional. The Hartree functional is explicitly known and is given by

$$E_H[n] = \frac{1}{2} \iint \frac{n(\mathbf{r})n(\mathbf{r}')}{|\mathbf{r} - \mathbf{r}'|} d\mathbf{r}d\mathbf{r}'. \quad (1.46)$$

Unfortunately, such an expression is not available for the exchange-correlation (xc) functional which is therefore the only remaining unknown quantity. It must take into account what is missing in the non-interacting kinetic functional and in the classical Hartree interaction

$$\begin{aligned} E_{xc}[n] &= T[n] - T_S[n] + W_{ee}[n] - E_H[n] \\ &= \langle \Psi | \hat{T} | \Psi \rangle - \langle \Phi | \hat{T} | \Phi \rangle + \langle \Psi | \hat{W}_{ee} | \Psi \rangle - E_H[n] \\ &= \langle \Psi | \hat{T} + \hat{W}_{ee} | \Psi \rangle - \langle \Phi | \hat{T} + \hat{W}_{ee} | \Phi \rangle + \langle \Phi | \hat{W}_{ee} | \Phi \rangle - E_H[n]. \end{aligned} \quad (1.47)$$

It is usually further decomposed into two contributions, an exchange functional

$$E_x[n] = \langle \Phi | \hat{W}_{ee} | \Phi \rangle - E_H[n] \quad (1.48)$$

which must account for the antisymmetry of the wave function with respect to the exchange of two electrons, and a correlation functional

$$E_c[n] = \langle \Psi | \hat{T} + \hat{W}_{ee} | \Psi \rangle - \langle \Phi | \hat{T} + \hat{W}_{ee} | \Phi \rangle, \quad (1.49)$$

which must describe the effects due to the correlated motion of the electrons.

Coming back to the definition of the pair density, this implies that the pair density can also be decomposed in a similar fashion

$$n_2(\mathbf{r}, \mathbf{r}') = n(\mathbf{r})n(\mathbf{r}') + n_{2,x}(\mathbf{r}, \mathbf{r}') + n_{2,c}(\mathbf{r}, \mathbf{r}') = n_2^{\text{KS}}(\mathbf{r}, \mathbf{r}') + n_{2,c}(\mathbf{r}, \mathbf{r}') \quad (1.50)$$

where $n_2^{\text{KS}}(\mathbf{r}, \mathbf{r}') = \langle \Phi | \hat{n}_2(\mathbf{r}, \mathbf{r}') | \Phi \rangle$ is the KS pair density. Therefore, the exchange and correlation pair densities can be expressed as $n_{2,x}(\mathbf{r}, \mathbf{r}') = n_2^{\text{KS}}(\mathbf{r}, \mathbf{r}') - n(\mathbf{r})n(\mathbf{r}')$ and $n_{2,c}(\mathbf{r}, \mathbf{r}') = n_2(\mathbf{r}, \mathbf{r}') - n_2^{\text{KS}}(\mathbf{r}, \mathbf{r}')$. In particular, this gives a convenient definition for the exchange functional as

$$E_x[n] = \frac{1}{2} \iint \frac{n_{2,x}(\mathbf{r}, \mathbf{r}')}{|\mathbf{r} - \mathbf{r}'|} d\mathbf{r} d\mathbf{r}'. \quad (1.51)$$

1.6 Local density approximation

1.6.1 Principle of the approximation

Since the KS scheme was proposed, the design of good approximations for the exchange-correlation functional has been a major subject of research. The first approximation was proposed by Kohn and Sham in the same paper. It is based on a model system, the uniform electron gas (UEG) in which electrons move on a positive uniformly charged background such that the total system is neutral and has an electron density n . This system is of particular interest because it defines in fact a series of systems where the exchange and correlation functionals are known either exactly or with very high accuracy for any constant density n . In other systems such as the hydrogen or the helium atom, the KS potential can also be numerically calculated by a Lieb optimization but provides only a solution for a specific density.

The exchange energy per particle in an UEG of density n is known explicitly:

$$\varepsilon_x(n(\mathbf{r})) = -\frac{3}{4} \left(\frac{3n(\mathbf{r})}{\pi} \right)^{1/3}, \quad (1.52)$$

and was originally derived by Dirac [27] and Slater [28]. Such an explicit expression is not known for the correlation part, but very accurate quantum Monte-Carlo calculations were performed by Ceperley and Alder [29] and lead to analytical expressions by interpolation, the most famous for molecules being the one by Vosko, Wilk and Nusair in 1980 [30] and the one by Perdew and Wang in 1992 [31].

The idea underlying the local-density approximation (LDA) is then to divide the real system onto a grid and substitute the exchange-correlation energy density on each volume element $d\mathbf{r}$ around the position \mathbf{r} by the one calculated for an uniform electron gas of density $n(\mathbf{r})$ as shown in Figure 1.2 such that the LDA exchange-correlation energy is

$$E_{xc}^{\text{LDA}}[n] = \int n(\mathbf{r}) \varepsilon_{xc}^{\text{UEG}}(n(\mathbf{r})) d\mathbf{r}. \quad (1.53)$$

The Hohenberg-Kohn theorems state that it is in principle possible to determine the

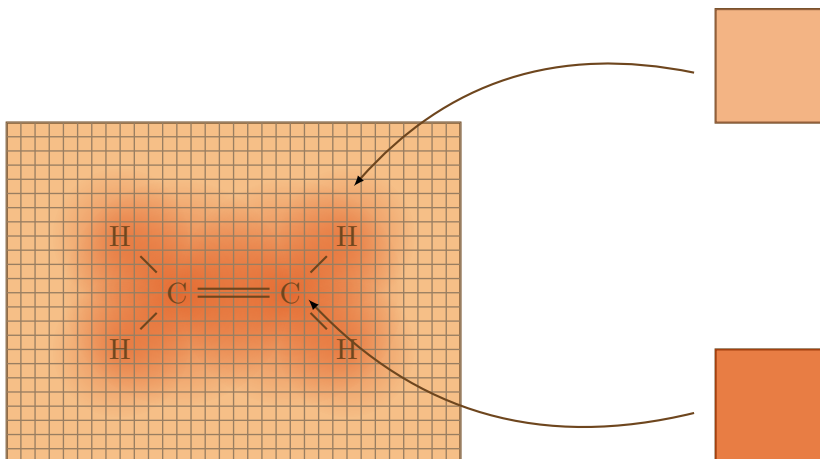


Figure 1.2 – Schematic representation of the LDA approximation, where the energy density functional at each grid point is replaced by the one of the uniform electron gas which has the same density.

total energy using only the total density and not the spin densities. However, when it comes to designing approximations for the exchange and correlation functionals, using the spin densities simplifies greatly the task, especially to reproduce the difference of stability between states of different spin. LDA was therefore extended to spin densities, which gave rise to the local-spin-density approximation (LSDA). Hereinafter, LSDA functionals are used but the spin-density dependence will be kept implicit.

1.6.2 Performance of the approximation

Realistic molecular systems are highly heterogeneous, therefore as the LDA functional relies on a homogeneous system, it would be expected to give disastrous results. However, this approximation turns out to behave extremely well given its level of complexity. In fact, the LDA functional usually overbinds molecules but gives reasonable structures [4, 32]. It benefits from an error compensation between the underestimation of the total exchange energy and the overestimation of the correlation. Moreover, in this approximation, the sum rule for the exchange-correlation hole is satisfied which can also be an explanation for its overall good performance.

A shortcoming of the LDA functional comes from the wrong asymptotic behavior of the xc potential at large distances. In fact, as the density decays exponentially, it is straightforward to show that it will also be the case for the LDA potential while it should decay as $-1/r$. This comes from the self-interaction error, as the exchange potential does not cancel the Hartree potential anymore in a 1-electron system. It also causes the Kohn-Sham orbital energies to be too low in magnitude and in particular, the ionization energy is largely underestimated.

It is difficult to provide a recipe to improve systematically the functionals. Introduction of gradient expansion corrections lead to the generalized-gradient approximations

(GGA) in an attempt to take into account the system inhomogeneity. The most famous GGA functionals are BLYP [33, 34] and PBE [35]. However, despite the gain of complexity, the overall improvement of these functionals with respect to the LDA remains modest [36, 37]. One reason for this is that the sum rule for the exchange-correlation hole is not fulfilled anymore with these functionals. Even more flexibility can be added by the introduction of the Laplacian of the density or the kinetic-energy density $\tau(\mathbf{r})$ in meta-GGA approximations, or by introducing some percentage of Hartree-Fock exchange in hybrid ones. In the continuity of the hybrid approximations, another approach relying on the range separation of the electronic interaction can be considered in order to introduce some exchange and correlation coming from wave-function methods.

1.7 Range separation of the two-electron interaction

1.7.1 Motivation

The local or semi-local approximations to the exchange and correlation functionals may seem well suited when electrons are close to each other but are less accurate when they are at large distance. Within these approximations, the DFT scheme seems therefore adapted to describe the electronic interaction only at short range and alternative methods should be considered for the long-range part of the interaction. Range-separated DFT is an extension of the Kohn-Sham formalism which provides in principle an exact scheme exploiting this statement [38, 39]. The starting point is not the non-interacting Kohn-Sham system but a partially interacting system where the long-range part of the Coulomb interaction is included. The Hartree-exchange-correlation functional must therefore describe what is missing, i.e. the short-range part of the interaction. In order to remain computationally interesting, not too much of the interaction should be included in the starting system or one would just end with a problem of the same complexity than the initial many-body problem. As some interaction is present in the starting system, its wave function is no longer a single Slater determinant and should require several (but not too many) determinants. Usual wave function methods such as configuration interaction (CI) are therefore required for its description [40, 41]. This method can therefore be seen as a multi-determinant expansion of Kohn-Sham theory which allows for the rigorous combination of wave-function and density-based methods as represented in Figure 1.3.

Moreover, one difficulty encountered in the wave function methods is the description of the electronic cusp when electrons are very close to each other. One advantage of the range-separated approach is that this phenomenon is described in the density functional part. In particular, this allows for a faster basis convergence in comparison with the complete treatment of the problem with pure wave function methods.

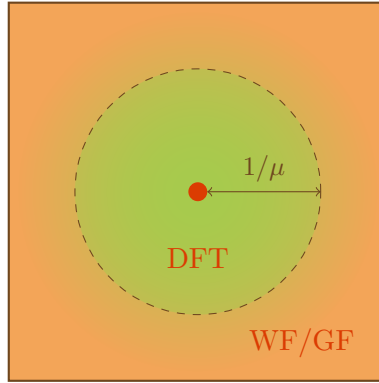


Figure 1.3 – Schematic representation of the range separation of the electron-electron interaction. At short-range, a DFT treatment is used, at long-range, a wave function (WF) method (or a manybody method based on Green’s function (GF)) is used. The range separation parameter μ can be seen as the inverse of the cut-off radius.

1.7.2 Range separation of the electronic interaction

In order to split the Coulomb interaction $w_{ee}(\mathbf{r}, \mathbf{r}') = 1/|\mathbf{r} - \mathbf{r}'|$ between an electron in \mathbf{r} and another one in \mathbf{r}' , into a short-range (sr) and a long-range (lr) part, several choices can be made. Introducing a radial function f , the only constraints are that it should vanish when the electron-electron distance is large and tends to 1 when the distance is short,

$$w_{ee}(\mathbf{r}, \mathbf{r}') = w_{ee}^{sr}(\mathbf{r}, \mathbf{r}') + w_{ee}^{lr}(\mathbf{r}, \mathbf{r}') = \frac{1 - f(|\mathbf{r} - \mathbf{r}'|)}{|\mathbf{r} - \mathbf{r}'|} + \frac{f(|\mathbf{r} - \mathbf{r}'|)}{|\mathbf{r} - \mathbf{r}'|}. \quad (1.54)$$

Among the different possibilities, one should mention in particular the use of the Yukawa potential $w_{ee}^{sr}(\mathbf{r}, \mathbf{r}') = e^{-\alpha|\mathbf{r} - \mathbf{r}'|}/|\mathbf{r} - \mathbf{r}'|$ [42–44], of the standard error function erf with or without the addition of a Gaussian function (erfgau) [45] or of a Gaussian attenuated potential [46].

In this thesis, range separation is made by using the standard error function erf

$$\text{erf}(x) = \frac{2}{\sqrt{\pi}} \int_0^x e^{-t^2} dt. \quad (1.55)$$

This choice is convenient since, within a Gaussian basis set, the evaluation of the two-electron integrals corresponding to the erf interaction requires only a simple change in the algorithm. In order to control the range of the separation, a range-separation parameter $\mu \in \mathbb{R}^+$ is introduced such that the radial function f is given by $f^\mu(|\mathbf{r} - \mathbf{r}'|) = \text{erf}(\mu|\mathbf{r} - \mathbf{r}'|)$. This parameter can be seen as the inverse of a smooth cut-off radius as shown in Figure 1.4. If the electron distance is smaller than $1/\mu$ then the short-range part is dominant, while the long-range part is for distances greater than $1/\mu$. The density is related to the inverse of the Wigner-Seitz radius

$$r_s = \left(\frac{3}{4\pi n} \right)^{1/3}, \quad (1.56)$$

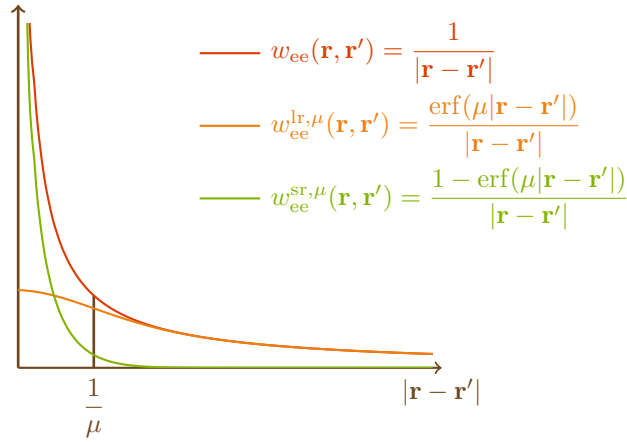


Figure 1.4 – Full-range, short-range and long-range part of the Coulomb interaction for a given range separation parameter μ in function of the electron-electron distance $|\mathbf{r} - \mathbf{r}'|$.

which can itself be related to the mean distance between particles. Although the range-separated approach is in principle exact for any μ , it is difficult to design approximate functionals which are able to treat such an inhomogeneous system as a molecule. Ideally, the range separation should depend locally on the density in each space point. However, the resolution of such a problem would be very tedious so the choice was made to perform the range separation globally with a compromise value of the range-separation parameter μ .

With this definition of range separation, it is then possible to define a short-range and a long-range interaction operator

$$\hat{W}_{ee}^{sr,\mu} = \frac{1}{2} \iint \hat{n}_2(\mathbf{r}, \mathbf{r}') w_{ee}^{sr,\mu}(\mathbf{r}, \mathbf{r}') d\mathbf{r} d\mathbf{r}' \quad \text{and} \quad \hat{W}_{ee}^{lr,\mu} = \frac{1}{2} \iint \hat{n}_2(\mathbf{r}, \mathbf{r}') w_{ee}^{lr,\mu}(\mathbf{r}, \mathbf{r}') d\mathbf{r} d\mathbf{r}', \quad (1.57)$$

where the corresponding interactions are given by

$$w_{ee}^{sr,\mu}(\mathbf{r}, \mathbf{r}') = \frac{1 - \text{erf}(\mu|\mathbf{r} - \mathbf{r}'|)}{|\mathbf{r} - \mathbf{r}'|} \quad \text{and} \quad w_{ee}^{lr,\mu}(\mathbf{r}, \mathbf{r}') = \frac{\text{erf}(\mu|\mathbf{r} - \mathbf{r}'|)}{|\mathbf{r} - \mathbf{r}'|}. \quad (1.58)$$

In particular, one should note that when $\mu \rightarrow 0$, the long-range interaction operator vanishes, and the short-range interaction tends to the real interaction, while when $\mu \rightarrow \infty$, it is the opposite.

1.7.3 Range-separation of the universal functional

In comparison with the usual KS formalism of section 1.5, the long-range part of the interaction is kept into the Lieb functional, which defines a long-range universal func-

tional

$$F^{\text{lr},\mu}[n] = \inf_{\Psi \rightarrow n} \langle \Psi | \hat{T} + \hat{W}_{\text{ee}}^{\text{lr},\mu} | \Psi \rangle. \quad (1.59)$$

Because of the presence of the long-range interaction operator, the minimizing wave function Ψ^μ is no longer a single Slater determinant. By analogy with the fully-interacting case, the long-range universal functional can be decomposed into its kinetic, Hartree, exchange and correlation contributions where the real interaction is replaced by its long-range equivalent

$$F^{\text{lr},\mu}[n] = T_{\text{S}}[n] + E_{\text{H}}^{\text{lr},\mu}[n] + E_{\text{x}}^{\text{lr},\mu}[n] + E_{\text{c}}^{\text{lr},\mu}[n], \quad (1.60)$$

where by analogy to Equations (1.46), (1.48) and (1.49),

$$\begin{aligned} E_{\text{H}}^{\text{lr},\mu}[n] &= \frac{1}{2} \iint n(\mathbf{r})n(\mathbf{r}')w_{\text{ee}}^{\text{lr},\mu}(\mathbf{r},\mathbf{r}')d\mathbf{r}d\mathbf{r}', \\ E_{\text{x}}^{\text{lr},\mu}[n] &= \langle \Phi | \hat{W}_{\text{ee}}^{\text{lr},\mu} | \Phi \rangle - E_{\text{H}}^{\text{lr},\mu}[n], \\ E_{\text{c}}^{\text{lr},\mu}[n] &= \langle \Psi^\mu | \hat{T} + \hat{W}_{\text{ee}}^{\text{lr},\mu} | \Psi^\mu \rangle - \langle \Phi | \hat{T} + \hat{W}_{\text{ee}}^{\text{lr},\mu} | \Phi \rangle. \end{aligned} \quad (1.61)$$

When μ goes to 0, the long-range energy functionals vanish and the KS universal functional $F^{\text{KS}}[n]$ is recovered. On the contrary, when $\mu \rightarrow \infty$, they tend to the full-range Hartree, exchange and correlation functionals and the long-range universal functional reduces to the full-range universal functional $F[n]$.

For a given μ , the total universal functional is recovered by addition of a complementary short-range functional $\bar{F}^{\text{sr},\mu}[n]$ which can also be decomposed into

$$\bar{F}^{\text{sr},\mu}[n] = E_{\text{H}}^{\text{sr},\mu}[n] + E_{\text{x}}^{\text{sr},\mu}[n] + \bar{E}_{\text{c}}^{\text{sr},\mu}[n], \quad (1.62)$$

where its Hartree, exchange and correlation contributions are given by

$$\begin{aligned} E_{\text{H}}^{\text{sr},\mu}[n] &= E_{\text{H}}[n] - E_{\text{H}}^{\text{lr},\mu}[n], \\ E_{\text{x}}^{\text{sr},\mu}[n] &= E_{\text{x}}[n] - E_{\text{x}}^{\text{lr},\mu}[n], \\ \bar{E}_{\text{c}}^{\text{sr},\mu}[n] &= E_{\text{c}}[n] - E_{\text{c}}^{\text{lr},\mu}[n]. \end{aligned} \quad (1.63)$$

For the correlation contribution, the complementary short-range functional is not equivalent to the one which would be obtained if the short-range part of the interaction was kept into the functional instead of the long-range one [47]

$$F^{\text{sr},\mu}[n] = \inf_{\Psi \rightarrow n} \langle \Psi | \hat{T} + \hat{W}_{\text{ee}}^{\text{sr},\mu} | \Psi \rangle. \quad (1.64)$$

To avoid any confusion, a bar is therefore used for the complementary functional.

1.7.4 Range-separated ground-state energy

Using these range-separated functionals, the ground-state energy of the system is then obtained by

$$\begin{aligned} E_0 &= \min_n \left\{ F^{\text{lr},\mu}[n] + \bar{F}^{\text{sr},\mu}[n] + \int v_{\text{ne}}(\mathbf{r})n(\mathbf{r})d\mathbf{r} \right\} \\ &= \min_n \left\{ \inf_{\Psi \rightarrow n} \langle \Psi | \hat{T} + \hat{W}_{\text{ee}}^{\text{lr},\mu} | \Psi \rangle + \bar{E}_{\text{Hxc}}^{\text{sr},\mu}[n] + \int v_{\text{ne}}(\mathbf{r})n(\mathbf{r})d\mathbf{r} \right\}. \end{aligned} \quad (1.65)$$

The minimizing wave function corresponds to the ground state solution of equation

$$\hat{H}^{\text{lr},\mu} |\Psi^\mu\rangle = \mathcal{E}^\mu |\Psi^\mu\rangle, \quad (1.66)$$

where $\hat{H}^{\text{lr},\mu} = \hat{T} + \hat{W}_{\text{ee}}^{\text{lr},\mu} + \hat{V}^{\text{sr},\mu}$ is the partially interacting Hamiltonian in which $\hat{V}^{\text{sr},\mu} = \int \hat{n}(\mathbf{r})v^{\text{sr},\mu}(\mathbf{r})$ is the complementary external potential operator which keeps the density constant. This potential can be split into its nucleus-electron, Hartree, exchange and correlation contributions $\bar{v}^{\text{sr},\mu}(\mathbf{r}) = v_{\text{ne}}(\mathbf{r}) + v_{\text{H}}^{\text{sr},\mu}(\mathbf{r}) + v_{\text{x}}^{\text{sr},\mu}(\mathbf{r}) + \bar{v}_{\text{c}}^{\text{sr},\mu}(\mathbf{r})$, where the short-range Hartree, exchange and correlation potentials are obtained by functional differentiation of the corresponding energy functionals

$$\bar{v}_{\text{Hxc}}^{\text{sr},\mu}[n](\mathbf{r}) = \frac{\delta \bar{E}_{\text{Hxc}}^{\text{sr},\mu}[n]}{\delta n(\mathbf{r})}. \quad (1.67)$$

Up to this point, the theory is exact. In practice, a density-functional approximation is usually used for $\bar{E}_{\text{Hxc}}^{\text{sr},\mu}[n]$. The minimizing multideterminantal wave function Ψ^μ can then be computed self-consistently with Equation (1.66) using the usual wave-function methods such as CI [40] or multiconfigurational self-consistent field (MCSCF) [48] or can be approximated to a single Slater determinant. The latter defines the range-separated-hybrid approximation (RSH) [43, 48, 49]. Due to the single determinant nature of the wave function, the ground-state energy then reduces to

$$E_{0,\text{RSH}}^\mu = \langle \Phi_0 | \hat{T} + \hat{V}_{\text{ne}} | \Phi_0 \rangle + E_{\text{H}}[n_0] + E_{\text{x,HF}}^{\text{lr},\mu}[\Phi_0] + \bar{E}_{\text{xc}}^{\text{sr},\mu}[n_0], \quad (1.68)$$

where Φ_0 and n_0 are the minimizing Slater determinant and associated electron density. In this approach, the long-range exchange is therefore treated at the Hartree-Fock level and the long-range correlation is neglected.

One main advantage of such an approach is that the presence of the HF long-range exchange potential ensures the correct asymptotic behavior of the xc potential in $-1/r$.

If the range separation is done on the exchange functional only, it defines the so-called long-range corrected functionals (LC) [50] which can also be referred to as RSHX [51]. In this case, the ground-state energy is given by

$$E_{0,\text{LC}}^\mu = \langle \Phi_0 | \hat{T} + \hat{V}_{\text{ne}} | \Phi_0 \rangle + E_{\text{H}}[n_0] + E_{\text{x,HF}}^{\text{lr},\mu}[\Phi_0] + E_{\text{x}}^{\text{sr},\mu}[n_0] + E_{\text{c}}[n_0]. \quad (1.69)$$

1.8 Conclusion

In this chapter, the time-independent density-functional theory and its range-separated extension were briefly reviewed. These methods are formally ground-state methods as they are based on the variational principle. However, the HK theorems state the ground-state density contain all the information on the system so in particular one should be able to extract the excitation energies. In the next chapters, we will therefore focus on how to extract these excitation energies in the framework of range separation.

Chapter 2

Excitation energies along a range-separated adiabatic connection

This chapter is the subject of a publication in collaboration with J. Toulouse, A. M. Teale, T. Helgaker and A. Savin, and has been submitted to the Journal of Chemical Physics.

In this chapter, we present a study of the variation of total energies and excitation energies along a range-separated adiabatic connection. This connection links the non-interacting Kohn-Sham electronic system to the physical interacting system by progressively switching on the electron-electron interactions whilst simultaneously adjusting a one-electron effective potential so as to keep the ground-state density constant. In this work the interactions are introduced in a range-dependent manner, first introducing predominantly long-range, and then all-range, interactions as the physical system is approached. Reference data are reported for the He and Be atoms and the H₂ molecule, obtained by calculating the short-range effective potential at the full configuration-interaction level using Lieb's Legendre-transform approach. As the strength of the electron-electron interactions increases, the excitation energies, calculated for the partially interacting systems along the adiabatic connection, offer increasingly accurate approximations to the exact excitation energies. Importantly, the excitation energies calculated at an intermediate point of the adiabatic connection are much better approximations to the exact excitation energies than are the corresponding Kohn-Sham excitation energies. This is particularly evident in situations involving strong static correlation effects and states with multiple excitation character, such as the dissociating H₂ molecule. These results highlight the utility of long-range interacting reference systems as a starting point for the calculation of excitation energies and are of interest for developing and analyzing practical approximate range-separated density-functional methodologies.

2.1 Introduction

Range-separated density-functional theory (see, e.g., Ref. [45]) constitutes an interesting alternative to standard Kohn-Sham (KS) density-functional theory (DFT) [19, 24]. In the standard KS approach, the physical interacting electronic Hamiltonian is replaced by an effective non-interacting Hamiltonian. By contrast, in range-separated DFT, the physical Hamiltonian is instead replaced by a partially interacting Hamiltonian that incorporates the long-range part of the electron-electron interaction. This corresponds to an intermediate point along a range-separated adiabatic connection [39, 45, 52–54]. The KS Hamiltonian is linked to the physical Hamiltonian by progressively switching on the long-range part of the two-electron interaction, whilst simultaneously modifying the one-electron potential so as to maintain a constant ground-state density. The ground-state energy of the physical system can then be extracted from the ground state of the long-range interacting Hamiltonian by using a short-range density functional describing the complementary short-range part of the electron-electron interaction.

Several short-range density-functional approximations have been developed [39, 45, 55–60] and a diverse range of approaches for calculating the ground state of the long-range interacting Hamiltonian have been explored. To aid in the description of static (or strong) correlation effects, which are poorly treated by standard density functionals, configuration-interaction [39–42, 45, 54, 61] multiconfiguration self-consistent-field (MC-SCF) [48, 62, 63], density-matrix functional theory (DMFT) [64–66], and constrained-pairing mean-field theory [67, 68] descriptions of the long-range interacting systems have been employed. To treat van der Waals interactions, second-order perturbation theory [49, 69–79], coupled-cluster theory [58, 60, 80–82], and random-phase approximations [83–93] have been used successfully.

Electronic excitation energies can also be calculated in range-separated DFT by using the linear-response approach with a time-dependent generalization of the static ground-state theory [94]. In this case, the excitation energies of the long-range interacting Hamiltonian act as starting approximations that are then corrected using a short-range density-functional kernel, just as the KS excitation energies act as starting approximations in linear-response time-dependent density-functional theory (TDDFT). Several such range-separated linear-response schemes have been developed in which the short-range part is described by an approximate adiabatic semilocal density-functional kernel and the long-range linear-response part is treated in Hartree-Fock [94–97], MCSCF [94, 97], second-order polarization-propagator approximation (SOPPA) [97], or DMFT [98]. These schemes aim at overcoming the limitations of standard linear-response TDDFT applied with usual adiabatic semilocal approximations for describing systems with static correlation [99], double or multiple excitations [100], and Rydberg and charge-transfer excitations [101, 102].

For the purpose of analyzing the above-mentioned linear-response range-separated DFT approaches, it is desirable to have accurate reference values of the excitation en-

ergies of the long-range interacting Hamiltonian along the range-separated adiabatic connection. In this work, we provide and analyze such accurate reference data for the He and Be atoms and the H₂ molecule. Short-range one-electron potentials keeping the ground-density constant along a range-separated adiabatic connection are calculated at the full configuration-interaction (FCI) level within Lieb’s Legendre-transform approach [21, 103, 104]. The excited-state energies of the long-range interacting Hamiltonian along the adiabatic connection are then calculated using the FCI method. Several accurate ground-state calculations have been performed in the past along the standard adiabatic connection [103–108] and range-separated adiabatic connections [45, 53, 108–110] for small atomic and molecular systems, but accurate calculations of excited-state energies along adiabatic connections are very scarce (see, however, Refs. [103, 111]).

The chapter is organized as follows. In Section 2.2, range-separated DFT is briefly reviewed and the definition of the excited states along the range-separated adiabatic connection is introduced. In Section 2.3, the behavior of the excited-state energies near the two endpoints of the adiabatic connection, the Kohn-Sham system and the physical system, is studied analytically. After giving computational details in Section 2.4, results along the full adiabatic-connection path are presented and discussed in Section 2.5. Finally, some concluding remarks are made in Section 2.6.

2.2 Range-separated density-functional theory

In range-separated DFT (see, e.g., Ref. [45]), the exact ground-state energy of an N -electron system is in principle obtained by the following minimization over normalized multi-determinantal wave functions Ψ :

$$E_0 = \min_{\Psi} \left\{ \langle \Psi | \hat{T} + \hat{V}_{\text{ne}} + \hat{W}_{\text{ee}}^{\text{lr},\mu} | \Psi \rangle + \bar{E}_{\text{Hxc}}^{\text{sr},\mu}[n_{\Psi}] \right\}. \quad (2.1)$$

This expression contains the kinetic-energy operator \hat{T} , the nuclear-electron interaction operator $\hat{V}_{\text{ne}} = \int v_{\text{ne}}(\mathbf{r})\hat{n}(\mathbf{r})d\mathbf{r}$ expressed in terms of the density operator $\hat{n}(\mathbf{r})$, and a long-range (lr) electron-electron interaction operator

$$\hat{W}_{\text{ee}}^{\text{lr},\mu} = \frac{1}{2} \iint w_{\text{ee}}^{\text{lr},\mu}(r_{12})\hat{n}_2(\mathbf{r}_1, \mathbf{r}_2)d\mathbf{r}_1d\mathbf{r}_2, \quad (2.2)$$

expressed in terms of the pair-density operator $\hat{n}_2(\mathbf{r}_1, \mathbf{r}_2)$. In the present work, we use the error-function interaction

$$w_{\text{ee}}^{\text{lr},\mu}(r_{12}) = \frac{\text{erf}(\mu r_{12})}{r_{12}}, \quad (2.3)$$

where μ controls the range of the separation, with $1/\mu$ acting as a smooth cut-off radius. The corresponding complementary short-range (sr) Hartree-exchange-correlation density functional $\bar{E}_{\text{Hxc}}^{\text{sr},\mu}[n_{\Psi}]$ is evaluated at the density of Ψ : $n_{\Psi}(\mathbf{r}) = \langle \Psi | \hat{n}(\mathbf{r}) | \Psi \rangle$.

The Euler-Lagrange equation for the minimization of Equation (2.1) leads to the (self-consistent) eigenvalue equation

$$\hat{H}^{\text{lr},\mu}|\Psi_0^\mu\rangle = \mathcal{E}_0^\mu|\Psi_0^\mu\rangle, \quad (2.4)$$

where Ψ_0^μ and \mathcal{E}_0^μ are the ground-state wave function and associated energy of the partially interacting Hamiltonian (with an explicit long-range electron-electron interaction)

$$\hat{H}^{\text{lr},\mu} = \hat{T} + \hat{V}_{\text{ne}} + \hat{W}_{\text{ee}}^{\text{lr},\mu} + \hat{V}_{\text{Hxc}}^{\text{sr},\mu}. \quad (2.5)$$

It contains the short-range Hartree-exchange-correlation potential operator, evaluated at the density $n_0(\mathbf{r}) = \langle \Psi_0^\mu | \hat{n}(\mathbf{r}) | \Psi_0^\mu \rangle$, which is equal to the ground-state density of the physical system for all μ ,

$$\hat{V}_{\text{Hxc}}^{\text{sr},\mu} = \int \bar{v}_{\text{Hxc}}^{\text{sr},\mu}[n_0](\mathbf{r}) \hat{n}(\mathbf{r}) d\mathbf{r}, \quad (2.6)$$

where

$$\bar{v}_{\text{Hxc}}^{\text{sr},\mu}[n](\mathbf{r}) = \frac{\delta \bar{E}_{\text{Hxc}}^{\text{sr},\mu}[n]}{\delta n(\mathbf{r})}. \quad (2.7)$$

For $\mu = 0$, $\hat{H}^{\text{lr},\mu}$ reduces to the standard non-interacting KS Hamiltonian, \hat{H}^{KS} , while for $\mu \rightarrow \infty$ it reduces to the physical Hamiltonian \hat{H} :

$$\hat{H}^{\text{KS}} = \hat{H}^{\text{lr},\mu=0} = \hat{T} + \hat{V}_{\text{ne}} + \hat{V}_{\text{Hxc}}, \quad (2.8)$$

$$\hat{H} = \hat{H}^{\text{lr},\mu=\infty} = \hat{T} + \hat{V}_{\text{ne}} + \hat{W}_{\text{ee}}. \quad (2.9)$$

Varying the parameter μ between these two limits, $\hat{H}^{\text{lr},\mu}$ defines a range-separated adiabatic connection, linking the non-interacting KS system to the physical system with the ground-state density kept constant (provided that the exact short-range Hartree-exchange-correlation potential $\bar{v}_{\text{Hxc}}^{\text{sr},\mu}(\mathbf{r})$ is used).

In this work we also consider the excited-state wave functions and energies of the long-range interacting Hamiltonian

$$\hat{H}^{\text{lr},\mu}|\Psi_k^\mu\rangle = \mathcal{E}_k^\mu|\Psi_k^\mu\rangle, \quad (2.10)$$

where $\hat{H}^{\text{lr},\mu}$ is Hamiltonian in Equation (2.5), with the short-range Hartree-exchange-correlation potential evaluated at the *ground-state density* n_0 . In range-separated DFT, these excited-state wave functions and energies provide a natural first approximation to the excited-state wave functions and energies of the physical system. For $\mu = 0$, they reduce to the single-determinant eigenstates and associated energies of the non-interacting KS Hamiltonian,

$$\hat{H}^{\text{KS}}|\Phi_k^{\text{KS}}\rangle = \mathcal{E}_k^{\text{KS}}|\Phi_k^{\text{KS}}\rangle, \quad (2.11)$$

while, for $\mu \rightarrow \infty$, they reduce to the excited-state wave functions and energies of the

physical Hamiltonian

$$\hat{H}|\Psi_k\rangle = E_k|\Psi_k\rangle. \quad (2.12)$$

Note that, since the ionization energy is related to the asymptotic decay of the ground-state density, the ionization energy of the Hamiltonian in Equation (2.10) is also independent of μ and is equal to the ionization energy of the physical system. This is an appealing feature since it sets the correct energy window for bound excited states. Finally, note that the excitation energies $\Delta\mathcal{E}_k^\mu = \mathcal{E}_k^\mu - \mathcal{E}_0^\mu$ calculated from Equation (2.10) constitute a starting point for range-separated linear-response theory based on the time-dependent generalization of Equation (2.1) [94].

2.3 Excited-state energies near the Kohn-Sham and physical systems

In this section, we study analytically the behavior of the excited-state energies \mathcal{E}_k^μ as a function of the range-separation parameter μ near the two endpoints of the adiabatic connection: the Kohn-Sham system at $\mu = 0$ and the physical system when $\mu \rightarrow \infty$. This study will aid in the understanding of the numerical results presented in Section 2.5.

2.3.1 Excited-state energies near the Kohn-Sham system

We first derive the expansion of the excited-state energies near $\mu = 0$, to see how the KS energies are affected by the introduction of the long-range electron-electron interaction. We assume that the system is spatially finite. All the details on the derivations of the Taylor expansions around the KS system are given in Appendix B.1

We rewrite the long-range interacting Hamiltonian of Equation (2.5) as

$$\hat{H}^{\text{lr},\mu} = \hat{H}^{\text{KS}} + \hat{W}_{\text{ee}}^{\text{lr},\mu} - \hat{V}_{\text{Hxc}}^{\text{lr},\mu}, \quad (2.13)$$

with the long-range Hartree-exchange-correlation potential operator

$$\hat{V}_{\text{Hxc}}^{\text{lr},\mu} = \hat{V}_{\text{Hxc}} - \hat{V}_{\text{Hxc}}^{\text{sr},\mu} = \int v_{\text{Hxc}}^{\text{lr},\mu}(\mathbf{r})\hat{n}(\mathbf{r})\text{d}\mathbf{r}. \quad (2.14)$$

The expansion of the long-range two-electron interaction is straightforward [45] (valid for $\mu r_{12} \ll 1$)

$$w_{\text{ee}}^{\text{lr},\mu}(r_{12}) = \frac{\text{erf}(\mu r_{12})}{r_{12}} = \frac{2\mu}{\sqrt{\pi}} + \mu^3 w_{\text{ee}}^{\text{lr},(3)}(r_{12}) + \mathcal{O}(\mu^5), \quad (2.15)$$

with

$$w_{\text{ee}}^{\text{lr},(3)}(r_{12}) = -\frac{2}{3\sqrt{\pi}}r_{12}^2. \quad (2.16)$$

Next, the expansion of the long-range Hartree-exchange-correlation potential

$$v_{\text{Hxc}}^{\text{lr},\mu}(\mathbf{r}) = \frac{\delta E_{\text{Hxc}}^{\text{lr},\mu}[n]}{\delta n(\mathbf{r})} \quad (2.17)$$

can be determined from the expansion of the corresponding energy functional $E_{\text{Hxc}}^{\text{lr},\mu}[n]$. As derived in Ref. [45], the expansion of the Hartree-exchange part begins at first order and may be written as

$$\begin{aligned} E_{\text{Hxc}}^{\text{lr},\mu}[n] &= \frac{\mu}{\sqrt{\pi}} \iint n_2^{\text{KS}}(\mathbf{r}_1, \mathbf{r}_2) d\mathbf{r}_1 d\mathbf{r}_2 \\ &+ \frac{\mu^3}{2} \iint n_2^{\text{KS}}(\mathbf{r}_1, \mathbf{r}_2) w_{\text{ee}}^{\text{lr},(3)}(r_{12}) d\mathbf{r}_1 d\mathbf{r}_2 + \mathcal{O}(\mu^5). \end{aligned} \quad (2.18)$$

where $n_2^{\text{KS}}(\mathbf{r}_1, \mathbf{r}_2)$ is the KS pair density, while the expansion of the correlation part only begins at sixth order (assuming a non-degenerate KS ground state)

$$E_c^{\text{lr},\mu}[n] = 0 + \mathcal{O}(\mu^6). \quad (2.19)$$

If the functional derivative of $E_{\text{Hxc}}^{\text{lr},\mu}[n]$ is taken with respect to density variations that preserve the number of electrons, $\int \delta n(\mathbf{r}) d\mathbf{r} = 0$, then the first-order term in Equation (2.18) does not contribute due to the fixed normalization of the KS pair density, $\iint n_2^{\text{KS}}(\mathbf{r}_1, \mathbf{r}_2) d\mathbf{r}_1 d\mathbf{r}_2 = N(N-1)$. The derivative is then defined up to an additive (μ -dependent) constant C^μ , which can be fixed by requiring that a distant electron experiences zero potential interaction in Equation (2.13), amounting to setting the zero-energy reference. The linear term in μ in the long-range Hartree-exchange-correlation potential can then be determined as follows.

To first order in μ , the long-range electron-electron interaction tends to a constant, $2\mu/\sqrt{\pi}$. A distant electron (with $1 \ll r_{12} \ll 1/\mu$) then experiences a constant interaction $2(N-1)\mu/\sqrt{\pi}$ with the remaining $N-1$ other electrons. This constant must be exactly compensated by the long-range Hartree-exchange-correlation potential in Equation (2.13), so that its first-order term in μ must also be $2(N-1)\mu/\sqrt{\pi}$. The expansion of $v_{\text{Hxc}}^{\text{lr},\mu}(\mathbf{r})$ therefore takes the form

$$v_{\text{Hxc}}^{\text{lr},\mu}(\mathbf{r}) = \frac{2(N-1)\mu}{\sqrt{\pi}} + \mu^3 v_{\text{Hxc}}^{\text{lr},(3)}(\mathbf{r}) + \mathcal{O}(\mu^5), \quad (2.20)$$

where $v_{\text{Hxc}}^{\text{lr},(3)}(\mathbf{r})$ is the third-order contribution.

Combining Equations (2.15) and (2.20), we arrive at the following expansion of the long-range interacting Hamiltonian of Equation (2.13):

$$\hat{H}^{\text{lr},\mu} = \hat{H}^{\text{KS}} + \mu \hat{H}^{\text{lr},(1)} + \mu^3 \hat{H}^{\text{lr},(3)} + \mathcal{O}(\mu^5), \quad (2.21)$$

with a constant first-order correction

$$\hat{H}^{\text{lr},(1)} = -\frac{N(N-1)}{\sqrt{\pi}} \quad (2.22)$$

and the following third-order correction

$$\hat{H}^{\text{lr},(3)} = \hat{W}_{\text{ee}}^{\text{lr},(3)} - \hat{V}_{\text{Hxc}}^{\text{lr},(3)}, \quad (2.23)$$

$$\hat{W}_{\text{ee}}^{\text{lr},(3)} = \frac{1}{2} \iint w_{\text{ee}}^{\text{lr},(3)}(r_{12}) \hat{n}_2(\mathbf{r}_1, \mathbf{r}_2) d\mathbf{r}_1 d\mathbf{r}_2, \quad (2.24)$$

$$\hat{V}_{\text{Hxc}}^{\text{lr},(3)} = \int v_{\text{Hxc}}^{\text{lr},(3)}(\mathbf{r}) \hat{n}(\mathbf{r}) d\mathbf{r}. \quad (2.25)$$

Since the first-order correction in the Hamiltonian is a constant, it does not affect the associated wave functions. The expansion of the wave functions therefore begins at third order in μ :

$$\Psi_k^\mu = \Phi_k^{\text{KS}} + \mu^3 \Psi_k^{(3)} + \mathcal{O}(\mu^5). \quad (2.26)$$

Using normalized KS wave functions $\langle \Phi_k^{\text{KS}} | \Phi_k^{\text{KS}} \rangle = 1$, the expansion of the total energy for the state k is then

$$\mathcal{E}_k^\mu = \mathcal{E}_k^{\text{KS}} - \frac{N(N-1)}{\sqrt{\pi}} \mu + \mu^3 \langle \Phi_k^{\text{KS}} | \hat{H}^{\text{lr},(3)} | \Phi_k^{\text{KS}} \rangle + \mathcal{O}(\mu^5). \quad (2.27)$$

The first-order contribution is the same for all states, cancelling out in the differences between the energies of two states. As a result, the corrections to the KS excitation energies are third order in μ .

For closed shells, the expansion of the difference between the singlet and triplet energies associated with the single excitation $i \rightarrow a$ can be obtained by applying Equation (2.27) with the spin-adapted KS wave functions ${}^1\Phi^{\text{KS}} = (\Phi_{i \rightarrow a}^{\text{KS}} + \Phi_{i \rightarrow \bar{a}}^{\text{KS}}) / \sqrt{2}$, for the singlet state, and ${}^{3,1}\Phi^{\text{KS}} = \Phi_{i \rightarrow a}^{\text{KS}}$, for the triplet state with spin projection $M_S = 1$. Only the two-electron term then contributes:

$$\begin{aligned} \Delta \mathcal{E}_{i \rightarrow a}^{\mu, 1-3} &= 2\mu^3 \langle ia | \hat{w}_{\text{ee}}^{\text{lr},(3)} | ai \rangle + \mathcal{O}(\mu^5) \\ &= \frac{8\mu^3}{3\sqrt{\pi}} |\langle i | \hat{\mathbf{r}} | a \rangle|^2 + \mathcal{O}(\mu^5), \end{aligned} \quad (2.28)$$

where we have used $r_{12}^2 = r_1^2 + r_2^2 - 2\mathbf{r}_1 \cdot \mathbf{r}_2$. The appearance of the transition dipole moment integral in Equation (2.28) means that, for an atomic system, the singlet-triplet energy splitting appears at third order in μ if the difference between the angular momentum of the orbitals φ_i and φ_a is $\Delta\ell = +1$ or -1 . Otherwise, the splitting appears at a higher order in μ .

2.3.2 Excited-state energies near the physical system

We now derive the asymptotic expansion of the excited-state energies when $\mu \rightarrow \infty$, which shows how the exact excited-state energies are affected by the removal of the very short-range part of the electron-electron interaction. All the details of the derivation can be found in Appendix B.2.

For this purpose, we rewrite the long-range interacting Hamiltonian of Equation (2.5) as

$$\hat{H}^{\text{lr},\mu} = \hat{H} - \hat{W}_{\text{ee}}^{\text{sr},\mu} + \hat{V}_{\text{Hxc}}^{\text{sr},\mu}, \quad (2.29)$$

where \hat{H} is the Hamiltonian of the physical system,

$$\hat{W}_{\text{ee}}^{\text{sr},\mu} = \frac{1}{2} \iint w_{\text{ee}}^{\text{sr},\mu}(r_{12}) \hat{n}_2(\mathbf{r}_1, \mathbf{r}_2) d\mathbf{r}_1 d\mathbf{r}_2 \quad (2.30)$$

is the short-range electron-electron interaction operator defined with the complementary error-function interaction

$$w_{\text{ee}}^{\text{sr},\mu}(r_{12}) = \frac{\text{erfc}(\mu r_{12})}{r_{12}}, \quad (2.31)$$

and $\hat{V}_{\text{Hxc}}^{\text{sr},\mu}$ is the short-range Hartree-exchange-correlation potential operator in Equation (2.6). The first term in the asymptotic expansion of $w_{\text{ee}}^{\text{sr},\mu}(r_{12})$ can be written in terms of a delta function [45] (valid for $\mu r_{12} \gg 1$)

$$w_{\text{ee}}^{\text{sr},\mu}(r_{12}) = \frac{\pi}{\mu^2} \delta(\mathbf{r}_{12}) + \mathcal{O}\left(\frac{1}{\mu^3}\right), \quad (2.32)$$

while the expansion of $\bar{v}_{\text{Hxc}}^{\text{sr},\mu}(\mathbf{r}) = \delta \bar{E}_{\text{Hxc}}^{\text{sr},\mu}[n] / \delta n(\mathbf{r})$ can be obtained from that of $\bar{E}_{\text{Hxc}}^{\text{sr},\mu}[n]$. As derived in Ref. [45], the expansion of the long-range Hartree-exchange energy is

$$E_{\text{Hx}}^{\text{sr},\mu}[n] = \frac{\pi}{2\mu^2} \int n_2^{\text{KS}}(\mathbf{r}, \mathbf{r}) d\mathbf{r} + \mathcal{O}\left(\frac{1}{\mu^4}\right), \quad (2.33)$$

where $n_2^{\text{KS}}(\mathbf{r}, \mathbf{r})$ is the KS on-top pair density, while the expansion of the long-range correlation energy is

$$\bar{E}_c^{\text{sr},\mu}[n] = \frac{\pi}{2\mu^2} \int n_{2,c}(\mathbf{r}, \mathbf{r}) d\mathbf{r} + \mathcal{O}\left(\frac{1}{\mu^3}\right), \quad (2.34)$$

where $n_{2,c}(\mathbf{r}, \mathbf{r})$ is the on-top correlation pair density of the physical system. Therefore, the expansion of the short-range Hartree-exchange-correlation potential takes the form

$$\bar{v}_{\text{Hxc}}^{\text{sr},\mu}(\mathbf{r}) = \frac{1}{\mu^2} \bar{v}_{\text{Hxc}}^{\text{sr},(-2)}(\mathbf{r}) + \mathcal{O}\left(\frac{1}{\mu^3}\right), \quad (2.35)$$

where $\bar{v}_{\text{Hxc}}^{\text{sr},(-2)}(\mathbf{r})$ is the μ^{-2} contribution formally obtained by taking the functional derivative of Equations (2.33) and (2.34).

Substituting Equations (2.32) and (2.35) into Equation (2.29), we obtain the asymp-

otic expansion of the long-range interacting Hamiltonian as

$$\hat{H}^{\text{lr},\mu} = \hat{H} + \frac{1}{\mu^2} \hat{H}^{\text{lr},(-2)} + \mathcal{O}\left(\frac{1}{\mu^3}\right), \quad (2.36)$$

where $\hat{H}^{\text{lr},(-2)} = -\hat{W}_{\text{ee}}^{\text{sr},(-2)} + \hat{V}_{\text{Hxc}}^{\text{sr},(-2)}$ is composed of an on-top two-electron term and a one-electron term:

$$\hat{W}_{\text{ee}}^{\text{sr},(-2)} = \frac{\pi}{2} \int \hat{n}_2(\mathbf{r}, \mathbf{r}) \text{d}\mathbf{r}, \quad (2.37)$$

$$\hat{V}_{\text{Hxc}}^{\text{sr},(-2)} = \int \bar{v}_{\text{Hxc}}^{\text{sr},(-2)}(\mathbf{r}) \hat{n}(\mathbf{r}) \text{d}\mathbf{r}. \quad (2.38)$$

The expansion of the Hamiltonian in Equation (2.36) suggests a similar expansion for the excited-state wave functions, $\Psi_k^\mu = \Psi_k + \mu^{-2} \Psi_k^{(-2)} + \mathcal{O}(\mu^{-3})$. However, as shown in Ref. [112], this expansion is not valid for $r_{12} \ll 1/\mu$. The contribution of the wave function for small r_{12} to the integral for the total energy $\mathcal{E}_k^\mu = \langle \Psi_k^\mu | \hat{H}^{\text{lr},\mu} | \Psi_k^\mu \rangle$ nevertheless vanishes in the limit $\mu \rightarrow \infty$, and the asymptotic expansion of the total energy of the state k is

$$\mathcal{E}_k^\mu = E_k + \frac{1}{\mu^2} \langle \Psi_k | \hat{H}^{\text{lr},(-2)} | \Psi_k \rangle + \mathcal{O}\left(\frac{1}{\mu^3}\right), \quad (2.39)$$

where the wave function Ψ_k is normalized to unity.

2.4 Computational details

The calculations were performed for the He and Be atoms and for the H₂ molecule with a development version of the DALTON program [113], using the implementation described in Refs. [104, 110]. First, a FCI calculation was performed to determine the exact ground-state density within the basis set considered, followed by a Lieb optimization [103] of the short-range potential $v^{\text{sr},\mu}(\mathbf{r}) = v_{\text{ne}}(\mathbf{r}) + \bar{v}_{\text{Hxc}}^{\text{sr},\mu}(\mathbf{r})$ also at the FCI level to reproduce the FCI ground-state density in the presence of the long-range electron-electron interaction $w_{\text{ee}}^{\text{lr},\mu}(r_{12})$. The FCI excited-state energies were then calculated using the partially interacting Hamiltonian with the interaction $w_{\text{ee}}^{\text{lr},\mu}(r_{12})$ and effective potential $v^{\text{sr},\mu}(\mathbf{r})$.

The Lieb maximization was performed using the short-range analogue of the algorithm of Wu and Yang [114], in which the potential is expanded as

$$v^{\text{sr},\mu}(\mathbf{r}) = v_{\text{ne}}(\mathbf{r}) + v_{\text{ref}}^{\text{sr},\mu}(\mathbf{r}) + \sum_t b_t g_t(\mathbf{r}). \quad (2.40)$$

where the reference potential is the short-range analogue of the Fermi-Amaldi potential

$$v_{\text{ref}}^{\text{sr},\mu}(\mathbf{r}) = \frac{N-1}{N} \int n_0(\mathbf{r}') w_{\text{ee}}^{\text{sr},\mu}(|\mathbf{r} - \mathbf{r}'|) \text{d}\mathbf{r}', \quad (2.41)$$

calculated for a fixed N -electron density n_0 , to ensure the correct asymptotic behaviour.

The same Gaussian basis set $\{g_t\}$ is used for the expansion of the potential and the molecular orbitals. The coefficients b_t are optimized by the Newton method, using a regularized Hessian with a truncated singular-value-decomposition cutoff of 10^{-7} for He and 10^{-6} for Be and H_2 .

Even-tempered Kaufmann basis sets [115] and uncontracted correlation consistent Dunning basis sets [116] augmented with diffuse functions were tested extensively for the He atom, especially to converge the lowest P state. No significant differences were observed using the two basis sets and only the Dunning basis sets are used in the following. The basis sets used are: uncontracted t-aug-cc-pV5Z for He, uncontracted d-aug-cc-pVDZ for Be, and uncontracted d-aug-cc-pVTZ Dunning basis sets for H_2 .

Calculations were performed for about 30 values of μ between 0 to 10 bohr $^{-1}$ (with about half the points between 0 and 1 where the energies vary the most). Cubic spline interpolation has been used on this calculated data when plotting the total and excitation energies as a function of μ . For later use, analytical expressions were also fitted to the calculated total energies and excitation energies. The forms used in the fitting were chosen to satisfy the expansions at small and large μ values as presented in Equations (2.27) and (2.39). The details of these fits are given in the supplementary material in Appendix C.

2.5 Results and discussion

2.5.1 Range-separated adiabatic connection for the helium atom

Total energies

The total energies of the ground state 1^1S and of the first Rydberg-like singlet and triplet S and P excited states of the He atom are plotted as a function of the range-separation parameter μ in Figure 2.1. At $\mu = 0$, the KS non-interacting total energies are obtained. Being sums of orbital energies with a resulting double counting of electron repulsion, these quantities are well above the total energies of the physical system (higher by about 1 hartree). When the long-range electron-electron interaction is added by increasing μ from $\mu = 0$, the total energies decrease linearly with μ with a slope of $-2/\sqrt{\pi}$, in accordance with the linear term in the expansion of Equation (2.27) for $N = 2$. For larger μ values, the total energy curves flatten and approach the energies of the physical system asymptotically as $1/\mu^2$ as $\mu \rightarrow \infty$, in accordance with Equation (2.39). The total energies along the adiabatic connection are poor approximations to the total energies of the physical system unless the range-separation parameter μ is large. Specifically, $\mu \gtrsim 6$ is required to be within 10 mhartree of the exact total energies.

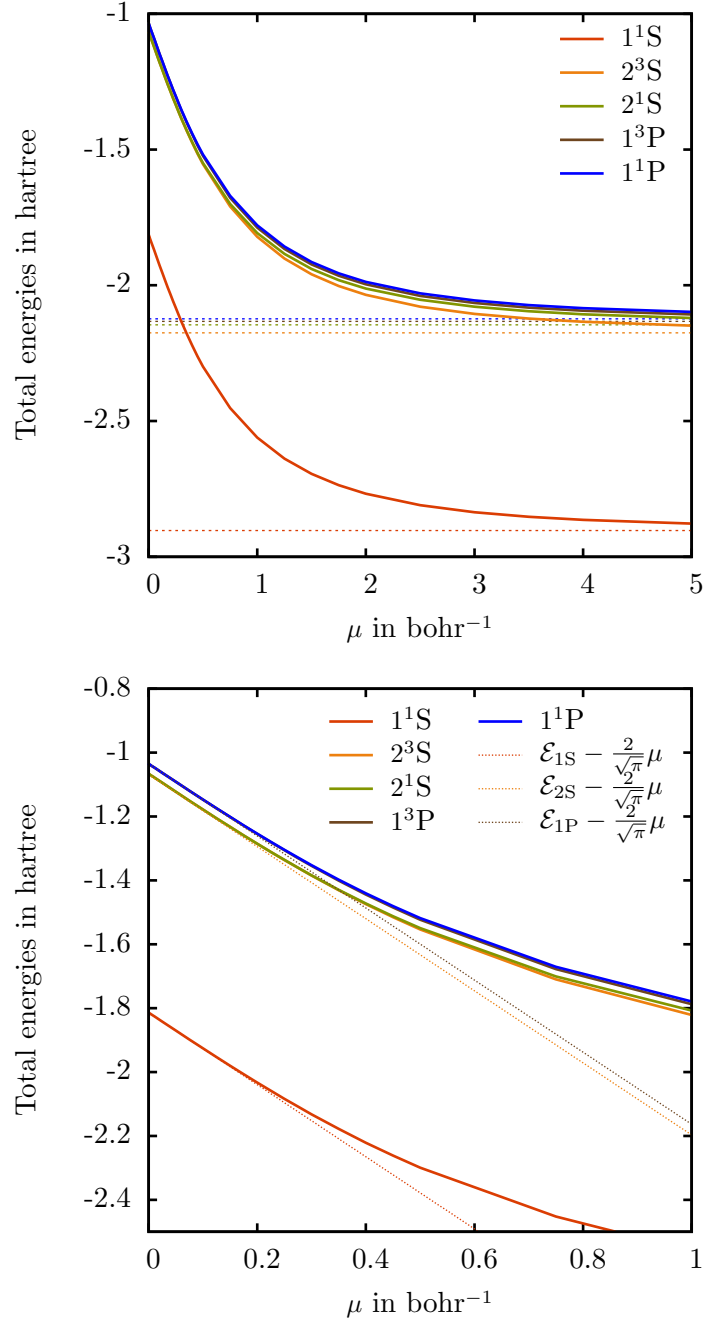


Figure 2.1 – Ground- and excited-state total energies \mathcal{E}_k^μ (in hartree) of the He atom as a function of μ (in bohr⁻¹). The total energies of the physical system $E_k = \mathcal{E}_k^{\mu \rightarrow \infty}$ are plotted as horizontal dotted lines (top). The slope at $\mu = 0$ is shown in dotted line (bottom).

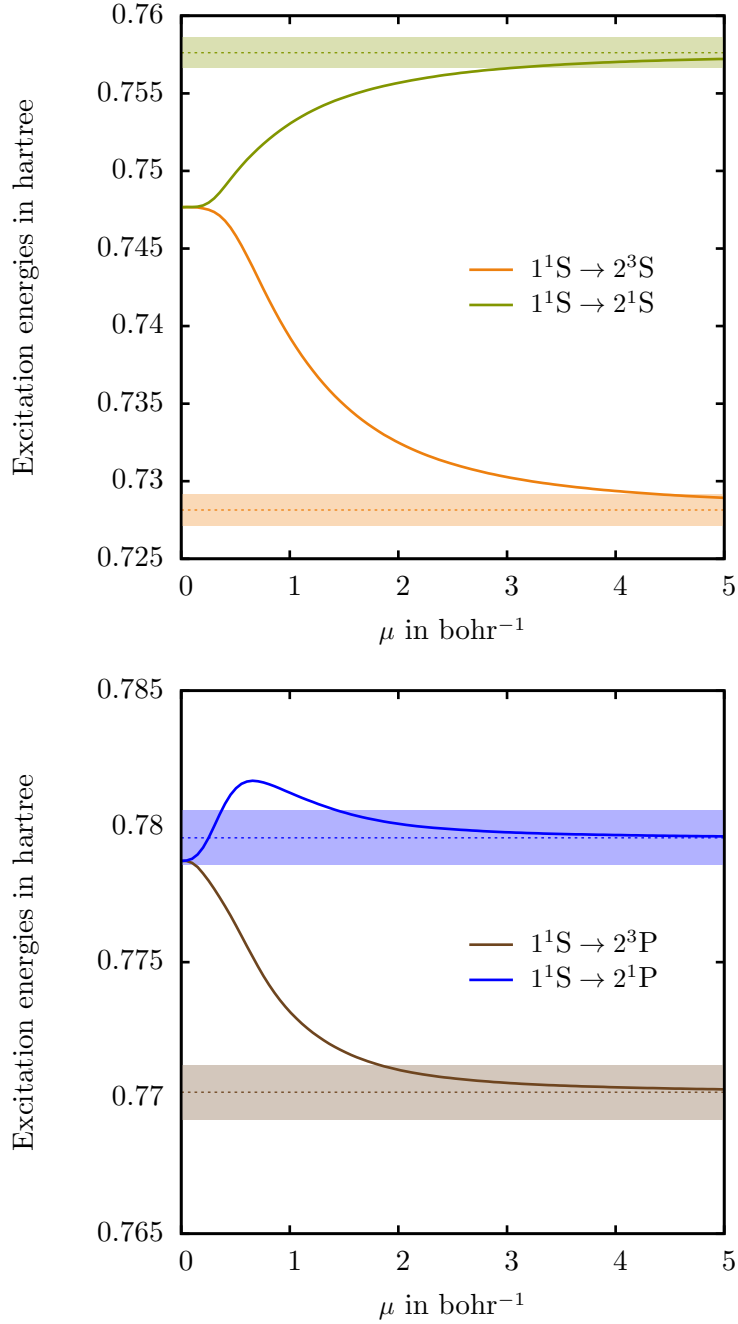


Figure 2.2 – First S (top) and P (bottom) excitation energies $\Delta\mathcal{E}_k^\mu = \mathcal{E}_k^\mu - \mathcal{E}_0^\mu$ (in hartree) of the He atom as a function of μ (in bohr⁻¹). The excitation energies of the physical system $\Delta E_k = \Delta\mathcal{E}_k^{\mu \rightarrow \infty}$ are plotted as horizontal dotted lines. An error of ± 1 mHartree is colored around each exact limit.

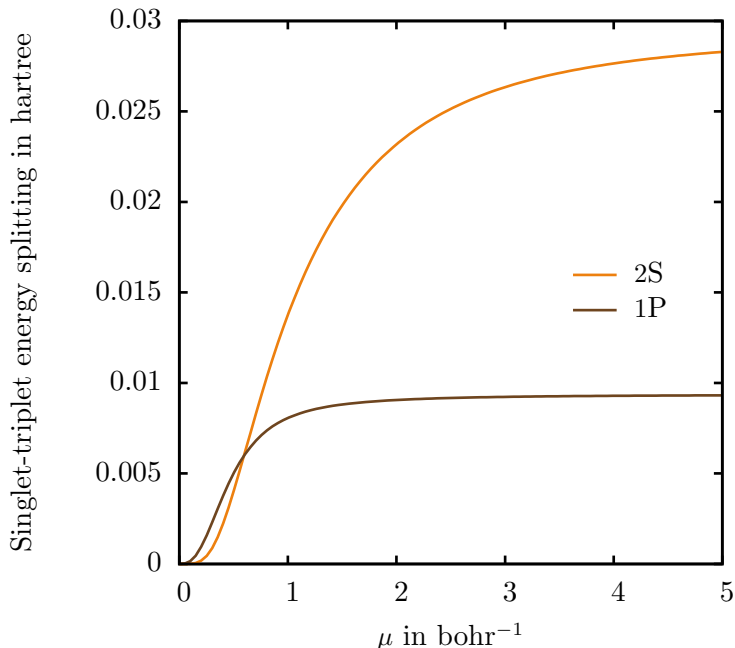


Figure 2.3 – Singlet-triplet energy splittings (in hartree) for the He atom as a function of μ (in bohr⁻¹).

Excitation energies

The lowest singlet and triplet excitation energies are plotted in Figure 2.2. The KS singlet and triplet excitation energies are degenerate and, as already observed for a few atomic systems in Refs. [117–119], are bracketed by the singlet and triplet excitation energies of the physical system. As μ increases from $\mu = 0$, the excitation energies vary as μ^3 since the linear term in Equation (2.27) cancels out for energy differences. The singlet-triplet degeneracy is lifted and the excitation energies converge to the exact singlet and triplet excitation energies when $\mu \rightarrow \infty$. Whereas a monotonic variation of the excitation energy with μ can be observed for the singlet and triplet $1S \rightarrow 2S$ excitations and for the triplet $1^1S \rightarrow 1^3P$ excitation, a non-monotonic variation is observed for the singlet $1^1S \rightarrow 1^1P$ excitation. This behaviour could be an artefact of the basis-set expansions (either orbital or potential), noting that a similar behaviour was observed for other excitations in a smaller basis set and was removed by enlarging the basis set. In line with previous observations in Refs. [117, 119] for the KS system, the excitation energies for Rydberg-type states along the adiabatic connection are rather good approximations to the excitation energies of the physical system (the maximal error is about 0.02 hartree at $\mu = 0$ for the triplet $1^1S \rightarrow 2^3S$ excitation), becoming better and better for high-lying states as they must eventually converge to the exact ionization energy.

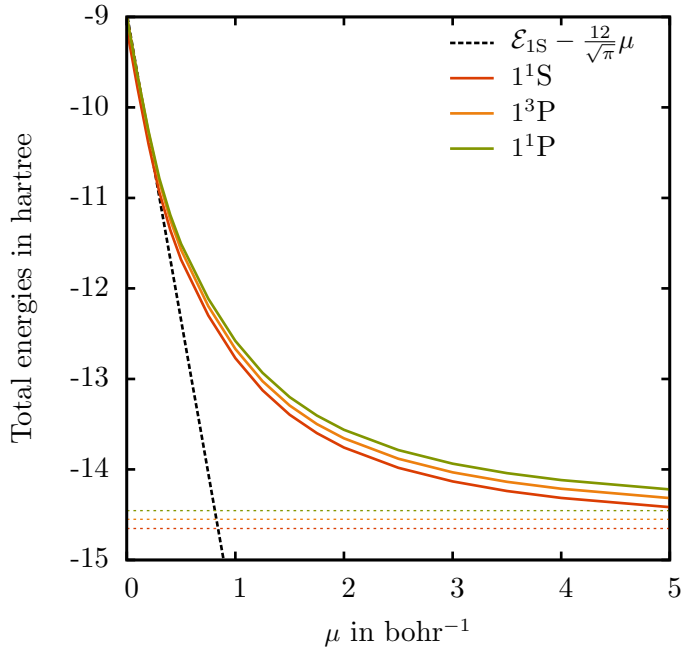


Figure 2.4 – Ground- and excited-state total energies \mathcal{E}_k^μ (in hartree) of the Be atom as a function of μ (in bohr $^{-1}$). The total energies of the physical system $E_k = \mathcal{E}_k^{\mu \rightarrow \infty}$ are plotted as horizontal dotted lines. The slope at $\mu = 0$ is shown in dashed line.

Singlet-triplet splitting

The singlet-triplet energy splittings for the 2S and 1P states are plotted in Figure 2.3. The expansion at small μ of Equation (2.28) predicts the singlet-triplet splitting to increase as μ^3 for the 1P state since it corresponds to the $1s \rightarrow 2p$ excitation in the KS system, so that $\Delta\ell = 1$. By contrast, the singlet-triplet splitting should increase at most as μ^5 for the 2S state since it corresponds to the $1s \rightarrow 2s$ excitation in the KS system, so that $\Delta\ell = 0$. This difference is clearly visible in Figure 2.3, where the 2S curve for the singlet-triplet splitting initially increases more slowly than the 1P curve.

2.5.2 Range-separated adiabatic connection for the valence excitation of the Beryllium atom

Total energies

The total energies of the ground state 1^1S and of the valence singlet and triplet 1P excited states of the Be atom are plotted in Figure 2.4. The KS total energies are approximately 6 hartree above the physical energies. At small μ , an initial slope of $-12/\sqrt{\pi}$ is observed for all states, in accordance with Equation (2.27) with $N = 4$. However, convergence to the physical energies with increasing μ is much slower than for the He atom, owing to the short inter-electronic distances in the Be $1s$ core region, which are consequently probed at larger μ values.

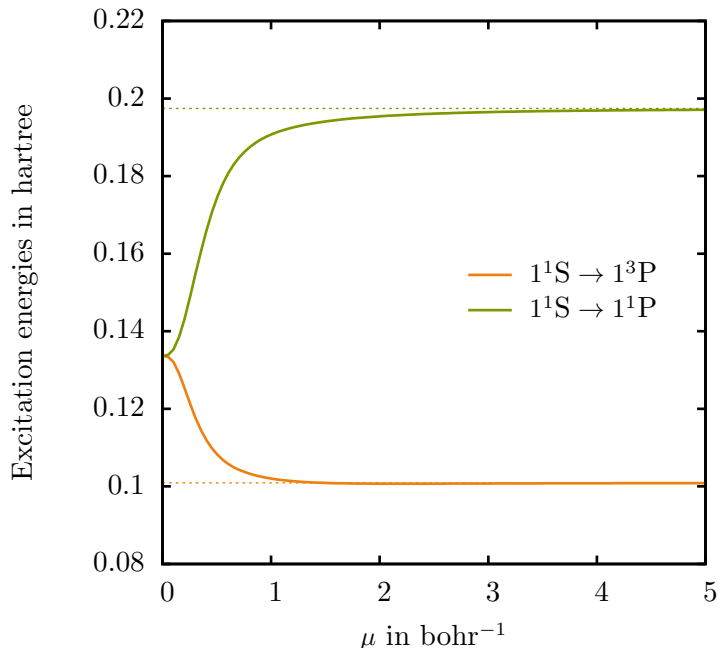


Figure 2.5 – Excitation energies $\Delta\mathcal{E}_k^\mu = \mathcal{E}_k^\mu - \mathcal{E}_0^\mu$ (in hartree) of the Be atom as a function of μ (in bohr⁻¹). The excitation energies of the physical system $\Delta E_k = \Delta\mathcal{E}_k^{\mu \rightarrow \infty}$ are plotted as horizontal dotted lines.

Excitation energies

The singlet and triplet excitation energies are plotted in Figure 2.5. As for He, the KS excitation energies are bracketed by the singlet and triplet excitation energies of the physical system. Not surprisingly, the KS excitation energies are poorer approximations to the exact excitation energies for these valence excitations in Be than for the Rydberg excitations in He. As μ increases, the KS excitation energies rapidly converge to the physical excitation energies. Clearly, the slow convergence of the core energies does not affect the convergence of the valence excitation energies.

Close to the KS system, at $\mu = 0$, the excitation energies are quite sensitive to the introduction of a small portion of electron-electron interaction in the Hamiltonian, which may be interpreted as a sign of static correlation. For $\mu \approx 0.4 - 0.5$, a typical μ value in range-separated DFT calculations [48, 51], the calculated excitation energies are significantly better approximations to the exact excitation energies than are the KS excitation energies. This observation justifies range-separated multi-determinantal linear-response DFT calculations, which take these excitation energies as a starting point.

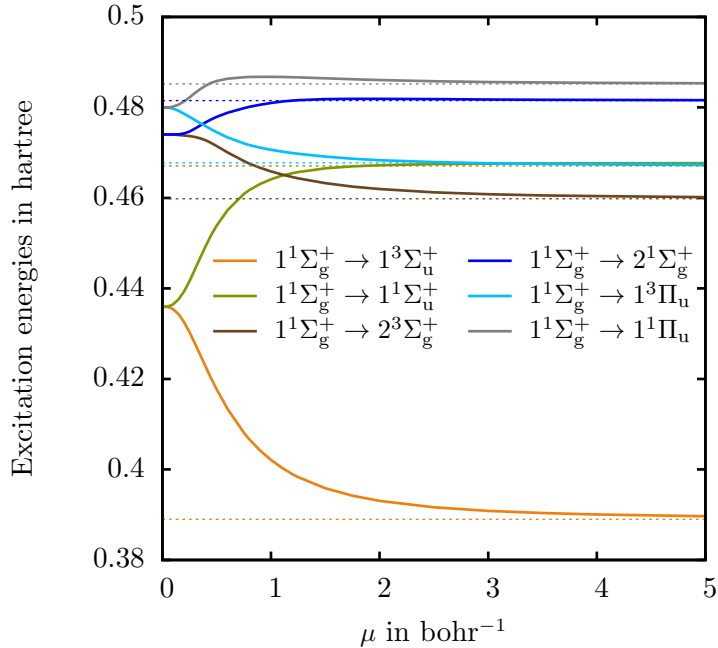


Figure 2.6 – Excitation energies $\Delta \mathcal{E}_k^\mu = \mathcal{E}_k^\mu - \mathcal{E}_0^\mu$ (in hartree) of the H₂ molecule at the equilibrium internuclear distance as a function of μ (in bohr⁻¹). The excitation energies of the physical system $\Delta E_k = \Delta \mathcal{E}_k^{\mu \rightarrow \infty}$ are plotted as horizontal dotted lines.

2.5.3 Range-separated adiabatic connection for the dihydrogen molecule along the dissociation

Equilibrium distance

The first few excitation energies of H₂ at the equilibrium bond distance are plotted against μ in Figure 2.6. As for the atoms, the valence excitation energies vary much more along the adiabatic connection than do the Rydberg-like excitation energies. Note also that the energetic ordering of the states changes along the adiabatic connection. With our choice of basis set, we also observe that the higher singlet excitation energies do not depend monotonically on μ , approaching the physical limits from above, as observed for He. Again, the excitation energies around $\mu \approx 0.4 - 0.5$ represent better approximations to the exact excitation energies than the KS excitation energies.

Stretched geometry

Finally, we consider the interesting case of the dissociation of the H₂ molecule. The first excitation energies at three times the equilibrium distance are shown in Figure 2.7. With increasing bond distance, the $1\sigma_g$ and $1\sigma_u$ molecular orbitals become degenerate. Consequently, the KS excitation energy for the single excitation $1\sigma_g \rightarrow 1\sigma_u$ goes to zero. Moreover, the KS excitation energy for the double excitation $(1\sigma_g)^2 \rightarrow (1\sigma_u)^2$ also goes to zero (albeit more slowly). This behaviour is in contrast to that of the physical system,

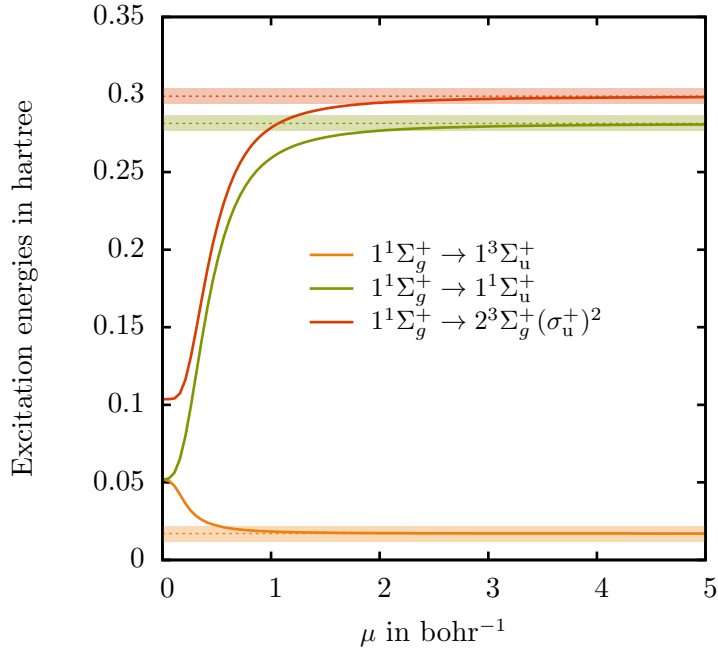


Figure 2.7 – Excitation energies $\Delta\mathcal{E}_k^\mu = \mathcal{E}_k^\mu - \mathcal{E}_0^\mu$ (in hartree) of the H_2 molecule at 3 times the equilibrium internuclear distance as a function of μ (in bohr⁻¹). The excitation energies of the physical system $\Delta E_k = \Delta\mathcal{E}_k^{\mu \rightarrow \infty}$ are plotted as horizontal dotted lines. An error of 5 mHartree is colored around these limits.

where only the excitation energy to the triplet $1^3\Sigma_u^+$ state goes to zero, whilst those to the singlet $1^1\Sigma_u^+$ state and the $2^1\Sigma_g^+$ state (the latter connected to the double excitation in the KS system) go to finite values.

Clearly, the excitation energies of KS theory are poor approximations to the exact excitation energies, making it difficult to recover from these poor starting values in practical linear-response TDDFT calculations. As μ increases from $\mu = 0$, the excitation energies to the singlet $1^1\Sigma_u^+$ and $2^1\Sigma_g^+$ states vary abruptly, rapidly approaching the physical values. This sensitivity to the inclusion of the electron-electron interaction is a clear signature of strong static correlation effects, emphasizing the importance of a multi-determinantal description in such situations. At $\mu \approx 0.4 - 0.5$, the $1^1\Sigma_u^+$ and $2^1\Sigma_g^+$ excitation energies, although still too low, are much better approximations than the KS excitation energies, constituting a strong motivation for range-separated multi-determinantal approaches in linear-response theory.

2.6 Conclusion

We have studied the variation of total energies and excitation energies along a range-separated adiabatic connection, linking the non-interacting KS system ($\mu = 0$) to the physical system ($\mu \rightarrow \infty$) by progressively switching on the long-range part of the

electron-electron interaction with the range-separation parameter μ , whilst keeping the ground-state density constant. This behaviour is of interest for the development and analysis of range-separated DFT schemes for the calculation of excitation energies, such as the linear-response range-separated schemes of Refs. [94, 95, 97].

Reference calculations were performed for the He and Be atoms and the H₂ molecule. Except when μ is large, the ground- and excited-state total energies along the adiabatic connection are poor approximations to the corresponding energies of the physical system. On the other hand, the excitation energies are good approximations to the excitation energies of the physical system for most of the adiabatic connection curve, except close to the KS system ($\mu = 0$). In particular, the excitation energies obtained at $\mu \approx 0.4 - 0.5$, typically used in range-separated DFT calculations, are significantly better approximations to the exact excitation energies than are the KS excitation energies. This behaviour appears to be particularly evident for situations involving strong static correlation effects and double excitations, as observed for the dissociating H₂ molecule.

These observations suggest that the excitation energies of the long-range interacting Hamiltonian in range-separated DFT may be useful as first estimates of the excitation energies of the physical system. However, if one cannot afford to use large μ values ($\mu > 2 - 3$), these excitation energies should be considered only as starting approximations, suitable for correction by, for example, linear-response range-separated theory.

In future work, we will utilize the present reference data to assess the approximations made in practical linear-response range-separated schemes, where the long-range contribution is treated, for example, at the Hartree-Fock, MCSCF or SOPPA levels of theory, while the short-range part is described by semi-local density-functional approximations. We will also use the results of this work to guide the development of time-independent range-separated DFT methods for the calculation of excitation energies as alternatives to linear-response schemes—in particular, for methods based on perturbation theories [112, 118] (see Chapter 3) or extrapolations [120, 121] along the adiabatic connection (see Chapter 4).

Chapter 3

Perturbation theory along the range-separated adiabatic connection

In this chapter, the effect of a first-order perturbative correction is assessed along the range-separated adiabatic connection. Starting from the energies of the partially interacting Hamiltonian defined in the previous chapter, a first-order correction is defined with two variants of perturbation theory: the “usual” perturbation theory, and an extension of the Görling-Levy one which has the advantage of keeping the ground-state density constant at each order of perturbation. Only the first, simpler, variant is tested on the systems defined in the previous chapter. The first-order correction within this perturbation theory improves significantly the total state energies of the different systems. However, the excitation energies are mostly deteriorated with respect to the zeroth-order ones which may be explained by the fact that the ionization energy is not correct anymore. The second variant of the perturbation theory should improve these results but has not been tested yet along the range-separated adiabatic connection.

3.1 Introduction

In density-functional theory (DFT) of quantum electronic systems, the most widely used approach for calculating excitation energies is nowadays linear-response time-dependent density-functional theory (TDDFT) (see, e.g., Refs. [122, 123]). However, in spite of many great successes, when applied with usual adiabatic semilocal approximations, linear-response TDDFT has serious limitations for describing systems with static (or strong) correlation [99], double or multiple excitations [100], and Rydberg and charge-transfer excitations [101, 102]. Besides, the Hohenberg-Kohn theorem [19] states that the time-independent ground-state density contains all the information on the system

so that time dependence is in principle not required to describe excited states. Several time-independent DFT approaches for calculating excitation energies exist and are still being developed.

A first strategy consists in simultaneously optimizing an ensemble of states. This ensemble DFT was pioneered by Theophilou [124] and Gross, Oliveira and Kohn [125] and is still a subject of current research [126–129], but it is hampered by the absence of appropriate approximate ensemble functionals. A second strategy consists in self-consistently optimizing a single excited state. This approach was started by Gunnarsson and Lundqvist [130] who extended ground-state DFT to the lowest-energy state in each symmetry class, and developed into the pragmatic (multiplet-sum) Δ SCF method [131, 132] (still in use today [133]) and related methods [134–136]. Great efforts have been made by Nagy, Görling, Levy, Ayers and others to formulate a rigorous self-consistent DFT theory of an arbitrary individual excited state [137–149] but one major difficulty is the need for development of approximate functionals for a specific excited state (see Ref. [150] for a proposal of such excited-state functionals). A third strategy, first proposed by Grimme, consists in using configuration-interaction (CI) schemes in which modified Hamiltonian matrix elements include information from DFT [151–154].

A fourth possible approach, proposed by Görling [155], is to calculate the excitation energies from Görling-Levy (GL) perturbation theory [156, 157] along the standard adiabatic connection using the non-interacting Kohn-Sham (KS) Hamiltonian as the zeroth-order Hamiltonian. In this approach, the zeroth-order approximation to the exact excitation energies is provided by KS orbital energy differences (which, for accurate KS potentials, is known to be already a fairly good approximation [119]). It can then be improved by perturbation theory at a given order in the coupling constant of the adiabatic connection. Filippi, Umrigar, and Gonze [118] showed that the GL first-order corrections provide a factor of two improvement to the KS zeroth-order excitation energies for the He, Li⁺, and Be atoms when using accurate KS potentials. For (near) degenerate states, Zhang and Burke [111] proposed to use degenerate second-order GL perturbation theory and showed that it works well on a simple one-dimensional model. This approach is conceptually simple as it uses the standard adiabatic connection along which the ground-state density is kept constant (in contrast to approaches introducing generalized adiabatic connections keeping an excited-state density constant [137, 138, 140, 145]). In spite of promising early results, this approach has not been further explored, maybe because it can be considered an approximation to TDDFT [158].

In this work, we explore further this density-functional perturbation theory approach for calculating excitation energies. We introduce one key modification in comparison to the earlier work of Refs. [118, 155]: As a zeroth-order Hamiltonian, instead of using the non-interacting KS Hamiltonian, we use a *partially interacting Hamiltonian* incorporating the *long-range* part of the Coulomb electron-electron interaction, and corresponding to an intermediate point along a range-separated adiabatic connection [39, 45, 52–54]. The partially interacting zeroth-order Hamiltonian is of course closer to the exact Hamil-

tonian than the non-interacting KS Hamiltonian is, and therefore less demand is put on perturbation theory. In particular, the zeroth-order Hamiltonian can already incorporate some static correlation. The downside of this is that a many-body method such as CI is required for finding the eigenstates and eigenvalues of the zeroth-order Hamiltonian. However, if the partial electron-electron interaction is only a relatively weak long-range interaction, one expects a faster convergence of the eigenstates and eigenvalues with respect to the one- and many-electron CI expansion than for the full Coulomb interaction [45], so that a small CI or multi-configuration self-consistent field (MCSCF) calculation would be sufficiently accurate. When using a semi-local density-functional approximation for the effective potential of the range-separated adiabatic connection, the presence of an explicit long-range electron-electron interaction in the zeroth-order Hamiltonian also has the advantage of avoiding the collapse of the high-lying Rydberg excitation energies. In contrast to adiabatic TDDFT, double or multiple excitations can be described with this density-functional perturbation theory approach, although this possibility was not explored in Refs. [118, 155]. Finally, approximate excited-state wave functions are obtained in this approach, which is useful for interpretative analysis and for the calculation of properties.

We envisage using this density-functional perturbation theory to calculate excited states after a range-separated ground-state calculation combining long-range CI [40, 41] or long-range MCSCF [48, 62] with a short-range density functional. This would be a simpler alternative to linear-response range-separated MCSCF [94, 97] for calculations of excitation energies. In this work, we study in details the two variants of range-separated density-functional perturbation theory and test the first, simpler variant on the He and Be atoms and on the H₂ molecule using accurate calculations along a range-separated adiabatic connection, without introducing density-functional approximations as done in Chapter 2.

The range-separated extension of both variants of the perturbation theory is presented in Section 3.2. In particular, Taylor expansions of the energies are given around the Kohn-Sham and the real systems for the first variant. Except for the finite basis approximation, no other approximation is introduced. The calculation are performed in the same manner than for the zeroth order and the results obtained for the helium and beryllium atoms, and for the dihydrogen molecule are discussed in Section 3.3.

3.2 Excited states from perturbation theory

In standard KS theory, the single-determinant eigenstates and associated energies of the non-interacting KS Hamiltonian,

$$\hat{H}^{\text{KS}}|\Phi_k^{\text{KS}}\rangle = \mathcal{E}_k^{\text{KS}}|\Phi_k^{\text{KS}}\rangle, \quad (3.1)$$

where $\hat{H}^{\text{KS}} = \hat{T} + \hat{V}_{\text{ne}} + \hat{V}_{\text{Hxc}}$, give a first approximation to the eigenstates and associated energies of the physical Hamiltonian. Two variants of perturbation theory using the KS Hamiltonian as zeroth-order Hamiltonian were proposed to calculate excitation energies [118, 155]. We provide below the extension of these two variants of perturbation theory to range-separated DFT. In this case, as a first approximation, it is natural to use the excited-state wave functions and energies of the long-range interacting Hamiltonian

$$\hat{H}^{\text{lr},\mu} |\Psi_k^\mu\rangle = \mathcal{E}_k^\mu |\Psi_k^\mu\rangle, \quad (3.2)$$

where $\hat{H}^{\text{lr},\mu} = \hat{T} + \hat{V}_{\text{ne}} + \hat{V}_{\text{Hxc}}^{\text{sr},\mu} + \hat{W}_{\text{ee}}^{\text{lr},\mu}$ is the same Hamiltonian as in Equation (2.5), i.e. where the short-range Hartree-exchange-correlation potential $\hat{V}_{\text{Hxc}}^{\text{sr},\mu} = \int \bar{v}_{\text{Hxc}}^{\text{sr},\mu}[n_0] \hat{n}(\mathbf{r}) d\mathbf{r}$, is evaluated at the ground-state density n_0 . These excited-state wave functions and energies can then be improved by defining perturbation theories in which the Hamiltonian $\hat{H}^{\text{lr},\mu}$ is used as zeroth-order Hamiltonian.

3.2.1 First variant of perturbation theory

The simplest way of defining such a perturbation theory is to introduce the following Hamiltonian depending on a coupling constant λ

$$\hat{H}^{\mu,\lambda} = \hat{H}^{\text{lr},\mu} + \lambda \hat{W}^{\text{sr},\mu}, \quad (3.3)$$

where the short-range perturbation operator $\hat{W}^{\text{sr},\mu}$ is

$$\hat{W}^{\text{sr},\mu} = \hat{W}_{\text{ee}}^{\text{sr},\mu} - \hat{V}_{\text{Hxc}}^{\text{sr},\mu}, \quad (3.4)$$

with the short-range electron-electron interaction $\hat{W}_{\text{ee}}^{\text{sr},\mu} = (1/2) \iint w_{\text{ee}}^{\text{sr},\mu}(r_{12}) \hat{n}_2(\mathbf{r}_1, \mathbf{r}_2) d\mathbf{r}_1 d\mathbf{r}_2$ defined with the complementary error-function interaction $w_{\text{ee}}^{\text{sr},\mu}(r) = \text{erfc}(\mu r)/r$. When varying λ , Equation (3.3) defines an adiabatic connection linking the long-range interacting Hamiltonian at $\lambda = 0$, $\hat{H}^{\mu,\lambda=0} = \hat{H}^{\text{lr},\mu}$, to the physical Hamiltonian at $\lambda = 1$, $\hat{H}^{\mu,\lambda=1} = \hat{H}$, for all μ , but the ground-state density is *not* kept constant along this adiabatic connection.

The exact eigenstates and associated eigenvalues of the physical Hamiltonian can then be found by standard Rayleigh-Schrödinger perturbation theory, i.e. Taylor expanding in λ the eigenstates and eigenvalues of the Hamiltonian $\hat{H}^{\mu,\lambda}$ and setting $\lambda = 1$

$$|\Psi_k\rangle = |\Psi_k^\mu\rangle + \sum_{n=1}^{\infty} |\Psi_k^{\mu,(n)}\rangle, \quad (3.5a)$$

$$E_k = \mathcal{E}_k^\mu + \sum_{n=1}^{\infty} E_k^{\mu,(n)}, \quad (3.5b)$$

in which $\Psi_k^\mu \equiv \Psi_k^{\mu,(0)}$ and $\mathcal{E}_k^\mu \equiv E_k^{\mu,(0)}$ act as zeroth-order eigenstates and energies. Using

orthonormalized zeroth-order eigenstates $\langle \Psi_k^\mu | \Psi_l^\mu \rangle = \delta_{kl}$ and assuming non-degenerate zeroth-order eigenstates, the first-order energy correction for the state k is

$$E_k^{\mu,(1)} = \langle \Psi_k^\mu | \hat{W}^{\text{sr},\mu} | \Psi_k^\mu \rangle, \quad (3.6)$$

so that, as usual, the zeroth+first-order energy is simply given by the expectation value of the physical Hamiltonian over the zeroth-order eigenstate

$$E_k^{\mu,(0+1)} = \mathcal{E}_k^\mu + E_k^{\mu,(1)} = \langle \Psi_k^\mu | \hat{H} | \Psi_k^\mu \rangle. \quad (3.7)$$

This last expression can be seen as a multi-determinantal extension of the exact-exchange KS energy expression for the state k , which was already proposed and studied for the ground state [57, 63, 159]. The second-order energy correction is

$$E_k^{\mu,(2)} = - \sum_{l \neq k} \frac{|\langle \Psi_l^\mu | \hat{W}^{\text{sr},\mu} | \Psi_k^\mu \rangle|^2}{\mathcal{E}_l^\mu - \mathcal{E}_k^\mu}, \quad (3.8)$$

and the first-order wave-function correction is (using intermediate normalization so that $\langle \Psi_k^\mu | \Psi_k^{\mu,(n)} \rangle = 0$ for all $n \geq 1$)

$$|\Psi_k^{\mu,(1)}\rangle = - \sum_{l \neq k} \frac{\langle \Psi_l^\mu | \hat{W}^{\text{sr},\mu} | \Psi_k^\mu \rangle}{\mathcal{E}_l^\mu - \mathcal{E}_k^\mu} |\Psi_l^\mu\rangle. \quad (3.9)$$

For $\mu = 0$, this perturbation theory reduces to the first variant of the KS perturbation theory studied by Filippi *et al.* [Equation (5) of Ref. [118]].

Taylor expansion of the energies around the KS system

The total energies up to the first order of the perturbation theory are given by the expectation value of the full Hamiltonian over the zeroth order wave functions in Equation (3.6). Using the Taylor expansion of the wave function $\Psi_k^\mu = \Phi_k^{\text{KS}} + \mu^3 \Psi_k^{(3)} + \mathcal{O}(\mu^5)$ around the KS wave function (cf. Equation (2.26)), it implies that the zeroth+first-order energies are thus given by

$$E_k^{\mu,(0+1)} = \langle \Phi_k^{\text{KS}} | \hat{H} | \Phi_k^{\text{KS}} \rangle + 2\mu^3 \langle \Phi_k^{\text{KS}} | \hat{H} | \Psi_k^{(3)} \rangle + \mathcal{O}(\mu^5), \quad (3.10)$$

where $\Psi_k^{(3)}$ is the contribution entering at the third power of μ in the zeroth-order wave function. With respect to the Taylor expansion of the zeroth-order energies given in Equation 2.27, no linear contribution in μ is present anymore and the energies are expanded around the corrected KS energies $\langle \Phi_k^{\text{KS}} | \hat{H} | \Phi_k^{\text{KS}} \rangle$ instead of the bare KS energies $\mathcal{E}_k = \langle \Phi_k^{\text{KS}} | \hat{H}^{\text{KS}} | \Phi_k^{\text{KS}} \rangle$.

Taylor expansion of the energies around the real system

From the Taylor expansion of the wave function $\Psi_k^\mu = \Psi_k + \mu^{-2}\Psi_k^{(-2)} + \mathcal{O}(\mu^{-3})$, which is valid almost everywhere (the coalescence needs to be treated carefully) given in Section 2.3.2, the first correction to the zeroth+first-order energies enter at the fourth power of μ

$$E_k^{\mu,(0+1)} = E_k + \frac{1}{\mu^4}E_k^{(0+1,-4)} + \mathcal{O}\left(\frac{1}{\mu^6}\right), \quad (3.11)$$

where $E_k^{(0+1,-4)}$ is the correction entering at the fourth power of $1/\mu$.

3.2.2 Second variant of perturbation theory

A second possibility is to define a perturbation theory based on a lightly more complicated adiabatic connection between the long-range interacting Hamiltonian and the physical Hamiltonian which keeps the ground-state density constant. This adiabatic connection is explained in Appendix D. The end result is that the Hamiltonian of Equation (3.3) is replaced by the following Hamiltonian

$$\hat{H}^{\mu,\lambda} = \hat{H}^{\text{lr},\mu} + \lambda\hat{W}^{\text{sr},\mu} - \hat{V}_{\text{c,md}}^{\text{sr},\mu,\lambda}, \quad (3.12)$$

where the operator $\hat{W}^{\text{sr},\mu}$ is now defined as

$$\hat{W}^{\text{sr},\mu} = \hat{W}_{\text{ee}}^{\text{sr},\mu} - \hat{V}_{\text{Hx,md}}^{\text{sr},\mu}, \quad (3.13)$$

with a short-range “multi-determinantal (md) Hartree-exchange” potential operator

$$\hat{V}_{\text{Hx,md}}^{\text{sr},\mu} = \int \frac{\delta E_{\text{Hx,md}}^{\text{sr},\mu}[n_0]}{\delta n(\mathbf{r})} \hat{n}(\mathbf{r}) d\mathbf{r}, \quad (3.14)$$

and an additional short-range “multi-determinantal correlation” potential operator

$$\hat{V}_{\text{c,md}}^{\text{sr},\mu,\lambda} = \int \frac{\delta E_{\text{c,md}}^{\text{sr},\mu,\lambda}[n_0]}{\delta n(\mathbf{r})} \hat{n}(\mathbf{r}) d\mathbf{r}, \quad (3.15)$$

which depends *non linearly* on λ in such a way so that the ground-state density n_0 is kept constant for all μ and λ . The density functionals $E_{\text{Hx,md}}^{\text{sr},\mu}[n]$ and $E_{\text{c,md}}^{\text{sr},\mu,\lambda}[n]$ are defined in Appendix D. One can show that, for non-degenerate ground-state wave functions Ψ_0^μ , the expansion of $\hat{V}_{\text{c,md}}^{\text{sr},\mu,\lambda}$ in λ for $\lambda \rightarrow 0$ starts at second order:

$$\hat{V}_{\text{c,md}}^{\text{sr},\mu,\lambda} = \lambda^2 \hat{V}_{\text{c,md}}^{\text{sr},\mu,(2)} + \dots. \quad (3.16)$$

Hence, the Hamiltonian of Equation (3.12) appropriately reduces to the long-range interacting Hamiltonian at $\lambda = 0$, $\hat{H}^{\mu,\lambda=0} = \hat{H}^{\text{lr},\mu}$. At $\lambda = 1$, it correctly reduces to the physical Hamiltonian, $\hat{H}^{\mu,\lambda=1} = \hat{H}$. This is so because the short-range Hartree-exchange-

correlation potential in the Hamiltonian $\hat{H}^{\text{lr},\mu}$ can be decomposed as

$$\hat{V}_{\text{Hxc}}^{\text{sr},\mu} = \hat{V}_{\text{Hx,md}}^{\text{sr},\mu} + \hat{V}_{\text{c,md}}^{\text{sr},\mu}, \quad (3.17)$$

where $\hat{V}_{\text{c,md}}^{\text{sr},\mu} = \hat{V}_{\text{c,md}}^{\text{sr},\mu,\lambda=1}$, and is therefore cancelled out by the perturbation terms for $\lambda = 1$. Equation (3.17) corresponds to an alternative decomposition of the short-range Hartree-exchange-correlation energy into ‘‘Hartree-exchange’’ and ‘‘correlation’’ contributions based on the multideterminant wave function Ψ_0^μ instead of the single-determinant KS wave function Φ_0^{KS} [57, 63, 159], which is a more natural decomposition in range-separated DFT. Here this decomposition is especially relevant since it separates the perturbation into a ‘‘Hartree-exchange’’ contribution that is linear in λ and a ‘‘correlation’’ contribution containing all the higher-order terms in λ .

The first-order energy correction is still given by Equation (3.6) using the perturbation operator of Equation (3.13). The zeroth+first-order energy is now given by

$$E_k^{\mu,(0+1)} = \mathcal{E}_k^\mu + E_k^{\mu,(1)} = \langle \Psi_k^\mu | \hat{H} + \hat{V}_{\text{c,md}}^{\text{sr},\mu} | \Psi_k^\mu \rangle. \quad (3.18)$$

The second-order energy correction of Equation (3.8) is replaced by

$$E_k^{\mu,(2)} = - \sum_{l \neq k} \frac{|\langle \Psi_l^\mu | \hat{W}^{\text{sr},\mu} | \Psi_k^\mu \rangle|^2}{\mathcal{E}_l^\mu - \mathcal{E}_k^\mu} - \langle \Psi_k^\mu | \hat{V}_{\text{c,md}}^{\text{sr},\mu,(2)} | \Psi_k^\mu \rangle,$$

and the expression of the first-order wave function correction is still given by Equation (3.9) using the perturbation operator of Equation (3.13).

For $\mu = 0$, this perturbation theory reduces to the second variant of the KS perturbation theory proposed by Görling [155] and studied by Filippi *et al.* [Equation (6) of Ref. [118]], which is nothing else than the application of GL perturbation theory [156, 157] to excited states. In Ref. [118], it was found that the first-order energy corrections in this second variant of KS perturbation theory provided on average a factor of two improvement to the KS zeroth-order excitation energies for the He, Li⁺, and Be atoms when using accurate KS potentials, whereas the first-order energy corrections in the first variant of KS perturbation theory deteriorated on average the KS excitation energies. The good results obtained with the second variant of KS perturbation theory may be at least partly explained by one good feature of GL perturbation theory which is that the ionization potential remains exact at all order in λ . This feature applies as well in the range-separation case, so that the second variant of range-separated perturbation theory should in principle be preferred. However, it requires the separation of the short-range Hartree-exchange-correlation potential into the ‘‘multideterminantal Hartree-exchange’’ and ‘‘multideterminantal correlation’’ contributions (according to Equation (3.17)), which we have not done for accurate potentials or calculations along the double adiabatic connection with a partial interaction defined by $\hat{W}_{\text{ee}}^{\text{lr},\mu} + \lambda \hat{W}_{\text{ee}}^{\text{sr},\mu}$ (cf. Appendix D). We thus only use the first variant of range-separated perturbation theory

in this work. Note, however, that the second variant of range-separated perturbation theory could easily be applied with density-functional approximations, using for example the local-density approximation that has been constructed for the “multideterminantal correlation” functional [59].

3.3 Results and discussion

In what follows, all the calculations were performed with the quantum chemistry package DALTON [113] with the same basis sets and the same thresholds as in Section 2.4. Starting from the zeroth-order energies obtained in Chapter 2, the first variant of perturbation theory detailed in Section 3.2 is applied on the helium and beryllium atoms and on the dihydrogen molecule in its equilibrium and stretched geometries.

3.3.1 Range-separated adiabatic connection for the helium atom

Total energies

The zeroth+first-order ground- and excited-state total energies of the helium atom along the range-separated adiabatic connection are shown in Figure 3.1. In the Kohn-Sham limit, when $\mu = 0$, the total state energies are significantly improved with respect to the zeroth-order ones given in Figure 2.1. In fact, as shown for the ground-state energy, the zeroth-order total energies were off by approximately 1.2 hartree with respect to the energies of the physical system. When the first-order correction is added, the error becomes smaller than 0.06 hartree for all the states. Moreover, for the excited states, the singlet and triplet energies are not degenerated anymore. When the range-separation parameter is increased, a faster convergence toward the total state energies of the physical system is also observed for all states. The description of the total energies is therefore much better with the first-order correction. In fact, the linear correction in μ is no longer present in the Taylor expansion of the energies at small μ (cf. Equation (3.10)) and the first correction enters at the third power of μ . At large μ , the error with respect to the physical energies enters in $1/\mu^4$ instead of $1/\mu^2$ in the zeroth-order case which explains the observed faster convergence with respect to the zeroth-order curves.

Excitation energies

The excitation energies of the helium atom at zeroth and zeroth+first order are given in Figure 3.2. For the KS system, at $\mu = 0$, the singlet and triplet excitation energies are degenerate at zeroth order. The introduction of the first-order correction allows one to open the gap between the singlet and triplet energies. However, the singlet and triplet excitation energies at zeroth+first order now overestimate the physical excitation energies of the system by 0.1-0.2 hartree such that the error is actually larger than at zeroth order. For the $1^1S \rightarrow 1^3P$ excitation energy, one can even note that the correction

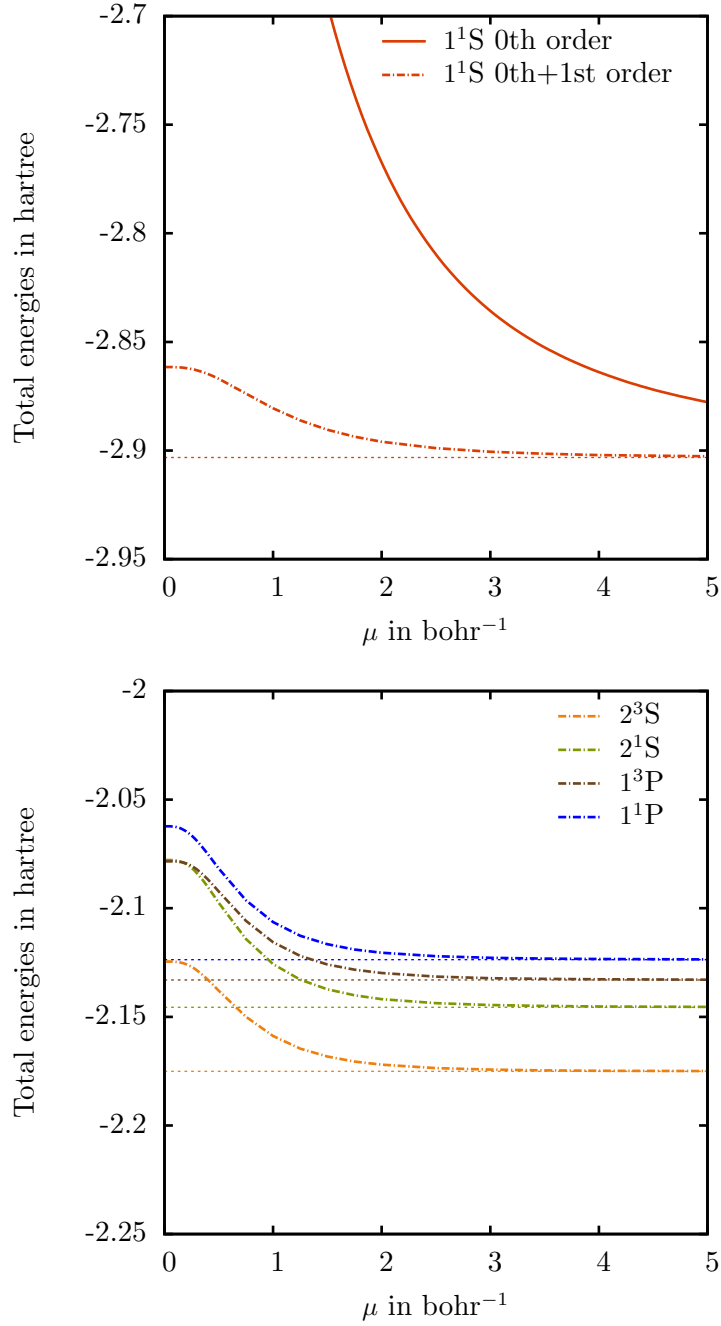


Figure 3.1 – Zeroth+first-order ground- (top) and excited-state (bottom) total energies $\mathcal{E}_k^{\mu,(0+1)}$ (in hartree) of the helium atom as a function of μ (in bohr⁻¹). The zeroth-order energy \mathcal{E}_0^μ is recalled for the ground state in plain line and the total energies of the physical system E_k are plotted as horizontal dotted lines.

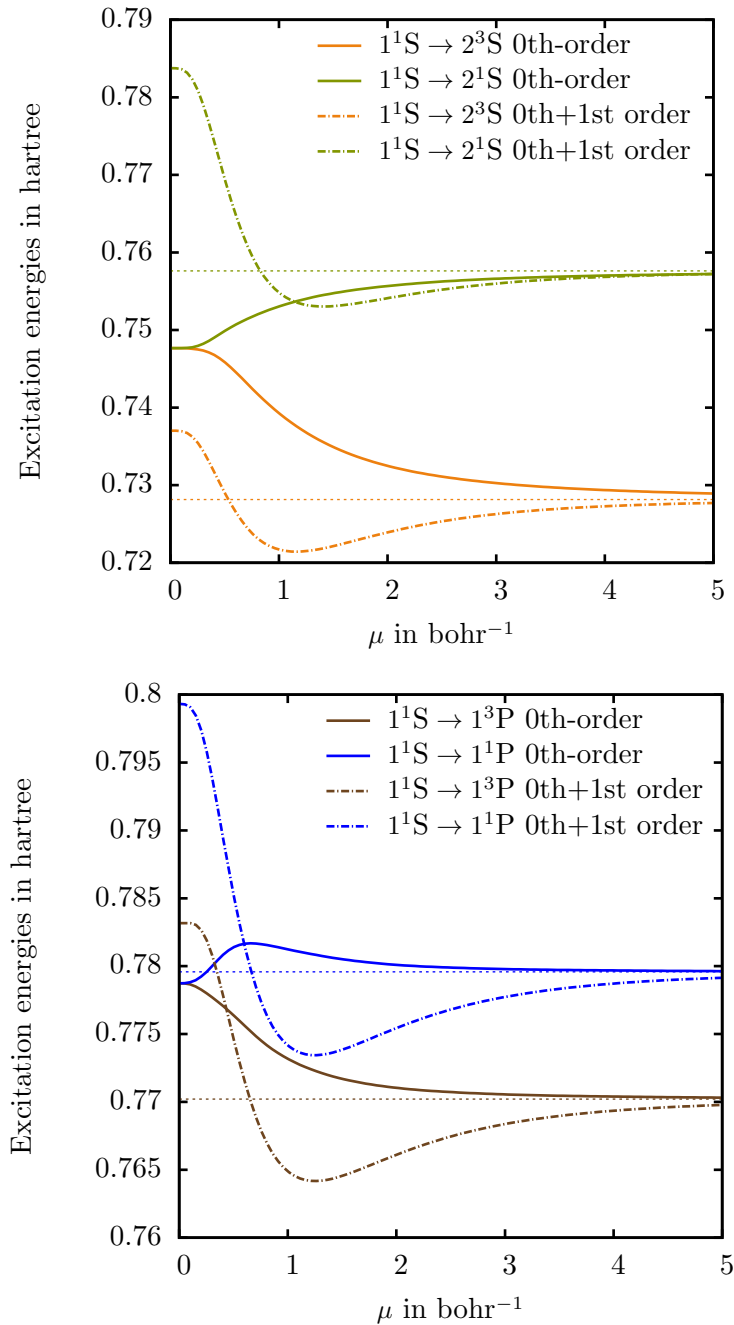


Figure 3.2 – Zeroth-order (plain line) excitation energies $\Delta\mathcal{E}_k^\mu$ and zeroth+first-order (dashed line) excitation energies $\Delta\mathcal{E}_k^{\mu,(0+1)}$ (in hartree) of the helium atom as a function of μ (in bohr⁻¹). The excitation energies of the physical system ΔE_k are plotted as horizontal dotted lines.

is going in the wrong direction. The singlet-triplet splitting is also too large by about a factor 1.5.

When the very long-range part of the Coulombic interaction is switched on, the initial overestimation is corrected. In fact, for small values of μ , all the excitation energies decrease in the third power of μ which is in agreement with Equation (3.10). Although, when $\mu \simeq 0.5-1$, this correction becomes too large and the excitation energies of the partially interacting system become lower than the energies of the physical system obtained when $\mu \rightarrow \infty$. If μ is further increased such that more and more interaction is included, the excitation energies begin to increase again and finally converge toward their exact limits from below. In the meanwhile, the zeroth-order excitation energies, which do not present this oscillation at small μ , converge monotonically toward their physical limit and are in average more accurate than the zeroth+first order excitation energies. Altogether, the first-order correction does not constitute an improvement for the excitation energies although the total energies were improved.

This failure of the first-order-correction to describe the excitation energies correctly should be connected to the fact that, as the ground-state density is not kept constant at each order of perturbation, the ionization potential is not constant anymore at the zeroth+first order along the adiabatic connection. This results in an unbalanced treatment between the ground state and the excited states. Moreover, the Rydberg excitation energies which are high in energy, are susceptible to be even more sensible to this effect and the higher they are, the more affected, as can be seen for the transitions to the P state. The second variant of perturbation theory should therefore improve this behavior as it keeps the density constant at each order as it was shown in the KS case [118, 157].

3.3.2 Range-separated adiabatic connection for the beryllium atom

The first-order perturbation correction is then applied to the ground state and valence excited states of the beryllium atom. The total energies are once again improved by the introduction of this perturbation but are not shown here. The valence excitation energies are shown in Figure 3.3 at the zeroth and the zeroth+first orders as a function of the range-separation parameter μ .

As valence excitations are concerned instead of Rydberg ones in the case of the helium atom, they are less sensitive to a bad description of the ionization energy. At $\mu = 0$, the singlet excitation energy is slightly improved by the introduction of the first-order correction. However, the triplet one is not described any better as instead of being overestimated at zeroth order, it is now underestimated by almost the same amount.

When the interaction is switched on, a bump is also observed for small values of μ for the singlet excitation energy but not the triplet excitation energy which goes monotonically to its physical limit. In this case the convergence of the energies with respect to μ is improved in comparison with the zeroth-order excitation energies, especially for the singlet one.

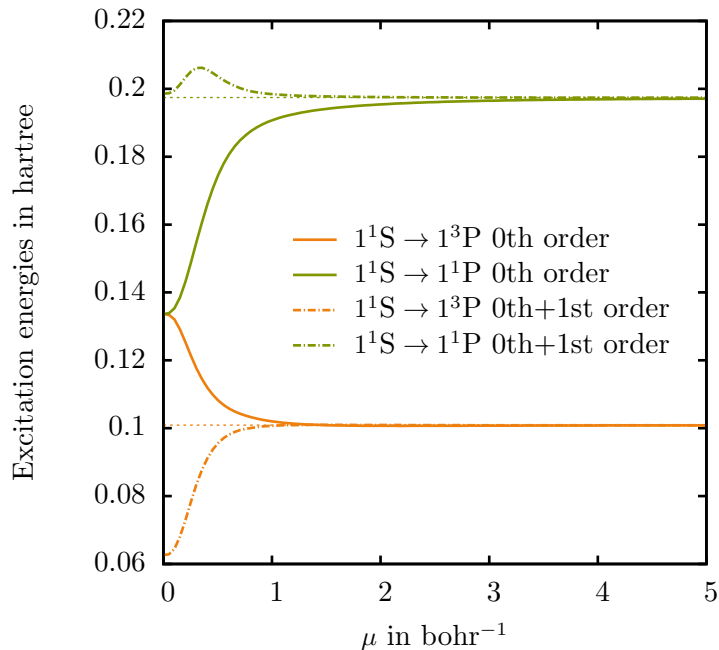


Figure 3.3 – Valence excitation energies of the beryllium atom (in hartree) at zeroth order $\Delta\mathcal{E}_k^\mu$ (plain line) and zeroth+first order $\Delta\mathcal{E}_k^{\mu,(0+1)}$ (dashed line), as a function of μ (in bohr⁻¹). The excitation energies of the physical system ΔE_k are plotted as horizontal dotted lines.

3.3.3 Range-separated adiabatic connection for the dihydrogen molecule

Finally, the first-order correction is applied to the excitation energies of the dihydrogen molecule at its equilibrium and a stretched geometry. The first excitation energies are shown in Figure 3.4 at the equilibrium distance R_{eq} (top) and in a stretched geometry at $3R_{\text{eq}}$ (bottom).

At the equilibrium geometry, the first-order correction works relatively well. It goes in the correct direction at $\mu = 0$, the triplet excitation energy is lowered while the singlet one is increased and the error is smaller than for the zeroth-order excitation energies for almost any value of μ . Unfortunately, when the bond is stretched, this is not the case anymore. At $3R_{\text{eq}}$, the first excitation energy $1^1\Sigma_g^+ \rightarrow 1^3\Sigma_u^+$ becomes negative for small values of μ and the error with respect to the physical excitation energy is higher than in the zeroth-order case. Moreover, the ordering of the two singlet excitation energies is incorrect at small μ and they present a strong oscillation when the interaction is switched on. Therefore, in this case, the zeroth-order excitation energies are in fact better approximations to the physical energies once again.

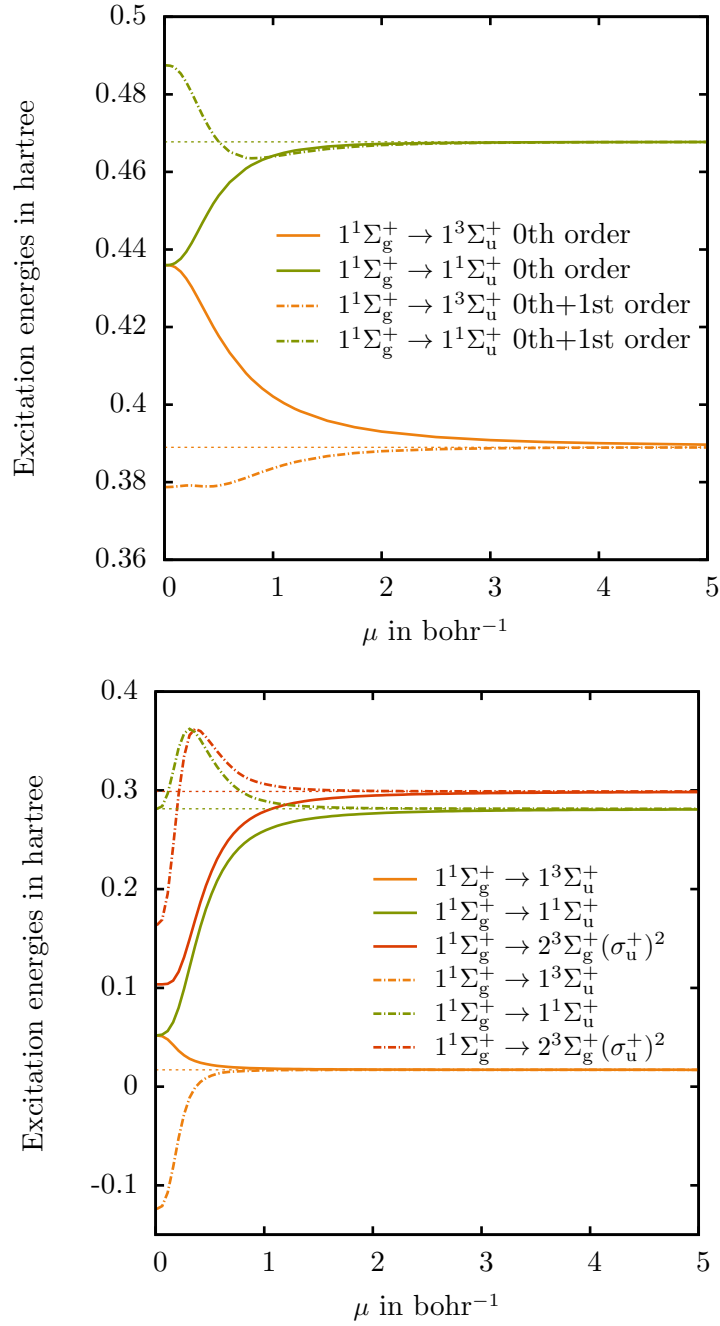


Figure 3.4 – Zeroth-order $\Delta\mathcal{E}_k^\mu$ (plain line) and zeroth+first-order $\Delta\mathcal{E}_k^{\mu,(0+1)}$ (dashed line) excitation energies of the dihydrogen molecule (in hartree) as a function of μ in bohr⁻¹ at the equilibrium distance (top) and three times the equilibrium distance (bottom). The excitation energies of the physical system ΔE_k are plotted as horizontal dotted lines.

3.4 Conclusion

In this chapter, we have developed two variants of a first-order perturbation theory along the range-separated adiabatic connection. The first, simpler, variant based on the usual Rayleigh-Schrödinger perturbation theory was tested on the helium and beryllium atoms and on the dihydrogen molecule at equilibrium and stretched geometries. It appears that although the total energies are improved with this first-order correction, this perturbation theory is not able to improve systematically the zeroth-order excitation energies as it does not keep the density constant along the adiabatic connection at each order of perturbation. In particular, it would be interesting to look at the evolution of the ionization potential in this case in order to understand better the effect of this variant of the perturbation theory on our systems of interest.

The second variant of the perturbation theory based on the Görling-Levy perturbation theory should in this sense improve significantly the results as by construction the ground-state density is kept constant at any order of the perturbation [157]. This perturbation theory was tested on the Kohn-Sham system and was proved to improve significantly the excitation energies [118]. However, its effects have not been explored along the range-separated adiabatic connection yet. It would be particularly interesting to test this variant on the different systems presented previously though we had not have time to explore this possibility yet.

An alternative to perturbation theory to improve the excitation energies along the adiabatic connection is provided by extrapolation schemes which make uses of the behavior of the energies around the physical system to estimate the exact energies from the energy of the partially interacting system at a given μ and its first-order derivative with respect to μ . This approach is explored in the next chapter.

Chapter 4

Energy extrapolation along the adiabatic connection

In this chapter, we propose an alternative method to improve the estimation of the energies of a physical system from the energies of a partially interacting one where only the long-range part of the Coulombic interaction is included. The energies of the partially interacting system have already been studied in Chapters 2 and 3 at zeroth- and zeroth+first-order of perturbation theory. From the analysis of their Taylor expansion around the physical system, the energies of the physical system can be further more extrapolated from the ones on the partially interacting system by using their first-order derivative with respect to the range-separation parameter μ . A similar scheme is also studied in the case of the linear adiabatic connection where it in fact becomes equivalent to the extension of first-order Görling-Levy perturbation theory on an intermediate point of this connection.

The extrapolation scheme is then applied on the zeroth-order range-separated energies of the helium and beryllium atoms and of the dihydrogen molecule at its equilibrium and stretched geometries. It improves significantly the convergence rate of the energies toward their exact limit with respect to the range-separation parameter and allows one to estimate the excitation energies of the physical system at the same accuracy with respect to the “bare” partially interacting excitation energies with a range-separation parameter divided by about a factor 2. When applied on the zeroth+first order excitation energies of the helium atom obtained along the range-separated adiabatic connection, the results remain disappointing as the quality of the starting point is inferior and the extrapolation correction is smaller than in the zeroth-order case. Finally, the extrapolation scheme was applied on the excitation energies of the helium atom along a linear adiabatic connection where the interaction is scaled by a factor λ going from 0 to 1. It works remarkably well in this case as both the starting energies are almost linear and therefore their behavior is easier to extrapolate.

4.1 Introduction

In order to calculate the excitation energies of a physical system in the time-independent DFT framework, a possible approach consists in starting from the KS orbital energy differences of the non-interacting system. In this case, Görling-Levy perturbation theory [118, 155–157] has been shown to successfully improve the description of the excitation energies as was mentioned in the previous chapter. Although, instead a starting from a non-interacting system, it is also possible to consider the excitation energies of a partially interacting system as the zeroth order of the perturbation theory. In this system, part of the interaction is already present so that its excitation energies are better approximations to the energies of the physical one. The adiabatic connection between the non-interacting and the physical system can be done linearly, where the interaction is scaled by a factor λ going from 0 to 1, or by including more and more of the long-range part of the Coulombic interaction with a range-separation parameter μ going from 0 to infinity. On both cases, the potential is adjusted in order to keep the ground-state density of the system constant.

The analysis of the Taylor expansions of the energies with respect to the range-separation parameter around the real system ($\mu \rightarrow \infty$) performed in Chapter 2, has shown that the energy of the partially interacting system were converging toward their physical limit in μ^{-2} . Using this information, it is possible to develop a scheme to extrapolate the energies of the physical system from the energies of the partially interacting one following the idea of Refs. [120, 121]. This extrapolation scheme involves the first-order derivative of the energies with respect to the range-separation parameter and constitutes an alternative to perturbation theory presented in Chapter 3 and to the linear-response time-dependent density-functional theory extended to the range-separation case which will be presented in the next part of this thesis.

Moreover, this extrapolation technique is not limited to the zeroth-order energies and could also be applied to the zeroth+first order energies resulting from a perturbation theory. From the Taylor expansions of the zeroth+first order energies studied in the first variant of perturbation theory in Chapter 3, an extrapolation scheme is thus proposed starting from these energies. Finally, a similar study is also performed on the linear adiabatic connection where the almost linear behavior of the excitation energies with respect to the scaling parameter λ is well-suited for such extrapolation techniques. The analysis of the excitation energies around $\lambda = 1$ provides then the required information and be exploited to improve the estimation of the energies of the physical system from an intermediate point of the connection.

The development of the extrapolation scheme is given in Section 4.2 both for the range-separated and the linear adiabatic connections. It is then applied to the range-separated energies obtained in the previous chapters on the helium and beryllium atoms and on the dihydrogen molecule at its equilibrium and stretched geometries, and on the helium atom along a linear adiabatic connection. The results are discussed in Section 4.3

starting either directly from the energies of the partially interacting system or from the energies where a perturbative first-order correction has already been applied.

4.2 Energy extrapolation

4.2.1 Range-separated adiabatic connection

Starting from the Hamiltonian of the partially interacting system $\hat{H}^{\text{lr},\mu} = \hat{T} + \hat{V}_{\text{ne}} + \hat{W}_{\text{ee}}^{\text{lr},\mu} + \hat{V}_{\text{Hxc}}^{\text{sr},\mu}$, where only the long-range interaction $\hat{W}_{\text{ee}}^{\text{lr},\mu}$ is included and where the short-range Hartree-exchange-correlation potential $\hat{V}_{\text{Hxc}}^{\text{sr},\mu}$ ensures that the ground-state density is kept constant along the adiabatic connection, the Taylor expansions of the partially interacting energies around the Kohn-Sham and the physical system were derived in Chapter 2. In particular, it was shown that they behave as

$$\mathcal{E}_k^\mu = E_k + \frac{1}{\mu^2} E_k^{(-2)} + \mathcal{O}\left(\frac{1}{\mu^3}\right), \quad (4.1)$$

around the physical system, where $E_k^{(-2)}$ is the correction entering at the second power of $1/\mu$. Following the scheme proposed in the recent articles [120, 121], it is possible to estimate the energy of the physical system E_k from the energy of the partially interacting system \mathcal{E}_k and its first-order derivative with respect to μ . From the Taylor expansion of the energies when $\mu \rightarrow \infty$, we know that the first-order derivative of the energies with respect to μ behave as

$$\frac{\partial \mathcal{E}_k^\mu}{\partial \mu} = -\frac{2}{\mu^3} E_k^{(-2)} + \mathcal{O}\left(\frac{1}{\mu^4}\right), \quad (4.2)$$

around the real system. Therefore, inserting this in Equation (2.39), the exact energy E_k can be written as a function of the energies along the adiabatic connection and of their first-order derivative as

$$E_k = \mathcal{E}_k^\mu + \frac{\mu}{2} \frac{\partial \mathcal{E}_k^\mu}{\partial \mu} + \mathcal{O}\left(\frac{1}{\mu^3}\right). \quad (4.3)$$

This therefore defines the extrapolated energies

$$E_k^{\text{EE},\mu} = \mathcal{E}_k^\mu + \frac{\mu}{2} \frac{\partial \mathcal{E}_k^\mu}{\partial \mu}, \quad (4.4)$$

which are correct up to the third power of $1/\mu$ with respect to the energies of the physical system. The correction given by the extrapolation scheme is null at $\mu = 0$ by construction, but should improve the description of the energies as soon as the interaction is switched on. More elaborated schemes could be developed by using higher-order derivatives or by using several points with different values of μ but in what follows only the simpler case is applied.

Similarly, for the zeroth+first order energies obtained in Chapter 3, using their Taylor

expansion around the physical system

$$E_k^{\mu,(0+1)} = E_k + \frac{1}{\mu^4} E_k^{(0+1,-4)} + \mathcal{O}\left(\frac{1}{\mu^6}\right), \quad (4.5)$$

given in Equation (3.11), it is possible to define an extrapolated energies at 0th+1st order. By differentiation of the energies with respect to μ ,

$$\frac{\partial E_k^{\mu,(0+1)}}{\partial \mu} = -\frac{4}{\mu^5} E_k^{(0+1,-4)} + \mathcal{O}\left(\frac{1}{\mu^7}\right), \quad (4.6)$$

the extrapolated zeroth+first-order energy is given as

$$E_k^{\text{EE},\mu,(0+1)} = E_k^{\mu,(0+1)} + \frac{\mu}{4} \frac{\partial E_k^{\mu,(0+1)}}{\partial \mu}, \quad (4.7)$$

which defines an extrapolation scheme for the first-order corrected energies. This extrapolated energy has a very similar form with respect to the zeroth-order one given in Equation (4.3) as only the prefactor of the correction changes from 1/2 to 1/4.

4.2.2 Linear adiabatic connection

If the more usual linear adiabatic connection is performed, then the partially interacting Hamiltonian is defined as $\hat{H}^\lambda = \hat{T} + \lambda \hat{W}_{\text{ee}} + \hat{V}^\lambda$ where \hat{V}^λ is adjusted to keep the ground-state density constant. This potential can be expressed in terms of the connecting parameter λ as

$$\hat{V}^\lambda = \hat{V}_{\text{ne}} + (1 - \lambda) \hat{V}_{\text{Hx}} + \hat{V}_{\text{c}} - \hat{V}_{\text{c}}^\lambda \quad (4.8)$$

where $\hat{V}_{\text{c}}^\lambda$ enters at second order in λ and is equal to \hat{V}_{c} at $\lambda = 1$. The energies of the partially interacting system can then be expanded around the physical system as

$$\mathcal{E}_k^\lambda = E_k + (1 - \lambda) E_k^{(1)} + \mathcal{O}((1 - \lambda)^2), \quad (4.9)$$

where $E_k^{(1)}$ is the contribution entering in the first power of $(1 - \lambda)$. Similarly to the range-separated case, by differentiation with respect to λ , it is then possible to extrapolate the energies of the physical system as

$$E_k^{\text{EE},\lambda} = \mathcal{E}_k^\lambda + (1 - \lambda) \frac{\partial \mathcal{E}_k^\lambda}{\partial \lambda}. \quad (4.10)$$

One should note that in this case, the extrapolation is equivalent to the first-order of the Görling-Levy perturbation theory [118, 157], i.e. the second variant of perturbation theory shown in Chapter 3.

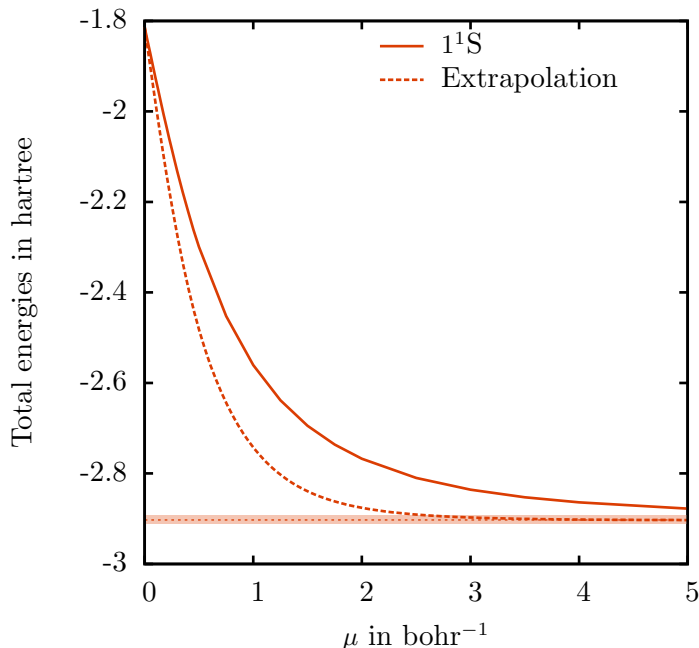


Figure 4.1 – Result of the extrapolation (dashed line) for the ground-state total energy of the helium atom (in hartree) as a function of μ (in bohr⁻¹). The “bare” energy is recalled in plain line, the energy of the physical system is given as an horizontal dotted line and an error of ± 10 millihartree around his limit is given by the colored region.

4.3 Results and discussion

The “bare” energies of the partially interacting systems are calculated with of the DALTON program [113] as detailed in Section 2.4 for the zeroth order and following the first variant of perturbation theory given in Chapter 3 for the zeroth+first order. The ground-state and excitation energies are then fitted following the procedure given in Appendix C. Starting from the analytical form of the fit, it is then straightforward to calculate the analytical derivative of the energies. The extrapolated energies are then calculated using Equations (4.3), (4.7) or (4.10) for the total and excitation energies of the helium and beryllium atoms and for the dihydrogen molecule at equilibrium and stretched geometries.

4.3.1 Range-separated extrapolation of the helium atom

Zeroth-order total energies

The result of the extrapolation scheme on the zeroth-order ground-state total energy of the helium atom is shown in Figure 4.1. By construction, the extrapolation correction has no effect at $\mu = 0$ so that the ground-state energy of the KS system is not affected by the extrapolation correction. However, for any non-zero value of μ , the extrapolated energy shows a systematic improvement with respect to the “bare” ground-state energy.

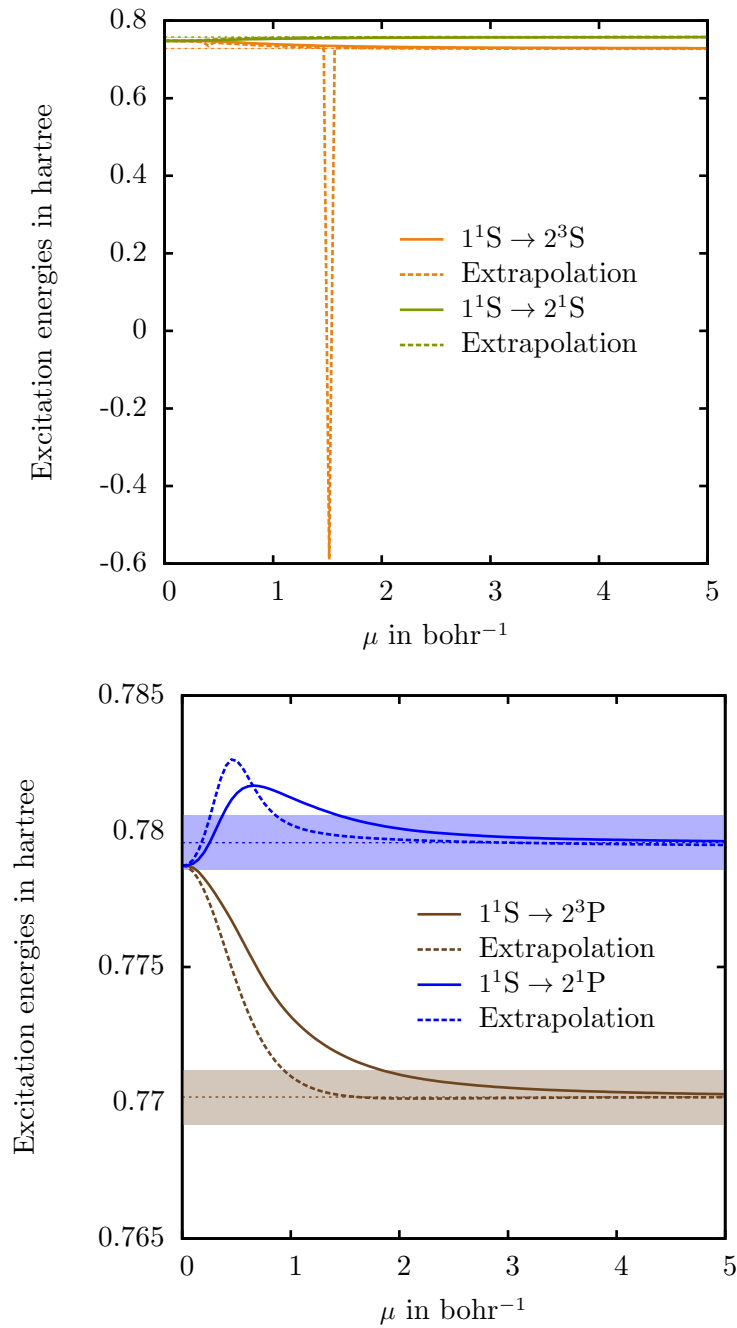


Figure 4.2 – Result of the extrapolation (dashed line) on the first S (top) and P (bottom) excitation energies (in hartree) of the helium atom as a function of μ (in bohr⁻¹). The “bare” excitation energies are recalled in plain line, the excitation energies of the physical system are given by horizontal dotted lines and an error of ± 1 millihartree is colored around each exact limit.

Without the extrapolation correction, a value of about 6 bohr⁻¹ was needed for the range-separation parameter in order to have an error smaller than 10 millihartree with respect to the energy of the physical system. When the extrapolation correction is added, a range-separation parameter greater than 2.8 bohr⁻¹ becomes sufficient to reproduce the same level of accuracy.

Moreover, the extrapolated energy is strictly decreasing with respect to the range-separation parameter μ and thus goes to its asymptotic limit from above. Due to this monotonic behavior, using the second-order derivative (or higher-order derivative) should in principle improve further more the results. Additionally, several points could be used to perform the extrapolation instead of one to increase the accuracy of the extrapolated energies.

Zeroth-order excitation energies

The extrapolation scheme is now applied on the first S and P excitation energies of the helium atom and the obtained extrapolated energies are shown in Figure 4.2. Both singlet and triplet S excitation energies have a monotonic behavior with respect to μ , the improvement due to the extrapolation correction is then systematic as the sign of the derivative pulls the excitation energies toward their physical limits. The triplet P excitation energy also has a monotonic behavior so the extrapolation also provides a systematic improvement. The 1¹S → 1¹P excitation energy, however, shows a non-monotonic behavior and presents a “bump” for small values of μ which is probably due to the size of the finite basis set as discussed earlier. As a consequence, this excitation energy goes to its physical limit from above and its first-order derivative changes sign at about 0.7 bohr⁻¹. In this region, the extrapolated energy becomes worse than the “bare” one. However, this only happens in a small region of the range-separation parameter and as soon as the excitation energy recovers a monotonic convergence towards its physical limit (i.e. for μ larger than 0.7 bohr⁻¹), the energy is improved by the extrapolation and converges faster to its physical limit. In all cases, a range-separation parameter of about 2 bohr⁻¹ becomes sufficient to have an error smaller than 1 millihartree on the excitation energies while a value of about 4 bohr⁻¹ is required otherwise.

Zeroth+first-order excitation energies

As shown in Equation (4.7), it is also possible to apply this extrapolation technique not starting from the zeroth-order energies of the partially interacting system but its zeroth+first-order energies. The extrapolated 1S → 2S excitation energies of the helium atom are shown in Figure 4.3. In this case, the effect of the extrapolation correction is less important as the derivative is multiplied by $\mu/4$ instead of $\mu/2$ in the zeroth-order case. Moreover, as the “bare” zeroth+first energies are worse starting points than the zeroth-order one, the correction should be more important to reproduce the physical energies of the system with a good accuracy.

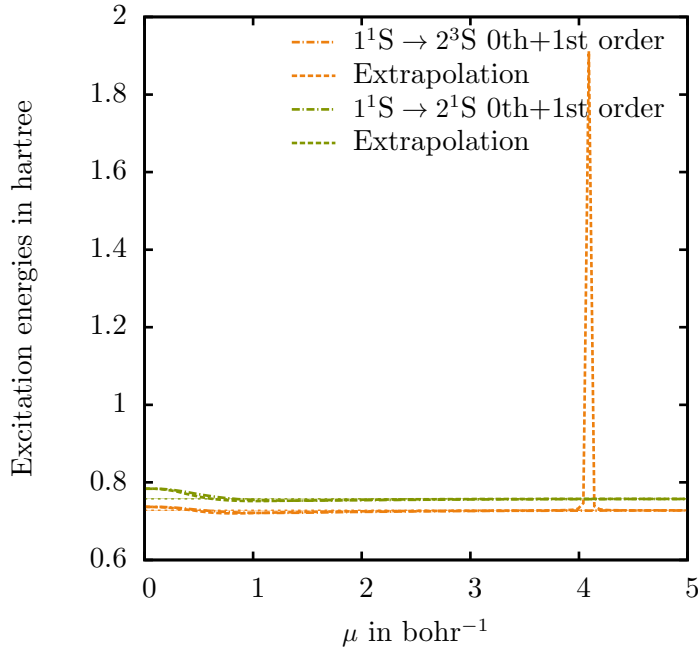


Figure 4.3 – Result of the extrapolation scheme (dashed line) along the range-separated adiabatic connection for the first excitation energies (in hartree) of the helium atom as a function of μ (in bohr^{-1}) starting from the zeroth+first order excitation energies. The “bare” excitation energies are recalled in dot-dashed line, the excitation energy of the physical system is given by an horizontal dotted line and the result of the first-order correction of the first variant of perturbation theory is given in dot-dashed line for comparison and an error of ± 1 millihartree is colored around each exact limit.

At small μ , the “bare” energies show an oscillation around their physical limit so that their first-order derivative changes sign. Because of this, the extrapolated energies are in fact worse than the “bare” energies around this region. However, as μ increases and that the “bare” energies begin to converge monotonically toward the physical energies of the system, then the extrapolation provides an improvement and allows to reproduce the exact energies with an error smaller than 1 millihartree for a range-separation parameter of 2.5 bohr^{-1} instead of 4 bohr^{-1} .

Consequently, it is better to perform the extrapolation on the zeroth-order curves, where the starting point is better and the correction larger by construction. In what follows, only zeroth-order extrapolated energies will therefore be shown.

4.3.2 Range-separated adiabatic connection for the valence excitation of the beryllium atom

The result of the extrapolation scheme is shown for the ground-state energy of the beryllium atom in Figure 4.4 (top). Once again, the convergence of the energy with respect to μ is systematically improved along the range-separated adiabatic connection with re-

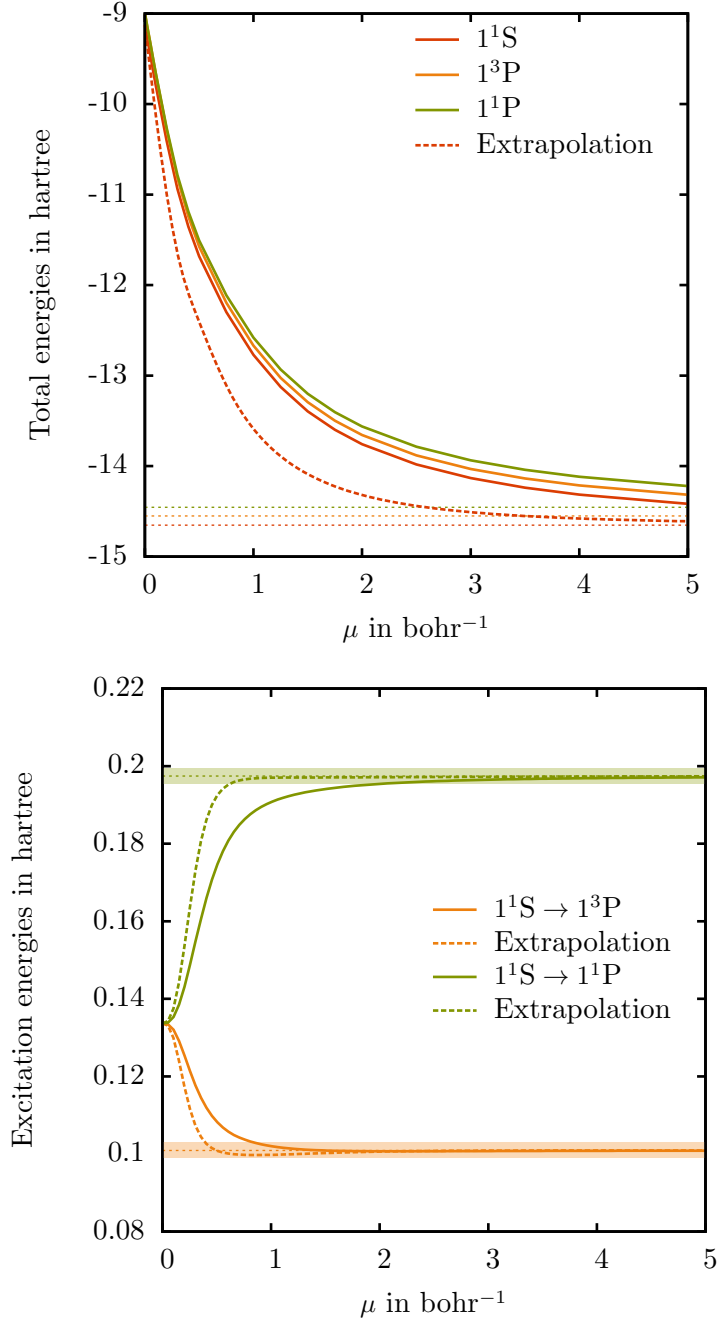


Figure 4.4 – Valence total state energies \mathcal{E}_k^μ (top) and excitation energies $\Delta\mathcal{E}_k^\mu = \mathcal{E}_k^\mu - \mathcal{E}_0^\mu$ of the beryllium atom (in hartree) as a function of μ (in bohr⁻¹). The “bare” energies are recalled in plain line, the result of the extrapolation for the ground-state energy is plotted in dashed line. The energies of the physical system are given as horizontal dotted lines and an error of ± 2 millihartree is colored around the physical excitation energies.

spect to the “bare” energy. As the beryllium atom has a core orbital, the convergence of the total energy is slower than in the helium atom as the density is more contracted and a larger range-separation parameter is needed to describe correctly this region. However, the extrapolation allows to recover an error smaller than 50 millihartree with respect to the ground-state energy of the physical system for a value of μ of about 5 bohr⁻¹ which is about ten times smaller than without the extrapolation correction but remains very large. Fortunately, the effect of the core cancels out in the excitation energies.

The effect of the extrapolation on the valence excitation energies of the beryllium atom is shown in Figure 4.4 (bottom). As the effect of the core orbitals disappears in the excitation energies, the “bare” energies already have a faster convergence toward their physical limits than the total energies. When the extrapolation correction is added, the value of μ required to ensure an error smaller than 2 millihartree is about 0.5 bohr⁻¹ which is particularly small as for the same value of μ , the total state energies of the beryllium atom are still off by about 4 hartrees. In this system, the static correlation plays a significant role and the multiconfigurational character of the wave function is quickly recovered when the interaction is switched on as shown in Ref. [48].

4.3.3 Range-separated adiabatic connection for the dihydrogen molecule along the dissociation

Finally, the extrapolation scheme is applied on the first zeroth-order energies of the dihydrogen molecule along the range-separated adiabatic connection both at equilibrium and at a stretched geometry. The result of the extrapolation on the singlet and triplet $\Sigma_g^+ \rightarrow \Sigma_u^+$ excitation energies of the dihydrogen molecule at its equilibrium geometry are shown in Figure 4.5 (top). The extrapolation correction provides a systematic improvement of the excitation energies toward their physical limit so that a value of 2 bohr⁻¹ for the range-separation parameter becomes sufficient to reproduce the physical energies with a maximum error of 1 millihartree. The internuclear bond of the dihydrogen molecule is then stretched to three times the equilibrium distance. The extrapolation scheme is then applied on the first three excitation energies corresponding to the first singlet and triplet excitations to the $1\Sigma_u^+$ state and to the double excitation to the $2\Sigma_g^+$ state. The extrapolated excitation energies are shown in the bottom of Figure 4.5. Once again, the improvement is systematic except for $\mu = 0$ where the correction is null. The triplet extrapolated energy shows a monotonic behavior with respect to μ while the singlet ones show a slight bump around 0.8 bohr⁻¹. However, all the extrapolated excitation energies present a faster convergence rate toward their physical limits than the “bare” ones which are recalled in plain lines. In this case, the extrapolation scheme works remarkably well as it allows one to recover an error smaller than 5 millihartree with respect to the physical limits for values of μ as small as 0.6 bohr⁻¹ when a range separation parameter of 2 bohr⁻¹ is needed otherwise. In particular, it allows one to describe the double excitation energy with a comparable accuracy than the single exci-

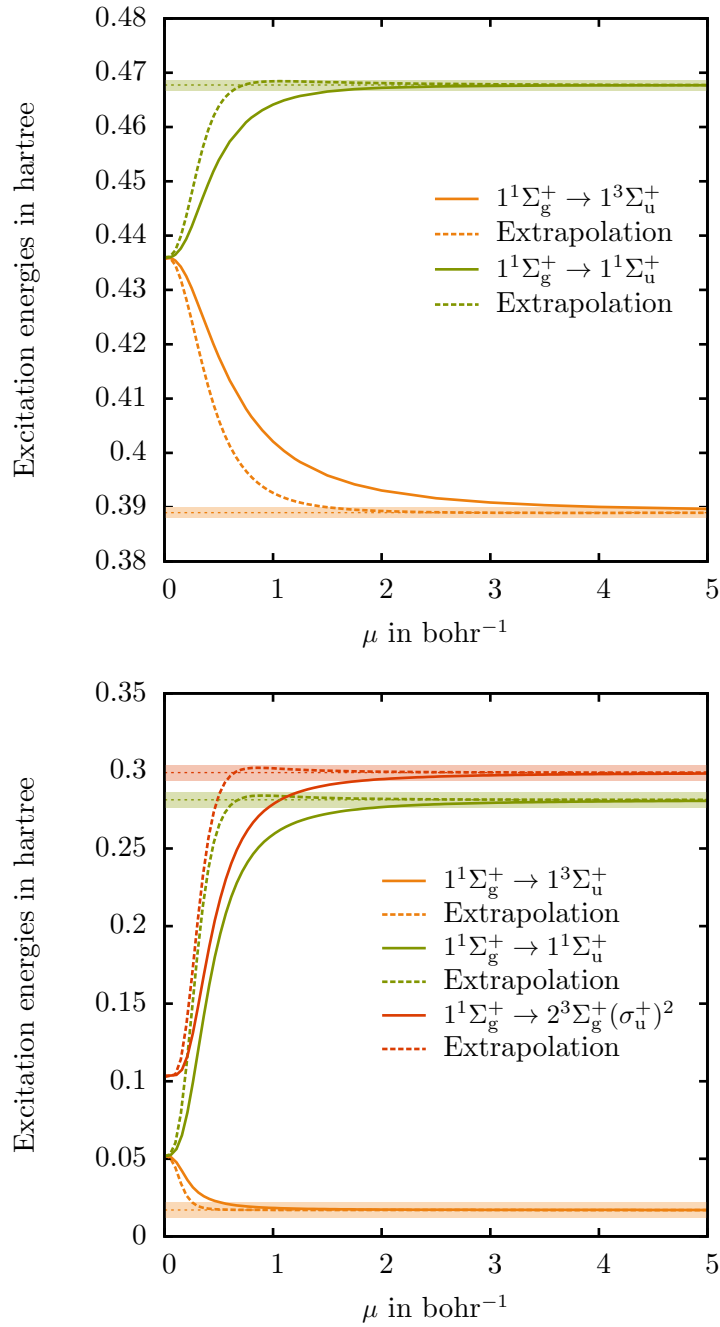


Figure 4.5 – Excitation energies $\Delta\mathcal{E}_k^\mu = \mathcal{E}_k^\mu - \mathcal{E}_0^\mu$ (in hartree) of the H₂ molecule at the equilibrium internuclear distance (top) and three times the equilibrium distance (bottom) as a function of μ (in bohr⁻¹). The excitation energies of the physical system $\Delta E_k = \Delta\mathcal{E}_k^{\mu \rightarrow \infty}$ are plotted as horizontal dotted lines. An error of ± 1 millihartree is colored around the physical excitation energies at equilibrium and an error of ± 5 millihartree at stretched geometry.

tation energies.

4.3.4 Linear adiabatic connection for the helium atom

In order to apply the extrapolation scheme on the linear adiabatic connection, the zeroth-order total and excitation energies of the helium atom along this connection are calculated following the procedure described in Chapter 2 and are shown in Figure 4.6.

Zeroth-order total energies

The total energies of the helium atom along the linear adiabatic connection are given in Figure 4.6 (top). When $\lambda = 0$, no interaction is included, so the KS energies are recovered as it was the case for $\mu = 0$. On the other hand, when $\lambda = 1$, the full interaction is present and the energies of the physical system are recovered, which corresponds to the limit $\mu \rightarrow \infty$. The two limit cases are therefore identical in the two methods but the way they are connected differs. The evolution of the total energies with respect to λ appears almost linear. Although, this behavior is easier to predict and should provide an efficient framework for extrapolations, the value of λ required to have an error of 10 millihartree is very close to 1 while in the range-separation case a intermediate value of μ was sufficient. As almost all the interaction would be included, the complexity of the calculation would therefore not be improved with respect to a FCI calculation.

Excitation energies

The excitation energies of the helium atom along the linear adiabatic connection are given in Figure 4.6 (bottom). Similarly to the total energies, the end points are common with the range-separated connection but the behavior of the energies along the connection is also more linear. One could note that as in the range-separation case, the singlet P energy does not have a monotonic behavior with respect to the connecting parameter. The basis set might be responsible for this behavior as discussed earlier.

Extrapolation and comparison with the range-separated case

The extrapolation scheme is then applied on the first excitation energy of the helium atom along the linear adiabatic connection and is also compared with the results obtained with the range-separated adiabatic connection in Figure 4.7. Without extrapolation, the value of the scaling parameter λ needs to be greater than 0.95 to reproduce correctly the energies with an error smaller than 1 millihartree, while for the range-separated one, as a small change of μ implies an important change in the energies when close to the KS, a range separation parameter of 2 bohr⁻¹ is sufficient to ensure the same accuracy. In a way, this means that the range-separated connection adds the most significant region of the interaction first, while the linear connection treats equally the interaction independently of its importance for the excitation energies. When the extrapolation

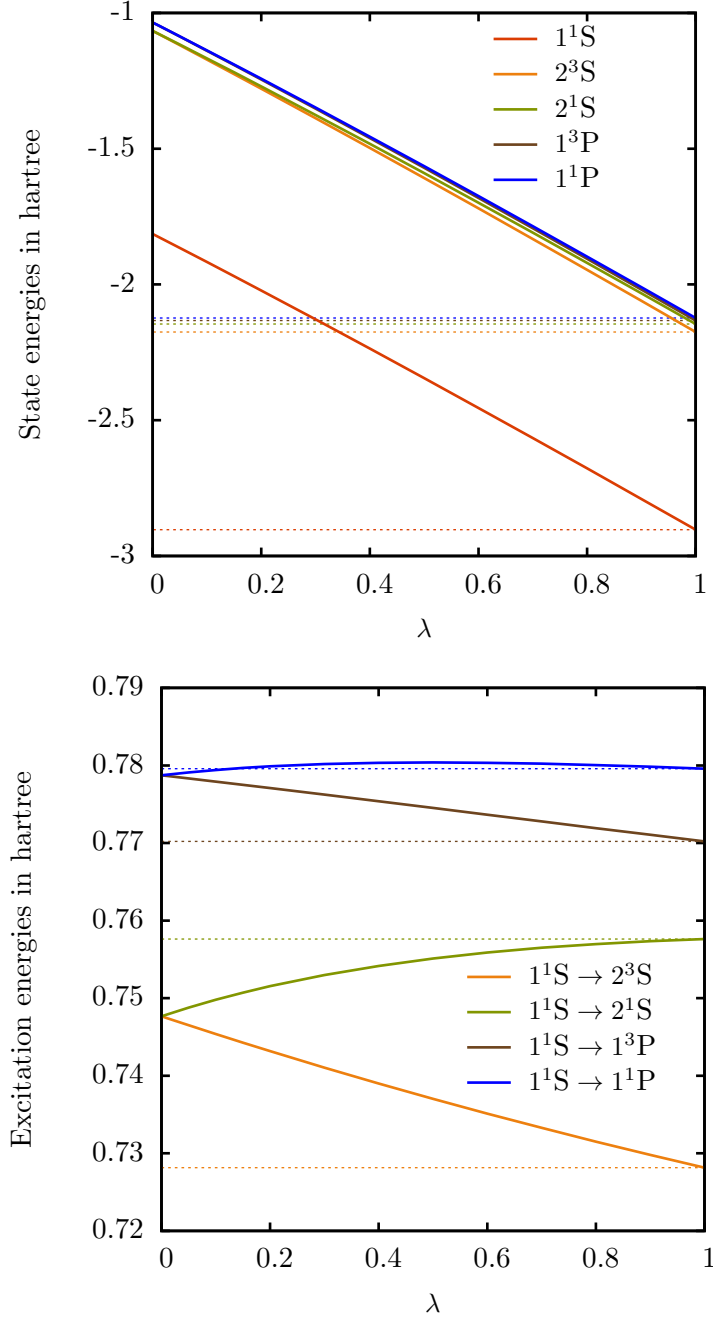


Figure 4.6 – Ground- and excited-state total energies \mathcal{E}_k^λ (top) and excitation energies $\Delta\mathcal{E}_k^\lambda = \mathcal{E}_k^\lambda - \mathcal{E}_0^\lambda$ of the He atom (in hartree) as a function of λ (in bohr⁻¹). The total energies of the physical system $E_k = \mathcal{E}_k^{\lambda=1}$ are plotted as horizontal dotted lines.

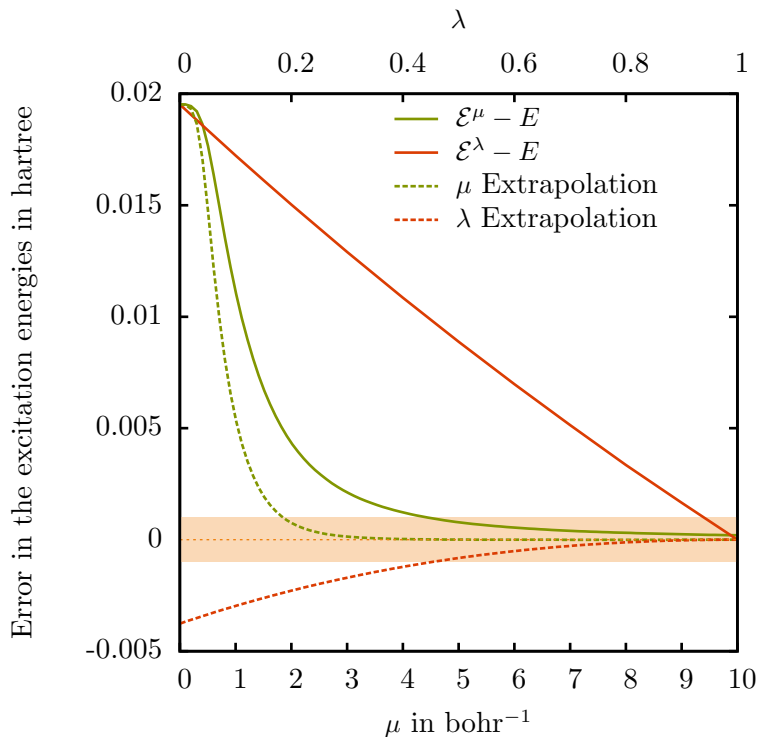


Figure 4.7 – Error on the triplet S excitation energy (in hartree) along the range-separated and linear adiabatic connections for the helium atom as functions of μ (in bohr $^{-1}$) or λ . The “bare” energies are given in plain lines and the extrapolated ones in dashed lines. An error smaller than 1 millihartree around the physical limit is given by the colored region.

correction is added, a systematic improvement of the energy is observed and the amount of interaction required to reproduce the physical limit with an accuracy of 1 millihartree now drops to 50%. Moreover one should note that contrary to the range-separated case, the KS extrapolated excitation energy also benefits from this correction as in this case the correction does not go to zero in this limit. At $\lambda = 0$, the extrapolated excitation energy matches the results obtained in [118] with the first-order Görling-Levy perturbation theory as expected.

For the KS system, it is obviously better to use the extrapolated linear connection as the extrapolation correction has no effect at $\mu = 0$. For a partially interacting system, it is difficult to compare the two connections, it seems however that the linear connection works in fact better than the range-separated one except for large values of λ .

4.4 Conclusion

In this chapter, we made use of the asymptotic behavior of the energies of a partially interacting system along the range-separated adiabatic connection to design an energy correction which allows us to extrapolate the physical energies of the system from its

partially interacting ones. The simplest possible extrapolation was obtained by using only the first-order derivative of the energies with respect to the range-separation parameter in one point. This extrapolation correction can be applied directly on the energies of the partially interacting system or after they have been corrected by a first-order perturbation.

This extrapolation scheme was tested on the helium and beryllium atom and on the dihydrogen molecule at both its equilibrium and a stretched geometry where no approximation were done except for the basis set. When applied on the zeroth-order energies, this extrapolation scheme was shown to be very successful as it improves significantly the convergence rate of the energies toward their physical limits. Moreover, this improvement is almost systematic, except at $\mu = 0$ where the extrapolation correction is null by construction and in some cases where the partially interacting energies present a “bump” at small μ which is probably due to the basis set. However, in all cases, the extrapolated energies were able to reproduce the physical energies of the system for a given accuracy with a range-separation parameter reduced by approximately a factor of 2 with respect to the “bare” energies.

When applied on the zeroth+first-order energies of the partially interacting system, the extrapolation correction overall improves their convergence rate. However, as the quality of the starting point is inferior than in the zeroth-order case as discussed in Chapter 3, and that the correction is smaller, the convergence is slower than in the previous case. Finally the extrapolation scheme was applied along the linear adiabatic connection where it also improves significantly the description of the excitation energies along the connection.

All these results have been obtained without any approximate functionals. The promising method should now be tested in a more pragmatic case where the potential is obtained from a (semi)local approximations. The effects of the inclusion of higher-order derivatives and of multiple points on this extrapolation should also be explored.

Bibliography

- [1] K. Capelle. 2006. *Brazilian J. Phys.* 36. Pp. 1318–1343.
- [2] A. Ruzsinszky and J. P. Perdew. 2011. *Comput. Theor. Chem.* 963. Pp. 2–6.
- [3] K. Burke. 2012. *J. Chem. Phys.* 136. P. 150901.
- [4] C. A. Ullrich and Z.-H. Yang. 2014. *Brazilian J. Phys.* 44. Pp. 154–188.
- [5] K. Burke and L. O. Wagner. 2013. *Int. J. Quantum Chem.* 113. Pp. 96–101.
- [6] R. G. Parr and W. Yang. *Density-Functional Theory of Atoms and Molecules*. Oxford university press, 1989.
- [7] R. M. Dreizler and E. K. U. Gross. *Density Functional Theory*. Berlin: Springer-Verlag, 1990.
- [8] W. Koch and M. C. Holthausen. *A Chemist’s Guide to Density Functional Theory*. Vol. 3. Wiley-VCH, 2000.
- [9] C. Fiolhais, F. Nogueira, M. Marques, and E. Engel. *A Primer in Density Functional Theory*. Ed. by C. Fiolhais, F. Nogueira, and M. A. L. Marques. Vol. 620 of Lecture Notes in Physics. Berlin: Springer, 2003, pp. 56–122.
- [10] D. Sholl and J. A. Steckel. *Density Functional Theory: A Practical Introduction*. Hoboken: Wiley-Interscience, Hoboken, 2009.
- [11] E. Engel and R. M. Dreizler. *Density Functional Theory: An Advanced Course*. Berlin: Springer, 2011, p. 546.
- [12] T. Helgaker. *Density-functional theory*. 2012. URL: http://qleap.au.dk/fileadmin/www.qleap.au.dk/Sommerskole2012/Density-functional%5C_Theory.pdf.
- [13] E. Besalú and J. Martí. 1998. *J. Chem. Educ.* 75. P. 105.
- [14] L. H. Thomas. 1927. *Math. Proc. Cambridge Philos. Soc.* 23. P. 542.
- [15] E. Fermi. 1927. *Rend. Accad. Naz. Lincei.* 6. Pp. 602–607.
- [16] T. Kato. 1957. *Commun. Pure Appl. Math.* 10. Pp. 151–177.
- [17] M. M. Morrell. 1975. *J. Chem. Phys.* 62. P. 549.
- [18] A. Nagy and C. Amovilli. 2008. *J. Chem. Phys.* 128. P. 114115.
- [19] P. Hohenberg and W. Kohn. 1964. *Phys. Rev.* 136. B834–B871.

BIBLIOGRAPHY

- [20] M. E. L. Levy. 1979. *Proc. Natl. Acad. Sci.* 76. Pp. 6062–6065.
- [21] E. H. Lieb. 1983. *Int. J. Quantum Chem.* 24. Pp. 243–277.
- [22] R. O. Jones and O. Gunnarson. 1989. *Rev. Mod. Phys.* 61. Pp. 689–746.
- [23] K. Burke. *ABC of DFT*. 2007.
- [24] W. Kohn and L. J. Sham. 1965. *Phys. Rev.* 140. A1133–A1138.
- [25] T. Koopmans. 1934. *Physica*. 1. Pp. 104–113.
- [26] J. P. Perdew, R. G. Parr, M. E. L. Levy, and J. L. Balduz. 1982. *Phys. Rev. Lett.* 49. P. 1691.
- [27] P. A. M. Dirac. 1930. *Math. Proc. Cambridge Philos. Soc.* 26. Pp. 376–385.
- [28] J. C. Slater. 1951. *Phys. Rev.* 81. Pp. 385–390.
- [29] D. D. M. Ceperley and B. J. B. Alder. 1980. *Phys. Rev. Lett.* 45. Pp. 566–569.
- [30] S. H. Vosko, L. Wilk, and M. Nusair. 1980. *Can. J. Phys.* 58. Pp. 1200–1211.
- [31] J. P. Perdew and Y. Wang. 1992. *Phys. Rev. B.* 45. Pp. 13244–13249.
- [32] V. N. Staroverov, G. E. Scuseria, J. Tao, and J. P. Perdew. 2003. *J. Chem. Phys.* 119. P. 12129.
- [33] C. Lee, W. Yang, and R. G. Parr. 1988. *Phys. Rev. B.* 37. P. 785.
- [34] A. D. Becke. 1988. *Phys. Rev. A.* 38. Pp. 3098–3100.
- [35] J. P. Perdew, K. Burke, and M. Ernzerhof. 1996. *Phys. Rev. Lett.* 77. P. 3865.
- [36] P. M. W. Gill, B. G. Johnson, J. A. Pople, and M. J. Frisch. 1992. *Chem. Phys. Lett.* 197. Pp. 499–505.
- [37] J. Paier, R. Hirschl, M. Marsman, and G. Kresse. 2005. *J. Chem. Phys.* 122. P. 234102.
- [38] A. Savin. “Beyond the Kohn-Sham determinant.” In: *Recent Adv. density Funct. methods*. Ed. by D. P. Chong. World Scientific, 1995, p. 129.
- [39] A. Savin. “On degeneracy, near-degeneracy and density functional theory”. In: *Recent Dev. Appl. Mod. Density Funct. Theory*. Ed. by J.M. Seminario. Amsterdam: Elsevier, 1996, p. 327.
- [40] T. Leininger, H. Stoll, H.-J. H.-j. Werner, and A. Savin. 1997. *Chem. Phys. Lett.* 275. Pp. 151–160.
- [41] R. Pollet, A. Savin, T. Leininger, and H. Stoll. 2002. *J. Chem. Phys.* 116. P. 1250.
- [42] A. Savin and H.-J. Flad. 1995. *Int. J. Quantum Chem.* 56. Pp. 327–332.
- [43] R. Baer and D. Neuhauser. 2005. *Phys. Rev. Lett.* 94. P. 43002.
- [44] Y. Akinaga and S. Ten-no. 2008. *Chem. Phys. Lett.* 462. Pp. 348–351.
- [45] J. Toulouse, F. Colonna, and A. Savin. 2004. *Phys. Rev. A.* 70. P. 062505.
- [46] J.-W. Song, K. Yamashita, and K. Hirao. 2012. *J. Chem. Phys.* 137. P. 244105.

-
- [47] J. Toulouse. “Extension multidéterminantale de la méthode de Kohn-Sham en théorie de la fonctionnelle de la densité par décomposition de l’interaction électronique en contributions de longue portée et de courte portée.” PhD thesis. Université Pierre et Marie Curie, 2005.
- [48] E. Fromager, J. Toulouse, and H. J. A. Jensen. 2007. *J. Chem. Phys.* 126. P. 074111.
- [49] J. G. Ángyán, I. Gerber, A. Savin, and J. Toulouse. 2005. *Phys. Rev. A.* 72. P. 012510.
- [50] H. Iikura, T. Tsuneda, T. Yanai, and K. Hirao. 2001. *J. Chem. Phys.* 115. P. 3540.
- [51] I. C. Gerber and J. G. Ángyán. 2005. *Chem. Phys. Lett.* 415. Pp. 100–105.
- [52] W. Yang. 1998. *J. Chem. Phys.* 109. P. 10107.
- [53] R. Pollet, F. Colonna, T. Leininger, et al. 2003. *Int. J. Quantum Chem.* 91. Pp. 84–93.
- [54] A. Savin, F. Colonna, and R. Pollet. 2003. *Int. J. Quantum Chem.* 93. P. 166.
- [55] J. Toulouse, A. Savin, and H.-J. Flad. 2004. *Int. J. Quantum Chem.* 100. P. 1047.
- [56] J. Toulouse, F. Colonna, and A. Savin. 2005. *J. Chem. Phys.* 122. P. 14110.
- [57] J. Toulouse, P. Gori-Giorgi, and A. Savin. 2005. *Theor. Chem. Acc.* 114. P. 305.
- [58] E. Goll, H.-J. Werner, and H. Stoll. 2005. *Phys. Chem. Chem. Phys.* 7. P. 3917.
- [59] S. Paziani, S. Moroni, P. Gori-Giorgi, and G. Bachelet. 2006. *Phys. Rev. B.* 73. P. 155111.
- [60] E. Goll, M. Ernst, F. Moegle-Hofacker, and H. Stoll. 2009. *J. Chem. Phys.* 130. P. 234112.
- [61] A. Savin. “Beyond the Kohn-Sham Determinant”. In: *Recent Adv. Density Funct. Theory*. Ed. by D. P. Chong. World Scientific, 1996.
- [62] E. Fromager, F. Réal, P. Wåhlin, et al. 2009. *J. Chem. Phys.* 131. P. 54107.
- [63] A. Stoyanova, A. M. Teale, J. Toulouse, et al. 2013. *J. Chem. Phys.* 139. P. 134113.
- [64] K. Pernal. 2010. *Phys. Rev. A.* 81. P. 52511.
- [65] D. R. Rohr, J. Toulouse, and K. Pernal. 2010. *Phys. Rev. A.* 82. P. 52502.
- [66] D. R. Rohr and K. Pernal. 2011. *J. Chem. Phys.* 135. P. 74104.
- [67] T. Tsuchimochi, G. E. Scuseria, and A. Savin. 2010. *J. Chem. Phys.* 132. P. 24111.
- [68] T. Tsuchimochi and G. E. Scuseria. 2011. *J. Chem. Phys.* 134. P. 64101.
- [69] I. C. Gerber and J. G. Ángyán. 2005. *Chem. Phys. Lett.* 416. P. 370.
- [70] I. C. Gerber and J. G. Ángyán. 2007. *J. Chem. Phys.* 126. P. 44103.
- [71] J. G. Ángyán. 2008. *Phys. Rev. A.* 78. P. 22510.
- [72] E. Fromager and H. J. A. Jensen. 2008. *Phys. Rev. A.* 78. P. 022504.

BIBLIOGRAPHY

- [73] E. Goll, T. Leininger, F. R. Manby, et al. 2008. *Phys. Chem. Chem. Phys.* 10. P. 3353.
- [74] B. G. Janesko and G. E. Scuseria. 2009. *Phys. Chem. Chem. Phys.* 11. P. 9677.
- [75] E. Fromager, R. Cimiraglia, and H. J. A. Jensen. 2010. *Phys. Rev. A.* 81. P. 24502.
- [76] S. Chabbal, H. Stoll, H.-J. Werner, and T. Leininger. 2010. *Mol. Phys.* 108. P. 3373.
- [77] S. Chabbal, D. Jacquemin, C. Adamo, et al. 2010. *J. Chem. Phys.* 133. P. 151104.
- [78] E. Fromager and H. Jensen. 2011. *J. Chem. Phys.* 135. P. 034116.
- [79] Y. Cornaton, A. Stoyanova, H. J. A. Jensen, and E. Fromager. 2013. *Phys. Rev. A.* 88. P. 022516.
- [80] E. Goll, H.-J. Werner, H. Stoll, et al. 2006. *Chem. Phys.* 329. P. 276.
- [81] E. Goll, H. Stoll, C. Thierfelder, and P. Schwerdtfeger. 2007. *Phys. Rev. A.* 76. P. 32507.
- [82] E. Goll, H.-J. Werner, and H. Stoll. 2008. *Chem. Phys.* 346. P. 257.
- [83] J. Toulouse, I. Gerber, G. Jansen, et al. 2009. *Phys. Rev. Lett.* 102. P. 096404.
- [84] B. G. Janesko, T. M. Henderson, and G. E. Scuseria. 2009. *J. Chem. Phys.* 130. P. 081105.
- [85] B. G. Janesko, T. M. Henderson, and G. E. Scuseria. 2009. *J. Chem. Phys.* 131. P. 34110.
- [86] B. G. Janesko and G. E. Scuseria. 2009. *J. Chem. Phys.* 131. P. 154106.
- [87] W. Zhu, J. Toulouse, A. Savin, and J. G. Ángyán. 2010. *J. Chem. Phys.* 132. P. 244108.
- [88] J. Toulouse, W. Zhu, J. G. Ángyán, and A. Savin. 2010. *Phys. Rev. A.* 82. P. 32502.
- [89] J. Paier, B. G. Janesko, T. M. Henderson, et al. 2010. *J. Chem. Phys.* 132. P. 094103.
- [90] J. Toulouse, W. Zhu, A. Savin, et al. 2011. *J. Chem. Phys.* 135. P. 84119.
- [91] J. G. Ángyán, R.-F. Liu, J. Toulouse, and G. Jansen. 2011. *J. Chem. Theory Comput.* 7. P. 3116.
- [92] R. M. Ireland, T. M. Henderson, and G. E. Scuseria. 2011. *J. Chem. Phys.* 135. P. 94105.
- [93] T. Gould and J. F. Dobson. 2011. *Phys. Rev. B.* 84. P. 241108.
- [94] E. Fromager, S. Knecht, and H. J. A. Jensen. 2013. *J. Chem. Phys.* 138. P. 084101.
- [95] E. Rebolini, A. Savin, and J. Toulouse. 2013. *Mol. Phys.* 111. Pp. 1219–1234.
- [96] J. Toulouse, E. Rebolini, T. Gould, et al. 2013. *J. Chem. Phys.* 138. P. 194106.
- [97] E. D. Hedegård, F. Heiden, S. Knecht, et al. 2013. *J. Chem. Phys.* 139. P. 184308.

-
- [98] K. Pernal. 2012. *J. Chem. Phys.* 136. P. 184105.
- [99] O. Gritsenko, S. V. Gisbergen, A. Görling, and E. J. Baerends. 2000. *J. Chem. Phys.* 113. Pp. 8478–8489.
- [100] N. T. Maitra, F. Zhang, R. J. Cave, and K. Burke. 2004. *J. Chem. Phys.* 120. P. 5932.
- [101] M. E. Casida, C. Jamorski, K. C. Casida, and D. R. Salahub. 1998. *J. Chem. Phys.* 108. P. 4439.
- [102] A. Dreuw, J. L. Weisman, and M. Head-Gordon. 2003. *J. Chem. Phys.* 119. P. 2943.
- [103] F. Colonna and A. Savin. 1999. *J. Chem. Phys.* 110. P. 2828.
- [104] A. M. Teale, S. Coriani, and T. Helgaker. 2009. *J. Chem. Phys.* 130. P. 104111.
- [105] D. P. Joubert and G. P. Strivastava. 1998. *J. Chem. Phys.* 109. P. 5212.
- [106] A. Savin, F. Colonna, and M. Allavena. 2001. *J. Chem. Phys.* 115. P. 6827.
- [107] A. M. Teale, S. Coriani, and T. Helgaker. 2010. *J. Chem. Phys.* 133. P. 164112.
- [108] M. D. Strømsheim, N. Kumar, S. Coriani, et al. 2011. *J. Chem. Phys.* 135. P. 194109.
- [109] J. Toulouse, F. F. Colonna, and A. Savin. 2005. *Mol. Phys.* 103. P. 2725.
- [110] A. M. Teale, S. Coriani, and T. Helgaker. 2010. *J. Chem. Phys.* 132. P. 164115.
- [111] F. Zhang and K. Burke. 2004. *Phys. Rev. A*. 69. P. 052510.
- [112] P. Gori-Giorgi and A. Savin. 2006. *Phys. Rev. A*. 73. P. 032506.
- [113] *DALTON, a molecular electronic structure program, Release Dalton2011 (2011)*. URL: <http://daltonprogram.org>.
- [114] Q. Wu and W. Yang. 2003. *J. Theor. Comput. Chem.* 02. Pp. 627–638.
- [115] K. Kaufmann. 1991. *J. Phys. B At. Mol. Opt. Phys.* 24. P. 2277.
- [116] T. H. Dunning. 1989. *J. Chem. Phys.* 90. P. 1007.
- [117] C. J. Umrigar, A. Savin, and X. Gonze. “Are unoccupied Kohn-Sham eigenvalues related to excitation energies?” In: *Electron. Density Funct. Theory Recent Prog. New Dir.* Ed. by J. F. Dobson, G. Vignale, and M. P. Das. N. Y.: Plenum, 1997.
- [118] C. Filippi, C. J. Umrigar, and X. Gonze. 1997. *J. Chem. Phys.* 107. P. 9994.
- [119] A. Savin, C. J. Umrigar, and X. Gonze. 1998. *Chem. Phys. Lett.* 288. P. 391.
- [120] A. Savin. 2011. *J. Chem. Phys.* 134. P. 214108.
- [121] A. Savin. 2014. *J. Chem. Phys.* 140.
- [122] M. E. Casida. 2009. *J. Mol. Struct. THEOCHEM.* 914. Pp. 3–18.
- [123] M. E. Casida and M. Huix-Rotllant. 2012. *Annu. Rev. Phys. Chem.* 63. P. 287.
- [124] A. Theophilou. 1979. *J. Phys. C Solid State Phys.* 5419.

BIBLIOGRAPHY

- [125] E. K. U. Gross, L. N. Oliveira, and W. Kohn. 1988. *Phys. Rev. A.* 37. P. 2809.
- [126] E. Pastorczak, N. I. Gidopoulos, and K. Pernal. 2013. *Phys. Rev. A.* 87. P. 62501.
- [127] O. Franck and E. Fromager. 2013. *Mol. Phys.*
- [128] Z.-H. Yang, J. Trail, and A. Pribram-Jones. 2014. *arXiv Prepr. arXiv1402.3209.*
- [129] A. Pribram-Jones, Z.-H. Yang, and J. Trail. 2014. *arXiv Prepr. arXiv1402.5444.*
- [130] O. Gunnarsson and B. I. Lundqvist. 1976. *Phys. Rev. B.* 13. Pp. 4274–4298.
- [131] T. Ziegler, A. Rauk, and E. Baerends. 1977. *Theor. Chim. Acta.* 271. P. 261.
- [132] U. von Barth. 1979. *Phys. Rev. A.* 20.
- [133] T. Kowalczyk, S. R. Yorst, and T. Van Voorhis. 2011. *J. Chem. Phys.* 134. P. 54128.
- [134] N. Ferré and X. Assfeld. 2002. *J. Chem. Phys.* 117. P. 4119.
- [135] M. Krykunov and T. Ziegler. 2013. *J. Chem. Theory Comput.* 9. P. 2761.
- [136] F. A. Evangelista, P. Shushkov, and J. C. Tully. 2013. *J. Phys. Chem. A.* 117. P. 7378.
- [137] A. Nagy. 1998. *Int. J. Quantum Chem.* 70. P. 681.
- [138] A. Görling. 1999. *Phys. Rev. A.* 59. Pp. 3359–3374.
- [139] M. Levy and Á. Nagy. 1999. *Phys. Rev. Lett.* 83. Pp. 4361–4364.
- [140] A. Görling. 2000. *Phys. Rev. Lett.* 85. P. 4229.
- [141] A. Nagy and M. Levy. 2001. *Phys. Rev. A.* 63. P. 52502.
- [142] A. Nagy. 2004. *Int. J. Quantum Chem.* 99. P. 256.
- [143] M. Harbola. 2004. *Phys. Rev. A.* 69. P. 042512.
- [144] V. Vitale, F. Della Salla, and A. Görling. 2005. *J. Chem. Phys.* 122. P. 244102.
- [145] A. Görling. 2005. *J. Chem. Phys.* 123. P. 62203.
- [146] P. Samal and M. K. Harbola. 2006. *J. Phys. B.* 39. P. 4065.
- [147] V. N. Glushkov and M. Levy. 2007. *J. Chem. Phys.* 126. P. 174106.
- [148] P. W. Ayers and M. Levy. 2009. *Phys. Rev. A.* 80. P. 12508.
- [149] P. W. Ayers, M. Levy, and A. Nagy. 2012. *Phys. Rev. A.* 85. P. 42518.
- [150] M. K. Harbola, M. Hemanadhan, M. Shamim, and P. Samal. 2012. *J. Phys. Conf. Ser.* 388. P. 012011.
- [151] S. Grimme. 1996. *Chem. Phys. Lett.* 259. P. 128.
- [152] S. Grimme and M. Waletzke. 1999. *J. Chem. Phys.* 111. P. 5645.
- [153] E. V. Beck, E. A. Stahlberg, L. W. Burggraf, and J.-P. Blaudeau. 2008. *Chem. Phys.* 349. P. 158.
- [154] B. Kaduk and T. Van Voorhis. 2010. *J. Chem. Phys.* 133. P. 61102.

- [155] A. Görling. 1996. *Phys. Rev. A.* 54. Pp. 3912–3915.
- [156] A. Görling and M. Levy. 1993. *Phys. Rev. B.* 47. P. 13105.
- [157] A. Görling and M. Levy. 1995. *Int. J. Quantum Chem.* 08. Pp. 93–108.
- [158] X. Gonze and M. Scheffler. 1999. *Phys. Rev. Lett.* 82. Pp. 4416–4419.
- [159] P. Gori-Giorgi and A. Savin. 2009. *Int. J. Quantum Chem.* 109. P. 1950.

Part II

Excitation energies from linear-response time-dependent density-functional theory

Chapter 5

Theoretical background on time-dependent linear-response density-functional theory

In this chapter, the time-dependent extension of density-functional theory is described and emphasis is placed on linear-response theory. This method is used to describe the response of a system initially in its ground state to a small time-dependent oscillatory perturbation, for instance a weak laser field. In particular, it allows one to extract the absorption spectrum of the system by providing both the excitation energies and the associated oscillator strengths. The theoretical foundations of the method are briefly recalled together with its formulation in the Kohn-Sham scheme. The usual adiabatic (semi-)local approximations are then discussed together with their successes and their limitations as in particular, they cannot deal with multiple excitations and/or charge-transfer excitations. Finally, the extension of the range-separated scheme to the time-dependent case is briefly sketched in its more common variant where separation is done on the exchange kernel only.

5.1 Introduction

In this original time-independent formulation, density-functional theory (DFT) is a ground-state method. However, the Hohenberg-Kohn theorem states that the ground-state electron density contains all the information on the system so that it is in principle possible to calculate any property of the system from this density, and in particular excitation energies. The most commonly used approach to compute excitation energies in the density-functional framework is to extend DFT to a time-dependent formalism and to use either real-time propagation or linear-response theory. In this thesis, we focus on the latter which is relevant when the system is subject to a weak electromagnetic field. In this case, a small time-dependent perturbation is applied on the system and its den-

sity response is analyzed. As the system has quantized energy levels, the response of the system is then intrinsically different if the frequency of the perturbation matches or not a level energy difference. This is the phenomenon which is exploited in linear-response time-dependent density-functional theory (TDDFT).

This chapter is intended to give a brief review of the TDDFT formalism within the linear-response framework. First, the time-dependent framework is laid down in Section 5.2, then the time-dependent KS scheme is explained in Section 5.3. As we are interested in reproducing the excitation energies of a system subject to a weak laser field, linear response can be used and is detailed in Section 5.4. Then the resolution in the case of finite molecular systems is given in Section 5.5 and the usual approximations, together with their deficiencies and possible remedies are given in Sections 5.6 and 5.7. More details can be found for instance in [1–8].

5.2 Time-dependent framework

5.2.1 Time-dependent Schrödinger equation

The stationary many-electron problem was introduced in Chapter 1 where the Hamiltonian of the system was time-independent. It allows one to obtain the eigenstates of the system by solving Equation (1.6). When the system evolves in a time-dependent field, its behavior is ruled by the time-dependent version of the Schrödinger equation given by

$$i\frac{\partial}{\partial t}\Psi_i(\mathbf{x}_1, \dots, \mathbf{x}_N, t) = \hat{H}(t)\Psi_i(\mathbf{x}_1, \dots, \mathbf{x}_N, t), \quad (5.1)$$

where the time-dependent Hamiltonian is $\hat{H}(t) = \hat{T} + \hat{V}(t) + \hat{W}_{ee}$. Its kinetic and electron-electron interaction operators are the same as in the static Hamiltonian (1.11), but the external potential operator is now explicitly time dependent,

$$\hat{V}(t) = \int \hat{n}(\mathbf{r})v(\mathbf{r}, t)d\mathbf{r}. \quad (5.2)$$

The time-dependent Schrödinger equation represents the propagation of an initial wave function of the system $\Psi(t_0)$ under the influence of a time-dependent potential $v(\mathbf{r}, t)$. Note that the initial wave function is not necessarily the ground state.

It is furthermore convenient to decompose the potential and the Hamiltonian into their time-independent and time-dependent parts

$$\begin{aligned} \hat{V}(t) &= \hat{V} + \delta\hat{V}(t) \\ \hat{H}(t) &= \hat{H} + \delta\hat{V}(t). \end{aligned} \quad (5.3)$$

The density of such a system is then also time dependent and is given by

$$n(\mathbf{r}, t) = \langle \Psi(t) | \hat{n}(\mathbf{r}) | \Psi(t) \rangle. \quad (5.4)$$

5.2.2 Representation of the time-dependent system

In order to describe the time evolution of the wave function and of the observables of the system, different representations can be used where either the states, the operators or both are evolving in time. One should note that these representations are also useful in the stationary case as, even if the Hamiltonian is time independent, the eigenstates evolve in time. Indeed, for an eigenstate Ψ_k of energy E_k , its phase rotates in time as $\Psi_k(t) = \Psi_k(t=0)e^{-iE_k t}$.

Schrödinger picture

In the Schrödinger representation, when calculating a time-dependent observable $\mathcal{P}(t) = \langle \Psi | \hat{\mathcal{P}} | \Psi \rangle$, the time evolution is contained in the state vectors and the operators are kept constant with respect to time. This evolution of the state vectors is described by the unitary time evolution operator $\hat{U}(t, t_0)$ (or just $\hat{U}(t)$ when $t_0 = 0$) such that

$$|\Psi(t)\rangle = \hat{U}(t, t_0)|\Psi(t_0)\rangle. \quad (5.5)$$

In the most general case, i.e. when the Hamiltonian is time dependent and the Hamiltonians at different times do not commute, this operator is given by

$$\hat{U}(t, t_0) = \hat{T} \exp \left(-i \int_{t_0}^t \hat{H}(t') dt' \right), \quad (5.6)$$

where \hat{T} is the Wick time-ordering operator [9, 10] which orders the operators with larger times on the left. Whereas if the Hamiltonian is time independent, the time evolution operator reduces simply to $\hat{U}(t, t_0) = \exp(-i\hat{H}(t - t_0))$.

Heisenberg picture

Another useful representation when time evolution is concerned is the Heisenberg picture. In this representation, the operators depend on time and the state vectors are time independent. In particular, the time-dependent creation and annihilation field operators are given by

$$\hat{\Psi}(1) = \hat{U}^\dagger(t_1, t_0) \hat{\Psi}_{\sigma_1}(\mathbf{r}_1) \hat{U}(t_1, t_0), \quad (5.7a)$$

$$\hat{\Psi}^\dagger(1) = \hat{U}^\dagger(t_1, t_0) \hat{\Psi}_{\sigma_1}^\dagger(\mathbf{r}_1) \hat{U}(t_1, t_0), \quad (5.7b)$$

where the variable 1 stands for the spin, space, and time coordinates of the electron $(\mathbf{r}_1, \sigma_1, t_1)$.

Interaction picture

The last possibility is given by the interaction picture where both the state vectors and the operators are time dependent. However, this picture will not be used hereinafter.

5.3 Time-dependent density-functional theory formalism

5.3.1 Runge-Gross theorem

Starting from an initial wave function $\Psi(t_0)$, if a time-dependent external perturbation $v(\mathbf{r}, t)$ is applied and propagated through the time-dependent Hamiltonian, the evolved wave function $\Psi(t)$ can be obtained at an ulterior time $t > t_0$. From this wave function, the time-dependent density $n(\mathbf{r}, t)$ can be calculated by applying the density operator. For a given $\Psi(t_0)$, there is thus a mapping $v(\mathbf{r}, t) \rightarrow n(\mathbf{r}, t)$, from the time-dependent potential to the time-dependent density.

The first Hohenberg-Kohn theorem states the invertibility of this mapping in the time-independent case and gives the formal foundations for density-functional theory. The analog of this theorem for time-dependent potential and density is the Runge-Gross theorem [11] which proves the existence of the reverse mapping.

Theorem 3 (Runge-Gross theorem). For a system of N interacting electrons, the densities $n(\mathbf{r}, t)$ and $n'(\mathbf{r}, t)$ evolving from a common initial state $\Psi_0 = \Psi(t_0)$ under the influence of two external time-dependent potentials $v(\mathbf{r}, t)$ and $v'(\mathbf{r}, t)$, are always different provided that the potentials differ by more than an additive spatially constant time-dependent function $c(t)$.

This theorem applies to potentials that are Taylor expandable about the initial time $t = t_0$, where t_0 is assumed to be finite, i.e.

$$v(\mathbf{r}, t) = \sum_{k=0}^{\infty} \frac{v^{(k)}(\mathbf{r})}{k!} (t - t_0)^k. \quad (5.8)$$

For such potentials, it provides a one-to-one mapping between the densities and the potentials. It thus allows one to express the time-dependent potential as a functional of the time-dependent density and of the initial state

$$v(\mathbf{r}, t) = v[n, \Psi_0](\mathbf{r}, t). \quad (5.9)$$

Moreover, if the initial wave function is the ground-state one then the first HK theorem states that it is also a functional of the ground-state density and the initial state dependence can therefore be dropped. The wave function $\Psi(t)$ is then determined up to a phase factor by n alone. The time-dependent Hamiltonian can then be written as a density functional, and the expectation value of a given operator $\hat{\mathcal{P}}$ is given by a unique functional of the density as the ambiguity in the phase of the wave function cancels out

$$\langle \Psi[n](t) | \hat{\mathcal{P}} | \Psi[n](t) \rangle = \mathcal{P}[n](t). \quad (5.10)$$

Some questions remain however unanswered by this theorem. For instance, it does not provide a way to treat potentials which are switched on adiabatically at $t_0 = -\infty$ [12] as

the Taylor expandability of these potentials about $t_0 = -\infty$ is not ensured anymore. The question of v -representability for time-dependent densities is also not dealt with. Van Leeuwen theorem [13–16] solves this issue in the case of a Kohn-Sham system. It relies on Taylor-expandable time-dependent densities and provides a formal framework for the time-dependent Kohn-Sham formalism. The Runge-Gross theorem of TDDFT has been proved for finite systems, where the density vanishes at infinity [15, 16]. However, it does not apply when a uniform homogeneous field acts on a periodic system [17]. This limitation of the Runge-Gross theorem can however be circumvented by using time-dependent current density-functional theory which also allows for the treatment of magnetic fields [17].

5.3.2 Variational principle

The time-dependent analog of the variational principle given by the second HK theorem is provided by a stationary condition on the quantum mechanical action integral. The solution of the time-dependent Schrödinger equation with the initial condition $\Psi(t_0) = \Psi_0$ corresponds to a stationary point of the action which is a density functional thanks to the Runge-Gross theorem

$$\mathcal{A}[n] = \int_{t_0}^{t_1} \langle \Psi[n](t) | i \frac{\partial}{\partial t} - \hat{H}(t) | \Psi[n](t) \rangle dt, \quad (5.11)$$

and can be rewritten as

$$\mathcal{A}[n] = \mathcal{B}[n] - \int_{t_0}^{t_1} \int v(\mathbf{r}, t) n(\mathbf{r}, t) d\mathbf{r} dt, \quad (5.12)$$

where the internal action \mathcal{B} is universal as it is independent of the external potential v . The correct density should then be obtained by applying the Dirac-Frenkel variational principle and solving the Euler equation

$$\frac{\delta \mathcal{A}[n]}{\delta n(\mathbf{r}, t)} = 0 \quad (5.13)$$

with appropriate boundary conditions. The potential would then be given by

$$v(\mathbf{r}, t) = \frac{\delta \mathcal{B}[n]}{\delta n(\mathbf{r}, t)}. \quad (5.14)$$

This implies that the external potential, which is a functional of the density from the Runge-Gross theorem, is the functional derivative of the internal action \mathcal{B} with respect to the density. However, this definition is problematic as it leads to a causality paradox [2] when calculating the response of a system to an external perturbation. In fact, it can be shown that the second derivative of the action with respect to density $\delta^2 \mathcal{A} / \delta n(\mathbf{r}, t) \delta n(\mathbf{r}', t')$ can be related to the response of the system. This derivative however is symmetric by the interchange of the time variables while the system should not respond to a perturbation

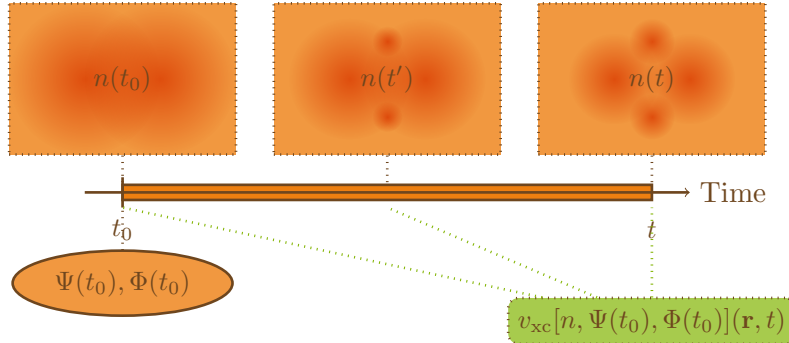


Figure 5.1 – The exchange-correlation potential at time t depends on all the densities at times $t_0 \leq t' \leq t$ and on the initial interacting and Kohn-Sham states. If the initial states are the ground states, then their dependence is included in the density dependence due to the HK theorems and can be omitted.

before it has actually happened. The problem arises from the fact that the Frenkel variational principle is valid only for variations of $|\Psi\rangle$ that vanish at the end points of the time interval under consideration. Several solutions were proposed to circumvent this paradox, the most famous being van Leeuwen’s Keldysh action [18, 19] and Vignale’s real-time resolution [20, 21]. As in this thesis TDDFT will be only applied within an adiabatic approximation discussed in Section 5.6.2, we will not explore this aspect of the theory any deeper.

5.3.3 Kohn-Sham approach

The Kohn-Sham scheme provides a very successful framework when time-independent calculations are concerned (cf. Section 1.5) and its time-dependent formulation is very similar. The one-to-one mapping between the time-dependent densities and potentials given by the Runge-Gross theorem is valid for any interaction and in particular in the case of non-interacting electrons. Therefore the exact time-dependent density can be reproduced by a system of N non-interacting electrons moving in a time-dependent effective potential $v^{\text{KS}}[n](t)$ which is uniquely determined. However, the Runge-Gross theorem ensures only the uniqueness of v^{KS} for all the v -representable densities but not its existence for an arbitrary time-dependent density $n(\mathbf{r}, t)$. Assuming the existence of such a potential, the time-dependent density is then given by

$$n(\mathbf{r}, t) = \sum_i |\varphi_i(\mathbf{r}, t)|^2 \quad (5.15)$$

where the time-dependent one-particle Kohn-Sham orbitals $\varphi_i(\mathbf{r}, t)$ are solutions of the set of time-dependent Kohn-Sham equations

$$i\frac{\partial}{\partial t}\varphi_i(\mathbf{r}, t) = \left[-\frac{\nabla^2}{2} + v^{\text{KS}}[n](\mathbf{r}, t)\right]\varphi_i(\mathbf{r}, t). \quad (5.16)$$

The time-dependent Kohn-Sham potential can be decomposed analogously to its time-independent counterpart into its external, Hartree, exchange and correlation parts, as

$$\begin{aligned} v^{\text{KS}}[n](\mathbf{r}, t) &= v[n](\mathbf{r}, t) + v_{\text{Hxc}}[n](\mathbf{r}, t) \\ &= v[n](\mathbf{r}, t) + v_{\text{H}}[n](\mathbf{r}, t) + v_{\text{x}}[n](\mathbf{r}, t) + v_{\text{c}}[n](\mathbf{r}, t), \end{aligned} \quad (5.17)$$

where the Hartree potential is given by

$$v_{\text{H}}[n](\mathbf{r}, t) = \int \frac{n(\mathbf{r}', t)}{|\mathbf{r} - \mathbf{r}'|} d\mathbf{r}', \quad (5.18)$$

and the exchange-correlation potential is unknown. In principle, this potential is a functional of the entire history of densities, and of the initial many-body and Kohn-Sham wave functions $\Psi(t_0)$ and $\Phi(t_0)$, as illustrated in Figure 5.1. If the initial state $\Psi(t_0)$ is the ground state, then the dependence $\Psi(t_0)$ and $\Phi(t_0)$ is embedded in the density dependence which allows us to write the potential as a functional of the time-dependent density only.

The history dependence of the time-dependent exchange-correlation potential increases greatly the complexity with respect to the time-independent case as the potential cannot even be related to the energy functional anymore. Therefore, even if the exact ground-state functional were known, the time-dependent potential would remain unknown.

5.4 Linear-response TDDFT

5.4.1 Linear-response theory

In usual absorption spectroscopy, one is interested to the response of the system (usually in its ground state) to a weak electromagnetic field. As the strength of the field is small, the exchange-correlation potential needs to be calculated only in the vicinity of the ground state and the well-known Rayleigh-Schrödinger perturbation theory can be used to calculate the response of the system and extract its excitation energies. On the other hand, if the strength of the laser field is of the same order of magnitude or greater than the potential due to the nuclei, then perturbation theory no longer applies and one falls into the field of real-time dynamics in non-perturbative fields. However, in this thesis, only the linear-response regime is considered. The derivation of the linear-response equations is done in the spin formalism. The conventions used for Fourier transforms can be found in Appendix A.2 together with a brief review of contour integration in the

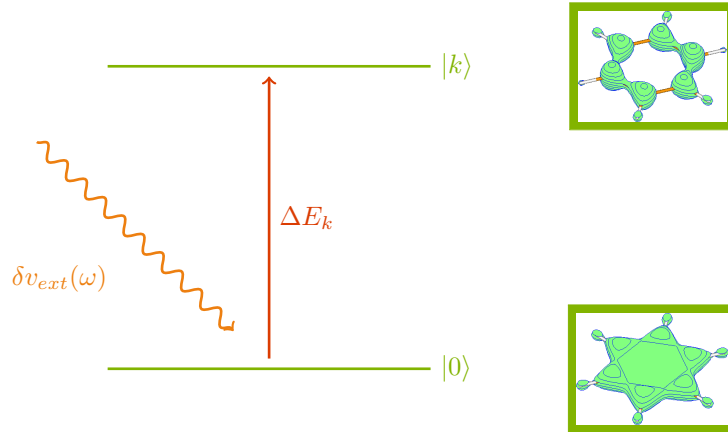


Figure 5.2 – Schematic representation of the density response of the benzene molecule to an external perturbation $\delta v(\omega)$.

framework of complex analysis.

Assume a system in its ground-state, with the spin densities $n_0(\mathbf{x})$. A real time-dependent external perturbation δv is switched on at time $t = t_0$, such that

$$v(\mathbf{x}, t) = \begin{cases} v(\mathbf{x}) & t \leq t_0 \\ v(\mathbf{x}) + \delta v(\mathbf{x}, t) & t > t_0. \end{cases} \quad (5.19)$$

This potential is related to its Fourier transform by

$$\delta v(\mathbf{x}, t) = \int \frac{d\omega}{2\pi} \delta v(\mathbf{x}, \omega) e^{-i\omega t}. \quad (5.20)$$

In particular, as $\delta v(\mathbf{x}, t)$ is real, its Fourier transform must satisfy the relation $\delta v(\mathbf{x}, \omega) = \delta v^*(\mathbf{x}, -\omega)$. When subject to such a perturbation, the system experiences some small time-dependent changes. In particular, the density becomes time dependent and can be expanded in order of perturbation as

$$n(\mathbf{x}, t) = n_0(\mathbf{x}) + n_1(\mathbf{x}, t) + n_2(\mathbf{x}, t) + \dots \quad (5.21)$$

where $n_0(\mathbf{x})$ is the initial time-independent density, $n_1(\mathbf{x}, t)$ is the first-order density, $n_2(\mathbf{x}, t)$ is the second-order one, etc. When the perturbation is small enough, the first order is then assumed to dominate. In linear-response theory, the change of density is therefore calculated up to the first order only

$$\delta n(\mathbf{x}, t) = n_1(\mathbf{x}, t). \quad (5.22)$$

The change in density in one spin-space point \mathbf{x} is not only due to the perturbation at this point but is the result of the perturbation on the whole system. How this perturbation is

propagated in time and space through the system is described by the retarded response function $\chi(\mathbf{x}, \mathbf{x}', t - t')$ such that the change of density is then given by

$$\delta n(\mathbf{x}, t) = \int_{t_0}^t \int \chi(\mathbf{x}, \mathbf{x}', t - t') \delta v(\mathbf{x}', t') d\mathbf{x}' dt', \quad (5.23)$$

where the response function depends only on the time difference because of time translation invariance. For excitation energy calculations, one is usually more interested by the frequency-dependent response function than the time-dependent one

$$\delta n(\mathbf{x}, \omega) = \int \chi(\mathbf{x}, \mathbf{x}', \omega) \delta v(\mathbf{x}', \omega) d\mathbf{x}', \quad (5.24)$$

where the explicit expressions of the Fourier transforms are given in the next section. The response function is therefore formally defined as the functional derivative of the density with respect to the external field evaluated at the external potential

$$\chi(\mathbf{x}, \mathbf{x}', \omega) = \left. \frac{\delta n(\mathbf{x}, \omega)}{\delta v(\mathbf{x}', \omega)} \right|_{v[n_0]}. \quad (5.25)$$

Before deriving the expression of this response function, some insights on its physical interpretation and how excitation energies can be extracted from it might be worth mentioning.

Suppose that the system is originally in its non-degenerate ground-state. Depending on the frequency of the perturbation, two cases can occur:

- either the frequency does not match any energy difference between an excited state and the ground state, then the change in density remains infinitesimal and the response function is finite;
- or the frequency matches an excitation energy from the ground state, then the system can change state and the change of density is important. This implies that the response function diverges for this frequency, i.e. it has a pole at this value of ω .

The basic idea of time-dependent linear-response density-functional theory is therefore to find the poles of the response function of the system to obtain the excitation energies, or equivalently to find the zeros of the inverse response function

$$\chi^{-1}(\mathbf{x}, \mathbf{x}', \omega) = \left. \frac{\delta v(\mathbf{x}, \omega)}{\delta n(\mathbf{x}', \omega)} \right|_{n_0}. \quad (5.26)$$

Expression of the linear response function

The initial Hamiltonian \hat{H} has eigenvectors $|k\rangle$ and eigenvalues E_k . In absence of any perturbation, these eigenstates evolve in time by a phase transformation depending on their energy, and at given time t , their expression is $|k(t)\rangle = e^{-iE_k t} |k\rangle$.

The time evolution of a state vector $|\Psi(t)\rangle$ of the time-dependent Hamiltonian $\hat{H}(t)$ can be given by a linear combination of the time-evolved unperturbed eigenvectors $|k(t)\rangle$

$$|\Psi(t)\rangle = \sum_k c_k(t)|k(t)\rangle = \sum_k c_k(t)e^{-iE_k t}|k\rangle. \quad (5.27)$$

The evolution of the coefficients $c_k(t)$ is obtained from the time-dependent Schrödinger equation (5.1) such that

$$c_k(t) = c_k(t_0) - i \sum_n \int_{t_0}^t \langle k|\delta\hat{V}(t')|n\rangle e^{-i(E_n - E_k)t'} c_n(t') dt'. \quad (5.28)$$

For an adiabatically switched potential at $t_0 \rightarrow -\infty$, the first-order corrections to the coefficients when the initial conditions are $c_0(t_0) = 1$ and $\forall k \neq 0, c_k(t_0) = 0$ are then given by

$$c_k^{(1)}(t) = -i \int_{-\infty}^t \langle k|\delta\hat{V}(t')|0\rangle e^{-i(E_0 - E_k)t'} dt', \quad k \neq 0. \quad (5.29)$$

The first-order expansion of the wave function at time t is given by $|\Psi(t)\rangle = |0(t)\rangle + |\Psi^{(1)}(t)\rangle$, where $|\Psi^{(1)}(t)\rangle = \sum_{k \neq 0} c_k^{(1)}(t)|k(t)\rangle$. The first-order change of the density is therefore

$$\delta n(\mathbf{x}, t) = \langle 0(t)|\hat{n}(\mathbf{x})|\Psi^{(1)}(t)\rangle + \langle \Psi^{(1)}(t)|\hat{n}(\mathbf{x})|0(t)\rangle. \quad (5.30)$$

Substituting the expression of the wave-function with its first-order coefficients, we get

$$\delta n(\mathbf{x}, t) = -i \int_{-\infty}^t \int \sum_{k \neq 0} \langle 0|\hat{n}(\mathbf{x})|k\rangle \langle k|\hat{n}(\mathbf{x}')|0\rangle e^{-i(E_k - E_0)(t-t')} \delta v(\mathbf{x}', t') dt' d\mathbf{x}' + \text{c.c.} \quad (5.31)$$

where c.c. stands for the complex conjugate. The upper bound of the integration can be extended to $+\infty$ by introduction of an Heaviside step function $\theta(t - t')$. The first-order change in density is then

$$\delta n(\mathbf{x}, t) = -i \iint \theta(t - t') \sum_{k \neq 0} \langle 0|\hat{n}(\mathbf{x})|k\rangle \langle k|\hat{n}(\mathbf{x}')|0\rangle e^{-i(E_k - E_0)(t-t')} \delta v(\mathbf{x}', t') dt' d\mathbf{x}' + \text{c.c.} \quad (5.32)$$

The Fourier transform of the first-order density is then

$$\delta n(\mathbf{x}, \omega) = \int \sum_{k \neq 0} \left[\frac{\langle 0|\hat{n}(\mathbf{x})|k\rangle \langle k|\hat{n}(\mathbf{x}')|0\rangle}{\omega - (E_k - E_0) + i0^+} - \frac{\langle 0|\hat{n}(\mathbf{x}')|k\rangle \langle k|\hat{n}(\mathbf{x})|0\rangle}{\omega + (E_k - E_0) + i0^+} \right] \delta v(\mathbf{x}', \omega) d\mathbf{x}'. \quad (5.33)$$

With the definition of the response function given in Equation (5.24) the Fourier-transformed linear response function is therefore

$$\chi(\mathbf{x}, \mathbf{x}', \omega) = \sum_{k \neq 0} \frac{\langle 0|\hat{n}(\mathbf{x})|k\rangle \langle k|\hat{n}(\mathbf{x}')|0\rangle}{\omega - (E_k - E_0) + i0^+} - \frac{\langle 0|\hat{n}(\mathbf{x}')|k\rangle \langle k|\hat{n}(\mathbf{x})|0\rangle}{\omega + (E_k - E_0) + i0^+}. \quad (5.34)$$

This function admits poles at the excitation energies $\omega_k = E_k - E_0$ and at the deexcitation energies $-\omega_k$. Therefore, assuming its invertibility, solving the equation $\chi^{-1}(\omega) = 0$ allows one to extract the excitation energies from the retarded response function.

5.4.2 Kohn-Sham response function

Within the Kohn-Sham framework, the external potential can be rewritten as the difference between the Kohn-Sham potential and the Hartree-exchange-correlation potential, which in the frequency space gives $v[n](\mathbf{x}, \omega) = v^{\text{KS}}[n](\mathbf{x}, \omega) - v_{\text{Hxc}}[n](\mathbf{x}, \omega)$. Using this decomposition in the expression of the inverse response function in Eq. (5.26), it gives

$$\begin{aligned} \chi^{-1}(\mathbf{x}, \mathbf{x}', \omega) &= \left. \frac{\delta v^{\text{KS}}[n](\mathbf{x}, \omega)}{\delta n(\mathbf{x}', \omega)} \right|_{n_0} - \left. \frac{\delta v_{\text{Hxc}}[n](\mathbf{x}, \omega)}{\delta n(\mathbf{x}', \omega)} \right|_{n_0} \\ &= \chi_{\text{KS}}^{-1}(\mathbf{x}, \mathbf{x}', \omega) - f_{\text{Hxc}}(\mathbf{x}, \mathbf{x}', \omega). \end{aligned} \quad (5.35)$$

The first part of the right hand side is the inverse of the Kohn-Sham response function $\chi_{\text{KS}}(\mathbf{x}, \mathbf{x}', \omega)$ which describe the response of the non-interacting electrons. As the states are single Slater determinants, its expression in the KS spin-orbital basis reduces to

$$\chi_{\text{KS}}(\mathbf{x}, \mathbf{x}', \omega) = \sum_{i,a} \left[\frac{\varphi_i^*(\mathbf{x})\varphi_a(\mathbf{x})\varphi_i(\mathbf{x}')\varphi_a^*(\mathbf{x}')}{\omega - (\varepsilon_a - \varepsilon_i) + i0^+} - \frac{\varphi_i(\mathbf{x})\varphi_a^*(\mathbf{x})\varphi_i^*(\mathbf{x}')\varphi_a(\mathbf{x}')}{\omega + (\varepsilon_a - \varepsilon_i) + i0^+} \right]. \quad (5.36)$$

The second part of the right hand side defines the Hartree-exchange-correlation kernel

$$f_{\text{Hxc}}(\mathbf{x}, \mathbf{x}', \omega) = \left. \frac{\delta v_{\text{Hxc}}[n](\mathbf{x}, \omega)}{\delta n(\mathbf{x}', \omega)} \right|_{n_0}, \quad (5.37)$$

which is in principle dependent of the spin densities, the initial states, two spin-space coordinates and the frequency and should describe all the effects due to the electronic interaction. This kernel is formally defined as the functional derivative of the frequency-dependent Hartree-exchange-correlation potential with respect to the time-dependent spin densities, evaluated at the ground-state spin densities. The zeros of χ^{-1} in Equation (5.35) give the excitation energies of the real system which are constructed from the excitation energies of the Kohn-Sham system corresponding to the poles of the Kohn-Sham response function corrected by the Hartree-exchange-correlation kernel. The Kohn-Sham response function is known, but one still need to deal with the Hartree-exchange-correlation kernel and time-dependent potential.

5.5 Resolution for a finite molecular system

5.5.1 Projection in a spin-orbital basis set

In a finite system framework, it is useful to reformulate this problem in a matrix form [1]. Consider the spin-orbital products $g_{ia}(\mathbf{x}_1, \mathbf{x}'_1) = \varphi_i^*(\mathbf{x}'_1)\varphi_a(\mathbf{x}_1)$ and $g_{ai}(\mathbf{x}_1, \mathbf{x}'_1) =$

$\varphi_a^*(\mathbf{x}'_1)\varphi_i(\mathbf{x}_1)$ which can be seen as excitation and de-excitation between φ_i and φ_a . They form a complete orthogonal basis with respect to the scalar product

$$\langle g_{pq}|g_{rs}\rangle = \int \varphi_p(\mathbf{x}'_1)\varphi_q^*(\mathbf{x}_1)\varphi_r^*(\mathbf{x}'_1)\varphi_s(\mathbf{x}_1)d\mathbf{x}_1d\mathbf{x}'_1 = \delta_{pr}\delta_{qs}. \quad (5.38)$$

In this basis, the Kohn-Sham response function can be rewritten as

$$\chi_{\text{KS}}(\mathbf{x}, \mathbf{x}', \omega) = \sum_{i,a} \left[\frac{g_{ia}(\mathbf{x}, \mathbf{x}')g_{ia}^*(\mathbf{x}', \mathbf{x})}{\omega - (\varepsilon_a - \varepsilon_i) + i0^+} - \frac{g_{ai}(\mathbf{x}, \mathbf{x}')g_{ai}^*(\mathbf{x}', \mathbf{x})}{\omega + (\varepsilon_a - \varepsilon_i) + i0^+} \right], \quad (5.39)$$

and can be represented by a diagonal matrix $\chi_{\text{KS}}(\omega)$ whose inverse is given by

$$\chi_{\text{KS}}^{-1}(\omega) = - \left[\begin{pmatrix} \Delta\varepsilon & 0 \\ 0 & \Delta\varepsilon \end{pmatrix} - \omega \begin{pmatrix} \mathbf{1} & 0 \\ 0 & -\mathbf{1} \end{pmatrix} \right], \quad (5.40)$$

with the first block corresponding to the g_{ia} functions and the second to the g_{ai} functions, and $\Delta\varepsilon_{ia,jb} = (\varepsilon_a - \varepsilon_i)\delta_{ij}\delta_{ab}$. To obtain the inverse response function of the real system, the contribution of the Hartree-exchange-correlation kernel is added via the coupling matrix \mathbf{K} whose matrix elements are obtained by projection of the kernel on the product basis

$$K_{ia,jb}(\omega) = \iint \varphi_i^*(\mathbf{x}_1)\varphi_a(\mathbf{x}_1)f_{\text{Hxc}}(\mathbf{x}_1, \mathbf{x}_2, \omega)\varphi_j(\mathbf{x}_2)\varphi_b^*(\mathbf{x}_2)d\mathbf{x}_1d\mathbf{x}_2 = \langle ib|f_{\text{Hxc}}(\omega)|aj\rangle. \quad (5.41)$$

As the potential is real-valued, it is straightforward to show that so is the kernel. In particular, this implies that

$$K_{ia,jb}(\omega) = K_{ai,bj}(-\omega)^*. \quad (5.42)$$

Using this relation, the matrix representation of the inverse response function is

$$\begin{aligned} \chi^{-1}(\omega) &= - \left[\begin{pmatrix} \mathbf{A}(\omega) & \mathbf{B}(\omega) \\ \mathbf{B}(-\omega)^* & \mathbf{A}(-\omega)^* \end{pmatrix} - \omega \begin{pmatrix} \mathbf{1} & 0 \\ 0 & -\mathbf{1} \end{pmatrix} \right] \\ &= - (\mathbf{A}(\omega) - \omega\mathbf{\Delta}), \end{aligned} \quad (5.43)$$

with $A_{ia,jb}(\omega) = (\varepsilon_a - \varepsilon_i)\delta_{ij}\delta_{ab} + K_{ia,jb}(\omega)$ and $B_{ia,jb}(\omega) = K_{ia,bj}(\omega)$. The name of the matrices \mathbf{A} and \mathbf{B} are inherited from the random phase approximation (RPA) theory also called time-dependent Hartree-Fock (TDHF). However, the presence of the exchange-correlation kernel $f_{\text{xc}}(\omega)$ changes significantly the problem as the matrix \mathbf{A} and \mathbf{B} are then frequency dependent. This forms therefore a non-linear problem where the number of solutions is greater than the size of the matrix. This is of crucial importance for the treatment of multiple excitations which is not possible otherwise. The zeros of Equation (5.43) are then obtained by solving the equation

$$\begin{pmatrix} \mathbf{A}(\omega) & \mathbf{B}(\omega) \\ \mathbf{B}(-\omega)^* & \mathbf{A}(-\omega)^* \end{pmatrix} \begin{pmatrix} \mathbf{X}(\omega) \\ \mathbf{Y}(\omega) \end{pmatrix} = \omega \begin{pmatrix} \mathbf{1} & 0 \\ 0 & -\mathbf{1} \end{pmatrix} \begin{pmatrix} \mathbf{X}(\omega) \\ \mathbf{Y}(\omega) \end{pmatrix}. \quad (5.44)$$

Finding the spectral decomposition of $\chi^{-1}(\omega)$ reduces therefore to solving the system

$$\begin{cases} \mathbf{A}(\omega)\mathbf{X}(\omega) + \mathbf{B}(\omega)\mathbf{Y}(\omega) = \omega\mathbf{X}(\omega) \\ \mathbf{B}(-\omega)^*\mathbf{X}(\omega) + \mathbf{A}(-\omega)^*\mathbf{Y}(\omega) = -\omega\mathbf{Y}(\omega), \end{cases} \quad (5.45)$$

which is invariant by conjugation and the transformation

$$\{\omega \rightarrow -\omega \quad ; \quad \mathbf{X}(\omega) \rightarrow \mathbf{Y}(-\omega)^* \quad ; \quad \mathbf{Y}(\omega) \rightarrow \mathbf{X}(-\omega)^*\}. \quad (5.46)$$

Its solutions thus come by pairs: the excitation energy ω_n associated with the eigenvector $(\mathbf{X}_n, \mathbf{Y}_n)$, and the deexcitation energy $-\omega_n$ associated with $(\mathbf{X}_{-n}, \mathbf{Y}_{-n})$. In practice, these equations should be solved self-consistently for each ω_n . When convergence is reached, each matrix $\mathbf{A}(\omega_n)$ has a set of eigenvalues and eigenvectors $\{\omega_k, (\mathbf{X}_k(\omega_n), \mathbf{Y}_k(\omega_n))\}$ such that it exists one k which satisfies $\omega_k = \omega_n$. The associated eigenvector $(\mathbf{X}_k(\omega_n), \mathbf{Y}_k(\omega_n))$ then defines $(\mathbf{X}_n, \mathbf{Y}_n)$. The eigenvector associated to the deexcitation energies $(\mathbf{X}_{-n}, \mathbf{Y}_{-n})$ is then obtained as $(\mathbf{Y}_n^*, \mathbf{X}_n^*)$.

5.5.2 Resolution for real orbitals

If the KS orbitals are real, the system of Equations (5.45) can be further reduced as $\mathbf{A}(-\omega)^* = \mathbf{A}(\omega)$ and $\mathbf{B}(-\omega)^* = \mathbf{B}(\omega)$. By addition and subtraction of its two equations, it can thus be rewritten as

$$\begin{cases} (\mathbf{A}(\omega) + \mathbf{B}(\omega))(\mathbf{X}(\omega) + \mathbf{Y}(\omega)) = \omega(\mathbf{X}(\omega) - \mathbf{Y}(\omega)) \\ (\mathbf{A}(\omega) - \mathbf{B}(\omega))(\mathbf{X}(\omega) - \mathbf{Y}(\omega)) = \omega(\mathbf{X}(\omega) + \mathbf{Y}(\omega)). \end{cases} \quad (5.47)$$

Moreover, if the matrix $(\mathbf{A}(\omega) - \mathbf{B}(\omega))$ is definite positive then

$$(\mathbf{A}(\omega) + \mathbf{B}(\omega))(\mathbf{X}(\omega) + \mathbf{Y}(\omega)) = \omega^2(\mathbf{A}(\omega) - \mathbf{B}(\omega))^{-1}(\mathbf{X}(\omega) + \mathbf{Y}(\omega)), \quad (5.48)$$

so that Equation (5.44) can conveniently be transformed into a half-size symmetric eigenvalue equation [1], although still non linear

$$\mathbf{M}(\omega)\mathbf{Z}(\omega) = \omega^2\mathbf{Z}(\omega), \quad (5.49)$$

with $\mathbf{M}(\omega) = (\mathbf{A}(\omega) - \mathbf{B}(\omega))^{1/2}(\mathbf{A}(\omega) + \mathbf{B}(\omega))(\mathbf{A}(\omega) - \mathbf{B}(\omega))^{1/2}$, and the normalized eigenvector $\mathbf{Z}(\omega) = \sqrt{\omega}(\mathbf{A}(\omega) - \mathbf{B}(\omega))^{-1/2}(\mathbf{X}(\omega) + \mathbf{Y}(\omega))$. Within this scheme, the vectors $\mathbf{X}(\omega)$ and $\mathbf{Y}(\omega)$ are not computed separately but as shown in the next section, their sum is in fact sufficient to calculate the relevant properties.

For the excitation and deexcitation energies to be real, the matrix \mathbf{M} needs to be definite positive which is the case if the two stability conditions, $(\mathbf{A}(\omega) + \mathbf{B}(\omega))$ and $(\mathbf{A}(\omega) - \mathbf{B}(\omega))$ definite positive, are satisfied.

5.5.3 Polarizability and oscillator strengths

The mean dynamic dipole polarizability $\bar{\alpha}(\omega)$ can be expressed using the sum-over-state theorem [1] of optical physics by

$$\bar{\alpha}(\omega) = \sum_{n \neq 0} \frac{f_n}{\omega_n^2 - \omega^2} \quad (5.50)$$

where f_n is the oscillator strength associated with the excited state Ψ_n and the excitation energy ω_n . It is given by the average of the diagonal elements of the polarizability tensor $\alpha(\omega)$ by $\bar{\alpha}(\omega) = \frac{1}{3} (\alpha_{xx}(\omega) + \alpha_{yy}(\omega) + \alpha_{zz}(\omega))$, where the qq component of the tensor is given by

$$\alpha_{qq}(\omega) = - \int \chi(\mathbf{r}, \mathbf{r}', \omega) r_q r'_q d\mathbf{r} d\mathbf{r}'. \quad (5.51)$$

Using the spectral decomposition of the response function for real KS orbitals, this element can be rewritten as

$$\alpha_{qq}(\omega) = \sum_n \sum_{ia, jb} \frac{2\omega_n \langle \varphi_i | \hat{q} | \varphi_a \rangle \langle \varphi_j | \hat{q} | \varphi_b \rangle (\mathbf{X}_n + \mathbf{Y}_n)_{ia} (\mathbf{X}_n + \mathbf{Y}_n)_{jb}}{\omega_n^2 - \omega^2}. \quad (5.52)$$

By identification in Equation (5.50), the oscillator strengths are then given by

$$f_n = \frac{2}{3} \sum_q \left(\sum_{ia} \langle \varphi_i | \hat{q} | \varphi_a \rangle (\mathbf{X}_n + \mathbf{Y}_n)_{ia} \right)^2 \omega_n. \quad (5.53)$$

In particular, they should fulfill the Thomas-Reiche-Kuhn (TRK) sum rule $\sum_n f_n = N$. They can be expressed in function of the transition moment thanks to Fermi golden rule

$$f_n = \frac{2}{3} \sum_q |\langle \Psi_0 | \hat{q} | \Psi_n \rangle|^2 \omega_n, \quad (5.54)$$

where the transition moments are

$$\langle \Psi_0 | \hat{q} | \Psi_n \rangle = \sum_{ia} \langle \varphi_i | \hat{q} | \varphi_a \rangle (\mathbf{X}_n + \mathbf{Y}_n)_{ia}. \quad (5.55)$$

5.6 Usual approximations

5.6.1 Tamm-Dancoff approximation

The Tamm-Dancoff approximation (TDA) [22] consists in neglecting the coupling between the excitations and the de-excitations, i.e. setting $\mathbf{B} = \mathbf{0}$ so that the TDDFT equations simply reduces to

$$\mathbf{A}(\omega_n) \mathbf{X}_n = \omega_n \mathbf{X}_n. \quad (5.56)$$

This approximation often helps to correct the deficiencies which are introduced by the approximations made on the exchange-correlation kernel. It therefore often gives bet-

ter excitation energies despite the fact that the sum rule is no longer satisfied. It is particularly efficient when a triplet instability arises [23]. We note in passing, that TDA can also be viewed as a non-self-consistent approximation to the static (multiplet-sum) Δ SCF method, which identifies the excited states with stationary points on the ground-state energy surface as a function of the orbital parameters [24, 25].

5.6.2 Adiabatic approximation

As shown in Section 5.3.3, the time-dependent exchange-correlation potential $v_{xc}[n](\mathbf{x}, t)$ depends, in principle, on densities everywhere in space and at all previous times $t' \leq t$. In order to provide a practical scheme for TDDFT calculations, the most widely used approximation is the *adiabatic approximation* where the potential is approximated to the ground-state potential evaluated at the instantaneous time-dependent density [1, 26]

$$v_{xc}[n](\mathbf{x}, t) \simeq v_{xc}[n(t)](\mathbf{x}). \quad (5.57)$$

and therefore is related to the exchange-correlation functional E_{xc} by

$$v_{xc}[n(t)](\mathbf{x}) = \left. \frac{\delta E_{xc}[n]}{\delta n(\mathbf{x}, t)} \right|_{n(\mathbf{x}, t)}. \quad (5.58)$$

The exchange-correlation kernel can thus be expressed as the second derivative of the energy with respect to the density as

$$f_{xc}(\mathbf{x}, \mathbf{x}', t, t') \simeq \delta(t - t') \left. \frac{\delta v_{xc}[n(t)](\mathbf{x})}{\delta n(\mathbf{x}', t)} \right|_{n_0} = \delta(t - t') \left. \frac{\delta^2 E_{xc}[n(t)]}{\delta n(\mathbf{x}, t) \delta n(\mathbf{x}', t)} \right|_{n_0}, \quad (5.59)$$

where the locality in time becomes even more obvious. The Fourier transform of the adiabatic exchange-correlation kernel is thus frequency independent and so are the matrices \mathbf{A} and \mathbf{B} . Equation (5.44) then turns into a linear problem

$$\begin{pmatrix} \mathbf{A} & \mathbf{B} \\ \mathbf{B}^* & \mathbf{A}^* \end{pmatrix} \begin{pmatrix} \mathbf{X}_n \\ \mathbf{Y}_n \end{pmatrix} = \omega_n \begin{pmatrix} \mathbf{1} & \mathbf{0} \\ \mathbf{0} & -\mathbf{1} \end{pmatrix} \begin{pmatrix} \mathbf{X}_n \\ \mathbf{Y}_n \end{pmatrix}. \quad (5.60)$$

Pseudo-hermiticity

Equation (5.60) can be reformulated as a pseudo-hermitian problem $\mathbf{\Delta}^{-1} \mathbf{\Lambda} \mathbf{C}_n = \omega_n \mathbf{C}_n$, where

$$\mathbf{\Lambda} = \begin{pmatrix} \mathbf{A} & \mathbf{B} \\ \mathbf{B}^* & \mathbf{A}^* \end{pmatrix} \quad \text{and} \quad \mathbf{\Delta} = \begin{pmatrix} \mathbf{1} & \mathbf{0} \\ \mathbf{0} & -\mathbf{1} \end{pmatrix}. \quad (5.61)$$

As \mathbf{A} is hermitian and \mathbf{B} is symmetric, the matrix $\mathbf{\Lambda}$ is hermitian, and so is $\mathbf{\Delta}$.

Definition (Pseudo-hermiticity). A matrix $\mathbf{\Pi}$ is said to be *pseudo-Hermitian* with respect to an invertible matrix \mathbf{Q} if and only if $\mathbf{\Pi}^\dagger = \mathbf{Q} \mathbf{\Pi} \mathbf{Q}^{-1}$.

Let $\mathbf{P} = \mathbf{\Delta}^{-1}\mathbf{\Lambda}$. It is easy to show that \mathbf{P} is pseudo-Hermitian with respect to $\mathbf{\Lambda}$

$$\mathbf{\Lambda}\mathbf{P}\mathbf{\Lambda}^{-1} = \mathbf{\Lambda}\mathbf{\Delta}^{-1}\mathbf{\Lambda}\mathbf{\Lambda}^{-1} = \mathbf{\Lambda}\mathbf{\Delta}^{-1} = (\mathbf{\Delta}^{-1}\mathbf{\Lambda})^\dagger = \mathbf{P}^\dagger. \quad (5.62)$$

Using this relation, if $\mathbf{\Lambda}$ is definite positive then we can define the pseudo-hermitian matrix $\mathbf{\Omega} = \mathbf{\Lambda}^{-1/2}\mathbf{P}^\dagger\mathbf{\Lambda}^{1/2}$ which is similar to \mathbf{P}

$$\mathbf{P} = \mathbf{\Lambda}^{-1}\mathbf{P}^\dagger\mathbf{\Lambda} = \mathbf{\Lambda}^{-1/2}\mathbf{\Omega}\mathbf{\Lambda}^{1/2}. \quad (5.63)$$

Consequently, as $\mathbf{\Omega}$ has real eigenvalues due to its hermiticity, so has \mathbf{P} . In other words, it means that the excitation and de-excitation energies are real if $\mathbf{\Lambda}$ is definite positive.

5.6.3 Adiabatic local-density approximation

Even if the adiabatic approximation already simplifies greatly the determination of the exchange-correlation kernel, further approximations are still required as it was the case for ground-state DFT. If the local-density approximation is used for the ground-state functional, this then gives rise the adiabatic local-density approximation (ALDA) where the kernel is not only local in time but also in space

$$f_{\text{Hxc}}(\mathbf{x}, \mathbf{x}', \omega) \xrightarrow[\text{Approx.}]{\text{Adiabatic}} f_{\text{Hxc}}(\mathbf{x}, \mathbf{x}') = \left. \frac{\delta^2 E_{\text{Hxc}}[n]}{\delta n(\mathbf{x})\delta n(\mathbf{x}')} \right|_{n_0} \xrightarrow[\text{Approx.}]{\text{Local Density}} f_{\text{Hxc}}(\mathbf{x})\delta(\mathbf{r} - \mathbf{r}'). \quad (5.64)$$

Semi-local and hybrid approximations can also be used instead of the LDA one in a similar way. In any case, the approximation on the kernel remains drastic and leads to a number of deficiencies which will be discussed in the next section together with some possible solutions.

5.7 Known deficiencies and remedies

The usual adiabatic (semi)-local approximations usually give reasonable results for the low-lying (valence) excitation energies with a mean absolute error of 0.3-0.4 eV [27] but break down for Rydberg excitations or when charge transfer or multiple excitations are involved [28]. In the following, the origin of these deficiencies is briefly analyzed together with how range separation can help in these matters.

5.7.1 Main deficiencies

Rydberg excitations

The first shortcoming encountered in TDDFT concerns the Rydberg excitation energies. As these states are high in energy, they are particularly sensible to the asymptotic behavior of the potential. In Section 1.6, we mentioned that the LDA potential decays exponentially while the exact exchange-correlation potential should decays as $-1/r$.

TDDFT inherits from this flaw of the potential which leads to a strong underestimation of the Rydberg excitation energies [29, 30]. This can be circumvented by a correction of the asymptotic behavior of the potential [31–34] or with the hybrid approximations where a fraction α of the HF exchange potential is present. The potential then decays as $-\alpha/r$ which, even if not exact, is still better than an exponential decay [35]. The long-range corrected functionals have, on the other hand, an exact asymptotic behavior as will be detailed in the next section.

Charge-transfer excitations

Another deficiency of TDDFT in the (semi)-local approximations is their inability to describe excitations with a charge-transfer character [23, 36–38]. In such excitations, the charge moves spatially from the donor (D) to the acceptor (A) which can be either two parts of the same molecule or two separated entities. For an initial neutral system, where the donor and the acceptor are separated by a large distance R , the excitation energy is given by the difference between the ionization potential of the donor \mathcal{E}_{IP} and the electronic affinity of the acceptor \mathcal{E}_{EA} plus the electrostatic interaction energy between the two fragments which are now charged

$$\omega(R) \xrightarrow{R \rightarrow \infty} \mathcal{E}_{IP} - \mathcal{E}_{EA} - \frac{1}{R}. \quad (5.65)$$

In TDDFT, however, within (semi)-local approximations, the overlap between the two main contributing orbitals exponentially vanishes and therefore the kernel contribution goes to 0. The excitation energy reduces then to the bare difference between the Kohn-Sham orbital energies $\varepsilon^A - \varepsilon^D$ which explains why the charge transfer is usually strongly underestimated with LDA or GGA functionals as their HOMO-LUMO gap is too low. To solve this problem, non-local exchange needs to be introduced. Hybrid approximations [35, 39] therefore behave much better and so do range-separated ones [40–42].

Double excitations

Another main problem encountered in TDDFT concerns the treatment of multiple excitations. One could think that these excitations are very high in energies and are of no interest when one wants only the lowest part of the spectrum. However, in some cases, they play an important role as for example in linear polyenes [43–45], during the dissociation of molecules (for instance the dihydrogen molecule [46]) or for radicals [47] and are completely missed in adiabatic TDDFT [48, 49]. This deficiency originates from the adiabatic approximation which turns the non-linear problem given in Equation (5.44) into a linear one. This implies that the number of solutions is exactly equals to the size of the matrix and that only excitations originating from single excitations in the KS system are described. Large efforts are made to circumvent the adiabatic approximation and at least treat double excitations. Several proposals can be found in the

literature for the treatment of molecular double excitations. One of them is dressed TDDFT [25, 43, 50–52] where a frequency-dependent kernel is build manually in a small subspace to describe the case where a double excitation mixes with a single one and is well separated from the others. However, this method is valid only in the limit of a weak electron-electron interaction and one need to know *a priori* where the double excitation is missing and to build the kernel explicitly for this particular excitation. Gritsenko *et al* [53] also proposed a non-adiabatic treatment of the double excitations based on the common energy denominator approximation (CEDA) [54, 55]. As the complete manifold of excited states is included in this kernel, it can be seen as an extension of the dressed TDDFT kernel.

Outside of the TDDFT framework (without talking of wave-function methods such as EOM-CCSD), other solutions are provided by many-body perturbation theory as for instance by the extended algebraic diagrammatic construction (ADC) [44, 56], by Green’s function based methods [57–59] or propagator-based methods such as SOPPA [60–64].

5.7.2 Range-separated methods

The success of range-separated functionals for ground-state calculations, due in particular to the inclusion of long-range Hartree-Fock exchange [65], lead to their extension to the time-dependent scheme in the case where range separation is done only on the exchange functional (LC methods). Starting from Equation (1.69), Tawada *et al.* proposed the LC-TDDFT method [40], where the LC kernel is given by

$$f_{\text{Hxc,LC}}^{\mu} = f_{\text{H}} + f_{\text{x,HF}}^{\text{lr},\mu} + f_{\text{x}}^{\text{sr},\mu} + f_{\text{c}}, \quad (5.66)$$

where f_{H} and f_{c} are the usual Hartree and correlation kernels, and where the exchange kernel has been divided in a short-range part $f_{\text{x}}^{\text{sr},\mu}$ treated by DFT and a long-range part $f_{\text{x,HF}}^{\text{lr},\mu}$ treated in HF. They proposed three functionals, LC-BOP, LC-PBEOP and LC-BLYP starting respectively from the pure functionals BOP [66, 67], PBEOP [68] and BLYP [69]. It was also explored by Yanai *et al* [70] which proposed the Coulomb-attenuating B3LYP (CAM-B3LYP) method and by Vydrov and Scuseria [71] who derived the functional LC- ω PBE starting from PBE. Head-Gordon and its collaborators proposed the ω B97 functionals [22, 72, 73] and extended it to double hybrid functionals [74]. A review of the behavior of these functionals is given in [75]. All these functionals are able to cope with the Rydberg and charge-transfer problems, however they still do not describe multiple excitations and may suffer from triplet instabilities because of the inclusion of the HF exchange.

5.8 Conclusion

In this chapter, we have briefly reviewed the TDDFT formalism and its successes and shortcomings when applied in the adiabatic (semi-)local approximation. Range separa-

tion of the exchange kernel is already able to make up for most of these shortcomings but the treatment of double- or higher-order excitations remains problematic. In the next chapter, we propose to extend the range separation to the correlation kernel in the same fashion as it is done in ground-state DFT within the RSH scheme. This does not solve the problem of double excitations but lays the appropriate framework for the perturbative addition of a long-range frequency-dependent correlation kernel as will be shown in the last part of this thesis.

Chapter 6

Electronic excitations from a linear-response range-separated hybrid scheme

This chapter is the subject of a publication in *Molecular Physics* (2013), 111, Pp. 1219–1234. in collaboration with A. Savin and J. Toulouse.

In this chapter, we study linear-response time-dependent density-functional theory (DFT) based on the single-determinant range-separated hybrid (RSH) scheme, i.e. combining a long-range Hartree-Fock exchange kernel with a short-range DFT exchange-correlation kernel, for calculating electronic excitation energies of molecular systems. It is an alternative to the more common long-range correction (LC) scheme which combines a long-range Hartree-Fock exchange kernel with a short-range DFT exchange kernel and a standard full-range DFT correlation kernel. We discuss the local-density approximation (LDA) to the short-range exchange and correlation kernels, and assess the performance of the linear-response RSH scheme for singlet \rightarrow singlet and singlet \rightarrow triplet valence and Rydberg excitations in the N_2 , CO , H_2CO , C_2H_4 , and C_6H_6 molecules, and for the first charge-transfer excitation in the C_2H_4 - C_2F_4 dimer. For these systems, the presence of long-range LDA correlation in the ground-state calculation and in the linear-response kernel has only a small impact on the excitation energies and oscillator strengths, so that the RSH method gives results very similar to the ones given by the LC scheme. Like in the LC scheme, the introduction of long-range HF exchange in the present method corrects the underestimation of charge-transfer and high-lying Rydberg excitation energies obtained with standard (semi-)local density-functional approximations, but also leads to underestimated excitation energies to low-lying spin-triplet valence states. This latter problem is largely cured by the Tamm-Dancoff approximation which leads to a relatively uniform accuracy for all excitation energies. This work thus suggests that the present linear-response RSH scheme is a reasonable starting approximation for describing electronic excitation energies, even before adding an explicit treatment of long-range correlation.

6.1 Introduction

Range-separated density-functional theory (see, e.g., Ref. [76] and references therein) constitutes an alternative to standard Kohn-Sham (KS) density-functional theory (DFT) [77] for ground-state electronic-structure calculations. It consists in combining wave-function-type approximations for long-range electron-electron interactions with density-functional approximations for short-range electron-electron interactions, using a controllable range-separation parameter. For example, in the single-determinant range-separated hybrid (RSH) scheme [78], the long-range Hartree-Fock (HF) exchange energy is combined with a short-range exchange-correlation density-functional approximation. The long-range correlation energy is missing in this scheme, but it can be added in a second step by many-body perturbation theory for describing van der Waals dispersion interactions for instance [78–83]. A simpler approach is the long-range correction (LC) scheme [65], also called RSHX [84], which consists in applying range separation on exchange only, i.e. combining the long-range HF exchange energy with a short-range exchange density-functional approximation and using a standard full-range correlation density functional. More complicated decompositions of the exchange energy have also been proposed, such as in the CAM-B3LYP approximation [70].

Range separation is also applied in linear-response time-dependent density-functional theory (TDDFT) [85] for calculating excitation energies and other response properties. The first and probably most widely used range-separated TDDFT approach is based on the LC scheme [40], and involves a long-range HF exchange kernel combined with a short-range DFT exchange kernel and a standard full-range DFT correlation kernel. It has also been proposed to use in this scheme an empirically modified correlation density functional depending on the range-separation parameter [86]. The CAM-B3LYP scheme and other similar schemes have also been applied in linear-response theory for calculating excitation energies [70, 72, 87–97]. In all these schemes, the presence of long-range HF exchange greatly improves Rydberg and charge-transfer excitation energies, in comparison to time-dependent Kohn-Sham (TDKS) calculations using standard local or semilocal density-functional approximations in which they are strongly underestimated (see, e.g., Ref. [28]).

In this chapter, we study a range-separated linear-response TDDFT method based on the RSH scheme, i.e. combining a long-range HF exchange kernel with a short-range DFT exchange-correlation kernel with no long-range correlation kernel. The motivation for this range-separated TDDFT approach is that, as for exchange, the long-range part of standard correlation density-functional approximations such as the local-density approximation (LDA) is usually inaccurate [76, 98, 99], so one may as well remove it. This can be viewed as a first-level approximation before adding a more accurate treatment of long-range correlation, e.g., by linear-response density-matrix functional theory (DMFT) [100] or linear-response multiconfiguration self-consistent field (MCSCF) theory [101]. These last approaches are capable of describing excited states of double excita-

tion character, which are out of reach within a single-determinant linear-response scheme using adiabatic exchange-correlation kernels (except in a spin-flip formulation [25, 102]).

The main goal of this chapter is to test whether the range-separated TDDFT method based on the RSH scheme is a reasonable starting approximation for calculating excitation energies of molecular systems, even before adding explicit long-range correlations. For this purpose, we apply the method to singlet \rightarrow singlet and singlet \rightarrow triplet valence and Rydberg excitations in the N_2 , CO , H_2CO , C_2H_4 , and C_6H_6 molecules, and to the first charge-transfer (CT) excitation in the C_2H_4 - C_2F_4 dimer, and compare with the LC scheme, as well as non-range-separated methods. In particular, we study the effect of dropping long-range LDA correlation in comparison to the LC scheme.

The chapter is organized as follows. The working equations of the linear-response RSH scheme are laid down in Section 6.2, and the short-range DFT exchange and correlation kernels are discussed in Section 6.3. After giving computational details in Section 6.4, we report and discuss our results in Section 6.5. Section 6.6 summarizes our conclusions. Technical details are given in Appendix E. Hartree atomic units are assumed throughout unless otherwise indicated.

6.2 Linear-response range-separated hybrid scheme

6.2.1 Ground-state range-separated scheme

In the RSH scheme [78], the ground-state energy is approximated as the following minimum over single-determinant wave functions Φ ,

$$E_{\text{RSH}}^\mu = \min_{\Phi} \left\{ \langle \Phi | \hat{T} + \hat{V}_{\text{ne}} | \Phi \rangle + E_{\text{H}}[n_{\Phi}] + E_{\text{x, HF}}^{\text{lr}, \mu}[\Phi] + E_{\text{xc}}^{\text{sr}, \mu}[n_{\Phi}, m_{\Phi}] \right\}, \quad (6.1)$$

where \hat{T} is the kinetic energy operator, \hat{V}_{ne} is the external potential operator due to the electron-nuclei interaction, $E_{\text{H}}[n]$ is the Hartree energy density functional,

$$E_{\text{H}}[n] = \frac{1}{2} \int n(\mathbf{r}_1)n(\mathbf{r}_2)w_{\text{ee}}(|\mathbf{r}_1 - \mathbf{r}_2|)d\mathbf{r}_1d\mathbf{r}_2, \quad (6.2)$$

with the Coulombic electron-electron interaction $w_{\text{ee}}(|\mathbf{r}_1 - \mathbf{r}_2|) = 1/|\mathbf{r}_1 - \mathbf{r}_2|$, $E_{\text{x, HF}}^{\text{lr}, \mu}[\Phi]$ is the long-range HF exchange energy

$$E_{\text{x, HF}}^{\text{lr}, \mu}[\Phi] = -\frac{1}{2} \int |\langle \Phi | \hat{n}_1(\mathbf{x}_1, \mathbf{x}_2) | \Phi \rangle|^2 w_{\text{ee}}^{\text{lr}, \mu}(|\mathbf{r}_1 - \mathbf{r}_2|)d\mathbf{x}_1d\mathbf{x}_2, \quad (6.3)$$

with the one-particle density-matrix operator $\hat{n}_1(\mathbf{x}_1, \mathbf{x}_2)$ and a long-range electron-electron interaction $w_{\text{ee}}^{\text{lr}, \mu}(|\mathbf{r}_1 - \mathbf{r}_2|)$, and $E_{\text{xc}}^{\text{sr}, \mu}[n, m]$ is the short-range exchange-correlation energy functional depending on the total density $n(\mathbf{r}) = n_{\uparrow}(\mathbf{r}) + n_{\downarrow}(\mathbf{r})$ and the (collinear) spin magnetization density $m(\mathbf{r}) = n_{\uparrow}(\mathbf{r}) - n_{\downarrow}(\mathbf{r})$, written with the spin densities $n_{\sigma}(\mathbf{r}) = n(\mathbf{x})$ for the space-spin coordinate $\mathbf{x} = (\mathbf{r}, \sigma)$. In this work, the long-range interaction will be taken as $w_{\text{ee}}^{\text{lr}, \mu}(r) = \text{erf}(\mu r)/r$, where the parameter μ can be interpreted as the inverse

of a smooth “cut-off” radius, but other interactions have also been considered [103–105]. What is neglected in Equation (6.1) is the long-range correlation energy $E_c^{\text{lr},\mu}$, but it can be added *a posteriori* by perturbative methods [78–83, 106, 107].

In the LC scheme [65], range separation is applied to the exchange energy only and the ground-state energy is expressed as

$$E_{\text{LC}}^\mu = \min_{\Phi} \left\{ \langle \Phi | \hat{T} + \hat{V}_{\text{ne}} | \Phi \rangle + E_{\text{H}}[n_{\Phi}] + E_{\text{x,HF}}^{\text{lr},\mu}[\Phi] + E_{\text{x}}^{\text{sr},\mu}[n_{\Phi}, m_{\Phi}] + E_{\text{c}}[n_{\Phi}, m_{\Phi}] \right\}, \quad (6.4)$$

where $E_{\text{x}}^{\text{sr},\mu}[n, m]$ is the short-range exchange energy functional, and $E_{\text{c}}[n, m]$ is the full-range correlation energy functional.

6.2.2 Linear-response theory

Just like in standard TDDFT [85], time-dependent linear-response theory applied to the RSH scheme leads to a familiar Dyson-like equation for the frequency-dependent 4-point linear response function $\chi(\mathbf{x}_1, \mathbf{x}_2; \mathbf{x}'_1, \mathbf{x}'_2; \omega)$ to a time-dependent perturbation (dropping the space-spin coordinates for simplicity)

$$\chi^{-1}(\omega) = \chi_0^{-1}(\omega) - f_{\text{H}} - f_{\text{x,HF}}^{\text{lr},\mu} - f_{\text{xc}}^{\text{sr},\mu}, \quad (6.5)$$

where $\chi_0(\omega)$ is the non-interacting RSH response function, f_{H} is the Hartree kernel,

$$f_{\text{H}}(\mathbf{x}_1, \mathbf{x}_2; \mathbf{x}'_1, \mathbf{x}'_2) = w_{\text{ee}}(|\mathbf{r}_1 - \mathbf{r}_2|) \delta(\mathbf{x}_1 - \mathbf{x}'_1) \delta(\mathbf{x}_2 - \mathbf{x}'_2), \quad (6.6)$$

$f_{\text{x,HF}}^{\text{lr},\mu}$ is the long-range HF exchange kernel,

$$f_{\text{x,HF}}^{\text{lr},\mu}(\mathbf{x}_1, \mathbf{x}_2; \mathbf{x}'_1, \mathbf{x}'_2) = -w_{\text{ee}}^{\text{lr},\mu}(|\mathbf{r}_1 - \mathbf{r}_2|) \delta(\mathbf{x}_1 - \mathbf{x}'_2) \delta(\mathbf{x}'_1 - \mathbf{x}_2), \quad (6.7)$$

and $f_{\text{xc}}^{\text{sr},\mu}$ is the short-range exchange-correlation kernel which is frequency independent in the adiabatic approximation,

$$f_{\text{xc}}^{\text{sr},\mu}(\mathbf{x}_1, \mathbf{x}_2; \mathbf{x}'_1, \mathbf{x}'_2) = f_{\text{xc}}^{\text{sr},\mu}(\mathbf{x}_1, \mathbf{x}_2) \delta(\mathbf{x}_1 - \mathbf{x}'_1) \delta(\mathbf{x}_2 - \mathbf{x}'_2), \quad (6.8)$$

with the 2-point kernel

$$f_{\text{xc}}^{\text{sr},\mu}(\mathbf{x}_1, \mathbf{x}_2) = \frac{\delta^2 E_{\text{xc}}^{\text{sr},\mu}[n, m]}{\delta n(\mathbf{x}_1) \delta n(\mathbf{x}_2)}. \quad (6.9)$$

Note that a 4-point formalism is required here because of the HF exchange kernel. The excitation energies are given by the poles of $\chi(\omega)$ in ω . Working in the basis of the RSH spin orbitals $\{\phi_k(\mathbf{x})\}$, the poles can be found by the pseudo-Hermitian eigenvalue problem [1]

$$\begin{pmatrix} \mathbf{A} & \mathbf{B} \\ \mathbf{B}^* & \mathbf{A}^* \end{pmatrix} \begin{pmatrix} \mathbf{X}_n \\ \mathbf{Y}_n \end{pmatrix} = \omega_n \begin{pmatrix} \mathbf{1} & \mathbf{0} \\ \mathbf{0} & -\mathbf{1} \end{pmatrix} \begin{pmatrix} \mathbf{X}_n \\ \mathbf{Y}_n \end{pmatrix}, \quad (6.10)$$

whose solutions come in pairs: the excitation energy ω_n associated with the eigenvector $(\mathbf{X}_n, \mathbf{Y}_n)$, and the deexcitation energy $-\omega_n$ associated with $(\mathbf{Y}_n^*, \mathbf{X}_n^*)$. The matrix elements of \mathbf{A} and \mathbf{B} are

$$\begin{aligned} A_{ia,jb} &= (\varepsilon_a - \varepsilon_i)\delta_{ij}\delta_{ab} + K_{ia,jb}, \\ B_{ia,jb} &= K_{ia,bj}, \end{aligned} \quad (6.11)$$

where i, j and a, b refer to occupied and virtual spin orbitals, respectively, ε_k is the energy of the spin orbital k , and \mathbf{K} is the coupling matrix accounting for the contributions of the different kernels,

$$\begin{aligned} K_{ia,jb} &= \langle aj|\hat{f}_{\text{H}}|ib\rangle + \langle aj|\hat{f}_{\text{x,HF}}^{\text{lr},\mu}|ib\rangle + \langle aj|\hat{f}_{\text{xc}}^{\text{sr},\mu}|ib\rangle \\ &= \langle aj|\hat{w}_{\text{ee}}|ib\rangle - \langle aj|\hat{w}_{\text{ee}}^{\text{lr},\mu}|bi\rangle + \langle aj|\hat{f}_{\text{xc}}^{\text{sr},\mu}|ib\rangle, \end{aligned} \quad (6.12)$$

where $\langle aj|\hat{w}_{\text{ee}}|ib\rangle$ and $\langle aj|\hat{w}_{\text{ee}}^{\text{lr},\mu}|bi\rangle$ are the two-electron integrals for the Coulombic and long-range interactions, respectively, and $\langle aj|\hat{f}_{\text{xc}}^{\text{sr},\mu}|ib\rangle$ are the matrix elements of the short-range exchange-correlation kernel,

$$\langle aj|\hat{f}_{\text{xc}}^{\text{sr},\mu}|ib\rangle = \int \phi_a^*(\mathbf{x}_1)\phi_j^*(\mathbf{x}_2)f_{\text{xc}}^{\text{sr},\mu}(\mathbf{x}_1, \mathbf{x}_2)\phi_i(\mathbf{x}_1)\phi_b(\mathbf{x}_2)d\mathbf{x}_1d\mathbf{x}_2. \quad (6.13)$$

For real-valued orbitals, and if $\mathbf{A} + \mathbf{B}$ and $\mathbf{A} - \mathbf{B}$ are positive definite, Equation (6.10) is conveniently transformed into a half-size symmetric eigenvalue equation [1]

$$\mathbf{M}\mathbf{Z}_n = \omega_n^2\mathbf{Z}_n, \quad (6.14)$$

with $\mathbf{M} = (\mathbf{A} - \mathbf{B})^{1/2}(\mathbf{A} + \mathbf{B})(\mathbf{A} - \mathbf{B})^{1/2}$ and the normalized eigenvectors $\mathbf{Z}_n = \sqrt{\omega_n}(\mathbf{A} - \mathbf{B})^{-1/2}(\mathbf{X}_n + \mathbf{Y}_n)$. The Tamm-Dancoff approximation (TDA) [22] consists in neglecting the coupling between the excitations and the de-excitations, i.e. setting $\mathbf{B} = \mathbf{0}$. We note, in passing, that the TDA can also be viewed as a non-self-consistent approximation to the static (multiplet-sum) Δ SCF method, which identifies the excited states with stationary points on the ground-state energy surface as a function of the orbital parameters [24, 25].

The same equations apply identically to the LC scheme except that the short-range correlation kernel $f_{\text{c}}^{\text{sr},\mu}$ has to be replaced by the full-range one f_{c} [40].

6.2.3 Spin adaptation for closed-shell systems

For spin-restricted closed-shell calculations, Equation (6.14) can be decoupled into two independent eigenvalue equations for singlet \rightarrow singlet excitations and for singlet \rightarrow triplet excitations, respectively [3, 26, 108] (see Appendix E.1). For simplicity, they will be referred to as “singlet excitations” and “triplet excitations”. The modifications for spin adaptation are located in the expression of the coupling matrix \mathbf{K} , which becomes,

for singlet excitations,

$${}^1K_{ia,jb} = 2\langle aj|\hat{w}_{ee}|ib\rangle - \langle aj|\hat{w}_{ee}^{\text{lr},\mu}|bi\rangle + 2\langle aj|{}^1\hat{f}_{xc}^{\text{sr},\mu}|ib\rangle, \quad (6.15)$$

and, for triplet excitations,

$${}^3K_{ia,jb} = -\langle aj|\hat{w}_{ee}^{\text{lr},\mu}|bi\rangle + 2\langle aj|{}^3\hat{f}_{xc}^{\text{sr},\mu}|ib\rangle, \quad (6.16)$$

where the indices i, j, a, b refer now to spatial orbitals and the singlet and triplet short-range exchange-correlation kernels are

$${}^1f_{xc}^{\text{sr},\mu}(\mathbf{r}_1, \mathbf{r}_2) = \frac{\delta^2 E_{xc}^{\text{sr},\mu}[n, m]}{\delta n(\mathbf{r}_1)\delta n(\mathbf{r}_2)}, \quad (6.17)$$

and

$${}^3f_{xc}^{\text{sr},\mu}(\mathbf{r}_1, \mathbf{r}_2) = \frac{\delta^2 E_{xc}^{\text{sr},\mu}[n, m]}{\delta m(\mathbf{r}_1)\delta m(\mathbf{r}_2)}, \quad (6.18)$$

where the derivatives are taken at zero spin magnetization density, $m(\mathbf{r}) = 0$. Because the spin-dependent exchange functional $E_x^{\text{sr},\mu}[n, m]$ is constructed from the spin-independent one $E_x^{\text{sr},\mu}[n] = E_x^{\text{sr},\mu}[n, m = 0]$ via the spin-scaling relation [109], $E_x^{\text{sr},\mu}[n, m] = (E_x^{\text{sr},\mu}[2n_\uparrow] + E_x^{\text{sr},\mu}[2n_\downarrow]) / 2$, one can show that the singlet and triplet exchange kernels are identical, and, for closed-shell systems, can be written with the spin-independent functional,

$$f_x^{\text{sr},\mu}(\mathbf{r}_1, \mathbf{r}_2) = {}^1f_x^{\text{sr},\mu}(\mathbf{r}_1, \mathbf{r}_2) = {}^3f_x^{\text{sr},\mu}(\mathbf{r}_1, \mathbf{r}_2) = \frac{\delta^2 E_x^{\text{sr},\mu}[n]}{\delta n(\mathbf{r}_1)\delta n(\mathbf{r}_2)}. \quad (6.19)$$

Therefore, contrary to the case of the correlation functional, the dependence on the spin magnetization density does not need to be considered in practice in the exchange functional for closed-shell systems.

The oscillator strength f_n for state n is zero for a triplet excitation, and it is calculated with the following formula for a singlet excitation (in the dipole length form) [1]

$$f_n = \frac{4}{3} \sum_{\alpha=x,y,z} \left(\sum_{ia} d_{\alpha,ia} \left[({}^1\mathbf{A} - {}^1\mathbf{B})^{1/2} {}^1\mathbf{Z}_n \right]_{ia} \right)^2, \quad (6.20)$$

where $d_{\alpha,ia} = \int \phi_i(\mathbf{r}) r_\alpha \phi_a(\mathbf{r}) d\mathbf{r}$ is the α -component of the transition dipole moment between the spatial occupied and virtual orbitals $\phi_i(\mathbf{r})$ and $\phi_a(\mathbf{r})$.

6.3 Short-range adiabatic exchange-correlation kernels

We will consider here the short-range adiabatic exchange and correlation kernels in the local-density approximation (LDA).

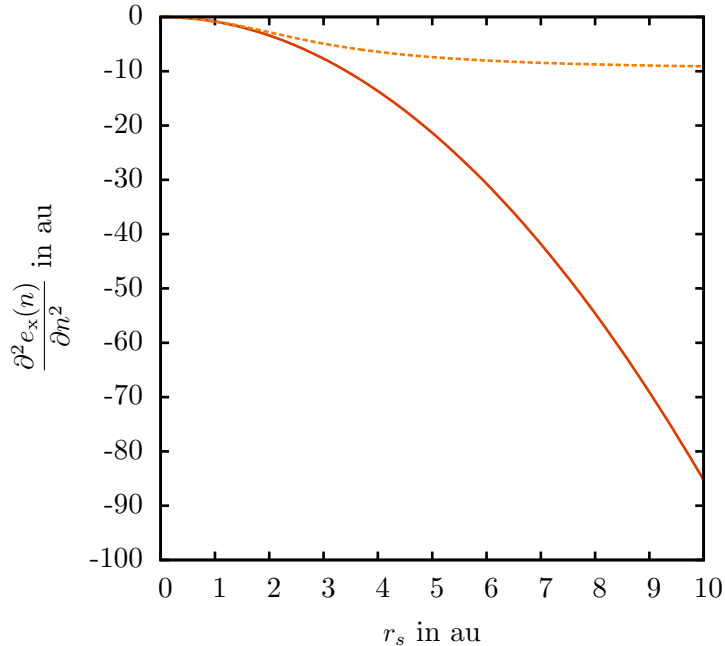


Figure 6.1 – Second-order derivatives of the full-range (full line) and short-range ($\mu = 0.4$, dashed line) LDA exchange energy density with respect to the density n as functions of the Wigner-Seitz radius r_s .

6.3.1 Exchange kernel

The short-range spin-independent LDA exchange energy functional is written as

$$E_{x,\text{LDA}}^{\text{sr},\mu}[n] = \int e_x^{\text{sr},\mu}(n(\mathbf{r})) d\mathbf{r}, \quad (6.21)$$

where $e_x^{\text{sr},\mu}(n) = n \epsilon_x^{\text{sr},\mu}(n)$ is the short-range energy density defined with the exchange energy per particle $\epsilon_x^{\text{sr},\mu}(n)$ of the homogeneous electron gas (HEG) with the short-range electron-electron interaction $w_{ee}^{\text{sr},\mu} = w_{ee} - w_{ee}^{\text{lr},\mu}$. The analytic expression of $\epsilon_x^{\text{sr},\mu}(n)$ is known [104, 110] and is recalled in Appendix E.2.1. The short-range adiabatic LDA exchange kernel is given by the second-order derivative of the energy density with respect to the density,

$$f_{x,\text{LDA}}^{\text{sr},\mu}(\mathbf{r}, \mathbf{r}') = \frac{\partial^2 e_x^{\text{sr},\mu}(n(\mathbf{r}))}{\partial n^2} \delta(\mathbf{r} - \mathbf{r}'). \quad (6.22)$$

Just like its full-range LDA counterpart, the short-range exchange LDA kernel is thus strictly local in space. However, this is here a less drastic approximation than for the full-range case. Indeed, by using the asymptotic expansion of the exact short-range spin-independent exchange density functional for $\mu \rightarrow \infty$ [76, 111], $E_x^{\text{sr},\mu}[n] = -\pi/(4\mu^2) \int n(\mathbf{r})^2 d\mathbf{r} + \mathcal{O}(1/\mu^4)$, one can see that the *exact* adiabatic short-range exchange

kernel has the following expansion in $1/\mu$,

$$f_x^{\text{sr},\mu}(\mathbf{r}, \mathbf{r}') = -\frac{\pi}{2\mu^2} \delta(\mathbf{r} - \mathbf{r}') + \mathcal{O}\left(\frac{1}{\mu^4}\right), \quad (6.23)$$

i.e., in the limit of a very short-range electron-electron interaction, it also becomes strictly local. More than that, the short-range LDA kernel of Equation (6.22) is exact for the leading term of Equation (6.23), as shown in Appendix E.2.1.

The short-range LDA exchange kernel for a fixed value of the range-separation parameter $\mu = 0.4$ is shown in Figure 6.1 as a function of the Wigner-Seitz radius $r_s = (3/(4\pi n))^{1/3}$ and compared with the full-range LDA exchange kernel. The LDA exchange kernel is always negative, which is a consequence of the concavity of the LDA exchange energy density curve as a function of the density n . For high enough densities such that $r_s \ll 1/\mu$, the short-range LDA exchange kernel reduces to the full-range one (see Appendix E.2.1). For larger values of r_s , the short-range LDA exchange kernel is reduced compared to the full-range one, and, in the low-density limit $r_s \rightarrow \infty$, it tends to the finite value of $-\pi/2\mu^2$ while the full-range LDA exchange kernel diverges to $-\infty$.

6.3.2 Correlation kernel

The short-range spin-dependent LDA correlation energy functional is written as

$$E_{c,\text{LDA}}^{\text{sr},\mu}[n, m] = \int e_c^{\text{sr},\mu}(n(\mathbf{r}), m(\mathbf{r})) d\mathbf{r}, \quad (6.24)$$

where $e_c^{\text{sr},\mu}(n, m) = n\epsilon_c(n, m) - n\epsilon_c^{\text{lr},\mu}(n, m)$ is the complement short-range correlation energy density, obtained from the correlation energy per particle of the standard homogeneous electron gas (HEG), $\epsilon_c(n, m)$, [112] and the correlation energy per particle of the HEG with the long-range electron-electron interaction, $\epsilon_c^{\text{lr},\mu}(n, m)$, as parametrized from quantum Monte Carlo calculations by Paziani *et al.* [113]. Its expression is recalled in Appendix E.2.2. The singlet and triplet short-range adiabatic LDA correlation kernels are local functions given by the second-order derivatives of the energy density with respect to the density n and the spin magnetization m , respectively,

$${}^1 f_{c,\text{LDA}}^{\text{sr},\mu}(\mathbf{r}, \mathbf{r}') = \frac{\partial^2 e_c^{\text{sr},\mu}(n(\mathbf{r}), m(\mathbf{r}))}{\partial n^2} \delta(\mathbf{r} - \mathbf{r}'), \quad (6.25)$$

$${}^3 f_{c,\text{LDA}}^{\text{sr},\mu}(\mathbf{r}, \mathbf{r}') = \frac{\partial^2 e_c^{\text{sr},\mu}(n(\mathbf{r}), m(\mathbf{r}))}{\partial m^2} \delta(\mathbf{r} - \mathbf{r}'). \quad (6.26)$$

For closed-shell systems, these kernels need to be evaluated only at zero spin magnetization, $m = 0$. Again, it can be argued that the strictly local form of the LDA correlation kernels of Equation (6.25) and (6.26) is more appropriate for the short-range kernels than for the full-range ones. Using the asymptotic expansion of the exact short-range correlation functional for $\mu \rightarrow \infty$ [76, 114], $E_c^{\text{sr},\mu}[n, m] = \pi/(2\mu^2) \int n_{2,c}(\mathbf{r}, \mathbf{r}) d\mathbf{r} + 2\sqrt{2\pi}/(3\mu^3) \int n_2(\mathbf{r}, \mathbf{r}) d\mathbf{r} + \mathcal{O}(1/\mu^4)$, and the total and correlation on-top pair densities in

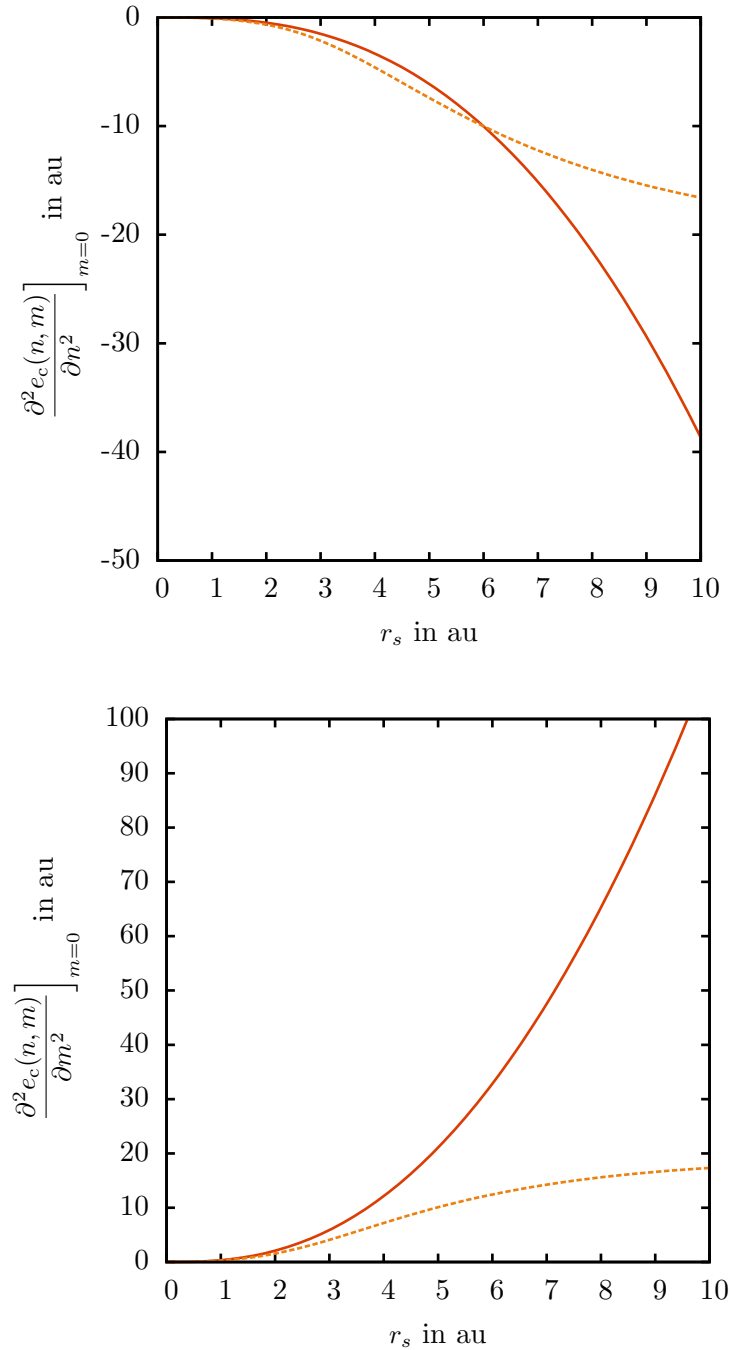


Figure 6.2 – Second-order derivatives of the full-range (full line) and short-range ($\mu = 0.4$, dashed line) LDA correlation energy densities with respect to the density n (top) and to the spin magnetization m (bottom) evaluated at $m = 0$ as functions of the Wigner-Seitz radius r_s .

the strong-interaction limit of the adiabatic connection $\lambda \rightarrow \infty$ (or for fully spin-polarized systems $n = |m|$) [115, 116], $n_2(\mathbf{r}, \mathbf{r}) \rightarrow 0$ and $n_{2,c}(\mathbf{r}, \mathbf{r}) \rightarrow -n(\mathbf{r})^2/2 + m(\mathbf{r})^2/2$, it is easy to show that the leading terms in the expansions of the *exact* adiabatic short-range correlation kernels for $\mu \rightarrow \infty$, in the strong-interaction (or low-density) limit, are strictly local

$${}^1 f_c^{\text{sr},\mu}(\mathbf{r}, \mathbf{r}') \xrightarrow{\lambda \rightarrow \infty} -\frac{\pi}{2\mu^2} \delta(\mathbf{r} - \mathbf{r}') + \mathcal{O}\left(\frac{1}{\mu^4}\right), \quad (6.27)$$

$${}^3 f_c^{\text{sr},\mu}(\mathbf{r}, \mathbf{r}') \xrightarrow{\lambda \rightarrow \infty} \frac{\pi}{2\mu^2} \delta(\mathbf{r} - \mathbf{r}') + \mathcal{O}\left(\frac{1}{\mu^4}\right). \quad (6.28)$$

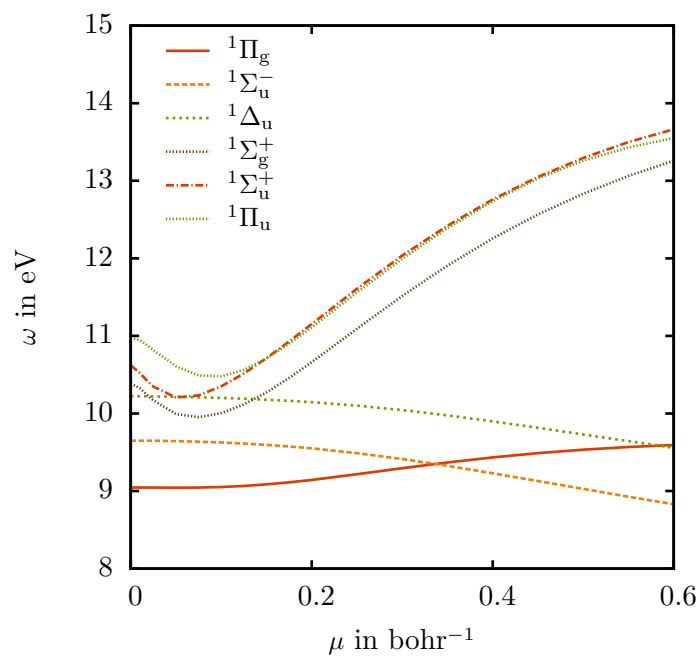
The short-range LDA correlation kernels of Equations (6.25) and (6.26), using the parametrization of Ref. [113], are exact for these leading terms.

The singlet and triplet short-range LDA correlation kernels are plotted in Figure 6.2, and compared with the full-range LDA correlation kernels. The singlet LDA correlation kernel is always negative while the triplet LDA correlation kernel is always positive, reflecting the fact that the LDA correlation energy density is concave when plotted as a function of the density n and convex when plotted as a function of the spin magnetization m . As for the exchange kernels, the singlet and triplet short-range LDA correlation kernels reduce to the full-range kernels in the high-density limit $r_s \rightarrow 0$ (see Appendix E.2.2). In the low-density limit $r_s \rightarrow \infty$, they tend to the finite values of $\mp\pi/2\mu^2$, while the full-range kernels diverge to $\mp\infty$.

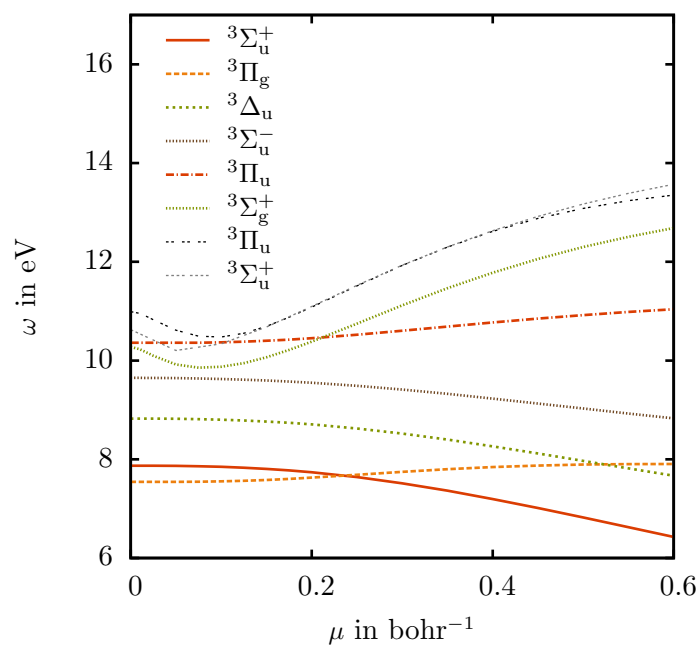
6.4 Computational details

The spin-adapted linear-response RSH scheme with the short-range LDA kernels has been implemented in a development version of the quantum chemistry program MOLPRO [118] for closed-shell systems. The implementation includes as special cases: standard TDKS with the LDA exchange-correlation functional, and time-dependent Hartree-Fock (TDHF). The implementation also includes the possibility to perform linear-response LC calculations (with the full-range LDA correlation functional). Each calculation is done in two steps: a self-consistent ground-state calculation is first performed with a chosen energy functional, and then a linear-response excited-state calculation is performed with a chosen kernel and using the previously calculated orbitals.

For compactness, “TD” will be dropped in the names of the methods and “LDA” will also be omitted in the names as it is the only density functional used here. Therefore, “KS” will denote a TDKS calculation using the LDA exchange-correlation functional, “HF” will stand for a TDHF calculation, “RSH” will denote a linear-response RSH calculation using the short-range LDA exchange-correlation functional, and “LC” will stand for a linear-response LC calculation using the short-range LDA exchange functional and the full-range LDA correlation functional. We will call “RSH-TDA” a linear-response RSH calculation with the Tamm-Dancoff approximation. For all these methods, the same functional is used for the ground-state energy calculation and the linear-response



(a) Singlet



(b) Triplet

Figure 6.3 – Singlet (a) and triplet (b) excitation energies of N₂ (in eV) with respect to the range-separation parameter μ (in bohr⁻¹) calculated by the linear-response RSH method with the short-range LDA exchange-correlation functional at the equilibrium geometry [117] and with the Sadlej+ basis set.

calculation. In addition, we will call “RSH-fHx” a linear-response RSH calculation where only the Hartree-exchange part of the RSH kernel is used (no correlation kernel) but evaluated with regular RSH orbitals (including the short-range correlation energy functional).

We calculate vertical excitation energies and oscillator strengths of five small molecules, N_2 , CO , H_2CO , C_2H_4 , and C_6H_6 , which have already been extensively studied theoretically [28, 29, 40, 61, 119, 120] and experimentally [121–124]. In order to have unique, comparable references, equation-of-motion coupled-cluster singles doubles (EOM-CCSD) calculations were done in the same basis with the quantum chemistry program Gaussian 09 [125]. For each molecule, we report the first 14 excited states found with the EOM-CCSD method. Following Ref. [1], we define the coefficient of the (spin-orbital) single excitation $i \rightarrow a$ in the wave function of the excited state n to be

$$c_{n,ia} = X_{n,ia} + Y_{n,ia} = \frac{1}{\sqrt{\omega_n}} [(\mathbf{A} - \mathbf{B})^{1/2} \mathbf{Z}_n]_{ia}, \quad (6.29)$$

but other choices for analyzing the eigenvectors are possible, such as defining the weight of the single excitation $i \rightarrow a$ to be $w_{n,ia} = X_{n,ia}^2 - Y_{n,ia}^2$ [126]. Each excited state was thus assigned by looking at its symmetry and the leading orbital contributions to the excitation. When several excited states of the same symmetry and the same leading orbital contributions were obtained, the assignment was done by increasing order of energy. Some assignments for C_2H_4 and C_6H_6 were difficult and are explained in Tables 6.4 and 6.5. The Sadlej basis sets [127, 128] were developed to describe the polarizability of valence-like states. As the description of Rydberg states requires more flexibility, they were augmented with more diffuse functions to form the Sadlej+ basis sets [29] that we use here. The molecules are taken in their experimental geometries [117, 129–131].

The C_2H_4 - C_2F_4 dimer [36, 40, 132] was studied in its cofacial configuration along the intermolecular distance coordinate R in the standard 6-31G* basis set. A geometry optimization was performed during the self-consistent ground-state calculation for each method. The CT excitation was identified by assigning the molecular orbitals involved in the excitations either to C_2H_4 or C_2F_4 , using the visualization program MOLDEN [133].

6.5 Results and discussion

6.5.1 Variation of the RSH excitation energies with the range-separation parameter

When the range-separation parameter is zero, $\mu = 0$, the long-range HF exchange vanishes and the short-range exchange-correlation functional reduces to the usual full-range one, therefore the RSH method is equivalent to the standard KS method in this limit. With the LDA functional, linear-response KS gives good results for the low-lying valence

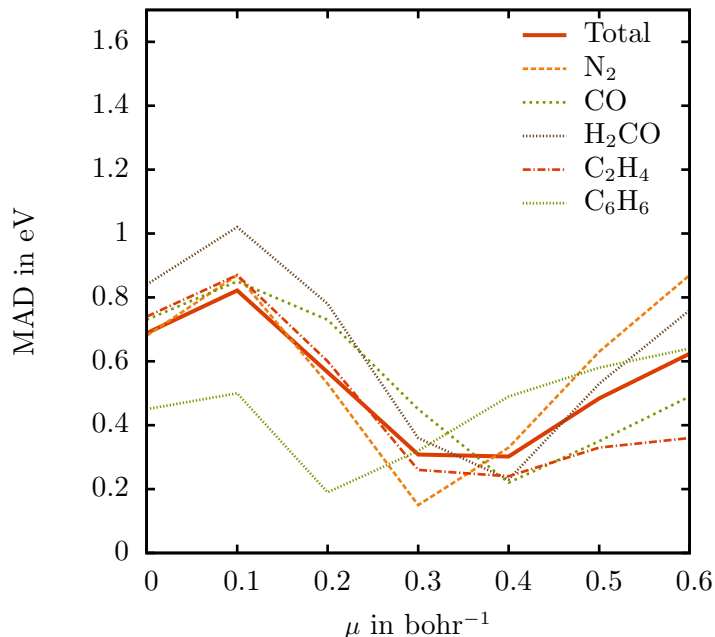
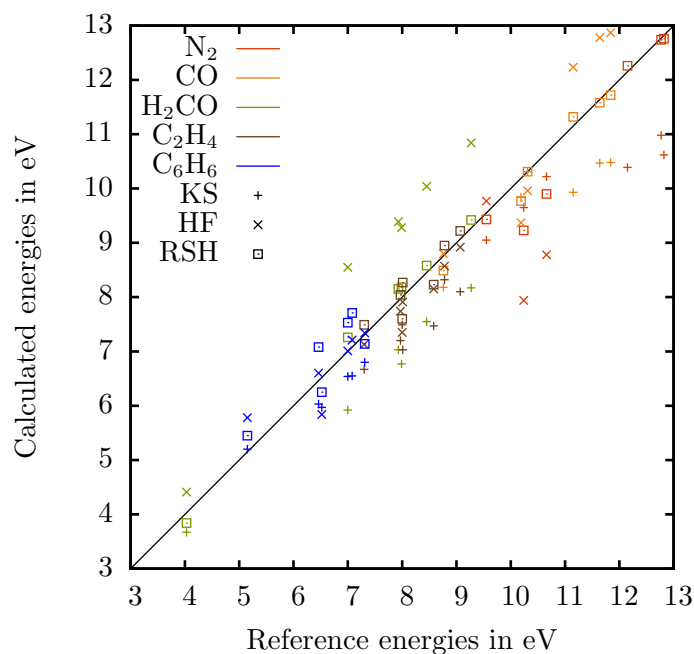


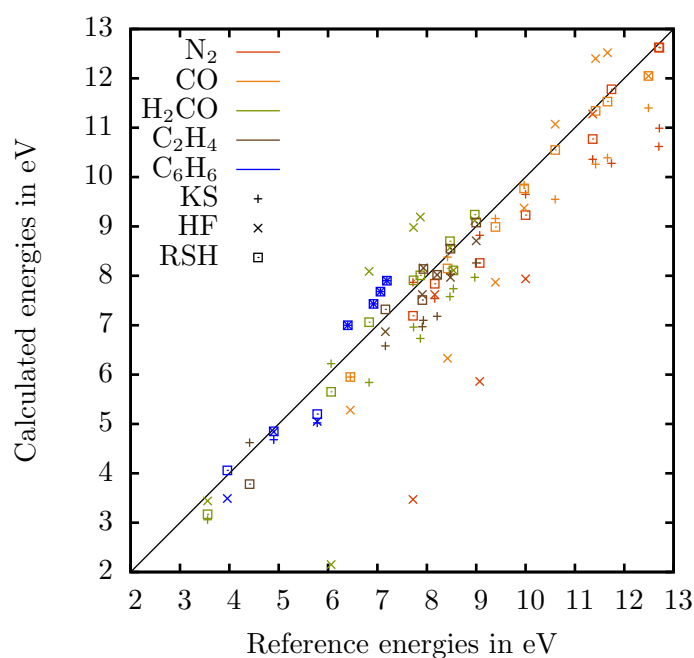
Figure 6.4 – Mean absolute deviation (MAD) in eV of the first 14 excitation energies of the N $_2$, CO, H $_2$ CO, C $_2$ H $_4$ and C $_6$ H $_6$ molecules calculated by the linear-response RSH method with the short-range LDA exchange-correlation functional with respect to the EOM-CCSD reference as a function of the range-separation parameter μ .

excitation energies but underestimates the high-lying Rydberg excitation energies. This underestimation is known to be due to the incorrect exponential asymptotic decay of the LDA exchange potential [29]. When μ increases, long-range HF exchange replaces LDA exchange and long-range LDA correlation is removed. In the limit $\mu \rightarrow +\infty$, RSH becomes equivalent to a HF calculation, in which Rydberg excitation energies are usually better described than in LDA but valence excitation energies can be poorly described, especially the triplet ones which can be strongly underestimated and can even become imaginary due to instabilities ($\mathbf{A} \pm \mathbf{B}$ in Equation (6.14) are no longer positive definite).

The variation of the first few singlet and triplet RSH excitation energies of N $_2$ with respect to the range-separation parameter μ is shown in Figure 6.3. The evolution of the excitation energies is similar for both spin states, however three different trends are seen for these excitations depending on their valence or Rydberg character and their spatial symmetry. The excitation energies to the Rydberg excited states ($^1\Sigma_g^+$, $^1\Pi_u$, $^1\Sigma_u^+$, $^3\Sigma_g^+$, $^3\Sigma_u^+$, $^3\Pi_u$) which are underestimated in KS show a significant increase with μ for $\mu \gtrsim 0.1$. This behavior is quite independent of the spin and spatial symmetry of the state. The valence excited states ($^1\Pi_g$, $^1\Sigma_u^-$, $^1\Delta_u$, $^3\Sigma_u^+$, $^3\Pi_g$, $^3\Delta_u$, $^3\Sigma_u^-$, $^3\Pi_u$) which are correctly described in KS are less affected by the introduction of long-range HF exchange. However, we observe two opposite behaviors depending on the orbital character of the excitation: all the valence Π states (corresponding to $\sigma \rightarrow \pi$ orbital transitions) have excitation



(a) Singlet



(b) Triplet

Figure 6.5 – Singlet (a) and triplet (b) excitation energies of N_2 , CO , H_2CO , C_2H_4 and C_6H_6 calculated by linear-response HF and KS (with the LDA functional), by the linear-response range-separated method RSH (with the short-range LDA functional and $\mu = 0.4 \text{ bohr}^{-1}$), as compared with the EOM-CCSD reference calculations.

energies that slowly increase with μ , while for valence Σ and Δ states (corresponding to $\pi \rightarrow \pi$ orbital transitions) the excitation energies decrease with μ . As a consequence, the ordering of the states changes significantly with μ . One should note that the variation of the excitation energies with μ have two causes: the variation of the orbital eigenvalues with μ in the ground-state calculation, and the variation of the kernel with μ in the linear-response calculation. Both effects can be significant.

The choice of the range-separation parameter μ is important. It has been proposed to adjust the value of μ for each system by imposing a self-consistent Koopmans’ theorem condition [41, 134]. This approach is appealing but it has the disadvantage of being non size-consistent, so we prefer to use a fixed value of μ , independent of the system. In Figure 6.4, the mean absolute deviation (MAD) of the RSH excitation energies with respect to the EOM-CCSD reference is plotted as a function of μ for each molecule and for the total set. The global minimum is obtained around $\mu \approx 0.3 - 0.4 \text{ bohr}^{-1}$. In all the following, we use a fixed value of $\mu = 0.4$, which is identical or similar to the value used in other range-separated TDDFT approaches [93, 100, 101]. We note however that the fact that the minimum of the MAD for C_6H_6 is around $\mu = 0.2$ shows that the optimal value of μ can substantially depend on the system. In particular, the presence of a triplet near-instability favors smaller values of μ .

6.5.2 Accuracy of the RSH excitation energies and oscillator strengths

The excitation energies and oscillator strengths for each method and each molecule are given in Tables 6.1-6.5. Mean absolute deviations with respect to the EOM-CCSD reference are also given for the valence, the Rydberg and all the excitation energies. We also report the position of the ionization threshold for each DFT method, as given by the opposite of the HOMO orbital energy. The excitation energies for all molecules are also plotted in Figure 6.5. As expected, KS gives reasonably small errors for the valence excitation energies (MAD between 0.36 and 0.73 eV) but deteriorates for the Rydberg ones (MAD between 0.49 and 1.83 eV) which are largely underestimated, as seen in Figure 6.5. As well known [29], in KS with the LDA functional, the ionization energy is much too small, resulting in most of the Rydberg states and some of the valence states being in the continuum above the ionization threshold, and which are thus very much dependent on the basis set. This problem is absent in HF and range-separated approaches which correctly push up the ionization threshold. The HF excitation energies are usually larger than the reference ones except for the first triplet excitation energies which are much too small or even imaginary because of the HF triplet (near-)instability. Overall, HF gives relatively large total MADs (between 0.59 and 1.62 eV).

The RSH excitation energies are in general intermediate between KS and HF ones and in good agreement with the EOM-CCSD ones. The valence and Rydberg excitation energies are treated with a more uniform accuracy (MAD between 0.06 and 0.61 eV). However, the first triplet excitation energies are affected by the HF triplet near-

instability and can be very underestimated. This effect is particularly important for the first triplet excitation energy of C_2H_4 and C_6H_6 as shown in Tables 6.4 and 6.5. This underestimation is largely cured by the Tamm-Dancoff approximation, as shown by the RSH-TDA results. The quality of the other excitation energies is not deteriorated with this approximation, so that RSH-TDA gives overall smallest MADs than RSH. However, the oscillator strengths which were relatively good in RSH tend to be overestimated for excitations to valence states in RSH-TDA. This has been connected with the fact that the TDA oscillator strengths violate the Thomas-Reiche-Kuhn sum rule. The present RSH results give thus very much the same trends already observed with other types of range-separated TDDFT approaches [40, 75, 86, 89, 135].

The first singlet CT excitation energy in the C_2H_4 - C_2F_4 dimer along the intermolecular distance coordinate R , for R between 5 and 10 Å (i.e. between 9.45 and 18.90 bohr), is given in Figure 6.6. This excitation corresponds to an electron transfer from the HOMO of C_2F_4 to the LUMO of C_2H_4 . Therefore, its energy must behave asymptotically as $I_{C_2F_4} - A_{C_2H_4} - 1/R$, where $I_{C_2F_4}$ is the ionization potential of the tetrafluoroethylene and $A_{C_2H_4}$ is the electron affinity of ethylene. A fit of the form $a + b/R$ was performed and the fitted parameters are shown in Figure 6.6. The well-known deficiency of KS with the LDA functional to describe the $-1/R$ dependence of such excitations is observed as it gives a parameter b close to zero, while HF and RSH both give the expected correct asymptotic behavior in $-1/R$ thanks to the non-locality of their exchange kernel [36].

6.5.3 Effect of the LDA correlation

Tables 6.1-6.5 also report results obtained with the LC scheme using the short-range exchange LDA functional and the full-range LDA correlation functional. The comparison with the RSH results allows one to see the global effect of long-range LDA correlation in the ground-state calculation and in the linear-response kernel. The RSH and LC excitation energies are globally quite close to each other, the largest difference being of 0.2 eV for the $^3\Pi$ Rydberg state of the CO molecule. In most cases, the LC excitation energies are slightly larger than the RSH ones. In comparison to the RSH scheme, the LC scheme gives slightly smaller MADs (by 0.01 to 0.08 eV) for valence excitation energies, but with the exception of CO it gives larger MADs (by 0.07 to 0.09 eV) for Rydberg excitation energies. The RSH and LC oscillator strengths are quite similar. This shows that long-range LDA correlation has a quite small effect for the systems and states considered here, and can be disregarded without much consequence.

The first CT excitation energy in the C_2H_4 - C_2F_4 dimer obtained with the LC scheme is also reported in Figure 6.6. Not surprisingly, the RSH and LC curves have the same $-1/R$ behavior, which is given by the long-range HF exchange kernel, and are essentially on-top on each other, showing that long-range LDA correlation has almost no effect on the HOMO and LUMO orbital energies.

To investigate the effect of the short-range LDA correlation kernel, Tables 6.1-6.5

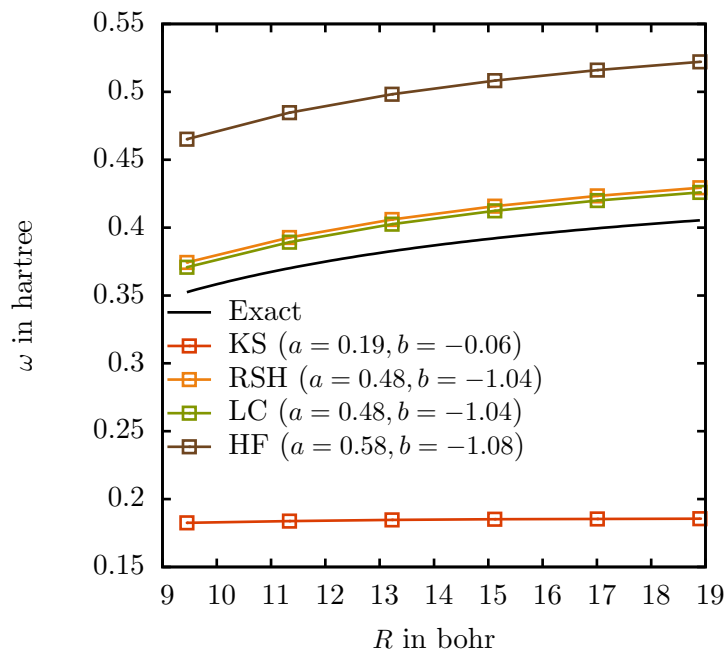


Figure 6.6 – First charge transfer excitation energy of the $\text{C}_2\text{H}_4\text{-C}_2\text{F}_4$ dimer calculated by linear-response HF and KS (with the LDA functional) and by the linear-response range-separated methods RSH and LC (with the short-range LDA functional and $\mu = 0.4 \text{ bohr}^{-1}$) using the 6-31G* basis. A fit of the form $a + b/R$ was performed. The fitted parameters a and b are given in atomic units.

also report RSH-fHx results obtained with regular RSH orbitals but no correlation kernel at all. Removing the short-range LDA correlation kernel tends to yield larger singlet excitation energies and smaller triplet excitation energies. This is not unexpected since the singlet LDA correlation kernel is negative and the triplet LDA correlation kernel is positive, as shown in Figure 6.2. In comparison to the RSH results, RSH-fHx gives quite similar singlet valence excitation energies and Rydberg excitation energies, but much lower triplet valence excitation energies (sometimes by as much as 0.5 eV), leading to significantly larger MADs for valence excitations. The short-range part of the LDA correlation kernel is thus important and cannot be neglected.

6.6 Conclusion

We have studied a linear-response range-separated scheme, which combines a long-range HF exchange kernel with a short-range LDA exchange-correlation kernel, for calculating electronic excitation energies and oscillator strengths of molecular systems. It is a first-level approximation before adding an explicit treatment of long-range correlation. It can also be seen as an alternative to the widely used linear-response LC scheme which combines a long-range HF exchange kernel with a short-range DFT exchange functional

and a full-range DFT correlation functional.

Tests on the N_2 , CO, H_2CO , C_2H_4 , and C_6H_6 molecules have shown that a reasonable value for the range-separation parameter is $\mu = 0.4 \text{ bohr}^{-1}$, which is consistent with what was previously reported in the literature for other types of range-separated TDDFT methods. Just like in the LC scheme, the introduction of long-range HF exchange in the present method corrects the well-known underestimation of high-lying Rydberg excitation energies of standard TDDFT using (semi)local density-functional approximations, but also leads to underestimated excitation energies to low-lying spin-triplet valence states. This latter problem is known to be associated with the presence of HF triplet near-instabilities and is largely cured by the Tamm-Dancoff approximation which leads to a relatively uniform accuracy for all excitation energies, but possibly at the cost of deteriorating the oscillator strengths. As expected, tests on the first CT excitation energy in the C_2H_4 - C_2F_4 have shown that the present range-separated TDDFT method also correctly describe this kind of excitations.

For the systems and states considered here the presence of long-range LDA correlation in the ground-state calculation and in the linear-response kernel has a quite small effect, so that the present method gives results very similar to the ones given by the LC scheme. Long-range LDA correlation can therefore be disregarded. In contrast, the short-range LDA correlation kernel is important for singlet \rightarrow triplet valence excitation energies and cannot be neglected. This work thus suggests that the present range-separated TDDFT scheme is a reasonable starting approximation for describing electronic excitation energies. The next step of this work is then to add to the present method an explicit frequency-dependent long-range correlation kernel derived from perturbation theory, e.g. in the spirit of Refs. [52, 57], which would add the possibility of describing double excitations.

State	Transition	KS	RSH	RSH-TDA	LC	RSH-fHx	HF	EOM-CCSD
Valence excitation energies (eV)								
$^3\Sigma_u^+$	$1\pi_u \rightarrow 1\pi_g$	7.87	7.19	7.63	7.31	6.65	3.47	7.72
$^3\Pi_g$	$3\sigma_g \rightarrow 1\pi_g$	7.54	7.84	7.90	7.88	7.67	7.62	8.16
$^3\Delta_u$	$1\pi_u \rightarrow 1\pi_g$	8.82	8.26	8.45	8.31	8.03	5.86	9.07
$^1\Pi_g$	$3\sigma_g \rightarrow 1\pi_g$	9.05	9.43	9.57	9.43	9.47	9.77	9.55
$^3\Sigma_u^-$	$1\pi_u \rightarrow 1\pi_g$	9.65	9.23	9.26	9.22	9.23	7.94	10.00
$^1\Sigma_u^-$	$1\pi_u \rightarrow 1\pi_g$	9.65	9.23	9.26	9.22	9.23	7.94	10.24
$^1\Delta_u$	$1\pi_u \rightarrow 1\pi_g$	10.22	9.90	9.91	9.90	9.95	8.78	10.66
$^3\Pi_u$	$2\sigma_u \rightarrow 1\pi_g$	10.36	10.77	10.86	10.82	10.53	11.28	11.36
Rydberg excitation energies (eV)								
$^3\Sigma_g^+$	$3\sigma_g \rightarrow 4\sigma_g$	10.28	11.78	11.79	11.94	11.73	13.05	11.74
$^1\Sigma_g^+$	$3\sigma_g \rightarrow 4\sigma_g$	<i>10.39</i>	12.26	12.29	12.38	12.26	13.98	12.15
$^3\Sigma_u^+$	$3\sigma_g \rightarrow 3\sigma_u$	<i>10.62</i>	12.63	12.64	12.87	12.59	14.16	12.70
$^3\Pi_u$	$3\sigma_g \rightarrow 2\pi_u$	<i>10.99</i>	12.62	12.62	12.83	12.59	14.56	12.71
$^1\Pi_u$	$3\sigma_g \rightarrow 2\pi_u$	<i>10.98</i>	12.74	12.74	12.87	12.75	13.21	12.77
$^1\Sigma_u^+$	$3\sigma_g \rightarrow 3\sigma_u$	<i>10.62</i>	12.76	12.77	12.89	12.78	14.00	12.82
Ionization threshold: $-\epsilon_{\text{HOMO}}$ (eV)								
		10.38	15.34	15.34	15.76	15.34	16.74	
MAD of excitation energies with respect to EOM-CCSD (eV)								
Valence		0.49	0.61	0.49	0.58	0.75	1.82	-
Rydberg		1.83	0.06	0.07	0.15	0.07	1.35	-
Total		1.06	0.38	0.31	0.40	0.46	1.62	-
Oscillator strengths ($\times 10^{-2}$)								
$^1\Pi_u$	$3\sigma_g \rightarrow 2\pi_u$	2.41	9.49	9.42	12.77	9.00	8.42	8.51
$^1\Sigma_u^+$	$3\sigma_g \rightarrow 3\sigma_u$	1.06	21.11	19.17	27.59	19.94	73.31	17.36

Table 6.1 – Excitation energies and oscillator strengths of N_2 calculated by linear-response HF and KS (with the LDA functional), by the linear-response range-separated methods RSH, RSH-TDA, LC, and RSH-fHx (with the short-range LDA functional and $\mu = 0.4 \text{ bohr}^{-1}$), and by EOM-CCSD taken as reference, using the Sadlej+ basis set. Excitation energies above the ionization threshold are indicated in italics.

State	Transition	KS	RSH	RSH-TDA	LC	RSH-fHx	HF	EOM-CCSD
Valence excitation energies (eV)								
$^3\Pi$	$5a_1(\sigma) \rightarrow 2e_1(\pi^*)$	5.95	5.95	6.10	6.06	5.62	5.28	6.45
$^3\Sigma^+$	$1e_1(\pi) \rightarrow 2e_1(\pi^*)$	8.38	8.15	8.43	8.22	7.72	6.33	8.42
$^1\Pi$	$5a_1(\sigma) \rightarrow 2e_1(\pi^*)$	8.18	8.49	8.73	8.49	8.55	8.80	8.76
$^3\Delta$	$1e_1(\pi) \rightarrow 2e_1(\pi^*)$	<i>9.16</i>	8.99	9.11	9.02	8.80	7.87	9.39
$^3\Sigma^-$	$1e_1(\pi) \rightarrow 2e_1(\pi^*)$	<i>9.84</i>	9.77	9.79	9.75	9.77	9.37	9.97
$^1\Sigma^-$	$1e_1(\pi) \rightarrow 2e_1(\pi^*)$	<i>9.84</i>	9.77	9.79	9.75	9.77	9.37	10.19
$^1\Delta$	$1e_1(\pi) \rightarrow 2e_1(\pi^*)$	<i>10.31</i>	10.31	10.31	10.29	10.35	9.96	10.31
$^3\Pi$	$4a_1(\sigma) \rightarrow 2e_1(\pi^*)$	<i>11.40</i>	12.05	12.10	12.05	11.91	13.05	12.49
Rydberg excitation energies (eV)								
$^3\Sigma^+$	$5a_1(\sigma) \rightarrow 6a_1(\sigma)$	<i>9.55</i>	10.55	10.57	10.72	10.46	11.07	10.60
$^1\Sigma^+$	$5a_1(\sigma) \rightarrow 6a_1(\sigma)$	<i>9.93</i>	11.32	11.38	11.36	11.34	12.23	11.15
$^3\Sigma^+$	$5a_1(\sigma) \rightarrow 7a_1(\sigma)$	<i>10.26</i>	11.34	11.35	11.51	11.29	12.40	11.42
$^1\Sigma^+$	$5a_1(\sigma) \rightarrow 7a_1(\sigma)$	<i>10.47</i>	11.58	11.59	11.63	11.60	12.78	11.64
$^3\Pi$	$5a_1(\sigma) \rightarrow 3e_1(\pi)$	<i>10.39</i>	11.53	11.54	11.73	11.49	12.52	11.66
$^1\Pi$	$5a_1(\sigma) \rightarrow 3e_1(\pi)$	<i>10.48</i>	11.72	11.73	11.81	11.73	12.87	11.84
Ionization threshold: $-\epsilon_{\text{HOMO}}$ (eV)								
		9.12	13.83	13.83	14.27	13.83	15.11	
MAD of excitation energies with respect to the EOM-CCSD calculation (eV)								
Valence		0.36	0.31	0.20	0.29	0.45	0.89	-
Rydberg		1.21	0.10	0.10	0.09	0.13	0.92	-
Total		0.73	0.22	0.16	0.20	0.31	0.91	-
Oscillator strengths ($\times 10^{-2}$)								
$^1\Pi$	$5a_1(\sigma) \rightarrow 2e_1(\pi^*)$	8.69	8.64	11.47	8.73	8.49	8.55	8.66
$^1\Sigma^+$	$5a_1(\sigma) \rightarrow 6a_1(\sigma)$	1.84	4.26	4.27	3.70	3.85	10.58	0.58
$^1\Sigma^+$	$5a_1(\sigma) \rightarrow 7a_1(\sigma)$	12.53	13.73	14.39	15.86	13.73	9.39	20.71
$^1\Pi$	$5a_1(\sigma) \rightarrow 3e_1(\pi)$	2.71	4.72	4.45	5.45	4.58	5.14	4.94

Table 6.2 – Excitation energies and oscillator strengths of CO calculated by linear-response HF and KS (with the LDA functional), by the linear-response range-separated methods RSH, RSH-TDA, LC, and RSH-fHx (with the short-range LDA functional and $\mu = 0.4 \text{ bohr}^{-1}$), and by EOM-CCSD taken as reference, using the Sadlej+ basis set. Excitation energies above the ionization threshold are indicated in italics.

State	Transition	KS	RSH	RSH-TDA	LC	RSH-fHx	HF	EOM-CCSD
Valence excitation energies (eV)								
3A_2	$2b_2(n) \rightarrow 2b_1(\pi^*)$	3.06	3.17	3.22	3.16	3.08	3.44	3.56
1A_2	$2b_2(n) \rightarrow 2b_1(\pi^*)$	3.67	3.84	3.88	3.82	3.86	4.41	4.03
3A_1	$1b_1(\pi) \rightarrow 2b_1(\pi^*)$	6.22	5.65	6.01	5.74	5.25	2.15	6.06
3B_1	$5a_1(\sigma) \rightarrow 2b_1(\pi^*)$	<i>7.74</i>	8.11	8.16	8.11	7.99	8.19	8.54
Rydberg excitation energies (eV)								
3B_2	$2b_2(n) \rightarrow 6a_1(\sigma)$	5.84	7.06	7.07	7.17	7.01	8.09	6.83
1B_2	$2b_2(n) \rightarrow 6a_1(\sigma)$	5.92	7.26	7.27	7.30	7.28	8.55	7.00
3B_2	$2b_2(n) \rightarrow 7a_1(\sigma)$	<i>6.96</i>	7.91	7.92	7.99	7.86	8.98	7.73
3A_1	$2b_2(n) \rightarrow 3b_2(\sigma)$	<i>6.73</i>	8.01	8.01	8.17	7.96	9.19	7.87
1B_2	$2b_2(n) \rightarrow 7a_1(\sigma)$	<i>7.04</i>	8.15	8.16	8.17	8.17	9.39	7.93
1A_1	$2b_2(n) \rightarrow 3b_2(\sigma)$	<i>6.77</i>	8.18	8.19	8.27	8.19	9.28	7.99
1A_2	$2b_2(n) \rightarrow 3b_1(\pi)$	<i>7.55</i>	8.58	8.58	8.67	8.58	10.04	8.45
3A_2	$2b_2(n) \rightarrow 3b_1(\pi)$	<i>7.58</i>	8.57	8.57	8.70	8.56	9.84	8.47
3B_2	$2b_2(n) \rightarrow 8a_1(\sigma)$	<i>7.97</i>	9.12	9.14	9.24	9.06	10.24	8.97
1B_2	$2b_2(n) \rightarrow 8a_1(\sigma)$	<i>8.17</i>	9.42	9.44	9.49	9.44	10.84	9.27
Ionization threshold: $-\epsilon_{\text{HOMO}}$ (eV)								
		6.30	10.63	10.63	11.06	10.63	12.04	
MAD of excitation energies with respect to EOM-CCSD (eV)								
Valence		0.46	0.36	0.23	0.34	0.50	1.19	-
Rydberg		1.00	0.18	0.19	0.26	0.16	1.39	-
Total		0.84	0.23	0.20	0.29	0.26	1.34	-
Oscillator strengths ($\times 10^{-2}$)								
1B_2	$2b_2(n) \rightarrow 6a_1(\sigma)$	3.13	1.77	1.91	1.88	1.69	2.99	2.15
1B_2	$2b_2(n) \rightarrow 7a_1(\sigma)$	2.05	4.58	4.77	5.04	4.47	4.46	4.12
1A_1	$2b_2(n) \rightarrow 3b_2(\sigma)$	4.34	5.35	5.82	6.07	5.18	21.31	5.70
1B_2	$2b_2(n) \rightarrow 8a_1(\sigma)$	4.27	4.01	4.45	4.08	3.88	6.65	4.22

Table 6.3 – Excitation energies and oscillator strengths of H_2CO calculated by linear-response HF and KS (with the LDA functional), by the linear-response range-separated methods RSH, RSH-TDA, LC, and RSH-fHx (with the short-range LDA functional and $\mu = 0.4$ bohr $^{-1}$), and by EOM-CCSD taken as reference, using the Sadlej+ basis set. The molecule is oriented in the yz plane along the z axis. Excitation energies above the ionization threshold are indicated in italics.

State	Transition	KS	RSH	RSH-TDA	LC	RSH-fHx	HF	EOM-CCSD
Valence excitation energies (eV)								
$^3B_{1u}$	$1b_{3u}(\pi) \rightarrow 1b_{2g}(\pi^*)$	4.62	3.78	4.24	3.92	4.01	0.16	4.41
$^1B_{1u}$	$1b_{3u}(\pi) \rightarrow 1b_{2g}(\pi^*)$	7.45	7.60	8.07	7.59	8.14	7.35	8.00
$^3B_{1g}$	$1b_{3g}(\sigma) \rightarrow 1b_{2g}(\pi^*)$	7.18	8.03	8.04	8.15	8.02	8.36	8.21
$^1B_{1g}$	$1b_{3g}(\sigma) \rightarrow 1b_{2g}(\pi^*)^{(a)}$	7.47	8.15	8.17	8.22	8.18	9.36	8.58
Rydberg excitation energies (eV)								
$^3B_{3u}$	$1b_{3u}(\pi) \rightarrow 4a_{1g}(\sigma)$	6.58	7.32	7.33	7.44	7.30	6.87	7.16
$^1B_{3u}$	$1b_{3u}(\pi) \rightarrow 4a_{1g}(\sigma)$	6.65	7.49	7.49	7.54	7.50	7.13	7.30
$^3B_{1g}$	$1b_{3u}(\pi) \rightarrow 2b_{2u}(\sigma)$	6.97	7.51	7.54	7.50	7.47	7.63	7.91
$^3B_{2g}$	$1b_{3u}(\pi) \rightarrow 3b_{1u}(\sigma)$	7.10	8.16	8.17	8.29	8.15	7.75	7.93
$^1B_{1g}$	$1b_{3u}(\pi) \rightarrow 2b_{2u}(\sigma)^{(b)}$	7.19	8.04	8.05	8.02	8.07	7.74	7.97
$^1B_{2g}$	$1b_{3u}(\pi) \rightarrow 3b_{1u}(\sigma)$	7.15	8.27	8.27	8.38	8.28	7.91	8.01
3A_g	$1b_{3u}(\pi) \rightarrow 2b_{3u}(\pi)$	8.03	8.55	8.56	8.76	8.51	7.97	8.48
1A_g	$1b_{3u}(\pi) \rightarrow 2b_{3u}(\pi)$	8.27	8.95	8.99	9.02	9.01	8.57	8.78
$^3B_{3u}$	$1b_{3u}(\pi) \rightarrow 5a_{1g}(\sigma)$	8.26	9.08	9.09	9.20	9.05	8.71	9.00
$^1B_{3u}$	$1b_{3u}(\pi) \rightarrow 5a_{1g}(\sigma)$	8.28	9.22	9.23	9.30	9.24	8.92	9.07
Ionization threshold: $-\epsilon_{\text{HOMO}}$ (eV)								
		6.89	10.61	10.61	11.07	10.61	10.23	
MAD of excitation energies with respect to EOM-CCSD (eV)								
Valence		0.73	0.41	0.20	0.33	0.28	1.46	-
Rydberg		0.71	0.18	0.19	0.27	0.18	0.24	-
Total		0.72	0.24	0.19	0.29	0.21	0.59	-
Oscillator strengths ($\times 10^{-2}$)								
$^1B_{1u}$	$1b_{3u}(\pi) \rightarrow 1b_{2g}(\pi^*)$	30.34	35.42	49.11	35.77	35.10	39.99	36.29
$^1B_{3u}$	$1b_{3u}(\pi) \rightarrow 4a_{1g}(\sigma)$	6.69	7.64	7.88	8.22	7.38	9.08	8.16
$^1B_{3u}$	$1b_{3u}(\pi) \rightarrow 5a_{1g}(\sigma)$	0.08	1.26	1.25	2.07	1.14	0.63	0.61

Table 6.4 – Excitation energies and oscillator strengths of C_2H_4 calculated by linear-response HF and KS (with the LDA functional), by the linear-response range-separated methods RSH, RSH-TDA, LC, and RSH-fHx (with the short-range LDA functional and $\mu = 0.4 \text{ bohr}^{-1}$), and by EOM-CCSD taken as reference, using the Sadlej+ basis set. The molecule is oriented in the yz plane along the z axis. Excitation energies above the ionization threshold are indicated in italics. ^(a) and ^(b): These two excitations mix heavily in LDA [32, 136] and the leading orbital contribution to the excitation changes with the range-separation parameter. Adiabatic curves respect to μ were followed to do the assignment, with state (b) defined as the lowest $^1B_{1g}$ state with orbital transitions $1b_{3g}(\sigma) \rightarrow 1b_{2g}(\pi^*)$ and $1b_{3u}(\pi) \rightarrow 2b_{2u}(\sigma)$, and state (a) defined as the second lowest one.

State	Transition	KS	RSH	RSH-TDA	LC	RSH-fHx	HF	EOM-CCSD
Valence excitation energies (eV)								
${}^3B_{1u}$	$1e_{1g}(\pi) \rightarrow 1e_{2u}(\pi^*)$	4.35	3.37	4.06	3.49	2.88	-	3.96
${}^3E_{1u}$	$1e_{1g}(\pi) \rightarrow 1e_{2u}(\pi^*)$	4.69	4.81	4.85	4.84	4.69	4.68	4.90
${}^1B_{2u}$	$1e_{1g}(\pi) \rightarrow 1e_{2u}(\pi^*)$	5.20	5.45	5.56	5.45	5.47	5.78	5.15
${}^3B_{2u}$	$1e_{1g}(\pi) \rightarrow 1e_{2u}(\pi^*)$	4.94	5.02	5.20	5.05	4.95	5.02	5.78
${}^1B_{1u}$	$1e_{1g}(\pi) \rightarrow 1e_{2u}(\pi^*)$	5.97	6.25	6.49	6.24	6.29	5.84	6.52
${}^1E_{1u}$	$1e_{1g}(\pi) \rightarrow 1e_{2u}(\pi^*)$	<i>6.80</i>	7.14	7.65	7.13	7.16	7.34	7.30
Rydberg excitation energies (eV)								
${}^3E_{1g}$	$1e_{1g}(\pi) \rightarrow 4a_{1g}(\sigma)$	6.01	7.00	7.00	7.10	7.00	6.46	6.40
${}^1E_{1g}$	$1e_{1g}(\pi) \rightarrow 4a_{1g}(\sigma)$	6.03	7.08	7.08	7.14	7.09	6.59	6.46
${}^3A_{2u}$	$1e_{1g}(\pi) \rightarrow 4e_{1u}(\sigma)$	<i>6.52</i>	7.43	7.43	7.56	7.43	6.87	6.92
${}^1A_{2u}$	$1e_{1g}(\pi) \rightarrow 4e_{1u}(\sigma)$	<i>6.54</i>	7.53	7.53	7.63	7.53	7.01	7.00
${}^3E_{2u}$	$1e_{1g}(\pi) \rightarrow 4e_{1u}(\sigma)$	<i>6.54</i>	7.68	7.68	7.83	7.68	7.17	7.06
${}^1E_{2u}$	$1e_{1g}(\pi) \rightarrow 4e_{1u}(\sigma)$	<i>6.55</i>	7.71	7.71	7.84	7.71	7.21	7.08
${}^1A_{1u}$	$1e_{1g}(\pi) \rightarrow 4e_{1u}(\sigma)$	<i>6.59</i>	7.90	7.90	8.05	7.90	7.43	7.18
${}^3A_{1u}$	$1e_{1g}(\pi) \rightarrow 4e_{1u}(\sigma)$	<i>6.59</i>	7.90	7.90	8.05	7.90	7.43	7.19
Ionization threshold: $-\epsilon_{\text{HOMO}}$ (eV)								
		6.50	9.72	9.72	10.18	9.72	9.15	
MAD of excitation energies with respect to EOM-CCSD (eV)								
Valence		0.39	0.32	0.22	0.29	0.43	0.93	-
Rydberg		0.49	0.61	0.62	0.74	0.62	0.12	-
Total		0.45	0.49	0.45	0.55	0.54	0.47	-
Oscillator strengths ($\times 10^{-2}$)								
${}^1E_{1u}$	$1e_{1g}(\pi) \rightarrow 1e_{2u}(\pi^*)$	55.78	62.74	91.09	63.00	62.42	71.49	66.41
${}^1A_{2u}$	$1e_{1g}(\pi) \rightarrow 4e_{1u}(\sigma)$	2.11	7.10	7.44	8.27	6.87	7.69	7.04

Table 6.5 – Excitation energies and oscillator strengths of C_6H_6 calculated by linear-response HF and KS (with the LDA functional), by the linear-response range-separated methods RSH, RSH-TDA, LC, and RSH-fHx (with the short-range LDA functional and $\mu = 0.4$ bohr $^{-1}$), and by EOM-CCSD taken as reference, using the Sadlej+ basis set. Excitation energies above the ionization threshold are indicated in italics. Except for the E_{1g} states whose assignments were trivial, all the other states correspond to the orbital transitions $e_{1g} \rightarrow e_{2u}$ and $e_{1g} \rightarrow e_{1u}$, which lead to $B_{1u} \oplus E_{1u} \oplus B_{2u}$ and $A_{1u} \oplus E_{2u} \oplus A_{2u}$ manifolds, respectively, in the D_{6h} symmetry point-group. Since the calculations were performed in the D_{2h} subgroup, some symmetry information for these states was lost but the assignment could be done using the degeneracy of the states.

Bibliography

- [1] M. Casida. “Time-Dependent Density-functional response theory for molecules”. In: *Recent Adv. Density Funct. Methods, Part I*. Ed. by D. P. Chong. Singapore: World Scientific, 1995, p. 155.
- [2] E. K. U. Gross, J. F. Dobson, and M. Petersilka. “Density Functional Theory of Time-Dependent Phenomena”. In: *Top. Curr. Chem.* Ed. by R. Nalewajski. Vol. 60. Topics in Current Chemistry. Berlin: Springer, 1996, p. 81.
- [3] M. Petersilka, U. J. Gossmann, and E. K. U. Gross. 1996. *Phys. Rev. Lett.* 76. P. 1212.
- [4] H. Appel, E. K. U. Gross, and K. Burke. 2003. *Phys. Rev. Lett.* 90. P. 043005.
- [5] M. E. Casida. 2009. *J. Mol. Struct. THEOCHEM.* 914. Pp. 3–18.
- [6] P. Elliott, K. Burke, and F. Furche. “Excited states from time-dependent density functional theory”. In: *Rev. Comput. Chem.* Ed. by K. B. Lipkowitz and T. R. Cundari. Vol. 26. 91. NJ: Wiley, Hoboken, 2009, pp. 91–165.
- [7] E. K. U. Gross and N. T. Maitra. *Fundamentals of Time-Dependent Density Functional Theory*. Ed. by M. A. Marques, N. T. Maitra, F. M. Nogueira, et al. Vol. 837. Lecture Notes in Physics. Berlin, Heidelberg: Springer Berlin Heidelberg, 2012.
- [8] C. A. Ullrich and Z.-H. Yang. 2014. *Brazilian J. Phys.* 44. Pp. 154–188.
- [9] G. Wick. 1950. *Phys. Rev.* 80. P. 268.
- [10] M. Dasgupta. *An introduction to quantum field theory*. 2008. URL: <http://cds.cern.ch/record/257493>.
- [11] E. Runge and E. K. U. Gross. 1984. *Phys. Rev. Lett.* 52. Pp. 997–1000.
- [12] E. K. U. Gross and W. Kohn. 1990. *Adv. Quantum Chem.*
- [13] R. van Leeuwen. 1999. *Phys. Rev. Lett.* 82. Pp. 3863–3866.
- [14] R. van Leeuwen. 2006. *Lect. Notes Phys.* 706. Pp. 17–31.
- [15] M. Ruggenthaler and R. van Leeuwen. 2011. *Europhys. Lett.* 95. Pp. 1–6.
- [16] M. Ruggenthaler, K. J. H. Giesbertz, M. Penz, and R. van Leeuwen. 2012. *Phys. Rev. A.* 85. Pp. 1–20.
- [17] G. Vignale. 2004. *Phys. Rev. B.* 70. P. 201102.

BIBLIOGRAPHY

- [18] R. van Leeuwen. 1998. *Phys. Rev. Lett.* 80. Pp. 1280–1283.
- [19] R. van Leeuwen. 2001. *Int. J. Mod. Phys. B.* 15. Pp. 1969–2023.
- [20] G. Vignale. 2008. *Phys. Rev. A.* 77. P. 062511.
- [21] M. A. Mosquera. 2013. *Phys. Rev. A.* 88. P. 022515.
- [22] S. Hirata and M. Head-Gordon. 1999. *Chem. Phys. Lett.* 314. Pp. 291–299.
- [23] M. E. Casida, F. Gutierrez, J. Guan, et al. 2000. *J. Chem. Phys.* 113. P. 7062.
- [24] T. Ziegler, M. Seth, M. Krykunov, et al. 2009. *J. Chem. Phys.* 130. P. 154102.
- [25] M. E. Casida and M. Huix-Rotllant. 2012. *Annu. Rev. Phys. Chem.* 63. P. 287.
- [26] R. Bauernschmitt and R. Ahlrichs. 1996. *Chem. Phys. Lett.* 2614.
- [27] J. Tao, S. Tretiak, and J.-X. Zhu. 2008. *J. Chem. Phys.* 128. P. 084110.
- [28] M. J. G. Peach, P. Benfield, T. U. Helgaker, and D. J. Tozer. 2008. *J. Chem. Phys.* 128. P. 044118.
- [29] M. E. Casida, C. Jamorski, K. C. Casida, and D. R. Salahub. 1998. *J. Chem. Phys.* 108. P. 4439.
- [30] A. Wasserman, N. Maitra, and K. Burke. 2003. *Phys. Rev. Lett.* 91. P. 263001.
- [31] D. Tozer and N. Handy. 1998. *J. Chem. Phys.* 109. Pp. 10180–10189.
- [32] M. E. Casida and D. R. Salahub. 2000. *J. Chem. Phys.* 113. Pp. 8918–8935.
- [33] M. J. Allen and D. J. Tozer. 2000. *J. Chem. Phys.* 113. P. 5185.
- [34] M. Grüning, O. V. Gritsenko, S. J. A. van Gisbergen, and E. J. Baerends. 2001. *J. Chem. Phys.* 114. P. 652.
- [35] Y. Zhao and D. G. Truhlar. 2006. *J. Phys. Chem. A.* 110. Pp. 13126–30.
- [36] A. Dreuw, J. L. Weisman, and M. Head-Gordon. 2003. *J. Chem. Phys.* 119. P. 2943.
- [37] A. Dreuw and M. Head-Gordon. 2004. *J. Am. Chem. Soc.* 126. Pp. 4007–4016.
- [38] N. Kuritz, T. Stein, R. Baer, and L. Kronik. 2011. *J. Chem. Theory Comput.* 7. Pp. 2408–2415.
- [39] Y. Zhao and D. G. Truhlar. 2006. *J. Chem. Phys.* 125. P. 194101.
- [40] Y. Tawada, T. Tsuneda, S. Yanagisawa, et al. 2004. *J. Chem. Phys.* 120. P. 8425.
- [41] T. Stein, L. Kronik, and R. Baer. 2009. *J. Am. Chem. Soc.* 131. Pp. 2818–20.
- [42] L. Kronik, T. Stein, S. Refaely-Abramson, and R. Baer. 2012. *J. Chem. Theory Comput.* 8. Pp. 1515–1531.
- [43] R. J. Cave, F. Zhang, N. T. Maitra, and K. Burke. 2004. *Chem. Phys. Lett.* 389. Pp. 39–42.
- [44] J. H. Starcke, M. Wormit, J. Schirmer, and A. Dreuw. 2006. *Chem. Phys.* 329. Pp. 39–49.

-
- [45] P. Elliott, S. Goldson, C. Canahui, and N. T. Maitra. 2011. *Chem. Phys.* 391. Pp. 110–119.
- [46] O. Gritsenko, S. V. Gisbergen, A. Görling, and E. J. Baerends. 2000. *J. Chem. Phys.* 113. Pp. 8478–8489.
- [47] S. Hirata and M. Head-Gordon. 1999. *Chem. Phys. Lett.* Pp. 375–382.
- [48] D. Tozer and N. Handy. 2000. *Phys. Chem. Chem. Phys.* Pp. 2117–2121.
- [49] C.-P. Hsu, S. Hirata, and M. Head-Gordon. 2001. *J. Phys. Chem. A.* 105. P. 451.
- [50] N. T. Maitra, F. Zhang, R. J. Cave, and K. Burke. 2004. *J. Chem. Phys.* 120. P. 5932.
- [51] M. E. Casida. 2005. *J. Chem. Phys.* 122. P. 54111.
- [52] M. Huix-Rotllant and M. E. Casida. 2010. *arXiv Prepr. arXiv1008.1478*.
- [53] O. V. Gritsenko and E. J. Baerends. 2009. *Phys. Chem. Chem. Phys.* 11. P. 4640.
- [54] O. V. Gritsenko and E. J. Baerends. 2001. *Phys. Rev. A.* 64. P. 042506.
- [55] M. Grüning, O. V. Gritsenko, S. J. a. van Gisbergen, and E. Jan Baerends. 2002. *J. Chem. Phys.* 116. P. 9591.
- [56] J. Schirmer. 1982. *Phys. Rev. A.* 26.
- [57] P. Romaniello, D. Sangalli, J. A. Berger, et al. 2009. *J. Chem. Phys.* 130. P. 044108.
- [58] D. Sangalli, P. Romaniello, G. Onida, and A. Marini. 2011. *J. Chem. Phys.* 134. P. 34115.
- [59] D. Zhang, S. N. Steinmann, and W. Yang. 2013. *J. Chem. Phys.* 139. P. 154109.
- [60] J. Oddershede. 1978. *Adv. Quantum Chem.* 11. P. 275.
- [61] E. S. Nielsen, P. Jørgensen, and J. Oddershede. 1980. *J. Chem. Phys.* 73. P. 499.
- [62] J. Oddershede, P. Jørgensen, and D. L. Yeager. 1984. *Comput. Phys. Reports.* 2. Pp. 33–92.
- [63] M. J. Packer, E. K. Dalskov, T. Enevoldsen, et al. 1996. *J. Chem. Phys.* 105. P. 5886.
- [64] M. Huix-Rotllant. “Improved correlation kernels for linear-response time-dependent density-functional theory”. PhD thesis. 2011.
- [65] H. Iikura, T. Tsuneda, T. Yanai, and K. Hirao. 2001. *J. Chem. Phys.* 115. P. 3540.
- [66] A. D. Becke. 1988. *Phys. Rev. A.* 38. Pp. 3098–3100.
- [67] T. Tsuneda, T. Suzumura, and K. Hirao. 1999. *J. Chem. Phys.* 110. P. 10664.
- [68] J. P. Perdew, K. Burke, and M. Ernzerhof. 1996. *Phys. Rev. Lett.* 77. P. 3865.
- [69] C. Lee, W. Yang, and R. G. Parr. 1988. *Phys. Rev. B.* 37. P. 785.
- [70] T. Yanai, D. P. Tew, and N. C. Handy. 2004. *Chem. Phys. Lett.* 393. Pp. 51–57.

BIBLIOGRAPHY

- [71] O. A. Vydrov and G. E. Scuseria. 2006. *J. Chem. Phys.* 125. P. 234109.
- [72] J.-D. Chai and M. Head-Gordon. 2008. *J. Chem. Phys.* 128. P. 084106.
- [73] J.-D. Chai and M. Head-Gordon. 2008. *Phys. Chem. Chem. Phys.* 10. P. 6615.
- [74] J.-D. Chai and M. Head-Gordon. 2009. *J. Chem. Phys.* 131. P. 174105.
- [75] G. Cui and W. Yang. 2010. *Mol. Phys.* 108. Pp. 2745–2750.
- [76] J. Toulouse, F. Colonna, and A. Savin. 2004. *Phys. Rev. A.* 70. P. 062505.
- [77] W. Kohn and L. J. Sham. 1965. *Phys. Rev.* 140. A1133–A1138.
- [78] J. G. Ángyán, I. Gerber, A. Savin, and J. Toulouse. 2005. *Phys. Rev. A.* 72. P. 012510.
- [79] E. Goll, H.-J. Werner, and H. Stoll. 2005. *Phys. Chem. Chem. Phys.* 7. P. 3917.
- [80] J. Toulouse, I. Gerber, G. Jansen, et al. 2009. *Phys. Rev. Lett.* 102. P. 096404.
- [81] B. G. Janesko, T. M. Henderson, and G. E. Scuseria. 2009. *J. Chem. Phys.* 130. P. 081105.
- [82] J. Toulouse, W. Zhu, J. G. Ángyán, and A. Savin. 2010. *Phys. Rev. A.* 82. P. 32502.
- [83] J. Toulouse, W. Zhu, A. Savin, et al. 2011. *J. Chem. Phys.* 135. P. 84119.
- [84] I. C. Gerber and J. G. Ángyán. 2005. *Chem. Phys. Lett.* 415. Pp. 100–105.
- [85] E. K. U. Gross and W. Kohn. 1985. *Phys. Rev. Lett.* 55. Pp. 2850–2852.
- [86] E. Livshits and R. Baer. 2007. *Phys. Chem. Chem. Phys.* 9. Pp. 2932–41.
- [87] T. Yanai, R. J. Harrison, and N. C. Handy. 2005. *Mol. Phys.* 103. Pp. 413–424.
- [88] M. J. G. Peach, T. Helgaker, P. Sałek, et al. 2006. *Phys. Chem. Chem. Phys.* 8. Pp. 558–62.
- [89] M. J. G. Peach, A. J. Cohen, and D. J. Tozer. 2006. *Phys. Chem. Chem. Phys.* 8. Pp. 4543–9.
- [90] A. W. Lange, M. A. Rohrdanz, and J. M. Herbert. 2008. *J. Phys. Chem. B.* 112. Pp. 6304–8.
- [91] M. A. Rohrdanz and J. M. Herbert. 2008. *J. Chem. Phys.* 129. P. 034107.
- [92] Y. Akinaga and S. Ten-no. 2008. *Chem. Phys. Lett.* 462. Pp. 348–351.
- [93] M. A. Rohrdanz, K. M. Martins, and J. M. Herbert. 2009. *J. Chem. Phys.* 130. P. 054112.
- [94] Y. Akinaga and S. Ten-no. 2009. *Int. J. Quantum Chem.* 109. P. 1905.
- [95] R. Peverati and D. G. Truhlar. 2011. *J. Phys. Chem. Lett.* 2. Pp. 2810–2817.
- [96] K. A. Nguyen, P. N. Day, and R. Pachter. 2011. *J. Chem. Phys.* 135. P. 074109.
- [97] Y.-S. Lin, C.-W. Tsai, G.-D. Li, and J.-D. Chai. 2012. *J. Chem. Phys.* 136. P. 154109.

-
- [98] J. Toulouse, F. Colonna, and A. Savin. 2005. *J. Chem. Phys.* 122. P. 14110.
- [99] J. Toulouse, F. F. Colonna, and A. Savin. 2005. *Mol. Phys.* 103. P. 2725.
- [100] K. Pernal. 2012. *J. Chem. Phys.* 136. P. 184105.
- [101] E. Fromager, S. Knecht, and H. J. A. Jensen. 2013. *J. Chem. Phys.* 138. P. 084101.
- [102] F. Wang and T. Ziegler. 2004. *J. Chem. Phys.* 121. Pp. 12191–6.
- [103] A. Savin and H.-J. Flad. 1995. *Int. J. Quantum Chem.* 56. Pp. 327–332.
- [104] A. Savin. “On degeneracy, near-degeneracy and density functional theory”. In: *Recent Dev. Appl. Mod. Density Funct. Theory*. Ed. by J.M. Seminario. Amsterdam: Elsevier, 1996, p. 327.
- [105] R. Baer and D. Neuhauser. 2005. *Phys. Rev. Lett.* 94. P. 43002.
- [106] E. Fromager and H. J. A. Jensen. 2008. *Phys. Rev. A.* 78. P. 022504.
- [107] J. Paier, B. G. Janesko, T. M. Henderson, et al. 2010. *J. Chem. Phys.* 132. P. 094103.
- [108] S. van Gisbergen, J. Snijders, and E. Baerends. 1999. *Comput. Phys. Commun.* 118. Pp. 119–138.
- [109] G. Oliver and J. Perdew. 1979. *Phys. Rev. A.* 20. P. 397.
- [110] J. Toulouse, A. Savin, and H.-J. Flad. 2004. *Int. J. Quantum Chem.* 100. P. 1047.
- [111] P. Gill and R. Adamson. 1996. *Chem. Phys. Lett.* 2614.
- [112] J. P. Perdew and Y. Wang. 1992. *Phys. Rev. B.* 45. Pp. 13244–13249.
- [113] S. Pazziani, S. Moroni, P. Gori-Giorgi, and G. Bachelet. 2006. *Phys. Rev. B.* 73. P. 155111.
- [114] P. Gori-Giorgi and A. Savin. 2006. *Phys. Rev. A.* 73. P. 032506.
- [115] K. Burke, J. P. Perdew, and M. Ernzerhof. 1998. *J. Chem. Phys.* 109. P. 3760.
- [116] P. Gori-Giorgi, M. Seidl, and A. Savin. 2008. *Phys. Chem. Chem. Phys.* 10. P. 3440.
- [117] K.-P. P. Huber and G. Herzberg. *Molecular Spectra and Molecular Structure - IV. Constants of Diatomic Molecules*. New York: Van Nostrand Reinhold, 1979.
- [118] H.-J. Werner, P. J. Knowles, G. Knizia, et al. *MOLPRO, version 2012.1, a package of ab initio programs*. Cardiff, UK, 2012.
- [119] O. Parisel and Y. Ellinger. 1996. *Chem. Phys.* 205. Pp. 323–349.
- [120] L. Serrano-Andrés, M. Merchán, I. Nebot-Gil, et al. 1993. *J. Chem. Phys.* 98. Pp. 3151–3162.
- [121] D. Wilden, P. Hicks, and J. Comer. 1979. *J. Phys. B.* 1579.
- [122] D. J. Clouthier and D. A. Ramsay. 1983. *Annu. Rev. Phys. Chem.* 34. Pp. 31–58.
- [123] S. Taylor, D. G. Wilden, and J. Comer. 1982. *Chem. Phys.* 70. Pp. 291–298.

BIBLIOGRAPHY

- [124] C. R. Lessard and D. C. Moule. 1977. *J. Chem. Phys.* 66. P. 3908.
- [125] M. J. Frisch, G. W. Trucks, H. B. Schlegel, et al. *Gaussian 09 Revision A.1.*
- [126] F. Furche and D. Rappoport. “Density functional methods for excited states: equilibrium structure and electronic spectra”. In: *Comput. Photochem.* Ed. by M. Olivucci. Theoretical and Computational Chemistry, Vol. 16. Amsterdam: Elsevier, 2005, pp. 93–128.
- [127] A. J. Sadlej. 1988. *Collect. Czechoslov. Chem. Commun.* 53. Pp. 1995–2016.
- [128] A. J. Sadlej and M. Urban. 1991. *J. Mol. Struct. THEOCHEM.* 234. Pp. 147–171.
- [129] A. Le Floch. 1991. *Mol. Phys.* 72. Pp. 133–144.
- [130] L. V. Gurvich, I. V. Veyts, and C. B. Alcock. *Thermodynamic Properties of Individual Substances, Fourth Edition.* Hemisphere Pub. Co., New York, 1989.
- [131] G. Herzberg. *Molecular spectroscopy and molecular structure; Electronic spectra and electronic structure of polyatomic molecules, vol. III.* New York: van Nostrand Reinhold, 1966.
- [132] N. Mardirossian, J. A. Parkhill, and M. Head-Gordon. 2011. *Phys. Chem. Chem. Phys.* 13. P. 19325.
- [133] G. Schaftenaar and J. H. Noordik. *Molden: a pre- and post-processing program for molecular and electronic structures.* 2000.
- [134] T. Stein, L. Kronik, and R. Baer. 2009. *J. Chem. Phys.* 131. P. 244119.
- [135] M. J. G. Peach and D. J. Tozer. 2012. *J. Phys. Chem. A.* 116. P. 9783.
- [136] S. Hamel, M. E. Casida, and D. R. Salahub. 2002. *J. Chem. Phys.* 116. P. 8276.

Part III

Excitation energies from Green's function methods

Chapter 7

Theoretical background on Green's function methods

An alternative approach to time-dependent density-functional theory (TDDFT) to compute electronic excitation energies is provided by many-body perturbation theory which is widely used in the condensed-matter physics community. One main advantage of this approach is that it is in principle able to describe double excitations which are absent in TDDFT within the usual adiabatic approximation, and that its formalism is close to the TDDFT one. In this chapter, we study its transfer from solids to finite molecular systems where the equations need to be projected onto a gaussian spin-orbital basis set, and where the validity of the approximations made in physics for solids has to be questioned. We introduce here the concepts of quasiparticle and of Green's functions on which is based this theory. We then recall the working equations of many-body perturbation theory for the one-particle case (Dyson equation) and the two-particle case (Bethe-Salpeter equation) and introduce the self-energy and Bethe-Salpeter kernel which are the key quantities of this method. The equations are derived in a four-point formalism in order to prepare for their applications to finite molecular systems and the correspondence with Feynman diagrams is made along the derivation. We then recall Hedin's equations which provide a set of five coupled equations which should in principle allows one to calculate the self-energy.

7.1 Introduction

Time-dependent density-functional theory (TDDFT) [1] within the linear-response formalism [2–4] is nowadays the most widely used approach to the calculation of electronic excitation energies of molecules and solids. Applied within the adiabatic approximation and with the usual local or semilocal density functionals, TDDFT gives indeed in many cases excitation energies with reasonable accuracy and low computational cost. However, several serious limitations of these approximations are known, e.g. for molecules: too low

charge-transfer excitation energies [5], lack of double excitations [6], and wrong behavior of the excited-state surface along a bond-breaking coordinate (see, e.g., Ref. [7]). Several remedies to these problems are actively being explored, including: long-range corrected TDDFT [8, 9] which improves charge-transfer excitation energies, dressed TDDFT [6, 10, 11] which includes double excitations, and time-dependent density-matrix functional theory (TDDMFT) [12–16] which tries to address all these problems.

In the condensed-matter physics community, the Bethe-Salpeter equation (BSE) applied within the GW approximation (see, e.g., Refs. [17–19]) is often considered as the most successful approach to overcome the limitations of TDDFT. Although it has been often used to describe excitons (bound electron-hole pair) in periodic systems, it is also increasingly applied to calculations of excitation energies in finite molecular systems [20–34]. In particular, the BSE approach is believed to give accurate charge-transfer excitation energies in molecules [29, 31], and when used with a frequency-dependent kernel it is in principle capable of describing double excitations [35, 36]. A second-order Bethe-Salpeter kernel was recently tested by Zhang *et al* [37] within the Tamm-Dancoff approximation, in a perturbative approach.

We start by giving a brief review of Green's function many-body theory for calculating excitation energies. For more details, see e.g. Refs. [17, 19, 38]. The concepts of one-particle and two-particle Green's functions are introduced in Sections 7.2 and 7.3. Their equations of motion, namely the Dyson and Bethe-Salpeter equations are derived in Sections 7.4 and 7.5. These equations involve the exchange-correlation self-energy as a main ingredient which calculation is possible by solving the coupled set of Hedin's equations as detailed in Section 7.6.

7.2 One-particle Green's function

Let $|N\rangle$ be the normalized ground-state wave function for a system of N electrons described by the Hamiltonian \hat{H} . The time-ordered one-particle equilibrium Green's function at zero temperature is defined as

$$\begin{aligned} iG(1,2) &= \langle N | \hat{T} [\hat{\Psi}(1) \hat{\Psi}^\dagger(2)] | N \rangle \\ &= \theta(t_1 - t_2) \langle N | \hat{\Psi}(1) \hat{\Psi}^\dagger(2) | N \rangle - \theta(t_2 - t_1) \langle N | \hat{\Psi}^\dagger(2) \hat{\Psi}(1) | N \rangle. \end{aligned} \quad (7.1)$$

Index 1 stands for space, spin and time coordinates $(\mathbf{r}_1, \sigma_1, t_1) = (\mathbf{x}_1, t_1)$. \hat{T} is the Wick time-ordering operator which orders the operators with larger times on the left and θ is the Heaviside step function. The whole time-dependence is contained in $\hat{\Psi}(1) = e^{i\hat{H}t_1} \hat{\Psi}(\mathbf{x}_1) e^{-i\hat{H}t_1}$ and $\hat{\Psi}^\dagger(2) = e^{i\hat{H}t_2} \hat{\Psi}^\dagger(\mathbf{x}_2) e^{-i\hat{H}t_2}$, the annihilation and creation field operators in the Heisenberg representation which were introduced in Section 5.2.

If t_1 is greater than t_2 , an electron is added at time t_2 at the position \mathbf{x}_2 to the system in its ground state. This extra negative charge interacts with its environment and create a depletion in the charge density around it to form a quasi-electron which

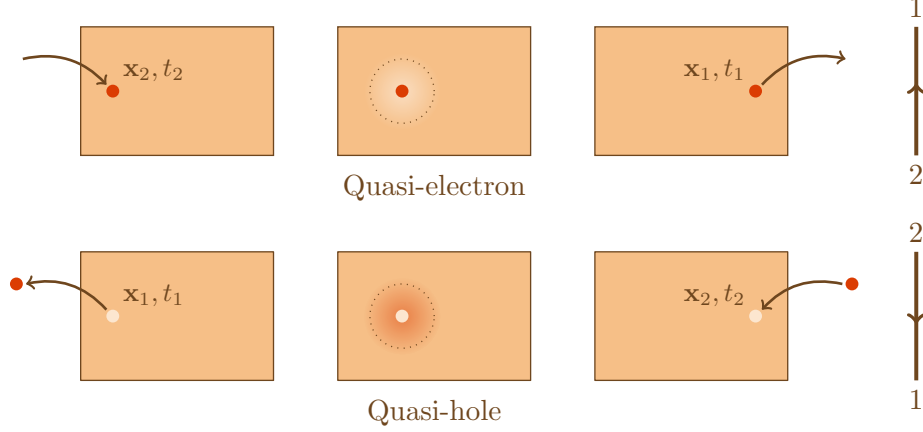


Figure 7.1 – Schematic and Feynman representation of the one-particle Green's function $G(1,2)$.

is propagated through the system. An electron is then removed at time t_1 and position \mathbf{x}_1 . The probability amplitude to find an electron in (\mathbf{x}_1, t_1) when an electron was added in (\mathbf{x}_2, t_2) is then given by the one-particle Green's function $G(1,2)$. Its Feynman representation is given a thick arrow going from 2 to 1 hereinafter, where the time axis is vertical as shown in Figure 7.1. On the other hand, if t_2 is greater than t_1 then $G(1,2)$ is the probability amplitude to find a hole in (\mathbf{x}_2, t_2) when an electron was removed in (\mathbf{x}_1, t_1) and represents the propagation of a quasi-hole in the system. Its Feynman representation is then a thick going down arrow. One should note that the one-particle Green's function is not defined if $t_1 = t_2$ and is related to the ground-state density by $n(\mathbf{x}_1) = -iG(1,1^+)$ where 1^+ stands for (\mathbf{x}_1, t_1^+) with $t_1^+ = t_1 + 0^+$.

In the absence of external potential, the system is invariant under time translation, therefore the Green's function depends only on $\tau = t_1 - t_2$. By introducing the closure relation for excited states with $N - 1$ or $N + 1$ particles, one can get

$$\begin{aligned}
 iG(\mathbf{x}_1, \mathbf{x}_2; \tau) = & \theta(\tau) \sum_A \langle N | \hat{\psi}(\mathbf{x}_1) | N + 1, A \rangle \langle N + 1, A | \hat{\psi}^\dagger(\mathbf{x}_2) | N \rangle e^{-i(E_{N+1,A} - E_N)\tau} \\
 & - \theta(-\tau) \sum_I \langle N | \hat{\psi}^\dagger(\mathbf{x}_2) | N - 1, I \rangle \langle N - 1, I | \hat{\psi}(\mathbf{x}_1) | N \rangle e^{-i(E_N - E_{N-1,I})\tau},
 \end{aligned} \tag{7.2}$$

where E_N , $E_{N+1,A}$ and $E_{N-1,I}$ are the energies of the ground state $|N\rangle$, of the A -th excited state with $N + 1$ particles $|N + 1, A\rangle$ and of the I -th excited state with $N - 1$ particles $|N - 1, I\rangle$, respectively. The Lehmann representation of the one-particle Green's function is obtained by Fourier transform

$$G(\mathbf{x}_1, \mathbf{x}_2; \omega) = \sum_A \frac{f_A(\mathbf{x}_1) f_A^*(\mathbf{x}_2)}{\omega - \mathcal{E}_A + i0^+} + \sum_I \frac{f_I(\mathbf{x}_1) f_I^*(\mathbf{x}_2)}{\omega - \mathcal{E}_I - i0^+}, \tag{7.3}$$

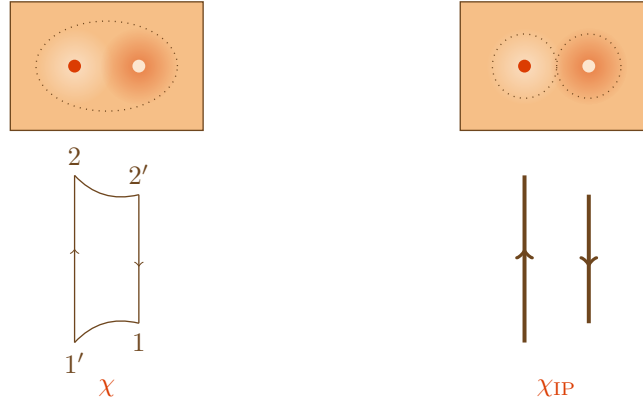


Figure 7.2 – Schematic and Feynman representations of the hole-electron full-interacting and independent-particle ph/hp propagators $\chi(1, 2; 1', 2')$ and $\chi_{IP}(1, 2; 1', 2')$.

where $f_A(\mathbf{x}) = \langle N | \hat{\psi}(\mathbf{x}) | N + 1, A \rangle$ and $f_I(\mathbf{x}) = \langle N - 1, I | \hat{\psi}(\mathbf{x}) | N \rangle$ form a complete basis set for the $N \pm 1$ -electron states, and $\mathcal{E}_A = E_{N+1,A} - E_N$ and $\mathcal{E}_I = E_N - E_{N-1,I}$ are minus the electron affinities and ionization energies, respectively. The conventions for Fourier transforms can be found in Appendix A.2.

As G is a one-particle quantity it seems natural that it describes one-particle processes only. However, as we are interested in electronic excitations which corresponds to the propagation of a hole and an electron simultaneously, a two-particle Green's function is therefore needed.

7.3 Two-particle Green's function

The time-ordered two-particle Green's function is defined as

$$i^2 G_2(1, 2; 1', 2') = \langle N | \hat{T} [\hat{\Psi}(1) \hat{\Psi}(2) \hat{\Psi}^\dagger(2') \hat{\Psi}^\dagger(1')] | N \rangle. \quad (7.4)$$

Depending on the time ordering, it describes the propagation of a pair of holes, of electrons or of a hole and an electron. In the case of optical absorption, one is only interested in the propagation of a hole-electron pair. Let χ be the 4-point polarizability,

$$\chi(1, 2; 1', 2') = iG_2(1, 2; 1', 2') - iG(1, 1')G(2, 2'). \quad (7.5)$$

It describes the coupled motion of two particles minus the motion of the independent ones. In order to describe the propagation of a hole and an electron, it requires $t'_2 > t_1$ and $t_2 > t'_1$ or the other way around. In this particular case, the 4-point polarizability reduces

to a particle-hole/hole-particle propagator where the times can be further contracted. If, in particular, the creation and annihilation of the hole and the electron are quasi-simultaneous, as in an electronic excitation, $t'_1 = t_1^+$ and $t'_2 = t_2^+$. In this case, the 4-point polarizability reduces to the linear response function¹

$$\chi(\mathbf{x}_1, \mathbf{x}_2; \mathbf{x}'_1, \mathbf{x}'_2; \tau) = \chi(\mathbf{x}_1, t_1, \mathbf{x}_2, t_2; \mathbf{x}'_1, t_1^+, \mathbf{x}'_2, t_2^+). \quad (7.6)$$

The Lehmann representation of the response function explicitly gives the excitation energies as poles in ω ,

$$\begin{aligned} \chi(\mathbf{x}_1, \mathbf{x}_2; \mathbf{x}'_1, \mathbf{x}'_2; \omega) = & \sum_{K \neq 0} \frac{\langle N | \hat{\Psi}^\dagger(\mathbf{x}'_1) \hat{\Psi}(\mathbf{x}_1) | N, K \rangle \langle N, K | \hat{\Psi}^\dagger(\mathbf{x}'_2) \hat{\Psi}(\mathbf{x}_2) | N \rangle}{\omega - (E_{N,K} - E_N) + i0^+} \\ & - \sum_{K \neq 0} \frac{\langle N | \hat{\Psi}^\dagger(\mathbf{x}'_2) \hat{\Psi}(\mathbf{x}_2) | N, K \rangle \langle N, K | \hat{\Psi}^\dagger(\mathbf{x}'_1) \hat{\Psi}(\mathbf{x}_1) | N \rangle}{\omega + (E_{N,K} - E_N) - i0^+}, \end{aligned} \quad (7.7)$$

where $|N, K\rangle$ is the K -th excited state with N particles of energy $E_{N,K}$. The ground state $|N, 0\rangle = |N\rangle$ is excluded from the sum.

It is also useful to define the independent-particle (IP) polarizability $\chi_{\text{IP}}(1, 2; 1', 2') = -iG(1, 2')G(2, 1')$ where the two particles propagate independently with each other but in interaction with the rest of the system². The schematic and Feynman representation of the full-interacting and independent-particle response functions are given in Figure 7.2 in the case of a hole-electron propagation. The Lehmann representation of the independent-particle response function is easily obtained by calculating $\chi_{\text{IP}}(\mathbf{x}_1, \mathbf{x}_2; \mathbf{x}'_1, \mathbf{x}'_2; \tau) = -iG(\mathbf{x}_1, \mathbf{x}'_2; \tau)G(\mathbf{x}_2, \mathbf{x}'_1; -\tau)$ with equation (7.2) and taking the Fourier transform

$$\begin{aligned} \chi_{\text{IP}}(\mathbf{x}_1, \mathbf{x}_2; \mathbf{x}'_1, \mathbf{x}'_2; \omega) = & \sum_{IA} \frac{f_I^*(\mathbf{x}'_1) f_A(\mathbf{x}_1) f_A^*(\mathbf{x}'_2) f_I(\mathbf{x}_2)}{\omega - (\mathcal{E}_A - \mathcal{E}_I) + i0^+} \\ & - \sum_{IA} \frac{f_I^*(\mathbf{x}'_2) f_A(\mathbf{x}_2) f_A^*(\mathbf{x}'_1) f_I(\mathbf{x}_1)}{\omega + (\mathcal{E}_A - \mathcal{E}_I) - i0^+}. \end{aligned} \quad (7.8)$$

Details of the Fourier transforms of the polarizability, propagator and response function are given in Appendix F. The distinction between polarizability, propagator and response function is made explicit in Figure 7.3 in the independent-particle case.

In practice, the one-particle and two-particle Green's function can be calculated with equations of motion, namely the Dyson and Bethe-Salpeter equations.

¹One should be aware that this defines a time-ordered quantity while in TDDFT a retarded response function is used. This distinction changes the position of the poles with respect to the real axis in the complex plane, however, when inverse response functions are considered, as will be done in the following, this distinction is not important anymore.

² χ_{IP} should rather be called an independent-quasi-particle polarizability but for the sake of consistency with the literature we will keep the usual denomination

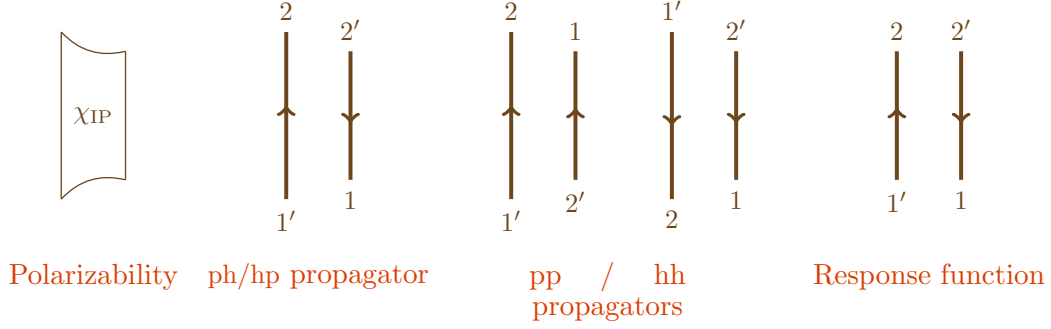


Figure 7.3 – Nomenclature for polarizability, propagators and response function for $\chi_{\text{IP}}(1, 2; 1', 2') = -iG(1, 2')G(2, 1')$. The one-particle Green's function is represented by a thick arrow. The time axis is going from the bottom to the top. As the time ordering is undetermined for the polarizability it is not represented in terms of Green's function. For the ph/hp propagator, $t'_2 > t_1$ and $t_2 > t'_1$ (or the other way around but not shown) but the respective positions of t_1 w.r.t. t'_1 and t_2 w.r.t. t'_2 are undefined. For the response function $t'_2 > t_1$ and $t_2 > t'_1$ (or the other way around but not shown) and $t'_1 = t_1^+$ and $t'_2 = t_2^+$. The particle-particle and hole-hole propagators (pp/hh) are also shown as they will be used in the next chapters.

7.4 Dyson equation

To make easier the connection with expressions in a finite spin-orbital basis, we systematically use 4-point indexes for all the two-electron quantities, however the more conventional 2-point derivation can be found for instance in [17]. The starting point is therefore a fully non-local time-dependent Hamiltonian,

$$\begin{aligned} \hat{H}(t_1) = & \int d\mathbf{x}_1 d1' \hat{\Psi}^\dagger(1) h(1, 1') \hat{\Psi}(1') \\ & + \frac{1}{2} \int d\mathbf{x}_1 d2d1' d2' \hat{\Psi}^\dagger(1) \hat{\Psi}^\dagger(2) w_{ee}(1, 2; 1', 2') \hat{\Psi}(1') \hat{\Psi}(2'), \end{aligned} \quad (7.9)$$

where $w_{ee}(1, 2; 1', 2') = w_{ee}(|\mathbf{r}_1 - \mathbf{r}_2|) \delta(t_1, t_2) \delta(1, 1') \delta(2, 2')$ is the spin-independent instantaneous Coulomb electron-electron interaction and $h(1, 1')$ is the one-electron Hamiltonian which contains the electron kinetic operator and the nuclei-electron interaction V_{ne} ,

$$h(1, 1') = -\delta(1, 1') \frac{\nabla_1^2}{2} + \delta(1, 1') V_{\text{ne}}(\mathbf{r}_1). \quad (7.10)$$

Using the equations of motion for the Heisenberg creation and annihilation operators in the expression of the derivative of G with respect to time [17], one can obtain the following equation,

$$\begin{aligned} i \int d3 \delta(1, 3) \frac{\partial}{\partial t_3} G(3, 2) - \int d3 h(1, 3) G(3, 2) \\ + i \int d3 d1' d3' w_{ee}(1, 3; 1', 3') G_2(1', 3'^+, 2, 3^{++}) = \delta(1, 2), \end{aligned} \quad (7.11)$$

where $^{++}$ stands for $t_3^+ + 0^+$. A whole series of equations can be derived for the Green's functions, relating the one-particle Green's function to the two-particle Green's function, the two-particle one to the three-particle one, etc. But solving this set of equations is not wanted.

To avoid this, one can use the Schwinger derivative technique [39, 40]. Introducing an external time-dependent potential $U(1, 1') = U(\mathbf{x}_1 t_1^+, \mathbf{x}'_1 t'_1) \delta(t_1, t'_1)$, one can express the two-particle Green's function in terms of the one-particle one and of its derivative with respect to U , evaluated at $U = 0$,

$$\frac{\delta G(1, 2)}{\delta U(3, 4)} = -G_2(1, 4; 2, 3) + G(1, 2)G(4, 3). \quad (7.12)$$

Using this relation in Equation (7.11), one can get

$$\begin{aligned} & \int d3 \left[i\delta(1, 3) \frac{\partial}{\partial t_3} - h(1, 3) \right] G(3, 2) \\ & + i \int d3 d1' d3' w_{ee}(1, 3; 1', 3') \left[G(1', 2)G(3', 3^{++}) - \frac{\delta G(1', 2)}{\delta U(3^{++}, 3'^+)} \right] = \delta(1, 2) \quad (7.13) \\ & \int d3 \left[i\delta(1, 3) \frac{\partial}{\partial t_3} - h(1, 3) \right] G(3, 2) - \int d3 \Sigma_{\text{Hxc}}(1, 3)G(3, 2) = \delta(1, 2), \end{aligned}$$

where $\Sigma_{\text{Hxc}}(1, 2)$ is the Hartree-exchange-correlation self-energy which takes into account all the two-particle effects. It can be decomposed into a Hartree contribution

$$\Sigma_{\text{H}}(1, 2) = -i \int d3 d3' w_{ee}(1, 3; 2, 3')G(3'^+, 3^{++}) \quad (7.14)$$

and an exchange-correlation one

$$\Sigma_{\text{xc}}(1, 2) = i \int d3 d1' d3' d4 w_{ee}(1, 3; 1', 3') \frac{\delta G(1', 4)}{\delta U(3^{++}, 3'^+)} G^{-1}(4, 2). \quad (7.15)$$

Note that these self-energies are functionals of the Green's function and should be written formally as $\Sigma_{\text{Hxc}}[G]$.

7.4.1 Non-interacting Green's function

One can define a Green's function G_h which shows no two-particle effects and therefore follows the equation of motion

$$\int d3 \left[i\delta(1, 3) \frac{\partial}{\partial t_1} - h(1, 3) \right] G_h(3, 2) = \delta(1, 2). \quad (7.16)$$

We choose its Feynman representation to be a dotted arrow. Using this relation in Equation (7.13), one finally gets the Dyson equation for the one-particle Green's function,

$$\int d3 [G_h^{-1}(1, 3) - \Sigma_{\text{Hxc}}[G](1, 3)] G(3, 2) = \delta(1, 2). \quad (7.17)$$

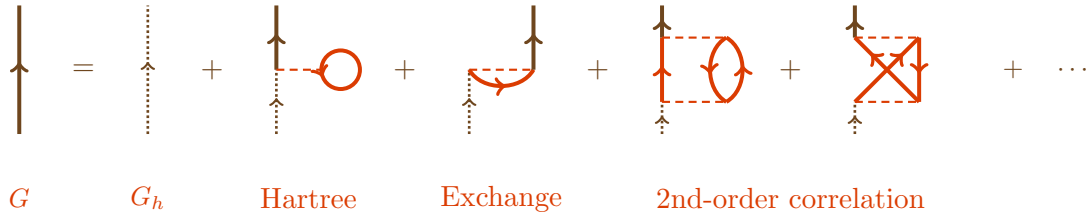


Figure 7.4 – Feynman representation of the perturbative expansion of the Dyson equation where Σ is expanded in order of w_{ee} but not G . The fully interacting Green's function is drawn as a thick arrow and the non-interacting one as a dotted one. The dashed line represents the Coulombic interaction. The self-energy is in red.

This equation is also often used under the forms

$$G(1, 2) = G_h(1, 2) + \int d3d4 G_h(1, 3) \Sigma_{\text{Hxc}}[G](3, 4) G(4, 2), \quad (7.18)$$

or

$$G^{-1}(1, 2) = G_h^{-1}(1, 2) - \Sigma_{\text{Hxc}}[G](1, 2). \quad (7.19)$$

It is convenient to use perturbation theory with respect to the electron-electron interaction to understand this equation. This is shown in Figure 7.4 up to the second order where the interaction is represented by a horizontal dashed line. At zeroth order, the particle does not interact with the system and is therefore represented by the non-interacting Green's function G_h . At first order, it interacts with the charge density of the system which is represented by a loop as $n(\mathbf{x}_3) = G(3, 3^+)$ and may be exchanged with another particle which gives rise to the Hartree and exchange terms. The higher orders of perturbation describe the correlation. At the second order, the particle can create a hole-electron pair via a first interaction and destroys it later via a second interaction where exchange may also occur. The fully interacting Green's function G can therefore be expanded around the non-interacting one. From Equation (7.18), the parts of diagram between the G_h arrow and the G arrow (in red) represents the self-energy. More details can be found in [41] for instance.

7.4.2 Hartree-Fock Green's function

In practice, the non-interacting Green's function G_h is rarely used and it is more common to encounter the Hartree-Fock (HF) Green's function for finite system (or Kohn-Sham Green's functions or even Hartree Green's functions in the case of solid-state physics)

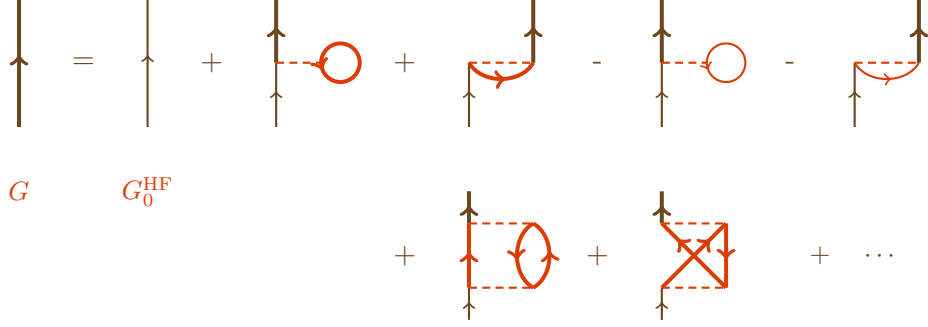


Figure 7.5 – Feynman representation of the perturbative expansion of the Dyson equation with the Hartree-Fock Green’s function as reference. The fully interacting Green’s function is drawn as a thick arrow and the Hartree-Fock one as a dotted arrow. The dashed line represents the Coulombic interaction. The self-energy is in red.

denoted by G_0^{HF} which satisfies the equation

$$\begin{aligned} \int d3 \left[i\delta(1,3) \frac{\partial}{\partial t_3} - h(1,3) - \Sigma_{\text{Hx}}^{\text{HF}}[G_0^{\text{HF}}](1,3) \right] G_0^{\text{HF}}(3,2) &= \delta(1,2) \\ \int d3 \left[G_h^{-1}(1,3) - \Sigma_{\text{Hx}}^{\text{HF}}[G_0^{\text{HF}}](1,3) \right] G_0^{\text{HF}}(3,2) &= \delta(1,2) \end{aligned} \quad (7.20)$$

where $\Sigma_{\text{Hx}}^{\text{HF}}[G_0^{\text{HF}}]$ is the HF Hartree-exchange self-energy. The HF Green’s function is thus related to the non-interacting one by

$$(G_0^{\text{HF}})^{-1}(1,2) = G_h^{-1}(1,2) - \Sigma_{\text{Hx}}^{\text{HF}}[G_0^{\text{HF}}](1,2). \quad (7.21)$$

where the HF self-energy is given by [38, 42]

$$\begin{aligned} \Sigma_{\text{Hx}}^{\text{HF}}[G_0^{\text{HF}}](1,2) &= -i \int d3d3' w_{ee}(1,3;2,3') G_0^{\text{HF}}(3'^+,3^{++}) \\ &+ i \int d3d3' w_{ee}(3,1;2,3') G_0^{\text{HF}}(3'^+,3^{++}). \end{aligned} \quad (7.22)$$

The consequences on the Dyson equation is schematically represented in Figure 7.5 for the HF Green’s function G_0^{HF} represented by a thin arrow. This also defines the HF polarizability,

$$\chi_0^{\text{HF}}(1,2;1',2') = -i G_0^{\text{HF}}(1,2') G_0^{\text{HF}}(2,1'), \quad (7.23)$$

where the particles are only interacting via a mean field. In what follows, the HF superscript is dropped for conciseness as only HF Green’s function will be considered.

7.5 Bethe-Salpeter Equation

In presence of the external time-dependent potential $U(1, 1')$ the Dyson equation (7.19), rewrites as

$$G^{-1}(1, 1') = G_h^{-1}(1, 1') - U(1, 1') - \Sigma_{\text{Hxc}}(1, 1'). \quad (7.24)$$

The polarizability³ of the system is then given by the change in the Green's function induced by the external potential U . Taking the derivative with respect to U of the Dyson equation and using the chain rule with respect to G , it becomes

$$\int d2d2' \frac{\delta G^{-1}(1, 1')}{\delta G(2, 2')} \frac{\delta G(2, 2')}{\delta U(3, 3')} = -\delta(1, 3)\delta(1', 3') - \int d2d2' \frac{\delta \Sigma_{\text{Hxc}}(1, 1')}{\delta G(2, 2')} \frac{\delta G(2, 2')}{\delta U(3, 3')}. \quad (7.25)$$

Using the derivative of the inverse (A.8) and the relation (A.5), the left-hand-side term can be written in terms of the independent response function

$$\frac{\delta G^{-1}(1, 1')}{\delta G(2, 2')} = -G^{-1}(1, 2')G^{-1}(2, 1') = i\chi_{\text{IP}}^{-1}(1, 2; 1', 2'). \quad (7.26)$$

As G_h^{-1} is independent of U , using the definition of the polarizability (7.5) together with Schwinger's relation (7.12), one can then get the so-called Bethe-Salpeter equation (see, e.g., Ref. [42])

$$\chi^{-1}(1, 2; 1', 2') = \chi_{\text{IP}}^{-1}(1, 2; 1', 2') - \Xi_{\text{Hxc}}(1, 2; 1', 2'), \quad (7.27)$$

or equivalently

$$\chi(1, 2; 1', 2') = \chi_{\text{IP}}(1, 2; 1', 2') + \int d3456 \chi_{\text{IP}}(1, 4; 1', 3)\Xi_{\text{Hxc}}(3, 6; 4, 5)\chi(5, 2; 6, 2'), \quad (7.28)$$

where Ξ_{Hxc} is the Hartree-exchange-correlation Bethe-Salpeter kernel, defined as

$$\Xi_{\text{Hxc}}(3, 6; 4, 5) = i \frac{\delta \Sigma_{\text{Hxc}}(3, 4)}{\delta G(5, 6)}. \quad (7.29)$$

Using once again in the perturbation picture, the fully interacting response function can be constructed from the independent-particle response function χ_{IP} as represented in Figure 7.6. At zeroth order, the particles interact with the rest of the system but not with each other. The interaction between the two quasi-particles can then be built in the order of the electron-electron interaction similarly to what was done for the self-energy in Figure 7.4.

7.6 Hedin's equations

We now have equations of motion for the one- and two-particle Green's functions. They depend on the Hartree-exchange-correlation self-energy. Its Hartree and exchange parts

³Beware that the times are implicitly ordered through the external potential.

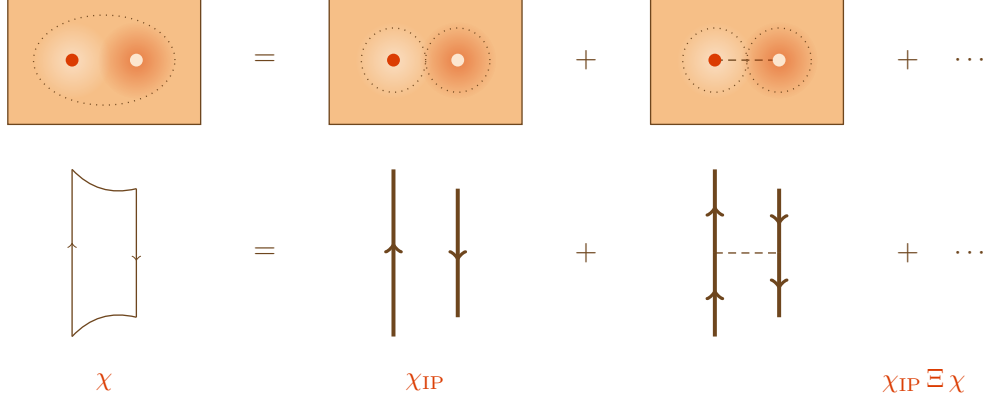


Figure 7.6 – Schematic and Feynman representation of the Bethe-Salpeter equation.

are known but a practical way of calculating its correlation part is needed. Hedin proposed a scheme which yields to a set of coupled equations and allows in principle for the calculation of the exact self-energy [43]. This scheme can be seen as a perturbation theory in terms of the screened interaction W instead of the bare Coulomb interaction w_{ee} . We show a generalization of this derivation for the case of a non-local potential.

Let $V(5, 6) = U(5, 6) - i \int d3d3' w_{ee}(5, 3; 6, 3') G(3', 3^+)$ be the non-local classical potential. Using the chain rule in the exchange-correlation self-energy, we get:

$$\begin{aligned} \Sigma_{xc}(1, 2) &= -i \int d3d1' d3' d4d5d6 w_{ee}(1, 3; 1', 3') G(1', 4) \frac{\delta G^{-1}(4, 2)}{\delta V(5, 6)} \frac{\delta V(5, 6)}{\delta U(3^{++}, 3'^+)} \\ &= i \int d3d1' d3' d4d5d6 w_{ee}(1, 3; 1', 3') G(1', 4) \tilde{\Gamma}(4, 6; 2, 5) \epsilon^{-1}(5, 3'; 6, 3^+). \end{aligned} \quad (7.30)$$

where the inverse dielectric function ϵ^{-1} which screens the bare Coulomb interaction w_{ee} and the irreducible vertex function $\tilde{\Gamma}$ are defined by

$$\epsilon^{-1}(1, 2; 3, 4) = \frac{\delta V(1, 3)}{\delta U(4, 2)} \quad \text{and} \quad \tilde{\Gamma}(1, 2; 3, 4) = -\frac{\delta G^{-1}(1, 3)}{\delta V(4, 2)}. \quad (7.31)$$

We can therefore define a dynamically screened potential

$$\begin{aligned} W(1, 2; 1', 2') &= \int d3d3' \epsilon^{-1}(1, 3; 1', 3^+) w_{ee}(2, 3'; 2', 3) \\ &= \int d3d3' \epsilon^{-1}(1, 3; 1', 3^+) w_{ee}(3', 2; 3, 2'), \end{aligned} \quad (7.32)$$

where the symmetry of the Coulomb interaction w_{ee} has been used, and we get the

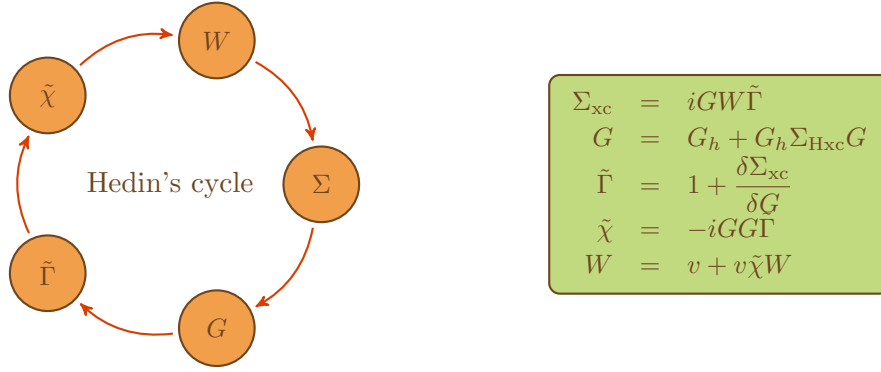


Figure 7.7 – Self-consistent solution of Hedin's set of coupled equations.

expression of the exchange-correlation self-energy,

$$\Sigma_{xc}(1, 2) = i \int d1' d3 d3' d4 G(1', 4) \tilde{\Gamma}(4, 3', 2, 3) W(3, 1; 3', 1'). \quad (7.33)$$

We still need to express the dielectric function and the irreducible vertex function without the use of V and U . To achieve this, we define the irreducible polarizability $\tilde{\chi}(1, 2; 3, 4) = -i\delta G(1, 3)/\delta V(4, 2)$, which, with the properties of the inverse and the definition of the vertex correction, can be rewritten as

$$\tilde{\chi}(1, 2; 3, 4) = -i \int d5 d5' G(1, 5) G(5', 3) \tilde{\Gamma}(5, 2; 5', 4). \quad (7.34)$$

Using this relation, one can rewrite the dielectric function as

$$\epsilon(1, 2; 3, 4) = \delta(1, 4)\delta(2, 3) - \int d5 d5' w_{ee}(1, 5; 3, 5') \tilde{\chi}(5', 2; 5^+, 4), \quad (7.35)$$

and the irreducible vertex correction as

$$\tilde{\Gamma}(1, 2; 3, 4) = \delta(1, 4)\delta(2, 3) - i \int d5 d6 \frac{\delta \Sigma_{xc}(1, 3)}{\delta G(5, 6)} \tilde{\chi}(5, 2; 6, 4). \quad (7.36)$$

We now have a set of five coupled equations (7.32) to (7.36) to calculate the self-energy which is represented in Figure 7.7.

7.7 Conclusion

In this chapter, we have introduced the one- and two-particle Green's function formalism and recalled the corresponding equations of motion for these two quantities, the Dyson equation and the Bethe-Salpeter equation. As in Kohn-Sham approach in density functional theory, a non-interacting system is taken as a reference system and the effects of the electron-electron interaction is included via the self-energy or the Bethe-Salpeter kernel. Hedin's equations provide an explicit approach to compute the self-energy which

can then be used to evaluate the Bethe-Salpeter kernel. With respect to the TDDFT kernel, the expression of the Bethe-Salpeter kernel is exactly known from the self-energy while the TDDFT kernel was explicitly related to the energy functional only within the adiabatic approximation which is therefore not required here. This implies that one can obtain a frequency-dependent kernel in this formalism. Moreover, TDDFT and BSE formalisms are very close so that a Bethe-Salpeter kernel could be used in the TDDFT formalism [19, 34–36, 44–50].

In practice, Hedin’s set of equations is never solved exactly and approximations are made for the derivation of the self-energy and of the kernel. The effects of these approximations are discussed in the following chapters and assessed on the model system given by H_2 in a minimal basis. In Chapter 8, the expressions of the self-energy is derived within the most famous approximation (GW) and one of its variants (GWx). The static Bethe-Salpeter kernel is then obtained by differentiation where part of the derivative is neglected as usually done is the condensed-matter physics community. It is projected onto a spin-orbital basis set and its performance is assessed on H_2 in a minimal basis for different starting Green’s functions. In Chapter 9, a perturbative approach is used in order to derive working equations for the static kernel up to the second order. In this case, all the terms are kept in the differentiation of the self-energy and their effects in assessed again with the model of system of H_2 . Finally, a dynamic Bethe-Salpeter kernel is discussed in Chapter 10 together with the quasiparticle effects due to the starting response function χ_{IP} or χ_0 on which the Bethe-Salpeter kernel is added.

Chapter 8

Static GW-BSE kernel in a finite orbital basis

Except for the part on the GWx approximation, this work was the subject to a publication in S. K. Ghosh & P. K. Chattaraj (Eds.), *Electronic Structure and Reactivity* (p. 367). CRC Press. (2013) in collaboration with J. Toulouse, and A. Savin.

The most widely used approximation in the context of Bethe-Salpeter calculations is the static GW approximation. In this approximation, the vertex corrections are neglected into the expression of the self-energy which is then obtained as the product of G and W and the Hedin's equations are not solved self-consistently but only one iteration of the cycle is performed.

In this chapter, the self-energy is computed in the GW approximation, and in a variant (GWx) where exchange is included in the definition of the dielectric matrix. In both cases, the kernel is then obtained in its static approximation by considering the screened interaction as local in time and the derivative of W with respect to G is neglected such that the response of the screening to the perturbation is neglected. As the self-energy is not build self-consistently, the choice of the starting Green's function plays a significant role and the effect of using the Hartree-Fock Green's function with respect to the exact one will be assessed. In each case, the equations are projected on a spin-orbital basis and applied on the model system of H_2 in a minimal basis.

8.1 Introduction

In the Bethe-Salpeter formalism, similarly to linear-response time-dependent density-functional theory, one can compute the neutral excitation energies of a system by the means of the poles of the response function. The Bethe-Salpeter equation links the response function of non-interacting quasi-particles to the one of the physical system

via the Hartree-exchange-correlation Bethe-Salpeter kernel which therefore contains all the effects due to the interaction. This kernel is explicitly related to the self-energy by first-order derivative and one has therefore to compute first this self-energy in order to access the kernel. Hedin's cycle provides a way to compute the self-energy by solving its five coupled equations as was mentioned in the previous chapter. However, when giving a closer look to these equations two difficulties emerge: first, as these equations are coupled, they should in principle be solved self consistently (with all the convergence issues that it implies), second, it involves the first-order derivative of the self-energy Σ with respect to the Green's function G . Therefore, one should first expand the self-energy with respect to G up to a given order analytically, take its first-order derivative and then numerically solve this already approximated set of equations self consistently without any guaranty that it will converge to the physical solution. It is needless to say that it requires a formidable analytic and computational effort. The simplest approximation was proposed by Hedin himself [43] and consists in assuming the vertex operator $\tilde{\Gamma}$ to be delta functions in spin, space and time so that the first-order derivative of Σ with respect to G is neglected. The exchange-correlation self-energy is then the product of G and W and the approximation is therefore called the *GW approximation*. Usually, the self-energy is not calculated self-consistently but with only one iteration of Hedin's cycle which hence defines the G_0W_0 approximation. For one-particle properties, these calculations [51–55] were shown to perform relatively well in comparison with self-consistent GW calculations [56–62]. However, the choice of the starting Green's function then plays an important role in the determination of the self-energy. Additionally, it is also possible to define a variant for the self-energy where exchange is included (GWx). In particular, this removes the self-screening effects which occur otherwise [63–65].

Once an approximate expression is chosen for the self-energy, the Bethe-Salpeter kernel can be found by functional differentiation with respect to G . Additional approximations can be made at this step, and the simplest case is obtained if the screened interaction is assumed to be static and if the derivative of W with respect to G is neglected. This approximation is called the static BSE-GW method and corresponds to the most widely used approximation for the kernel in the context of solids [66–69]. In this chapter, we are interested into the applications of these different approximations for a molecular finite system. The expressions of the G_0W_0 and G_0W_0x self-energies and of the corresponding static kernels are first derived in real space in Section 8.2 and are then projected in a spin-orbital basis in Section 8.3. Finally, they are applied on the model system of H_2 in a minimal basis in Section 8.4 with either the Hartree-Fock Green's function as a starting point, or the exact one obtained from a full configuration-interaction calculation in order to assess the effect of the starting Green's function.

8.2 Static GW approximation

In the GW approximation, the vertex function is assumed to be diagonal in spin, space and time coordinates $\tilde{\Gamma}(1, 2; 3, 4) = \delta(1, 4)\delta(2, 3)$ which simplifies greatly Hedin's equations. The irreducible polarizability becomes $\tilde{\chi}(1, 2; 3, 4) = -iG(1, 4)G(2, 3) = \chi_{\text{IP}}(1, 2; 3, 4)$ and contains only the response of the quasi-particles but does not take into account how their interaction is affected by the change of potential. The exchange-correlation self-energy becomes

$$\Sigma_{\text{xc}}(1, 2) = i \int d1' d3 G(1', 3) W(3, 1; 2, 1') \quad (8.1)$$

where in comparison to the Hartree-Fock case, the bare interaction w_{ee} has been replaced by a dynamically screened interaction W . If the derivative of W with respect to G is further neglected, as usually done, the corresponding Bethe-Salpeter kernel is then

$$\Xi_{\text{Hxc}}(1, 2; 1', 2') = w_{\text{ee}}(1, 2; 1', 2') - W(2, 1; 1', 2'), \quad (8.2)$$

where W is obtained from Equation (7.32) and ϵ^{-1} with Equation (7.35) in which $\tilde{\chi}$ is replaced by χ_{IP} . The Coulomb interaction is instantaneous and the one-particle Green's functions depends only of the time difference, therefore the time dependence of the screened interaction is

$$W(1, 2; 1', 2') = W(\mathbf{x}_1, \mathbf{x}_2; \mathbf{x}'_1, \mathbf{x}'_2; \tau) \delta(t_1, t'_1) \delta(t_2, t'_2), \quad (8.3)$$

where $\tau = t_1 - t_2$. If one considers the time dependence in W , the Fourier transform of the Bethe-Salpeter equation is not straightforward [35]. We will only consider here the usual COHSEX approximation where the screened interaction is static, i.e.,

$$W(1, 2; 1', 2') = W(\mathbf{x}_1, \mathbf{x}_2; \mathbf{x}'_1, \mathbf{x}'_2) \delta(t_1, t'_1) \delta(t_2, t'_2) \delta(t_1, t_2). \quad (8.4)$$

To summarize, the Fourier-space Bethe-Salpeter equation in the static GW approximation writes

$$\chi^{-1}(\mathbf{x}_1, \mathbf{x}_2; \mathbf{x}_3, \mathbf{x}_4; \omega) = \chi_{\text{IP}}^{-1}(\mathbf{x}_1, \mathbf{x}_2; \mathbf{x}_3, \mathbf{x}_4; \omega) - \Xi_{\text{Hxc}}(\mathbf{x}_1, \mathbf{x}_2; \mathbf{x}_3, \mathbf{x}_4), \quad (8.5)$$

where the kernel $\Xi_{\text{Hxc}}(\mathbf{x}_1, \mathbf{x}_2; \mathbf{x}_3, \mathbf{x}_4) = w_{\text{ee}}(\mathbf{x}_1, \mathbf{x}_2; \mathbf{x}_3, \mathbf{x}_4) - W(\mathbf{x}_2, \mathbf{x}_1; \mathbf{x}_3, \mathbf{x}_4)$ contains the static screened interaction W calculated from

$$W(\mathbf{x}_1, \mathbf{x}_2; \mathbf{x}'_1, \mathbf{x}'_2) = \int d\mathbf{x}_3 d\mathbf{x}'_3 \epsilon^{-1}(\mathbf{x}_1, \mathbf{x}_3; \mathbf{x}'_1, \mathbf{x}'_3) w_{\text{ee}}(\mathbf{x}'_3, \mathbf{x}_2; \mathbf{x}_3, \mathbf{x}'_2), \quad (8.6)$$

and

$$\begin{aligned} \epsilon(\mathbf{x}_1, \mathbf{x}_2; \mathbf{x}_3, \mathbf{x}_4) &= \delta(\mathbf{x}_1, \mathbf{x}_4) \delta(\mathbf{x}_2, \mathbf{x}_3) \\ &\quad - \int d\mathbf{x}_5 d\mathbf{x}'_5 w_{\text{ee}}(\mathbf{x}_1, \mathbf{x}_5; \mathbf{x}_3, \mathbf{x}'_5) \chi_{\text{IP}}(\mathbf{x}'_5, \mathbf{x}_2; \mathbf{x}_5, \mathbf{x}_4; \omega = 0). \end{aligned} \quad (8.7)$$

We will refer to the approach of Equations (8.5)-(8.7) as the BSE-GW method. Although Hedin's equations may be solved self-consistently in the GW approximation [56, 60, 70–72], it is not usually the case. When only one iteration of the cycle is performed, the one-particle Green's function G in $\chi_{\text{IP}} = -iGG$ has to be specified. Different choices can be made. The simplest option is to use a non-interacting Green's function G_0 from a Hartree-Fock (HF) or Kohn-Sham (KS) calculation. In this case, $\chi_{\text{IP}} = -iG_0G_0 = \chi_0$ is just the non-interacting HF or KS response function. In the condensed-matter physics literature, the usual recipe is to use χ_0 in Equation (8.7) but an improved χ_{IP} in Equation (8.5) from a GW calculation. In the case of H_2 in a minimal basis, it is simple enough to use χ_{IP} constructed with the exact one-particle Green's function G .

We note that the dielectric function of Equation (8.7) could be alternatively derived by including the HF exchange in addition to the Coulomb interaction, i.e. using the antisymmetrized electron-electron interaction $\bar{w}_{\text{ee}}(\mathbf{x}_1, \mathbf{x}_5; \mathbf{x}_3, \mathbf{x}'_5) = w_{\text{ee}}(\mathbf{x}_1, \mathbf{x}_5; \mathbf{x}_3, \mathbf{x}'_5) - w_{\text{ee}}(\mathbf{x}_5, \mathbf{x}_1; \mathbf{x}_3, \mathbf{x}'_5)$ (see, e.g., Ref. [55]), which removes the “self-screening error” for one-electron systems [64]. A bar will be added to the quantities where exchange is included. The dielectric function therefore becomes:

$$\begin{aligned} \bar{\epsilon}(\mathbf{x}_1, \mathbf{x}_2; \mathbf{x}_3, \mathbf{x}_4) \\ = \delta(\mathbf{x}_1, \mathbf{x}_4)\delta(\mathbf{x}_2, \mathbf{x}_3) - \int d\mathbf{x}_5 d\mathbf{x}'_5 \bar{w}_{\text{ee}}(\mathbf{x}_1, \mathbf{x}_5; \mathbf{x}_3, \mathbf{x}'_5) \chi_{\text{IP}}(\mathbf{x}'_5, \mathbf{x}_2; \mathbf{x}_5, \mathbf{x}_4; \omega = 0). \end{aligned} \quad (8.8)$$

This method will be referred to as BSE-GW_x.

8.3 Expressions in a finite orbital basis

8.3.1 Spin-orbital basis

In order to solve the Bethe-Salpeter equation for finite systems, all the equations are projected onto an orthonormal spin-orbital basis $\{\phi_p\}$. As the equations are 4-point equations relating two-particle quantities, they are in fact projected onto the basis of products of two spin orbitals. Each matrix element is thus indexed by two double indices.

We consider the simplest case for which $\chi_{\text{IP}} = \chi_0$. The Lehmann representation of χ_0 is

$$\chi_0(\mathbf{x}_1, \mathbf{x}_2; \mathbf{x}'_1, \mathbf{x}'_2; \omega) = \sum_{ia} \frac{\phi_i^*(\mathbf{x}'_1)\phi_a(\mathbf{x}_1)\phi_a^*(\mathbf{x}'_2)\phi_i(\mathbf{x}_2)}{\omega - (\varepsilon_a - \varepsilon_i) + i0^+} - \frac{\phi_i^*(\mathbf{x}'_2)\phi_a(\mathbf{x}_2)\phi_a^*(\mathbf{x}'_1)\phi_i(\mathbf{x}_1)}{\omega + (\varepsilon_a - \varepsilon_i) - i0^+}, \quad (8.9)$$

where ϕ_i is the i -th occupied spin-orbital of energy ε_i and ϕ_a is the a -th virtual spin-orbital of energy ε_a . One can notice that χ_0 is expanded only on occupied-virtual (ov) and virtual-occupied (vo) products of spin-orbitals. The matrix elements of χ_0 are given by

$$[\chi_0(\omega)]_{pq,rs} = \int d\mathbf{x}_1 d\mathbf{x}'_1 d\mathbf{x}_2 d\mathbf{x}'_2 \phi_p(\mathbf{x}'_1)\phi_q^*(\mathbf{x}_1)\chi_0(\mathbf{x}_1, \mathbf{x}_2; \mathbf{x}'_1, \mathbf{x}'_2; \omega)\phi_r^*(\mathbf{x}_2)\phi_s(\mathbf{x}'_2). \quad (8.10)$$

The matrix representation of its inverse, in the (ov,vo) subspace, is

$$\chi_0^{-1}(\omega) = - \left[\begin{pmatrix} \Delta\epsilon & \mathbf{0} \\ \mathbf{0} & \Delta\epsilon \end{pmatrix} - \omega \begin{pmatrix} \mathbf{1} & \mathbf{0} \\ \mathbf{0} & -\mathbf{1} \end{pmatrix} \right], \quad (8.11)$$

where $\Delta\epsilon_{ia,jb} = \Delta\epsilon_{ai,bj} = (\epsilon_a - \epsilon_i)\delta_{ij}\delta_{ab}$, where i, j refer to occupied spin-orbitals and a, b to virtual orbitals. The dimension of the matrix is thus $2M_oM_v \times 2M_oM_v$ where M_o and M_v are the numbers of occupied and virtual spin orbitals, respectively. To build the matrix χ^{-1} , one then needs to construct the matrix elements of the Bethe-Salpeter kernel Ξ_{Hxc} which are given by

$$(\Xi_{\text{Hxc}})_{pq,rs} = w_{ee,pq,rs} - W_{pr,qs}, \quad (8.12)$$

where $w_{ee,pq,rs} = \langle qr|ps \rangle$ are the usual two-electron integrals, and the matrix elements of W can be obtained from Equation (8.6)

$$\begin{aligned} W_{pq,rs} &= \int d\mathbf{x}_1 d\mathbf{x}'_1 d\mathbf{x}_2 d\mathbf{x}'_2 \phi_p(\mathbf{x}'_1) \phi_q^*(\mathbf{x}_1) W(\mathbf{x}_1, \mathbf{x}_2; \mathbf{x}'_1, \mathbf{x}'_2) \phi_r^*(\mathbf{x}_2) \phi_s(\mathbf{x}'_2) \\ &= \int d\mathbf{x}_1 d\mathbf{x}'_1 d\mathbf{x}_2 d\mathbf{x}'_2 d\mathbf{x}_3 d\mathbf{x}'_3 \phi_p(\mathbf{x}'_1) \phi_q^*(\mathbf{x}_1) \epsilon^{-1}(\mathbf{x}_1, \mathbf{x}_3; \mathbf{x}'_1, \mathbf{x}'_3) \\ &\quad \times w_{ee}(\mathbf{x}'_3, \mathbf{x}_2; \mathbf{x}_3, \mathbf{x}'_2) \phi_r^*(\mathbf{x}_2) \phi_s(\mathbf{x}'_2). \end{aligned} \quad (8.13)$$

To decouple the common coordinates in ϵ^{-1} and w_{ee} , one can introduce two delta functions $\delta(\mathbf{x}_3, \mathbf{x}_4)$ and $\delta(\mathbf{x}'_3, \mathbf{x}'_4)$ and use the closure relations $\delta(\mathbf{x}_3, \mathbf{x}_4) = \sum_t \phi_t^*(\mathbf{x}_3) \phi_t(\mathbf{x}_4)$ and $\delta(\mathbf{x}'_3, \mathbf{x}'_4) = \sum_u \phi_u(\mathbf{x}'_3) \phi_u^*(\mathbf{x}'_4)$. By doing so, the matrix elements of v and ϵ^{-1} appear explicitly and we get

$$W_{pq,rs} = \sum_{tu} \epsilon_{pq,tu}^{-1} w_{ee,tu,rs}. \quad (8.14)$$

Similarly, for the dielectric function, we have

$$\epsilon_{pq,rs} = \delta_{pr}\delta_{qs} - \sum_{tu} w_{ee,pq,tu} [\chi_0(\omega=0)]_{tu,rs} = \delta_{pr}\delta_{qs} - w_{ee,pq,rs} [\chi_0(\omega=0)]_{rs,rs}, \quad (8.15)$$

where the last equality comes from the fact that χ_0 has only diagonal elements. It can be seen that the static screened interaction consists of an infinite-order perturbation expansion in the Coulomb interaction, namely using matrix notations,

$$\begin{aligned} \mathbf{W} &= \epsilon^{-1} \cdot \mathbf{w}_{ee} \\ &= \mathbf{w}_{ee} + \mathbf{w}_{ee} \cdot \chi_0(\omega=0) \cdot \mathbf{w}_{ee} + \mathbf{w}_{ee} \cdot \chi_0(\omega=0) \cdot \mathbf{w}_{ee} \cdot \chi_0(\omega=0) \cdot \mathbf{w}_{ee} + \dots, \end{aligned} \quad (8.16)$$

the first term in this expansion corresponding to linear-response time-dependent Hartree-Fock (TDHF). The matrix representation of the inverse of the interacting response func-

tion, in the (ov,vo) subspace, is then

$$\chi^{-1}(\omega) = - \left[\begin{pmatrix} \mathbf{A} & \mathbf{B} \\ \mathbf{B}^* & \mathbf{A}^* \end{pmatrix} - \omega \begin{pmatrix} \mathbf{1} & \mathbf{0} \\ \mathbf{0} & -\mathbf{1} \end{pmatrix} \right], \quad (8.17)$$

with the matrices

$$A_{ia,jb} = \Delta\varepsilon_{ia,jb} + w_{ee,ia,jb} - W_{ij,ab}, \quad (8.18a)$$

$$B_{ia,jb} = w_{ee,ia,bj} - W_{ib,aj}. \quad (8.18b)$$

The block structure of Equation (8.17) is a consequence of the symmetry of the Coulomb interaction, $w_{ee,qp,rs} = w_{ee,pq,rs}^*$, and of the static screened interaction, $W_{qs,pr} = W_{pr,qs}^*$. Moreover, the matrix \mathbf{A} is Hermitian (because $w_{ee,ia,jb} = w_{ee,jb,ia}^*$ and $W_{ij,ab} = W_{ji,ba}^*$) and the matrix \mathbf{B} is symmetric (because $w_{ee,ia,bj} = w_{ee,jb,ai}$ and $W_{ib,aj} = W_{ja,bi}$). The excitation energies ω_n are thus found by solving the usual linear-response pseudo-Hermitian eigenvalue equation, just as in TDDFT,

$$\begin{pmatrix} \mathbf{A} & \mathbf{B} \\ \mathbf{B}^* & \mathbf{A}^* \end{pmatrix} \begin{pmatrix} \mathbf{X}_n \\ \mathbf{Y}_n \end{pmatrix} = \omega_n \begin{pmatrix} \mathbf{1} & \mathbf{0} \\ \mathbf{0} & -\mathbf{1} \end{pmatrix} \begin{pmatrix} \mathbf{X}_n \\ \mathbf{Y}_n \end{pmatrix}, \quad (8.19)$$

whose solutions come in pairs: excitation energies ω_n with eigenvectors $(\mathbf{X}_n, \mathbf{Y}_n)$, and de-excitation energies $-\omega_n$ with eigenvectors $(\mathbf{Y}_n^*, \mathbf{X}_n^*)$. For real spin-orbitals and if $\mathbf{A} + \mathbf{B}$ and $\mathbf{A} - \mathbf{B}$ are positive definite, the eigenvalues are guaranteed to be real numbers and the pseudo-Hermitian eigenvalue equation (8.19) can be transformed into a half-size symmetric eigenvalue equation [3].

If instead of starting from χ_0 , one starts from $\chi_{\text{IP}} = -iGG$ with the exact one-particle Green's function G , the equations get more complicated since the matrix representation of χ_{IP} is generally not diagonal and not only has contributions in the (ov,vo) subspace of spin-orbital products but also in the occupied-occupied (oo) and virtual-virtual (vv) subspace of spin-orbital products. The dimension of the matrices thus becomes $M^2 \times M^2$ where M is the total number of (occupied and virtual) spin orbitals. In this case, the number of solutions of the response equations is generally higher than the number of single excitations, and in particular double excitations might be obtained even without a frequency-dependent kernel. Spurious excitations can also be found. This is similar to what happens in linear-response TDDMFT [12–15]. We will show this later in the case of H_2 in a minimal basis.

When exchange is included, similar equations can be derived, where $W_{pq,rs}$ is substituted by $\bar{W}_{pq,rs}$ with

$$\bar{W}_{pq,rs} = \sum_{tu} w_{ee,pq,tu} \bar{\epsilon}_{tu,rs}^{-1} \quad (8.20)$$

and

$$\bar{\epsilon}_{pq,rs}^{-1} = \delta_{pr}\delta_{qs} - \bar{w}_{ee,pq,rs} [\chi_0(\omega = 0)]_{rs,rs} \quad (8.21)$$

where the $\bar{w}_{ee,pq,rs} = \langle qr || ps \rangle$ are the usual antisymmetrized two-electron integrals.

8.3.2 Spin adaptation

We give now the expressions for spin-restricted closed-shell calculations. For four fixed spatial orbitals referred to as p, q, r, s , the Bethe-Salpeter kernel has the following spin structure

$$\begin{pmatrix} \Xi_{p\uparrow q\uparrow, r\uparrow s\uparrow} & \Xi_{p\uparrow q\uparrow, r\downarrow s\downarrow} & 0 & 0 \\ \Xi_{p\downarrow q\downarrow, r\uparrow s\uparrow} & \Xi_{p\downarrow q\downarrow, r\downarrow s\downarrow} & 0 & 0 \\ 0 & 0 & \Xi_{p\uparrow q\downarrow, r\uparrow s\downarrow} & \Xi_{p\uparrow q\downarrow, r\downarrow s\uparrow} \\ 0 & 0 & \Xi_{p\downarrow q\uparrow, r\uparrow s\downarrow} & \Xi_{p\downarrow q\uparrow, r\downarrow s\uparrow} \end{pmatrix}, \quad (8.22)$$

which can be brought to a diagonal form after rotation (see, e.g., Refs. [42, 73, 74])

$$\begin{pmatrix} {}^1\Xi_{pq,rs} & 0 & 0 & 0 \\ 0 & {}^3\Xi_{pq,rs} & 0 & 0 \\ 0 & 0 & {}^3\Xi_{pq,rs} & 0 \\ 0 & 0 & 0 & {}^3\Xi_{pq,rs} \end{pmatrix}, \quad (8.23)$$

with a spin-singlet term ${}^1\Xi_{pq,rs} = 2w_{ee,pq,rs} - W_{pr,qs}$ and three degenerate spin-triplet terms ${}^3\Xi_{pq,rs} = -W_{pr,qs}$. It has been used that the Coulomb interaction v and the screened interaction W are spin independent: $w_{ee,pq,rs} = w_{ee,p\uparrow q\uparrow, r\uparrow s\uparrow} = w_{ee,p\uparrow q\uparrow, r\downarrow s\downarrow} = w_{ee,p\downarrow q\downarrow, r\uparrow s\uparrow} = w_{ee,p\downarrow q\downarrow, r\downarrow s\downarrow}$ and $W_{pq,rs} = W_{p\uparrow q\uparrow, r\uparrow s\uparrow} = W_{p\uparrow q\uparrow, r\downarrow s\downarrow} = W_{p\downarrow q\downarrow, r\uparrow s\uparrow} = W_{p\downarrow q\downarrow, r\downarrow s\downarrow}$. The spin-adapted screened interaction is obtained by

$$W_{pq,rs} = \sum_{tu} {}^1\epsilon_{pq,tu}^{-1} w_{ee,tu,rs}, \quad (8.24)$$

where t and u refer to spatial orbitals, and the singlet dielectric function ${}^1\epsilon_{pq,rs} = \epsilon_{p\uparrow q\uparrow, r\uparrow s\uparrow} + \epsilon_{p\uparrow q\uparrow, r\downarrow s\downarrow}$ is given by

$${}^1\epsilon_{pq,rs} = \delta_{pr}\delta_{qs} - {}^1w_{ee,pq,rs} [\chi_0(\omega = 0)]_{rs,rs}, \quad (8.25)$$

where the singlet interaction is given by ${}^1w_{ee,pq,rs} = 2w_{ee,pq,rs}$. The bottom line is that the linear-response eigenvalue equation (8.19) fully decouples into a singlet eigenvalue equation

$$\begin{pmatrix} {}^1\mathbf{A} & {}^1\mathbf{B} \\ {}^1\mathbf{B}^* & {}^1\mathbf{A}^* \end{pmatrix} \begin{pmatrix} {}^1\mathbf{X}_n \\ {}^1\mathbf{Y}_n \end{pmatrix} = {}^1\omega_n \begin{pmatrix} \mathbf{1} & \mathbf{0} \\ \mathbf{0} & -\mathbf{1} \end{pmatrix} \begin{pmatrix} {}^1\mathbf{X}_n \\ {}^1\mathbf{Y}_n \end{pmatrix}, \quad (8.26)$$

with the matrices

$${}^1A_{ia,jb} = \Delta\varepsilon_{ia,jb} + 2w_{ee,ia,jb} - W_{ij,ab}, \quad (8.27a)$$

$${}^1B_{ia,jb} = 2w_{ee,ia,bj} - W_{ib,aj}, \quad (8.27b)$$

and a triplet eigenvalue equation

$$\begin{pmatrix} {}^3\mathbf{A} & {}^3\mathbf{B} \\ {}^3\mathbf{B}^* & {}^3\mathbf{A}^* \end{pmatrix} \begin{pmatrix} {}^3\mathbf{X}_n \\ {}^3\mathbf{Y}_n \end{pmatrix} = {}^3\omega_n \begin{pmatrix} \mathbf{1} & \mathbf{0} \\ \mathbf{0} & -\mathbf{1} \end{pmatrix} \begin{pmatrix} {}^3\mathbf{X}_n \\ {}^3\mathbf{Y}_n \end{pmatrix}, \quad (8.28)$$

with the matrices

$${}^3A_{ia,jb} = \Delta\varepsilon_{ia,jb} - W_{ij,ab}, \quad (8.29a)$$

$${}^3B_{ia,jb} = -W_{ib,aj}, \quad (8.29b)$$

where the absence of the Hartree contribution is responsible for the singlet-triplet splitting in the excitation energies. When exchange is included, the spin-adapted screened interaction is obtained by

$$\bar{W}_{pq,rs} = \sum_{tu} {}^1\bar{\epsilon}_{pq,tu}^{-1} w_{ee,tu,rs}, \quad (8.30)$$

where

$${}^1\bar{\epsilon}_{pq,rs} = \delta_{pr}\delta_{qs} - {}^1\bar{w}_{ee,pq,rs} [\chi_0(\omega = 0)]_{rs,rs}. \quad (8.31)$$

where ${}^1\bar{w}_{ee,pq,rs} = (2w_{ee,pq,rs} - w_{ee,pr,qs})$.

8.4 Example of H₂ in a minimal basis

As a pedagogical example, we apply the BSE-GW method to the calculation of the excitation energies of H₂ in a minimal basis consisting of two Slater basis functions, φ_a and φ_b , centered on each hydrogen atom and with the same exponent $\zeta = 1$. This is a closed-shell molecule, therefore all the calculations are done with spin adaptation in a spatial orbital basis. The molecular orbitals are $\psi_1 = (\varphi_a + \varphi_b)/\sqrt{2(1 + S_{ab})}$ (symmetry σ_g) and $\psi_2 = (\varphi_a - \varphi_b)/\sqrt{2(1 - S_{ab})}$ (symmetry σ_u) where S_{ab} is the overlap between φ_a and φ_b . The matrix representations of all two-electron quantities in the space of spatial-orbital products are of the following form

$$\mathbf{P} = \left(\begin{array}{cc|cc} P_{11,11} & P_{11,22} & P_{11,12} & P_{11,21} \\ P_{22,11} & P_{22,22} & P_{22,12} & P_{22,21} \\ \hline P_{12,11} & P_{12,22} & P_{12,12} & P_{12,21} \\ P_{21,11} & P_{21,22} & P_{21,12} & P_{21,21} \end{array} \right), \quad (8.32)$$

and we refer to the upper left block as the (oo,vv) block, and to the bottom right block as the (ov,vo) block. All the values of the integrals as a function of the internuclear distance R can be found in Ref. [75]. Note that, in the condensed-matter physics literature, a simplified version of H₂ in a minimal basis with only on-site Coulomb interaction is often

used under the name “half-filled two-site Hubbard model” (see, e.g., Refs. [64, 76, 77]), where with the notations used here, the Hubbard model is obtained for $\Delta\varepsilon = 2t$ and $J_{11} = J_{22} = K_{12} = J_{12} = U/2$ where t is the hopping parameter and U is the on-site Coulomb interaction.

8.4.1 BSE-GW method using the non-interacting Green’s function

The simplest approximation in the BSE-GW method is to start from the non-interacting HF Green’s function G_0 , leading to the non-interacting HF linear response function $\chi_{\text{IP}} = -iG_0G_0 = \chi_0$ whose matrix representation reads

$$\chi_0(\omega) = \left(\begin{array}{cc|cc} 0 & 0 & 0 & 0 \\ 0 & 0 & 0 & 0 \\ \hline 0 & 0 & \frac{1}{\omega - \Delta\varepsilon} & 0 \\ 0 & 0 & 0 & \frac{-1}{\omega + \Delta\varepsilon} \end{array} \right), \quad (8.33)$$

where $\Delta\varepsilon = \varepsilon_2 - \varepsilon_1$ is the difference between the energies of the molecular orbitals ψ_2 and ψ_1 . The non-interacting linear response function has non-vanishing matrix elements only in the (ov,vo) block, but it will be necessary to consider the other blocks as well for the screened interaction W . The matrix of the Coulomb interaction is

$$\mathbf{w}_{\text{ee}} = \left(\begin{array}{cc|cc} J_{11} & J_{12} & 0 & 0 \\ J_{12} & J_{22} & 0 & 0 \\ \hline 0 & 0 & K_{12} & K_{12} \\ 0 & 0 & K_{12} & K_{12} \end{array} \right), \quad (8.34)$$

where $J_{pq} = \langle pq|pq \rangle$ and $K_{pq} = \langle pq|qp \rangle$ are the usual Coulomb and exchange two-electron integrals over the molecular orbitals ψ_1 and ψ_2 . The off-diagonal blocks of v are zero by symmetry for H₂ in a minimal basis, but this is not the case in general. By matrix product and inversion, we get the static singlet dielectric matrix

$${}^1\epsilon = \left(\begin{array}{cc|cc} 1 & 0 & 0 & 0 \\ 0 & 1 & 0 & 0 \\ \hline 0 & 0 & 1 + \frac{2K_{12}}{\Delta\varepsilon} & \frac{2K_{12}}{\Delta\varepsilon} \\ 0 & 0 & \frac{2K_{12}}{\Delta\varepsilon} & 1 + \frac{2K_{12}}{\Delta\varepsilon} \end{array} \right), \quad (8.35)$$

which, in this case, is block diagonal with the (oo,vv) block being the identity. By using its inverse, we finally get the static screened interaction matrix

$$\mathbf{W} = \left(\begin{array}{cc|cc} J_{11} & J_{12} & 0 & 0 \\ J_{12} & J_{22} & 0 & 0 \\ \hline 0 & 0 & \frac{K_{12}}{1+4K_{12}/\Delta\varepsilon} & \frac{K_{12}}{1+4K_{12}/\Delta\varepsilon} \\ 0 & 0 & \frac{K_{12}}{1+4K_{12}/\Delta\varepsilon} & \frac{K_{12}}{1+4K_{12}/\Delta\varepsilon} \end{array} \right), \quad (8.36)$$

which is block diagonal and the (oo,vv) block is just the bare Coulomb interaction in the case of H_2 in a minimal basis, but this is not generally true. We have then everything to construct the 1A and 1B matrices of Equation (8.26) for singlet excitations, which in the present case are just one-dimensional

$${}^1A = \Delta\varepsilon + 2K_{12} - J_{12}, \quad (8.37a)$$

$${}^1B = 2K_{12} - \frac{K_{12}}{1+4K_{12}/\Delta\varepsilon}. \quad (8.37b)$$

and the 3A and 3B matrices of Equation (8.28) for triplet excitations

$${}^3A = \Delta\varepsilon - J_{12}, \quad (8.38a)$$

$${}^3B = -\frac{K_{12}}{1+4K_{12}/\Delta\varepsilon}. \quad (8.38b)$$

Solving then the response equations by the standard Casida approach [3], we get the singlet excitation energy

$${}^1\omega = \sqrt{\left(\Delta\varepsilon + 4K_{12} - J_{12} - \frac{K_{12}}{1+4K_{12}/\Delta\varepsilon}\right) \left(\Delta\varepsilon - J_{12} + \frac{K_{12}}{1+4K_{12}/\Delta\varepsilon}\right)}, \quad (8.39)$$

and the triplet excitation energy

$${}^3\omega = \sqrt{\left(\Delta\varepsilon - J_{12} - \frac{K_{12}}{1+4K_{12}/\Delta\varepsilon}\right) \left(\Delta\varepsilon - J_{12} + \frac{K_{12}}{1+4K_{12}/\Delta\varepsilon}\right)}. \quad (8.40)$$

Note that, for this simple system, the A terms have the usual TDHF or configuration interaction singles (CIS) forms, and the screening has an effect only on the B terms, decreasing the exchange integral K_{12} by a factor of $1+4K_{12}/\Delta\varepsilon$. Therefore, in the Tamm-Dancoff approximation [78], which consists in neglecting B , the effect of screening would be lost and the method would be equivalent to CIS. It is interesting to analyze the effect of the screening as a function of the internuclear distance R . For small R , the orbital

energy difference $\Delta\varepsilon$ is much greater than the exchange integral K_{12} , so the screening factor $1 + 4K_{12}/\Delta\varepsilon$ is close to 1 and TDHF excitation energies are recovered. For large R (dissociation limit), $\Delta\varepsilon$ goes to zero, so the screening factor diverges and the term $K_{12}/(1 + 4K_{12}/\Delta\varepsilon)$ vanishes.

The excitation energies from the ground state $^1\Sigma_g^+$ to the first singlet $^1\Sigma_u^+$ and triplet $^3\Sigma_u^+$ excited states are plotted as a function of R in Figure 8.1. The reference curves are from a full configuration-interaction (FCI) calculation giving the exact excitation energies in this basis. In a minimal basis, the singlet $^1\Sigma_u^+$ excited state is constrained to dissociate into the ionic configuration $H^- \dots H^+$, and so in the dissociation limit $R \rightarrow \infty$ the exact singlet excitation energy goes to a constant, $I - A \approx 0.625$ hartree where I and A are the ionization energy and electron affinity of the hydrogen atom. The triplet $^3\Sigma_u^+$ dissociates into the neutral configuration $H^\bullet \dots H^\bullet$, as does the ground state, and so the exact triplet excitation energy goes to zero in the dissociation limit. TDHF gives accurate excitation energies for small R , but gives qualitatively wrong curves in the dissociation limit. For the singlet state, the TDHF excitation energy goes to zero, a wrong behavior inherited from the vanishing $\Delta\varepsilon$ in this limit. For the triplet state, the TDHF response equation suffers from a triplet instability for $R \geq 4$ bohr and the excitation energy becomes imaginary. It is known that TDDFT with standard density-functional approximations gives similarly incorrect energy curves [7, 76, 79–81]. The BSE-GW method using the non-interacting HF Green's function G_0 gives accurate excitation energies at small R , but fails in the dissociation limit. The singlet excitation energy becomes imaginary for $R \geq 4.9$ bohr. Indeed, in the dissociation limit, $\Delta\varepsilon$ goes to zero and Equation (8.39) leads to a negative term under the square root: $^1\omega \rightarrow \sqrt{(4K_{12} - J_{12})(-J_{12})}$. Similarly, the BSE-GW triplet excitation energy is imaginary between $R = 4.0$ and $R = 4.9$ bohr, and incorrectly tends to a non-zero value in the dissociation limit.

8.4.2 BSE-GWx method using the non-interacting Green's function

In what follows, the effect of adding exchange in the dielectric matrix is investigated. The singlet electron-electron interaction is then given by $\bar{w}_{ee}(\mathbf{x}_1, \mathbf{x}_5; \mathbf{x}_3, \mathbf{x}'_5) = w_{ee}(\mathbf{x}_1, \mathbf{x}_5; \mathbf{x}_3, \mathbf{x}'_5) - w_{ee}(\mathbf{x}_5, \mathbf{x}_1; \mathbf{x}_3, \mathbf{x}'_5)$. Its spin-adapted matrix representation in the minimal basis set is then

$$^1\bar{\mathbf{w}}_{ee} = \left(\begin{array}{cc|cc} J_{11} & 2J_{12} - K_{12} & 0 & 0 \\ 2J_{12} - K_{12} & J_{22} & 0 & 0 \\ \hline 0 & 0 & 2K_{12} - J_{12} & K_{12} \\ 0 & 0 & K_{12} & 2K_{12} - K_{12} \end{array} \right). \quad (8.41)$$

With respect to the matrix of the interaction when the antisymmetrization is not taken into account, the self-screening has been removed in this representation. The non-interacting response function is unchanged so the antisymmetrized dielectric matrix

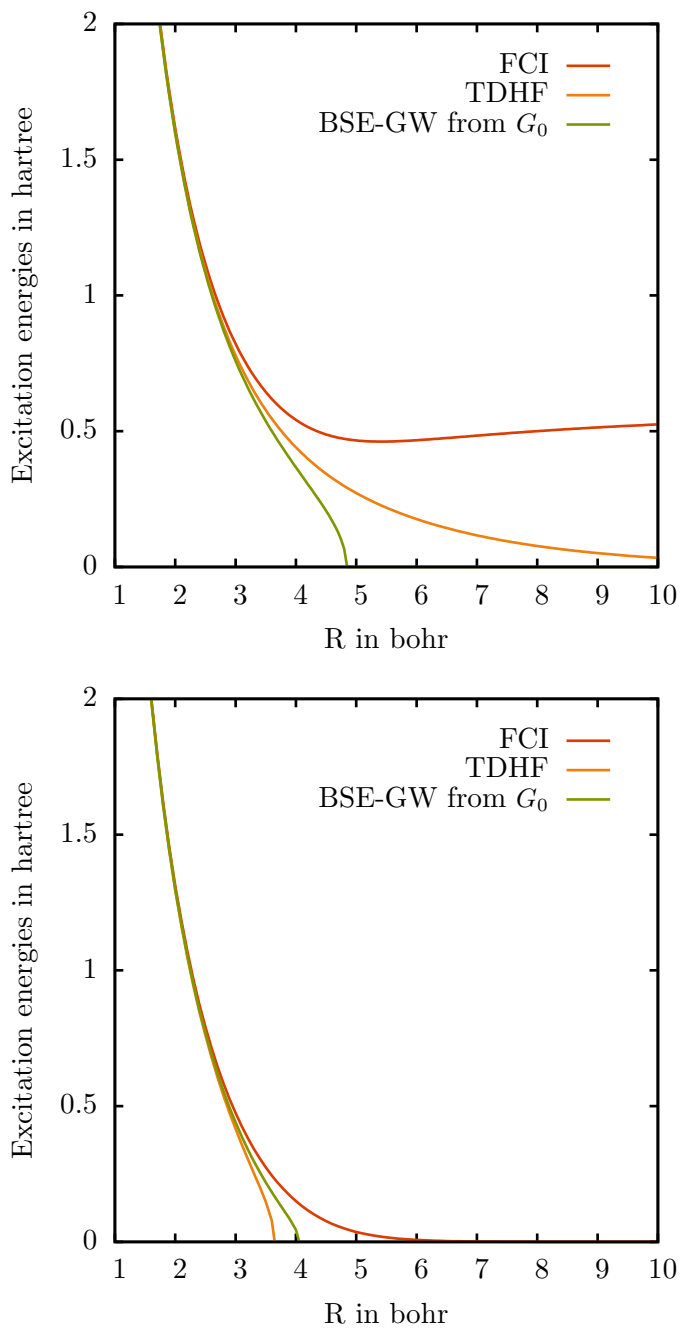


Figure 8.1 – Excitation energies of the singlet $^1\Sigma_u^+$ (top) and the triplet $^3\Sigma_u^+$ (bottom) states of H_2 in a minimal basis as a function of the internuclear distance R calculated by FCI, TDHF, and BSE-GW with the non-interacting HF Green’s function G_0 .

is

$${}^1\bar{\epsilon} = \left(\begin{array}{cc|cc} 1 & 0 & 0 & 0 \\ 0 & 1 & 0 & 0 \\ \hline 0 & 0 & 1 + \frac{2K_{12} - J_{12}}{\Delta\epsilon} & \frac{K_{12}}{\Delta\epsilon} \\ 0 & 0 & \frac{K_{12}}{\Delta\epsilon} & 1 + \frac{2K_{12} - J_{12}}{\Delta\epsilon} \end{array} \right) \quad (8.42)$$

and the matrix of the screening is

$$\bar{\mathbf{W}} = \left(\begin{array}{cc|cc} J_{11} & J_{12} & 0 & 0 \\ J_{12} & J_{22} & 0 & 0 \\ \hline 0 & 0 & \bar{W}_{12} & \bar{W}_{12} \\ 0 & 0 & \bar{W}_{12} & \bar{W}_{12} \end{array} \right) \quad (8.43)$$

where $\bar{W}_{12} = \frac{K_{12}}{1 + (3K_{12} - J_{12})/\Delta\epsilon}$. With respect to the BSE-GW case where no exchange was accounted for, the exchange integral K_{12} is now screened by $1 + (3K_{12} - J_{12})/\Delta\epsilon$ instead of $1 + 4K_{12}/\Delta\epsilon$. The screening is therefore reduced by $K_{12} + J_{12}$ as the self-screening has been removed. Using this screened interaction into Equations (8.26) and (8.28), the singlet and triplet matrices \mathbf{A} and \mathbf{B} can be constructed and are given by

$$\begin{aligned} {}^1A &= \Delta\epsilon + 2K_{12} - J_{12} \\ {}^1B &= 2K_{12} - \frac{K_{12}}{1 + (3K_{12} - J_{12})/\Delta\epsilon} \end{aligned} \quad (8.44)$$

in the singlet case, and by

$$\begin{aligned} {}^3A &= \Delta\epsilon - J_{12} \\ {}^3B &= -\frac{K_{12}}{1 + (3K_{12} - J_{12})/\Delta\epsilon}, \end{aligned} \quad (8.45)$$

in the triplet case. Solving Casida's equation [3], the singlet excitation is then

$${}^1\omega = \sqrt{\left(\Delta\epsilon + 4K_{12} - J_{12} - \frac{K_{12}}{1 + \frac{3K_{12} - J_{12}}{\Delta\epsilon}} \right) \left(\Delta\epsilon - J_{12} + \frac{K_{12}}{1 + \frac{3K_{12} - J_{12}}{\Delta\epsilon}} \right)} \quad (8.46)$$

and the triplet equation is

$${}^3\omega = \sqrt{\left(\Delta\epsilon - J_{12} - \frac{K_{12}}{1 + \frac{3K_{12} - J_{12}}{\Delta\epsilon}} \right) \left(\Delta\epsilon - J_{12} + \frac{K_{12}}{1 + \frac{3K_{12} - J_{12}}{\Delta\epsilon}} \right)}. \quad (8.47)$$

These excitation energies are plotted in Figure 8.2 together with the FCI and TDHF curves for the sake of comparison. With respect to the initial curves given in Figure 8.1, very similar patterns are observed. The excitation energies still become imaginary when

the bond is stretched but at slightly different values of the internuclear distance. The singlet excitation energy becomes imaginary at $R = 5.3$ bohr when it was 4.9 bohr when exchange was not included and is not significantly improved. The triplet excitation energy on the other hand, is slightly worsened as it now becomes imaginary at $R=3.7$ bohr instead of 4 bohr. The overall effect of the inclusion of exchange in the dielectric matrix is therefore rather small in this case.

The BSE-GW method using the non-interacting HF Green's function G_0 thus badly fails for H_2 in the dissociation limit, with or without exchange in the dielectric matrix. As this method is based on a single-determinant reference, this should not come as a surprise. Moreover, the double excitation is also completely absent from this method. However, the BSE approach also allows one to start from an interacting Green's function G taking into account the multiconfigurational character of stretched H_2 . We will now test this alternative approach.

8.4.3 BSE-GW method using the exact Green's function

Independent-particle response function

We apply the BSE-GW equations (8.5)-(8.7) with the independent-particle response function $\chi_{IP} = -iGG$ constructed from the exact one-particle Green's function G , and which can be calculated by the Lehmann formula (7.8) using the N -electron ground state and the $(N \pm 1)$ -electron states. The states to consider for H_2 in a minimal basis are given in Figure 8.3. The ground state is composed of two Slater determinants, its energy is $E_N = 2\varepsilon_1 - J_{11} + E_c$ where $E_c = \Delta - \sqrt{\Delta^2 + K_{12}^2}$ is the correlation energy with $2\Delta = 2\Delta\varepsilon + J_{11} + J_{22} - 4J_{12} + 2K_{12}$. The coefficients of the determinants are determined by $c_2 = c_1 K_{12} / (\Delta + \sqrt{K_{12}^2 + \Delta^2})$ and $c_1^2 + c_2^2 = 1$. The energies of the two $(N + 1)$ -electron states are: $E_{N+1,1} = 2\varepsilon_1 + \varepsilon_2 - J_{11}$ and $E_{N+1,2} = 2\varepsilon_2 + \varepsilon_1 - J_{11} + J_{22} - 2J_{12} + K_{12}$. The energies of the two $(N - 1)$ -electron states are: $E_{N-1,1} = \varepsilon_1 - J_{11}$ and $E_{N-1,2} = \varepsilon_2 - 2J_{12} + K_{12}$. We thus obtain four poles for the exact one-particle Green's function. Two of them correspond to minus the electron affinities,

$$\mathcal{E}_2 = E_{N+1,1} - E_N = \varepsilon_2 - E_c, \quad (8.48a)$$

$$\mathcal{E}'_2 = E_{N+1,2} - E_N = 2\varepsilon_2 - \varepsilon_1 + J_{22} - 2J_{12} + K_{12} - E_c, \quad (8.48b)$$

and the other two correspond to minus the ionization energies,

$$\mathcal{E}_1 = E_N - E_{N-1,1} = \varepsilon_1 + E_c, \quad (8.49a)$$

$$\mathcal{E}'_1 = E_N - E_{N-1,2} = 2\varepsilon_1 - \varepsilon_2 - J_{11} + 2J_{12} - K_{12} + E_c. \quad (8.49b)$$

In condensed-matter physics, \mathcal{E}_1 and \mathcal{E}_2 are associated with “quasi-particle” peaks of photoelectron spectra, while \mathcal{E}'_1 and \mathcal{E}'_2 are associated with “satellites”. The Dyson

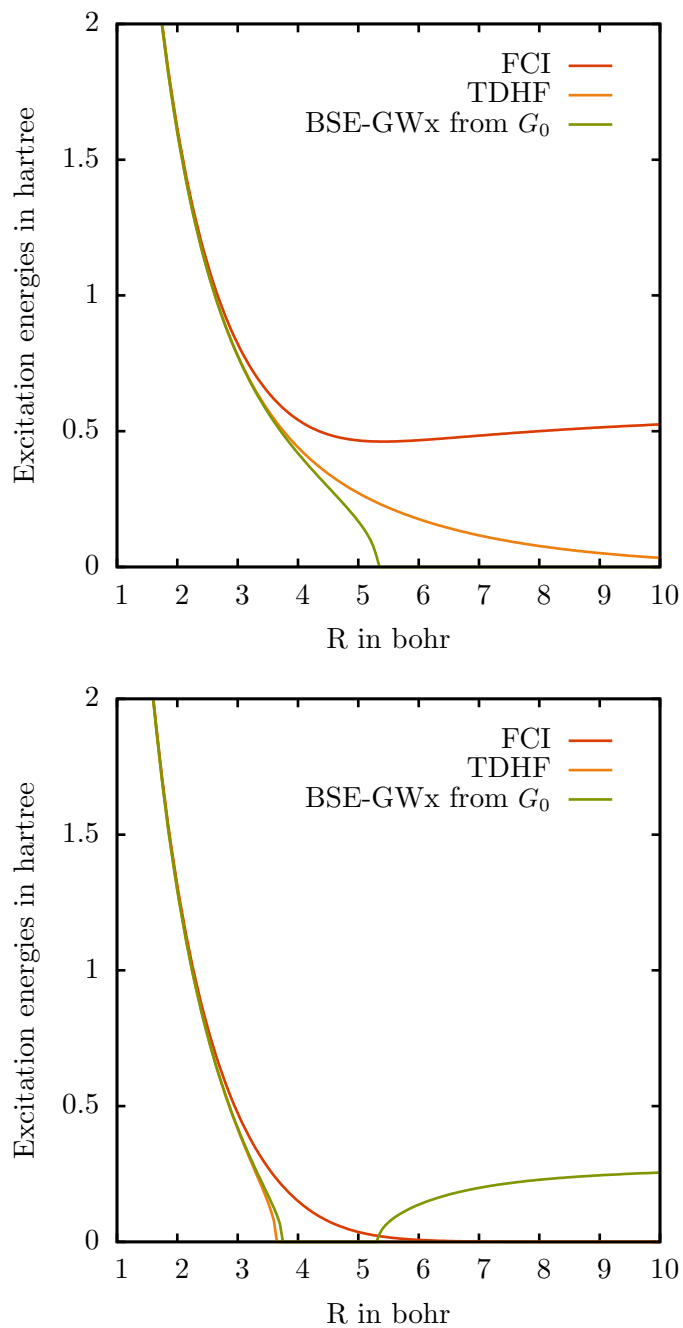


Figure 8.2 – Excitation energies of the singlet $^1\Sigma_u^+$ (top) and the triplet $^3\Sigma_u^+$ (bottom) states of H₂ in a minimal basis as a function of the internuclear distance R calculated by FCI, TDHF, and BSE-GW_x with the non-interacting HF Green’s function G_0 .

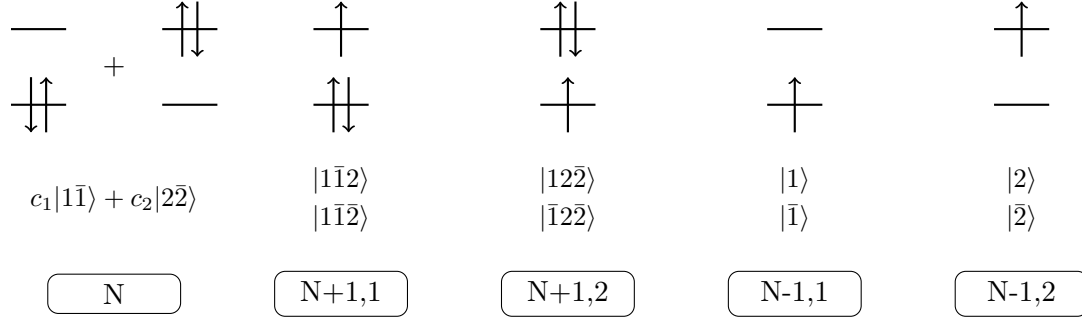


Figure 8.3 – N -electron ground state, and $(N \pm 1)$ -electron states for H_2 in a minimal basis.

orbitals are also easily calculated, and we finally arrive at the matrix representation of χ_{IP} in the basis of the products of spatial orbitals

$$\chi_{\text{IP}}(\omega) = \left(\begin{array}{cc|cc} \chi_{\text{IP},11}(\omega) & 0 & 0 & 0 \\ 0 & \chi_{\text{IP},22}(\omega) & 0 & 0 \\ \hline 0 & 0 & \chi_{\text{IP},12}(\omega) & 0 \\ 0 & 0 & 0 & \chi_{\text{IP},21}(\omega) \end{array} \right), \quad (8.50)$$

with the matrix elements

$$\chi_{\text{IP},11}(\omega) = \frac{c_1^2 c_2^2}{\omega - (\mathcal{E}'_2 - \mathcal{E}_1)} - \frac{c_1^2 c_2^2}{\omega + (\mathcal{E}'_2 - \mathcal{E}_1)}, \quad (8.51a)$$

$$\chi_{\text{IP},22}(\omega) = \frac{c_1^2 c_2^2}{\omega - (\mathcal{E}_2 - \mathcal{E}'_1)} - \frac{c_1^2 c_2^2}{\omega + (\mathcal{E}_2 - \mathcal{E}'_1)}, \quad (8.51b)$$

$$\chi_{\text{IP},12}(\omega) = \frac{c_1^4}{\omega - (\mathcal{E}_2 - \mathcal{E}_1)} - \frac{c_2^4}{\omega + (\mathcal{E}'_2 - \mathcal{E}'_1)}, \quad (8.51c)$$

$$\chi_{\text{IP},21}(\omega) = \frac{c_2^4}{\omega - (\mathcal{E}'_2 - \mathcal{E}'_1)} - \frac{c_1^4}{\omega + (\mathcal{E}_2 - \mathcal{E}_1)}. \quad (8.51d)$$

Therefore, whereas $\chi_0(\omega)$ has only one positive pole, $\chi_{\text{IP}}(\omega)$ has four distinct positive poles (and four symmetric negative poles). These poles are plotted in Figure 8.4. The lowest one, $\mathcal{E}_2 - \mathcal{E}_1$, called fundamental gap in the condensed-matter physics literature, can be considered as an approximation to a neutral single excitation energy since in the limit of non-interacting particles it equals the difference of the orbital eigenvalues $\Delta\varepsilon = \varepsilon_2 - \varepsilon_1$. The two intermediate poles, $\mathcal{E}'_2 - \mathcal{E}_1$ and $\mathcal{E}_2 - \mathcal{E}'_1$, can be interpreted as approximations to a double excitation energy since they reduce to $2\Delta\varepsilon$ in the limit of non-interacting particles. Surprisingly, the highest pole, $\mathcal{E}'_2 - \mathcal{E}'_1$, reduces to $3\Delta\varepsilon$ in this limit and it is thus tempting to associate it with a triple excitation even though the system contains only two electrons! In the dissociation limit $R \rightarrow \infty$, the four poles tends to the same value, i.e. $I - A \approx 0.625$ hartree which is also minus twice the correlation energy $-2E_c$, showing that the non-vanishing fundamental gap in this limit is a correlation effect. Note that

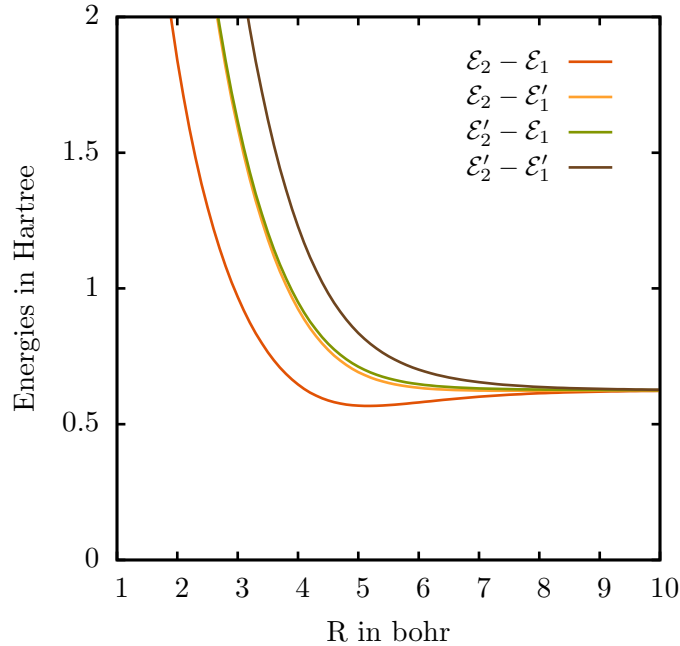


Figure 8.4 – Positive poles of the independent-particle linear response function in function of the internuclear distance R

it has been shown [64] that the non-self-consistent GW approximation (G_0W_0) to the one-particle Green's function gives a fundamental gap which is too small by a factor of 2 in the dissociation limit, so we do not consider this approximation here.

Excitation energies

Having calculated the independent-particle response function, the next steps of the BSE-GW calculation of the excitation energies proceed similarly as in Section 8.4.1, even though the expressions get more complicated. From the matrix $\chi_{IP}(\omega = 0)$ and the Coulomb interaction matrix (8.34), we calculate the singlet dielectric matrix which is still block diagonal but the upper left block is no longer the identity matrix. We calculate then the static screened interaction matrix which is still block diagonal but the elements of its upper left block are now also affected by screening. We can then construct the corresponding singlet and triplet Bethe-Salpeter kernel ${}^1\Xi$ and ${}^3\Xi$. The response eigenvalue equations (8.26) and (8.28) are no longer applicable, so the singlet excitation energies are found by searching the values of ω giving vanishing eigenvalues of the inverse singlet linear-response matrix ${}^1\chi(\omega)^{-1} = \chi_{IP}(\omega)^{-1} - {}^1\Xi$, and the triplet excitation energies are found by searching the values of ω giving vanishing eigenvalues of the inverse triplet linear-response matrix ${}^3\chi(\omega)^{-1} = \chi_{IP}(\omega)^{-1} - {}^3\Xi$. For H_2 in a minimal basis, ${}^1\chi(\omega)^{-1}$ and ${}^3\chi(\omega)^{-1}$ are 4×4 matrices which are block diagonal, the (oo, vv) block being uncoupled to the (ov, vo) block. For both the singlet and triplet cases, the four positive poles of $\chi_{IP}(\omega)$ transform into four excitation energies (plus four symmetric de-excitation energies).

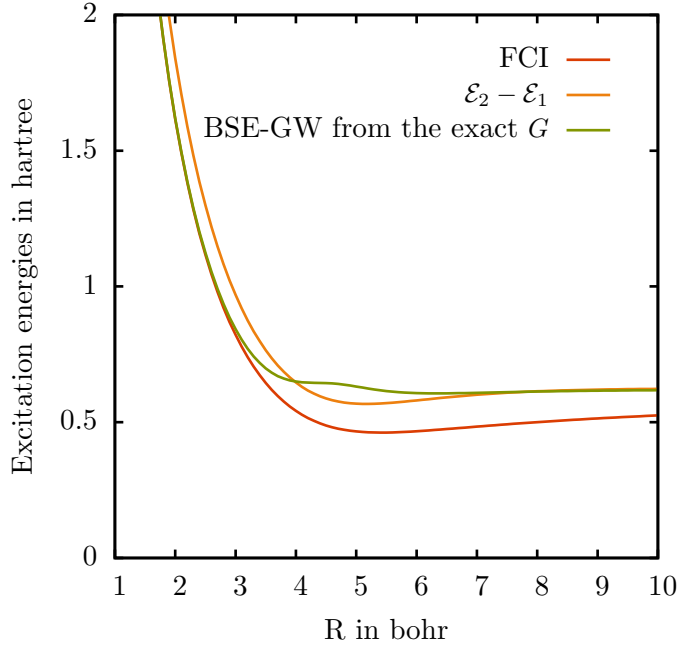


Figure 8.5 – Excitation energy of the singlet ${}^1\Sigma_u^+$ state of H_2 in a minimal basis as a function of the internuclear distance R calculated by FCI and BSE-GW with the exact Green’s function. The lowest pole of $\chi_{\text{IP}}(\omega)$, the fundamental gap $\mathcal{E}_2 - \mathcal{E}_1$, is also plotted for comparison.

Among the two positive excitation energies coming from the (ov,vo) block of the matrix ${}^1\chi(\omega)^{-1}$, the lowest one is identified with the first singlet ${}^1\Sigma_u^+$ excitation energy, which is called the optical gap. It is plotted in Figure 8.5 and compared with the reference FCI excitation energy and also with the fundamental gap $\mathcal{E}_2 - \mathcal{E}_1$ to highlight the effect of the Bethe-Salpeter kernel. At small internuclear distance, $R \leq 3$ bohr, the Bethe-Salpeter kernel brings the BSE-GW curve very close to the FCI curve. For large R , the BSE-GW excitation energy follows the curve of the fundamental gap, which slightly overestimates the excitation energy at $R = 10$ bohr but eventually goes to the correct limit $I - A$ when $R \rightarrow \infty$. Thus, contrary to the BSE-GW method using the non-interacting Green’s function, the obtained excitation energy curve has now a correct shape. This relies on the fundamental gap being a good starting approximation to the optical gap. As regards the second excitation energy coming from the (ov,vo) block of the matrix ${}^1\chi(\omega)^{-1}$ which is connected to highest pole $\mathcal{E}'_2 - \mathcal{E}'_1$ of $\chi_{\text{IP}}(\omega)$, it is a spurious excitation due to the approximate Bethe-Salpeter kernel used.

The lowest positive excitation energy coming from the (oo,vv) block of the matrix ${}^1\chi(\omega)^{-1}$ is identified with the second singlet ${}^1\Sigma_g^+$ excited state which has a double excitation character. It is plotted in Figure 8.6 and compared with the FCI excitation energy for this state and with the poles $\mathcal{E}'_2 - \mathcal{E}_1$ and $\mathcal{E}_2 - \mathcal{E}'_1$ of $\chi_{\text{IP}}(\omega)$. It is noteworthy that the BSE-GW method starting from $\chi_{\text{IP}}(\omega)$ instead of $\chi_0(\omega)$ but using a frequency-

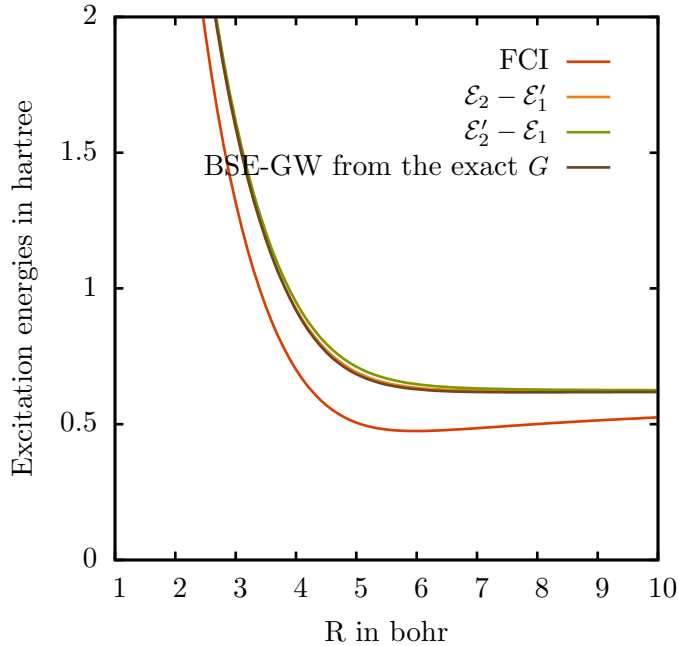


Figure 8.6 – Excitation energy of the second singlet ${}^1\Sigma_g^+$ state of H₂ in a minimal basis as a function of the internuclear distance R calculated by FCI and BSE-GW with the exact Green’s function. The poles $\mathcal{E}'_2 - \mathcal{E}_1$ and $\mathcal{E}_2 - \mathcal{E}'_1$ of $\chi_{\text{IP}}(\omega)$ are also plotted for comparison.

independent kernel does describe this double-excitation state with an overall correct shape for the energy curve. However, the BSE-GW excitation energy is almost identical to the two poles $\mathcal{E}'_2 - \mathcal{E}_1$ and $\mathcal{E}_2 - \mathcal{E}'_1$. The Bethe-Salpeter kernel in the static GW approximation thus brings virtually no improvement for this state over the starting poles of $\chi_{\text{IP}}(\omega)$. The (oo,vv) block of the matrix ${}^1\chi(\omega)^{-1}$ also gives a second higher excitation energy that is spurious.

We finally consider the triplet excited state ${}^3\Sigma_u^+$. The lowest positive excitation energy coming from the (ov,vo) block of the matrix ${}^3\chi(\omega)^{-1}$ should be identified with this state. It is plotted in Figure 8.7 and compared with the FCI excitation energy for this state and with the fundamental gap $\mathcal{E}_2 - \mathcal{E}_1$. For small internuclear distances, $R \leq 3$ bohr, the BSE-GW method gives an accurate excitation energy, but for larger R , instead of going to zero, the BSE-GW excitation energy follows the fundamental gap until the excitation energy becomes imaginary for $R \geq 6.5$ bohr. The problem is that the poles of $\chi_{\text{IP}}(\omega)$ are the same for both the singlet and triplet cases, and the fundamental gap $\mathcal{E}_2 - \mathcal{E}_1$ is not a good starting approximation to the triplet excitation energy in the dissociation limit. The Bethe-Salpeter kernel in the static GW approximation is not able of compensating for this bad starting point. In addition to this excitation energy, the BSE-GW method gives three other spurious triplet excitation energies.

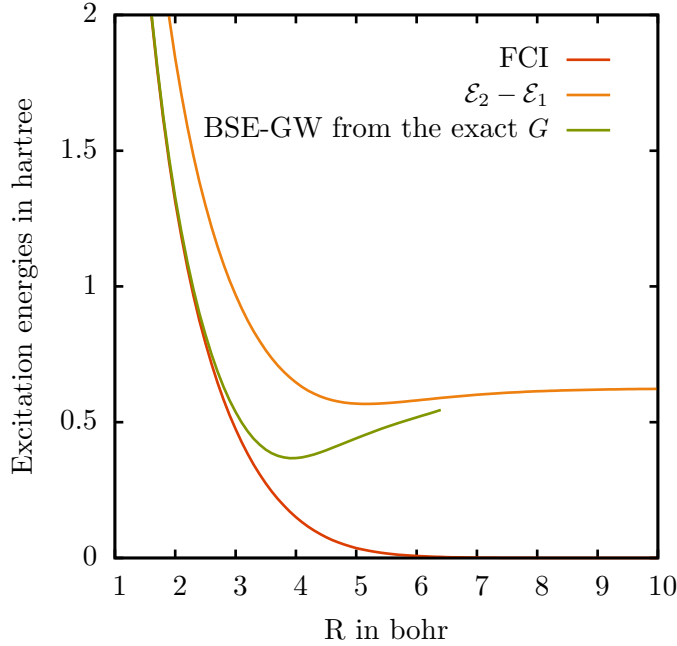


Figure 8.7 – Excitation energy of the triplet ${}^3\Sigma_u^+$ state of H_2 in a minimal basis as a function of the internuclear distance R calculated by FCI and BSE-GW with the exact Green’s function. The lowest pole of $\chi_{\text{IP}}(\omega)$, the fundamental gap $\mathcal{E}_2 - \mathcal{E}_1$, is also plotted for comparison.

Effect of the inclusion of exchange

A similar study was performed when exchange is included in the dielectric response function as was done in the non-interacting case. The excitation energy to the singlet ${}^1\Sigma_u^+$ state is shown in Figure 8.8. It does not present a bump anymore but its large R value overestimates the exact FCI energy. Its asymptotic limit is higher than without exchange which was already too high. However, the effect of the kernel does not cancel out anymore at large R but goes in the wrong direction with the respect of the poles of the non-interacting response function. The excitation energy to the second singlet ${}^1\Sigma_g^+$ state is shown in Figure 8.9. As for the singlet ${}^1\Sigma_u^+$ excitation, its behavior at large R is not improved by the inclusion of the exchange. The effect of the kernel does not cancel anymore at large R but goes in the wrong direction with respect to the poles of χ_{IP} . The excitation energy to the triplet ${}^3\Sigma_u^+$ state is shown in Figure 8.10. It becomes imaginary for a smaller value of R than without exchange as was also observed with the non-interacting Green’s function.

In all these cases, the correct asymptotic limit is not recovered for the excitation energies. In fact, as will be seen in the next chapter in the perturbative framework, the inclusion of exchange in the dielectric matrix needs to be done together with the inclusion of the derivative of W with respect to G in order to have a consistent expression for the kernel.

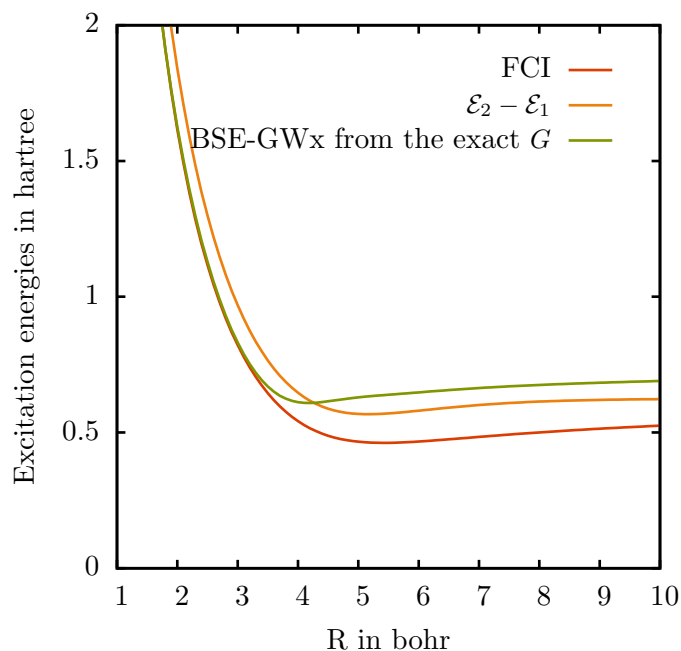


Figure 8.8 – Excitation energy of the singlet ${}^1\Sigma_u^+$ state of H₂ in a minimal basis as a function of the internuclear distance R calculated by FCI and BSE-GWx with the exact Green’s function. The lowest pole of $\chi_{\text{IP}}(\omega)$, the fundamental gap $\varepsilon_2 - \varepsilon_1$, is also plotted for comparison.

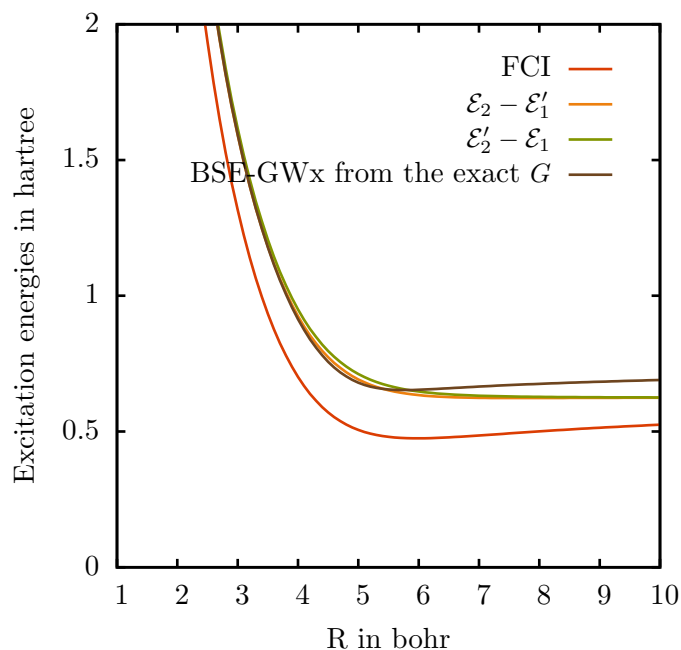


Figure 8.9 – Excitation energy of the second singlet ${}^1\Sigma_g^+$ state of H₂ in a minimal basis as a function of the internuclear distance R calculated by FCI and BSE-GWx with the exact Green’s function. The poles $\varepsilon_2' - \varepsilon_1$ and $\varepsilon_2 - \varepsilon_1'$ of $\chi_{\text{IP}}(\omega)$ are also plotted for comparison.

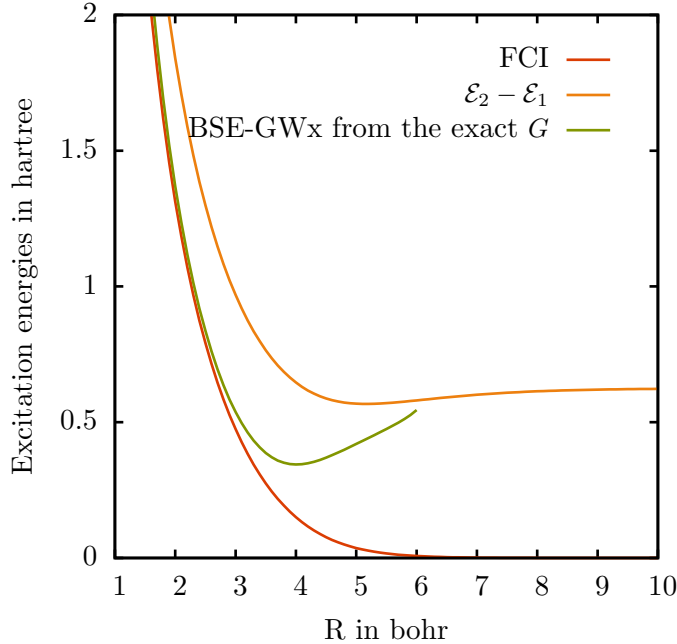


Figure 8.10 – Excitation energy of the triplet ${}^3\Sigma_u^+$ state of H_2 in a minimal basis as a function of the internuclear distance R calculated by FCI and BSE-GWx with the exact Green’s function. The lowest pole of $\chi_{\text{IP}}(\omega)$, the fundamental gap $\mathcal{E}_2 - \mathcal{E}_1$, is also plotted for comparison.

8.5 Conclusion

In this chapter, we have applied the BSE approach in the static GW approximation for the calculation of the excitation energies on the toy model of H_2 in a minimal basis. We were essentially interested to the effects of the different approximations that are made on the self-energy but did not investigate the ones made during the derivation of the kernel. We have tested two variants for the starting one-particle Green’s function: the non-interacting HF one and the exact one, and have also assessed the effect of the inclusion of exchange in the dielectric matrix for these two variants. Around the equilibrium internuclear distance, both variants give accurate excitation energies to the first singlet ${}^1\Sigma_u^+$ and triplet ${}^3\Sigma_u^+$ excited states. In the dissociation limit, however, the two variants differ. The first variant, starting from the non-interacting one-particle Green’s function, badly fails in this limit for both the singlet and triplet states, giving imaginary excitation energies. The second variant, starting from the exact one-particle Green’s function, gives a qualitatively correct energy curve for the singlet ${}^1\Sigma_u^+$ excited state up to the dissociation limit. This relies on the fact that the fundamental gap (given by the one-particle Green’s function) is a good starting approximation to the first singlet excitation energy. However, the same variant gives an incorrect energy curve for the triplet ${}^3\Sigma_u^+$ excited state in the dissociation limit. In this case, the fundamental gap is a bad starting approximation to the first triplet excitation energy. The inclusion

of exchange in the GWx variant does not help with these deficiencies and even gives imaginary excitation energies for smaller intermolecular distances.

The second BSE variant using the exact one-particle Green's function gives more excitation energies than the first BSE variant. Most of them are spurious excitations due to the approximate Bethe-Salpeter kernel which is used and is not number conserving when the derivative of the self-energy is dropped [35, 36, 82, 83]. However, one of them can be identified with the excitation energy to the singlet ${}^1\Sigma_g^+$ excited state which has a double excitation character. It is remarkable that such a double excitation can be described at all within a static approximation. This was made possible by using a multi-configurational wave function for the construction of the Green's function. However, the Bethe-Salpeter kernel in the static GW approximation is insufficient to describe accurately the energy curve of this state, even around the equilibrium distance.

Staying in the static approximation, one major approximation remains on kernel as the derivative of W with respect to G was neglected up to this point. Its effect is assessed in the next chapter in a perturbative approach where all the quantities are given up to the second order of the interaction.

Chapter 9

Second-order static BSE kernel

In this chapter, the self-energy and static Bethe-Salpeter kernel are expanded in a perturbative way up to second order with respect to the bare electron-electron interaction. The derivation is first done in real space where the exchange may or may not be included in the self-energy and where the derivative of W with respect to G is or is not included. The resulting equations are then projected onto a spin-orbital basis. The inclusion of exchange into the correlation self-energy leads to a spin-orbital representation where the two-electron integrals are antisymmetrized but is not sufficient by itself to ensure the same for the second-order correlation Bethe-Salpeter kernel. In fact, for the Bethe-Salpeter kernel, a fully antisymmetrized form is obtained only when both the exchange in the correlation self-energy and the term $\delta W/\delta G$ in its derivative are included. In this case, the conservation laws are fulfilled. If only one of these contributions is taken into account an unbalanced expression where only part of the integrals is antisymmetrized is obtained. This confirms that both effects have to be taken into account together in order to treat finite molecular systems for which the exchange terms are important. This antisymmetrized static second-order kernel is once again illustrated on H_2 in a minimal basis set where in the static approximation it is found to have a non-physical form. Most of the technical details can be found in Appendix G.

9.1 Introduction

The response function of a system describes how it is affected by a change potential, for instance by addition of an electromagnetic field. In the Bethe-Salpeter approach, the description of this response involves a kernel which describes the interaction between the quasi-particles and how this interaction is affected by the perturbation. It is formally given by differentiation of the self-energy which can be calculated in principle via the exact set of coupled equations provided by Hedin's cycle (cf Chapter 7). As it is not possible to find a straightforward solution to this problem, different kinds of approximations can be introduced for the construction of the self-energy depending on

the physical system to describe and/or the available computational power. The GW approximation was introduced in the last chapter and consists in neglecting the vertex corrections which account for the change of interaction of the quasi-particles induced by a change of potential. Other approximations can be made by expressing Hedin's equations as either finite or infinite series of the non-interacting (or Hartree-Fock) Green's function G_0 and of the bare interaction w_{ee} [17, 84, 85], or of the screened interaction W [45, 48, 86]. When such approximations are designed, one has to make sure that they are conserving approximations [39, 87, 88] which means that given quantities such as the number of particles or the total energy will be conserved by these approximations. These conservation laws can be related to the Thomas-Reiche-Kuhn sum rule present in time-dependent density-functional theory (TDDFT). In particular, when the kernel is derived from the self-energy, the first-order derivative of W with respect to G is often dropped, which means that the change in screening due to the perturbation is neglected. However, in order to design a conserving approximation, this term should in principle be kept.

In the framework of finite molecular systems, we expand the correlation self-energy (in Section 9.2) and Bethe-Salpeter kernel (in Section 9.3) up to second order with respect to the bare Coulomb interaction w_{ee} and the Hartree-Fock Green's function G_0 and project them onto a spin-orbital basis. The effects of the inclusion of exchange into the correlation self-energy (GWx) and of the inclusion of the derivative of W with respect to G into the kernel are assessed. As the resulting correlation Bethe-Salpeter kernel is frequency dependent, it requires in principle to solve the dynamical Bethe-Salpeter equation. However, in this chapter, a static approximation of the kernel is used by setting ω to 0 in the correlation kernel and is inserted in the Bethe-Salpeter equation. The effects of the inclusion of exchange in the self-energy and of the derivative of W with respect to G are tracked through the derivation in order to show their respective importance. The dynamical case will be treated in the next chapter. The effects of the second-order approximation is then assessed on the model system of H_2 in a minimal basis in Section 9.4 and compared to the results obtained in Chapter 8 when neither the exchange or $\delta W/\delta G$ are included. Then, the kernel, where both contributions are included, is also illustrated on this model system. Technical details of the derivation of the second-order self-energy and kernel can be found in Appendix G.

This perturbative expansion in terms of the bare electron-electron interaction will be especially interesting in the range-separated context where the interaction will be replaced by its (smaller) long-range part as our end goal, afterall, is to design a long-range correlation Bethe-Salpeter kernel which will be added perturbatively to the range-separated TDDFT kernel (cf Chapter 6). This could also justify why an expansion in terms of the bare interaction is performed and not in terms of the screened interaction.

9.2 Second-order self-energy

9.2.1 Second-order self-energy in real space

From the previous chapter, the Hartree-exchange-correlation self-energy, within the GWx approximation, is given in the time domain by

$$\Sigma_{\text{Hxc}}[G](1, 2) = -i \int d3d3' w_{\text{ee}}(1, 3; 2, 3') G(3'^+, 3^{++}) + i \int d1' d3 G(1', 3) \bar{W}(3, 1; 2, 1'), \quad (9.1)$$

where the screened potential \bar{W} is given by

$$\bar{W}(1, 2; 1', 2') = \int d3d3' \bar{\epsilon}^{-1}(1, 3; 1', 3') w_{\text{ee}}(3', 2; 3, 2'), \quad (9.2)$$

and the antisymmetrized dielectric function is

$$\bar{\epsilon}(1, 2; 3, 4) = \delta(1, 4)\delta(2, 3) - \int d5d5' \bar{w}_{\text{ee}}(1, 5; 3, 5') \chi_{\text{IP}}(5', 2; 5^+, 4). \quad (9.3)$$

In order to expand the self-energy at second order with respect to the electron-electron interaction w_{ee} , the inverse dielectric function needs to be expanded up to the first order and is then given by

$$(\bar{\epsilon}^{(1)})^{-1}(1, 2; 3, 4) = \delta(1, 4)\delta(2, 3) + \int d5d5' \bar{w}_{\text{ee}}(1, 5; 3, 5') \chi_{\text{IP}}(5', 2; 5^+, 4). \quad (9.4)$$

When inserted into the expression of the Hartree-exchange-correlation self-energy, it gives rise to four contributions: the Hartree self-energy

$$\Sigma_{\text{H}}[G](1, 2) = -i \int d3d3' w_{\text{ee}}(1, 3; 2, 3') G(3'^+, 3^{++}), \quad (9.5)$$

and the exchange self-energy

$$\Sigma_{\text{x}}[G](1, 2) = i \int d1' d3 G(1', 3) w_{\text{ee}}(3, 1; 2, 1') \quad (9.6)$$

which contribute at first order with respect to w_{ee} , the second-order direct correlation self-energy

$$\Sigma_{\text{c}}^{(2\text{d})}[G](1, 2) = i \int d1' d3d4d4' d5d5' G(1', 3) w_{\text{ee}}(3, 5; 2, 5') \chi_{\text{IP}}(5', 4; 5^+, 4'^+) w_{\text{ee}}(4', 1; 4, 1') \quad (9.7)$$

and the second-order “exchanged” correlation self-energy

$$\Sigma_{\text{c}}^{(2\text{x})}[G](1, 2) = -i \int d1' d3d4d4' d5d5' G(1', 3) w_{\text{ee}}(5, 3; 2, 5') \chi_{\text{IP}}(5', 4; 5^+, 4'^+) w_{\text{ee}}(4', 1; 4, 1'), \quad (9.8)$$

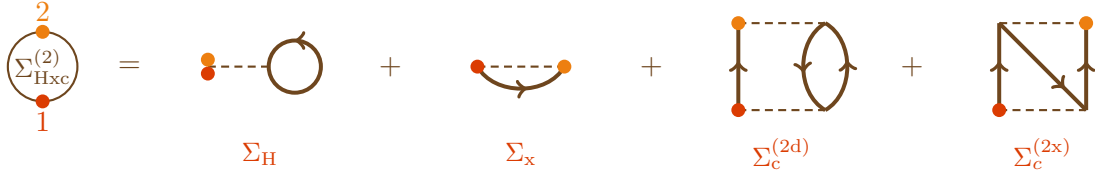


Figure 9.1 – Feynman diagrams of the second-order self-energy. The colored dots are the outer variables. These diagrams represents in fact the self-energy contributions to the Green’s function of an electron. In order to have the full diagrammatic expansion of the self-energy, diagrams with reverse arrows should also be included to account for the contributions of the Green’s function of a hole.

which arise from the antisymmetrisation of the two-electron interaction in the dielectric function. The Feynman diagrams of these contributions are recalled in Figure 9.1 where the order of perturbation can be easily found by counting the number of interaction lines (dashed line) which enter in each diagram. If the dielectric function is not antisymmetrized, the “exchanged” correlation contribution disappears, i.e. the last diagram in Figure 9.1 is removed. In here, we have kept the explicit functional dependence of the self-energy with respect to the full-interacting Green’s function G as to obtain the kernel, we need to differentiate with respect to G . However, if one’s goal is to get the self-energy at second order, then the self-energy has to be evaluated at $G = G_0$.

As the Hartree and exchange self-energy are not affected by the second-order expansion and have already been given in the previous chapter, only the second-order correlation will be detailed hereinafter.

9.2.2 Projection onto a spin-orbital basis

In what follows, we are interested in the projection onto the spin-orbital basis set of the Fourier transform of the second-order self-energy evaluated at $G = G_0$. The convention for the Fourier transform can be found in Appendix A.2. The matrix elements are then obtained in the spin-orbital basis with the convention

$$\Sigma_{uv}(\omega) = \iint d\mathbf{x}_1 d\mathbf{x}_2 \Sigma(\mathbf{x}_1, \mathbf{x}_2, \omega) \varphi_u^*(\mathbf{x}_1) \varphi_v(\mathbf{x}_2). \quad (9.9)$$

The details of the derivation can be found in Appendix G.1.

Direct correlation self-energy

The real-space expression of the direct correlation self-energy in the time domain is given by Equation (9.7). When the time variables are made explicit, it can be rewritten as

$$\Sigma_c^{(2d)}[G](\mathbf{x}_1, \mathbf{x}_2, \tau) = G(\mathbf{x}_1, \mathbf{x}_2, \tau) \int d\mathbf{x}_4 d\mathbf{x}_5 G(\mathbf{x}_5, \mathbf{x}_4, -\tau) G(\mathbf{x}_4, \mathbf{x}_5, \tau - 0^+) w_{ee}(\mathbf{r}_2, \mathbf{r}_5) w_{ee}(\mathbf{r}_4, \mathbf{r}_1), \quad (9.10)$$

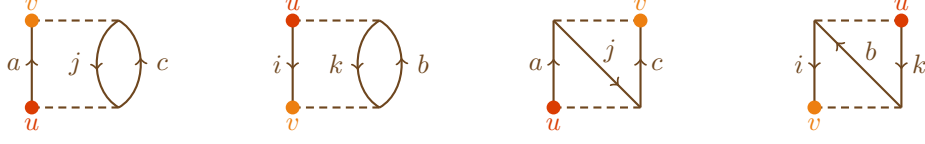


Figure 9.2 – Spin-orbital interpretation of the diagrammatic expansion of the second-order correlation self-energy.

where $\tau = t_1 - t_2$. When evaluated at $G = G_0$, the matrix elements of its Fourier transform in the spin-orbital basis set are then given by

$$\begin{aligned} \Sigma_{c,uv}^{(2d)}(\omega) &= \sum_{ajc} \frac{\langle ac|vj\rangle\langle uj|ac\rangle}{\omega - (\varepsilon_a - \varepsilon_j + \varepsilon_c) + i0^+} + \sum_{ibk} \frac{\langle ik|vb\rangle\langle ub|ik\rangle}{\omega - (\varepsilon_i - \varepsilon_b + \varepsilon_k) - i0^+} \\ &= \sum_{ajc} \frac{\langle ac|vj\rangle\langle uj|ac\rangle}{\omega - \varepsilon_a + \varepsilon_j - \varepsilon_c + i0^+} - \sum_{ibk} \frac{\langle ik|vb\rangle\langle ub|ik\rangle}{-\omega + (\varepsilon_i - \varepsilon_b + \varepsilon_k) + i0^+}. \end{aligned} \quad (9.11)$$

These two terms correspond to the first two diagrams of Figure 9.2. The two two-electron integrals in the numerator corresponds to the two interaction lines present in each diagram. The three orbital energies correspond to the particle and hole lines where an occupied orbital is given by an down-going arrow and a virtual orbital corresponds to an up-going arrow. The outer variables 1 and 2 have been replaced by their corresponding orbitals u and v following the convention given in Equation (9.9). On these diagrams, one can also “read” the two-electron integrals. For instance, for the top interaction line of the first diagram, the orbitals a and v are integrated together and so are the orbitals j and c , this can then be “translated” in the equation by the term $\langle ac|vj\rangle$.

In this expression however, the two-electron integrals are not antisymmetrized as only the direct part of the correlation self-energy was taken into account. Let now consider the “exchanged” part.

“Exchanged” correlation self energy

Similarly to the direct case, the real-space expression of the “exchanged” correlation self-energy with explicit time variables is given by

$$\Sigma_c^{(2x)}[G](\mathbf{x}_1, \mathbf{x}_2, \tau) = - \int d\mathbf{x}_3 d\mathbf{x}_4 G(\mathbf{x}_1, \mathbf{x}_3, \tau) G(\mathbf{x}_3, \mathbf{x}_4, -\tau) G(\mathbf{x}_4, \mathbf{x}_2, \tau) w_{ee}(\mathbf{r}_2, \mathbf{r}_3) w_{ee}(\mathbf{r}_4, \mathbf{r}_1). \quad (9.12)$$

Its matrix elements in the frequency space when evaluated at $G = G_0$ are then given by

$$\begin{aligned} \Sigma_{c,uv}^{(2x)}(\omega) &= - \sum_{ajc} \frac{\langle ca|vj\rangle\langle uj|ac\rangle}{\omega - (\varepsilon_a - \varepsilon_j + \varepsilon_c) + i0^+} - \sum_{ibk} \frac{\langle ki|vb\rangle\langle ub|ik\rangle}{\omega - (\varepsilon_i - \varepsilon_b + \varepsilon_k) - i0^+} \\ &= - \sum_{ajc} \frac{\langle ca|vj\rangle\langle uj|ac\rangle}{\omega - \varepsilon_a + \varepsilon_j - \varepsilon_c + i0^+} + \sum_{ibk} \frac{\langle ki|vb\rangle\langle ub|ik\rangle}{-\omega + \varepsilon_i - \varepsilon_b + \varepsilon_k + i0^+}, \end{aligned} \quad (9.13)$$

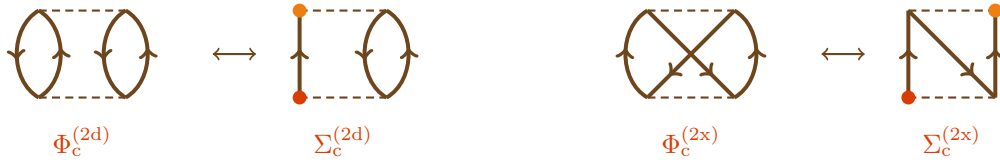


Figure 9.3 – Feynman diagrams of the function Φ from which the correlation self-energy can be obtained by differentiation with respect to G .

which corresponds to the antisymmetric counterpart of the direct correlation self-energy. These two terms correspond to the last two diagrams of Figure 9.2. As in the direct case, a spin-orbital interpretation of the diagrams can be made and matches the expression found in Equation (9.13). The minus sign comes from the absence of loop in these diagrams with respect to the direct ones.

Total second-order correlation self-energy

When both the direct and the “exchanged” contributions are taken together, the matrix elements of the total second-order correlation self-energy evaluated at $G = G_0$ are therefore

$$\Sigma_{c,uv}^{(2)}(\omega) = \frac{1}{2} \sum_{ajc} \frac{\langle ac||vj\rangle\langle uj||ac\rangle}{\omega - (\varepsilon_a - \varepsilon_j + \varepsilon_c) + i0^+} + \frac{1}{2} \sum_{ibk} \frac{\langle ik||vb\rangle\langle ub||ik\rangle}{\omega - (\varepsilon_i - \varepsilon_b + \varepsilon_k) - i0^+}, \quad (9.14)$$

where $\langle pq||rs\rangle = \langle pq|rs\rangle - \langle pq|sr\rangle$ so that all the two-electron integrals are now antisymmetrized. Taking either the direct correlation only or the total correlation, can be a relevant approximation depending on either one is dealing with a finite or infinite system. Moreover, each of these two possibilities constitutes a conserving approximation which means that they are consistent with the general (number, momentum and energy) conservation laws. A sufficient condition on the self-energy operator to be a conserving approximation is to be Φ -derivable, i.e. there exists a functional Φ of G such that $\Sigma = \delta\Phi/\delta G$ [87]. This condition can also be checked diagrammatically following the rules introduced by Baym [88]. The Feynman diagrams of the direct and “exchanged” part of the function Φ are given in Figure 9.3 and are homomorphic to the well-known Goldstone diagrams for the Møller-Plesset correlation energy at second order [89–91].

9.3 Second-order Bethe-Salpeter kernel

9.3.1 Second-order Bethe-Salpeter kernel in real space

Knowing the second-order self-energy, the second-order Hartree-exchange-correlation Bethe-Salpeter kernel can then be obtained as

$$\Xi_{\text{Hxc}}^{(2)}(1, 6; 2, 5) = i \left. \frac{\delta \Sigma_{\text{Hxc}}^{(2)}[G](1, 2)}{\delta G(5, 6)} \right|_{G=G_0}, \quad (9.15)$$

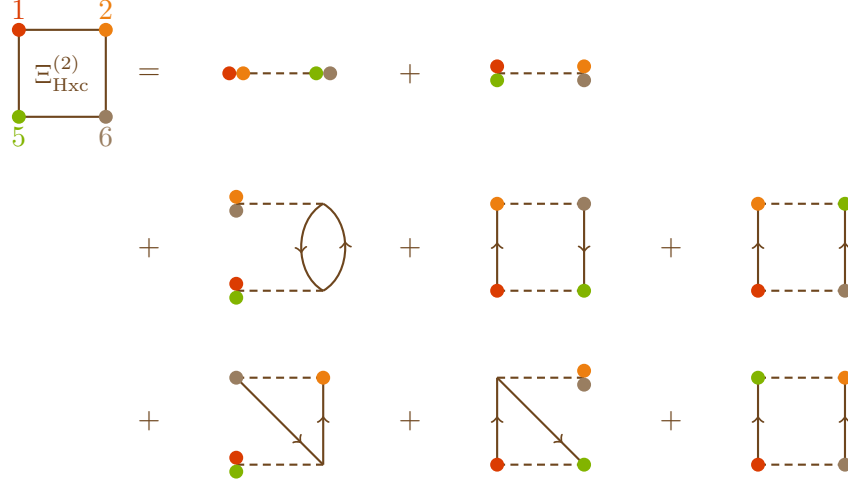


Figure 9.4 – Feynman representation of the second-order Bethe-Salpeter kernel. The colored dots are the outer variables. In order to have the full diagrammatic expansion, the diagrams with reverse Green’s functions should also be accounted for.

if the exchange and the derivative of W with respect to G are included then the corresponding Feynman diagrams are given in Figure 9.4 where “differentiating with respect to G ” can be interpreted as removing a G arrow from the self-energy diagrams. The tail of the removed arrow is replaced by a brown point corresponding to the variable 6 and the head is replaced by a green point corresponding to the variable 5. Therefore, starting with the diagrammatic expansion of the self-energy given in Figure 9.1, one can obtain the kernel by removing the G arrow in the Hartree and exchange parts and by removing either one of the three G arrows for the direct and exchanged correlation self-energy which gives rise to six diagrams for the correlation part of the kernel. Similarly to the self-energy, an approximation to the kernel is said to be conserving if there exists a functional Φ such that the kernel can be expressed as the second-order derivative of Φ with respect to G . Therefore, starting from a conserving approximation of the self-energy, the kernel will be conserving if all the terms are kept in the differentiation of Σ with respect to G .

As we are interested in the matrix elements of the frequency-dependent kernel, the algebraic derivation of the kernel is a two-step procedure: first, the Fourier transform is performed following the conventions given in Appendix A.2, and then the matrix elements are obtained with the convention

$$\Xi_{pq,rs}(\omega) = \int d\mathbf{x}_1 d\mathbf{x}_2 d\mathbf{x}_5 d\mathbf{x}_6 \varphi_p(\mathbf{x}_2) \varphi_q^*(\mathbf{x}_1) \Xi(\mathbf{x}_1, \mathbf{x}_6; \mathbf{x}_2, \mathbf{x}_5; \omega) \varphi_r^*(\mathbf{x}_6) \varphi_s(\mathbf{x}_5). \quad (9.16)$$

Hartree kernel

With explicit time variables, the Hartree kernel is given in real space as

$$\Xi_{\text{H}}(1, 6; 2; 5) = i \frac{\delta \Sigma_{\text{H}}(1, 2)}{\delta G(5, 6)} = \delta(1, 2) \delta(5, 6) \delta(t_1 - t_5) w_{\text{ee}}(\mathbf{r}_1, \mathbf{r}_5), \quad (9.17)$$

and is local in time. It corresponds to the first diagram of the right-hand-side of Figure 9.4. With the convention given in Equation (9.16), its matrix elements are simply given by the two-electron integrals $\Xi_{\text{H},pq,rs} = \langle qr | ps \rangle$.

Exchange kernel

In the same way, the exchange kernel is given by

$$\Xi_{\text{x}}(1, 6; 2; 5) = i \frac{\delta \Sigma_{\text{x}}(1, 2)}{\delta G(5, 6)} = -\delta(6, 2) \delta(1, 5) \delta(t_1 - t_2) w_{\text{ee}}(\mathbf{r}_1, \mathbf{r}_2), \quad (9.18)$$

and is also local in time. It corresponds to the second diagram of the right-hand-side of Figure 9.4 where the points 2 and 5 have been exchanged with respect to the Hartree term. Its matrix elements are then given by $\Xi_{\text{x},pq,rs} = -\langle qr | sp \rangle$, and corresponds to the antisymmetric counterpart of the Hartree kernel.

Correlation kernel

The second-order correlation Bethe-Salpeter kernel can be split into a direct and an “exchanged part”, coming naturally from the decomposition of the self-energy

$$\begin{aligned} \Xi_{\text{c}}^{(2)}(1, 6; 2; 5) &= \Xi_{\text{c}}^{(2\text{d})}(1, 6; 2; 5) + \Xi_{\text{c}}^{(2\text{x})}(1, 6; 2; 5) \\ &= i \frac{\delta \Sigma_{\text{c}}^{(2\text{d})}(1, 2)}{\delta G(5, 6)} \Bigg|_{G=G_0} + i \frac{\delta \Sigma_{\text{c}}^{(2\text{x})}(1, 2)}{\delta G(5, 6)} \Bigg|_{G=G_0}. \end{aligned} \quad (9.19)$$

Each of these parts will be treated separately in the following. Moreover, as the second-order self-energy is a product G times the second-order screened interaction $\bar{W}^{(2)}$, in each differentiation, two terms occur, one coming from $(\delta G / \delta G) \bar{W}^{(2)}$ which will be denoted as $\triangleright \Xi$ and one coming from $G (\delta \bar{W}^{(2)} / \delta G)$ which is denoted as $\triangleleft \Xi$. A summary of the decompositions is given in Figure 9.5 in terms of Feynman diagrams. The first contribution $\triangleright \Xi$ corresponds to the interaction between the quasi-hole and the quasi-electron and is represented by the “bubble” diagram (and its antisymmetrized counterpart) in Figure 9.5. The second contribution $\triangleleft \Xi$ takes into accounts the change in the interaction induced by the perturbation and corresponds to the “ladder” diagrams in Figure 9.5. The distinction between these two contributions is made explicit in order to be able to identify the effects of the derivative of W with respect to G which is usually neglected in the literature for solid systems. However, it can be forgotten if one is not interested in this comparison. Finally, the kernels also decompose into in a ph/hp part which corre-

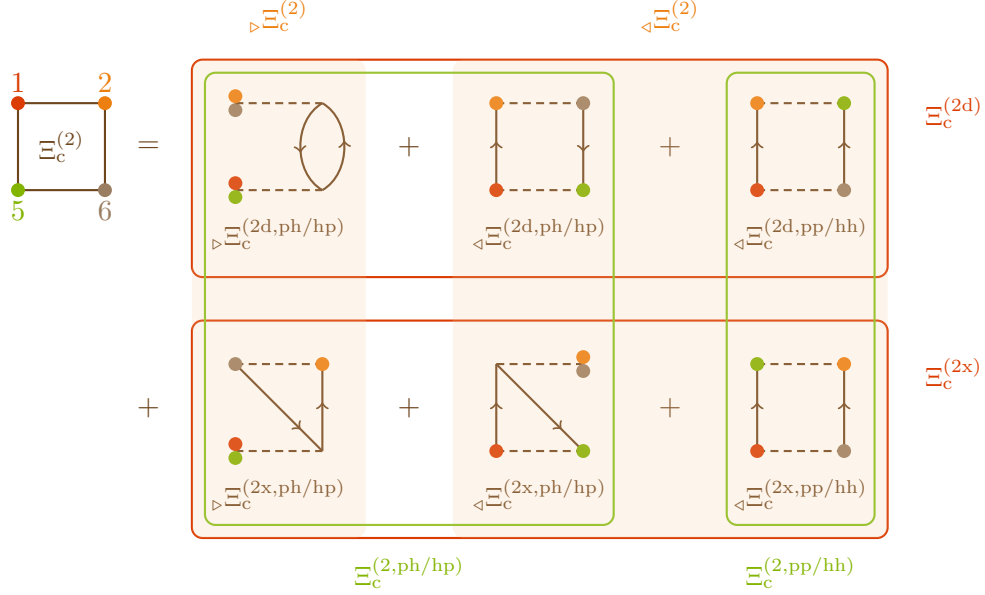


Figure 9.5 – Diagrammatic decomposition of the second-order Bethe-Salpeter correlation kernel, into direct and exchanged part (in red), into pp/hh and ph/ph contributions (in green) and into the parts coming from W and from $G\delta W/\delta G$ (in orange).

sponds to the propagation of an electron and a hole and a pp/hh where either two holes or two electrons are propagated simultaneously. The details of the derivations are given in Appendix G.2.

Direct correlation BSE kernel The direct correlation Bethe-Salpeter kernel can be split into three contributions

$$\begin{aligned}
 \Xi_c^{(2d)}(1, 6; 2; 5) = & \delta(t_2, t_6)\delta(t_1, t_5) \triangleright \Xi_c^{(2d,ph/hp)}(\mathbf{x}_1, \mathbf{x}_6; \mathbf{x}_2, \mathbf{x}_5; t_1 - t_2) \\
 & + \delta(t_2, t_6)\delta(t_1, t_5) \triangleleft \Xi_c^{(2d,ph/hp)}(\mathbf{x}_1, \mathbf{x}_6; \mathbf{x}_2, \mathbf{x}_5; t_1 - t_2) \\
 & + \delta(t_2, t_5)\delta(t_1, t_6) \triangleleft \Xi_c^{(2d,pp/hh)}(\mathbf{x}_1, \mathbf{x}_6; \mathbf{x}_2, \mathbf{x}_5; t_1 - t_2).
 \end{aligned} \tag{9.20}$$

The first two terms are ph/hp terms and have the same delta functions on the time variables. They correspond to the propagation of a hole and an electron together. The third term has different delta functions on the time variables and corresponds to the propagation of either two holes or two electrons together, it is thus a pp/hh term. These terms will need to be treated separately when the Fourier transform is performed as detailed in Appendix G.2 and when inserted in the Bethe-Salpeter equation except in the static case where an additional delta function on t_1 and t_2 solves this issue. Moreover, one should note that $\triangleleft \Xi_c^{(d,pp/hh)}[G]$ and $\triangleleft \Xi_c^{(d,ph/hp)}[G]$ arise from the derivative of W with respect to G and are usually neglected in the literature of condensed-matter physics.

With the convention given by Equation (9.16), the matrix elements of the frequency-

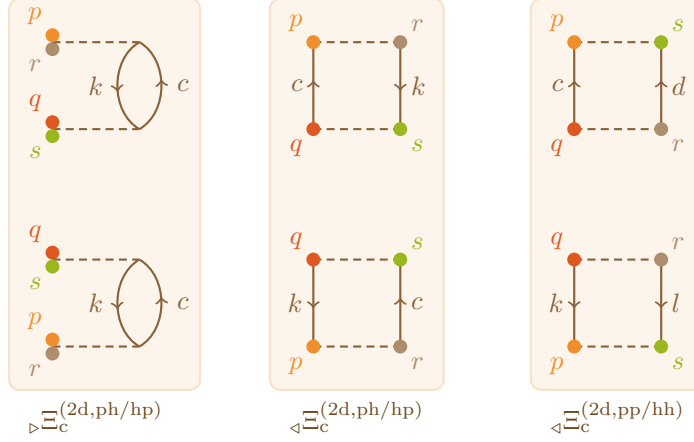


Figure 9.6 – Spin-orbital interpretation of the diagrammatic expansion of the direct second-order correlation kernel.

dependent second-order direct correlation kernel are then given by

$$\triangleright\Xi_{c,pq,rs}^{(2d,ph/hp)}(\omega) = - \sum_{kc} \frac{\langle qk|sc\rangle\langle rc|pk\rangle}{\omega - (\varepsilon_c - \varepsilon_k) + i0^+} + \sum_{kc} \frac{\langle rk|pc\rangle\langle qc|sk\rangle}{\omega + (\varepsilon_c - \varepsilon_k) - i0^+}, \quad (9.21)$$

which corresponds to the top and bottom left diagrams of Figure 9.6,

$$\triangleleft\Xi_{c,pq,rs}^{(2d,ph/hp)}(\omega) = - \sum_{kc} \frac{\langle cr|pk\rangle\langle qk|cs\rangle}{\omega - (\varepsilon_c - \varepsilon_k) + i0^+} + \sum_{kc} \frac{\langle kr|pc\rangle\langle qc|ks\rangle}{\omega + (\varepsilon_c - \varepsilon_k) - i0^+}, \quad (9.22)$$

which corresponds to the middle diagrams of Figure 9.6 and

$$\triangleleft\Xi_{c,pq,rs}^{(2d,pp/hh)}(\omega) = \sum_{cd} \frac{\langle cd|ps\rangle\langle qr|cd\rangle}{\omega - (\varepsilon_c + \varepsilon_d) + i0^+} - \sum_{kl} \frac{\langle kl|ps\rangle\langle qr|kl\rangle}{\omega - (\varepsilon_k + \varepsilon_l) - i0^+}, \quad (9.23)$$

for the right diagrams. As in the self-energy case, it is possible to make a spin-orbital interpretation of the diagrams and the diagrammatic and algebraic formulations are equivalent.

“Exchanged” correlation BSE kernel A similar decomposition can be done for the second-order “exchanged” correlation kernel such that

$$\begin{aligned} \Xi_c^{(2x)}(1, 6; 2; 5) &= \delta(t_2, t_6)\delta(t_1, t_5)\triangleright\Xi_c^{(2x,ph/hp)}(\mathbf{x}_1, \mathbf{x}_6; \mathbf{x}_2, \mathbf{x}_5; t_1 - t_2) \\ &\quad + \delta(t_2, t_6)\delta(t_1, t_5)\triangleleft\Xi_c^{(2x,ph/hp)}(\mathbf{x}_1, \mathbf{x}_6; \mathbf{x}_2, \mathbf{x}_5; t_1 - t_2) \\ &\quad + \delta(t_2, t_5)\delta(t_1, t_6)\triangleleft\Xi_c^{(2x,pp/hh)}(\mathbf{x}_1, \mathbf{x}_6; \mathbf{x}_2, \mathbf{x}_5; t_1 - t_2), \end{aligned} \quad (9.24)$$

which also has ph/hp and pp/hh contributions. Once the Fourier transform is performed as detailed in Appendix G.2, the matrix elements of the frequency-dependent second-order “exchanged” correlation kernel are obtained by projection onto the spin-orbital

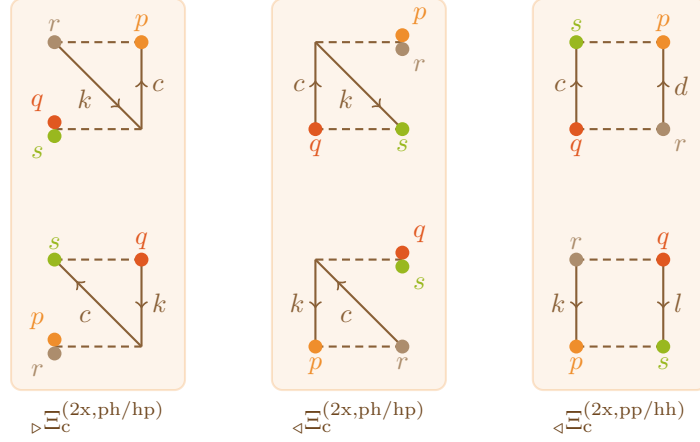


Figure 9.7 – Spin-orbital interpretation of the diagrammatic expansion of the “exchanged” second-order correlation kernel.

basis and are given by

$$\triangleright \Xi_{c,pq,rs}^{(2x,ph/hp)}(\omega) = \sum_{kc} \frac{\langle cr|pk\rangle\langle qk|sc\rangle}{\omega - (\varepsilon_c - \varepsilon_k) + i0^+} - \sum_{kc} \frac{\langle kr|pc\rangle\langle qc|sk\rangle}{\omega + (\varepsilon_c - \varepsilon_k) - i0^+}, \quad (9.25a)$$

$$\triangleleft \Xi_{c,pq,rs}^{(2x,ph/hp)}(\omega) = \sum_{kc} \frac{\langle rc|pk\rangle\langle qk|cs\rangle}{\omega - (\varepsilon_c - \varepsilon_k) + i0^+} - \sum_{kc} \frac{\langle rk|pc\rangle\langle qc|ks\rangle}{\omega + (\varepsilon_c - \varepsilon_k) - i0^+}. \quad (9.25b)$$

$$\Xi_{c,pq,rs}^{(2x,pp/hh)}(\omega) = - \sum_{cd} \frac{\langle cd|ps\rangle\langle qr|cd\rangle}{\omega - (\varepsilon_c + \varepsilon_d) + i0^+} + \sum_{kl} \frac{\langle kl|ps\rangle\langle qr|lk\rangle}{\omega - (\varepsilon_k + \varepsilon_l) - i0^+}, \quad (9.25c)$$

which correspond respectively to the left, middle and right diagrams of Figure 9.7. These terms correspond to the antisymmetric counterpart of the direct terms which diagrammatic expansions were given in Figure 9.6.

Total correlation kernel By combination of the direct and exchanged terms, the total second-order correlation kernel is therefore given by

$$\begin{aligned} \Xi_{c,pq,rs}^{(2)}(\omega) = & - \sum_{kc} \frac{\langle rc|pk\rangle\langle qk|sc\rangle}{\omega - (\varepsilon_c - \varepsilon_k) + i0^+} + \sum_{kc} \frac{\langle rk|pc\rangle\langle qc|sk\rangle}{\omega + (\varepsilon_c - \varepsilon_k) - i0^+} \\ & + \frac{1}{2} \sum_{cd} \frac{\langle qr|cd\rangle\langle cd|ps\rangle}{\omega - (\varepsilon_c + \varepsilon_d) + i0^+} - \frac{1}{2} \sum_{kl} \frac{\langle qr|kl\rangle\langle kl|ps\rangle}{\omega - (\varepsilon_k + \varepsilon_l) - i0^+}. \end{aligned} \quad (9.26)$$

The first two contributions constitute the ph/hp part while the last two terms are the pp/hh part. In this equation, all the electron-electron integrals are antisymmetrized. If neither the antisymmetrization of the self-energy nor the derivative of W with respect to G are included, then the kernel is given by Equation (9.21). If only one of these contributions is accounted for, then an unbalanced form is obtained where only half of the integrals are antisymmetrized. This acknowledges the fact that both contributions have to be taken into account together in order to have a kernel in which direct and

exchanged terms are treated on an equal footing. Moreover, as the second-order self-energy provides a conserving approximation and that all the terms were accounted for in its differentiation, this kernel is also conserving.

Spin adaptation For spin-restricted closed-shell calculations, the spin-adapted kernel is obtained by rotation in spin-space as was done in Section 8.3.2. For four fixed spatial orbitals referred to as p, q, r, s , the spin-singlet kernel is therefore obtained by

$${}^1\Xi_{c,pq,rs}^{(2)}(\omega) = \Xi_{c,p\uparrow q\uparrow, r\uparrow s\uparrow}^{(2)}(\omega) + \Xi_{c,p\uparrow q\uparrow, r\downarrow s\downarrow}^{(2)}(\omega) \quad (9.27)$$

and the triplet kernel by

$${}^3\Xi_{c,pq,rs}^{(2)}(\omega) = \Xi_{c,p\uparrow q\uparrow, r\uparrow s\uparrow}^{(2)}(\omega) - \Xi_{c,p\uparrow q\uparrow, r\downarrow s\downarrow}^{(2)}(\omega). \quad (9.28)$$

The term $\Xi_{c,p\uparrow q\uparrow, r\uparrow s\uparrow}^{(2)}(\omega)$ and $\Xi_{c,p\uparrow q\uparrow, r\downarrow s\downarrow}^{(2)}(\omega)$ are calculated in Appendix G.3 for the ph/hp and the pp/hh contributions to the kernel. The singlet and triplet ph/hp kernels are then obtained by sum and difference, and are given by

$$\begin{aligned} {}^1\Xi_{c,pq,rs}^{(2,\text{ph/hp})}(\omega) = & \\ & - \sum_{kc} \frac{2w_{ee,pr,ck}w_{ee,sq,kc} - w_{ee,pr,ck}w_{ee,cq,ks} - w_{ee,kr,cp}w_{ee,sq,kc} + 2w_{ee,kr,cp}w_{ee,cq,ks}}{\omega - (\varepsilon_c - \varepsilon_k) + i0^+} \\ & + \sum_{kc} \frac{2w_{ee,pr,kc}w_{ee,sq,ck} - w_{ee,pr,kc}w_{ee,kq,cs} - w_{ee,cr,kp}w_{ee,sq,ck} + 2w_{ee,cr,kp}w_{ee,kq,cs}}{\omega + (\varepsilon_c - \varepsilon_k) - i0^+}, \end{aligned} \quad (9.29a)$$

$$\begin{aligned} {}^3\Xi_{c,pq,rs}^{(2,\text{ph/hp})}(\omega) = & - \sum_{kc} \frac{2w_{ee,pr,ck}w_{ee,sq,kc} - w_{ee,pr,ck}w_{ee,cq,ks} - w_{ee,kr,cp}w_{ee,sq,kc}}{\omega - (\varepsilon_c - \varepsilon_k) + i0^+} \\ & + \sum_{kc} \frac{2w_{ee,pr,kc}w_{ee,sq,ck} - w_{ee,pr,kc}w_{ee,kq,cs} - w_{ee,cr,kp}w_{ee,sq,ck}}{\omega + (\varepsilon_c - \varepsilon_k) - i0^+}. \end{aligned} \quad (9.29b)$$

Similarly, the spin-adapted pp/hh kernels are given by

$$\begin{aligned} {}^1\Xi_{c,pq,rs}^{(2,\text{pp/hh})}(\omega) = & \\ = & \frac{1}{2} \sum_{cd} \frac{2w_{ee,cq,rd}w_{ee,pc,ds} - w_{ee,cq,rd}w_{ee,sc,dp} - w_{ee,dq,rc}w_{ee,pc,ds} + 2w_{ee,dq,rc}w_{ee,sc,dp}}{\omega - (\varepsilon_c + \varepsilon_d) + i0^+} \\ & - \frac{1}{2} \sum_{kl} \frac{2w_{ee,kq,rl}w_{ee,pk,ls} - w_{ee,kq,rl}w_{ee,sk,lp} - w_{ee,lq,rk}w_{ee,pk,ls} + 2w_{ee,lq,rk}w_{ee,sk,lp}}{\omega - (\varepsilon_k + \varepsilon_l) - i0^+}, \end{aligned} \quad (9.30a)$$

$$\begin{aligned} {}^3\Xi_{c,pq,rs}^{(2,\text{pp/hh})}(\omega) = & - \frac{1}{2} \sum_{cd} \frac{w_{ee,cq,rd}w_{ee,sc,dp} + w_{ee,dq,rc}w_{ee,pc,ds}}{\omega - (\varepsilon_c + \varepsilon_d) + i0^+} \\ & + \frac{1}{2} \sum_{kl} \frac{w_{ee,kq,rl}w_{ee,sk,lp} + w_{ee,lq,rk}w_{ee,pk,ls}}{\omega - (\varepsilon_k + \varepsilon_l) - i0^+}. \end{aligned} \quad (9.30b)$$

As this kernel is frequency-dependent, it cannot be inserted straightforwardly into the Bethe-Salpeter equation and convolution products in frequency space need to be done.

However, it is already interesting to look at its behavior in the static approximation. First, this allows us to evaluate the effects of the second-order approximation in comparison to the kernel derived in Chapter 8. Moreover, it is also possible to study the effect of the inclusion of the derivative of W . The effects of the second-order kernel are thus illustrated on our usual model system given by H₂ in a minimal basis set.

9.4 Application to H₂ in a minimal basis

9.4.1 Effects of the perturbative expansion

In order to have comparable quantities, the second-order correlation kernel where neither the antisymmetrized self-energy nor the derivative of W are included, is considered and is applied with G_0 as a starting Green's function, this method will be referred to as $G_0W_0^{(2)}$. It is compared to the G_0W_0 method detailed in the Chapter 8 where the same ingredients are included but where the kernel was not truncated at second order. In this case, the singlet excitation energy was given by

$${}^1\omega = \sqrt{\left(\Delta\varepsilon + 4K_{12} - J_{12} - \frac{K_{12}}{1 + 4K_{12}/\Delta\varepsilon}\right) \left(\Delta\varepsilon - J_{12} + \frac{K_{12}}{1 + 4K_{12}/\Delta\varepsilon}\right)}, \quad (9.31)$$

and the triplet excitation energy by

$${}^3\omega = \sqrt{\left(\Delta\varepsilon - J_{12} - \frac{K_{12}}{1 + 4K_{12}/\Delta\varepsilon}\right) \left(\Delta\varepsilon - J_{12} + \frac{K_{12}}{1 + 4K_{12}/\Delta\varepsilon}\right)}. \quad (9.32)$$

In the second-order case, the inverse of the dielectric matrix is expanded for small K_{12} . It is straightforward to see that such an expansion will not be valid when H₂ is dissociated as the difference of orbital energies goes to 0 but K_{12} does not such that $\Delta\varepsilon \ll K_{12}$. The singlet excitation energy is then given as

$${}^1\omega^{(2)} = \sqrt{\left(\Delta\varepsilon + 3K_{12} - J_{12} + \frac{4K_{12}^2}{\Delta\varepsilon}\right) \left(\Delta\varepsilon - J_{12} + K_{12} - \frac{4K_{12}^2}{\Delta\varepsilon}\right)}, \quad (9.33)$$

and the triplet one as

$${}^3\omega^{(2)} = \sqrt{\left(\Delta\varepsilon - J_{12} - K_{12} + \frac{4K_{12}^2}{\Delta\varepsilon}\right) \left(\Delta\varepsilon - J_{12} + K_{12} - \frac{4K_{12}^2}{\Delta\varepsilon}\right)}. \quad (9.34)$$

These energies are plotted in Figure 9.8 together with the TDHF and FCI references. Around the equilibrium distance, where $\Delta\varepsilon$ is large, the second-order energies reproduce correctly the non-perturbative energies. However, when the bond is stretched and that the orbital energy difference smaller and smaller, the singlet excitation energy becomes imaginary for a smaller internuclear distance than is the non-perturbative case, at about 4 bohr instead of 4.8 bohr. The triplet excitation energy becomes also imaginary for

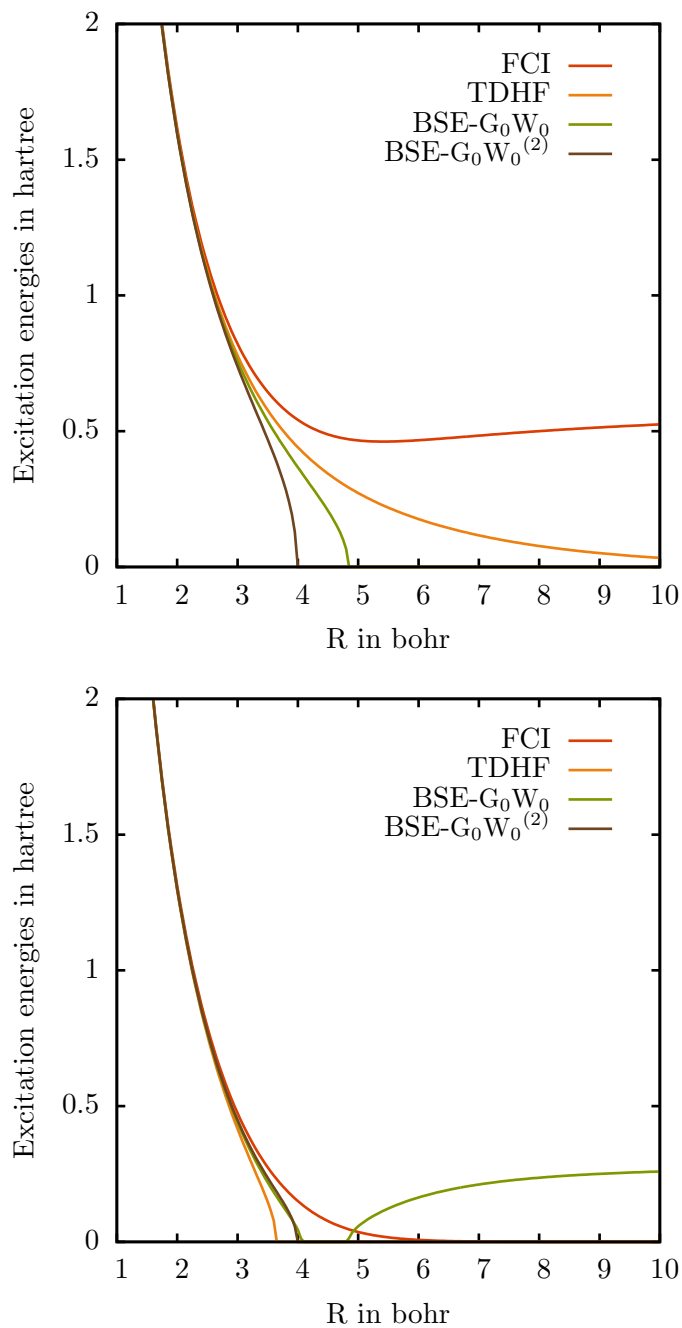


Figure 9.8 – Excitation energies of the singlet $^1\Sigma_u^+$ (top) and the triplet $^3\Sigma_u^+$ (bottom) states of H_2 in a minimal basis as a function of the internuclear distance R calculated by FCI, TDHF, G_0W_0 and $G_0W_0^{(2)}$.

the same value of R of about 4 bohr which corresponds to the distance where $\Delta\varepsilon - J_{12} + K_{12} - 4K_{12}^2/\Delta\varepsilon = 0$. However, in this case, the non-perturbative triplet excitation energy is not behaving any better and both curves are very similar.

Comparison with the FCI perturbative expansion

It is also insightful to compare these expansions with an expansion of the FCI energies at second order with respect to the electron-electron interaction. The ground- and excited-state FCI energies are given by

$$\begin{aligned} E_0 &= 2\varepsilon_1 - \lambda J_{11} + E_c \\ {}^1E_1 &= \varepsilon_1 + \varepsilon_2 - \lambda(J_{11} + J_{12} - 2K_{12}) \\ {}^3E_1 &= \varepsilon_1 + \varepsilon_2 - \lambda(J_{11} + J_{12}) \end{aligned} \quad (9.35)$$

where λ is an ordering parameter and $E_c = \Delta - \sqrt{\Delta^2 + \lambda^2 K_{12}^2}$ such that

$$\Delta = \varepsilon_2 - \varepsilon_1 + \lambda \frac{J_{11} + J_{22} - 4J_{12} + 2K_{12}}{2}. \quad (9.36)$$

Therefore, the Taylor expansion of the excitation energies up to the second order are given by

$$\begin{aligned} {}^1\omega^{\text{FCI},(2)} &= \Delta\varepsilon + \lambda(-J_{12} + 2K_{12}) + \lambda^2 \frac{K_{12}^2}{2\Delta\varepsilon} + \mathcal{O}(\lambda^3) \\ {}^3\omega^{\text{FCI},(2)} &= \Delta\varepsilon - \lambda(J_{12}) + \lambda^2 \frac{K_{12}^2}{2\Delta\varepsilon} + \mathcal{O}(\lambda^3). \end{aligned} \quad (9.37)$$

If a similar expansion is performed for the Bethe-Salpeter second-order energies, one can obtain

$$\begin{aligned} {}^1\omega^{(2)} &= \Delta\varepsilon + \lambda(-J_{12} + 2K_{12}) - \lambda^2 \frac{K_{12}^2}{2\Delta\varepsilon} + \mathcal{O}(\lambda^3) \\ {}^3\omega^{(2)} &= \Delta\varepsilon - \lambda(J_{12}) - \lambda^2 \frac{K_{12}^2}{2\Delta\varepsilon} + \mathcal{O}(\lambda^3). \end{aligned} \quad (9.38)$$

The second order correction goes in the wrong direction as pointed out by Brand *et al* [92] in the TDHF case. This means that at this level some terms are missing in the second-order expansion or are not described properly within the static approximation.

9.4.2 Effects of the derivative of W

Matrix elements of the correlation kernel

As the matrix representation of the electron-electron is diagonal by block in the case of H₂ in a minimal basis set, the matrix elements $\Xi_{c,1\uparrow 2\uparrow,1\uparrow 2\uparrow}(\omega)$ and $\Xi_{c,1\uparrow 2\uparrow,1\downarrow 2\downarrow}(\omega)$ are equal to 0 and therefore the correlation kernel does not contribute in the block **A** as it was also the case in Section 8.4.1 and 8.4.2. In the block **B** however, its contribution remains

and in the static approximation is given by

$${}^1\Xi_{c,12,21}^{(2)}(\omega = 0) = K_{12} \left(\frac{2(K_{12} + J_{12})}{\Delta\varepsilon} - \frac{J_{22}}{2\varepsilon_2} + \frac{J_{11}}{2\varepsilon_1} \right) \quad (9.39)$$

in the singlet case, and by

$${}^3\Xi_{c,12,21}^{(2)}(\omega = 0) = K_{12} \left(\frac{2(K_{12} - J_{12})}{\Delta\varepsilon} + \frac{J_{22}}{2\varepsilon_2} - \frac{J_{11}}{2\varepsilon_1} \right). \quad (9.40)$$

in the triplet case. The matrix **A** and **B** are then given by

$$\begin{aligned} {}^1A &= \Delta\varepsilon + 2K_{12} - J_{12} \\ {}^1B &= 2K_{12} - K_{12} \left(1 - \frac{2(K_{12} + J_{12})}{\Delta\varepsilon} + \frac{J_{22}}{2\varepsilon_2} - \frac{J_{11}}{2\varepsilon_1} \right) \\ {}^3A &= \Delta\varepsilon - J_{12} \\ {}^3B &= -K_{12} \left(1 - \frac{2(K_{12} - J_{12})}{\Delta\varepsilon} - \frac{J_{22}}{2\varepsilon_2} + \frac{J_{11}}{2\varepsilon_1} \right) \end{aligned} \quad (9.41)$$

Excitation energies

The singlet excitation energy in the static approximation at second order with exchange and with the inclusion of the derivative of W with respect to **G** is therefore given by

$$\begin{aligned} {}^1\omega &= \sqrt{\Delta\varepsilon + 4K_{12} - J_{12} - K_{12} \left(1 - \frac{2(K_{12} + J_{12})}{\Delta\varepsilon} + \frac{J_{22}}{2\varepsilon_2} - \frac{J_{11}}{2\varepsilon_1} \right)} \\ &\quad \times \sqrt{\Delta\varepsilon - J_{12} + K_{12} \left(1 - \frac{2(K_{12} + J_{12})}{\Delta\varepsilon} + \frac{J_{22}}{2\varepsilon_2} - \frac{J_{11}}{2\varepsilon_1} \right)} \end{aligned} \quad (9.42)$$

and the triplet one is given by

$$\begin{aligned} {}^3\omega &= \sqrt{\Delta\varepsilon - J_{12} - K_{12} \left(1 - \frac{2(K_{12} - J_{12})}{\Delta\varepsilon} - \frac{J_{22}}{2\varepsilon_2} + \frac{J_{11}}{2\varepsilon_1} \right)} \\ &\quad \times \sqrt{\Delta\varepsilon - J_{12} + K_{12} \left(1 - \frac{2(K_{12} - J_{12})}{\Delta\varepsilon} - \frac{J_{22}}{2\varepsilon_2} + \frac{J_{11}}{2\varepsilon_1} \right)}. \end{aligned} \quad (9.43)$$

These excitation energies show an unphysical form where the ε_1 and ε_2 are present by themselves while only the orbital energy difference $\Delta\varepsilon$ should be present. This effect is due to the static approximation as the kernel is not convoluted with the response functions in the Bethe-Salpeter equation. In fact, as will be shown in the next chapter, if the convolution is properly done, then the correlation kernel depends only on energy differences between occupied and virtual orbitals as one would expect.

The singlet and triplet excitation energies are plotted for the dihydrogen molecule as functions of the internuclear distance R in Figure 9.9. Due to their unphysical expression, they probably provide the worse results among all the approximations tested up to this

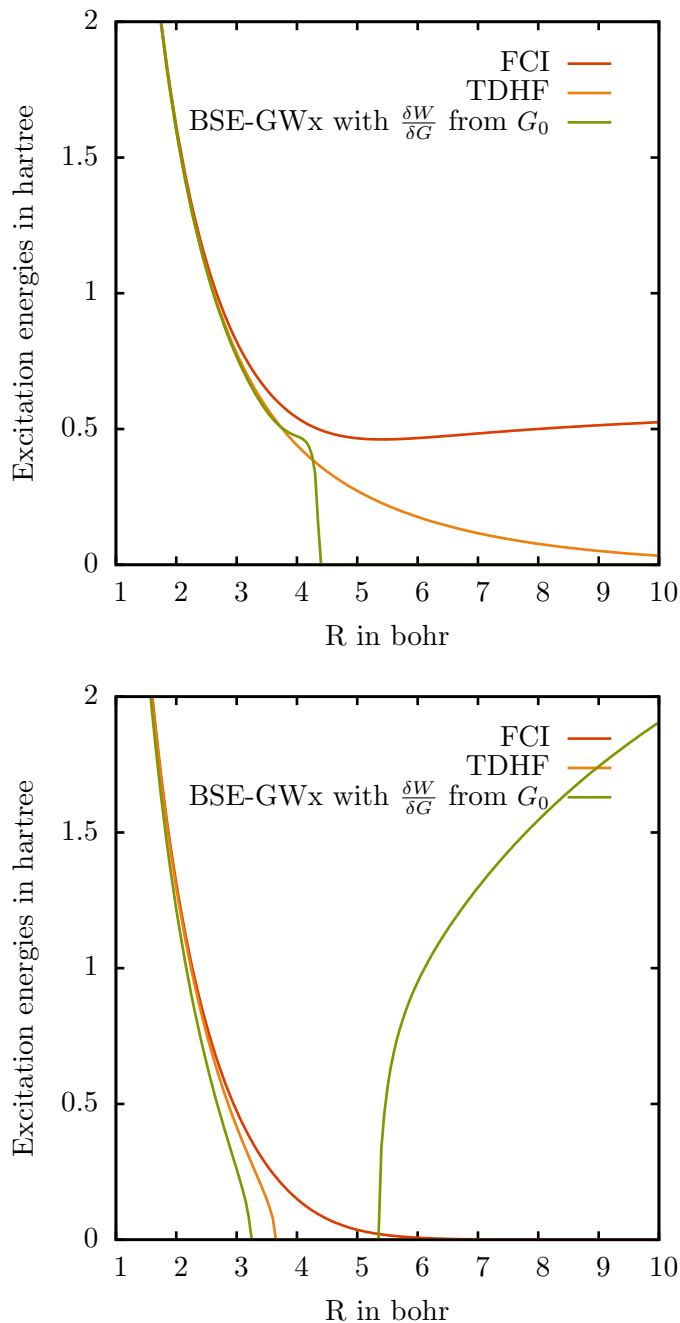


Figure 9.9 – Excitation energies of the singlet $1\Sigma_u^+$ (top) and the triplet $3\Sigma_u^+$ (bottom) states of H₂ in a minimal basis as a function of the internuclear distance R calculated by FCI, TDHF, and BSE-GWx with the derivative of W with respect to G with the non-interacting HF Green's function G_0 .

point. The singlet excitation energy is very similar to the TDHF excitation energy up to 3.5 bohr, then show a slight improvement up to 4 bohr and finally goes abruptly to 0 and becomes imaginary for distances larger than 4.3 bohr. In the meanwhile, the triplet excitation energy is worse than the TDHF reference for any value of the internuclear distance and becomes imaginary for $R = 3.2$ bohr which is the smallest breaking distance ever encountered so far. After 5.2 bohr, an unphysical solution corresponding in fact to the deexcitation appears.

9.5 Conclusion

In this chapter, a second-order correlation Bethe-Salpeter kernel has been derived and illustrated on the model system of H_2 in a minimal basis in the static approximation. In order to get a conserving approximation well-suited for finite molecular system, it was shown that both the antisymmetrization of the electron-electron interaction in the correlation self-energy and the totality of the contribution in its first-order derivative with respect to G were to be taken into account conjointly.

The effect of the truncation at second order was assessed on the dihydrogen molecule and shows no effect around the equilibrium distance where the G_0W_0 approximation works correctly but has a larger effect when the bond is stretched for the singlet excitation in the region where the G_0W_0 approximation is also breaking down. However as the second-order expansion is valid when the electron-electron integrals are much smaller than the orbital energy difference, it is obvious that such a level of approximation would not be able to describe correctly the dissociation of H_2 or similar systems where strong correlation plays a significant role.

Still at second order with respect to the electron-electron interaction, the effect of the inclusion of exchange into the dielectric function and of the derivative of the self-energy with respect to G was then assessed. This defines a conserving approximation for the Bethe-Salpeter kernel. However, within the static approximation, it shows a very unphysical form as the excitation energies do not depend only on energy differences but also on orbitals energies by themselves. The singlet and triplet excitation energies of the dihydrogen molecule obtained with this kernel shows a good agreement with the FCI reference calculation around equilibrium distance but then deteriorate rapidly when the bond is stretched.

This confirms that a static second-order Bethe-Salpeter correlation kernel is not well-suited to describe systems like H_2 along the dissociation for two reasons, the first being the second-order expansion and the second being the static approximation. However, if such a strongly-correlated system is not at stake and one is interested only in describing excitations where a double contribution is important, using a second-order correlation kernel makes sense but only with a dynamical treatment. The derivation of such a second-order dynamical kernel is the subject of the next chapter.

Chapter 10

Range-separated dynamical second-order BSE kernel

In this chapter, we develop an effective dynamical second-order Bethe-Salpeter correlation kernel both in real space and in a spin-orbital basis set. In order to ensure a number-conserving approximation in the framework of finite molecular systems, exchange was included in the dielectric matrix and all terms were kept in the construction of the kernel from the second-order self-energy. When the Bethe-Salpeter equation is solved in a dynamical fashion, the frequency-dependent second-order kernel obtained in the previous chapter needs to be convoluted with two two-frequency propagators. This convolution product can be reformulated as a product of two response functions and of an effective kernel. As this effective kernel depends only on one frequency, it can be used in TDDFT-like equations in order to calculate the poles of the response function. If constructed on a range-separated Green's function and with the long-range part of the interaction, this kernel can also be used in the framework of range-separated TDDFT as an effective long-range frequency-dependent correlation kernel which can be added perturbatively to the TDRSH kernel discussed in Chapter 6. In both cases, the inclusion of a frequency-dependent kernel raises some computational issues as one needs to solve a non-linear eigenvalue problem. A perturbative approach within the Tamm-Dancoff approximation is therefore used in the calculations. The behavior of the kernel is first illustrated on the model system of H_2 in a minimal basis. In this case, the very symmetric nature of this system leads to the annihilation of the frequency-dependent part of the kernel. However, the comparison of the expansion of the excitation energies up to second order with respect to the interaction, with the expansions of the corresponding FCI energies highlights what is missing in this dynamical kernel. The kernel is then applied to the calculation of the first singlet and triplet excitation energies of N_2 , CO , H_2CO and C_2H_4 both with and without range separation. For these systems, the addition of the perturbative kernel induces a systematic increase of the excitation energies. It leads to a strong deterioration of the excitation energies in the non range-separated case but improves both the mean absolute deviation and the maximum error when used with range separation. Details of the derivation and of the implementation can be found in Appendices H and I.

10.1 Introduction

It is now well-established in the literature that a frequency-dependent kernel is required to describe multiple excitations [35, 36, 47, 86] at least when starting from a single-reference Green's function. In order to compute the excitation energies of a finite molecular system, a second-order correlation kernel was developed in the previous chapter where exchange was included in the dielectric matrix and where the effects of the perturbation on the screened interaction were taken into account. When used in the static approximation, this kernel was proven to have a non-physical form and thus requires a dynamical treatment. In this case, the Fourier transform of the Bethe-Salpeter equation is not trivial anymore as convolution products need to be performed in the frequency space between the kernel and two two-frequency propagators. The Fourier transform of the Bethe-Salpeter equation is performed in Section 10.2 where it is shown that the previous convolution product can be rewritten as the product of an effective kernel $\tilde{\Xi}^{(2)}(\omega)$ and of two response functions. The expressions of the matrix elements of the singlet and triplet correlation effective kernels are then derived in a spin-orbital basis set. With such a kernel, solving the Bethe-Salpeter equation reduces to solving a non-linear eigenvalue problem similar to the one encountered in time-dependent density-functional theory without the adiabatic approximation (cf. Chapter 5). This kernel has been recently studied by Zhang *et al* [37] although their approach is slightly different and they limited themselves to the Tamm-Dancoff case starting from a Hartree-Fock (HF) Green's function with a quasi-particle GW correction.

Our goal however is to design a long-range frequency-dependent correlation kernel in order to add it perturbatively to the range-separated-hybrid (RSH) kernel

$$f_{\text{Hxc}}^{\mu, \text{RSH}} = f_{\text{H}} + f_{\text{x, HF}}^{\text{lr}, \mu} + f_{\text{xc}}^{\text{sr}, \mu} \quad (10.1)$$

designed in Chapter 6 so that we could take into account the effects of the double excitations entering in the description of the single ones. Such a long-range kernel can easily be obtained from a full-range kernel by substituting the electron-electron interaction by its long-range part only and the HF orbital energies by the RSH ones. The HF case is then recovered in the limit when the range-separation parameter μ goes to infinity. As the orbital energy differences of the range-separated Green's function are expected to be a good starting point for the calculation of excitation energies, no quasi-particle GW correction is performed prior to the Bethe-Salpeter calculation. The (long-range) second-order effective correlation kernel $\tilde{\Xi}_{\text{c}}^{\text{lr}, \mu, (2)}(\omega)$ depends only on the external frequency ω such that the Bethe-Salpeter equation can be written in the form

$$\chi^{-1}(\omega) = \chi_0^{-1}(\omega) - \left(f_{\text{Hxc}}^{\mu, \text{RSH}} + \tilde{\Xi}_{\text{c}}^{\text{lr}, \mu, (2)}(\omega) \right). \quad (10.2)$$

In this case, an efficient resolution scheme needs to be designed as the usual Casida's resolution scheme does not hold anymore with a frequency-dependent kernel. This equa-

tion defines in fact a non-linear eigenvalue problem which should in principle be solved self-consistently. However, in this work a simpler approach will be explored. Following the work of Zhang *et al*, a perturbative resolution within the Tamm-Dancoff approximation is given in Section 10.3 both with and without range separation. To illustrate the behavior of the dynamical kernel, it is once again applied on the model system given by the hydrogen molecule in a minimal basis. Even though, the kernel is not expected to describe correctly the dissociation as it was designed perturbatively at second order, useful insights can be obtained by comparing for instance the second-order expansions of the excitation energies with respect to the ones obtained by the exact full-CI method. This analysis is detailed in Section 10.4. Finally, this dynamical kernel is applied to the calculation of the first lowest excitation energies of four small molecules N_2 , CO , H_2CO and C_2H_4 and compared to the results obtained in Chapter 6 without the long-range correlation kernel. The computational details are given in Section 10.5 and Section 10.6. In this chapter, only the main steps of the derivation are given and are sketched in terms of Feynman diagrams. More details on the derivation can be found in Appendix H. The calculation were performed on a homemade software which is briefly described in Appendix I.

10.2 Dynamical second-order Bethe-Salpeter kernel

10.2.1 Fourier transform of the Bethe-Salpeter Equation

When a dynamical kernel is introduced in the Bethe-Salpeter equation, its Fourier transform requires some additional efforts. The general Bethe-Salpeter equation in time domain is given by

$$\chi(1, 2; 1', 2') = \chi_{IP}(1, 2; 1', 2') + \int d3456 \chi_{IP}(1, 4; 1', 3) \Xi_{Hxc}(3, 6; 4, 5) \chi(5, 2; 6, 2'), \quad (10.3)$$

where χ and χ_{IP} are 4 point-polarizabilities. In the context of excitation energies, such general quantities are not needed and response functions are sufficient. Hence, the times are constraint to the case $t'_1 = t_1^+$ and $t'_2 = t_2^+$, so the Bethe-Salpeter equation rewrites as

$$\begin{aligned} \chi(\mathbf{x}_1 t_1, \mathbf{x}_2 t_2; \mathbf{x}'_1 t_1^+, \mathbf{x}'_2 t_2^+) &= \chi_{IP}(\mathbf{x}_1 t_1, \mathbf{x}_2 t_2; \mathbf{x}'_1 t_1^+, \mathbf{x}'_2 t_2^+) \\ &+ \int d\mathbf{x}_3 dt_3 d\mathbf{x}_4 dt_4 d\mathbf{x}_5 dt_5 d\mathbf{x}_6 dt_6 \chi_{IP}(\mathbf{x}_1 t_1, \mathbf{x}_4 t_4; \mathbf{x}'_1 t_1^+, \mathbf{x}_3 t_3) \\ &\quad \Xi_{Hxc}(\mathbf{x}_3 t_3, \mathbf{x}_6 t_6; \mathbf{x}_4 t_4, \mathbf{x}_5 t_5) \chi(\mathbf{x}_5 t_5, \mathbf{x}_2 t_2; \mathbf{x}_6 t_6, \mathbf{x}'_2 t_2^+). \end{aligned} \quad (10.4)$$

Although the left-hand side and the first term of the right-hand side of this equation are response functions (depending of only one time difference), the last term involves propagators depending of two time differences because of the presence of a dynamical kernel. Their Fourier transform and their matrix elements are given in Appendix F.

When expanded at second order with respect to the electron-electron interaction and

evaluated at $G = G_0$, this equation can be rewritten as

$$\begin{aligned} \chi(\mathbf{x}_1 t_1, \mathbf{x}_2 t_2; \mathbf{x}'_1 t_1^+, \mathbf{x}'_2 t_2^+) &= \chi_0(\mathbf{x}_1 t_1, \mathbf{x}_2 t_2; \mathbf{x}'_1 t_1^+, \mathbf{x}'_2 t_2^+) \\ &+ \int d\mathbf{x}_3 dt_3 d\mathbf{x}_4 dt_4 d\mathbf{x}_5 dt_5 d\mathbf{x}_6 dt_6 \chi_0(\mathbf{x}_1 t_1, \mathbf{x}_4 t_4; \mathbf{x}'_1 t_1^+, \mathbf{x}_3 t_3) \\ &\quad \Xi_{\text{Hxc}}^{(2)}(\mathbf{x}_3 t_3, \mathbf{x}_6 t_6; \mathbf{x}_4 t_4, \mathbf{x}_5 t_5) \chi(\mathbf{x}_5 t_5, \mathbf{x}_2 t_2; \mathbf{x}_6 t_6, \mathbf{x}'_2 t_2^+). \end{aligned} \quad (10.5)$$

As the Hartree and exchange kernels are local in time, only the correlation part of the right-hand side will be detailed here. In the previous chapter, it has been shown that the second-order correlation kernel can be decoupled into a ph/hp and a pp/hh parts which exhibit different delta functions on the time variables (cf. Equations (9.20) and (9.24)) such that the second-order correlation kernel is given by

$$\begin{aligned} \Xi_c^{(2)}(3, 6; 4, 5) &= \delta(t_4, t_6) \delta(t_3, t_5) \Xi_c^{(2, \text{ph/hp})}(\mathbf{x}_3, \mathbf{x}_6; \mathbf{x}_4, \mathbf{x}_5; t_3 - t_4) \\ &+ \delta(t_4, t_5) \delta(t_3, t_6) \Xi_c^{(2, \text{pp/hh})}(\mathbf{x}_3, \mathbf{x}_6; \mathbf{x}_4, \mathbf{x}_5; t_3 - t_4), \end{aligned} \quad (10.6)$$

where the terms $\Xi_c^{(2, \text{ph/hp})}$ and $\Xi_c^{(2, \text{pp/hh})}$ include both direct and exchanged contributions and where the derivative of W was also taken into account. As the delta functions are different for the ph/ph and pp/hh terms, they need to be treated separately when the Fourier transform is performed. The details of the Fourier transforms of both contributions are given in Appendix H.1. Finally, the Fourier transform of the Bethe-Salpeter equation is given by

$$\begin{aligned} \chi(\mathbf{x}_1, \mathbf{x}_2; \mathbf{x}'_1, \mathbf{x}'_2; \omega) &= \chi_0(\mathbf{x}_1, \mathbf{x}_2; \mathbf{x}'_1, \mathbf{x}'_2; \omega) \\ &+ \int d\mathbf{x}_3 d\mathbf{x}_4 d\mathbf{x}_5 d\mathbf{x}_6 \chi_0(\mathbf{x}_1, \mathbf{x}_4; \mathbf{x}'_1, \mathbf{x}_3; \omega) \Xi_{\text{Hxc}}(\mathbf{x}_3, \mathbf{x}_6; \mathbf{x}_4, \mathbf{x}_5) \chi(\mathbf{x}_5, \mathbf{x}_2; \mathbf{x}_6, \mathbf{x}'_2, \omega) \\ &+ \int \frac{d\omega'}{2\pi} \int \frac{d\omega''}{2\pi} \int d\mathbf{x}_3 d\mathbf{x}_4 d\mathbf{x}_5 d\mathbf{x}_6 \chi_0(\mathbf{x}_1, \mathbf{x}_4; \mathbf{x}'_1, \mathbf{x}_3; -\eta, \omega', \omega) \\ &\quad \Xi_c^{(2, \text{ph/hp})}(\mathbf{x}_3, \mathbf{x}_6; \mathbf{x}_4, \mathbf{x}_5; \omega' - \omega'') \chi(\mathbf{x}_5, \mathbf{x}_2; \mathbf{x}_6, \mathbf{x}'_2; \omega'', -\eta, \omega) \\ &+ \int \frac{d\omega'}{2\pi} \int \frac{d\omega''}{2\pi} \int d\mathbf{x}_3 d\mathbf{x}_4 d\mathbf{x}_5 d\mathbf{x}_6 \chi_0(\mathbf{x}_1, \mathbf{x}_4; \mathbf{x}'_1, \mathbf{x}_3; -\eta, \omega', \omega) \\ &\quad \Xi_c^{(2, \text{pp/hh})}(\mathbf{x}_3, \mathbf{x}_6; \mathbf{x}_4, \mathbf{x}_5; \omega' + \omega'') \chi(\mathbf{x}_5, \mathbf{x}_2; \mathbf{x}_6, \mathbf{x}'_2; \omega'', -\eta, \omega), \end{aligned} \quad (10.7)$$

where η is a small positive quantity. This equation involves the convolution product of two-frequency propagators and the one-frequency pp/hh and ph/hp Bethe-Salpeter kernels. This convolution product can then be rewritten in a product of two response functions and of an effective kernel as pointed out by Romaniello *et al* in Ref [35, 36]. The main steps of this transformation is recalled in the following and is applied in order to compute the matrix elements of the effective second-order correlation kernel.

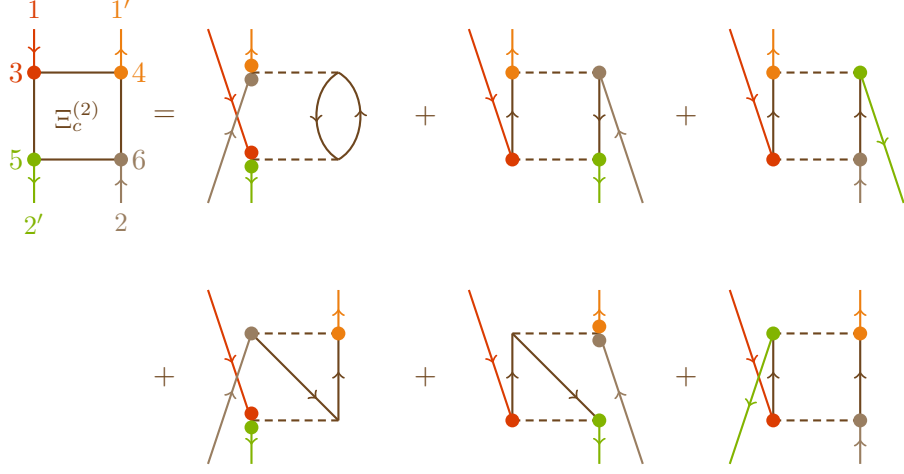


Figure 10.1 – Feynman representation of $T^{\text{ph/hp}}$ and $T^{\text{pp/hh}}$ obtained by convolution of the second-order correlation Bethe-Salpeter kernel with the non-interacting response functions.

10.2.2 Effective second-order correlation kernel

An effective correlation kernel is then defined by introducing the products $\chi_0(\omega)\chi_0^{-1}(\omega)$ on the left and $\chi(\omega)^{-1}\chi(\omega)$ on the right in Equation (10.7)

$$\begin{aligned}
 \chi(\omega) &= \chi_0(\omega) + \chi_0(\omega)\Xi_{\text{Hx}}\chi(\omega) \\
 &+ \chi_0(\omega)\chi_0^{-1}(\omega) \int \frac{d\omega'}{2\pi} \frac{d\omega''}{2\pi} \chi_0(-\eta, \omega', \omega) \Xi_c^{(2, \text{ph/hp})}(\omega' - \omega'') \chi(\omega'', -\eta, \omega) \chi(\omega)^{-1} \chi(\omega) \\
 &+ \chi_0(\omega)\chi_0^{-1}(\omega) \int \frac{d\omega'}{2\pi} \frac{d\omega''}{2\pi} \chi_0(-\eta, \omega', \omega) \Xi_c^{(2, \text{pp/hh})}(\omega' + \omega'') \chi(\omega'', -\eta, \omega) \chi(\omega)^{-1} \chi(\omega),
 \end{aligned} \tag{10.8}$$

so that the Bethe-Salpeter equation rewrites as

$$\chi(\omega) = \chi_0(\omega) + \chi_0(\omega)\Xi_{\text{Hx}}\chi(\omega) + \chi_0(\omega)\tilde{\Xi}_c^{(2, \text{ph/hp})}(\omega)\chi(\omega) + \chi_0(\omega)\tilde{\Xi}_c^{(2, \text{pp/hh})}(\omega)\chi(\omega), \tag{10.9}$$

where the spin-space variables have been kept implicit for conciseness. When evaluated at $G = G_0$, to be consistent with the order of perturbation, the ph/hp and pp/hh second-order effective correlation kernels are therefore defined as

$$\begin{aligned}
 \tilde{\Xi}_c^{(2, \text{ph/hp})}(\omega) &= \chi_0^{-1}(\omega) \int \frac{d\omega'}{2\pi} \frac{d\omega''}{2\pi} \chi_0(-\eta, \omega', \omega) \Xi_c^{(2, \text{ph/hp})}(\omega' - \omega'') \chi_0(\omega'', -\eta, \omega) \chi_0(\omega)^{-1} \\
 &= \chi_0^{-1}(\omega) T^{\text{ph/hp}}(\omega) \chi_0(\omega)^{-1},
 \end{aligned} \tag{10.10a}$$

$$\begin{aligned}
 \tilde{\Xi}_c^{(2,\text{pp/hh})}(\omega) &= \chi_0^{-1}(\omega) \int \frac{d\omega'}{2\pi} \frac{d\omega''}{2\pi} \chi_0(-\eta, \omega', \omega) \Xi_c^{(2,\text{pp/hh})}(\omega' + \omega'') \chi_0(\omega'', -\eta, \omega) \chi_0(\omega)^{-1} \\
 &= \chi_0^{-1}(\omega) T^{\text{pp/hh}}(\omega) \chi_0(\omega)^{-1}.
 \end{aligned} \tag{10.10b}$$

These kernels are then computed in a two-step procedure: first, the inner terms $T^{\text{ph/hp}}$ and $T^{\text{pp/hh}}$ are calculated by convoluting the second-order Bethe-Salpeter kernel with two non-interacting response functions in real space, then their matrix elements are evaluated and a matrix multiplication is done with the matrices of the inverse non-interacting response functions.

The details of the first step of the derivation can be found in Appendix H.2. This convolution product is represented diagrammatically in Figure 10.1. The second-order correlation kernel $\Xi_c^{(2)}(3, 6; 4, 5)$ derived in the previous chapter is represented in brown and is multiplied by the two non-interacting response functions $\chi_0(1, 4; 1', 3) = -iG_0(1, 3)G_0(4, 1')$ and $\chi_0(5, 2, 6, 2') = -iG_0(5, 2')G_0(2, 6)$ which are each represented by two G_0 arrows.

10.2.3 Expression in a spin-orbital basis

We then evaluate the matrix elements in the ph/hp and pp/hh inner terms in the (ov,ov) block (corresponding to \mathbf{A}) and the (ov,vo) block (corresponding to \mathbf{B}). The complete diagrammatic expansion of the matrix elements of the block \mathbf{A} are shown in Figure 10.2 where the time ordering of t_1 and t_2 has been chosen in order to make sure that i and j are represented by hole Green's function (down-going arrows) and that a and b are represented by electron Green's functions (up-going arrows).

Finally, as the matrix elements of the two-frequency non-interacting response functions $\chi_0(-\eta, \omega', \omega)$ and $\chi_0(\omega'', -\eta, \omega)$ can be rewritten in function of the matrix elements of $\chi_0(\omega)$ (cf. Appendix F), it is easy to extract the matrix elements of the effective second-order correlation Bethe-Salpeter kernel as shown in Figure 10.3 for the first term of the expansion. Following this procedure, the matrix elements of the effective correlation kernel in the \mathbf{A} block are then given by

$$\begin{aligned}
 \tilde{\Xi}_{c,ia,jb}^{(2)}(\omega) &= - \sum_{kc} \left(\frac{\langle jk||ic\rangle \langle ac||bk\rangle}{\omega - \varepsilon_a + \varepsilon_k - \varepsilon_c + \varepsilon_j + i0^+} + \frac{\langle jc||ik\rangle \langle ak||bc\rangle}{\omega + \varepsilon_i - \varepsilon_c + \varepsilon_k - \varepsilon_b + i0^+} \right) \\
 &\quad + \frac{1}{2} \left(\sum_{kl} \frac{\langle aj||kl\rangle \langle kl||ib\rangle}{\omega - (\varepsilon_a + \varepsilon_b) + (\varepsilon_k + \varepsilon_l) + i0^+} + \sum_{cd} \frac{\langle aj||cd\rangle \langle cd||ib\rangle}{\omega + (\varepsilon_i + \varepsilon_j) - (\varepsilon_c + \varepsilon_d) + i0^+} \right),
 \end{aligned} \tag{10.11}$$

and depends on the frequency ω , four orbital energies ε and two antisymmetrized electron-electron integrals $\langle pq||rs\rangle = \langle pq|rs\rangle - \langle pq|sr\rangle$, which is consistent with the order of expansion. This kernel is identical to the one recently proposed by Zhang *et al* [37] and shows some similitude with the SOPPA kernel [93–95] which however contains additional terms. A clue to understand the differences between this Bethe-Salpeter kernel and the SOPPA kernel comes from the definition of the second-order expansion. In here, the

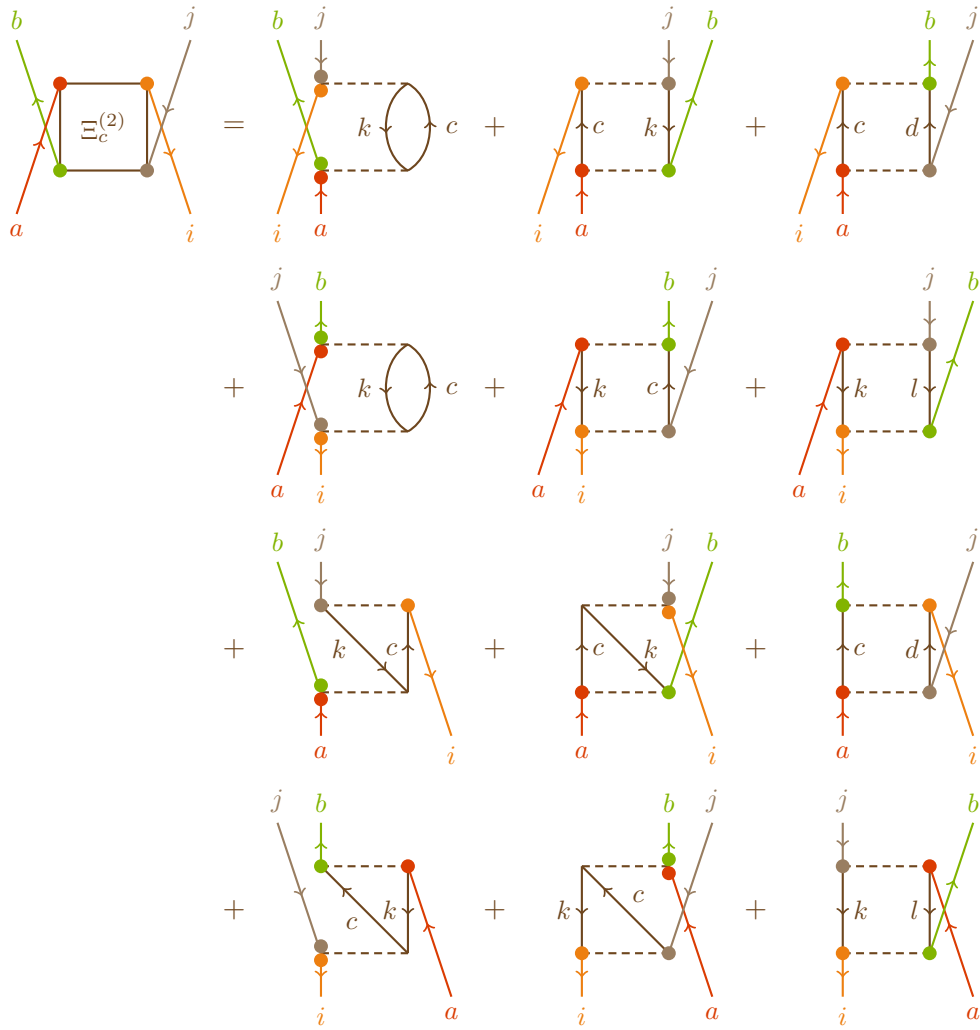


Figure 10.2 – Spin-orbital representation of the convolution of the Bethe-Salpeter kernel with the response functions in the **A** block.

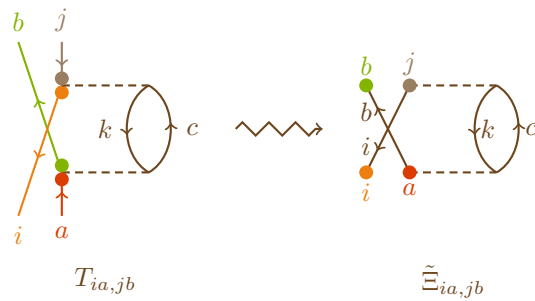


Figure 10.3 – Spin-orbital representation of the effective Bethe-Salpeter kernel in the **A** block.

expansion is done with respect to the electron-electron interaction, leaving the Green's function G intact, and then evaluating the obtained expression at $G = G_0$ so that the independent-particle response function χ_{IP} reduces to the non-interacting response function χ_0 . However, an alternative approach would be to develop the interacting Green's function G in terms of G_0 and Σ and to truncate this expansion at second order with respect to the the electron-electron interaction. In this case, the independent-particle response function χ_{IP} has additional contributions with respect to χ_0 coming from the self-energy corrections up to the second order:

$$\begin{aligned} \chi_{\text{IP}}(1, 2; 1', 2') &= \chi_0(1, 2; 1', 2') - iG_0(2, 1') \int d3d4 G_0(1, 3) \Sigma_c^{(2)}(3, 4) G_0(4, 2') \\ &\quad - iG_0(1, 2') \int d3d4 G_0(2, 3) \Sigma_c^{(2)}(3, 4) G_0(4, 1'). \end{aligned} \quad (10.12)$$

We are currently exploring this aspect, however it will not be reported hereinafter.

In the **B** block, the matrix elements of the effective kernel are given by

$$\begin{aligned} \tilde{\Xi}_{c,ia,bj}^{(2)} &= \sum_{kc} \left(\frac{\langle bk||ic\rangle \langle ac||jk\rangle}{-\varepsilon_a + \varepsilon_k - \varepsilon_c + \varepsilon_j + i0^+} + \frac{\langle bc||ik\rangle \langle ak||jc\rangle}{\varepsilon_i - \varepsilon_c + \varepsilon_k - \varepsilon_b + i0^+} \right) \\ &\quad + \frac{1}{2} \left(\sum_{kl} \frac{\langle ab||kl\rangle \langle kl||ij\rangle}{(\varepsilon_a + \varepsilon_b) - (\varepsilon_k + \varepsilon_l) - i0^+} + \sum_{cd} \frac{\langle ab||cd\rangle \langle cd||ij\rangle}{(\varepsilon_c + \varepsilon_d) - (\varepsilon_i + \varepsilon_j) - i0^+} \right), \end{aligned} \quad (10.13)$$

and do not depend on the frequency. This can be understood in terms of diagrams as the indices j and b are exchanged. Therefore, in order to still ensure an up-arrow for j and a down-arrow for b , the times need to be further contracted and the kernel becomes local in time and thus frequency independent.

The second-order effective correlation kernel display sums over either one occupied and one virtual orbital for the ph/hp part or over two occupied or two virtual orbitals for the pp/hh. The latter scales as $N_o^2 N_v^4$ where N_o is the number of occupied orbitals and N_v the number of virtual ones. This term will be particularly expensive in a large basis set as the number of virtual orbitals is important. Moreover, we can note that the contribution of the kernel in the **A** block will be particularly important if a double excitation contributes to the excitation energy ω . As shown by Sangalli *et al* in Ref. [36] such a kernel can be related to the second RPA approach [96] by Löwdin partitioning [97] and therefore defines a number-conserving approximation where no spurious excitations will enter. The Löwdin partitioning technique is recalled briefly in the following as it could also be used to “unfold” the problem so that a linear eigenvalue problem would be recovered.

Löwdin partitioning and second RPA approach

Suppose an eigenvalue problem

$$\begin{pmatrix} \mathbf{S} & \mathbf{C} \\ \mathbf{C}^\dagger & \mathbf{D} \end{pmatrix} \begin{pmatrix} \mathbf{X} \\ \mathbf{Y} \end{pmatrix} = \omega \begin{pmatrix} \mathbf{X} \\ \mathbf{Y} \end{pmatrix}, \quad (10.14)$$

where \mathbf{S} spans the Fock space of the single excitations, \mathbf{D} the Fock space of double excitations and \mathbf{C} is a coupling matrix between the singles and the doubles. Assuming \mathbf{C} is non-zero and $\mathbf{D} - \omega \mathbf{1}$ is invertible with $\mathbf{1}$ the identity matrix, this eigenvalue problem can be rewritten as

$$(\mathbf{S} + \mathbf{C}(\omega \mathbf{1} - \mathbf{D})^{-1} \mathbf{C}^\dagger) \mathbf{X} = \omega \mathbf{X}. \quad (10.15)$$

The second-order correlation kernel in the block \mathbf{A} given by Equation (10.11) has a similar form where the coupling matrices are provided by the matrix of the two-electron interaction and the matrix \mathbf{D} is given by the differences of four orbital energies ε . However, and it will be important in the following, the single and double excitations must couple with each other in order to have such a folding.

10.2.4 Range-separated kernel

As the kernel is not constructed self-consistently, the starting Green's function has an important impact and should be chosen carefully. In this sense, the Hartree-Fock Green's function G_0^{HF} may not be the best choice as the orbital energy differences are not good approximations to the excitation energies of the system. The local-density approximation in the DFT framework is also known to underestimate the gap and, without GW corrections, does not provide a satisfactory starting point either.

On the other hand, the orbital energy differences obtained within range-separated DFT with the an appropriately chosen range-separation parameter μ can provide much better approximations so that the corresponding RSH Green's function G_0^{RSH} would be a better starting point for the kernel. Moreover, in the TDRSH framework, the short-range part of the correlation kernel is already accounted for, such that the Bethe-Salpeter kernel must describe the long-range part of the correlation only. It is thus obtained by substituting the full-range electron-electron interaction w_{ee} by its long-range part $w_{ee}^{\text{lr},\mu}$. This defines a second-order dynamical correlation kernel $\tilde{\Xi}_c^{\text{lr},\mu,(2)}(\omega)$ which can then be added perturbatively to the RSH kernel detailed in Chapter 6 such that the total dynamical RSH kernel is given by

$$f_{\text{Hxc}}^\mu(\omega) = f_{\text{H}} + f_{\text{x,HF}}^{\text{lr},\mu} + f_{\text{xc}}^{\text{sr},\mu} + \tilde{\Xi}_c^{\text{lr},\mu,(2)}(\omega), \quad (10.16)$$

where f_{H} is the Hartree kernel, $f_{\text{x,HF}}^{\text{lr},\mu}$ is the long-range Hartree-Fock exchange kernel and $f_{\text{xc}}^{\text{sr},\mu}$ is the short-range DFT exchange-correlation kernel. This is of particular interest as it allows one to recover a frequency-dependent kernel in the TDDFT framework.

10.3 Resolution of the Bethe-Salpeter equation

In what follows, the derivation is given in the range-separated case, the HF case being recovered when μ goes to infinity. As the Hartree, exchange and short-range correlation kernels are frequency independent, and the long-range effective second-order correlation kernel depends only on the external frequency ω , the inverse response function in the frequency space can be written as

$$\chi^{-1}(\omega) = \chi_0^{-1}(\omega) - f_{\text{Hxc}}^\mu(\omega), \quad (10.17)$$

where $\chi_0^{-1}(\omega)$ is the range-separated response function constructed on the RSH orbitals and $f_{\text{Hxc}}^\mu(\omega)$ is the corrected RSH kernel given in Equation (10.16).

10.3.1 Matrix representation of the Bethe-Salpeter equation

For a finite system, this equation is projected onto an orthonormal spin-orbital basis set $\{\varphi_p\}$ as was done in the static case. This leads to the construction of the matrices \mathbf{A} and \mathbf{B} where \mathbf{A} is now frequency dependent due to the long-range correlation Bethe-Salpeter kernel. The resolution of the Bethe-Salpeter equation is thus equivalent to the resolution of the following non-linear eigenvalue problem

$$\begin{pmatrix} \mathbf{A}(\omega_n) & \mathbf{B} \\ \mathbf{B}^* & \mathbf{A}(-\omega_n)^* \end{pmatrix} \begin{pmatrix} \mathbf{X}_n \\ \mathbf{Y}_n \end{pmatrix} = \omega_n \begin{pmatrix} \mathbf{1} & \mathbf{0} \\ \mathbf{0} & -\mathbf{1} \end{pmatrix} \begin{pmatrix} \mathbf{X}_n \\ \mathbf{Y}_n \end{pmatrix}, \quad (10.18)$$

where the matrix elements of \mathbf{A} and \mathbf{B} are given by

$$\begin{aligned} A_{ia,jb}(\omega) &= \Delta\varepsilon_{ia,jb} + w_{ee,ia,jb} - w_{ee,ij,ab}^{\text{lr},\mu} + f_{\text{xc},ia,jb}^{\text{sr},\mu} + \tilde{\Xi}_{c,ia,jb}^{\text{lr},\mu,(2)}(\omega), \\ B_{ia,jb} &= w_{ee,ia,bj} - w_{ee,ib,aj}^{\text{lr},\mu} + f_{\text{xc},ia,bj}^{\text{sr},\mu} + \tilde{\Xi}_{c,ia,bj}^{\text{lr},\mu,(2)}. \end{aligned} \quad (10.19)$$

The resolution of such a problem is much more complicated than in the static case as the matrix \mathbf{A} depends on the eigenvalue ω_n . It is therefore not possible anymore to use the standard Casida's resolution scheme [3] and this equation should in principle be solved self-consistently. A first simplification of this problem consists in using the Tamm-Dancoff approximation, i.e. setting the \mathbf{B} block to zero so that the coupling between the excitations and the de-excitations is neglected. In this case, the problem reduces to

$$\mathbf{A}(\omega_n)\mathbf{X}_n = \omega_n\mathbf{X}_n. \quad (10.20)$$

Although, this problem is simpler than the initial one, this equation remains complex as it still defines a non-linear problem and has to be solved self-consistently. Assume convergence is reached, the excitation energies would then satisfy the relation

$$\omega_n = \mathbf{X}_n^\dagger \mathbf{A}(\omega_n) \mathbf{X}_n. \quad (10.21)$$

Perturbative treatment

Within the Tamm-Dancoff approximation, the simplest way to cope with Equation (10.21) is to use a perturbative resolution in terms of ω as was done in [37]. The matrix $\mathbf{A}(\omega)$ can easily be decomposed into a frequency-independent and a frequency-dependent parts

$$\mathbf{A}(\omega) = \mathbf{A}^{\text{RSH},\mu} + \tilde{\mathbf{E}}_c^{\text{lr},\mu,(2)}(\omega), \quad (10.22)$$

where \mathbf{A}^{RSH} corresponds to the matrix \mathbf{A} obtained with the TDRSH method detailed in Chapter 6 and $\tilde{\mathbf{E}}_c^{\text{lr},\mu,(2)}(\omega)$ is the matrix of the effective long-range second-order Bethe-Salpeter correlation kernel. The excitation energies ω_n can then be expanded around the TDRSH excitation energies $\omega_{0,n}$ as

$$\omega_n = \omega_{0,n} + \mathbf{X}_{0,n}^\dagger \tilde{\mathbf{E}}_c^{(2)}(\omega_{0,n}) \mathbf{X}_{0,n} + \mathbf{X}_{0,n}^\dagger \left. \frac{\partial \tilde{\mathbf{E}}_c^{\text{lr},\mu,(2)}(\omega)}{\partial \omega} \right|_{\omega=\omega_{0,n}} \mathbf{X}_{0,n} (\omega_n - \omega_{0,n}), \quad (10.23)$$

such that, with the normalization factor Z_n given by

$$Z_n = \left(1 - \mathbf{X}_{0,n}^\dagger \left. \frac{\partial \tilde{\mathbf{E}}_c^{\text{lr},\mu,(2)}(\omega)}{\partial \omega} \right|_{\omega=\omega_{0,n}} \mathbf{X}_{0,n} \right)^{-1}, \quad (10.24)$$

the corrected excitation energies are obtained as

$$\omega_n = \omega_{0,n} + Z_n \mathbf{X}_{0,n}^\dagger \tilde{\mathbf{E}}_c^{\text{lr},\mu,(2)}(\omega_{0,n}) \mathbf{X}_{0,n}. \quad (10.25)$$

An alternative to this perturbative resolution would be to unfold the matrix into the Fock space of the single and double excitations as mentioned above. However the size of the matrix would grow rapidly with the number of virtual orbitals which could cause some other computational issues.

10.3.2 Spin adaptation

As with the static kernels, it is possible to decouple this problem into a singlet and a triplet case such that solving the Bethe-Salpeter equation becomes equivalent to solving the singlet and triplet non-linear eigenvalue equations

$${}^1\mathbf{A}({}^1\omega_n){}^1\mathbf{X}_n = {}^1\omega_n {}^1\mathbf{X}_n, \quad (10.26)$$

$${}^3\mathbf{A}({}^3\omega_n){}^3\mathbf{X}_n = {}^3\omega_n {}^3\mathbf{X}_n. \quad (10.27)$$

Within the perturbative treatment, the matrix elements of the singlet and triplet \mathbf{A}^{RSH} matrices are given by

$$\begin{aligned} {}^1A_{ia,jb}^{\text{RSH}} &= \Delta\varepsilon_{ia,jb} + 2w_{ee,ia,jb} - w_{ee,ij,ab}^{\text{lr},\mu} + 2{}^1J_{xc,ia,jb}^{\text{sr},\mu}, \\ {}^3A_{ia,jb}^{\text{RSH}} &= \Delta\varepsilon_{ia,jb} - w_{ee,ij,ab}^{\text{lr},\mu} + 2{}^3J_{xc,ia,jb}^{\text{sr},\mu}. \end{aligned} \quad (10.28)$$

The spin adaptation of the effective correlation kernel is performed in Appendix H.2. The matrix elements of the singlet and triplet second-order effective kernels in the block \mathbf{A} are then given by

$$\begin{aligned} {}^1\Xi_{c,ia,jb}^{\text{lr},\mu,(2)}(\omega) &= \\ &- \sum_{kc} \frac{2w_{ee,ij,kc}^{\text{lr},\mu} w_{ee,ba,ck}^{\text{lr},\mu} - w_{ee,ij,kc}^{\text{lr},\mu} w_{ee,ka,cb}^{\text{lr},\mu} - w_{ee,cj,ki}^{\text{lr},\mu} w_{ee,ba,ck}^{\text{lr},\mu} + 2w_{ee,cj,ki}^{\text{lr},\mu} w_{ee,ka,cb}^{\text{lr},\mu}}{\omega - \varepsilon_a + \varepsilon_k - \varepsilon_c + \varepsilon_j} \\ &- \sum_{kc} \frac{2w_{ee,ij,ck}^{\text{lr},\mu} w_{ee,ba,kc}^{\text{lr},\mu} - w_{ee,ij,ck}^{\text{lr},\mu} w_{ee,ca,kb}^{\text{lr},\mu} - w_{ee,kj,ci}^{\text{lr},\mu} w_{ee,ba,kc}^{\text{lr},\mu} + 2w_{ee,kj,ci}^{\text{lr},\mu} w_{ee,ca,kb}^{\text{lr},\mu}}{\omega + \varepsilon_i - \varepsilon_c + \varepsilon_k - \varepsilon_b} \\ &+ \frac{1}{2} \sum_{cd} \frac{2w_{ee,ca,jd}^{\text{lr},\mu} w_{ee,ic,db}^{\text{lr},\mu} - w_{ee,ca,jd}^{\text{lr},\mu} w_{ee,bc,di}^{\text{lr},\mu} - w_{ee,da,jc}^{\text{lr},\mu} w_{ee,ic,db}^{\text{lr},\mu} + 2w_{ee,da,jc}^{\text{lr},\mu} w_{ee,bc,di}^{\text{lr},\mu}}{\omega + (\varepsilon_i + \varepsilon_j) - (\varepsilon_c + \varepsilon_d)} \\ &+ \frac{1}{2} \sum_{kl} \frac{2w_{ee,ka,jl}^{\text{lr},\mu} w_{ee,ik,lb}^{\text{lr},\mu} - w_{ee,ka,jl}^{\text{lr},\mu} w_{ee,bk,li}^{\text{lr},\mu} - w_{ee,la,jk}^{\text{lr},\mu} w_{ee,ik,lb}^{\text{lr},\mu} + 2w_{ee,la,jk}^{\text{lr},\mu} w_{ee,bk,li}^{\text{lr},\mu}}{\omega - (\varepsilon_a + \varepsilon_b) + (\varepsilon_k + \varepsilon_l)}, \end{aligned} \quad (10.29a)$$

$$\begin{aligned} {}^3\Xi_{c,ia,jb}^{\text{lr},\mu,(2)}(\omega) &= - \sum_{kc} \frac{2w_{ee,ij,kc}^{\text{lr},\mu} w_{ee,ba,ck}^{\text{lr},\mu} - w_{ee,ij,kc}^{\text{lr},\mu} w_{ee,ka,cb}^{\text{lr},\mu} - w_{ee,cj,ki}^{\text{lr},\mu} w_{ee,ba,ck}^{\text{lr},\mu}}{\omega - \varepsilon_a + \varepsilon_k - \varepsilon_c + \varepsilon_j} \\ &- \sum_{kc} \frac{2w_{ee,ij,ck}^{\text{lr},\mu} w_{ee,ba,kc}^{\text{lr},\mu} - w_{ee,ij,ck}^{\text{lr},\mu} w_{ee,ca,kb}^{\text{lr},\mu} - w_{ee,kj,ci}^{\text{lr},\mu} w_{ee,ba,kc}^{\text{lr},\mu}}{\omega + \varepsilon_i - \varepsilon_c + \varepsilon_k - \varepsilon_b} \\ &- \frac{1}{2} \sum_{cd} \frac{w_{ee,ca,jd}^{\text{lr},\mu} w_{ee,bc,di}^{\text{lr},\mu} + w_{ee,da,jc}^{\text{lr},\mu} w_{ee,ic,db}^{\text{lr},\mu}}{\omega + (\varepsilon_i + \varepsilon_j) - (\varepsilon_c + \varepsilon_d)} \\ &- \frac{1}{2} \sum_{kl} \frac{w_{ee,ka,jl}^{\text{lr},\mu} w_{ee,bk,li}^{\text{lr},\mu} + w_{ee,la,jk}^{\text{lr},\mu} w_{ee,ik,lb}^{\text{lr},\mu}}{\omega - (\varepsilon_a + \varepsilon_b) + (\varepsilon_k + \varepsilon_l)}. \end{aligned} \quad (10.29b)$$

The spin-adapted matrix elements of the effective kernel in the \mathbf{B} block are not used in this Tamm-Dancoff perturbative approach but can be found in Appendix H.

10.4 Application to H_2 in a minimal basis

As usual, we first assess the behavior of the kernel on the model system of H_2 in a minimal basis set. Unfortunately, due to its very symmetric nature, the two-electron interaction matrix is block diagonal in this system. This implies in particular that the contribution of the correlation kernel in the block \mathbf{A} is zero and as it is the only frequency-dependent contribution to the second-order Bethe-Salpeter kernel, the only “double” effects will

occur through **B**.

The matrix elements of the singlet and triplet correlation kernel in the block **B** are given by

$${}^1\tilde{\Xi}_{c,12,21}^{(2)} = -K_{12} \left(\frac{2(K_{12} + J_{12}) - J_{22} - J_{11}}{2\Delta\varepsilon} \right) \quad (10.30a)$$

$${}^3\tilde{\Xi}_{c,12,21}^{(2)} = -K_{12} \left(\frac{2(K_{12} - J_{12}) + J_{22} + J_{11}}{2\Delta\varepsilon} \right). \quad (10.30b)$$

Although, this kernel is frequency-independent, it still differs from its static approximation given in Equations (9.39) and (9.40), which expressions are recalled here:

$${}^1\Xi_{c,12,21}^{(2)}(\omega = 0) = K_{12} \left(\frac{2(K_{12} + J_{12})}{\Delta\varepsilon} - \frac{J_{22}}{2\varepsilon_2} + \frac{J_{11}}{2\varepsilon_1} \right), \quad (10.31a)$$

$${}^3\Xi_{c,12,21}^{(2)}(\omega = 0) = K_{12} \left(\frac{2(K_{12} - J_{12})}{\Delta\varepsilon} + \frac{J_{22}}{2\varepsilon_2} - \frac{J_{11}}{2\varepsilon_1} \right). \quad (10.31b)$$

Two main differences emerge from this comparison:

- the presence of energy differences $\Delta\varepsilon$ for all the contributions of the dynamical kernel instead of orbital energies ε_2 and ε_1 for the last two terms of Equations (10.31a) and (10.31b). This form of the kernel is therefore much more physical than the static one ;
- the sign of the correction changes between the static and the dynamical kernel.

The matrices **A** and **B** are then given by

$$\begin{aligned} {}^1A &= \Delta\varepsilon + 2K_{12} - J_{12} \\ {}^1B &= 2K_{12} - K_{12} \left(1 + \frac{2(K_{12} + J_{12}) - J_{22} - J_{11}}{2\Delta\varepsilon} \right) \\ {}^3A &= \Delta\varepsilon - J_{12} \\ {}^3B &= -K_{12} \left(1 + \frac{2(K_{12} - J_{12}) + J_{22} + J_{11}}{2\Delta\varepsilon} \right) \end{aligned} \quad (10.32)$$

such that the singlet excitation energy is given by

$$\begin{aligned} {}^1\omega &= \sqrt{\Delta\varepsilon + 4K_{12} - J_{12} - K_{12} \left(1 + \frac{2(K_{12} + J_{12}) - J_{22} - J_{11}}{2\Delta\varepsilon} \right)} \\ &\quad \times \sqrt{\Delta\varepsilon - J_{12} + K_{12} \left(1 + \frac{2(K_{12} + J_{12}) - J_{22} - J_{11}}{2\Delta\varepsilon} \right)}, \end{aligned} \quad (10.33)$$

and the triplet one by

$$\begin{aligned}
 {}^3\omega &= \sqrt{\Delta\varepsilon - J_{12} - K_{12} \left(1 + \frac{2(K_{12} - J_{12}) + J_{22} + J_{11}}{2\Delta\varepsilon} \right)} \\
 &\quad \times \sqrt{\Delta\varepsilon - J_{12} + K_{12} \left(1 + \frac{2(K_{12} - J_{12}) + J_{22} + J_{11}}{2\Delta\varepsilon} \right)}.
 \end{aligned} \tag{10.34}$$

As was done for the static kernel, it is interesting to compare the Taylor expansions of these energies with respect to the electron-electron interaction to the expansions of the FCI energies at the same order recalled here:

$$\begin{aligned}
 {}^1\omega^{\text{FCI},(2)} &= \Delta\varepsilon + \lambda(-J_{12} + 2K_{12}) + \lambda^2 \frac{K_{12}^2}{2\Delta\varepsilon} + \mathcal{O}(\lambda^3) \\
 {}^3\omega^{\text{FCI},(2)} &= \Delta\varepsilon - \lambda(J_{12}) + \lambda^2 \frac{K_{12}^2}{2\Delta\varepsilon} + \mathcal{O}(\lambda^3).
 \end{aligned} \tag{10.35}$$

If a similar expansion is performed for the dynamical Bethe-Salpeter second-order energies, the same expansion then in the static case is recovered despite the change of sign of the kernel

$$\begin{aligned}
 {}^1\omega^{(2)} &= \Delta\varepsilon + \lambda(-J_{12} + 2K_{12}) - \lambda^2 \frac{K_{12}^2}{2\Delta\varepsilon} + \mathcal{O}(\lambda^3) \\
 {}^3\omega^{(2)} &= \Delta\varepsilon - \lambda(J_{12}) - \lambda^2 \frac{K_{12}^2}{2\Delta\varepsilon} + \mathcal{O}(\lambda^3).
 \end{aligned} \tag{10.36}$$

The second-order contribution exhibits therefore a wrong behavior with respect to the FCI case. When giving a closer look to the origin of the different contributions of this expansion, it appears that the second-order contribution comes only from the exchange kernel. In fact, as the correlation kernel contributes only in the **B** block, its second-order contribution cancels out in the excitation energies. This highlights the fact that some important second-order contributions seem to be missing in this second-order kernel. This deficiency can have several origins: the GW approximation, the lack of self-consistency, the choice of the starting Green's function and the absence of self-energy corrections in the non-interacting response function. A priori, the GW approximation can be ruled out as it is redundant with the second-order truncation. Given the fact that the interaction matrix is block diagonal, the self-consistency is not responsible either. It thus remains only the choice of the starting point and the self-energy corrections which are in fact related to each other. We are currently assessing the effects of the later which could to a partial compensation of the dynamical effects [98], however this study is still under progress and in the following these corrections are not accounted for.

The singlet and triplet excitation energies are shown as functions of the internuclear distance R in Figure 10.4. The FCI and TDHF curves are recalled for the sake of comparison. With this kernel, the singlet excitation energy is improved with respect to the TDHF one up to 6 bohr⁻¹, then breaks down and becomes rapidly imaginary.

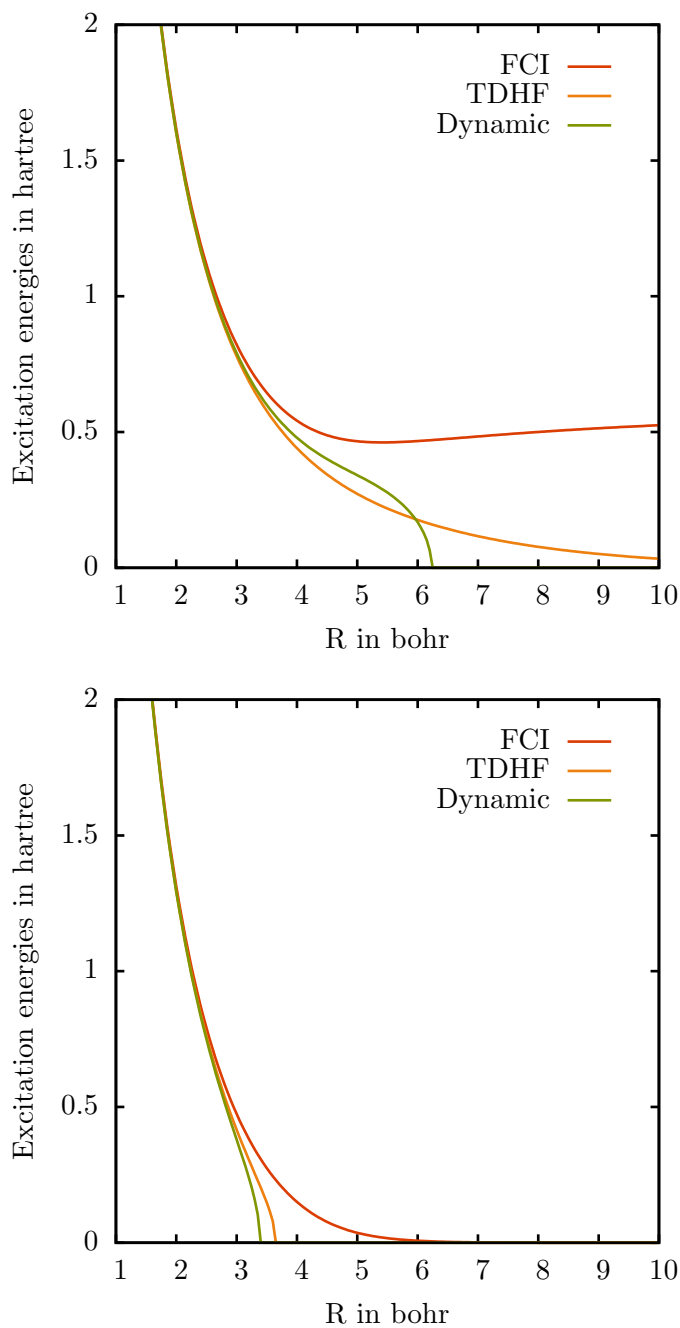


Figure 10.4 – Excitation energies of the singlet $^1\Sigma_u^+$ (top) and the triplet $^3\Sigma_u^+$ (bottom) states of H₂ in a minimal basis as a function of the internuclear distance R calculated by FCI, TDHF, and the dynamic second-order BSE-GWx with the derivative of W with respect to G with the non-interacting HF Green's function G_0 .

This was to be expected as the second-order expansion is not valid anymore when the bond is stretched too much as the orbital energy difference becomes small with respect to the two-electron integrals. The triplet excitation energy however is deteriorated by the correlation kernel with respect to the TDHF reference and becomes imaginary for a smaller internuclear distance.

However, this model system seems not to be sufficient to really assess the behavior of the kernel as the frequency dependence is lost because of its symmetric nature and of the size of the basis set, it is thus necessary to go to larger systems.

10.5 Computational details

Starting from a TDRSH calculation in the Tamm-Dancoff approximation with a short-range LDA functional, the long-range correlation kernel is then added perturbatively, following the procedure detailed in Section 10.3.1. This is a three-step calculation. First, a self-consistent ground-state calculation is performed with a development version of the quantum chemistry program MOLPRO [99] and the orbital energies, the two-electron integrals and the matrix elements of the singlet and triplet short-range LDA kernels are dumped into several text files. We then used a homemade software to do the next two steps, namely the time-dependent range-separated calculation (TDRSH) within the Tamm-Dancoff approximation and the evaluation of the correction due to the dynamical long-range correlation kernel using the previously calculated orbitals and two-electron integrals.

For compactness, “TD” will be dropped in the names of the methods and “LDA” will also be omitted in the names as it is the only density functional used here. Moreover, all the results are obtained within the Tamm-Dancoff approximation within the perturbative scheme. Therefore, “KS” will denote a TDKS calculation using the LDA exchange-correlation functional with the Tamm-Dancoff approximation, “HF” will stand for a TDHF calculation with the Tamm-Dancoff approximation (equivalent to the CI single method), “RSH” will denote a linear-response RSH calculation using the short-range LDA exchange-correlation functional with the Tamm-Dancoff approximation. When the (long-range) second-order Bethe-Salpeter correlation kernel is added perturbatively on top of the HF (or RSH) calculation, the suffix “BSE2” is appended to the name of the initial method, following the notation set by Zhang *et al* [37]. If the normalization factor Z_n is set to 1, it is denoted “BSE2’ ”.

We study four small molecules N_2 , CO, H_2CO and C_2H_4 in the same geometry (experimental) and with the same basis set (Sadlej+) than in Chapter 6. The details on the reference data and basis set can therefore be found in Section 6.4. Results are not available for C_6H_6 and the C_2H_4 - C_2F_4 dimer yet as this method is computationally expensive especially in term of memory as the full interaction matrix is needed. As the range-separation parameter μ has been optimized in absence of the long-range correlation kernel in Chapter 6, it is necessary to check if this optimized value still holds with

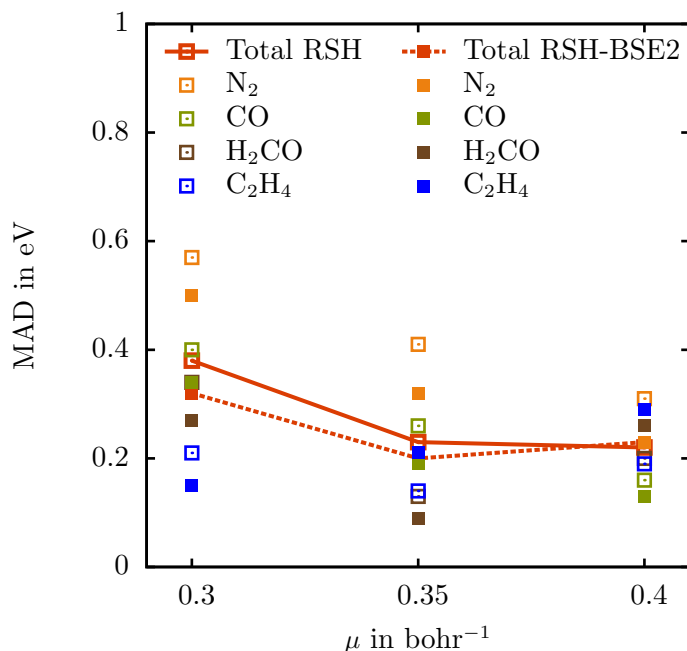


Figure 10.5 – Mean absolute deviation (MAD) in eV of the first 14 excitation energies of the N_2 , CO, H_2CO and C_2H_4 molecules calculated by the RSH and RSH-BSE2 methods with the short-range LDA exchange-correlation functional with respect to the EOM-CCSD reference as a function of the range-separation parameter μ .

the addition of this kernel. The results of this optimization are shown in Figure 10.5. Without the kernel, the optimal μ for this set of molecule is equal to 0.4 bohr⁻¹, however, with the inclusion of the long-range dynamical kernel, this value is slightly reduced to 0.35 bohr⁻¹. Therefore, all the results are shown with this value of the range-separation parameter in the following.

10.6 Results and discussion

The excitation energies for each method and each molecule are given in Tables 10.1-10.4. Mean absolute deviations and maximum absolute deviations with respect to the EOM-CCSD reference are also given for the valence, the Rydberg and all the excitation energies. Whatever the starting point, RSH or HF, the correction due to the perturbative correlation kernel is always positive. Therefore, if the excitation energies were already too high with respect to the reference, they are deteriorated by the correction, and if they were too low it depends on the magnitude of the correction.

10.6.1 Effect of the correction on the HF excitation energies

When applied on the excitation energies obtained at the HF level in the Tamm-Dancoff approximation, the correction due to the correlation kernel is especially large for the

valence excitation energies and increases them by 2 to 3.7 eV. Although, the valence excitation energies are often underestimated in HF, the magnitude of the correction is way too high with respect to the error present in HF which leads to an overall overestimation of the valence excitation energies by 1.65-3.15 eV. The Rydberg excitation energies calculated in HF are usually already too high, therefore when the correction is applied, they increase furthermore and are deteriorated. However, the magnitude of the correction is much smaller for the Rydberg excitation energies (0.19-1.75 eV) than for the valence ones such that their deterioration is less significant. In this case, the effect of the inclusion of the normalization factor is also important for the valence excitation energies (up to 0.27 eV) although it remains small for the Rydberg ones.

The difference of magnitude in the valence and Rydberg corrections can be understood as follows. The smallest denominator in the kernel correction is obtained for the HOMO-LUMO contribution and is given by $\omega_{0,n} - 2\varepsilon^{\text{LUMO}} + 2\varepsilon^{\text{HOMO}}$. As all the TDHF energies are well below the ionization threshold, the effect of the variation of $\omega_{0,n}$ is not very significant and in a first approximation, we could consider that the matrix of the effective second-order correlation is sensibly the same for all the excitations and have predominant contributions for orbitals close to the HOMO and the LUMO, i.e. valence orbitals. What changes significantly however when going from a valence to a Rydberg is the eigenvector $\mathbf{X}_{0,n}$ which multiplies the effective kernel in Equation (10.25). For a valence excitation energy, this eigenvector has its major contributions in the subspace of valence excitations and overlaps significantly with the effective kernel, while in the Rydberg case, this overlap is much smaller and so is the correction to a Rydberg excitation.

10.6.2 Effect of the correction on the RSH excitation energies

When applied on the Tamm-Dancoff range-separated excitation energies, the long-range correlation correction induces a moderate increase of the excitation energies of 0.04 to 0.30 eV. As in the HF case, the correction is more important for the valence excitation energies than for the Rydberg ones. The difference of magnitude of the RSH correction with respect to the HF case is to be attributed to the substitution of the full-range electron-electron interaction by its long-range part. In this case, the effect of the normalization factor Z_n is almost indiscernible because it is very close to 1 and multiply a correction which is much smaller than in the HF case. For the chosen value of the range-separation parameter μ of 0.35 bohr⁻¹, the excitation energies of the considered system were mostly slightly underestimated such that the correction overall improves their description as the global mean absolute deviation decreases by 0.04 to 0.09 eV except for ethylene where it increases by 0.07 eV such that globally, the MAD is reduced by about 0.03 eV which is a pretty small improvement. However, when looking at the maximum absolute deviation, the long-range correction actually provides a systematic improvement for all the systems which means that the description of the excitation energies is more even with this method than in standard TDRSH.

10.7 Conclusion

In this chapter, we have derived an effective second-order Bethe-Salpeter long-range dynamical correlation kernel which depends only on the external frequency and can be applied within the range-separated TDDFT framework. When projected into a spin-orbital basis set, it appears that the frequency-dependence is in fact only present in the **A** block and that the **B** block remains frequency independent. In the **A** block, this kernel has now a physical form with respect to its static approximation explored in the previous chapter which involves a product of two antisymmetrized two-electron integrals and poles corresponding to double excitation energies in terms of orbital energy differences. Such a kernel should therefore contribute significantly when the excitation energy is close to a double excitation.

As the use of such a kernel implies that the resolution of the Bethe-Salpeter equation defines a non-linear eigenvalue problem, a perturbative resolution was used to circumvent this issue as a first approximation although the use of Löwdin partitioning technique should allow one to unfold the matrix and recover a linear eigenvalue problem so that a self-consistent calculation could be avoided. We have not explored this approach yet but work is under progress on this aspect. The resolution was done in the Tamm-Dancoff approximation following the scheme proposed by Zhang *et al*, however, it would be of particular interest to be able to solve the Bethe-Salpeter equation without this approximation. As we have the matrix elements of the effective correlation kernel in the **B** block, and they do not depend on the frequency, this step should be relatively straightforward, although computationally demanding.

We have illustrated the behavior of this kernel on the model system given by the hydrogen molecule in a minimal basis and seen that some second-order contributions were missing in order to recover correctly the second-order limit in the excitation energies with respect to the one obtained in full-CI. We have identified this phenomenon to the neglect of the self-energy corrections coming from the independent-particle response function and are currently exploring this deficiency of the method, both on the model system and in the general case. This should allow us to recover additional contributions to the second-order kernel which expression would then be closer to the one of the SOPPA kernel.

However, the second-order dynamical kernel derived here constitutes a conserving approximation and improves the description of the excitation energies when applied perturbatively within the Tamm-Dancoff approximation to the first lowest excitation energies of the four small molecules studied here. However, the excitations studied here did not present important contributions from double excitations and it should be interesting to test this approach on a system where double excitations are important.

State	Transition	KS	RSH	RSH-BSE2'	RSH-BSE2	HF	HF-BSE2'	HF-BSE2	EOM-CCSD
Valence excitation energies (eV)									
$^3\Sigma_u^+$	$1\pi_u \rightarrow 1\pi_g$	8.08	7.74	7.93	7.93	6.23	8.76	8.88	7.72
$^3\Pi_g$	$3\sigma_g \rightarrow 1\pi_g$	7.58	7.85	8.05	8.05	7.99	10.80	10.97	8.16
$^3\Delta_u$	$1\pi_u \rightarrow 1\pi_g$	8.88	8.54	8.73	8.74	7.32	9.84	9.96	9.07
$^1\Pi_g$	$3\sigma_g \rightarrow 1\pi_g$	9.17	9.50	9.68	9.68	10.02	12.31	12.43	9.55
$^3\Sigma_u^-$	$1\pi_u \rightarrow 1\pi_g$	9.65	9.34	9.53	9.53	8.50	10.67	10.77	10.00
$^1\Sigma_u^-$	$1\pi_u \rightarrow 1\pi_g$	9.65	9.34	9.53	9.53	8.50	10.73	10.84	10.24
$^1\Delta_u$	$1\pi_u \rightarrow 1\pi_g$	10.25	9.98	10.18	10.18	9.06	11.20	11.30	10.66
$^3\Pi_u$	$2\sigma_u \rightarrow 1\pi_g$	10.42	10.77	10.97	10.97	11.74	14.63	14.82	11.36
Rydberg excitation energies (eV)									
$^3\Sigma_{g0}^+$	$3\sigma_g \rightarrow 4\sigma_g$	10.28	11.47	11.56	11.56	13.12	13.93	13.94	11.74
$^1\Sigma_{g0}^+$	$3\sigma_g \rightarrow 4\sigma_g$	10.40	11.94	11.98	11.98	14.01	14.22	14.22	12.15
$^3\Sigma_u^+$	$3\sigma_g \rightarrow 3\sigma_u$	10.63	12.30	12.40	12.40	14.21	15.05	15.07	12.70
$^3\Pi_u$	$3\sigma_g \rightarrow 2\pi_u$	10.99	12.30	12.36	12.36	13.04	13.42	13.43	12.71
$^1\Pi_u$	$3\sigma_g \rightarrow 2\pi_u$	10.98	12.39	12.44	12.44	13.23	13.45	13.45	12.77
$^1\Sigma_u^+$	$3\sigma_g \rightarrow 3\sigma_u$	10.62	12.43	12.51	12.51	14.31	15.02	15.04	12.82
Ionization threshold: $-\epsilon_{\text{HOMO}}$ (eV)									
		6.30	14.94	14.94	14.94	16.74	16.74	16.74	
MAD of excitation energies with respect to EOM-CCSD (eV)									
Valence		0.48	0.47	0.35	0.35	1.14	1.52	1.65	-
Rydberg		1.83	0.34	0.27	0.27	1.17	1.70	1.71	-
Total		1.06	0.41	0.32	0.32	1.15	1.60	1.68	-
Maximum absolute deviation of excitation energies with respect to EOM-CCSD (eV)									
		2.19	0.90	0.71	0.71	1.86	3.28	3.47	-

Table 10.1 – Excitation energies of N_2 calculated by linear-response HF and KS (with the LDA functional), by the linear-response range-separated methods RSH, RSH-BSE2' and RSH-BSE2 (with the short-range LDA functional and $\mu = 0.35 \text{ bohr}^{-1}$) within the Tamm-Dancoff approximation, and by EOM-CCSD taken as reference, using the Sadlej+ basis set.

State	Transition	KS	RSH	RSH-BSE2'	RSH-BSE2	HF	HF-BSE2'	HF-BSE2	EOM-CCSD
Valence excitation energies (eV)									
$^3\Pi$	$5a_1(\sigma) \rightarrow 2e_1(\pi^*)$	6.04	6.10	6.32	6.32	5.85	8.15	8.27	6.45
$^3\Sigma^+$	$1e_1(\pi) \rightarrow 2e_1(\pi^*)$	8.54	8.45	8.63	8.63	7.79	10.26	10.38	8.42
$^1\Pi$	$5a_1(\sigma) \rightarrow 2e_1(\pi^*)$	8.42	8.68	8.88	8.88	9.08	10.86	10.94	8.76
$^3\Delta$	$1e_1(\pi) \rightarrow 2e_1(\pi^*)$	9.20	9.13	9.31	9.31	8.74	11.08	11.19	9.39
$^3\Sigma^-$	$1e_1(\pi) \rightarrow 2e_1(\pi^*)$	9.84	9.80	9.97	9.98	9.73	11.68	11.76	9.97
$^1\Sigma^-$	$1e_1(\pi) \rightarrow 2e_1(\pi^*)$	9.84	9.80	9.98	9.98	9.73	11.73	11.82	10.19
$^1\Delta$	$1e_1(\pi) \rightarrow 2e_1(\pi^*)$	10.33	10.32	10.50	10.50	10.15	11.98	12.05	10.31
$^3\Pi$	$4a_1(\sigma) \rightarrow 2e_1(\pi^*)$	11.43	11.96	12.12	12.12	13.31	15.59	15.70	12.49
Rydberg excitation energies (eV)									
$^3\Sigma^+$	$5a_1(\sigma) \rightarrow 6a_1(\sigma)$	9.56	10.34	10.46	10.46	11.18	12.07	12.09	10.60
$^1\Sigma^+$	$5a_1(\sigma) \rightarrow 6a_1(\sigma)$	9.95	11.12	11.20	11.20	12.27	12.61	12.61	11.15
$^3\Sigma^+$	$5a_1(\sigma) \rightarrow 7a_1(\sigma)$	10.26	11.08	11.17	11.17	12.42	12.82	12.83	11.42
$^1\Sigma^+$	$5a_1(\sigma) \rightarrow 7a_1(\sigma)$	10.50	11.30	11.38	11.38	12.79	12.91	12.91	11.64
$^3\Pi$	$5a_1(\sigma) \rightarrow 3e_1(\pi)$	10.39	11.26	11.34	11.34	12.60	13.19	13.20	11.66
$^1\Pi$	$5a_1(\sigma) \rightarrow 3e_1(\pi)$	10.50	11.45	11.52	11.52	12.88	13.21	13.21	11.84
Ionization threshold: $-\epsilon_{\text{HOMO}}$ (eV)									
		9.12	13.49	13.49	13.49	15.11	15.11	15.11	
MAD of excitation energies with respect to the EOM-CCSD calculation (eV)									
Valence		0.33	0.23	0.16	0.16	0.49	1.92	2.02	-
Rydberg		1.19	0.29	0.22	0.22	0.97	1.42	1.42	-
Total		0.70	0.26	0.19	0.19	0.69	1.70	1.76	-
Maximum absolute deviation of excitation energies with respect to EOM-CCSD (eV)									
		1.34	0.53	0.37	0.36	1.16	3.10	3.22	-

Table 10.2 – Excitation energies of CO calculated by linear-response HF and KS (with the LDA functional), by the linear-response range-separated methods RSH, RSH-BSE2' and RSH-BSE2 (with the short-range LDA functional and $\mu = 0.35$ bohr $^{-1}$) within the Tamm-Dancoff approximation, and by EOM-CCSD taken as reference, using the Sadlej+ basis set.

State	Transition	KS	RSH	RSH-BSE2'	RSH-BSE2	HF	HF-BSE2'	HF-BSE2	EOM-CCSD
Valence excitation energies (eV)									
3A_2	$2b_2(n) \rightarrow 2b_1(\pi^*)$	3.08	3.17	3.45	3.45	3.76	6.66	6.86	3.56
1A_2	$2b_2(n) \rightarrow 2b_1(\pi^*)$	3.70	3.82	4.11	4.11	4.58	7.20	7.37	4.03
3A_1	$1b_1(\pi) \rightarrow 2b_1(\pi^*)$	6.35	6.08	6.39	6.39	4.96	8.08	8.30	6.06
3B_1	$5a_1(\sigma) \rightarrow 2b_1(\pi^*)$	7.77	8.09	8.39	8.40	8.60	12.01	12.28	8.54
Rydberg excitation energies (eV)									
3B_2	$2b_2(n) \rightarrow 6a_1(\sigma)$	5.85	6.83	6.92	6.92	8.17	8.63	8.63	6.83
1B_2	$2b_2(n) \rightarrow 6a_1(\sigma)$	5.93	7.01	7.07	7.08	8.56	8.72	8.72	7.00
3B_2	$2b_2(n) \rightarrow 7a_1(\sigma)$	6.96	7.69	7.81	7.81	9.04	9.83	9.85	7.73
3A_1	$2b_2(n) \rightarrow 3b_2(\sigma)$	6.73	7.77	7.83	7.83	9.24	9.58	9.58	7.87
1B_2	$2b_2(n) \rightarrow 7a_1(\sigma)$	7.04	7.91	8.00	8.00	9.41	9.78	9.78	7.93
1A_1	$2b_2(n) \rightarrow 3b_2(\sigma)$	6.78	7.93	7.97	7.97	9.53	10.00	10.01	7.99
1A_2	$2b_2(n) \rightarrow 3b_1(\pi)$	7.55	8.32	8.39	8.39	10.04	10.26	10.26	8.45
3A_2	$2b_2(n) \rightarrow 3b_1(\pi)$	7.58	8.31	8.38	8.38	9.93	11.04	11.07	8.47
3B_2	$2b_2(n) \rightarrow 8a_1(\sigma)$	7.97	8.90	8.98	8.98	10.21	11.89	11.96	8.97
1B_2	$2b_2(n) \rightarrow 8a_1(\sigma)$	8.19	9.17	9.25	9.25	10.86	11.05	11.05	9.27
Ionization threshold: $-\epsilon_{\text{HOMO}}$ (eV)									
		6.30	10.33	10.33	10.33	12.04	12.04	12.04	
MAD of excitation energies with respect to the EOM-CCSD calculation (eV)									
Valence		0.47	0.27	0.17	0.17	0.48	2.94	3.15	-
Rydberg		0.99	0.07	0.06	0.06	1.45	2.03	2.04	-
Total		0.84	0.13	0.09	0.09	1.17	2.29	2.36	-
Maximum absolute deviation of excitation energies with respect to EOM-CCSD (eV)									
		1.21	0.45	0.33	0.33	1.59	3.47	3.74	-

Table 10.3 – Excitation energies of H_2CO calculated by linear-response HF and KS (with the LDA functional), by the linear-response range-separated methods RSH, RSH-BSE2' and RSH-BSE2 (with the short-range LDA functional and $\mu = 0.35 \text{ bohr}^{-1}$) within the Tamm-Dancoff approximation, and by EOM-CCSD taken as reference, using the Sadlej+ basis set.

State	Transition	KS	RSH	RSH-BSE2'	RSH-BSE2	HF	HF-BSE2'	HF-BSE2	EOM-CCSD
Valence excitation energies (eV)									
$^3B_{1u}$	$1b_{3u}(\pi) \rightarrow 1b_{2g}(\pi^*)$	4.74	4.35	4.73	4.73	3.54	5.92	6.06	4.41
$^1B_{1u}$	$1b_{3u}(\pi) \rightarrow 1b_{2g}(\pi^*)$	7.91	8.07	8.37	8.38	7.70	9.05	9.11	8.00
$^3B_{1g}$	$1b_{3g}(\sigma) \rightarrow 1b_{2g}(\pi^*)$	7.18	7.92	8.04	8.04	8.48	10.33	10.43	8.21
$^1B_{1g}$	$1b_{3g}(\sigma) \rightarrow 1b_{2g}(\pi^*)$	7.48	8.04	8.24	8.24	9.23	10.74	10.81	8.58
Rydberg excitation energies (eV)									
$^3B_{3u}$	$1b_{3u}(\pi) \rightarrow 4a_{1g}(\sigma)$	6.59	7.21	7.35	7.35	6.91	7.36	7.37	7.16
$^1B_{3u}$	$1b_{3u}(\pi) \rightarrow 4a_{1g}(\sigma)$	6.65	7.36	7.48	7.48	7.14	7.42	7.43	7.30
$^3B_{1g}$	$1b_{3u}(\pi) \rightarrow 2b_{2u}(\sigma)$	6.98	7.42	7.77	7.78	7.66	8.10	8.10	7.91
$^3B_{2g}$	$1b_{3u}(\pi) \rightarrow 3b_{1u}(\sigma)$	7.10	8.03	8.11	8.11	7.79	8.06	8.07	7.93
$^1B_{1g}$	$1b_{3u}(\pi) \rightarrow 2b_{2u}(\sigma)$	7.19	7.92	8.17	8.17	7.75	8.09	8.09	7.97
$^1B_{2g}$	$1b_{3u}(\pi) \rightarrow 3b_{1u}(\sigma)$	7.15	8.13	8.20	8.20	7.92	8.07	8.07	8.01
3A_g	$1b_{3u}(\pi) \rightarrow 2b_{3u}(\pi)$	8.03	8.46	8.60	8.60	8.02	8.62	8.64	8.48
1A_g	$1b_{3u}(\pi) \rightarrow 2b_{3u}(\pi)$	8.30	8.87	8.99	8.99	8.61	8.88	8.88	8.78
$^3B_{3u}$	$1b_{3u}(\pi) \rightarrow 5a_{1g}(\sigma)$	8.26	8.97	9.12	9.12	8.74	9.26	9.26	9.00
$^1B_{3u}$	$1b_{3u}(\pi) \rightarrow 5a_{1g}(\sigma)$	8.28	9.09	9.20	9.20	8.92	9.13	9.13	9.07
Ionization threshold: $-\epsilon_{\text{HOMO}}$ (eV)									
		6.89	10.45	10.45	10.45	10.23	10.23	10.23	
MAD of excitation energies with respect to the EOM-CCSD calculation (eV)									
Valence		0.64	0.24	0.30	0.30	0.52	1.71	1.80	-
Rydberg		0.71	0.10	0.17	0.17	0.21	0.14	0.14	-
Total		0.69	0.14	0.21	0.21	0.30	0.59	0.62	-
Maximum absolute deviation of excitation energies with respect to EOM-CCSD (eV)									
		1.10	0.54	0.37	0.38	0.87	2.16	2.23	-

Table 10.4 – Excitation energies of C_2H_4 calculated by linear-response HF and KS (with the LDA functional), by the linear-response range-separated methods RSH, RSH-BSE2' and RSH-BSE2 (with the short-range LDA functional and $\mu = 0.35$ bohr $^{-1}$) within the Tamm-Dancoff approximation, and by EOM-CCSD taken as reference, using the Sadlej+ basis set.

Bibliography

- [1] E. Runge and E. K. U. Gross. 1984. *Phys. Rev. Lett.* 52. Pp. 997–1000.
- [2] E. K. U. Gross and W. Kohn. 1985. *Phys. Rev. Lett.* 55. Pp. 2850–2852.
- [3] M. Casida. “Time-Dependent Density-functional response theory for molecules”. In: *Recent Adv. Density Funct. Methods, Part I*. Ed. by D. P. Chong. Singapore: World Scientific, 1995, p. 155.
- [4] M. Petersilka, U. J. Gossmann, and E. K. U. Gross. 1996. *Phys. Rev. Lett.* 76. P. 1212.
- [5] A. Dreuw, J. L. Weisman, and M. Head-Gordon. 2003. *J. Chem. Phys.* 119. P. 2943.
- [6] N. T. Maitra, F. Zhang, R. J. Cave, and K. Burke. 2004. *J. Chem. Phys.* 120. P. 5932.
- [7] O. Gritsenko, S. V. Gisbergen, A. Görling, and E. J. Baerends. 2000. *J. Chem. Phys.* 113. Pp. 8478–8489.
- [8] Y. Tawada, T. Tsuneda, S. Yanagisawa, et al. 2004. *J. Chem. Phys.* 120. P. 8425.
- [9] L. Kronik, T. Stein, S. Refaely-Abramson, and R. Baer. 2012. *J. Chem. Theory Comput.* 8. Pp. 1515–1531.
- [10] M. E. Casida. 2005. *J. Chem. Phys.* 122. P. 54111.
- [11] M. Huix-Rotllant and M. E. Casida. 2010. *arXiv Prepr. arXiv1008.1478*.
- [12] K. Pernal, O. Gritsenko, and E. J. Baerends. 2007. *Phys. Rev. A.* 75. P. 12506.
- [13] K. Pernal, K. Giesbertz, O. Gritsenko, and E. J. Baerends. 2007. *J. Chem. Phys.* 127. P. 214101.
- [14] K. Giesbertz, E. Baerends, and O. Gritsenko. 2008. *Phys. Rev. Lett.* 101. P. 033004.
- [15] K. J. H. Giesbertz, K. Pernal, O. V. Gritsenko, and E. J. Baerends. 2009. *J. Chem. Phys.* 130. P. 114104.
- [16] K. Pernal. 2012. *J. Chem. Phys.* 136. P. 184105.
- [17] G. Strinati. 1988. *La Riv. del Nuovo Cim.* 11. Pp. 1–86.
- [18] M. Rohlfing and S. G. Louie. 2000. *Phys. Rev. B.* 62. P. 4927.

BIBLIOGRAPHY

- [19] G. Onida, L. Reining, and A. Rubio. 2002. *Rev. Mod. Phys.* 74. P. 601.
- [20] M. Rohlfing. 2000. *Int. J. Quantum. Chem.* 80. P. 807.
- [21] J. C. Grossman, M. Rohlfing, L. Mitas, et al. 2001. *Phys. Rev. Lett.* 86. P. 472.
- [22] M. L. Tiago and J. R. Chelikowsky. 2005. *Solid State Commun.* 136. P. 333.
- [23] P. H. Hahn, W. G. Schmidt, and F. Bechstedt. 2005. *Phys. Rev. B.* 72. P. 245425.
- [24] M. L. Tiago and J. R. Chelikowsky. 2006. *Phys. Rev. B.* 73. P. 205334.
- [25] M. L. Tiago, P. R. C. Kent, R. Q. Hood, and F. A. Reboredo. 2008. *J. Chem. Phys.* 129. P. 84311.
- [26] M. Grüning, A. Marini, and X. Gonze. 2009. *Nano Lett.* 9. P. 2820.
- [27] Y. Ma, M. Rohlfing, and C. Molteni. 2009. *Phys. Rev. B.* 80. P. 241405.
- [28] Y. Ma, M. Rohlfing, and C. Molteni. 2010. *J. Chem. Theory Comput.* 6. P. 257.
- [29] D. Rocca, D. Lu, and G. Galli. 2010. *J. Chem. Phys.* 133. P. 164109.
- [30] M. Grüning, A. Marini, and X. Gonze. 2011. *Comput. Mater. Sci.* 50. P. 2148.
- [31] X. Blase and C. Attaccalite. 2011. *Appl. Phys. Lett.* 99. P. 171909.
- [32] C. Faber, P. Boulanger, I. Duchemin, et al. 2013. *J. Chem. Phys.* 139. P. 194308.
- [33] P. Boulanger and D. Jacquemin. 2014. *J. Chem. Theory Comput.*
- [34] C. Faber, P. Boulanger, C. Attaccalite, et al. 2014. *Philos. Trans. A. Math. Phys. Eng. Sci.* 372. P. 20130271.
- [35] P. Romaniello, D. Sangalli, J. A. Berger, et al. 2009. *J. Chem. Phys.* 130. P. 044108.
- [36] D. Sangalli, P. Romaniello, G. Onida, and A. Marini. 2011. *J. Chem. Phys.* 134. P. 34115.
- [37] D. Zhang, S. N. Steinmann, and W. Yang. 2013. *J. Chem. Phys.* 139. P. 154109.
- [38] F. Bruneval. “Exchange and Correlation in the Electronic Structure of Solids, from Silicon to Cuprous Oxide: GW Approximation and beyond”. PhD thesis. Ecole Polytechnique, 2005.
- [39] P. Martin and J. Schwinger. 1959. *Phys. Rev.* 139.
- [40] T. Kato, T. Kobayashi, and M. Namiki. 1960. *Prog. Theor. Phys. Suppl.* 15. Pp. 3–60.
- [41] R. D. Mattuck. *A guide to Feynman diagrams in the many-body problem*. Courier Dover Publications, 1976.
- [42] J. Toulouse, W. Zhu, J. G. Ángyán, and A. Savin. 2010. *Phys. Rev. A.* 82. P. 32502.
- [43] L. Hedin. 1965. *Phys. Rev.* 139. A796–A823.
- [44] L. Reining, V. Olevano, A. Rubio, and G. Onida. 2002. *Phys. Rev. Lett.* 88. P. 066404.

-
- [45] R. Del Sole, G. Adragna, V. Olevano, and L. Reining. 2003. *Phys. Rev. B.* 67. P. 045207.
- [46] F. Sottile, V. Olevano, and L. Reining. 2003. *Phys. Rev. Lett.* 91. P. 056402.
- [47] A. Marini, R. Del Sole, and A. Rubio. 2003. *Phys. Rev. Lett.* 91. P. 256402.
- [48] A. Marini, R. Del Sole, and A. Rubio. “Optical Properties of Solids and Nanostructures from a Many-Body”. In: *Lect. Notes Phys.* Vol. 706. Berlin, Heidelberg: Springer-Verlag, 2006, pp. 301–316.
- [49] A. Marini, R. Del Sole, and A. Rubio. “Approximate Functionals from Many-Body Perturbation Theory”. In: *Lect. Notes Phys.* Vol. 706. Berlin, Heidelberg: Springer-Verlag, 2006, pp. 161–180.
- [50] M. Tiago, J. Idrobo, S. Ögüt, et al. 2009. *Phys. Rev. B.* 79. P. 155419.
- [51] M. Hybertsen and S. Louie. 1985. *Phys. Rev. Lett.* 55. Pp. 1418–1421.
- [52] M. Hybertsen and S. Louie. 1986. *Phys. Rev. B.* 34. P. 5390.
- [53] F. Aryasetiawan and O. Gunnarsson. 1998. *Rep. Prog. Phys.* 61. P. 237.
- [54] W. G. Aulbur, L. Jönsson, and J. W. Wilkins. 1999. *Solid State Phys.* 54. Pp. 1–218.
- [55] E. L. Shirley and R. M. Martin. 1993. *Phys. Rev. B.* 47. P. 15404.
- [56] B. Holm and U. von Barth. 1998. *Phys. Rev. B.* 57. Pp. 2108–2117.
- [57] B. Holm and F. Aryasetiawan. 2000. *Phys. Rev. B.* 62. Pp. 4858–4865.
- [58] S. Faleev, M. V. Schilfgaard, and T. Kotani. 2004. *Phys. Rev. Lett.* 93. P. 126406.
- [59] T. Kotani, M. V. Schilfgaard, and S. Faleev. 2007. *Phys. Rev. B.* 76. P. 165106.
- [60] C. Rostgaard, K. W. Jacobsen, and K. S. Thygesen. 2010. *Phys. Rev. B.* 81. P. 085103.
- [61] M. Strange, C. Rostgaard, H. Häkkinen, and K. S. Thygesen. 2011. *Phys. Rev. B.* 83. P. 115108.
- [62] F. Caruso, P. Rinke, X. Ren, et al. 2012. *Phys. Rev. B.* 86. P. 081102.
- [63] M. Shishkin, M. Marsman, and G. Kresse. 2007. *Phys. Rev. Lett.* 99. P. 246403.
- [64] P. Romaniello, S. Guyot, and L. Reining. 2009. *J. Chem. Phys.* 131. P. 154111.
- [65] F. Aryasetiawan, R. Sakuma, and K. Karlsson. 2012. *Phys. Rev. B.* 85. P. 035106.
- [66] G. Onida, L. Reining, and R. Godby. 1995. *Phys. Rev. Lett.* 75. Pp. 818–821.
- [67] S. Albrecht, G. Onida, and L. Reining. 1997. *Phys. Rev. B.* 55. Pp. 278–281.
- [68] S. Albrecht, L. Reining, R. D. Sole, and G. Onida. 1998. *Phys. Rev. Lett.* 80. P. 4510.
- [69] S. Albrecht and L. Reining. 1998. *Phys. Status Solidi A.* 170. Pp. 189–198.
- [70] S. Faleev, M. van Schilfgaard, and T. Kotani. 2004. *Phys. Rev. Lett.* 93. P. 126406.

BIBLIOGRAPHY

- [71] M. van Schilfgaarde, T. Kotani, and S. Faleev. 2006. *Phys. Rev. Lett.* 96. P. 226402.
- [72] A. Stan, N. E. Dahlen, and R. van Leeuwen. 2006. *Europhys. Lett.* 76. P. 298.
- [73] J. Toulouse, W. Zhu, A. Savin, et al. 2011. *J. Chem. Phys.* 135. P. 84119.
- [74] J. G. Ángyán, R.-F. Liu, J. Toulouse, and G. Jansen. 2011. *J. Chem. Theory Comput.* 7. P. 3116.
- [75] M. J. S. Dewar and J. Kelemen. 1971. *J. Chem. Educ.* 48. P. 494.
- [76] F. Aryasetiawan, O. Gunnarsson, and A. Rubio. 2002. *Eur. Lett.* 57. P. 683.
- [77] T. Olsen and K. S. Thygesen. 2013.
- [78] S. Hirata and M. Head-Gordon. 1999. *Chem. Phys. Lett.* Pp. 375–382.
- [79] Z.-L. Cai and J. R. Reimers. 2000. *J. Chem. Phys.* 112. P. 527.
- [80] M. E. Casida, F. Gutierrez, J. Guan, et al. 2000. *J. Chem. Phys.* 113. P. 7062.
- [81] K. J. H. Giesbertz and E. J. Baerends. 2008. *Chem. Phys. Lett.* 461. P. 338.
- [82] N. Bickers and D. Scalapino. 1989. *Ann. Phys. (N. Y.)*. 193. Pp. 206–251.
- [83] N. Bickers, D. Scalapino, and S. White. 1989. *Phys. Rev. Lett.* 62. Pp. 961–964.
- [84] A. A. Abrikosov, L. P. Gorkov, and I. E. Dzialoshinskii. *Methods of quantum field theory in statistical physics*. 1963.
- [85] A. L. Fetter and J. D. Walecka. *Quantum Theory of Many-Particle Systems*. Dover, 1971.
- [86] A. Marini and R. Del Sole. 2003. *Phys. Rev. Lett.* 91. P. 176402.
- [87] G. Baym and L. Kadanoff. 1961. *Phys. Rev.* 124.
- [88] G. Baym. 1962. *Phys. Rev.* 127. P. 1391.
- [89] C. Moller and M. Plesset. 1934. *Phys. Rev.* 46. P. 618.
- [90] A. Szabo and N. Ostlund. *Modern quantum chemistry*. Mineola, New York: Dover Publications, 1989.
- [91] T. Helgaker, P. Jorgensen, and J. Olsen. *Molecular electronic-structure theory*. Chichester: Wiley, 2002.
- [92] J. Brand and L. Cederbaum. 1998. *Phys. Rev. A*. Pp. 1–16.
- [93] E. S. Nielsen, P. Jorgensen, and J. Oddershede. 1980. *J. Chem. Phys.* 73. P. 499.
- [94] M. J. Packer, E. K. Dalskov, T. Enevoldsen, et al. 1996. *J. Chem. Phys.* 105. P. 5886.
- [95] M. Huix-Rotllant. “Improved correlation kernels for linear-response time-dependent density-functional theory”. PhD thesis. 2011.
- [96] J. Wambach. 1988. *Reports Prog. Phys.* P. 989.
- [97] P. Löwdin. 1963. *J. Mol. Spectrosc.* 33. Pp. 12–33.

- [98] F. Bechstedt, K. Tenelsen, B. Adolph, and R. Del Sole. 1997. *Phys. Rev. Lett.* 78. Pp. 1528–1531.
- [99] H.-J. Werner, P. J. Knowles, G. Knizia, et al. *MOLPRO, version 2012.1, a package of ab initio programs*. Cardiff, UK, 2012.

General conclusion and perspectives

This thesis constitutes a contribution to the treatment of molecular excitation energies by range-separated methods. By separation of the electron-electron interaction into a short and a long-range part, these methods allow one to rigorously combine density-functional methods and wave-function or Green's function methods. They have been extensively studied in the ground-state case but are still the object of investigations for their application to excited-state calculations. The field of calculations of excitation energies from density functional theory is undeniably lead by linear-response time-dependent density-functional theory. However, it is not the only available option and many time-independent methods are also explored. In this thesis, range separation was applied both in the time-independent and the time-dependent case but not with the same end goal. In the zoo of methods which are nowadays available it is often difficult to find the origin of a deficiency as many approximations are done simultaneously, the first part of this thesis was therefore aimed at studying the effect of range separation on the excitation energies without further approximations. The second and third parts were in this way much more pragmatic as they were designed to tackle the problem of multiple excitations present in time-dependent density-functional theory within the adiabatic approximation. In this case, a local-density approximation was used for the density functional and a single-determinant approximation was performed for the wave function part and finally a long-range correlation kernel is added perturbatively.

Range-separated time-independent density-functional theory

The effects of the adiabatic approximation are difficult to assess in the time-dependent case. Moreover from the Hohenberg-Kohn theorem, the time-independent ground-state density is in principle able to describe all the properties of the system and in particular the excitation energies. We therefore first placed ourselves in the time-independent case where our goal was not to provide a pragmatic method to calculate excitation energies with range separation, at least not in the short term, but more to come back to the fundamentals with minimum approximations, and to do an analytic and numerical study on some small systems. In this study, the only approximation was the one-electron basis, so that hopefully with large enough basis sets, our observations could be attributed to range separation only. This was the object of the first part of this thesis where the excitation energies of a partially interacting system were followed along a range-separated adiabatic connection linking the non-interacting Kohn-Sham system to the physical system. The Taylor expansions of the energies around the two end points of this connection allowed us to propose an extrapolation scheme able to improve the description of the excitation energies of the physical system from an intermediate point of the connection. It also provided some exact conditions that an approximate potential should fulfill around these two limits. In particular, it allowed us to assess how much of the long-range interaction should be included in order to describe properly the excitation energies of the physical system. We are currently assessing how the local-density approximation

(LDA) and a single-determinant approximation as used in range-separated hybrid methods (RSH) affect these energies. We hope that this work could help the development of range-separated methods for excitation energies, either in the time-independent or in the time-dependent case.

Range-separated time-dependent density-functional theory

The second part of this thesis focused on the application of range separation to time-dependent density-functional theory (TDDFT) within the adiabatic local density approximation. When applied on the exchange part of the Hartree-exchange-correlation kernel (which should take into account all the effects coming from the electron-electron interaction), range separation has been proven to be very successful to overcome several flaws of TDDFT such as the description of Rydberg or charge-transfer excitation energies. However, until recently, the correlation kernel was left untouched so that multiple excitations were still missed by this approach. In the RSH approach where the wave function is approximated to a single Slater determinant, the long-range part of the correlation kernel vanishes. We thus derived the short-range LDA singlet and triplet kernels, implement them in the quantum chemistry software Molpro and analyze the effects of the removal of the long-range LDA correlation on the excitation energies of five small molecules and of the first charge-transfer excitation of a small dimer. It appeared that this removal has almost no effect on the energies so that the obtained energies provided a good starting point for the perturbative addition of a long-range correlation kernel. In order to design a long-range correlation kernel able to take into account the effect of double excitations, a frequency-dependent one is required. Such a kernel was then constructed in the last part of this thesis, using a Green's function approach.

Long-range second-order Bethe-Salpeter correlation kernel

In order to design a frequency-dependent correlation kernel, the Bethe-Salpeter approach used in condensed-matter physics seemed very promising as it provides an explicit frequency-dependent formalism which is very close to the TDDFT one. In the third part of this thesis, we thus undertook the construction of an effective second-order correlation kernel in this formalism. As the mapping between the physicist formalism for periodic systems to the chemist formalism for finite molecular systems was not straightforward, a first step consisted in transposing the Green's function formalism to a spin-orbital formulation and to assess the validity of the usual approximations performed in the condensed-matter physics community to our systems of interest. It appeared that in the framework of finite molecular system, the Hartree and exchange contributions should be treated together in the construction of the dielectric matrix and that the effect of the perturbation on the screened interaction should not be neglected contrary to what is done for solids. A second-order correlation Bethe-Salpeter kernel was then constructed and first tested in its static approximation. It appeared that in this case a non-physical

kernel was obtained and that a dynamic treatment was indeed required. This dynamical kernel required additional efforts in order to get an effective second-order kernel which could be added to the RSH kernel perturbatively. Throughout the derivation, the model system given by the dihydrogen molecule in a minimal basis was used to illustrate the main developments. In particular, the effect of the starting Green's function, of the inclusion of exchange, of the second-order approximation and of the static approximation were assessed on this model. The effective second-order correlation kernel was then implemented in a perturbative fashion within the Tamm-Dancoff approximation and tested on four small molecules with and without range separation. In these cases, when applied in a range-separated scheme, the excitation energies were overall improved by the addition of the perturbative long-range effective Bethe-Salpeter kernel. However in these systems, no excitation presented a significant double-excitation contribution which is the very case where the kernel is expected to play an important role.

Open issues

It is hard to put a final point to this thesis where there is still so much to understand and to do. In the following, I will try to summarize the perspectives which have been raised by this work and remain on my "TO DO" list.

Concerning the time-independent part, the usual approximations need to be reintroduced one by one in order to follow their effects on the excitation energies and on the ionization potential. We have seen in the case of the first-order perturbation theory that a poor description of the ionization potential could have dramatic effects on the excitation energies, such an effect is also expected with a local density approximation. The effect of a single-determinant approximation or the use of a truncated configuration interaction (CI) instead of the full CI are also to be explored. It could provide insights on the recently-proposed TD-MC-srDFT method which mixes TDDFT at short range and multi-configurational self-consistent field at long range for the calculation of excited states and could allow for further developments.

Concerning the second part of this thesis, the derivation and the implementation of the short-range LDA kernels has been done only in the closed-shell case and it should be of interest for many applications to have an open-shell code. Short-range GGA kernels would also be useful.

The last part of this thesis is probably the most frustrating one for me as so much remains to be done and I will attempt to make a list of what I would have wished to do if I had a fourth year...

- First of all, the second-order kernel needs to be tested more extensively, and on systems known to have double excitations in the lower part of their excitation spectrum.
- Next, a non-perturbative resolution based on a Löwdin "unfolding" would be nice, also without the Tamm-Dancoff approximation. Moreover, the code was designed

CONCLUSION

more in an exploratory perspective than in a efficient way. If the kernel is confirmed to be of interest, the module should be integrated to a “real” quantum chemistry program.

- Finally, the second-order truncation was done with respect to the electron-electron interaction but without taking into account the self-energy corrections which enter in the independent-particle response function and also contribute to the second order. We are currently working on this aspect. A first step would be to assess them on the model system given by H_2 in a minimal basis and then in the general case. This would be of particular interest to understand the link between the second-order polarization propagator approach and this work.

This list could probably be longer and I would like that some on these points will be solved in the short term either by me or my collaborators. I hope that this work will be of some use for future developments on similar projects.

Paris, 28th April 2014

List of publications

- *Electronic excitations from a linear-response range-separated hybrid scheme.*
Rebolini, E., Savin, A., and Toulouse, J.
Molecular Physics, 111, Pp. 1219–1234 (2013).
- *Electronic excitation energies of molecular systems from the Bethe-Salpeter equation: Example of the H₂ molecule.*
Rebolini, E., Toulouse, J., and Savin, A.
In S. K. Ghosh & P. K. Chattaraj (Eds.), Electronic Structure and Reactivity (p. 367). CRC Press. (2013).
- *Assessment of range-separated time-dependent density-functional theory for calculating C₆ dispersion coefficients.*
Toulouse, J., Rebolini, E., Gould, T., Dobson, J. F., Seal, P., and Ángyán, J. G.
Journal of Chemical Physics, 138, p.194106 (2013).
- *Décrire la structure électronique avec des fonctionnelles de la densité.*
Adamo, C., Rebolini, E., and Savin, A.
L'actualité chimique, 382-383, Pp. 22–28 (2014).
- *Excitation energies along a range-separated adiabatic connection.*
Rebolini, E., Toulouse, J., Teale, A. M., Helgaker, T., and Savin, A.
Journal of Chemical Physics, (2014) *submitted*
- *First-order corrected excitation energies along a range-separated adiabatic connection.*
Rebolini, E., Toulouse, J., Teale, A. M., Helgaker, T., and Savin, A.
in preparation
- *Extrapolated excitation energies along a range-separated and a linear adiabatic connection.*
Rebolini, E., Toulouse, J., Teale, A. M., Helgaker, T., and Savin, A.
in preparation
- *Electronic excitation energies of molecular systems from a dynamical range-separated second-order Bethe-Salpeter kernel.*
Rebolini, E., Toulouse, J., and Savin, A.
in preparation

Appendices

Appendix A

Mathematical tools

In this appendix, the main mathematical tools used throughout this thesis are defined. Especially, the main formulas of functional calculus are recalled together with the definition of the underlying Banach space. As many Fourier transforms are done between the time and frequency spaces, the conventions used for the Fourier transform together with the contour integration techniques in the framework of complex analysis are also briefly recalled in the following.

A.1 Functionals

Most of this thesis uses the mathematical concept of functional, either of the density, of the potential or of a Green's function. We therefore recall here the definition of a functional and of the underlying spaces which are encountered here.

Definition (Functional). A functional F is a function from a vector space V usually of functions into its underlying scalar field

$$F : f \mapsto F[f]. \tag{A.1}$$

A functional can be seen as a function of a function f and is denoted with bracket notations $F[f]$. It is the key quantity of functional analysis which studies complete normed vector spaces over the real or complex numbers, i.e. *Banach spaces*. In this thesis, two special kinds of Banach spaces are used:

- Hilbert spaces: where the norm arises from an inner product.
- L^p spaces: where the norm is an L^p -norm.

Definition (L^p -norm). Given a vector $\mathbf{r} = (r_1, r_2, \dots, r_n)$ in the n -dimensional real vector space \mathbb{R}^n , for a real number $p \geq 1$, the p -norm or L^p -norm of \mathbf{r} is

$$\|\mathbf{r}\|_p = (r_1^p + r_2^p + \dots + r_n^p)^{\frac{1}{p}} \quad (\text{A.2})$$

Throughout the different derivations present in this thesis, a few functional calculus rules are used and are given here: the functional derivative, the inverse and the chain rule.

Definition (Functional derivative). Given a Banach space M representing the set of functions f and a functional $F : M \mapsto \mathbb{R}$, the functional derivative (or Fréchet derivative) of F with respect to f , denoted $\frac{\delta F}{\delta f}$, is defined by

$$\delta F[f] = \int \frac{\delta F[f]}{\delta f(x)} \delta f(x) dx. \quad (\text{A.3})$$

If the change in f is localized, $\delta f(x) = \epsilon \delta(x - x_0)$, then a more conventional definition can be given

$$\frac{\delta F[f]}{\delta f(x_0)} = \lim_{\epsilon \rightarrow 0} \frac{F[f + \epsilon \delta(x - x_0)] - F[f]}{\epsilon}. \quad (\text{A.4})$$

In the case of a two-point quantity, one should note in particular that

$$\frac{\delta G(1, 2)}{\delta G(4, 3)} = \delta(1, 4) \delta(2, 3). \quad (\text{A.5})$$

As for usual functions, a chain rule can be defined for functional derivatives

$$\frac{\delta F[G[H]](1)}{\delta H(2)} = \int d3 \frac{\delta F[G](1)}{\delta G(3)} \frac{\delta G[H](3)}{\delta H(2)}. \quad (\text{A.6})$$

Another useful object in the framework of this thesis is the inverse of a two- and four-point functional. For a two-point functional, the inverse is defined by

$$\int d3 F(1, 3) F^{-1}(3, 2) = \int d3 F^{-1}(1, 3) F(3, 2) = \delta(1, 2), \quad (\text{A.7})$$

and its derivative is given by

$$\frac{\delta F(1, 2)}{\delta G(4, 3)} = - \int d5 d6 F(1, 5) \frac{\delta F^{-1}(5, 6)}{\delta G(4, 3)} G(6, 2). \quad (\text{A.8})$$

The inverse of a four-point functional is given by

$$\begin{aligned} \int d3 d3' H(1, 3; 1', 3') H^{-1}(3', 2; 3, 2') &= \int d3 d3' H^{-1}(1, 3; 1', 3') H(3', 2; 3, 2') \\ &= \delta(1, 2') \delta(2, 1'). \end{aligned} \quad (\text{A.9})$$

A.2 Fourier transform and complex analysis

A very brief review of complex analysis is given for the application of Fourier integral evaluation. More details can be found for instance in [1].

A.2.1 Conventions for Fourier transforms

We use the following convention for the Fourier transform of the function f

$$f(t) = \int \frac{d\omega}{2\pi} f(\omega) e^{-i\omega t}, \quad (\text{A.10})$$

which inverse transform is given by

$$f(\omega) = \int dt f(t) e^{i\omega t}. \quad (\text{A.11})$$

In particular, it is worth mentioning that the Fourier transform of the Heaviside step function is given by

$$\theta(\tau) = - \int \frac{d\omega}{2\pi i} \frac{e^{-i\omega\tau}}{\omega + i0^+} \quad \text{and} \quad \theta(-\tau) = \int \frac{d\omega}{2\pi i} \frac{e^{-i\omega\tau}}{\omega - i0^+}, \quad (\text{A.12})$$

A.2.2 Method of contour integral

A very powerful approach to evaluate the integral of complex functions is given by the contour integration technique in the framework of complex analysis. It is briefly recalled here for our particular case of interest. A few definitions are needed in order to establish the central theorem of this theory, the Cauchy's residue theorem.

Definition (Holomorphic function). Suppose Ω is a simply connected open subset of \mathbb{C} , the function $f : \Omega \rightarrow \mathbb{C}$ is holomorphic on Ω if it is complex differentiable on every point z_0 of Ω , i.e. the limit

$$f'(z_0) = \lim_{z \rightarrow z_0} \frac{f(z) - f(z_0)}{z - z_0}, \quad (\text{A.13})$$

exists for every z_0 in Ω .

Definition (Winding number). Suppose γ is a closed curve in Ω , the winding number of γ around a complex number a is

$$I_\gamma(a) = \frac{1}{2\pi i} \oint_\gamma \frac{dz}{z - a}. \quad (\text{A.14})$$

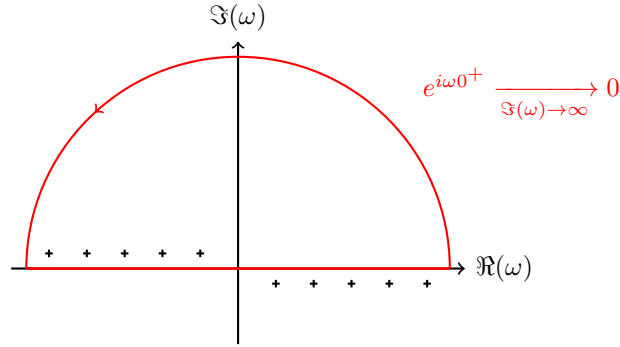


Figure A.1 – Contour integration on the upper half-plane.

Definition (Residue). Suppose a punctured disk $D = \{z | 0 < |z - c| < R\}$ in the complex plane is given and f is a holomorphic function defined on D . The residue $\text{Res}(f, c)$ of f at c is the coefficient a_{-1} of $(z - c)^{-1}$ in the Laurent series expansion of f around c .

We now have all the definitions needed to state the main theorem underlying this theory, the Cauchy's residue theorem.

Theorem 4 (Cauchy's residue theorem). Suppose Ω is a simply connected open subset of the complex plane, and a_1, \dots, a_n are finitely many points of Ω and f is a function which is defined and holomorphic on $\{\Omega \setminus \{a_1, \dots, a_n\}\}$. If γ is a closed curve in Ω which does not meet any of the a_k , and whose start point equals its endpoint, then

$$\oint_{\gamma} f(z) dz = 2\pi i \sum_{k=1}^n I_{\gamma}(a_k) \text{Res}(f, a_k). \quad (\text{A.15})$$

Application to Fourier integrals

The idea, when one wants to evaluate an integral on \mathbb{R} , is to take only a part of the integral on $[-R, R]$ and to close the path in the complex plane, usually by a half-circle, controlling that the additional part will not contribute to the integral. This is possible thanks to Jordan's lemma

Lemma. Jordan's Lemma. Suppose $f : \mathbb{C} \rightarrow \mathbb{C}$ is a continuous function on

$$\mathcal{S} = \{re^{i\theta}; t \geq 0; 0 \leq \theta_1 \leq \theta \leq \theta_2 \leq \pi\}, \quad (\text{A.16})$$

such that $\lim_{z \in \mathcal{S} \rightarrow \infty} f(z) = 0$. If we note $\gamma(r) = \{re^{i\theta}; \theta_1 \leq \theta \leq \theta_2\}$ then $\lim_{r \rightarrow \infty} \int_{\gamma(r)} f(z) e^{iz} dz = 0$.

To evaluate an integral

$$\mathcal{I} = \int f(x)e^{ikx} dx, \quad \text{with } k \in \mathbb{R}, \quad (\text{A.17})$$

the sign of k is important as the integral on the upper half-plane of $f(x)e^{ikz}$ goes to 0 when $r \rightarrow \infty$ only if the real part of ikz is negative. Therefore, if k is positive, the contour will be closed on the upper half-plane as shown in Figure A.1, and if k is negative, it will be closed on the lower half-plane, such that

$$\int f(x)e^{ikx} dx = \begin{cases} 2i\pi \sum_{\substack{a \text{ singularity} \\ \text{in the upper half-plane}}} \text{Res}(f(x)e^{ikx}, a) & \text{if } k > 0 \\ 2i\pi \sum_{\substack{a \text{ singularity} \\ \text{in the lower half-plane}}} \text{Res}(f(x)e^{ikx}, a) & \text{if } k < 0. \end{cases} \quad (\text{A.18})$$

A.3 Spherical mean

A last definition which is useful in the framework is the definition of the spherical mean given in the following:

Definition (Spherical mean). Consider an open set U in the Euclidean space \mathbb{R}_n and a continuous function u defined on U with real or complex values. Let x be a point in U and $r > 0$ be such that the closed ball $B(x, r)$ of center x and radius r is contained in U . The spherical mean over the sphere of radius r centered at x is defined as

$$\tilde{u}(x, r) = \frac{1}{\omega_{n-1}(r)} \int_{\partial B(x, r)} u(y) dS(y) \quad (\text{A.19})$$

where $\partial B(x, r)$ is the $(n - 1)$ -sphere forming the boundary of $B(x, r)$, dS denotes integration with respect to spherical measure and $\omega_{n-1}(r)$ is the “surface area” of this $(n - 1)$ -sphere.

Alternatively,

$$\tilde{u}(x, r) = \frac{1}{\omega_{n-1}} \int_{\|y\|=1} u(x + ry) dS(y) \quad (\text{A.20})$$

where $\omega_{n-1}(r) = \omega_{n-1} r^{n-1}$ is the area of the $(n - 1)$ -sphere of radius 1.

Appendix B

Taylor expansions of the range-separated energies

In this appendix, the details of the Taylor expansions of the Hartree-exchange-correlation potential, of the Hamiltonian, of the wave function and of the energies are given around the KS and the physical systems for the range-separated adiabatic connection. It is to be read together with Chapter 2.

B.1 Taylor expansions around the KS system

In the limit where the range-separation parameter μ goes to 0, the system is very close to the Kohn-Sham system. It is then convenient to develop its Hamiltonian around the Kohn-Sham Hamiltonian as

$$\begin{aligned}\hat{H}^{\text{lr},\mu} &= \hat{T} + \int v_{\text{ne}}(\mathbf{r})\hat{n}(\mathbf{r})d\mathbf{r} + \int \bar{v}_{\text{Hxc}}^{\text{sr},\mu}(\mathbf{r})\hat{n}(\mathbf{r})d\mathbf{r} + \frac{1}{2} \iint w_{\text{ee}}^{\text{lr},\mu}(r_{12})\hat{n}_2(\mathbf{r}_1, \mathbf{r}_2)d\mathbf{r}_1d\mathbf{r}_2 \\ &= \hat{H}^{\text{KS}} - \int v_{\text{Hxc}}^{\text{lr},\mu}(\mathbf{r})\hat{n}(\mathbf{r})d\mathbf{r} + \frac{1}{2} \iint w_{\text{ee}}^{\text{lr},\mu}(r_{12})\hat{n}_2(\mathbf{r}_1, \mathbf{r}_2)d\mathbf{r}_1d\mathbf{r}_2.\end{aligned}\tag{B.1}$$

The Maclaurin series of the long-range interaction around $\mu = 0$ is exactly known and is given by

$$\begin{aligned}w_{\text{ee}}^{\text{lr},\mu}(r) &= \frac{2}{\sqrt{\pi}} \sum_{n=0}^{\infty} \frac{(-1)^n}{n!(2n+1)} r^{2n} \mu^{2n+1} = \sum_{n=0}^{\infty} w_{\text{ee}}^{(2n+1)}(r) \mu^{2n+1} \\ &= \frac{2}{\sqrt{\pi}} \mu - \frac{2}{3\sqrt{\pi}} r^2 \mu^3 + \mathcal{O}(\mu^5).\end{aligned}\tag{B.2}$$

The Taylor expansion of the long-range interaction operator $\hat{W}_{\text{ee}}^{\text{lr},\mu}$ is therefore straightforward but the potential contribution needs to be evaluated.

By definition, the long-range Hartree-exchange-correlation potential is the functional

derivative of the corresponding ground-state energy functional with respect to the density. If calculated at N fixed, it is then defined up to an additive constant C^μ which is a constant with respect to \mathbf{r} but can depend on μ . The expressions of the long-range energy functionals are recalled in the following but can also be found in Refs. [2, 3].

B.1.1 Long-range Hartree-exchange-coorelation functionals

Long-range Hartree energy functional

The Hartree energy is given by

$$E_H[n] = \frac{1}{2} \iint \frac{n(\mathbf{r}_1)n(\mathbf{r}_2)}{r_{12}} d\mathbf{r}_1 d\mathbf{r}_2. \quad (\text{B.3})$$

The long-range Hartree energy functional is obtained by substituting the usual electron-electron interaction $1/r_{12}$ by its long-range counterpart $w_{ee}^{\text{lr},\mu}(r_{12})$. By doing so, and using the Taylor expansion of the interaction (B.2), we get

$$\begin{aligned} E_H^{\text{lr},\mu}[n] &= \frac{1}{2} \iint n(\mathbf{r}_1)n(\mathbf{r}_2)w_{ee}^{\text{lr},\mu}(r_{12})d\mathbf{r}_1 d\mathbf{r}_2 \\ &= \frac{1}{\sqrt{\pi}} \sum_{n=0}^{\infty} \frac{(-1)^n}{n!(2n+1)} \mu^{2n+1} \iint n(\mathbf{r}_1)n(\mathbf{r}_2)r_{12}^{2n} d\mathbf{r}_1 d\mathbf{r}_2 \\ &= \frac{N^2[n]}{\sqrt{\pi}} \mu - \frac{1}{3\sqrt{\pi}} \mu^3 \iint n(\mathbf{r}_1)n(\mathbf{r}_2)r_{12}^2 d\mathbf{r}_1 d\mathbf{r}_2 + \mathcal{O}(\mu^5). \end{aligned} \quad (\text{B.4})$$

Long-range exchange energy functional

The long-range exchange energy is given by

$$\begin{aligned} E_x^{\text{lr},\mu}[n] &= \frac{1}{2} \iint n_{2,x}(\mathbf{r}_1, \mathbf{r}_2)w_{ee}^{\text{lr},\mu}(r_{12})d\mathbf{r}_1 d\mathbf{r}_2 \\ &= \frac{1}{\sqrt{\pi}} \sum_{n=0}^{\infty} \frac{(-1)^n}{n!(2n+1)} \mu^{2n+1} \iint n_{2,x}(\mathbf{r}_1, \mathbf{r}_2)r_{12}^{2n} d\mathbf{r}_1 d\mathbf{r}_2 \\ &= \frac{1}{\sqrt{\pi}} \mu \iint n_{2,x}(\mathbf{r}_1, \mathbf{r}_2)d\mathbf{r}_1 d\mathbf{r}_2 - \frac{1}{3\sqrt{\pi}} \mu^3 \iint n_{2,x}(\mathbf{r}_1, \mathbf{r}_2)r_{12}^2 d\mathbf{r}_1 d\mathbf{r}_2 + \mathcal{O}(\mu^5). \end{aligned} \quad (\text{B.5})$$

Except for the one-electron case where $n_{2,x}(\mathbf{r}_1, \mathbf{r}_2) = -n(\mathbf{r}_1)n(\mathbf{r}_2)$ and the two-electron case where $n_{2,x}(\mathbf{r}_1, \mathbf{r}_2) = -n(\mathbf{r}_1)n(\mathbf{r}_2)/2$, the exchange pair density cannot be expressed as an explicit functional of n . Using the expression of the exchange pair density in terms of the exchange hole, the long-range exchange energy rewrites as

$$E_x^{\text{lr},\mu}[n] = \frac{1}{\sqrt{\pi}} \mu \int d\mathbf{r}_1 n(\mathbf{r}_1) \int d\mathbf{r}_2 h_x(\mathbf{r}_1, \mathbf{r}_2) - \frac{1}{3\sqrt{\pi}} \mu^3 \iint n_{2,x}(\mathbf{r}_1, \mathbf{r}_2)r_{12}^2 d\mathbf{r}_1 d\mathbf{r}_2 + \mathcal{O}(\mu^5) \quad (\text{B.6})$$

where $h_x(\mathbf{r}_1, \mathbf{r}_2)$ is the exchange hole which is normalized to -1 i.e. $\int d\mathbf{r}_2 h_x(\mathbf{r}_1, \mathbf{r}_2) = -1$. Using this normalization, the long-range exchange energy reduces to

$$E_x^{\text{lr},\mu}[n] = -\frac{N[n]}{\sqrt{\pi}}\mu - \frac{1}{3\sqrt{\pi}}\mu^3 \iint n_{2,x}(\mathbf{r}_1, \mathbf{r}_2)r_{12}^2 d\mathbf{r}_1 d\mathbf{r}_2 + \mathcal{O}(\mu^5). \quad (\text{B.7})$$

Long-range correlation energy functional

The long-range correlation energy requires integration along the adiabatic connection as the correlation part of the two-particle density $n_{2,c}$ depends on μ . It is therefore given by

$$E_c^{\text{lr},\mu}[n] = \frac{1}{2} \int_0^\mu \iint n_{2,c}^\xi(\mathbf{r}_1, \mathbf{r}_2) \frac{\partial w_{ee}^{\text{lr},\xi}(r_{12})}{\partial \xi} d\mathbf{r}_1 d\mathbf{r}_2 d\xi \quad (\text{B.8})$$

Considering that $n_{2,c}^\xi$ can be expanded around $\xi = 0$ as

$$n_{2,c}^\xi(\mathbf{r}_1, \mathbf{r}_2) = \sum_{k=1}^{\infty} \frac{1}{k!} \left. \frac{\partial^k n_{2,c}^\xi(\mathbf{r}_1, \mathbf{r}_2)}{\partial \xi^k} \right|_{\xi=0} \xi^k \quad (\text{B.9})$$

then the long-range correlation energy becomes

$$\begin{aligned} E_c^{\text{lr},\mu}[n] &= \frac{1}{\sqrt{\pi}} \sum_{n=1}^{\infty} \sum_{k=1}^{\infty} \frac{(-1)^n}{n!k!(2n+k+1)} \mu^{2n+k+1} \iint \left. \frac{\partial^k n_{2,c}^\mu(\mathbf{r}_1, \mathbf{r}_2)}{\partial \mu^k} \right|_{\mu=0} r_{12}^{2n} d\mathbf{r}_1 d\mathbf{r}_2 \\ &= 0 + \mathcal{O}(\mu^6) \end{aligned} \quad (\text{B.10})$$

in the case of a non-degenerate Kohn-Sham ground state, where the term at $n = 0$ is dropped because $\int n_{2,c}(\mathbf{r}_1, \mathbf{r}_2) d\mathbf{r}_1 d\mathbf{r}_2 = 0$ and the terms $k = 1, 2, 4$ are zero by identification in the Taylor expansion of the wave function as shown in [3].

B.1.2 Long-range Hartree-exchange-correlation potential

If the functional derivative of $E_{\text{Hxc}}^{\text{lr},\mu}[n]$ is taken with respect to density variations that preserve the number of electrons, $\int \delta n(\mathbf{r}) d\mathbf{r} = 0$, then $\delta N / \delta n = 0$. The derivative is then defined up to an additive (μ -dependent) constant C^μ . To first order in μ , the long-range electron-electron interaction tends to a constant, $2\mu/\sqrt{\pi}$. A distant electron (with $1 \ll r_{12} \ll 1/\mu$) then experiences a constant interaction $2(N-1)\mu/\sqrt{\pi}$ with the remaining $N-1$ other electrons. This constant must be exactly compensated by the long-range Hartree-exchange-correlation potential, so that its first-order term in μ must also be $2(N-1)\mu/\sqrt{\pi}$. The expansion of $v_{\text{Hxc}}^{\text{lr},\mu}(\mathbf{r})$ therefore takes the form

$$v_{\text{Hxc}}^{\text{lr},\mu}(\mathbf{r}) = \frac{2(N-1)\mu}{\sqrt{\pi}} + \mu^3 v_{\text{Hxc}}^{\text{lr},(3)}(\mathbf{r}) + \mathcal{O}(\mu^5), \quad (\text{B.11})$$

where $v_{\text{Hxc}}^{\text{lr},(3)}(\mathbf{r})$ is the third-order contribution. Note that the constant C^μ should also affect the third- and higher-contributions of the potential and develops as

$$C^\mu = C^{(1)}\mu + C^{(3)}\mu^3 + \dots \quad (\text{B.12})$$

B.1.3 Taylor expansion of the Hamiltonian

Substituting Equations (B.2), (B.11) in (B.1), we get the following Taylor expansion for the Hamiltonian around $\mu = 0$:

$$\begin{aligned} \hat{H}^{\text{lr},\mu} &= \hat{H}^{\text{KS}} + \frac{1}{2} \iint \left[\frac{2}{\sqrt{\pi}}\mu + w_{\text{ee}}^{\text{lr},(3)}(r_{12})\mu^3 \right] \hat{n}_2(\mathbf{r}_1, \mathbf{r}_2) d\mathbf{r}_1 d\mathbf{r}_2 \\ &\quad - \int \left[\frac{2(N-1)}{\sqrt{\pi}}\mu + v_{\text{Hxc}}^{\text{lr},(3)}(\mathbf{r})\mu^3 \right] \hat{n}(\mathbf{r}) d\mathbf{r} + \mathcal{O}(\mu^5) \\ &= \hat{H}^{\text{KS}} - \frac{N(N-1)}{\sqrt{\pi}}\mu + \mu^3 \left(\hat{W}_{\text{ee}}^{\text{lr},(3)} - \hat{V}_{\text{Hxc}}^{\text{lr},(3)} \right) + \mathcal{O}(\mu^5) \end{aligned} \quad (\text{B.13})$$

where

$$\hat{W}_{\text{ee}}^{\text{lr},(3)} = -\frac{1}{2} \iint \frac{2r_{12}^2}{3\sqrt{\pi}} \hat{n}_2(\mathbf{r}_1, \mathbf{r}_2) d\mathbf{r}_1 d\mathbf{r}_2. \quad (\text{B.14})$$

The linear correction in μ is a constant. Consequently it affects the energies but not the wave functions so their first correction is cubic in μ :

$$|\Psi_k^\mu\rangle = |\Phi_k^{\text{KS}}\rangle + |\Psi_k^{(3)}\rangle\mu^3 + \mathcal{O}(\mu^5). \quad (\text{B.15})$$

B.1.4 Taylor expansion of the energies

The energies corresponding to the state $|\Psi_k^\mu\rangle$ are by definition given by

$$\mathcal{E}_k^\mu = \frac{\langle \Psi_k^\mu | \hat{H}^{\text{lr},\mu} | \Psi_k^\mu \rangle}{\langle \Psi_k^\mu | \Psi_k^\mu \rangle} \quad (\text{B.16})$$

where the numerator is

$$\begin{aligned} \langle \Psi_k^\mu | \hat{H}^{\text{lr},\mu} | \Psi_k^\mu \rangle &= \mathcal{E}_k^{\text{KS}} - \frac{N(N-1)}{\sqrt{\pi}}\mu \\ &\quad + \mu^3 \left(2\mathcal{E}_k^{\text{KS}} \langle \Psi_k^{(3)} | \Phi_k^{\text{KS}} \rangle + \langle \Phi_k^{\text{KS}} | \hat{W}_{\text{ee}}^{\text{lr},(3)} - \hat{V}_{\text{Hxc}}^{\text{lr},(3)} | \Phi_k^{\text{KS}} \rangle \right) + \mathcal{O}(\mu^5) \end{aligned} \quad (\text{B.17})$$

and the denominator is $\langle \Psi_k^\mu | \Psi_k^\mu \rangle = 1 + 2\mu^3 \langle \Psi_k^{(3)} | \Phi_k^{\text{KS}} \rangle + \mathcal{O}(\mu^5)$. Therefore, the Taylor expansions of the energies around $\mu = 0$ are

$$\mathcal{E}_k^\mu = \mathcal{E}_k^{\text{KS}} - \frac{N(N-1)}{\sqrt{\pi}}\mu + \mu^3 \langle \Phi_k^{\text{KS}} | \hat{W}_{\text{ee}}^{\text{lr},(3)} - \hat{V}_{\text{Hxc}}^{\text{lr},(3)} | \Phi_k^{\text{KS}} \rangle + \mathcal{O}(\mu^5). \quad (\text{B.18})$$

In Equation (B.18), the linear correction is state-independent and depends only of the number of electrons of the system. Therefore in the excitation energies, this term cancels

out and only the correction in μ^3 remains.

$$\mathcal{E}_k^\mu - \mathcal{E}_0^\mu = \mu^3 \left[\langle \Phi_k^{\text{KS}} | \hat{W}_{\text{ee}}^{\text{lr},(3)} - \hat{V}_{\text{Hxc}}^{\text{lr},(3)} | \Phi_k^{\text{KS}} \rangle - \langle \Phi_0^{\text{KS}} | \hat{W}_{\text{ee}}^{\text{lr},(3)} - \hat{V}_{\text{Hxc}}^{\text{lr},(3)} | \Phi_0^{\text{KS}} \rangle \right] + \mathcal{O}(\mu^4). \quad (\text{B.19})$$

This correction can be divided into a one-electron and a two-electron part where the one-electron contribution is given by $\langle \Phi_k^{\text{KS}} | \hat{V}_{\text{Hxc}}^{\text{lr},(3)} | \Phi_k^{\text{KS}} \rangle$ and the two-electron contribution is given by

$$\langle \Phi_k^{\text{KS}} | \hat{W}_{\text{ee}}^{\text{lr},(3)} | \Phi_k^{\text{KS}} \rangle = -\frac{1}{3\sqrt{\pi}} \langle \Phi_k^{\text{KS}} | \iint \hat{n}_2(\mathbf{r}_1, \mathbf{r}_2) r_{12}^2 d\mathbf{r}_1 d\mathbf{r}_2 | \Phi_k^{\text{KS}} \rangle. \quad (\text{B.20})$$

Moreover, using the definition of the pair density operator $\hat{n}_2(\mathbf{r}_1, \mathbf{r}_2) = \hat{n}(\mathbf{r}_1)\hat{n}(\mathbf{r}_2) - \hat{n}(\mathbf{r}_1)\delta(\mathbf{r}_1 - \mathbf{r}_2)$, the latter rewrites as

$$\begin{aligned} \langle \Phi_k^{\text{KS}} | \hat{W}_{\text{ee}}^{\text{lr},(3)} | \Phi_k^{\text{KS}} \rangle &= -\frac{1}{3\sqrt{\pi}} \langle \Phi_k^{\text{KS}} | \iint \hat{n}(\mathbf{r}_1)\hat{n}(\mathbf{r}_2) r_{12}^2 d\mathbf{r}_1 d\mathbf{r}_2 | \Phi_k^{\text{KS}} \rangle \\ &\quad + \frac{1}{3\sqrt{\pi}} \langle \Phi_k^{\text{KS}} | \iint \hat{n}(\mathbf{r}_1)\delta(\mathbf{r}_1 - \mathbf{r}_2) r_{12}^2 d\mathbf{r}_1 d\mathbf{r}_2 | \Phi_k^{\text{KS}} \rangle \\ &= -\frac{1}{3\sqrt{\pi}} \langle \Phi_k^{\text{KS}} | \iint \hat{n}(\mathbf{r}_1)\hat{n}(\mathbf{r}_2) r_{12}^2 d\mathbf{r}_1 d\mathbf{r}_2 | \Phi_k^{\text{KS}} \rangle. \end{aligned} \quad (\text{B.21})$$

Using the scalar product of \mathbf{r}_1 and \mathbf{r}_2 , r_{12}^2 can be rewritten as $r_{12}^2 = r_1^2 + r_2^2 - 2\mathbf{r}_1 \cdot \mathbf{r}_2$

$$\begin{aligned} \langle \Phi_k^{\text{KS}} | \hat{W}_{\text{ee}}^{\text{lr},(3)} | \Phi_k^{\text{KS}} \rangle &= -\frac{1}{3\sqrt{\pi}} \langle \Phi_k^{\text{KS}} | \iint \hat{n}(\mathbf{r}_1)\hat{n}(\mathbf{r}_2)(r_1^2 + r_2^2) d\mathbf{r}_1 d\mathbf{r}_2 | \Phi_k^{\text{KS}} \rangle \\ &\quad + \frac{2}{3\sqrt{\pi}} \langle \Phi_k^{\text{KS}} | \iint \hat{n}(\mathbf{r}_1)\hat{n}(\mathbf{r}_2)\mathbf{r}_1 \cdot \mathbf{r}_2 d\mathbf{r}_1 d\mathbf{r}_2 | \Phi_k^{\text{KS}} \rangle \\ &= -\frac{2N}{3\sqrt{\pi}} \int n_k(\mathbf{r}) r^2 d\mathbf{r} + \frac{2}{3\sqrt{\pi}} \langle \Phi_k^{\text{KS}} | \int \hat{n}(\mathbf{r}_1) \mathbf{r}_1 d\mathbf{r}_1 \cdot \int \hat{n}(\mathbf{r}_2) \mathbf{r}_2 d\mathbf{r}_2 | \Phi_k^{\text{KS}} \rangle \\ &= -\frac{2N}{3\sqrt{\pi}} \int n_k(\mathbf{r}) r^2 d\mathbf{r} + \frac{2}{3\sqrt{\pi}} \sum_j \left| \langle \Phi_k^{\text{KS}} | \int \hat{n}(\mathbf{r}) \mathbf{r} d\mathbf{r} | \Phi_j^{\text{KS}} \rangle \right|^2, \end{aligned} \quad (\text{B.22})$$

where n_k is the density of the KS state $|\Phi_k^{\text{KS}}\rangle$ and where the resolution of identity has been used in the last line.

Taylor expansion of the singlet-triplet splitting

For closed shells, the expansion of the difference between the singlet and triplet energies associated with the single excitation $i \rightarrow a$ can be obtained by applying Equation (B.18) with the spin-adapted KS wave functions ${}^1\Phi^{\text{KS}} = (\Phi_{i \rightarrow a}^{\text{KS}} + \Phi_{i \rightarrow \bar{a}}^{\text{KS}})/\sqrt{2}$, for the singlet state, and ${}^3,1\Phi^{\text{KS}} = \Phi_{i \rightarrow a}^{\text{KS}}$, for the triplet state with spin projection $M_S = 1$. As all the determinants are constructed on the some KS orbitals, the one-electron contribution vanishes and only the two-electron term then contributes:

$$\Delta\mathcal{E}_{i \rightarrow a}^{\mu,1-3} = \mu^3 \left[\langle {}^1\Phi^{\text{KS}} | \hat{W}_{\text{ee}}^{\text{lr},(3)} | {}^1\Phi^{\text{KS}} \rangle - \langle {}^3\Phi^{\text{KS}} | \hat{W}_{\text{ee}}^{\text{lr},(3)} | {}^3\Phi^{\text{KS}} \rangle \right] + \mathcal{O}(\mu^5). \quad (\text{B.23})$$

ε_a	\uparrow	\uparrow	\downarrow	\downarrow
ε_i	\uparrow	\downarrow	\uparrow	\downarrow
M_s	1	0	0	-1
	$\Phi_{i \rightarrow a}^{\text{KS}}$	$\Phi_{i \rightarrow \bar{a}}^{\text{KS}}$	$\Phi_{i \rightarrow a}^{\text{KS}}$	$\Phi_{i \rightarrow \bar{a}}^{\text{KS}}$

Figure B.1 – Spin configurations for the single excitation $i \rightarrow a$ starting from the Kohn-Sham ground-state.

which then gives

$$\begin{aligned}
 \Delta \mathcal{E}_{i \rightarrow a}^{\mu, 1-3} &= 2\mu^3 \langle ia | \hat{w}_{\text{ee}}^{\text{lr}, (3)} | ai \rangle + \mathcal{O}(\mu^5) \\
 &= \frac{8\mu^3}{3\sqrt{\pi}} |\langle i | \hat{\mathbf{r}} | a \rangle|^2 + \mathcal{O}(\mu^5),
 \end{aligned} \tag{B.24}$$

where we have used $r_{12}^2 = r_1^2 + r_2^2 - 2\mathbf{r}_1 \cdot \mathbf{r}_2$. The appearance of the transition dipole moment integral in Equation (B.24) means that, for an atomic system, the singlet-triplet energy splitting appears at third order in μ if the difference between the angular moment of the orbitals φ_i and φ_a is $\Delta\ell = +1$ or -1 . Otherwise, the splitting appears at a higher order in μ .

B.2 Taylor expansions near the real system

The Taylor expansion of the short-range interaction when $\mu \rightarrow \infty$ is given by [2]:

$$\begin{aligned}
 w_{\text{ee}}^{\text{sr}, \mu}(\mathbf{r}) &= 4\sqrt{\pi} \sum_{n=0}^m \frac{(-1)^n \Gamma\left(\frac{n+3}{2}\right)}{n!(n+2)\mu^{n+2}} \delta^{(n)}(\mathbf{r}) + \mathcal{O}\left(\frac{1}{\mu^{m+3}}\right) \\
 &= \frac{\pi}{\mu^2} \delta(\mathbf{r}) - \frac{4\sqrt{\pi}}{3\mu^3} \delta^{(1)}(\mathbf{r}) + \frac{3\pi}{8\mu^4} \delta^{(2)}(\mathbf{r}) + \mathcal{O}\left(\frac{1}{\mu^5}\right)
 \end{aligned} \tag{B.25}$$

B.2.1 Derivative of the short-range Hartree functional

With the definition of the spherical mean given in Appendix A.3, the spherical average of the density around \mathbf{r}_1 on the sphere of radius r_{12} is

$$\tilde{n}(\mathbf{r}_1, r_{12}) = \frac{1}{4\pi} \iint n(\mathbf{r}_1 + r_{12}\mathbf{y}) dS(\mathbf{y}). \tag{B.26}$$

Using this and the change of variable $\mathbf{r}_2 \rightarrow \mathbf{r}_{12}$, the short-range Hartree energy becomes

$$\begin{aligned}
 E_{\text{H}}^{\text{sr}, \mu}[n] &= \frac{1}{2} \iint n(\mathbf{r}_1) n(\mathbf{r}_2) w_{\text{ee}}^{\text{sr}, \mu}(r_{12}) d\mathbf{r}_1 d\mathbf{r}_2 \\
 &= \frac{1}{2} \iint 4\pi r_{12}^2 n(\mathbf{r}_1) \tilde{n}(\mathbf{r}_1, r_{12}) w_{\text{ee}}^{\text{sr}, \mu}(r_{12}) d\mathbf{r}_1 dr_{12}.
 \end{aligned} \tag{B.27}$$

and its Taylor expansion when $\mu \rightarrow \infty$ is then

$$E_{\text{H}}^{\text{sr},\mu}[n] = 2\sqrt{\pi} \sum_{n=0}^m \frac{(-1)^n \Gamma\left(\frac{n+3}{2}\right)}{n!(n+2)\mu^{n+2}} \iint \delta^{(n)}(\mathbf{r}_{12}) n(\mathbf{r}_1) \tilde{n}(\mathbf{r}_1, r_{12}) d\mathbf{r}_1 dr_{12} + \mathcal{O}\left(\frac{1}{\mu^{m+3}}\right) \quad (\text{B.28})$$

Moreover, for a \mathcal{C}^∞ function f , using successive integrations by parts, one can show

$$\int f(r) \delta^{(n)}(\mathbf{r}) d\mathbf{r} = (-1)^n f^{(n)}(0). \quad (\text{B.29})$$

The Taylor expansion of the spherical average of the density around $r_{12} = 0$ is given by

$$\tilde{n}(\mathbf{r}_1, r_{12}) = \left(1 + \frac{1}{3!} r_{12}^2 \nabla_{r_{12}}^2 + \frac{1}{5!} r_{12}^4 \nabla_{r_{12}}^4 + \dots\right) n(\mathbf{r}_1 + \mathbf{r}_{12})|_{r_{12}=0} \quad (\text{B.30})$$

Using this relation and the fact that, the spherical mean of the density only develops in even power of r_{12} around $r_{12} = 0$,

$$E_{\text{H}}^{\text{sr},\mu}[n] = 2\sqrt{\pi} \sum_{n=0}^m \frac{\Gamma\left(\frac{2n+3}{2}\right)}{(2n)!(2n+2)\mu^{2n+2}} \int \tilde{n}^{(2n)}(\mathbf{r}_1, 0) n(\mathbf{r}_1) d\mathbf{r}_1 + \mathcal{O}\left(\frac{1}{\mu^{2m+4}}\right) \quad (\text{B.31})$$

where

$$\tilde{n}^{(2n)}(\mathbf{r}_1, 0) = \left(\frac{\partial^{2n} \tilde{n}(\mathbf{r}_1, r_{12})}{\partial r_{12}^{2n}}\right)_{r_{12}=0}, \quad (\text{B.32})$$

and in particular, $\tilde{n}^{(0)}(\mathbf{r}_1, 0) = n(\mathbf{r}_1)$. The Taylor expansion of the short-range Hartree energy is therefore

$$\begin{aligned} E_{\text{H}}^{\text{sr},\mu}[n] &= \frac{\sqrt{\pi}}{\mu^2} \Gamma\left(\frac{3}{2}\right) \int n(\mathbf{r})^2 d\mathbf{r} + \mathcal{O}\left(\frac{1}{\mu^4}\right) \\ &= \frac{\pi}{2\mu^2} \int n(\mathbf{r})^2 d\mathbf{r} + \mathcal{O}\left(\frac{1}{\mu^4}\right) \end{aligned} \quad (\text{B.33})$$

and is an explicit functional of n . The Taylor expansion of the short-range Hartree potential is thus

$$v_{\text{H}}^{\text{sr},\mu}[n](\mathbf{r}) = \frac{\pi}{\mu^2} n(\mathbf{r}) + \mathcal{O}\left(\frac{1}{\mu^4}\right). \quad (\text{B.34})$$

B.2.2 Derivative of the short-range exchange functional

With the same method, for the exchange energy,

$$\begin{aligned} E_{\text{x}}^{\text{sr},\mu}[n] &= \frac{1}{2} \iint \tilde{n}_{2,x}(\mathbf{r}_1, r_{12}) w_{\text{ee}}^{\text{sr},\mu}(r_{12}) d\mathbf{r}_1 dr_{12} \\ &= 2\sqrt{\pi} \sum_{n=0}^m \frac{\Gamma\left(\frac{2n+3}{2}\right)}{(2n)!(2n+2)\mu^{2n+2}} \iint n_{2,x}^{(2n)}(\mathbf{r}, \mathbf{r}) d\mathbf{r} + \mathcal{O}\left(\frac{1}{\mu^{2m+4}}\right), \end{aligned} \quad (\text{B.35})$$

where $n_{2,x}(\mathbf{r}, \mathbf{r})$ is the exchange on-top pair density, given by $-\sum_{\sigma} n_{\sigma}^2(\mathbf{r})$. The short-range energy is then:

$$E_x^{\text{sr},\mu}[n] = \frac{\pi}{2\mu^2} \int n_{2,x}(\mathbf{r}, \mathbf{r}) d\mathbf{r} + \mathcal{O}\left(\frac{1}{\mu^4}\right). \quad (\text{B.36})$$

The Taylor expansion of the short-range exchange potential is then

$$v_x^{\text{sr},\mu}[n](\mathbf{r}) = \frac{\pi}{2\mu^2} \int \frac{\delta n_{2,x}(\mathbf{r}', \mathbf{r}')}{\delta n(\mathbf{r})} d\mathbf{r}' + \mathcal{O}\left(\frac{1}{\mu^4}\right). \quad (\text{B.37})$$

B.2.3 Derivative of the short-range correlation functional

By definition, the short-range correlation energy functional is obtained by

$$\begin{aligned} \bar{E}_c^{\text{sr},\mu}[n] &= -\frac{1}{2} \int_{\mu}^{\infty} d\xi \iint n_{2,c}^{\xi}(\mathbf{r}_1, \mathbf{r}_2) \partial_{\xi} w_{ee}^{\text{sr},\xi}(r_{12}) d\mathbf{r}_1 d\mathbf{r}_2 \\ &= -\int_{\mu}^{\infty} d\xi \frac{\partial}{\partial \xi} \bar{E}_c^{\text{sr},\xi}[n]. \end{aligned} \quad (\text{B.38})$$

The derivative of the long-range correlation energy with respect to ξ is given by

$$\begin{aligned} \frac{\partial}{\partial \xi} \bar{E}_c^{\text{sr},\xi}[n] &= \frac{1}{2} \iint n_{2,c}^{\xi}(\mathbf{r}_1, \mathbf{r}_2) \frac{\partial w_{ee}^{\text{sr},\mu}(r_{12})}{\partial \xi} d\mathbf{r}_1 d\mathbf{r}_2 \\ &= -\frac{1}{\sqrt{\pi}} \iint 4\pi r_{12}^2 \tilde{n}_{2,c}^{\xi}(\mathbf{r}_1, r_{12}) e^{-\xi^2 r_{12}^2} d\mathbf{r}_1 dr_{12} \end{aligned} \quad (\text{B.39})$$

where $\tilde{n}_{2,c}^{\xi}$ is the spherically-averaged correlation pair density and where the derivative of the short-range interaction with respect to ξ was taken as:

$$\frac{\partial w_{ee}^{\text{sr},\xi}(r_{12})}{\partial \xi} = -\frac{2}{\sqrt{\pi}} e^{-\xi^2 r_{12}^2}. \quad (\text{B.40})$$

However, if one uses directly the asymptotic expansion of the exponential in Equation (B.39), each term of the serie diverges. Therefore, the integration and the summation cannot be swapped [4]. We define the system-averaged pair density

$$f^{\xi}(r_{12}) = \int \tilde{n}_{2,c}^{\xi}(\mathbf{r}_1, r_{12}) d\mathbf{r}_1 \quad (\text{B.41})$$

and its correlated part $f_c^{\xi}(r_{12}) = f^{\xi}(r_{12}) - f^{\text{KS}}(r_{12})$. From the cusp condition at the coalescence, Gori-Giorgi *et al* [4] showed that the system-averaged pair density for the modified interaction should behave as

$$f^{\xi}(r_{12}) = f(0) \left(1 + 2r_{12} p_1(\xi r_{12}) + \frac{2}{\sqrt{\pi}\xi} \right) \quad (\text{B.42})$$

and that the wave-function of the system expands as

$$\Psi_i^\mu(r_{12}) = \Psi_i(0) \left[1 + r_{12}p_1(\mu r_{12}) + \frac{1}{\sqrt{\pi\mu}} + \dots \right] \quad (\text{B.43})$$

where $f(0)$ is the system-averaged on-top pair density and where the function p_1 is given by

$$p_1(y) = \frac{e^{-y^2} - 2}{2\sqrt{\pi}y} + \left(\frac{1}{2} + \frac{1}{4y^2} \right) \text{erf}(y). \quad (\text{B.44})$$

By integration over r_{12} in Equation (B.39) where Equation (B.42) has been used, the first terms of the Taylor expansion of the derivative of the short-range correlation energy with respect to ξ are given by

$$\frac{\partial}{\partial \xi} \bar{E}_c^{\text{sr},\xi}[n] = -\pi \frac{f_c(0)}{\xi^3} - 2\sqrt{2\pi} \frac{f(0)}{\xi^4} + \mathcal{O}\left(\frac{1}{\xi^5}\right). \quad (\text{B.45})$$

By integration along the adiabatic connection, the Taylor expansion of the short-range correlation energy is thus

$$\begin{aligned} \bar{E}_c^{\text{sr},\mu}[n] &= \pi \frac{f_c(0)}{2\mu^2} + 2\sqrt{2\pi} \frac{f(0)}{3\mu^3} + \mathcal{O}\left(\frac{1}{\mu^4}\right) \\ &= \frac{\pi}{2\mu^2} \int n_{2,c}(\mathbf{r}, \mathbf{r}) d\mathbf{r} + \frac{2\sqrt{2\pi}}{3\mu^3} \int n_2(\mathbf{r}, \mathbf{r}) d\mathbf{r} + \mathcal{O}\left(\frac{1}{\mu^4}\right). \end{aligned} \quad (\text{B.46})$$

The corresponding potential is therefore

$$\bar{v}_c^{\text{sr},\mu}[n](\mathbf{r}) = \frac{\pi}{2\mu^2} \int \frac{\delta n_{2,c}(\mathbf{r}', \mathbf{r}')}{\delta n(\mathbf{r})} d\mathbf{r}' + \frac{2\sqrt{2\pi}}{3\mu^3} \int \frac{\delta n_2(\mathbf{r}', \mathbf{r}')}{\delta n(\mathbf{r})} d\mathbf{r}' + \mathcal{O}\left(\frac{1}{\mu^4}\right). \quad (\text{B.47})$$

Finally, the Taylor expansion of the short-range Hartree-exchange-correlation potential near the real system is given by

$$\bar{v}_{\text{Hxc}}^{\text{sr},\mu}[n](\mathbf{r}) = \frac{\pi}{2\mu^2} \int \frac{\delta n_2(\mathbf{r}', \mathbf{r}')}{\delta n(\mathbf{r})} d\mathbf{r}' + \frac{2\sqrt{2\pi}}{3\mu^3} \int \frac{\delta n_2(\mathbf{r}', \mathbf{r}')}{\delta n(\mathbf{r})} d\mathbf{r}' + \mathcal{O}\left(\frac{1}{\mu^4}\right). \quad (\text{B.48})$$

B.2.4 Taylor expansion of the Hamiltonian:

By substituting Equations (B.25) and (B.48) into the expression of the Hamiltonian, it becomes

$$\begin{aligned} \hat{H}^{\text{lr},\mu} &= \hat{H} - \iint \left[\frac{\pi}{2\mu^2} \delta(\mathbf{r}_{12}) - \frac{2\sqrt{\pi}}{3\mu^3} \delta^{(1)}(\mathbf{r}_{12}) \right] \hat{n}_2(\mathbf{r}_1, \mathbf{r}_2) d\mathbf{r}_1 d\mathbf{r}_2 \\ &\quad + \left[\frac{\pi}{2\mu^2} + \frac{2\sqrt{2\pi}}{3\mu^3} \right] \iint \frac{\delta n_2(\mathbf{r}', \mathbf{r}')}{\delta n(\mathbf{r})} \hat{n}(\mathbf{r}) d\mathbf{r} d\mathbf{r}' + \mathcal{O}\left(\frac{1}{\mu^4}\right) \\ &= \hat{H} + \frac{1}{\mu^2} \hat{H}^{(-2)} + \mathcal{O}\left(\frac{1}{\mu^3}\right) \end{aligned} \quad (\text{B.49})$$

B.2.5 Taylor expansion of the energies

In order to evaluate the energies, we divide the integration over r_{12} into two regions, one going from 0 to $1/\mu$ and one going from $1/\mu$ to ∞ . In the first region, the Taylor expansion of $\Psi_k^\mu(r_{12})w_{ee}^{\text{lr},\mu}(r_{12})\Psi_k^\mu(r_{12})$ around $r_{12} = 0$ is given by

$$\Psi_k^\mu(r_{12})w_{ee}^{\text{lr},\mu}(r_{12})\Psi_k^\mu(r_{12}) = \Psi_k(0)^2 \left(\frac{2\mu}{\sqrt{\pi}} + \frac{2}{\pi^{3/2}\mu} + \frac{4}{\pi} \right) + \mathcal{O}(r_{12}) \quad (\text{B.50})$$

and a contribution in $1/\mu$ is present. However, when integrated, it is multiplied by the volume element which goes to 0 when μ goes to ∞ and will not contribute in the energies. In the second region, $r_{12} > 1/\mu$ so the Taylor expansion of $\Psi_k^\mu(r_{12})w_{ee}^{\text{lr},\mu}(r_{12})\Psi_k^\mu(r_{12})$ around $\mu \rightarrow \infty$ is given by

$$\Psi_k^\mu(r_{12})w_{ee}^{\text{lr},\mu}(r_{12})\Psi_k^\mu(r_{12}) = \Psi_k(0)^2 \left(1 + \frac{1}{r_{12}} + \frac{1}{4}r_{12} + \frac{1}{2\mu^2 r_{12}^2} + \frac{1}{4\mu^2 r_{12}} \right) + \mathcal{O}\left(\frac{1}{\mu^3}\right) \quad (\text{B.51})$$

where the first contribution appears in $1/\mu^2$. Therefore, the Taylor expansion of the energies around the real system is given by

$$\mathcal{E}_k^\mu = E_k + \frac{1}{\mu^2}E_k^{(-2)} + \mathcal{O}\left(\frac{1}{\mu^3}\right) \quad (\text{B.52})$$

Appendix C

Fit of the energies along the adiabatic connection

In this appendix, the details of the fit performed on the energies along the range-separated adiabatic connection are given. The fitted parameters obtained for the helium and beryllium atoms and for the dihydrogen molecule at equilibrium and stretched geometries are also given. It is to be read together with Chapter 2 and Chapter 4 as the first-order derivative of the energies with respect to the range-separation parameter are calculated analytically from the form of the fit.

C.1 Form of the fit

The total energies \mathcal{E}_k^μ and excitation energies $\Delta\mathcal{E}_k^\mu = \mathcal{E}_k^\mu - \mathcal{E}_0^\mu$ of the partially-interacting Hamiltonian given in Equation (2.5) have been calculated with the DALTON program as a function of the range-separation parameter μ for the helium and beryllium atoms and for the dihydrogen molecule. The computational details can be found in Section 2.4. The total ground-state energies were then fitted to the following analytical expression which satisfies the form of the expansions at small μ and large μ given in Equations (2.27) and (2.39)

$$\mathcal{E}_0^\mu = E_0 + \frac{\mathcal{E}_0^{\text{KS}} - E_0 + c_1\mu + c_2\mu^2 + c_3\mu^3}{1 + d_1\mu + d_2\mu^2 + d_3\mu^3 + d_4\mu^4 + d_5\mu^5},$$

where $c_1 = -N(N-1)/\sqrt{\pi} + (\mathcal{E}_0^{\text{KS}} - E_0)d_1$ and $c_2 = -N(N-1)d_1/\sqrt{\pi} + (\mathcal{E}_0^{\text{KS}} - E_0)d_2$ are fixed by the small- μ expansion, E_0 and $\mathcal{E}_0^{\text{KS}}$ give the ground-state total energies of the physical system and of the Kohn-Sham (KS) system, and N is the number of electrons. The excitation energies were fitted to the expression

$$\Delta\mathcal{E}_k^\mu = \Delta E_k + \frac{\Delta\mathcal{E}_k^{\text{KS}} - \Delta E_k + c_1\mu + c_2\mu^2 + c_3\mu^3}{1 + d_1\mu + d_2\mu^2 + d_3\mu^3 + d_4\mu^4 + d_5\mu^5},$$

where $c_1 = d_1(\Delta\mathcal{E}_k^{\text{KS}} - \Delta E_k)$ and $c_2 = d_2(\Delta\mathcal{E}_k^{\text{KS}} - \Delta E_k)$ to ensure the correct behavior at small μ , and ΔE_k and $\Delta\mathcal{E}_k^{\text{KS}}$ give the excitation energies of the physical system and of the KS system.

C.2 Fitted parameters

The fits were performed on about 30 points for a range of μ going from 0 to 10 bohr⁻¹. The parameters of the fit can be found in Tables C.1, C.2, C.3 and C.4, and reproduce the calculated curves shown in the article with a maximum error of about 0.1 mhartree. All the energies are in hartree and μ is in bohr⁻¹.

Table C.1 – Fitted parameters of the ground-state and excitation energies along the range-separated adiabatic connection for the helium atom using an uncontracted triple-augmented quintuple zeta basis set and a truncated singular-value decomposition cutoff of 10^{-7} .

Ground-state	$\mathcal{E}_0^{\text{KS}}$	E_0	c_3	d_1	d_2	d_3	d_4	d_5
1^1S	-1.813977	-2.902589	0.2886122	-0.5256672	1.267965	0.7302989	1.729618	0.6215862
Transition	$\Delta\mathcal{E}_k^{\text{KS}}$	ΔE_k	c_3	d_1	d_2	d_3	d_4	d_5
$1^1\text{S} \rightarrow 2^3\text{S}$	0.7476677	0.7281453	0.06186663	-1.148460	0.7875350	3.601280	-0.8453350	3.279870
$1^1\text{S} \rightarrow 2^1\text{S}$	0.7476670	0.7576321	-0.09598863	-1.799520	3.139774	9.153716	6.331953	8.164700
$1^1\text{S} \rightarrow 1^3\text{P}$	0.7787323	0.7701976	0.2572886	-4.517757	11.06152	37.53672	-27.73374	90.37671
$1^1\text{S} \rightarrow 1^1\text{P}$	0.7787322	0.7795772	0.05426567	11.97447	-47.11893	114.6076	-82.48554	51.72106

Table C.2 – Fitted parameters of the ground-state and excitation energies along the range-separated adiabatic connection for the beryllium atom using an uncontracted double-augmented double zeta basis set and a truncated singular-value decomposition cutoff of 10^{-6} .

Ground-state	$\mathcal{E}_0^{\text{KS}}$	E_0	c_3	d_1	d_2	d_3	d_4	d_5
1^1S	-9.124165	-14.65438	46.83671	-0.2090221	-1.923411	3.658671	10.96260	5.215731
Transition	$\Delta\mathcal{E}_k^{\text{KS}}$	ΔE_k	c_3	d_1	d_2	d_3	d_4	d_5
$1^1\text{S} \rightarrow 1^3\text{P}$	0.1336714	0.1009080	-0.02498641	2.675899	-1.103249	66.59735	-39.94845	24.42414
$1^1\text{S} \rightarrow 1^1\text{P}$	0.1336461	0.1974410	-0.3142418	2.670149	-5.243878	40.77140	-44.04497	36.69480

Table C.3 – Fitted parameters of the excitation energies along the range-separated adiabatic connection for the dihydrogen molecule at the equilibrium distance using an uncontracted double-augmented triple zeta basis set and a truncated singular-value decomposition cutoff of 10^{-6} .

Transition	$\Delta\mathcal{E}_k^{\text{KS}}$	ΔE_k	c_3	d_1	d_2	d_3	d_4	d_5
$1^1\Sigma_g^+ \rightarrow 1^3\Sigma_u^+$	0.4359619	0.3890173	0.2799389	1.767023	13.40149	19.23359	24.79910	19.29466
$1^1\Sigma_g^+ \rightarrow 1^1\Sigma_u^+$	0.4359571	0.4677408	-0.01241781	1.264479	-0.4431237	21.85013	-16.49858	12.33904
$1^1\Sigma_g^+ \rightarrow 2^3\Sigma_g^+$	0.4740336	0.4598110	0.2481387	0.9229492	-10.10530	21.52073	-16.87971	25.28795
$1^1\Sigma_g^+ \rightarrow 2^1\Sigma_g^+$	0.4740150	0.4814739	0.04156341	-5.018161	10.11410	-3.755105	-2.033443	8.145262
$1^1\Sigma_g^+ \rightarrow 1^3\Pi_u$	0.480003	0.4670848	0.1376852	30.80894	-13.52176	121.4909	-67.14926	32.50543
$1^1\Sigma_g^+ \rightarrow 1^1\Pi_u$	0.4799835	0.4852236	0.01995048	0.5766261	-5.036269	37.87564	-20.46073	10.75388

Table C.4 – Fitted parameters of the excitation energies along the range-separated adiabatic connection for the dihydrogen molecule at three times the equilibrium distance using an uncontracted double-augmented triple zeta basis set and a truncated singular-value decomposition cutoff of 10^{-6} .

Transition	$\Delta\mathcal{E}_k^{\text{KS}}$	ΔE_k	c_3	d_1	d_2	d_3	d_4	d_5
$1^1\Sigma_g^+ \rightarrow 1^3\Sigma_u^+$	0.05176212	0.01700837	0.6515038	-1.415220	4.923966	118.7312	-176.1438	667.7109
$1^1\Sigma_g^+ \rightarrow 1^1\Sigma_u^+$	0.05174852	0.2813186	-9.042050	-9.080417	27.82670	57.35565	-188.3668	718.6815
$1^1\Sigma_g^+ \rightarrow 2^3\Sigma_g^+(\sigma_u^+)^2$	0.1034820	0.2988327	-8.364428	-6.876502	37.68192	51.86662	-151.0807	783.8883

Appendix D

Double adiabatic connection keeping the density constant

In this appendix, we present a double adiabatic connection, depending on two parameters, which keeps the ground-state density constant. The second variant of perturbation theory of Section 3.2.2 is based on this double adiabatic connection. Another form of a double adiabatic connection keeping the density constant was previously considered in Refs. [5, 6].

The Levy–Lieb universal density functional for the Coulomb electron–electron interaction \hat{W}_{ee} writes [7–9]

$$\begin{aligned} F[n] &= \min_{\Psi \rightarrow n} \langle \Psi | \hat{T} + \hat{W}_{\text{ee}} | \Psi \rangle \\ &= \langle \Psi[n] | \hat{T} + \hat{W}_{\text{ee}} | \Psi[n] \rangle, \end{aligned} \quad (\text{D.1})$$

where \hat{T} is the kinetic energy operator. We generalize it to the interaction $\hat{W}_{\text{ee}}^{\text{lr},\mu} + \lambda \hat{W}_{\text{ee}}^{\text{sr},\mu}$ where $\hat{W}_{\text{ee}}^{\text{lr},\mu}$ and $\hat{W}_{\text{ee}}^{\text{sr},\mu}$ are long-range and short-range electron–electron interactions, respectively, which depends on both a range-separation parameter μ , and on a linear parameter λ ,

$$\begin{aligned} F^{\mu,\lambda}[n] &= \min_{\Psi \rightarrow n} \langle \Psi | \hat{T} + \hat{W}_{\text{ee}}^{\text{lr},\mu} + \lambda \hat{W}_{\text{ee}}^{\text{sr},\mu} | \Psi \rangle \\ &= \langle \Psi^{\mu,\lambda}[n] | \hat{T} + \hat{W}_{\text{ee}}^{\text{lr},\mu} + \lambda \hat{W}_{\text{ee}}^{\text{sr},\mu} | \Psi^{\mu,\lambda}[n] \rangle. \end{aligned} \quad (\text{D.2})$$

The Coulomb universal density functional $F[n]$ is then decomposed into the functional $F^{\mu,\lambda}[n]$ and a μ - and λ -dependent complement short-range Hartree–exchange–correlation density functional $\bar{E}_{\text{Hxc}}^{\text{sr},\mu,\lambda}[n]$

$$F[n] = F^{\mu,\lambda}[n] + \bar{E}_{\text{Hxc}}^{\text{sr},\mu,\lambda}[n], \quad (\text{D.3})$$

APPENDIX D. DOUBLE ADIABATIC CONNECTION

leading to following expression for the exact ground-state energy of an electronic system

$$E_0 = \min_{\Psi} \left\{ \langle \Psi | \hat{T} + \hat{V}_{\text{ne}} + \hat{W}_{\text{ee}}^{\text{lr},\mu} + \lambda \hat{W}_{\text{ee}}^{\text{sr},\mu} | \Psi \rangle + \bar{E}_{\text{Hxc}}^{\text{sr},\mu,\lambda}[n_{\Psi}] \right\}, \quad (\text{D.4})$$

where \hat{V}_{ne} is the nuclei-electron interaction operator and the minimization is performed over normalized multideterminant wave functions. The Euler-Lagrange equation corresponding to this minimization is

$$\hat{H}^{\mu,\lambda} |\Psi_0^{\mu,\lambda}\rangle = \mathcal{E}_0^{\mu,\lambda} |\Psi_0^{\mu,\lambda}\rangle, \quad (\text{D.5})$$

where $\Psi_0^{\mu,\lambda}$ and $\mathcal{E}_0^{\mu,\lambda}$ are the ground-state wave function and energy of the Hamiltonian

$$\hat{H}^{\mu,\lambda} = \hat{T} + \hat{V}_{\text{ne}} + \hat{W}_{\text{ee}}^{\text{lr},\mu} + \lambda \hat{W}_{\text{ee}}^{\text{sr},\mu} + \hat{V}_{\text{Hxc}}^{\text{sr},\mu,\lambda}, \quad (\text{D.6})$$

where $\hat{V}_{\text{Hxc}}^{\text{sr},\mu,\lambda} = \int \delta \bar{E}_{\text{Hxc}}^{\text{sr},\mu,\lambda}[n_0] / \delta n(\mathbf{r}) \hat{n}(\mathbf{r}) d\mathbf{r}$ is short-range Hartree-exchange-correlation potential operator, evaluated at the density $n_0(\mathbf{r}) = \langle \Psi_0^{\mu,\lambda} | \hat{n}(\mathbf{r}) | \Psi_0^{\mu,\lambda} \rangle$ which is the ground-state density of the physical system for all μ and λ . The Hamiltonian $\hat{H}^{\mu,\lambda}$ of Equation (D.6) thus defines a double adiabatic connection keeping the ground-state density constant.

The range-separated ground-state DFT formalism of Section 2.2 is recovered in the limit $\lambda = 0$. For the purpose of applying a perturbation theory in λ starting from this limit $\lambda = 0$, we want to rewrite the Hamiltonian $\hat{H}^{\mu,\lambda}$ of Equation (D.6) as the sum of the Hamiltonian at $\lambda = 0$, $\hat{H}^{\text{lr},\mu} = \hat{H}^{\mu,\lambda=0}$, and a perturbation operator. For this, the density functional $\bar{E}_{\text{Hxc}}^{\text{sr},\mu,\lambda}[n]$ is written as

$$\bar{E}_{\text{Hxc}}^{\text{sr},\mu,\lambda}[n] = \bar{E}_{\text{Hxc}}^{\text{sr},\mu,\lambda=0}[n] - E_{\text{Hxc}}^{\text{sr},\mu,\lambda}[n], \quad (\text{D.7})$$

which defines a new density functional $E_{\text{Hxc}}^{\text{sr},\mu,\lambda}[n]$. The Hamiltonian $\hat{H}^{\mu,\lambda}$ can then be rewritten as

$$\hat{H}^{\mu,\lambda} = \hat{H}^{\text{lr},\mu} + \lambda \hat{W}_{\text{ee}}^{\text{sr},\mu} - \hat{V}_{\text{Hxc}}^{\text{sr},\mu,\lambda}, \quad (\text{D.8})$$

where $\hat{V}_{\text{Hxc}}^{\text{sr},\mu,\lambda} = \int \delta E_{\text{Hxc}}^{\text{sr},\mu,\lambda}[n_0] / \delta n(\mathbf{r}) \hat{n}(\mathbf{r}) d\mathbf{r}$ is the short-range Hartree-exchange-correlation potential operator associated with the density functional $E_{\text{Hxc}}^{\text{sr},\mu,\lambda}[n]$ introduced in Equation (D.7). The dependence on λ of this density functional can be made more explicit. It is easy to show that $E_{\text{Hxc}}^{\text{sr},\mu,\lambda}[n]$ has the following expression

$$\begin{aligned} E_{\text{Hxc}}^{\text{sr},\mu,\lambda}[n] &= \langle \Psi^{\mu,\lambda}[n] | \hat{T} + \hat{W}_{\text{ee}}^{\text{lr},\mu} + \lambda \hat{W}_{\text{ee}}^{\text{sr},\mu} | \Psi^{\mu,\lambda}[n] \rangle \\ &\quad - \langle \Psi^{\mu,\lambda=0}[n] | \hat{T} + \hat{W}_{\text{ee}}^{\text{lr},\mu} | \Psi^{\mu,\lambda=0}[n] \rangle, \end{aligned} \quad (\text{D.9})$$

which leads to the following decomposition

$$E_{\text{Hxc}}^{\text{sr},\mu,\lambda}[n] = \lambda E_{\text{Hx,md}}^{\text{sr},\mu}[n] + E_{\text{c,md}}^{\text{sr},\mu,\lambda}[n], \quad (\text{D.10})$$

where $E_{\text{Hx,md}}^{\text{sr},\mu}[n] = \langle \Psi^{\mu,\lambda=0}[n] | \hat{W}_{\text{ee}}^{\text{sr},\mu} | \Psi^{\mu,\lambda=0}[n] \rangle$ is a multideterminantal (md) generalization of the usual short-range Hartree-exchange functional [10–12]. Using the variational property of the wave function $\Psi^{\mu,\lambda}[n]$, and for non-degenerate wave functions $\Psi^{\mu,\lambda=0}[n]$, the expansion in λ of $E_{\text{c,md}}^{\text{sr},\mu,\lambda}[n]$ at $\lambda = 0$ starts at second order: $E_{\text{c,md}}^{\text{sr},\mu,\lambda}[n] = \lambda^2 E_{\text{c,md}}^{\text{sr},\mu,(2)}[n] + \dots$, as in standard G6riling-Levy (GL) perturbation theory [13, 14]. The Hamiltonian $\hat{H}^{\mu,\lambda}$ of Equation (D.8) can then be rewritten as

$$\hat{H}^{\mu,\lambda} = \hat{H}^{\text{lr},\mu} + \lambda \hat{W}^{\text{sr},\mu} - \hat{V}_{\text{c,md}}^{\text{sr},\mu,\lambda}, \quad (\text{D.11})$$

where the perturbation operator $\hat{W}^{\text{sr},\mu} = \hat{W}_{\text{ee}}^{\text{sr},\mu} - \hat{V}_{\text{Hx,md}}^{\text{sr},\mu}$ with $\hat{V}_{\text{Hx,md}}^{\text{sr},\mu} = \int \delta E_{\text{Hx,md}}^{\text{sr},\mu}[n_0] / \delta n(\mathbf{r}) \hat{n}(\mathbf{r}) d\mathbf{r}$ has been introduced to collect all the linear terms in λ , and the remaining perturbation operator $\hat{V}_{\text{c,md}}^{\text{sr},\mu,\lambda} = \int \delta E_{\text{c,md}}^{\text{sr},\mu,\lambda}[n_0] / \delta n(\mathbf{r}) \hat{n}(\mathbf{r}) d\mathbf{r}$ contains all the higher-order terms in λ .

Appendix E

Range-separated kernels

In this appendix, the spin adaptation of the short-range exchange and correlation kernels is given. Details of their derivation in the LDA case together with their asymptotic behavior close to the KS and the physical kernel are also given. This appendix is to be read together with Chapter 6.

E.1 Spin-adapted kernels

For spin-restricted closed-shell calculations, spin-singlet and spin-triplet excitations can be decoupled [15–17] (see also Refs. [18, 19]). The non-spin-flip part of the coupling matrix \mathbf{K} of Eq. (6.12) has the following spin block structure

$$\mathbf{K} = \begin{pmatrix} \mathbf{K}_{\uparrow,\uparrow} & \mathbf{K}_{\uparrow,\downarrow} \\ \mathbf{K}_{\downarrow,\uparrow} & \mathbf{K}_{\downarrow,\downarrow} \end{pmatrix}, \quad (\text{E.1})$$

where the matrix blocks $\mathbf{K}_{\sigma,\sigma'}$ have elements of the form $\mathbf{K}_{i\sigma a\sigma, j\sigma' b\sigma'}$ with i, j , and a, b referring to occupied and virtual spatial orbitals, respectively. The matrix \mathbf{K} can be brought to a block diagonal form by rotation in spin space

$$\tilde{\mathbf{K}} = \begin{pmatrix} {}^1\mathbf{K} & \mathbf{0} \\ \mathbf{0} & {}^3\mathbf{K} \end{pmatrix}, \quad (\text{E.2})$$

with a singlet component

$${}^1\mathbf{K} = \frac{\mathbf{K}_{\uparrow,\uparrow} + \mathbf{K}_{\uparrow,\downarrow} + \mathbf{K}_{\downarrow,\uparrow} + \mathbf{K}_{\downarrow,\downarrow}}{2}, \quad (\text{E.3})$$

and a triplet component

$${}^3\mathbf{K} = \frac{\mathbf{K}_{\uparrow,\uparrow} - \mathbf{K}_{\uparrow,\downarrow} - \mathbf{K}_{\downarrow,\uparrow} + \mathbf{K}_{\downarrow,\downarrow}}{2}. \quad (\text{E.4})$$

This directly leads to the singlet and triplet RSH coupling matrices of Eqs. (6.15) and (6.16), where the singlet and triplet short-range exchange-correlation kernels are defined as

$${}^1 f_{\text{xc}}^{\text{sr},\mu}(\mathbf{r}_1, \mathbf{r}_2) = \frac{f_{\text{xc},\uparrow\uparrow}^{\text{sr},\mu}(\mathbf{r}_1, \mathbf{r}_2) + f_{\text{xc},\uparrow\downarrow}^{\text{sr},\mu}(\mathbf{r}_1, \mathbf{r}_2) + f_{\text{xc},\downarrow\uparrow}^{\text{sr},\mu}(\mathbf{r}_1, \mathbf{r}_2) + f_{\text{xc},\downarrow\downarrow}^{\text{sr},\mu}(\mathbf{r}_1, \mathbf{r}_2)}{4}, \quad (\text{E.5})$$

and

$${}^3 f_{\text{xc}}^{\text{sr},\mu}(\mathbf{r}_1, \mathbf{r}_2) = \frac{f_{\text{xc},\uparrow\uparrow}^{\text{sr},\mu}(\mathbf{r}_1, \mathbf{r}_2) - f_{\text{xc},\uparrow\downarrow}^{\text{sr},\mu}(\mathbf{r}_1, \mathbf{r}_2) - f_{\text{xc},\downarrow\uparrow}^{\text{sr},\mu}(\mathbf{r}_1, \mathbf{r}_2) + f_{\text{xc},\downarrow\downarrow}^{\text{sr},\mu}(\mathbf{r}_1, \mathbf{r}_2)}{4}. \quad (\text{E.6})$$

The different spin components of the kernel can be expressed with the second-order functional derivatives of the corresponding energy functional $E_{\text{xc}}^{\text{sr},\mu}[n, m]$ with respect to the density n and the spin magnetization density m ,

$$f_{\text{xc},\uparrow\uparrow}^{\text{sr},\mu}(\mathbf{r}_1, \mathbf{r}_2) = \frac{\delta^2 E_{\text{xc}}^{\text{sr},\mu}[n, m]}{\delta n_{\uparrow}(\mathbf{r}_1) \delta n_{\uparrow}(\mathbf{r}_2)} = \frac{\delta^2 E_{\text{xc}}^{\text{sr},\mu}[n, m]}{\delta n(\mathbf{r}_1) \delta n(\mathbf{r}_2)} + 2 \frac{\delta^2 E_{\text{xc}}^{\text{sr},\mu}[n, m]}{\delta n(\mathbf{r}_1) \delta m(\mathbf{r}_2)} + \frac{\delta^2 E_{\text{xc}}^{\text{sr},\mu}[n, m]}{\delta m(\mathbf{r}_1) \delta m(\mathbf{r}_2)}, \quad (\text{E.7})$$

and

$$f_{\text{xc},\uparrow\downarrow}^{\text{sr},\mu}(\mathbf{r}_1, \mathbf{r}_2) = f_{\text{xc},\downarrow\uparrow}^{\text{sr},\mu}(\mathbf{r}_1, \mathbf{r}_2) = \frac{\delta^2 E_{\text{xc}}^{\text{sr},\mu}[n, m]}{\delta n_{\uparrow}(\mathbf{r}_1) \delta n_{\downarrow}(\mathbf{r}_2)} = \frac{\delta^2 E_{\text{xc}}^{\text{sr},\mu}[n, m]}{\delta n(\mathbf{r}_1) \delta n(\mathbf{r}_2)} - \frac{\delta^2 E_{\text{xc}}^{\text{sr},\mu}[n, m]}{\delta m(\mathbf{r}_1) \delta m(\mathbf{r}_2)}, \quad (\text{E.8})$$

and

$$f_{\text{xc},\downarrow\downarrow}^{\text{sr},\mu}(\mathbf{r}_1, \mathbf{r}_2) = \frac{\delta^2 E_{\text{xc}}^{\text{sr},\mu}[n, m]}{\delta n_{\downarrow}(\mathbf{r}_1) \delta n_{\downarrow}(\mathbf{r}_2)} = \frac{\delta^2 E_{\text{xc}}^{\text{sr},\mu}[n, m]}{\delta n(\mathbf{r}_1) \delta n(\mathbf{r}_2)} - 2 \frac{\delta^2 E_{\text{xc}}^{\text{sr},\mu}[n, m]}{\delta n(\mathbf{r}_1) \delta m(\mathbf{r}_2)} + \frac{\delta^2 E_{\text{xc}}^{\text{sr},\mu}[n, m]}{\delta m(\mathbf{r}_1) \delta m(\mathbf{r}_2)}. \quad (\text{E.9})$$

The mixed derivative with respect to n and m cancels out in Eqs. (E.5) and (E.6) and we finally obtain the singlet and triplet kernels of Eqs. (6.17) and (6.18).

E.2 Short-range LDA exchange-correlation functional

E.2.1 Short-range LDA exchange

The short-range spin-independent LDA exchange energy density is a function of the density n (or equivalently of the Wigner-Seitz radius $r_s = (3/(4\pi n))^{1/3}$) and of the range-separation parameter μ , and writes

$$e_{\text{x}}^{\text{sr},\mu} = n(\epsilon_{\text{x}} - \epsilon_{\text{x}}^{\text{lr},\mu}), \quad (\text{E.10})$$

where ϵ_{x} is the full-range exchange energy per particle of the homogeneous electron gas,

$$\epsilon_{\text{x}} = -\frac{27\alpha^2}{16 r_s}, \quad (\text{E.11})$$

with $\alpha = (4/(9\pi))^{1/3}$, and $\epsilon_x^{\text{lr},\mu}$ is the long-range exchange energy per particle of the homogeneous electron gas [20, 21]

$$\epsilon_x^{\text{lr},\mu} = -\frac{9\alpha^2 A}{r_s} \left[\sqrt{\pi} \operatorname{erf} \left(\frac{1}{2A} \right) + (2A - 4A^3) e^{-1/(4A^2)} - 3A + 4A^3 \right], \quad (\text{E.12})$$

with $A = \alpha \mu r_s / 2$.

Large μ behavior

In the limit of a very short-range interaction ($\mu \rightarrow +\infty$) or in the low-density limit ($n \rightarrow 0$ or $r_s \rightarrow \infty$), i.e. $A \rightarrow \infty$, the short-range exchange energy density $e_x^{\text{sr},\mu}$ goes to zero with the following asymptotic expansion

$$e_x^{\text{sr},\mu} = -\frac{3n}{16r_s^3 \mu^2} + \frac{9n}{320\alpha^2 r_s^5 \mu^4} + O\left(\frac{1}{\mu^6}\right), \quad (\text{E.13})$$

and the corresponding short-range exchange kernel, i.e. the second-order derivative with respect to n , expands as

$$\frac{\partial^2 e_x^{\text{sr},\mu}}{\partial n^2} = -\frac{\pi}{2\mu^2} + \frac{\pi}{6\alpha^2 r_s^2 \mu^4} + O\left(\frac{1}{\mu^6}\right). \quad (\text{E.14})$$

Small μ behavior

In the limit of the Coulombic interaction ($\mu \rightarrow 0$) or in the high-density limit ($n \rightarrow +\infty$ or $r_s \rightarrow 0$), i.e. $A \rightarrow 0$, the short-range exchange energy density $e_x^{\text{sr},\mu}$ reduces to the full-range exchange energy density $e_x = n \epsilon_x$ with the following expansion

$$e_x^{\text{sr},\mu} = e_x + \frac{\mu n}{\sqrt{\pi}} - \frac{3\alpha r_s \mu^2 n}{2\pi} + \frac{\mu^4}{6\pi^3} + O\left(e^{-1/\mu^2}\right), \quad (\text{E.15})$$

and the short-range exchange kernel behaves as

$$\frac{\partial^2 e_x^{\text{sr},\mu}}{\partial n^2} = \frac{\partial^2 e_x}{\partial n^2} + \pi \alpha^4 r_s^4 \mu^2 + O\left(e^{-1/\mu^2}\right), \quad (\text{E.16})$$

with the full-range exchange kernel

$$\frac{\partial^2 e_x}{\partial n^2} = -\pi \alpha^2 r_s^2. \quad (\text{E.17})$$

Taking the ratio of Eqs. (E.16) and (E.17), it is seen the short-range exchange kernel reduces to the full-range one when

$$\alpha^2 \mu^2 r_s^2 \ll 1, \quad (\text{E.18})$$

i.e. $r_s \ll 4.8$ for $\mu = 0.4$.

E.2.2 Short-range LDA correlation

The short-range spin-dependent LDA correlation energy density is a function of the density n , the spin magnetization density m (or equivalently of r_s and $\zeta = m/n$), and of the range-separation parameter μ , and writes

$$e_c^{\text{sr},\mu} = n(\epsilon_c - \epsilon_c^{\text{lr},\mu}), \quad (\text{E.19})$$

where ϵ_c is the full-range correlation energy per particle of the homogeneous electron gas [22], and $\epsilon_c^{\text{lr},\mu}$ is the correlation energy per particle of a homogeneous electron gas with the long-range electron-electron interaction, as fitted by Paziani *et al.* [23] on quantum Monte Carlo calculations with imposed exact limits,

$$\epsilon_c^{\text{lr},\mu} = \frac{\phi_2(\zeta)^3 Q\left(\frac{\mu\sqrt{r_s}}{\phi_2(\zeta)}\right) + a_1(r_s, \zeta)\mu^3 + a_2(r_s, \zeta)\mu^4 + a_3(r_s, \zeta)\mu^5 + a_4(r_s, \zeta)\mu^6 + a_5(r_s, \zeta)\mu^8}{(1 + b_0^2(r_s)\mu^2)^4}, \quad (\text{E.20})$$

where $\phi_2(\zeta) = [(1 + \zeta)^{2/3} + (1 - \zeta)^{2/3}]/2$ and the other functions are given in Ref. [23].

The derivatives of $e_c^{\text{sr},\mu}$ with respect to n and m are easily expressed in terms of the derivatives of $\epsilon_c^{\text{sr},\mu}$ with respect to r_s and ζ . The first-order derivatives are

$$\begin{aligned} \frac{\partial e_c^{\text{sr},\mu}}{\partial n} &= -\frac{r_s}{3} \frac{\partial \epsilon_c^{\text{sr},\mu}}{\partial r_s} + \epsilon_c^{\text{sr},\mu}, \\ \frac{\partial e_c^{\text{sr},\mu}}{\partial m} &= \frac{\partial \epsilon_c^{\text{sr},\mu}}{\partial \zeta}, \end{aligned} \quad (\text{E.21})$$

and the second-order derivatives are

$$\begin{aligned} \frac{\partial^2 e_c^{\text{sr},\mu}}{\partial n^2} &= -\frac{r_s}{9n} \left(2 \frac{\partial \epsilon_c^{\text{sr},\mu}}{\partial r_s} - r_s \frac{\partial^2 \epsilon_c^{\text{sr},\mu}}{\partial r_s^2} \right), \\ \frac{\partial^2 e_c^{\text{sr},\mu}}{\partial m^2} &= \frac{1}{n} \frac{\partial^2 \epsilon_c^{\text{sr},\mu}}{\partial \zeta^2}. \end{aligned} \quad (\text{E.22})$$

For spin-restricted closed-shell calculations, we just need to evaluate them at $\zeta = 0$.

Large μ behavior

The leading terms of the asymptotic expansion for $\mu \rightarrow +\infty$ of the short-range correlation energy density $e_c^{\text{sr},\mu}$ can be expressed with the on-top pair-density of the homogeneous electron gas [23]. In the low-density limit $r_s \rightarrow +\infty$ (or the strong-interaction limit $\lambda \rightarrow +\infty$ of the adiabatic connection), it simplifies to

$$e_c^{\text{sr},\mu} \Big|_{r_s \rightarrow +\infty} = -\frac{3(1 - \zeta^2)n}{16r_s^3\mu^2} + O\left(\frac{1}{\mu^4}\right). \quad (\text{E.23})$$

In this limit, the associated singlet and triplet short-range correlation kernels, i.e. the second-order derivatives of $e_c^{\text{sr},\mu}$ with respect to n and m evaluated at $\zeta = 0$, have the following expansions

$$\left. \frac{\partial^2 e_c^{\text{sr},\mu}}{\partial n^2} \right|_{\zeta=0, r_s \rightarrow +\infty} = -\frac{\pi}{2\mu^2} + O\left(\frac{1}{\mu^4}\right), \quad (\text{E.24})$$

$$\left. \frac{\partial^2 e_c^{\text{sr},\mu}}{\partial m^2} \right|_{\zeta=0, r_s \rightarrow +\infty} = \frac{\pi}{2\mu^2} + O\left(\frac{1}{\mu^4}\right). \quad (\text{E.25})$$

Small μ behavior

In the limit $\mu \rightarrow 0$, the short-range correlation energy density $e_c^{\text{sr},\mu}$ reduces to the full-range correlation energy density $e_c = n \epsilon_c$ with the following expansion [23]

$$e_c^{\text{sr},\mu} = e_c + \frac{3\alpha \phi_2(\zeta) r_s \mu^2 n}{2\pi} + O(\mu^3). \quad (\text{E.26})$$

It can easily be shown that the singlet and triplet short-range correlation kernels, evaluated at $\zeta = 0$, approach the corresponding full-range kernels with the same leading term

$$\left. \frac{\partial^2 e_c^{\text{sr},\mu}}{\partial n^2} \right|_{\zeta=0} = \left. \frac{\partial^2 e_c}{\partial n^2} \right|_{\zeta=0} - \pi \alpha^4 r_s^4 \mu^2 + O(\mu^3), \quad (\text{E.27})$$

$$\left. \frac{\partial^2 e_c^{\text{sr},\mu}}{\partial m^2} \right|_{\zeta=0} = \left. \frac{\partial^2 e_c}{\partial m^2} \right|_{\zeta=0} - \pi \alpha^4 r_s^4 \mu^2 + O(\mu^3). \quad (\text{E.28})$$

In the high-density limit $r_s \rightarrow 0$, the expansion of the full-range correlation energy density has the form [22]

$$e_c = n [c_0(\zeta) \ln r_s - c_1(\zeta) + O(r_s \ln r_s)]. \quad (\text{E.29})$$

The expansion of the singlet full-range correlation kernels is

$$\left. \frac{\partial^2 e_c}{\partial n^2} \right|_{\zeta=0} = -c_0(0) \pi^2 \alpha^3 r_s^3 + O(r_s^4 \ln r_s), \quad (\text{E.30})$$

with $c_0(0) = (1 - \ln 2)/\pi^2$, and the expansion of the triplet full-range correlation kernels is found from the correlation part of the spin stiffness $\alpha_c(r_s) = (\partial^2 \epsilon_c / \partial \zeta^2)_{\zeta=0}$

$$\begin{aligned} \left. \frac{\partial^2 e_c}{\partial m^2} \right|_{\zeta=0} &= 3\pi^2 \alpha^3 r_s^3 \alpha_c(r_s) \\ &= 3\pi^2 \alpha^3 r_s^3 [A_\alpha \ln r_s + C_\alpha + O(r_s \ln r_s)], \end{aligned} \quad (\text{E.31})$$

where $A_\alpha = -1/(6\pi^2)$ and $C_\alpha = 0.0354744$ [24]. Comparing Eqs. (E.27) and (E.30), it is

seen the singlet short-range correlation kernel reduces to the full-range one when

$$\frac{\pi \alpha r_s \mu^2}{1 - \ln 2} \ll 1, \quad (\text{E.32})$$

i.e. $r_s \ll 1.2$ for $\mu = 0.4$, and, comparing Eqs. (E.28) and (E.31), the triplet short-range correlation kernel reduces to the full-range one when

$$\frac{\alpha r_s \mu^2}{3\pi(A_\alpha \ln r_s + C_\alpha)} \ll 1, \quad (\text{E.33})$$

i.e. $r_s \ll 2.4$ for $\mu = 0.4$.

Appendix F

Fourier transform of the non-interacting polarizability

In this appendix, the Fourier transforms of the non-interacting polarizability, propagators and response function are given since they are often used throughout this thesis. The case of the propagation of a hole and a particle is first detailed, with different degrees of contraction on the time variables, then the propagation of two holes or two electrons is studied. The matrix elements of the different quantities in the frequency space are also given and are summarized at the end of this appendix.

F.1 Non-interacting polarizability

When the time variables are made explicit, the non-interacting polarizability is given by

$$\chi_0(\mathbf{x}_1 t_1, \mathbf{x}_2 t_2; \mathbf{x}'_1 t'_1, \mathbf{x}'_2 t'_2) = -i G_0(\mathbf{x}_1, t_1, \mathbf{x}'_2, t'_2) G_0(\mathbf{x}_2, t_2, \mathbf{x}'_1, t'_1). \quad (\text{F.1})$$

When the times are contracted, two situations can occur,

- either t_1 is contracted with t'_1 , and t_2 is contracted with t'_2 : in this case, the Green's functions have an opposite time ordering and χ_0 corresponds to the propagation of a hole and an electron. This term will be denoted ph/hp for particle-hole/hole-particle propagator ;
- or t_1 is contracted with t_2 and t'_1 with t'_2 : in this case, both Green's function have the same time ordering and χ_0 corresponds to the propagation of either two holes or two electrons. This term is thus denoted pp/hh which stands for particle-particle/hole-hole propagation.

The first case is by far more common when optical transition are concerned and is detailed in the next section.

F.2 Particle-hole or hole-particle propagator

When a particle-hole propagator is concerned, it is convenient to express it in terms of time differences. It then rewrites as

$$\chi_0(\mathbf{x}_1 t_1, \mathbf{x}_2 t_2; \mathbf{x}'_1 t'_1, \mathbf{x}'_2 t'_2) = \chi_0(\mathbf{x}_1, \mathbf{x}_2; \mathbf{x}'_1, \mathbf{x}'_2, \tau_1, \tau_2, \tau) \quad (\text{F.2})$$

with $\tau_1 = t_1 - t'_1$, $\tau_2 = t_2 - t'_2$ and $\tau = \frac{t_1 + t'_1}{2} - \frac{t_2 + t'_2}{2}$. With these conventions, the propagator can be written in terms of Green's function as

$$\chi_0(\mathbf{x}_1, \mathbf{x}_2; \mathbf{x}'_1, \mathbf{x}'_2, \tau_1, \tau_2, \tau) = -iG_0\left(\mathbf{x}_1, \mathbf{x}'_2; \frac{\tau_1 + \tau_2}{2} + \tau\right) G_0\left(\mathbf{x}_2, \mathbf{x}'_1; \frac{\tau_1 + \tau_2}{2} - \tau\right). \quad (\text{F.3})$$

As it depends on three time differences, its Fourier transform is therefore defined as

$$\chi_0(\mathbf{x}_1, \mathbf{x}_2; \mathbf{x}'_1, \mathbf{x}'_2, \omega'', \omega', \omega) = \int d\tau_1 d\tau_2 d\tau e^{i\omega''\tau_1} e^{i\omega'\tau_2} e^{i\omega\tau} \chi_0(\mathbf{x}_1, \mathbf{x}_2; \mathbf{x}'_1, \mathbf{x}'_2, \tau_1, \tau_2, \tau). \quad (\text{F.4})$$

By successive changes of variables, this can be rewritten as

$$\begin{aligned} \chi_0(\mathbf{x}_1, \mathbf{x}_2; \mathbf{x}'_1, \mathbf{x}'_2, \omega'', \omega', \omega) &= -i \int d\tau_1 d\tau_2 d\tau e^{i(\omega'' + \omega/2)\tau} e^{i(\omega'' - \omega/2)\tau_1} e^{i(\omega' - \omega'')\tau_2} G_0(\mathbf{x}_1, \mathbf{x}'_2; \tau) G_0(\mathbf{x}_2, \mathbf{x}'_1, \tau_1) \\ &= -iG_0\left(\mathbf{x}_1, \mathbf{x}'_2; \omega'' + \frac{\omega}{2}\right) G_0\left(\mathbf{x}_2, \mathbf{x}'_1, \omega'' - \frac{\omega}{2}\right) 2\pi\delta(\omega' - \omega''). \end{aligned} \quad (\text{F.5})$$

In the context of this thesis, some particular cases are of interest and are detailed hereinafter.

F.2.1 Case $t'_1 = t_1^+$

By definition of the Fourier transform given in Equation (A.10), the propagator is given in this case by

$$\begin{aligned} \chi_0(\mathbf{x}_1, \mathbf{x}_2; \mathbf{x}'_1, \mathbf{x}'_2, \tau_1 = -\eta, \omega', \omega) &= \int \frac{d\omega''}{2\pi} e^{i\omega''\eta} \chi_0(\mathbf{x}_1, \mathbf{x}_2; \mathbf{x}'_1, \mathbf{x}'_2, \omega'', \omega', \omega) \\ &= -iG_0\left(\mathbf{x}_1, \mathbf{x}'_2; \omega' + \frac{\omega}{2}\right) G_0\left(\mathbf{x}'_1, \mathbf{x}_2; \omega' - \frac{\omega}{2}\right) e^{i\omega'\eta}. \end{aligned} \quad (\text{F.6})$$

Spin-orbital expression

Using the Lehmann representation of the non-interacting Green's function

$$G_0(\mathbf{x}_1, \mathbf{x}_2, \omega) = \sum_a \frac{\varphi_a(\mathbf{x}_1)\varphi_a^*(\mathbf{x}_2)}{\omega - \varepsilon_a + i0^+} + \sum_i \frac{\varphi_i(\mathbf{x}_1)\varphi_i^*(\mathbf{x}_2)}{\omega - \varepsilon_i - i0^+}, \quad (\text{F.7})$$

in Equation (F.6) and using the relation

$$\frac{1}{(\omega - a)(\omega - b)} = \frac{1}{a - b} \left(\frac{1}{\omega - a} - \frac{1}{\omega - b} \right), \quad (\text{F.8})$$

the propagator reduces to

$$\begin{aligned} & \chi_0(\mathbf{x}_1, \mathbf{x}_2; \mathbf{x}'_1, \mathbf{x}'_2, -\eta, \omega', \omega) \\ &= -i \sum_{ab} \frac{\varphi_a(\mathbf{x}_1) \varphi_a^*(\mathbf{x}'_2) \varphi_b(\mathbf{x}_2) \varphi_b^*(\mathbf{x}'_1)}{-\omega + \varepsilon_a - \varepsilon_b} \left(\frac{1}{\omega' + \frac{\omega}{2} - \varepsilon_a + i0^+} - \frac{1}{\omega' - \frac{\omega}{2} - \varepsilon_b + i0^+} \right) e^{i\omega'\eta} \\ & - i \sum_{aj} \frac{\varphi_a(\mathbf{x}_1) \varphi_a^*(\mathbf{x}'_2) \varphi_j(\mathbf{x}_2) \varphi_j^*(\mathbf{x}'_1)}{-\omega + \varepsilon_a - \varepsilon_j - i0^+} \left(\frac{1}{\omega' + \frac{\omega}{2} - \varepsilon_a + i0^+} - \frac{1}{\omega' - \frac{\omega}{2} - \varepsilon_j - i0^+} \right) e^{i\omega'\eta} \quad (\text{F.9}) \\ & - i \sum_{ib} \frac{\varphi_i(\mathbf{x}_1) \varphi_i^*(\mathbf{x}'_2) \varphi_b(\mathbf{x}_2) \varphi_b^*(\mathbf{x}'_1)}{-\omega + \varepsilon_i - \varepsilon_b + i0^+} \left(\frac{1}{\omega' + \frac{\omega}{2} - \varepsilon_i - i0^+} - \frac{1}{\omega' - \frac{\omega}{2} - \varepsilon_b + i0^+} \right) e^{i\omega'\eta} \\ & - i \sum_{ij} \frac{\varphi_i(\mathbf{x}_1) \varphi_i^*(\mathbf{x}'_2) \varphi_j(\mathbf{x}_2) \varphi_j^*(\mathbf{x}'_1)}{-\omega + \varepsilon_i - \varepsilon_j} \left(\frac{1}{\omega' + \frac{\omega}{2} - \varepsilon_i - i0^+} - \frac{1}{\omega' - \frac{\omega}{2} - \varepsilon_j - i0^+} \right) e^{i\omega'\eta} \end{aligned}$$

In particular, its matrix elements in the (ov,ov) block and in the (vo,vo) block can be expressed in terms of the matrix elements of the one-frequency response function as

$$\chi_{0,ja,ja}(-\eta, \omega', \omega) = i\chi_{0,ja,ja}(\omega) \left(\frac{1}{\omega' + \frac{\omega}{2} - \varepsilon_a + i0^+} - \frac{1}{\omega' - \frac{\omega}{2} - \varepsilon_j - i0^+} \right) e^{i\omega'\eta} \quad (\text{F.10a})$$

$$\chi_{0,bi,bi}(-\eta, \omega', \omega) = i\chi_{0,bi,bi}(\omega) \left(\frac{1}{\omega' + \frac{\omega}{2} - \varepsilon_i - i0^+} - \frac{1}{\omega' - \frac{\omega}{2} - \varepsilon_b + i0^+} \right) e^{i\omega'\eta}, \quad (\text{F.10b})$$

where

$$\chi_{0,ja,ja}(\omega) = \frac{1}{\omega - \varepsilon_a + \varepsilon_j + i0^+}, \quad (\text{F.11a})$$

$$\chi_{0,bi,bi}(\omega) = -\frac{1}{\omega - \varepsilon_i + \varepsilon_b - i0^+}. \quad (\text{F.11b})$$

F.2.2 Case $t'_2 = t_2^+$

A similar derivation can be done in the case where $t'_2 = t_2^+$. The propagator is then given by

$$\begin{aligned} \chi_0(\mathbf{x}_1, \mathbf{x}_2; \mathbf{x}'_1, \mathbf{x}'_2, \omega'', \tau_2 = -\eta, \omega) &= \int \frac{d\omega'}{2\pi} e^{i\omega'\eta} \chi_0(\mathbf{x}_1, \mathbf{x}_2; \mathbf{x}'_1, \mathbf{x}'_2, \omega'', \omega', \omega) \\ &= -iG_0(\mathbf{x}_1, \mathbf{x}'_2; \omega'' + \frac{\omega}{2})G_0(\mathbf{x}_2, \mathbf{x}'_1; \omega'' - \frac{\omega}{2})e^{i\omega''\eta} \quad (\text{F.12}) \\ &= \chi_0(\mathbf{x}_1, \mathbf{x}_2; \mathbf{x}'_1, \mathbf{x}'_2, \tau_1 = -\eta, \omega'', \omega) \end{aligned}$$

and has the same spin-orbital expression than in the case $t'_1 = t_1^+$.

F.2.3 Case $t'_1 = t_1^+$ and $t'_2 = t_2^+$

If both times are contracted, then the response function is obtained as

$$\chi_0(\mathbf{x}_1, \mathbf{x}_2; \mathbf{x}'_1, \mathbf{x}'_2, -\eta, -\eta, \omega) = -i \int \frac{d\omega'}{2\pi} e^{i\omega\eta} e^{i\omega'\eta} G_0(\mathbf{x}_1, \mathbf{x}'_2; \omega' + \frac{\omega}{2}) G_0(\mathbf{x}_2, \mathbf{x}'_1; \omega' - \frac{\omega}{2}) \quad (\text{F.13})$$

which by integration over ω' in the upper half complex plane gives

$$\begin{aligned} \chi_0(\mathbf{x}_1, \mathbf{x}_2; \mathbf{x}'_1, \mathbf{x}'_2, \tau_1 = -\eta, \tau_2 = -\eta, \omega) \\ = \sum_{aj} \frac{\varphi_a(\mathbf{x}_1) \varphi_a^*(\mathbf{x}'_2) \varphi_j(\mathbf{x}_2) \varphi_j^*(\mathbf{x}'_1)}{\omega - \varepsilon_a + \varepsilon_j + i0^+} e^{i\omega\eta} - \sum_{ib} \frac{\varphi_i(\mathbf{x}_1) \varphi_i^*(\mathbf{x}'_2) \varphi_b(\mathbf{x}_2) \varphi_b^*(\mathbf{x}'_1)}{\omega - \varepsilon_i + \varepsilon_b - i0^+} e^{i\omega\eta}. \end{aligned} \quad (\text{F.14})$$

F.3 Particle-particle or hole-hole propagator

A pp/hh propagator can also be encountered in the derivation of the Bethe-Salpeter kernel in the case $\chi_{IP}(\mathbf{x}_1 t_1, \mathbf{x}_6 t_1; \mathbf{x}_5 t_2^+, \mathbf{x}_2 t_2)$. In terms of time differences, this propagator rewrites as

$$\chi_0(\mathbf{x}_1 t_1, \mathbf{x}_6 t_1; \mathbf{x}_5 t_2^+, \mathbf{x}_2 t_2) = -i G_0(\mathbf{x}_1, \mathbf{x}_2, \tau) G_0(\mathbf{x}_6, \mathbf{x}_5, \tau - \eta) \quad (\text{F.15})$$

where $\tau = t_1 - t_2$. Its Fourier transform is thus given by

$$\begin{aligned} \chi_0(\mathbf{x}_1, \mathbf{x}_6; \mathbf{x}_5, \mathbf{x}_2; \omega) &= -i \int d\tau e^{i\omega\tau} G_0(\mathbf{x}_1, \mathbf{x}_2, \tau) G_0(\mathbf{x}_6, \mathbf{x}_5, \tau - \eta) \\ &= -i \int \frac{d\omega'}{2\pi} e^{i\omega'\eta} G_0(\mathbf{x}_1, \mathbf{x}_2, \omega - \omega') G_0(\mathbf{x}_6, \mathbf{x}_5, \omega'), \end{aligned} \quad (\text{F.16})$$

which by integration over ω' over the upper half complex plane gives

$$\chi_0(\mathbf{x}_1, \mathbf{x}_6; \mathbf{x}_5, \mathbf{x}_2, \omega) = - \sum_{ab} \frac{\varphi_a(\mathbf{x}_1) \varphi_a^*(\mathbf{x}_2) \varphi_b(\mathbf{x}_6) \varphi_b^*(\mathbf{x}_5)}{\omega - (\varepsilon_a + \varepsilon_b) + i0^+} + \sum_{ij} \frac{\varphi_i(\mathbf{x}_1) \varphi_i^*(\mathbf{x}_2) \varphi_j(\mathbf{x}_6) \varphi_j^*(\mathbf{x}_5)}{\omega - (\varepsilon_i + \varepsilon_j) - i0^+}. \quad (\text{F.17})$$

F.4 Summary

- ph/hp propagator in the general case

$$\chi_0(\mathbf{x}_1, \mathbf{x}_2; \mathbf{x}'_1, \mathbf{x}'_2, \omega'', \omega', \omega) = -iG_0\left(\mathbf{x}_1, \mathbf{x}'_2; \omega'' + \frac{\omega}{2}\right) G_0\left(\mathbf{x}_2, \mathbf{x}'_1, \omega'' - \frac{\omega}{2}\right) 2\pi\delta(\omega' - \omega''). \quad (\text{F.18})$$

- ph/hp propagator when one time difference is contracted

$$\begin{aligned} \chi_0(\mathbf{x}_1, \mathbf{x}_2; \mathbf{x}'_1, \mathbf{x}'_2, -\eta, \omega', \omega) &= \chi_0(\mathbf{x}_1, \mathbf{x}_2; \mathbf{x}'_1, \mathbf{x}'_2, \omega', -\eta, \omega) \\ &= -i \sum_{ab} \frac{\varphi_a(\mathbf{x}_1)\varphi_a^*(\mathbf{x}'_2)\varphi_b(\mathbf{x}_2)\varphi_b^*(\mathbf{x}'_1)}{-\omega + \varepsilon_a - \varepsilon_b} \left(\frac{1}{\omega' + \frac{\omega}{2} - \varepsilon_a + i0^+} - \frac{1}{\omega' - \frac{\omega}{2} - \varepsilon_b + i0^+} \right) e^{i\omega'\eta} \\ &\quad - i \sum_{aj} \frac{\varphi_a(\mathbf{x}_1)\varphi_a^*(\mathbf{x}'_2)\varphi_j(\mathbf{x}_2)\varphi_j^*(\mathbf{x}'_1)}{-\omega + \varepsilon_a - \varepsilon_j - i0^+} \left(\frac{1}{\omega' + \frac{\omega}{2} - \varepsilon_a + i0^+} - \frac{1}{\omega' - \frac{\omega}{2} - \varepsilon_j - i0^+} \right) e^{i\omega'\eta} \\ &\quad - i \sum_{ib} \frac{\varphi_i(\mathbf{x}_1)\varphi_i^*(\mathbf{x}'_2)\varphi_b(\mathbf{x}_2)\varphi_b^*(\mathbf{x}'_1)}{-\omega + \varepsilon_i - \varepsilon_b + i0^+} \left(\frac{1}{\omega' + \frac{\omega}{2} - \varepsilon_i - i0^+} - \frac{1}{\omega' - \frac{\omega}{2} - \varepsilon_b + i0^+} \right) e^{i\omega'\eta} \\ &\quad - i \sum_{ij} \frac{\varphi_i(\mathbf{x}_1)\varphi_i^*(\mathbf{x}'_2)\varphi_j(\mathbf{x}_2)\varphi_j^*(\mathbf{x}'_1)}{-\omega + \varepsilon_i - \varepsilon_j} \left(\frac{1}{\omega' + \frac{\omega}{2} - \varepsilon_i - i0^+} - \frac{1}{\omega' - \frac{\omega}{2} - \varepsilon_j - i0^+} \right) e^{i\omega'\eta}. \end{aligned} \quad (\text{F.19})$$

- ph/hp response function

$$\begin{aligned} \chi_0(\mathbf{x}_1, \mathbf{x}_2; \mathbf{x}'_1, \mathbf{x}'_2, -\eta, -\eta, \omega) \\ = \sum_{aj} \frac{\varphi_a(\mathbf{x}_1)\varphi_a^*(\mathbf{x}'_2)\varphi_j(\mathbf{x}_2)\varphi_j^*(\mathbf{x}'_1)}{\omega - \varepsilon_a + \varepsilon_j + i0^+} e^{i\omega\eta} - \sum_{ib} \frac{\varphi_i(\mathbf{x}_1)\varphi_i^*(\mathbf{x}'_2)\varphi_b(\mathbf{x}_2)\varphi_b^*(\mathbf{x}'_1)}{\omega - \varepsilon_i + \varepsilon_b - i0^+} e^{i\omega\eta}. \end{aligned} \quad (\text{F.20})$$

- pp/hh response function

$$\chi_0(\mathbf{x}_1, \mathbf{x}_6; \mathbf{x}_5, \mathbf{x}_2, \omega) = - \sum_{ab} \frac{\varphi_a(\mathbf{x}_1)\varphi_a^*(\mathbf{x}_2)\varphi_b(\mathbf{x}_6)\varphi_b^*(\mathbf{x}_5)}{\omega - (\varepsilon_a + \varepsilon_b) + i0^+} + \sum_{ij} \frac{\varphi_i(\mathbf{x}_1)\varphi_i^*(\mathbf{x}_2)\varphi_j(\mathbf{x}_6)\varphi_j^*(\mathbf{x}_5)}{\omega - (\varepsilon_i + \varepsilon_j) - i0^+}. \quad (\text{F.21})$$

Appendix G

Second-order self-energy and static BSE kernel

In this appendix, the details of the derivation of the second-order correlation self-energy and Bethe-Salpeter kernel are given. It requires the Fourier transform conventions given in Appendix A.2 and the Fourier transforms of the response functions with different possible time ordering given in Appendix F. A summary of the formulas of interest for the rest of this thesis is given at the end of this appendix.

G.1 Correlation self-energy

G.1.1 Direct correlation self-energy

The second-order direct correlation self-energy is by definition

$$\Sigma_c^{(2d)}[G](1, 2) = i \int d1' d3 d4 d4' d5 d5' G(1', 3) w_{ee}(3, 5; 2, 5') \chi_{IP}(5', 4; 5^+, 4'^+) w_{ee}(4', 1; 4, 1'). \quad (\text{G.1})$$

With the explicit time dependence, it becomes

$$\begin{aligned} \Sigma_c^{(2d)}[G](\mathbf{x}_1, \mathbf{x}_2, \tau) \\ = i \int d\mathbf{x}_4 d\mathbf{x}_5 G(\mathbf{x}_1, \mathbf{x}_2, \tau) \chi_{IP}(\mathbf{x}_5, \mathbf{x}_4; \mathbf{x}_5, \mathbf{x}_4; -\eta, -\eta, -\tau) w_{ee}(\mathbf{r}_2, \mathbf{r}_5) w_{ee}(\mathbf{r}_4, \mathbf{r}_1) \end{aligned} \quad (\text{G.2})$$

where $\tau = t_1 - t_2$ and $\eta = 0^+$ is a small real positive quantity. Following the conventions given in Appendix A.2, its Fourier transform is thus given by

$$\begin{aligned} \Sigma_c^{(2d)}[G](\mathbf{x}_1, \mathbf{x}_2, \omega) \\ = i \int d\mathbf{x}_4 d\mathbf{x}_5 d\tau e^{i\omega\tau} G(\mathbf{x}_1, \mathbf{x}_2, \tau) \chi_{IP}(\mathbf{x}_5, \mathbf{x}_4; \mathbf{x}_5, \mathbf{x}_4; -\eta, -\eta, -\tau) w_{ee}(\mathbf{r}_2, \mathbf{r}_5) w_{ee}(\mathbf{r}_4, \mathbf{r}_1) \end{aligned} \quad (\text{G.3})$$

By making explicit the Fourier transform of χ_{IP} and using this in G , it then becomes

$$\begin{aligned}
 \Sigma_c^{(2d)}[G](\mathbf{x}_1, \mathbf{x}_2, \omega) &= i \int d\mathbf{x}_4 d\mathbf{x}_5 d\tau \frac{d\omega'}{2\pi} e^{i\omega\tau} e^{i\omega'\tau} G(\mathbf{x}_1, \mathbf{x}_2, \tau) \chi_{\text{IP}}(\mathbf{x}_5, \mathbf{x}_4; \mathbf{x}_5, \mathbf{x}_4; -\eta, -\eta, \omega') w_{\text{ee}}(\mathbf{r}_2, \mathbf{r}_5) w_{\text{ee}}(\mathbf{r}_4, \mathbf{r}_1) \\
 &= i \int d\mathbf{x}_4 d\mathbf{x}_5 \frac{d\omega'}{2\pi} G(\mathbf{x}_1, \mathbf{x}_2, \omega + \omega') \chi_{\text{IP}}(\mathbf{x}_5, \mathbf{x}_4; \mathbf{x}_5, \mathbf{x}_4; -\eta, -\eta, \omega') w_{\text{ee}}(\mathbf{r}_2, \mathbf{r}_5) w_{\text{ee}}(\mathbf{r}_4, \mathbf{r}_1),
 \end{aligned} \tag{G.4}$$

which by integration over ω' over the upper half complex plane becomes

$$\begin{aligned}
 \Sigma_c^{(2d)}[G](\mathbf{x}_1, \mathbf{x}_2, \omega) &= \sum_{AJC} \int d\mathbf{x}_4 d\mathbf{x}_5 \frac{f_A(\mathbf{x}_1) f_A^*(\mathbf{x}_2) f_J(\mathbf{x}_5) f_J^*(\mathbf{x}_4) f_C(\mathbf{x}_4) f_C^*(\mathbf{x}_5)}{\omega - (\mathcal{E}_A - \mathcal{E}_J + \mathcal{E}_C) + i0^+} w_{\text{ee}}(\mathbf{r}_2, \mathbf{r}_5) w_{\text{ee}}(\mathbf{r}_4, \mathbf{r}_1) \\
 &+ \sum_{IBK} \int d\mathbf{x}_4 d\mathbf{x}_5 \frac{f_I(\mathbf{x}_1) f_I^*(\mathbf{x}_2) f_B(\mathbf{x}_5) f_B^*(\mathbf{x}_4) f_K(\mathbf{x}_4) f_K^*(\mathbf{x}_5)}{\omega - (\mathcal{E}_I - \mathcal{E}_B + \mathcal{E}_K) - i0^+} w_{\text{ee}}(\mathbf{r}_2, \mathbf{r}_5) w_{\text{ee}}(\mathbf{r}_4, \mathbf{r}_1).
 \end{aligned} \tag{G.5}$$

When evaluated for $G = G_0$, its matrix elements are therefore given by

$$\begin{aligned}
 \Sigma_{c,uv}^{(2d)}(\omega) &= \iint d\mathbf{x}_1 d\mathbf{x}_2 \Sigma_c^{(2d)}(\mathbf{x}_1, \mathbf{x}_2, \omega) \varphi_u^*(\mathbf{x}_1) \varphi_v(\mathbf{x}_2) \\
 &= \sum_{ajc} \frac{\langle ac|vj\rangle \langle uj|ac\rangle}{\omega - (\varepsilon_a - \varepsilon_j + \varepsilon_c) + i0^+} + \sum_{ibk} \frac{\langle ik|vb\rangle \langle ub|ik\rangle}{\omega - (\varepsilon_i - \varepsilon_b + \varepsilon_k) - i0^+}.
 \end{aligned} \tag{G.6}$$

G.1.2 Exchanged correlation self-energy

The exchanged correlation self-energy is by definition

$$\Sigma_c^{(2x)}[G](1, 2) = -i \int d1' d3 d4 d4' d5 d5' G(1', 3) w_{\text{ee}}(5, 3; 2, 5') \chi_{\text{IP}}(5', 4; 5^+, 4'^+) w_{\text{ee}}(4', 1; 4, 1'). \tag{G.7}$$

With explicit time variables, it is thus given by

$$\begin{aligned}
 \Sigma_c^{(2x)}[G](\mathbf{x}_1, \mathbf{x}_2, \tau) &= -i \int d\mathbf{x}_3 d\mathbf{x}_4 G(\mathbf{x}_1, \mathbf{x}_3, \tau) \chi_{\text{IP}}(\mathbf{x}_3, \mathbf{x}_4; \mathbf{x}_2, \mathbf{x}_4, -\eta, -\eta, -\tau) w_{\text{ee}}(\mathbf{r}_2, \mathbf{r}_3) w_{\text{ee}}(\mathbf{r}_4, \mathbf{r}_1),
 \end{aligned} \tag{G.8}$$

which by Fourier transform leads to

$$\begin{aligned}
 \Sigma_c^{(2x)}[G](\mathbf{x}_1, \mathbf{x}_2, \omega) &= - \sum_{AJC} \int d\mathbf{x}_3 d\mathbf{x}_4 \frac{f_A(\mathbf{x}_1) f_A^*(\mathbf{x}_3) f_J(\mathbf{x}_3) f_J^*(\mathbf{x}_4) f_C(\mathbf{x}_4) f_C^*(\mathbf{x}_2)}{\omega - (\mathcal{E}_A - \mathcal{E}_J + \mathcal{E}_C) + i0^+} w_{\text{ee}}(\mathbf{r}_2, \mathbf{r}_3) w_{\text{ee}}(\mathbf{r}_4, \mathbf{r}_1) \\
 &- \sum_{IBK} \int d\mathbf{x}_3 d\mathbf{x}_4 \frac{f_I(\mathbf{x}_1) f_I^*(\mathbf{x}_3) f_B(\mathbf{x}_3) f_B^*(\mathbf{x}_4) f_K(\mathbf{x}_4) f_K^*(\mathbf{x}_2)}{\omega - (\mathcal{E}_I - \mathcal{E}_B + \mathcal{E}_K) - i0^+} w_{\text{ee}}(\mathbf{r}_2, \mathbf{r}_3) w_{\text{ee}}(\mathbf{r}_4, \mathbf{r}_1).
 \end{aligned} \tag{G.9}$$

When evaluated at $G = G_0$, its matrix elements are

$$\Sigma_{c,uv}^{(2x)}(\omega) = - \sum_{ajc} \frac{\langle ca|vj\rangle\langle uj|ac\rangle}{\omega - (\varepsilon_a - \varepsilon_j + \varepsilon_c) + i0^+} - \sum_{ibk} \frac{\langle ki|vb\rangle\langle ub|ik\rangle}{\omega - (\varepsilon_i - \varepsilon_b + \varepsilon_k) - i0^+}, \quad (\text{G.10})$$

such that the total second-order self-energy is given by

$$\Sigma_{c,uv}^{(2)}(\omega) = \frac{1}{2} \sum_{ajc} \frac{\langle ac||vj\rangle\langle uj||ac\rangle}{\omega - (\varepsilon_a - \varepsilon_j + \varepsilon_c) + i0^+} + \frac{1}{2} \sum_{ibk} \frac{\langle ik||vb\rangle\langle ub||ik\rangle}{\omega - (\varepsilon_i - \varepsilon_b + \varepsilon_k) - i0^+}. \quad (\text{G.11})$$

G.2 Correlation kernel

G.2.1 Direct correlation kernel

By differentiating the second-order direct correlation self-energy with respect to G and evaluating this derivative at $G = G_0$, the second-order direct correlation kernel is obtained as

$$\begin{aligned} \Xi_c^{(2d)}(1, 6; 2; 5) &= - \int d1' d3 d4 d4' d7 d7' \delta(1', 5) \delta(3, 6) w_{ee}(3, 7; 2, 7') \chi_0(7', 4; 7^+, 4'^+) w_{ee}(4', 1; 4, 1') \\ &\quad - \int d1' d3 d4 d4' d5 d5' G(1', 3) \left. \frac{\delta [w_{ee}(3, 7; 2, 7') \chi_{IP}(7', 4; 7^+, 4'^+) w_{ee}(4', 1; 4, 1')]}{\delta G(5, 6)} \right|_{G=G_0} \end{aligned} \quad (\text{G.12})$$

and can be decoupled into two parts, $\triangleright\Xi_c^{(2d)}$ which corresponds to the first term of the r.h.s. of this equation and arise from $(\delta G/\delta G)W$, and $\triangleleft\Xi_c^{(2d)}$ which corresponds to the second term and comes from $G(\delta W/\delta G)$.

The first part of the derivative is given by

$$\begin{aligned} \triangleright\Xi_c^{(2d)}(1, 6; 2, 5) &= - \delta(t_2, t_6) \delta(t_1, t_5) \delta(\mathbf{x}_6, \mathbf{x}_2) \delta(\mathbf{x}_1, \mathbf{x}_5) \\ &\quad \int d\mathbf{x}_3 d\mathbf{x}_4 w_{ee}(\mathbf{r}_2, \mathbf{r}_3) \chi_0(\mathbf{x}_3 t_2, \mathbf{x}_4 t_1; \mathbf{x}_3 t_2^+, \mathbf{x}_4 t_1^+) w_{ee}(\mathbf{r}_4, \mathbf{r}_1) \\ &= \delta(t_2, t_6) \delta(t_1, t_5) \triangleright\Xi_c^{(2d, \text{ph/hp})}(\mathbf{x}_1, \mathbf{x}_6; \mathbf{x}_2, \mathbf{x}_5; t_1 - t_2) \end{aligned} \quad (\text{G.13})$$

which defines $\triangleright\Xi_c^{(2d, \text{ph/hp})}(\mathbf{x}_1, \mathbf{x}_6; \mathbf{x}_2, \mathbf{x}_5; t_1 - t_2)$ by taking out the delta functions on the times. The time ordering in the response function corresponds to the propagation of a hole and an electron, therefore this term is denoted ph/hp.

The second part of the derivative corresponds to the term $G\delta W/\delta G$

$$\begin{aligned} \triangleleft\Xi_c^{(2d)}(1, 6; 2; 5) &= - G(1, 2) \int d4 d7 w_{ee}(\mathbf{r}_2, \mathbf{r}_7) \delta(t_2, t_7) \left. \frac{\delta \chi_{IP}(7, 4; 7^+, 4^+)}{\delta G(5, 6)} \right|_{G=G_0} w_{ee}(\mathbf{r}_4, \mathbf{r}_1) \delta(t_1, t_4). \end{aligned} \quad (\text{G.14})$$

When the differentiation is done, two kinds of terms arise depending on the time ordering

of the response functions,

$$\begin{aligned} \triangleleft \Xi_c^{(2d)}(1, 6; 2; 5) &= iG(1, 2) \int d4d7 w_{ee}(\mathbf{r}_2, \mathbf{r}_7) \delta(t_2, t_7) \delta(4, 5) \delta(7^+, 6) G(7, 4^+) w_{ee}(\mathbf{r}_4, \mathbf{r}_1) \delta(t_1, t_4) \\ &+ iG(1, 2) \int d4d7 w_{ee}(\mathbf{r}_2, \mathbf{r}_7) \delta(t_2, t_7) \delta(7, 5) \delta(4^+, 6) G(4, 7^+) w_{ee}(\mathbf{r}_4, \mathbf{r}_1) \delta(t_1, t_4). \end{aligned} \quad (\text{G.15})$$

If the time variables are made explicit, this rewrites as

$$\begin{aligned} \triangleleft \Xi_c^{(2d)}(1, 6; 2; 5) &= iG(\mathbf{x}_1 t_1, \mathbf{x}_2 t_2) w_{ee}(\mathbf{r}_2, \mathbf{r}_6) \delta(t_2^+, t_6) G(\mathbf{x}_6 t_2, \mathbf{x}_5 t_1^+) w_{ee}(\mathbf{r}_5, \mathbf{r}_1) \delta(t_1, t_5) \\ &+ iG(\mathbf{x}_1 t_1, \mathbf{x}_2 t_2) w_{ee}(\mathbf{r}_2, \mathbf{r}_5) \delta(t_2, t_5) G(\mathbf{x}_6 t_1, \mathbf{x}_5 t_2^+) w_{ee}(\mathbf{r}_6, \mathbf{r}_1) \delta(t_1^+, t_6) \\ &= \delta(t_2^+, t_6) \delta(t_1, t_5) \triangleleft \Xi_c^{(2d, \text{ph/hp})}(\mathbf{x}_1, \mathbf{x}_6; \mathbf{x}_2, \mathbf{x}_5; t_1 - t_2) \\ &+ \delta(t_2, t_5) \delta(t_1^+, t_6) \triangleleft \Xi_c^{(2d, \text{pp/hh})}(\mathbf{x}_1, \mathbf{x}_6; \mathbf{x}_2, \mathbf{x}_5; t_1 - t_2), \end{aligned} \quad (\text{G.16})$$

where the first

$$\triangleleft \Xi_c^{(2d, \text{ph/hp})}(\mathbf{x}_1, \mathbf{x}_6; \mathbf{x}_2, \mathbf{x}_5; t_1 - t_2) = -w_{ee}(\mathbf{r}_2, \mathbf{r}_6) \chi_0(\mathbf{x}_1 t_1, \mathbf{x}_6 t_2; \mathbf{x}_5 t_1^+, \mathbf{x}_2 t_2) w_{ee}(\mathbf{r}_5, \mathbf{r}_1), \quad (\text{G.17})$$

corresponds to a ph/hp term as the time ordering is different in the two Green's function, while the second term

$$\triangleleft \Xi_c^{(2d, \text{pp/hh})}(\mathbf{x}_1, \mathbf{x}_6; \mathbf{x}_2, \mathbf{x}_5; t_1 - t_2) = -w_{ee}(\mathbf{r}_2, \mathbf{r}_5) \chi_0(\mathbf{x}_1 t_1, \mathbf{x}_6 t_1; \mathbf{x}_5 t_2^+, \mathbf{x}_2 t_2) w_{ee}(\mathbf{r}_6, \mathbf{r}_1), \quad (\text{G.18})$$

is a pp/hh term as the time difference is the same in both Green's functions. Using the Fourier transforms of the ph/hp and pp/hh propagators given in Appendix A.2, the Fourier transforms of the contributions of the direct second-order kernel are therefore

$$\begin{aligned} \triangleright \Xi_c^{(2d, \text{ph/hp})}(\mathbf{x}_1, \mathbf{x}_6; \mathbf{x}_2, \mathbf{x}_5; \omega) &= \delta(\mathbf{x}_6, \mathbf{x}_2) \delta(\mathbf{x}_1, \mathbf{x}_5) \int d\mathbf{x}_3 d\mathbf{x}_4 w_{ee}(\mathbf{r}_2, \mathbf{r}_3) w_{ee}(\mathbf{r}_4, \mathbf{r}_1) \\ &\sum_{kc} \left[\frac{\varphi_k(\mathbf{x}_4) \varphi_k^*(\mathbf{x}_3) \varphi_c(\mathbf{x}_3) \varphi_c^*(\mathbf{x}_4)}{\omega + (\varepsilon_c - \varepsilon_k) - i0^+} - \frac{\varphi_c(\mathbf{x}_4) \varphi_c^*(\mathbf{x}_3) \varphi_k(\mathbf{x}_3) \varphi_k^*(\mathbf{x}_4)}{\omega - (\varepsilon_c - \varepsilon_k) + i0^+} \right], \end{aligned} \quad (\text{G.19a})$$

$$\begin{aligned} \triangleleft \Xi_c^{(2d, \text{ph/hp})}(\mathbf{x}_1, \mathbf{x}_6; \mathbf{x}_2, \mathbf{x}_5; \omega) &= w_{ee}(\mathbf{r}_2, \mathbf{r}_6) w_{ee}(\mathbf{r}_5, \mathbf{r}_1) \\ &\sum_{kc} \left[\frac{\varphi_k(\mathbf{x}_1) \varphi_k^*(\mathbf{x}_2) \varphi_c(\mathbf{x}_6) \varphi_c^*(\mathbf{x}_5)}{\omega + (\varepsilon_c - \varepsilon_k) - i0^+} - \frac{\varphi_c(\mathbf{x}_1) \varphi_c^*(\mathbf{x}_2) \varphi_k(\mathbf{x}_6) \varphi_k^*(\mathbf{x}_5)}{\omega - (\varepsilon_c - \varepsilon_k) + i0^+} \right] \end{aligned} \quad (\text{G.19b})$$

$$\begin{aligned} \triangleleft \Xi_c^{(2d, \text{pp/hh})}(\mathbf{x}_1, \mathbf{x}_6; \mathbf{x}_2, \mathbf{x}_5; \omega) &= w_{ee}(\mathbf{r}_2, \mathbf{r}_5) w_{ee}(\mathbf{r}_6, \mathbf{r}_1) \\ &\left[\sum_{cd} \frac{\varphi_c(\mathbf{x}_1) \varphi_c^*(\mathbf{x}_2) \varphi_d(\mathbf{x}_6) \varphi_d^*(\mathbf{x}_5)}{\omega - (\varepsilon_c + \varepsilon_d) + i0^+} - \sum_{kl} \frac{\varphi_k(\mathbf{x}_1) \varphi_k^*(\mathbf{x}_2) \varphi_l(\mathbf{x}_6) \varphi_l^*(\mathbf{x}_5)}{\omega - (\varepsilon_k + \varepsilon_l) - i0^+} \right] \end{aligned} \quad (\text{G.19c})$$

Therefore, the corresponding matrix elements are given by

$$\triangleright \Xi_{c, pq, rs}^{(2d, \text{ph/hp})}(\omega) = - \sum_{kc} \frac{\langle qk|sa\rangle \langle ra|pk\rangle}{\omega - (\varepsilon_c - \varepsilon_k) + i0^+} + \sum_{kc} \frac{\langle rk|pa\rangle \langle qa|sk\rangle}{\omega + (\varepsilon_c - \varepsilon_k) - i0^+}, \quad (\text{G.20a})$$

$$\triangleleft \Xi_{c,pq,rs}^{(2d,ph/hp)}(\omega) = - \sum_{kc} \frac{\langle ar|pk\rangle \langle qk|as\rangle}{\omega - (\varepsilon_c - \varepsilon_k) + i0^+} + \sum_{kc} \frac{\langle kr|pa\rangle \langle qa|ks\rangle}{\omega + (\varepsilon_c - \varepsilon_k) - i0^+} \quad (\text{G.20b})$$

$$\triangleleft \Xi_{c,pq,rs}^{(2d,pp/hh)}(\omega) = \sum_{cd} \frac{\langle ab|ps\rangle \langle qr|ab\rangle}{\omega - (\varepsilon_c + \varepsilon_d) + i0^+} - \sum_{kl} \frac{\langle kl|ps\rangle \langle qr|kl\rangle}{\omega - (\varepsilon_k + \varepsilon_l) - i0^+} \quad (\text{G.20c})$$

G.2.2 Exchanged correlation kernel

A similar derivation is performed for the the second-order exchanged correlation kernel. By differentiation of the corresponding self-energy and evaluation at $G = G_0$, the exchanged correlation kernel is then obtained as

$$\begin{aligned} & \Xi_c^{(2x)}(1, 6; 2; 5) \\ &= \int d1' d3 d4 d4' d7 d7' \delta(1', 5) \delta(3, 6) w_{ee}(7, 3; 2, 7') \chi_0(7', 4; 7^+, 4'^+) w_{ee}(4', 1; 4, 1') \\ & \quad + \int d1' d3 d4 d4' d7 d7' G(1', 3) w_{ee}(7, 3; 2, 7') \left. \frac{\delta \chi_{IP}(7', 4; 7^+, 4'^+)}{\delta G(5, 6)} \right|_{G=G_0} w_{ee}(4', 1; 4, 1') \\ &= \triangleright \Xi_c^{(2x)}(1, 6; 2; 5) + \triangleleft \Xi_c^{(2x)}(1, 6; 2; 5), \end{aligned} \quad (\text{G.21})$$

which can be decoupled into two parts coming either from the derivative of G or the derivative of W . The first part of the exchanged second-order correlation kernel is therefore

$$\begin{aligned} & \triangleright \Xi_c^{(2x)}(1, 6; 2, 5) \\ &= \delta(t_2, t_6) \delta(t_1, t_5) \delta(\mathbf{x}_1, \mathbf{x}_5) \int d\mathbf{x}_4 w_{ee}(\mathbf{r}_2, \mathbf{r}_6) \chi_0(\mathbf{x}_4 t_1, \mathbf{x}_6 t_2; \mathbf{x}_4 t_1^+, \mathbf{x}_2 t_2^+) w_{ee}(\mathbf{r}_4, \mathbf{r}_1) \\ &= \delta(t_2, t_6) \delta(t_1, t_5) \triangleright \Xi_c^{(2x,ph/hp)}(\mathbf{x}_1, \mathbf{x}_6; \mathbf{x}_2, \mathbf{x}_5; t_1 - t_2), \end{aligned} \quad (\text{G.22})$$

where $\triangleright \Xi_c^{(2x,ph/hp)}$ is obtained by taking the delta functions on the time variables out,

$$\begin{aligned} & \triangleright \Xi_c^{(2x,ph/hp)}(\mathbf{x}_1, \mathbf{x}_6; \mathbf{x}_2, \mathbf{x}_5; t_1 - t_2) \\ &= \delta(\mathbf{x}_1, \mathbf{x}_5) \int d\mathbf{x}_4 w_{ee}(\mathbf{r}_2, \mathbf{r}_6) \chi_0(\mathbf{x}_4 t_1, \mathbf{x}_6 t_2; \mathbf{x}_4 t_1^+, \mathbf{x}_2 t_2^+) w_{ee}(\mathbf{r}_4, \mathbf{r}_1). \end{aligned} \quad (\text{G.23})$$

It is a ph/hp term as the time ordering in the response function corresponds to the propagation of a hole and an electron together. Its Fourier transform is thus given by

$$\begin{aligned} \triangleright \Xi_c^{(2x,ph/hp)}(\mathbf{x}_1, \mathbf{x}_6; \mathbf{x}_2, \mathbf{x}_5, \omega) &= \delta(\mathbf{x}_1, \mathbf{x}_5) \int d\mathbf{x}_4 w_{ee}(\mathbf{r}_2, \mathbf{r}_6) w_{ee}(\mathbf{r}_4, \mathbf{r}_1) \\ & \quad \left[\sum_{kc} \frac{\varphi_c(\mathbf{x}_4) \varphi_c^*(\mathbf{x}_2) \varphi_k(\mathbf{x}_6) \varphi_k^*(\mathbf{x}_4)}{\omega - (\varepsilon_c - \varepsilon_k) + i0^+} - \frac{\varphi_k(\mathbf{x}_4) \varphi_k^*(\mathbf{x}_2) \varphi_c(\mathbf{x}_6) \varphi_c^*(\mathbf{x}_4)}{\omega + (\varepsilon_c - \varepsilon_k) - i0^+} \right], \end{aligned} \quad (\text{G.24})$$

and its matrix elements are given by

$$\triangleright \Xi_{c,pq,rs}^{(2x,ph/hp)}(\omega) = \sum_{kc} \frac{\langle ar|pk\rangle \langle qk|sa\rangle}{\omega - (\varepsilon_c - \varepsilon_k) + i0^+} - \sum_{kc} \frac{\langle kr|pa\rangle \langle qa|sk\rangle}{\omega + (\varepsilon_c - \varepsilon_k) - i0^+} \quad (\text{G.25})$$

The second part of the the exchanged correlation kernel arise from the derivative of W and is given by

$$\begin{aligned} & \triangleleft \Xi_c^{(2x)}(1, 6; 2, 5) \\ &= -i \int d3d4 G_0(1, 3) w_{ee}(\mathbf{r}_2, \mathbf{r}_3) \delta(t_3, t_2) G_0(4, 2^+) \delta(3, 5) \delta(4^+, 6) w_{ee}(\mathbf{r}_4, \mathbf{r}_1) \delta(t_1, t_4) \quad (\text{G.26}) \\ & \quad - i \int d3 G_0(1, 3) w_{ee}(\mathbf{r}_2, \mathbf{r}_3) \delta(t_3, t_2) \delta(2^+, 6) G_0(3, 5^+) w_{ee}(\mathbf{r}_5, \mathbf{r}_1) \delta(t_1, t_5). \end{aligned}$$

By making the time variables explicit, it rewrites as

$$\begin{aligned} & \triangleleft \Xi_c^{(2x)}(1, 6; 2, 5) \\ &= -i G_0(\mathbf{x}_1 t_1, \mathbf{x}_5 t_2) w_{ee}(\mathbf{r}_2, \mathbf{r}_5) \delta(t_5, t_2) G_0(\mathbf{x}_6 t_1, \mathbf{x}_2 t_2^+) w_{ee}(\mathbf{r}_6, \mathbf{r}_1) \delta(t_1^+, t_6) \\ & \quad - i \int d\mathbf{x}_3 G_0(\mathbf{x}_1 t_1, \mathbf{x}_3, t_2) w_{ee}(\mathbf{r}_2, \mathbf{r}_3) \delta(t_2^+, t_6) G_0(\mathbf{x}_3 t_2, \mathbf{x}_5 t_1^+) w_{ee}(\mathbf{r}_5, \mathbf{r}_1) \delta(t_1, t_5) \quad (\text{G.27}) \\ &= \delta(t_5, t_2) \delta(t_1, t_6) \triangleleft \Xi_c^{(2x, pp/hh)}(\mathbf{x}_1, \mathbf{x}_6; \mathbf{x}_2, \mathbf{x}_5; t_1 - t_2) \\ & \quad + \delta(t_1, t_5) \delta(t_2, t_6) \triangleleft \Xi_c^{(2x, ph/hp)}(\mathbf{x}_1, \mathbf{x}_6; \mathbf{x}_2, \mathbf{x}_5; t_1 - t_2) \end{aligned}$$

where

$$\begin{aligned} & \triangleleft \Xi_c^{(2x, pp/hh)}(\mathbf{x}_1, \mathbf{x}_6; \mathbf{x}_2, \mathbf{x}_5; t_1 - t_2) \\ &= w_{ee}(\mathbf{r}_2, \mathbf{r}_5) \chi_0(\mathbf{x}_6 t_1, \mathbf{x}_1 t_1; \mathbf{x}_5 t_2, \mathbf{x}_2 t_2^+) w_{ee}(\mathbf{r}_6, \mathbf{r}_1) \end{aligned} \quad (\text{G.28})$$

and

$$\begin{aligned} & \triangleleft \Xi_c^{(2x, ph/hp)}(\mathbf{x}_1, \mathbf{x}_6; \mathbf{x}_2, \mathbf{x}_5; t_1 - t_2) \\ &= \delta(\mathbf{x}_2, \mathbf{x}_6) \int d\mathbf{x}_3 w_{ee}(\mathbf{r}_2, \mathbf{r}_3) \chi_0(\mathbf{x}_1 t_1, \mathbf{x}_3 t_2; \mathbf{x}_5 t_1^+, \mathbf{x}_3 t_2) w_{ee}(\mathbf{r}_5, \mathbf{r}_1) \end{aligned} \quad (\text{G.29})$$

Their Fourier transforms are then given by

$$\begin{aligned} & \triangleleft \Xi_c^{(2x, pp/hh)}(\mathbf{x}_1, \mathbf{x}_6; \mathbf{x}_2, \mathbf{x}_5; \omega) \\ &= w_{ee}(\mathbf{r}_2, \mathbf{r}_5) w_{ee}(\mathbf{r}_6, \mathbf{r}_1) \\ & \quad \left[- \sum_{cd} \frac{\varphi_c(\mathbf{x}_6) \varphi_c^*(\mathbf{x}_2) \varphi_d(\mathbf{x}_1) \varphi_d^*(\mathbf{x}_5)}{\omega - (\varepsilon_c + \varepsilon_d) + i0^+} + \sum_{kl} \frac{\varphi_k(\mathbf{x}_6) \varphi_k^*(\mathbf{x}_2) \varphi_l(\mathbf{x}_1) \varphi_l^*(\mathbf{x}_5)}{\omega - (\varepsilon_k + \varepsilon_l) - i0^+} \right], \end{aligned} \quad (\text{G.30a})$$

$$\begin{aligned} & \triangleleft \Xi_c^{(2x, ph/hp)}(\mathbf{x}_1, \mathbf{x}_6; \mathbf{x}_2, \mathbf{x}_5; \omega) \\ &= \delta(\mathbf{x}_2, \mathbf{x}_6) \int d\mathbf{x}_3 w_{ee}(\mathbf{r}_2, \mathbf{r}_3) w_{ee}(\mathbf{r}_5, \mathbf{r}_1) \\ & \quad \left[\sum_{kc} \frac{\varphi_c(\mathbf{x}_1) \varphi_c^*(\mathbf{x}_3) \varphi_k(\mathbf{x}_3) \varphi_k^*(\mathbf{x}_5)}{\omega - (\varepsilon_c - \varepsilon_k) + i0^+} - \frac{\varphi_k(\mathbf{x}_1) \varphi_k^*(\mathbf{x}_3) \varphi_c(\mathbf{x}_3) \varphi_c^*(\mathbf{x}_5)}{\omega + (\varepsilon_c - \varepsilon_k) - i0^+} \right]. \end{aligned} \quad (\text{G.30b})$$

and their matrix elements are

$$\langle \Xi_{c,pq,rs}^{(2x,pp/hh)}(\omega) = - \sum_{cd} \frac{\langle cd|ps\rangle\langle qr|dc\rangle}{\omega - (\varepsilon_c + \varepsilon_d) + i0^+} + \sum_{kl} \frac{\langle kl|ps\rangle\langle qr|lk\rangle}{\omega - (\varepsilon_k + \varepsilon_l) - i0^+}, \quad (\text{G.31a})$$

$$\langle \Xi_{c,pq,rs}^{(2x,ph/hp)}(\omega) = \sum_{kc} \frac{\langle rc|pk\rangle\langle qk|cs\rangle}{\omega - (\varepsilon_c - \varepsilon_k) + i0^+} - \sum_{kc} \frac{\langle rk|pc\rangle\langle qc|ks\rangle}{\omega + (\varepsilon_c - \varepsilon_k) - i0^+}. \quad (\text{G.31b})$$

G.2.3 Total correlation kernel

Combining the direct and exchanged contributions, the ph/hp contribution to the correlation kernel is thus given by

$$\Xi_{c,pq,rs}^{2,ph/hp}(\omega) = - \sum_{kc} \frac{\langle rc||pk\rangle\langle qk||sc\rangle}{\omega - (\varepsilon_c - \varepsilon_k) + i0^+} + \sum_{kc} \frac{\langle rk||pc\rangle\langle qc||sk\rangle}{\omega + (\varepsilon_c - \varepsilon_k) - i0^+}, \quad (\text{G.32})$$

and the pp/hh contribution by

$$\Xi_{c,pq,rs}^{2,pp/hh}(\omega) = \frac{1}{2} \sum_{cd} \frac{\langle qr||cd\rangle\langle cd||ps\rangle}{\omega - (\varepsilon_c + \varepsilon_d) + i0^+} - \frac{1}{2} \sum_{kl} \frac{\langle qr||kl\rangle\langle kl||ps\rangle}{\omega - (\varepsilon_k + \varepsilon_l) - i0^+}. \quad (\text{G.33})$$

G.3 Spin-adaptation of the correlation kernel

For spin-restricted closed-shell calculations, the spin-adapted kernel is obtained by rotation in the spin space as was done in Section 8.3.2. For four fixed spatial orbitals referred to as p, q, r, s , the spin-singlet and triplet kernels are therefore obtained by

$${}^1\Xi_{c,pq,rs}^{(2)}(\omega) = \Xi_{c,p\uparrow q\uparrow, r\uparrow s\uparrow}^{(2)}(\omega) + \Xi_{c,p\uparrow q\uparrow, r\downarrow s\downarrow}^{(2)}(\omega), \quad (\text{G.34a})$$

$${}^3\Xi_{c,pq,rs}^{(2)}(\omega) = \Xi_{c,p\uparrow q\uparrow, r\uparrow s\uparrow}^{(2)}(\omega) - \Xi_{c,p\uparrow q\uparrow, r\downarrow s\downarrow}^{(2)}(\omega). \quad (\text{G.34b})$$

G.3.1 Ph/hp spin-adapted kernel

With the convention

$$w_{ee,pq,rs}(\omega) = \int d\mathbf{x}_1 d\mathbf{x}_2 d\mathbf{x}_5 d\mathbf{x}_6 \varphi_p(\mathbf{x}_2) \varphi_q^*(\mathbf{x}_1) w_{ee}(\mathbf{x}_1, \mathbf{x}_6; \mathbf{x}_2, \mathbf{x}_5; \omega) \varphi_r^*(\mathbf{x}_6) \varphi_s(\mathbf{x}_5), \quad (\text{G.35})$$

the spin contribution to the ph/hp kernel are obtained from Equation (G.40) when the sum over i and a is done for all possible spins and are given by

$$\begin{aligned} \Xi_{c,p\uparrow q\uparrow, r\uparrow s\uparrow}^{(2,ph/hp)}(\omega) = & \\ & - \sum_{kc} \frac{2w_{ee,pr,ck}w_{ee,sq,kc} - w_{ee,pr,ck}w_{ee,cq,ks} - w_{ee,kr,cp}w_{ee,sq,kc} + w_{ee,kr,cp}w_{ee,cq,ks}}{\omega - (\varepsilon_c - \varepsilon_k) + i0^+} \\ & + \sum_{kc} \frac{2w_{ee,pr,kc}w_{ee,sq,ck} - w_{ee,pr,kc}w_{ee,kq,cs} - w_{ee,cr,kp}w_{ee,sq,ck} + w_{ee,cr,kp}w_{ee,kq,cs}}{\omega + (\varepsilon_c - \varepsilon_k) - i0^+}, \end{aligned} \quad (\text{G.36a})$$

$$\Xi_{c,p\uparrow q\uparrow,r\downarrow s\downarrow}^{(2)}(\omega) = - \sum_{kc} \frac{w_{ee,kr,cp}w_{ee,cq,ks}}{\omega - (\varepsilon_c - \varepsilon_k) + i0^+} + \sum_{kc} \frac{w_{ee,cr,kp}w_{ee,kq,cs}}{\omega + (\varepsilon_c - \varepsilon_k) - i0^+}. \quad (\text{G.36b})$$

The singlet and triplet ph/hp kernels are then obtained by sum and difference of these two terms and are given by

$$\begin{aligned} {}^1\Xi_{c,pq,rs}^{(2,\text{ph/hp})}(\omega) = & \\ & - \sum_{kc} \frac{2w_{ee,pr,ck}w_{ee,sq,kc} - w_{ee,pr,ck}w_{ee,cq,ks} - w_{ee,kr,cp}w_{ee,sq,kc} + 2w_{ee,kr,cp}w_{ee,cq,ks}}{\omega - (\varepsilon_c - \varepsilon_k) + i0^+} \\ & + \sum_{kc} \frac{2w_{ee,pr,kc}w_{ee,sq,ck} - w_{ee,pr,kc}w_{ee,kq,cs} - w_{ee,cr,kp}w_{ee,sq,ck} + 2w_{ee,cr,kp}w_{ee,kq,cs}}{\omega + (\varepsilon_c - \varepsilon_k) - i0^+}, \end{aligned} \quad (\text{G.37a})$$

$$\begin{aligned} {}^3\Xi_{c,pq,rs}^{(2,\text{ph/hp})}(\omega) = & - \sum_{kc} \frac{2w_{ee,pr,ck}w_{ee,sq,kc} - w_{ee,pr,ck}w_{ee,cq,ks} - w_{ee,kr,cp}w_{ee,sq,kc}}{\omega - (\varepsilon_c - \varepsilon_k) + i0^+} \\ & + \sum_{kc} \frac{2w_{ee,pr,kc}w_{ee,sq,ck} - w_{ee,pr,kc}w_{ee,kq,cs} - w_{ee,cr,kp}w_{ee,sq,ck}}{\omega + (\varepsilon_c - \varepsilon_k) - i0^+}. \end{aligned} \quad (\text{G.37b})$$

G.3.2 Pp/hh spin-adapted kernel

Similarly, in Equation (G.41), the sums are performed over all spin-orbitals. The term $\Xi_{c,p\uparrow q\uparrow,r\uparrow s\uparrow}^{(2,\text{pp/hh})}(\omega)$ and $\Xi_{c,p\uparrow q\uparrow,r\downarrow s\downarrow}^{(2,\text{pp/hh})}(\omega)$ are given by

$$\Xi_{c,p\uparrow q\uparrow,r\uparrow s\uparrow}^{(2,\text{pp/hh})}(\omega) = \frac{1}{2} \sum_{cd} \frac{\bar{w}_{ee,cq,rd}\bar{w}_{ee,pc,ds}}{\omega - (\varepsilon_c + \varepsilon_d) + i0^+} - \frac{1}{2} \sum_{kl} \frac{\bar{w}_{ee,kq,rl}\bar{w}_{ee,pk,ls}}{\omega - (\varepsilon_k + \varepsilon_l) - i0^+}, \quad (\text{G.38a})$$

$$\begin{aligned} \Xi_{c,p\uparrow q\uparrow,r\downarrow s\downarrow}^{(2,\text{pp/hh})}(\omega) = & \frac{1}{2} \sum_{cd} \frac{w_{ee,cq,rd}w_{ee,pc,ds} + w_{ee,dq,rc}w_{ee,sc,dp}}{\omega - (\varepsilon_c + \varepsilon_d) + i0^+} \\ & - \frac{1}{2} \sum_{kl} \frac{w_{ee,kq,rl}w_{ee,pk,ls} + w_{ee,lq,rk}w_{ee,sk,lp}}{\omega - (\varepsilon_k + \varepsilon_l) - i0^+}, \end{aligned} \quad (\text{G.38b})$$

where $\bar{w}_{ee,pq,rs}$ stands for $w_{ee,pq,rs} - w_{ee,pr,qs}$. The spin-adapted pp/hh kernels are thus given by

$$\begin{aligned} {}^1\Xi_{c,pq,rs}^{(2,\text{pp/hh})}(\omega) = & \\ = & \frac{1}{2} \sum_{cd} \frac{2w_{ee,cq,rd}w_{ee,pc,ds} - w_{ee,cq,rd}w_{ee,sc,dp} - w_{ee,dq,rc}w_{ee,pc,ds} + 2w_{ee,dq,rc}w_{ee,sc,dp}}{\omega - (\varepsilon_c + \varepsilon_d) + i0^+} \\ & - \frac{1}{2} \sum_{kl} \frac{2w_{ee,kq,rl}w_{ee,pk,ls} - w_{ee,kq,rl}w_{ee,sk,lp} - w_{ee,lq,rk}w_{ee,pk,ls} + 2w_{ee,lq,rk}w_{ee,sk,lp}}{\omega - (\varepsilon_k + \varepsilon_l) - i0^+}, \end{aligned} \quad (\text{G.39a})$$

$$\begin{aligned} {}^3\Xi_{c,pq,rs}^{(2,\text{pp/hh})}(\omega) = & - \frac{1}{2} \sum_{cd} \frac{w_{ee,cq,rd}w_{ee,sc,dp} + w_{ee,dq,rc}w_{ee,pc,ds}}{\omega - (\varepsilon_c + \varepsilon_d) + i0^+} \\ & + \frac{1}{2} \sum_{kl} \frac{w_{ee,kq,rl}w_{ee,sk,lp} + w_{ee,lq,rk}w_{ee,pk,ls}}{\omega - (\varepsilon_k + \varepsilon_l) - i0^+}. \end{aligned} \quad (\text{G.39b})$$

G.4 Summary

- ph/hp second-order correlation kernel

$$\Xi_{c,pq,rs}^{2,\text{ph/hp}}(\omega) = - \sum_{kc} \frac{\langle rc||pk\rangle\langle qk||sc\rangle}{\omega - (\varepsilon_c - \varepsilon_k) + i0^+} + \sum_{kc} \frac{\langle rk||pc\rangle\langle qc||sk\rangle}{\omega + (\varepsilon_c - \varepsilon_k) - i0^+}, \quad (\text{G.40})$$

- pp/hh second-order correlation kernel

$$\Xi_{c,pq,rs}^{2,\text{pp/hh}}(\omega) = \frac{1}{2} \sum_{cd} \frac{\langle qr||cd\rangle\langle cd||ps\rangle}{\omega - (\varepsilon_c + \varepsilon_d) + i0^+} - \frac{1}{2} \sum_{kl} \frac{\langle qr||kl\rangle\langle kl||ps\rangle}{\omega - (\varepsilon_k + \varepsilon_l) - i0^+}. \quad (\text{G.41})$$

- ph/hp singlet second-order correlation kernel

$$\begin{aligned} {}^1\Xi_{c,pq,rs}^{(2,\text{ph/hp})}(\omega) = & \\ & - \sum_{kc} \frac{2w_{ee,pr,ck}w_{ee,sq,kc} - w_{ee,pr,ck}w_{ee,cq,ks} - w_{ee,kr,cp}w_{ee,sq,kc} + 2w_{ee,kr,cp}w_{ee,cq,ks}}{\omega - (\varepsilon_c - \varepsilon_k) + i0^+} \\ & + \sum_{kc} \frac{2w_{ee,pr,kc}w_{ee,sq,ck} - w_{ee,pr,kc}w_{ee,kq,cs} - w_{ee,cr,kp}w_{ee,sq,ck} + 2w_{ee,cr,kp}w_{ee,kq,cs}}{\omega + (\varepsilon_c - \varepsilon_k) - i0^+}, \end{aligned} \quad (\text{G.42})$$

- ph/hp triplet second-order correlation kernel

$$\begin{aligned} {}^3\Xi_{c,pq,rs}^{(2,\text{ph/hp})}(\omega) = & - \sum_{kc} \frac{2w_{ee,pr,ck}w_{ee,sq,kc} - w_{ee,pr,ck}w_{ee,cq,ks} - w_{ee,kr,cp}w_{ee,sq,kc}}{\omega - (\varepsilon_c - \varepsilon_k) + i0^+} \\ & + \sum_{kc} \frac{2w_{ee,pr,kc}w_{ee,sq,ck} - w_{ee,pr,kc}w_{ee,kq,cs} - w_{ee,cr,kp}w_{ee,sq,ck}}{\omega + (\varepsilon_c - \varepsilon_k) - i0^+}. \end{aligned} \quad (\text{G.43})$$

- pp/hh singlet second-order correlation kernel

$$\begin{aligned} {}^1\Xi_{c,pq,rs}^{(2,\text{pp/hh})}(\omega) = & \\ = & \frac{1}{2} \sum_{cd} \frac{2w_{ee,cq,rd}w_{ee,pc,ds} - w_{ee,cq,rd}w_{ee,sc,dp} - w_{ee,dq,rc}w_{ee,pc,ds} + 2w_{ee,dq,rc}w_{ee,sc,dp}}{\omega - (\varepsilon_c + \varepsilon_d) + i0^+} \\ & - \frac{1}{2} \sum_{kl} \frac{2w_{ee,kq,rl}w_{ee,pk,ls} - w_{ee,kq,rl}w_{ee,sk,lp} - w_{ee,lq,rk}w_{ee,pk,ls} + 2w_{ee,lq,rk}w_{ee,sk,lp}}{\omega - (\varepsilon_k + \varepsilon_l) - i0^+}, \end{aligned} \quad (\text{G.44})$$

- pp/hh triplet second-order correlation kernel

$$\begin{aligned} {}^3\Xi_{c,pq,rs}^{(2,\text{pp/hh})}(\omega) = & - \frac{1}{2} \sum_{cd} \frac{w_{ee,cq,rd}w_{ee,sc,dp} + w_{ee,dq,rc}w_{ee,pc,ds}}{\omega - (\varepsilon_c + \varepsilon_d) + i0^+} \\ & + \frac{1}{2} \sum_{kl} \frac{w_{ee,kq,rl}w_{ee,sk,lp} + w_{ee,lq,rk}w_{ee,pk,ls}}{\omega - (\varepsilon_k + \varepsilon_l) - i0^+}. \end{aligned} \quad (\text{G.45})$$

Appendix H

Dynamic BSE

In this appendix, the details of the Fourier transform of the Bethe-Salpeter equation with a dynamical second-order kernel which depends on one frequency are given. The derivation of the effective second-order dynamical Bethe-Salpeter kernel in a spin-orbital basis set is also detailed. This appendix is to be read with Chapter 10 and requires the equations derived in Appendices F and G. A summary of the main formulas is given at the end of this appendix.

H.1 Fourier transform of the Bethe-Salpeter Equation

In this section, we are interested in evaluating the Fourier transform of the response function χ at second-order with respect to the electronic interaction defined through the Bethe-Salpeter equation as

$$\begin{aligned} \chi(\mathbf{x}_1 t_1, \mathbf{x}_2 t_2; \mathbf{x}'_1 t_1^+, \mathbf{x}'_2 t_2^+) &= \chi_0(\mathbf{x}_1 t_1, \mathbf{x}_2 t_2; \mathbf{x}'_1 t_1^+, \mathbf{x}'_2 t_2^+) \\ &+ \int d\mathbf{x}_3 dt_3 d\mathbf{x}_4 dt_4 d\mathbf{x}_5 dt_5 d\mathbf{x}_6 dt_6 \chi_0(\mathbf{x}_1 t_1, \mathbf{x}_4 t_4; \mathbf{x}'_1 t_1^+, \mathbf{x}_3 t_3) \quad (\text{H.1}) \\ &\Xi_{Hxc}^{(2)}(\mathbf{x}_3 t_3, \mathbf{x}_6 t_6; \mathbf{x}_4 t_4, \mathbf{x}_5 t_5) \chi(\mathbf{x}_5 t_5, \mathbf{x}_2 t_2; \mathbf{x}_6 t_6, \mathbf{x}'_2 t_2^+). \end{aligned}$$

As the Hartree and exchange kernels are static, only the correlation part is detailed hereinafter. From Chapter 9, we know that the second-order correlation kernel can be decoupled into a ph/hp and a pp/hh part which exhibits different delta functions on the time variables

$$\begin{aligned} \Xi_c^{(2)}(3, 6; 4, 5) &= \delta(t_4, t_6) \delta(t_3, t_5) \Xi_c^{(2, \text{ph/hp})}(\mathbf{x}_3, \mathbf{x}_6; \mathbf{x}_4, \mathbf{x}_5; t_3 - t_4) \\ &+ \delta(t_4, t_5) \delta(t_3, t_6) \Xi_c^{(2, \text{pp/hh})}(\mathbf{x}_3, \mathbf{x}_6; \mathbf{x}_4, \mathbf{x}_5; t_3 - t_4). \quad (\text{H.2}) \end{aligned}$$

In this equation, the terms $\Xi_c^{(2, \text{ph/hp})}$ and $\Xi_c^{(2, \text{pp/hh})}$ include both direct and exchanged contributions, where the derivative of W was also taken into account. As the delta

functions are different for the ph/hp and pp/hh terms, they need to be treated separately when the Fourier transform is performed.

H.1.1 Evaluation of the particle-hole term

We first evaluate the ph/hp contribution to the Bethe-Salpeter equation given by

$$\begin{aligned}
 T^{\text{ph/hp}}(\mathbf{x}_1, \mathbf{x}_2, \mathbf{x}'_1, \mathbf{x}'_2; t_1 - t_2) \\
 = \int d\mathbf{x}_3 dt_3 d\mathbf{x}_4 dt_4 d\mathbf{x}_5 dt_5 d\mathbf{x}_6 dt_6 \chi_0(\mathbf{x}_1 t_1, \mathbf{x}_4 t_4; \mathbf{x}'_1 t_1^+, \mathbf{x}_3 t_3) \\
 \delta(t_4, t_6) \delta(t_3, t_5) \Xi_c^{(2, \text{ph/hp})}(\mathbf{x}_3, \mathbf{x}_6; \mathbf{x}_4, \mathbf{x}_5; t_3 - t_4) \chi(\mathbf{x}_5 t_5, \mathbf{x}_2 t_2; \mathbf{x}_6 t_6, \mathbf{x}'_2 t_2^+),
 \end{aligned} \tag{H.3}$$

which will be referred as $T^{\text{ph/hp}}$ in the following. In terms of time differences, it becomes

$$\begin{aligned}
 T^{\text{ph/hp}}(\mathbf{x}_1, \mathbf{x}_2, \mathbf{x}'_1, \mathbf{x}'_2; t_1 - t_2) \\
 = \int d\mathbf{x}_3 dt_3 d\mathbf{x}_4 dt_4 d\mathbf{x}_5 d\mathbf{x}_6 \chi_0 \left(\mathbf{x}_1, \mathbf{x}_4; \mathbf{x}'_1, \mathbf{x}_3; -\eta, t_4 - t_3, \frac{2t_1 - \eta}{2} - \frac{t_3 + t_4}{2} \right) \\
 \Xi_c^{(2, \text{ph})}(\mathbf{x}_3, \mathbf{x}_6; \mathbf{x}_4, \mathbf{x}_5; t_3 - t_4) \chi(\mathbf{x}_5, \mathbf{x}_2; \mathbf{x}_6, \mathbf{x}'_2; t_3 - t_4, -\eta, \frac{t_3 + t_4}{2} - \frac{2t_2 - \eta}{2}).
 \end{aligned} \tag{H.4}$$

In order to perform the Fourier transform of this quantity, it is convenient to do a change of variables given by

$$t_3 \rightarrow \tau_3 = t_3 - t_4 \quad ; \quad t_4 \rightarrow \tau_4 = t_4 - t_2 + \frac{\tau_3 + \eta}{2} \quad ; \quad \tau = t_1 - t_2, \tag{H.5}$$

such that it can be rewritten as

$$\begin{aligned}
 T^{\text{ph/hp}}(\mathbf{x}_1, \mathbf{x}_2; \mathbf{x}'_1, \mathbf{x}'_2; \tau) = \int d\mathbf{x}_3 d\tau_3 d\mathbf{x}_4 d\tau_4 d\mathbf{x}_5 d\mathbf{x}_6 \chi_0(\mathbf{x}_1, \mathbf{x}_4; \mathbf{x}'_1, \mathbf{x}_3; -\eta, -\tau_3, \tau - \tau_4) \\
 \Xi_c^{(2, \text{ph/hp})}(\mathbf{x}_3, \mathbf{x}_6; \mathbf{x}_4, \mathbf{x}_5; \tau_3) \chi(\mathbf{x}_5, \mathbf{x}_2; \mathbf{x}_6, \mathbf{x}'_2; \tau_3, -\eta, \tau_4).
 \end{aligned} \tag{H.6}$$

As it depends only on one time difference, its Fourier transform is then given by

$$\begin{aligned}
 T^{\text{ph/hp}}(\mathbf{x}_1, \mathbf{x}_2; \mathbf{x}'_1, \mathbf{x}'_2; \omega) = \int d\tau e^{i\omega\tau} \int d\mathbf{x}_3 d\tau_3 d\mathbf{x}_4 d\tau_4 d\mathbf{x}_5 d\mathbf{x}_6 \chi_0(\mathbf{x}_1, \mathbf{x}_4; \mathbf{x}'_1, \mathbf{x}_3; -\eta, -\tau_3, \tau - \tau_4) \\
 \Xi_c^{(2, \text{ph/hp})}(\mathbf{x}_3, \mathbf{x}_6; \mathbf{x}_4, \mathbf{x}_5; \tau_3) \chi(\mathbf{x}_5, \mathbf{x}_2; \mathbf{x}_6, \mathbf{x}'_2; \tau_3, -\eta, \tau_4).
 \end{aligned} \tag{H.7}$$

Making explicit the Fourier transform of χ_0 and Ξ , it becomes

$$\begin{aligned}
 T^{\text{ph/hp}}(\mathbf{x}_1, \mathbf{x}_2; \mathbf{x}'_1, \mathbf{x}'_2; \omega) = \int d\tau d\tau_3 d\tau_4 \frac{d\omega'}{2\pi} \frac{d\omega''}{2\pi} \frac{d\omega'''}{2\pi} d\mathbf{x}_3 d\mathbf{x}_4 d\mathbf{x}_5 d\mathbf{x}_6 \\
 \chi_0(\mathbf{x}_1, \mathbf{x}_4; \mathbf{x}'_1, \mathbf{x}_3; -\eta, \omega', \omega'') \Xi_c^{(2, \text{ph/hp})}(\mathbf{x}_3, \mathbf{x}_6; \mathbf{x}_4, \mathbf{x}_5; \omega''') \\
 \chi(\mathbf{x}_5, \mathbf{x}_2; \mathbf{x}_6, \mathbf{x}'_2; \tau_3, -\eta, \tau_4) e^{-i(\omega'' - \omega)\tau} e^{-i(\omega''' - \omega')\tau_3} e^{i\omega''\tau_4},
 \end{aligned} \tag{H.8}$$

which by integration over the time variables and ω'' gives

$$T^{\text{ph/hp}}(\mathbf{x}_1, \mathbf{x}_2; \mathbf{x}'_1, \mathbf{x}'_2; \omega) = \int \frac{d\omega'}{2\pi} \frac{d\omega''}{2\pi} d\mathbf{x}_3 d\mathbf{x}_4 d\mathbf{x}_5 d\mathbf{x}_6 \chi_0(\mathbf{x}_1, \mathbf{x}_4; \mathbf{x}'_1, \mathbf{x}_3; -\eta, \omega', \omega) \Xi_c^{(2, \text{ph/hp})}(\mathbf{x}_3, \mathbf{x}_6; \mathbf{x}_4, \mathbf{x}_5; \omega' - \omega'') \chi(\mathbf{x}_5, \mathbf{x}_2; \mathbf{x}_6, \mathbf{x}'_2; \omega'', -\eta, \omega) \quad (\text{H.9})$$

In the second-order approximation, only the zeroth-order term contributes in χ as the correlation kernel contributes at the second order. Therefore, making advantage of the diagonal character of χ_0 , the matrix elements of this term are

$$T_{pq,rs}^{\text{ph/hp}}(\omega) = \int \frac{d\omega'}{2\pi} \frac{d\omega''}{2\pi} \chi_{0,pq,pq}(-\eta, \omega', \omega) \Xi_c^{(2, \text{ph/hp})}(\omega' - \omega'') \chi_{0,rs,rs}(\omega'', -\eta, \omega). \quad (\text{H.10})$$

H.1.2 Evaluation of the particle-particle/hole-hole term

We note $T^{\text{pp/hh}}$ the term coming from the convolution of the pp/hh correlation kernel, given by

$$T^{\text{pp/hh}}(\mathbf{x}_1, \mathbf{x}_2, \mathbf{x}'_1, \mathbf{x}'_2; t_1 - t_2) = \int d\mathbf{x}_3 dt_3 d\mathbf{x}_4 dt_4 d\mathbf{x}_5 d\mathbf{x}_6 \chi_0(\mathbf{x}_1 t_1, \mathbf{x}_4 t_4; \mathbf{x}'_1 t_1^+, \mathbf{x}_3 t_3) \Xi_c^{(2, \text{pp/hh})}(\mathbf{x}_3, \mathbf{x}_6; \mathbf{x}_4, \mathbf{x}_5; t_3 - t_4) \chi(\mathbf{x}_5 t_4, \mathbf{x}_2 t_2; \mathbf{x}_6 t_3, \mathbf{x}'_2 t_2^+). \quad (\text{H.11})$$

In terms of time differences, and with the change of variables

$$\tau_4 = t_4 - t_3 \quad ; \quad \tau_3 = t_3 - t_2 + \frac{\tau_4 + \eta}{2} \quad ; \quad \tau = t_1 - t_2, \quad (\text{H.12})$$

it can be rewritten as

$$T^{\text{pp/hh}}(\mathbf{x}_1, \mathbf{x}_2, \mathbf{x}'_1, \mathbf{x}'_2; \tau) = \int d\mathbf{x}_3 d\tau_3 d\mathbf{x}_4 d\tau_4 d\mathbf{x}_5 d\mathbf{x}_6 \chi_0(\mathbf{x}_1, \mathbf{x}_4; \mathbf{x}'_1, \mathbf{x}_3; -\eta, \tau_4, \tau - \tau_3) \Xi_c^{(2, \text{pp/hh})}(\mathbf{x}_3, \mathbf{x}_6; \mathbf{x}_4, \mathbf{x}_5; -\tau_4) \chi(\mathbf{x}_5, \mathbf{x}_2; \mathbf{x}_6, \mathbf{x}'_2; \tau_4, -\eta, \tau_3). \quad (\text{H.13})$$

Similarly to the ph/ph case, its Fourier transform is therefore

$$T^{\text{pp/hh}}(\mathbf{x}_1, \mathbf{x}_2, \mathbf{x}'_1, \mathbf{x}'_2; \omega) = \int \frac{d\omega'}{2\pi} \int \frac{d\omega''}{2\pi} \int d\mathbf{x}_3 d\mathbf{x}_4 d\mathbf{x}_5 d\mathbf{x}_6 \chi_0(\mathbf{x}_1, \mathbf{x}_4; \mathbf{x}'_1, \mathbf{x}_3; -\eta, \omega', \omega) \Xi_c^{(2, \text{pp/hh})}(\mathbf{x}_3, \mathbf{x}_6; \mathbf{x}_4, \mathbf{x}_5; \omega' + \omega'') \chi(\mathbf{x}_5, \mathbf{x}_2; \mathbf{x}_6, \mathbf{x}'_2; \omega'', -\eta, \omega), \quad (\text{H.14})$$

and its matrix elements are given by

$$T_{pq,rs}^{\text{pp/hh}}(\omega) = \int \frac{d\omega'}{2\pi} \frac{d\omega''}{2\pi} \chi_{0,pq,pq}(-\eta, \omega', \omega) \Xi_c^{(2, \text{pp/hh})}(\omega' + \omega'') \chi_{0,rs,rs}(\omega'', -\eta, \omega). \quad (\text{H.15})$$

H.2 Matrix elements of the effective kernel

In a first step, the integral over ω' is evaluated in the case $pq = ja$, where the matrix elements of χ_0 are given in Equation (F.10a). Then, the integration over ω'' is done either with $rs = ib$ for the matrix elements of the block (ov,ov) corresponding to the matrix **A**, or with $rs = bi$ for the matrix elements of the block (ov,vo) which correspond to the **B** block.

H.2.1 Particle-hole effective kernel

Integration over ω' for $pq = ia$

Using the expression of the matrix elements of χ_0 given in Equation (F.10a), and of the ph/ph correlation kernel given in Equation (G.40), the matrix elements of $T^{\text{ph/hp}}$ are

$$T_{ia,rs}^{\text{ph/hp}}(\omega) = i \sum_{kc} \int \frac{d\omega'}{2\pi} \frac{d\omega''}{2\pi} \chi_{0,ia,ia}(\omega) \chi_{0,rs,rs}(\omega'', -\eta, \omega) e^{i\omega'\eta} \left(\frac{1}{\omega' + \frac{\omega}{2} - \varepsilon_a + i0^+} - \frac{1}{\omega' - \frac{\omega}{2} - \varepsilon_i - i0^+} \right) \left(\frac{\langle rk||ic\rangle \langle ac||sk\rangle}{\omega' - \omega'' + (\varepsilon_c - \varepsilon_k) - i0^+} - \frac{\langle rc||ik\rangle \langle ak||sc\rangle}{\omega' - \omega'' - (\varepsilon_c - \varepsilon_k) + i0^+} \right). \quad (\text{H.16})$$

Using the relation (F.8) and by integration on the upper complex half-plane, it gives

$$T_{ia,rs}^{\text{ph/hp}}(\omega) = \sum_{kc} \int \frac{d\omega''}{2\pi} \chi_{0,ia,ia}(\omega) \chi_{0,rs,rs}(\omega'', -\eta, \omega) \left(\frac{\langle rk||ic\rangle \langle ac||sk\rangle}{-\omega'' - \frac{\omega}{2} + \varepsilon_a + \varepsilon_c - \varepsilon_k - i0^+} - \frac{\langle rc||ik\rangle \langle ak||sc\rangle}{-\omega'' + \frac{\omega}{2} + \varepsilon_i - \varepsilon_c + \varepsilon_k + i0^+} \right). \quad (\text{H.17})$$

Integration over ω'' for $rs = jb$

The matrix elements in the (ov,ov) block are then obtained by doing the second integration over ω'' in the case $rs = jb$, using Equation (F.10a) for the matrix elements of χ_0 . In this case, the matrix elements of the ph/ph term are given by

$$T_{ia,jb}^{\text{ph/hp}}(\omega) = -i \int \frac{d\omega''}{2\pi} \sum_{kc} \chi_{0,ia,ia}(\omega) \chi_{0,jb,jb}(\omega) \left(\frac{\langle jk||ic\rangle \langle ac||bk\rangle}{\omega'' + \frac{\omega}{2} - \varepsilon_a - \varepsilon_c + \varepsilon_k + i0^+} - \frac{\langle jc||ik\rangle \langle ak||bc\rangle}{\omega'' - \frac{\omega}{2} - \varepsilon_i + \varepsilon_c - \varepsilon_k - i0^+} \right) \left(\frac{1}{\omega'' + \frac{\omega}{2} - \varepsilon_b + i0^+} - \frac{1}{\omega'' - \frac{\omega}{2} - \varepsilon_j - i0^+} \right) e^{i\omega''\eta} \quad (\text{H.18})$$

and by integration over the upper complex plane, it finally gives

$$T_{ia,jb}^{\text{ph/hp}}(\omega) = -\chi_{0,ia,ia}(\omega)\chi_{0,jb,jb}(\omega) \sum_{kc} \left(\frac{\langle jk||ic\rangle\langle ac||bk\rangle}{\omega - \varepsilon_a + \varepsilon_k - \varepsilon_c + \varepsilon_j + i0^+} + \frac{\langle jc||ik\rangle\langle ak||bc\rangle}{\omega + \varepsilon_i - \varepsilon_c + \varepsilon_k - \varepsilon_b + i0^+} \right). \quad (\text{H.19})$$

Integration over ω'' for $rs = bj$

In order to have the (ov,vo) matrix elements, the second integration is now done with $rs = bj$ instead of $rs = bj$. The matrix elements of χ_0 are now given by Equation (F.10b). The matrix elements of the term ph/ph in the (ov,vo) block are thus obtained by

$$T_{ia,bj}^{\text{ph/hp}}(\omega) = -i \int \frac{d\omega''}{2\pi} \sum_{kc} \chi_{0,ia,ia}(\omega)\chi_{0,bj,bj}(\omega) \left(\frac{\langle bk||ic\rangle\langle ac||jk\rangle}{\omega'' + \frac{\omega}{2} - \varepsilon_a - \varepsilon_c + \varepsilon_k + i0^+} - \frac{\langle bc||ik\rangle\langle ak||jc\rangle}{\omega'' - \frac{\omega}{2} - \varepsilon_i + \varepsilon_c - \varepsilon_k - i0^+} \right) \left(\frac{1}{\omega'' + \frac{\omega}{2} - \varepsilon_j - i0^+} - \frac{1}{\omega'' - \frac{\omega}{2} - \varepsilon_b + i0^+} \right) e^{i\omega''\eta}. \quad (\text{H.20})$$

and by integration over the upper complex plane, it finally gives

$$T_{ia,bj}^{\text{ph/hp}}(\omega) = -\chi_{0,ia,ia}(\omega)\chi_{0,bj,bj}(\omega) \sum_{kc} \left(\frac{\langle bk||ic\rangle\langle ac||jk\rangle}{\varepsilon_a - \varepsilon_k + \varepsilon_c - \varepsilon_j - i0^+} - \frac{\langle bc||ik\rangle\langle ak||jc\rangle}{\varepsilon_i - \varepsilon_c + \varepsilon_k - \varepsilon_b + i0^+} \right). \quad (\text{H.21})$$

It is worth mentioning that this term depends on ω only via the two response functions which means that the ph/ph effective kernel does not depend on ω in the **B** block at the second order of perturbation.

Effective ph/hp correlation kernel

This therefore defines an effective ph/hp kernel $\tilde{\Xi}_c^{(2,\text{ph/hp})}$ which matrix elements in the block **A** are given by

$$\tilde{\Xi}_{c,ia,jb}^{(2,\text{ph/hp})}(\omega) = -\sum_{kc} \left(\frac{\langle jk||ic\rangle\langle ac||bk\rangle}{\omega - \varepsilon_a + \varepsilon_k - \varepsilon_c + \varepsilon_j + i0^+} + \frac{\langle jc||ik\rangle\langle ak||bc\rangle}{\omega + \varepsilon_i - \varepsilon_c + \varepsilon_k - \varepsilon_b + i0^+} \right), \quad (\text{H.22})$$

and in the block **B** by

$$\tilde{\Xi}_{c,ia,bj}^{(2,\text{ph/hp})} = \sum_{kc} \left(\frac{\langle bk||ic\rangle\langle ac||jk\rangle}{-\varepsilon_a + \varepsilon_k - \varepsilon_c + \varepsilon_j + i0^+} + \frac{\langle bc||ik\rangle\langle ak||jc\rangle}{\varepsilon_i - \varepsilon_c + \varepsilon_k - \varepsilon_b + i0^+} \right). \quad (\text{H.23})$$

It is straightforward to show that the kernel contribution to the block **A** is then hermitian such that $\tilde{\Xi}_{c,ia,jb}^{(2,\text{ph/hp})}(\omega) = \tilde{\Xi}_{c,jb,ia}^{(2,\text{ph/hp})}(\omega)^*$, and symmetric and frequency-independent for the

block **B**, i.e. $\tilde{\Xi}_{c,ia,bj}^{(2,\text{ph}/\text{hp})} = \tilde{\Xi}_{c,jb,ai}^{(2,\text{ph}/\text{hp})}$.

Spin adaptation

Following the same procedure as in Appendix G.3, the matrix elements of the singlet and triplet ph/hp effective correlation kernels in the block **A** are given by

$$\begin{aligned} {}^1\tilde{\Xi}_{c,ia,jb}^{(2,\text{ph}/\text{hp})}(\omega) = & \\ & - \sum_{kc} \frac{2w_{ee,ij,kc}w_{ee,ba,ck} - w_{ee,ij,kc}w_{ee,ka,cb} - w_{ee,cj,ki}w_{ee,ba,ck} + 2w_{ee,cj,ki}w_{ee,ka,cb}}{\omega - \varepsilon_a + \varepsilon_k - \varepsilon_c + \varepsilon_j + i0^+} \\ & - \sum_{kc} \frac{2w_{ee,ij,ck}w_{ee,ba,kc} - w_{ee,ij,ck}w_{ee,ca,kb} - w_{ee,kj,ci}w_{ee,ba,kc} + 2w_{ee,kj,ci}w_{ee,ca,kb}}{\omega + \varepsilon_i - \varepsilon_c + \varepsilon_k - \varepsilon_b + i0^+}, \end{aligned} \quad (\text{H.24a})$$

$$\begin{aligned} {}^3\tilde{\Xi}_{c,ia,jb}^{(2,\text{ph}/\text{hp})}(\omega) = & - \sum_{kc} \frac{2w_{ee,ij,kc}w_{ee,ba,ck} - w_{ee,ij,kc}w_{ee,ka,cb} - w_{ee,cj,ki}w_{ee,ba,ck}}{\omega - \varepsilon_a + \varepsilon_k - \varepsilon_c + \varepsilon_j + i0^+} \\ & - \sum_{kc} \frac{2w_{ee,ij,ck}w_{ee,ba,kc} - w_{ee,ij,ck}w_{ee,ca,kb} - w_{ee,kj,ci}w_{ee,ba,kc}}{\omega + \varepsilon_i - \varepsilon_c + \varepsilon_k - \varepsilon_b + i0^+}, \end{aligned} \quad (\text{H.24b})$$

and the matrix elements of the singlet and triplet ph/hp effective correlation kernels in the block **B** are given by

$$\begin{aligned} {}^1\tilde{\Xi}_{c,ia,bj}^{(2,\text{ph}/\text{hp})} = & \\ & \sum_{kc} \frac{2w_{ee,ib,kc}w_{ee,ja,ck} - w_{ee,ib,kc}w_{ee,ka,cj} - w_{ee,cb,ki}w_{ee,ja,ck} + 2w_{ee,cb,ki}w_{ee,ka,cj}}{-\varepsilon_a + \varepsilon_k - \varepsilon_c + \varepsilon_j + i0^+} \\ & + \sum_{kc} \frac{2w_{ee,ib,ck}w_{ee,ja,kc} - w_{ee,ib,ck}w_{ee,ca,kj} - w_{ee,cb,ci}w_{ee,ja,kc} + 2w_{ee,cb,ci}w_{ee,ca,kj}}{\varepsilon_i - \varepsilon_c + \varepsilon_k - \varepsilon_b + i0^+}, \end{aligned} \quad (\text{H.25a})$$

$$\begin{aligned} {}^3\tilde{\Xi}_{c,ia,bj}^{(2,\text{ph}/\text{hp})} = & \sum_{kc} \frac{2w_{ee,ib,kc}w_{ee,ja,ck} - w_{ee,ib,kc}w_{ee,ka,cj} - w_{ee,cb,ki}w_{ee,ja,ck}}{-\varepsilon_a + \varepsilon_k - \varepsilon_c + \varepsilon_j + i0^+} \\ & + \sum_{kc} \frac{2w_{ee,ib,ck}w_{ee,ja,kc} - w_{ee,ib,ck}w_{ee,ca,kj} - w_{ee,cb,ci}w_{ee,ja,kc}}{\varepsilon_i - \varepsilon_c + \varepsilon_k - \varepsilon_b + i0^+}. \end{aligned} \quad (\text{H.25b})$$

H.2.2 Particle-particle/hole-hole effective kernel

Its matrix elements to the second-order of perturbation are given by

$$T_{pq,rs}^{\text{pp}/\text{hh}}(\omega) = \int \frac{d\omega'}{2\pi} \int \frac{d\omega''}{2\pi} \chi_{0,pq,pq}(-\eta, \omega', \omega) \Xi_{c,pq,rs}^{(2,\text{pp}/\text{hh})}(\omega' + \omega'') \chi_{0,rs,rs}(\omega'', -\eta, \omega). \quad (\text{H.26})$$

where the matrix elements of the different contributions are given in Equations (G.41), (F.10a) and (F.10b). Following the same steps as in the ph/ph case, its matrix elements in the (ov—ov) and (ov—vo) blocks are therefore given by

$$\begin{aligned} T_{ia,jb}^{\text{pp}/\text{hh}}(\omega) = & \chi_{0,ia,ia}(\omega) \chi_{0,jb,jb}(\omega) \\ & \frac{1}{2} \left(\sum_{kl} \frac{\langle aj||kl\rangle \langle kl||ib\rangle}{\omega - (\varepsilon_a + \varepsilon_b) + (\varepsilon_k + \varepsilon_l) + i0^+} + \sum_{cd} \frac{\langle aj||cd\rangle \langle cd||ib\rangle}{\omega + (\varepsilon_i + \varepsilon_j) - (\varepsilon_c + \varepsilon_d) + i0^+} \right) \end{aligned} \quad (\text{H.27a})$$

$$T_{ia,bj}^{\text{pp/hh}}(\omega) = \chi_{0,ia,ia}(\omega)\chi_{0,bj,bj}(\omega) \frac{1}{2} \left(\sum_{kl} \frac{\langle ab||kl\rangle\langle kl||ij\rangle}{(\varepsilon_a + \varepsilon_b) - (\varepsilon_k + \varepsilon_l) - i0^+} + \sum_{cd} \frac{\langle ab||cd\rangle\langle cd||ij\rangle}{(\varepsilon_c + \varepsilon_d) - (\varepsilon_i + \varepsilon_j) - i0^+} \right). \quad (\text{H.27b})$$

The matrix elements of the effective pp/hh correlation kernel are thus

$$\tilde{\Xi}_{c,ia,jb}^{(2,\text{pp/hh})}(\omega) = \frac{1}{2} \left(\sum_{kl} \frac{\langle aj||kl\rangle\langle kl||ib\rangle}{\omega - (\varepsilon_a + \varepsilon_b) + (\varepsilon_k + \varepsilon_l) + i0^+} + \sum_{cd} \frac{\langle aj||cd\rangle\langle cd||ib\rangle}{\omega + (\varepsilon_i + \varepsilon_j) - (\varepsilon_c + \varepsilon_d) + i0^+} \right) \quad (\text{H.28a})$$

$$\tilde{\Xi}_{c,ia,bj}^{(2,\text{pp/hh})} = \frac{1}{2} \left(\sum_{kl} \frac{\langle ab||kl\rangle\langle kl||ij\rangle}{(\varepsilon_a + \varepsilon_b) - (\varepsilon_k + \varepsilon_l) - i0^+} + \sum_{cd} \frac{\langle ab||cd\rangle\langle cd||ij\rangle}{(\varepsilon_c + \varepsilon_d) - (\varepsilon_i + \varepsilon_j) - i0^+} \right). \quad (\text{H.28b})$$

As it was the case for the ph/hp effective kernel, the contributions to the **A** block are hermitian, and are frequency-independent and symmetric in the block **B**.

Spin adaptation

The matrix elements of the singlet and triplet pp/hh effective correlation kernels in the block **A** are given by

$$1\tilde{\Xi}_{c,ia,jb}^{(2,\text{pp/hh})}(\omega) = \frac{1}{2} \sum_{cd} \frac{2w_{ee,ca,jd}w_{ee,ic,db} - w_{ee,ca,jd}w_{ee,bc,di} - w_{ee,da,jc}w_{ee,ic,db} + 2w_{ee,da,jc}w_{ee,bc,di}}{\omega + (\varepsilon_i + \varepsilon_j) - (\varepsilon_c + \varepsilon_d) + i0^+} + \frac{1}{2} \sum_{kl} \frac{2w_{ee,ka,jl}w_{ee,ik,lb} - w_{ee,ka,jl}w_{ee,bk,li} - w_{ee,la,jk}w_{ee,ik,lb} + 2w_{ee,la,jk}w_{ee,bk,li}}{\omega - (\varepsilon_a + \varepsilon_b) + (\varepsilon_k + \varepsilon_l) + i0^+}, \quad (\text{H.29a})$$

$$3\tilde{\Xi}_{c,ia,jb}^{(2,\text{pp/hh})}(\omega) = -\frac{1}{2} \sum_{cd} \frac{w_{ee,ca,jd}w_{ee,bc,di} + w_{ee,da,jc}w_{ee,ic,db}}{\omega + (\varepsilon_i + \varepsilon_j) - (\varepsilon_c + \varepsilon_d) + i0^+} - \frac{1}{2} \sum_{kl} \frac{w_{ee,ka,jl}w_{ee,bk,li} + w_{ee,la,jk}w_{ee,ik,lb}}{\omega - (\varepsilon_a + \varepsilon_b) + (\varepsilon_k + \varepsilon_l) + i0^+}, \quad (\text{H.29b})$$

and in the block **B** by

$$1\tilde{\Xi}_{c,ia,bj}^{(2,\text{pp/hh})} = -\frac{1}{2} \sum_{cd} \frac{2w_{ee,ca,bd}w_{ee,ic,dj} - w_{ee,ca,bd}w_{ee,jc,di} - w_{ee,da,bc}w_{ee,ic,dj} + 2w_{ee,da,bc}w_{ee,jc,di}}{(\varepsilon_i + \varepsilon_j) - (\varepsilon_c + \varepsilon_d) + i0^+} - \frac{1}{2} \sum_{kl} \frac{2w_{ee,ka,bl}w_{ee,ik,lj} - w_{ee,ka,bl}w_{ee,jk,li} - w_{ee,la,bk}w_{ee,ik,lj} + 2w_{ee,la,bk}w_{ee,jk,li}}{-(\varepsilon_a + \varepsilon_b) + (\varepsilon_k + \varepsilon_l) + i0^+}, \quad (\text{H.30a})$$

$$3\tilde{\Xi}_{c,ia,bj}^{(2,\text{pp/hh})} = \frac{1}{2} \sum_{cd} \frac{w_{ee,ca,bd}w_{ee,jc,di} + w_{ee,da,bc}w_{ee,ic,dj}}{(\varepsilon_i + \varepsilon_j) - (\varepsilon_c + \varepsilon_d) + i0^+} + \frac{1}{2} \sum_{kl} \frac{w_{ee,ka,bl}w_{ee,jk,li} + w_{ee,la,bk}w_{ee,ik,lj}}{-(\varepsilon_a + \varepsilon_b) + (\varepsilon_k + \varepsilon_l) + i0^+}. \quad (\text{H.30b})$$

H.3 Summary

- second-order correlation kernel in the block **A**

$$\begin{aligned} \tilde{\Xi}_{c,ia,jb}^{(2)}(\omega) = & \\ & - \sum_{kc} \left(\frac{\langle jk||ic\rangle\langle ac||bk\rangle}{\omega - \varepsilon_a + \varepsilon_k - \varepsilon_c + \varepsilon_j + i0^+} + \frac{\langle jc||ik\rangle\langle ak||bc\rangle}{\omega + \varepsilon_i - \varepsilon_c + \varepsilon_k - \varepsilon_b + i0^+} \right) \\ & + \frac{1}{2} \left(\sum_{kl} \frac{\langle aj||kl\rangle\langle kl||ib\rangle}{\omega - (\varepsilon_a + \varepsilon_b) + (\varepsilon_k + \varepsilon_l) + i0^+} + \sum_{cd} \frac{\langle aj||cd\rangle\langle cd||ib\rangle}{\omega + (\varepsilon_i + \varepsilon_j) - (\varepsilon_c + \varepsilon_d) + i0^+} \right). \end{aligned} \quad (\text{H.31})$$

- second-order correlation kernel in the block **B**

$$\begin{aligned} \tilde{\Xi}_{c,ia,bj}^{(2)} = & \sum_{kc} \left(\frac{\langle bk||ic\rangle\langle ac||jk\rangle}{-\varepsilon_a + \varepsilon_k - \varepsilon_c + \varepsilon_j + i0^+} + \frac{\langle bc||ik\rangle\langle ak||jc\rangle}{\varepsilon_i - \varepsilon_c + \varepsilon_k - \varepsilon_b + i0^+} \right) \\ & + \frac{1}{2} \left(\sum_{kl} \frac{\langle ab||kl\rangle\langle kl||ij\rangle}{(\varepsilon_a + \varepsilon_b) - (\varepsilon_k + \varepsilon_l) - i0^+} + \sum_{cd} \frac{\langle ab||cd\rangle\langle cd||ij\rangle}{(\varepsilon_c + \varepsilon_d) - (\varepsilon_i + \varepsilon_j) - i0^+} \right). \end{aligned} \quad (\text{H.32})$$

- singlet second-order correlation kernel in the block **A**

$$\begin{aligned} {}^1\tilde{\Xi}_{c,ia,jb}^{(2)}(\omega) = & \\ & - \sum_{kc} \frac{2w_{ee,ij,kc}w_{ee,ba,ck} - w_{ee,ij,kc}w_{ee,ka,cb} - w_{ee,cj,ki}w_{ee,ba,ck} + 2w_{ee,cj,ki}w_{ee,ka,cb}}{\omega - \varepsilon_a + \varepsilon_k - \varepsilon_c + \varepsilon_j + i0^+} \\ & - \sum_{kc} \frac{2w_{ee,ij,ck}w_{ee,ba,kc} - w_{ee,ij,ck}w_{ee,ca,kb} - w_{ee,kj,ci}w_{ee,ba,kc} + 2w_{ee,kj,ci}w_{ee,ca,kb}}{\omega + \varepsilon_i - \varepsilon_c + \varepsilon_k - \varepsilon_b + i0^+} \\ & + \frac{1}{2} \sum_{cd} \frac{2w_{ee,ca,jd}w_{ee,ic,db} - w_{ee,ca,jd}w_{ee,bc,di} - w_{ee,da,jc}w_{ee,ic,db} + 2w_{ee,da,jc}w_{ee,bc,di}}{\omega + (\varepsilon_i + \varepsilon_j) - (\varepsilon_c + \varepsilon_d) + i0^+} \\ & + \frac{1}{2} \sum_{kl} \frac{2w_{ee,ka,jl}w_{ee,ik,lb} - w_{ee,ka,jl}w_{ee,bk,li} - w_{ee,la,jk}w_{ee,ik,lb} + 2w_{ee,la,jk}w_{ee,bk,li}}{\omega - (\varepsilon_a + \varepsilon_b) + (\varepsilon_k + \varepsilon_l) + i0^+}, \end{aligned} \quad (\text{H.33})$$

- triplet second-order correlation kernel in the block **A**

$$\begin{aligned} {}^3\tilde{\Xi}_{c,ia,jb}^{(2)}(\omega) = & - \sum_{kc} \frac{2w_{ee,ij,kc}w_{ee,ba,ck} - w_{ee,ij,kc}w_{ee,ka,cb} - w_{ee,cj,ki}w_{ee,ba,ck}}{\omega - \varepsilon_a + \varepsilon_k - \varepsilon_c + \varepsilon_j + i0^+} \\ & - \sum_{kc} \frac{2w_{ee,ij,ck}w_{ee,ba,kc} - w_{ee,ij,ck}w_{ee,ca,kb} - w_{ee,kj,ci}w_{ee,ba,kc}}{\omega + \varepsilon_i - \varepsilon_c + \varepsilon_k - \varepsilon_b + i0^+} \\ & - \frac{1}{2} \sum_{cd} \frac{w_{ee,ca,jd}w_{ee,bc,di} + w_{ee,da,jc}w_{ee,ic,db}}{\omega + (\varepsilon_i + \varepsilon_j) - (\varepsilon_c + \varepsilon_d) + i0^+} \\ & - \frac{1}{2} \sum_{kl} \frac{w_{ee,ka,jl}w_{ee,bk,li} + w_{ee,la,jk}w_{ee,ik,lb}}{\omega - (\varepsilon_a + \varepsilon_b) + (\varepsilon_k + \varepsilon_l) + i0^+}, \end{aligned} \quad (\text{H.34})$$

- singlet second-order correlation kernel in the block **B**

$$\begin{aligned}
1\Xi_{c,ia,bj}^{(2)} = & \sum_{kc} \frac{2w_{ee,ib,kc}w_{ee,ja,ck} - w_{ee,ib,kc}w_{ee,ka,cj} - w_{ee,cb,ki}w_{ee,ja,ck} + 2w_{ee,cb,ki}w_{ee,ka,cj}}{-\varepsilon_a + \varepsilon_k - \varepsilon_c + \varepsilon_j + i0^+} \\
& + \sum_{kc} \frac{2w_{ee,ib,ck}w_{ee,ja,kc} - w_{ee,ib,ck}w_{ee,ca,kj} - w_{ee,kb,ci}w_{ee,ja,kc} + 2w_{ee,kb,ci}w_{ee,ca,kj}}{\varepsilon_i - \varepsilon_c + \varepsilon_k - \varepsilon_b + i0^+} \\
& - \frac{1}{2} \sum_{cd} \frac{2w_{ee,ca,bd}w_{ee,ic,dj} - w_{ee,ca,bd}w_{ee,jc,di} - w_{ee,da,bc}w_{ee,ic,dj} + 2w_{ee,da,bc}w_{ee,jc,di}}{(\varepsilon_i + \varepsilon_j) - (\varepsilon_c + \varepsilon_d) + i0^+} \\
& - \frac{1}{2} \sum_{kl} \frac{2w_{ee,ka,bl}w_{ee,ik,lj} - w_{ee,ka,bl}w_{ee,jk,li} - w_{ee,la,bk}w_{ee,ik,lj} + 2w_{ee,la,bk}w_{ee,jk,li}}{-(\varepsilon_a + \varepsilon_b) + (\varepsilon_k + \varepsilon_l) + i0^+},
\end{aligned} \tag{H.35}$$

- triplet second-order correlation kernel in the block **B**

$$\begin{aligned}
3\Xi_{c,ia,bj}^{(2)} = & \sum_{kc} \frac{2w_{ee,ib,kc}w_{ee,ja,ck} - w_{ee,ib,kc}w_{ee,ka,cj} - w_{ee,cb,ki}w_{ee,ja,ck}}{-\varepsilon_a + \varepsilon_k - \varepsilon_c + \varepsilon_j + i0^+} \\
& + \sum_{kc} \frac{2w_{ee,ib,ck}w_{ee,ja,kc} - w_{ee,ib,ck}w_{ee,ca,kj} - w_{ee,kb,ci}w_{ee,ja,kc}}{\varepsilon_i - \varepsilon_c + \varepsilon_k - \varepsilon_b + i0^+} \\
& + \frac{1}{2} \sum_{cd} \frac{w_{ee,ca,bd}w_{ee,jc,di} + w_{ee,da,bc}w_{ee,ic,dj}}{(\varepsilon_i + \varepsilon_j) - (\varepsilon_c + \varepsilon_d) + i0^+} \\
& + \frac{1}{2} \sum_{kl} \frac{w_{ee,ka,bl}w_{ee,jk,li} + w_{ee,la,bk}w_{ee,ik,lj}}{-(\varepsilon_a + \varepsilon_b) + (\varepsilon_k + \varepsilon_l) + i0^+}.
\end{aligned} \tag{H.36}$$

Appendix I

MolExc manual

In this appendix, a user manual is provided for my program MolExc. This program relies on Molpro for the SCF calculation in order to get the two-electron integrals over the molecular orbitals, the orbital energies and the matrix elements of the short-range kernels. MolExc is then able to perform the linear-response calculation for HF, RSH, static and dynamic second-order BSE. Typical inputs for MolExc and for Molpro are given here.

I.1 Presentation

MolExc is a homemade package able to deal with the linear-response part of a quantum chemistry calculation. It was designed in order to test the different variants of the Bethe-Salpeter kernels. For now, it relies on a development version of Molpro [25] for the ground-state SCF calculations in order to get the two-electron integrals on the molecular orbitals via the `FCIdump` [26, 27], the orbital energies and the matrix elements of the short-range kernels. However, it could be interfaced with any quantum software able to “dump” these quantities. MolExc is able to perform linear-response time-dependent RSH calculations with or without the Tamm-Dancoff approximation, different variants of static Bethe-Salpeter calculation (with or without the inclusion of exchange and of the derivative of W with respect to G , with or without range separation, or in TDA) and dynamical second-order (range-separated) Bethe-Salpeter calculations within the TDA perturbative approach detailed in Chapter 10.

As the ground-state calculation is done with Molpro, the two-electron integrals, the orbital energies and eventually the matrix elements of the short-range singlet and triplet kernels must be given in the input file, together with the kind of calculation to be performed. It is possible to ask for specific excitations to be calculated or a given number of excitations.

This software was developed using the OCaml programming language [28] and in particular the package Lacaml [29] which provides a binding to the BLAS and LAPACK

libraries. It uses the IRP programming technique proposed by Colonna *et al* [30–32].

I.2 MolExc input syntax

MolExc takes a unique file in input which should contain several fields. The order of the fields is not important, but each field should be on written on a new line. The input format is case insensitive. A typical input file is

```
method = RSH_dynamic_bsegw
tda
int_file = N2_sadlejplus.dump2
eps_file = N2_sadlejplus.out
erf_file = N2_sadlejplus.dump
ker_sing_file = N2_sadlejplus.kersing
ker_trip_file = N2_sadlejplus.kertrip
acc_eps_file = N2_sadlejplus.eps
exc = 1
```

I.2.1 The method field

The `method` field can accept different method names:

- `tdhf`: Time-dependent Hartree-Fock
- `tdrsh`: Time-dependent RSH
- `bse-gw` | `bsegw` | `bse_gw`: Static BSE-GW calculation
- `rsh_bsegw`: Static range-separated BSE-GW calculation
- `dynamic_bsegw`: Dynamic second-order BSE-GW calculation
- `rsh_dynamic_bsegw`: Dynamic range-separated second-order BSE-GW calculation

The static (range-separated) BSE-GW calculation can take additional options to control which contributions are included in the kernel when the keyword `with` is used on the same line. The available options are `exchange`, `order_2`, `direct_order_2`, `dwdg`, `static_freq`. The Tamm-Dancoff approximation is available for all the methods and the key `tda` should be written on a separate line.

I.2.2 The integral, orbital energies and kernel files

The following fields give the files where the orbital energies, the matrix elements of the two-electron integrals and of the singlet and triplet exchange-correlation kernels. Without range separation, only the `int_file` and `eps_file` are required. The `int_file`

is the FCIDUMP file produced by Molpro when the command `{fci;dump}` is called. It contains the matrix elements of all two-electron integrals in the format

```
float int1 int2 int3 int4
```

where the float is the value of the integral and the four integers are the orbital indices. Only non-redundant elements are given. The convention for the indices ordering is that the two first indices correspond to electron 1 and the last two correspond to electron 2 in decreasing order. The header of the FCIDUMP file contains the symmetry of the orbitals. It is possible to use symmetry for non range-separated calculations but some issues remain for range-separated ones.

The `eps_file` is just the output file of Molpro. The orbital energies and occupation are recovered in this file. However, the default precision of the orbital energies is low. It is therefore possible to provide an additional file where accurate orbital energies are given in `acc_eps_file`. Molpro was modified in order to produce this file in the `rpa-tddft` routine when the option `ker=dump` is given, together with the short-range singlet and triplet kernels in the case of a range-separation calculation.

I.2.3 debug, nexc and exc options

It is possible to print intermediate matrices, essentially for debugging. As they are usually huge, only a subblock is printed via the `debug =n` command where n is the size of the submatrices to be printed.

It is also possible to ask for the n first excitation energies of a system via the command `nexc=n`. It affects only the printing for static calculations but for dynamical BSE calculations only the corrections to the first n excitation energies (the costly part of the calculation) are computed.

Similarly, it is possible to ask for specific excitations with the keyword `exc=i,j,k` where i,j and k are the indices of the excitation energies to be computed. This is possible only for the dynamical part.

I.3 Molpro input syntax

Concerning the SCF calculation with Molpro, after definition of the molecule and of the basis, the syntax is:

```
! Fix the range-separation parameter
mu=0.35

! Compute long-range two-electron integrals
{int
 erf,mu;
 save}
```

```
! orbital record
orbrec=2101.2

! RSH calculation
{rks,exerf,ecerf;
rangehybrid;
orbital,orbrec;
orbprint,100;}

! Dump long-range two-electron integrals
{fci;
orbit,orbrec
core,0
thr,1.d-10
dump;}

! Compute full-range two-electron integrals
int

! Dump full-range two-electron integrals
{fci;
orbit,orbrec
core,0
thr,1.d-10
dump;}

! Reset the range-separation parameter to mu=0.35
setmu,mu;

! Dump orbital energies, singlet and triplet sr xc kernels
{rpa-tddft;
orb,orbrec;
core,0;
excit,method=rs-tddft,ker=dump;
kernelxc,ldaxerf,ldacerf}
```

When entering the `rpa-tddft` routine with the `ker=dump` option, the orbital epsilons are dumped, the singlet and triplet exchange-correlation kernel are evaluated and dumped into two separate files but the calculation of the excitation energies is not performed in order to save time.

MolExc is licensed under the GNU General Public License and can be found at <http://www.lct.jussieu.fr/pagesperso/rebolini/molexc/>.

Bibliography

- [1] W. Appel. *Mathématiques pour la physique et les physiciens*. H K, 2002.
- [2] J. Toulouse, F. Colonna, and A. Savin. 2004. *Phys. Rev. A*. 70. P. 062505.
- [3] J. Toulouse. “Extension multidéterminantale de la méthode de Kohn-Sham en théorie de la fonctionnelle de la densité par décomposition de l’interaction électronique en contributions de longue portée et de courte portée.” PhD thesis. Université Pierre et Marie Curie, 2005.
- [4] P. Gori-Giorgi and A. Savin. 2006. *Phys. Rev. A*. 73. P. 032506.
- [5] J. Toulouse, P. Gori-Giorgi, and A. Savin. 2006. *Int. J. Quantum Chem.* 106. P. 2026.
- [6] Y. Cornaton and E. Fromager. 2013. *arXiv Prepr. arXiv1312.0409*. Pp. 1–24.
- [7] M. Levy. 1979. *Proc. Natl. Acad. Sci. U.S.A.* 76. P. 6062.
- [8] M. Levy. 1982. *Phys. Rev. A*. 26. P. 1200.
- [9] E. H. Lieb. 1983. *Int. J. Quantum Chem.* 24. Pp. 243–277.
- [10] J. Toulouse, P. Gori-Giorgi, and A. Savin. 2005. *Theor. Chem. Acc.* 114. P. 305.
- [11] P. Gori-Giorgi and A. Savin. 2009. *Int. J. Quantum Chem.* 109. P. 1950.
- [12] A. Stoyanova, A. M. Teale, J. Toulouse, et al. 2013. *J. Chem. Phys.* 139. P. 134113.
- [13] A. Görling and M. Levy. 1993. *Phys. Rev. B*. 47. P. 13105.
- [14] A. Görling and M. Levy. 1995. *Int. J. Quantum Chem.* 08. Pp. 93–108.
- [15] M. Petersilka, U. J. Gossmann, and E. K. U. Gross. 1996. *Phys. Rev. Lett.* 76. P. 1212.
- [16] R. Bauernschmitt and R. Ahlrichs. 1996. *Chem. Phys. Lett.* 2614.
- [17] S. van Gisbergen, J. Snijders, and E. Baerends. 1999. *Comput. Phys. Commun.* 118. Pp. 119–138.
- [18] J. Toulouse, W. Zhu, A. Savin, et al. 2011. *J. Chem. Phys.* 135. P. 84119.
- [19] J. G. Ángyán, R.-F. Liu, J. Toulouse, and G. Jansen. 2011. *J. Chem. Theory Comput.* 7. P. 3116.
- [20] A. Savin. “On degeneracy, near-degeneracy and density functional theory”. In: *Recent Dev. Appl. Mod. Density Funct. Theory*. Ed. by J.M. Seminario. Amsterdam: Elsevier, 1996, p. 327.

BIBLIOGRAPHY

- [21] J. Toulouse, A. Savin, and H.-J. Flad. 2004. *Int. J. Quantum Chem.* 100. P. 1047.
- [22] J. P. Perdew and Y. Wang. 1992. *Phys. Rev. B.* 45. Pp. 13244–13249.
- [23] S. Pazziani, S. Moroni, P. Gori-Giorgi, and G. Bachelet. 2006. *Phys. Rev. B.* 73. P. 155111.
- [24] S. H. Vosko, L. Wilk, and M. Nusair. 1980. *Can. J. Phys.* 58. Pp. 1200–1211.
- [25] H.-J. Werner, P. J. Knowles, G. Knizia, F. R. Manby, M. Schütz, and others. *MOLPRO, version 2012.1, a package of ab initio programs.*
- [26] P. J. Knowles and N. C. Handy. 1984. *Chem. Phys. Lett.* 111. Pp. 315–321.
- [27] P. J. Knowles and N. C. Handy. 1989. 54. Pp. 75–83.
- [28] *OCaml programming language.* URL: <http://ocaml.org/>.
- [29] *LACAML - Linear Algebra for OCaml.* URL: <https://bitbucket.org/mmott1/lacaml>.
- [30] F. Colonna, L.-H. Jolly, R. a. Poirier, et al. 1994. *Comput. Phys. Commun.* 81. Pp. 293–317.
- [31] F. Colonna. 2006. *arXiv Prepr. cs/0601035.* Pp. 1–21.
- [32] A. Scemama. 2009. *arXiv Prepr. arXiv0909.5012.*

Résumé en français

Introduction

L'étude des phénomènes induits par l'interaction lumière-matière constitue une étape clé pour la compréhension globale de notre environnement immédiat. La lumière est constituée de photons qui transportent des quanta d'énergie. L'interaction entre la matière et un photon peut donner lieu à des phénomènes complexes tels que l'absorption, l'émission ou la diffusion. À l'échelle d'une molécule, la physique classique ne s'applique plus et une description quantique de la matière est requise dans laquelle les niveaux d'énergies sont discrets. Si l'on considère un système dans son état fondamental (son état de plus basse énergie), l'absorption d'un photon entraîne l'excitation du système vers un état de plus haute énergie. Plusieurs phénomènes peuvent alors avoir lieu :

- Le système peut retourner dans son état fondamental (ou dans un niveau de plus basse énergie) par une transition non-radiative (par relaxation vibrationnelle, par croisement inter-systèmes ou par conversion interne), ou par une transition radiative où un photon est émis (soit par fluorescence, soit par phosphorescence). Dans tous ces processus, aucune liaison chimique n'est brisée ou créée et le système conserve son intégrité. Ceci définit par conséquent la famille des processus photophysiques. Ces mécanismes sont extrêmement intéressants car ils sont responsables de nombreux phénomènes tels que l'émission lumineuse des étoiles ou la couleur des objets, et interviennent notamment dans la conception des panneaux photovoltaïques où un matériau (souvent un semi-conducteur) convertit l'énergie lumineuse en une différence de potentiel. Les processus photophysiques sont aussi largement utilisés à des fins analytiques puisqu'ils permettent de sonder les états de la matière. Selon le dispositif expérimental (la gamme d'énergie ou la direction d'observation), différents types d'informations peuvent être obtenus comme par exemple la position des niveaux électroniques (qui décrivent la configuration électronique du système) ou, dans le cas d'une molécule en phase gaz, celle des niveaux ro-vibroniques qui caractérisent les rotations et les vibrations de cette molécule.
- Dans certains cas, le système excité ne retourne pas dans son état initial et utilise cette énergie supplémentaire pour initier une réaction chimique, seul (photoisomérisation) ou avec d'autres réactifs (photoactivation). La photochimie est la branche de la chimie responsable de l'étude de ce type de processus. L'exemple le plus connu est probablement la photosynthèse mais en réalité de nombreuses réactions nécessitent une photoactivation comme par exemple la synthèse de la vitamine D ou la dégradation des matières plastiques. Grâce aux progrès technologiques réalisés ces dernières années, un nouveau champ de recherche a également

vu le jour et a pour but d'utiliser la lumière pour contrôler une réaction afin de favoriser la formation d'un certain produit et donc d'augmenter son rendement. Comme moins de réactifs sont consommés et que moins de déchets sont produits, cette approche est particulièrement intéressante dans le cadre de la chimie verte.

Dans tous les phénomènes mentionnés ci-dessus, le nombre d'électrons dans le système reste constant. Cependant si on augmente suffisamment la quantité d'énergie apportée au système, un électron peut également être éjecté comme par exemple dans la spectroscopie de photo-émission. Cela permet alors d'extraire d'autres types d'informations comme par exemple les affinités électroniques. Cependant, dans le cadre de cette thèse, de tels phénomènes ne seront pas abordés et nous nous concentrerons uniquement sur les énergies d'excitation électroniques dans le cas de systèmes moléculaires. La gamme d'énergie de ces excitations correspond à la partie visible du spectre et aux rayonnements ultra-violet. Elles sont donc étudiées expérimentalement par spectroscopie UV-visible.

La prédiction ou l'analyse d'un spectre UV-visible par un calcul sur ordinateur constitue à présent un domaine de recherche actif, soit pour aider les expérimentateurs dans l'interprétation de leurs résultats, soit pour la conception de nouveaux composés d'intérêt biologique ou industriel, soit enfin pour étudier des environnements hostiles pour lesquels il est difficile voire impossible de réaliser des expériences (par exemple dans l'espace, dans des conditions extrêmes de température et de pression ou dans des champs magnétiques intenses). Afin d'obtenir des résultats quantitatifs, les théoriciens ont alors besoin de méthodes fiables avec un coût de calcul faible pour pouvoir étudier des systèmes relativement grands. Afin de simuler un spectre UV-visible, deux types d'information sont nécessaires, les énergies d'excitation électroniques et la probabilité que ces excitations aient lieu (ce qui est donné en pratique par les forces d'oscillateur). La probabilité d'une transition électronique peut varier énormément dans une gamme d'énergie très restreinte et influence donc significativement l'allure finale du spectre. Ces probabilités sont reliées au concept de transitions permises ou interdites présent en spectroscopie et aux règles de sélection qui en découlent.

En pratique, le calcul des énergies d'excitation d'un système se fait généralement en deux étapes. Dans un premier temps, le système est étudié dans son état fondamental, puis des énergies de transition verticales sont calculées en gardant la géométrie du système fixée et en considérant que le phénomène d'excitation est instantané par rapport à l'échelle de temps du mouvement des noyaux. Cependant, la géométrie la plus stable du système dans un état excité diffère en général de celle de l'état fondamental ce qui implique qu'une surface d'énergie potentielle est en principe nécessaire pour décrire précisément la physique du système. De plus, pour reproduire un spectre expérimental, les effets des niveaux ro-vibroniques et d'élargissement des raies devraient être pris en

compte. Cependant dans cette thèse, nous nous intéressons uniquement au calcul des énergies d'excitation électroniques et des forces d'oscillateur d'une molécule en phase gaz, à température nulle et à géométrie fixée.

Toute la difficulté d'un calcul quantique réside dans la description du mouvement corrélé des électrons à cause de leur interaction et de leur nature quantique intrinsèque. Historiquement, les chimistes théoriciens ont utilisés des méthodes basées sur la fonction d'onde électronique en raffinant de plus en plus la méthode Hartree-Fock (HF) dans laquelle le traitement de la corrélation est complètement absent. Les méthodes post-HF et multi-configurationnelles réintroduisent (en partie) cette corrélation et ont l'avantage indéniable de pouvoir être améliorées de façon systématique et de pouvoir produire des résultats très précis. Cependant, ces méthodes sont très gourmandes en temps de calcul car elles dépendent des coordonnées de chaque électron. Leur complexité polynomiale par rapport à la taille du système les rend donc rapidement inutilisables pour des calculs sur des systèmes de grande taille comme des solides ou des protéines. Néanmoins, elles font l'objet d'une recherche active afin de réduire leur coût de calcul par des méthodes de « density-fitting » ou en exploitant la localisation des orbitales.

Un autre type d'approche est proposée par la théorie de la fonctionnelle de la densité (DFT) qui est basée sur la densité électronique du système dans son état fondamental au lieu de sa fonction d'onde. La densité électronique représente le nombre moyen d'électrons par élément de volume et ne dépend que d'une seule coordonnée d'espace et de spin quelque soit le nombre d'électrons dans le système. Une telle approche réduit donc significativement le coût de calcul. Cependant, le prix à payer est que toute la complexité du calcul est maintenant cachée dans une fonctionnelle d'énergie inconnue. Dans l'approche de Kohn et Sham, le calcul est réalisé en utilisant un système auxiliaire fictif d'électrons sans interaction mais reproduisant la densité électronique du système réel. L'idée dans cette approche est de calculer de façon exacte la majorité de l'énergie afin que la partie inconnue soit la plus petite possible et donc en principe plus facile à approximer. Pour reproduire le système physique, il reste donc à prendre en compte les effets de l'interaction électronique qui sont alors décrits par la fonctionnelle de Hartree-échange-corrélation. De nombreuses fonctionnelles approchées ont été développées depuis quelques dizaines d'années, basées essentiellement sur des approximations locales (LDA) ou semi-locales (GGA). Elles permettent à la DFT de produire de bons résultats avec un coût de calcul moindre ce qui a permis son essor rapide.

Dans sa formulation originelle, indépendante du temps, la DFT permet de calculer la densité électronique et l'énergie de l'état fondamental. Cependant, les théorèmes de Hohenberg et Kohn montrent que la densité du fondamental contient la totalité de l'information sur le système et donc en particulier ses énergies d'excitation. L'introduction

d'une dépendance en temps permet d'extraire ces énergies d'excitation à partir de la densité en utilisant par exemple la théorie de la réponse linéaire. Dans cette approche, on étudie la réponse de la densité du système à une perturbation périodique dépendante du temps. Si la fréquence de cette perturbation correspond à une différence d'énergie entre l'état fondamental et un état excité du système, celui-ci change d'état et sa densité électronique est donc fortement affectée alors qu'à une fréquence quelconque le changement de densité est faible. La méthode de la théorie de la fonctionnelle de la densité dépendante du temps (TDDFT) en réponse linéaire exploite ce phénomène et détecte les énergies d'excitation comme les fréquences où la densité du système change beaucoup.

Comme dans le cas indépendant du temps, cette méthode nécessite une fonctionnelle approchée pour décrire les effets de l'interaction électronique. Cette fonctionnelle est appelée le noyau de Hartree-échange-corrélation. En toute rigueur, ce noyau ne peut pas être calculé à partir de la fonctionnelle d'énergie. Cependant, en pratique, une approximation adiabatique est utilisée pour contourner cette difficulté. Dans cette approximation, le noyau devient indépendant de la fréquence de la perturbation ce qui entraîne un certain nombre de problèmes. Avec les approximations usuelles, les énergies d'excitation vers les états de valence (bas en énergie) sont néanmoins généralement bien décrites mais celles vers les états de Rydberg (plus hauts en énergie) sont largement sous-estimées. De plus les excitations à transfert de charge ou à caractère multiple ne sont pas reproduites correctement.

La mauvaise description des excitations de Rydberg et à transfert de charge est essentiellement due au mauvais comportement asymptotique du potentiel à longue distance inter-électronique dans les approximations locales et semi-locales. La non-description des excitations multiples est en revanche directement liée à l'approximation adiabatique. Dans le cas d'un système isolé à sa géométrie d'équilibre, les excitations doubles (ou plus généralement multiples) ne sont pas fréquentes dans la partie basse du spectre d'excitation. Elles interviennent par exemple dans les polyènes linéaires mais ne jouent pas un rôle important dans la plupart des systèmes. Cependant, lorsqu'on s'intéresse à la réactivité chimique et à la description d'un mécanisme réactionnel, les choses se compliquent. En effet, lorsque les liaisons sont étirées, les états excités peuvent se croiser ou produire des intersections coniques. Au voisinage de ces régions, les excitations multiples sont plus probables puisque plusieurs états peuvent être extrêmement proches. Il est alors important de pouvoir les prendre en compte afin de décrire ces régions correctement, d'autant plus que ces dernières sont en général cruciales pour comprendre le mécanisme réactionnel. La TDDFT dans l'approximation adiabatique n'est pas capable de décrire ces excitations multiples et peut produire des résultats de qualités médiocres dans ces régions.

Un angle d'attaque possible pour résoudre (au moins partiellement) ces différents problèmes est de diviser l'interaction électronique en une partie de courte portée quand les électrons sont proches et une partie de longue portée lorsqu'ils sont éloignés. Dans les approximations usuelles, la DFT décrit relativement bien la partie de courte portée mais échoue pour la longue portée. Dans l'approche à séparation de portée, cette partie est donc traitée par des méthodes fonction d'onde ou de théorie de la perturbation à plusieurs corps, qui sont plus adaptées. La portée de la séparation peut être ajustée par un paramètre de séparation de portée. Cette approche a été appliquée avec succès pour des calculs sur l'état fondamental et est explorée depuis quelques années pour les états excités. Quand elle est appliquée sur le noyau d'échange, par introduction d'un noyau d'échange HF de longue portée, elle permet d'améliorer la description des excitations de Rydberg et à transfert de charge puisque le bon comportement du potentiel est alors assuré.

Dans cette thèse, nous voulons explorer les effets de la séparation de portée sur la description des énergies d'excitation à la fois dans une approche dépendante du temps et dans une approche indépendante du temps. En particulier, nous voulons appliquer la séparation de portée au noyau de corrélation TDDFT afin d'améliorer la description des excitations présentant des contributions doubles, en introduisant un noyau de corrélation dépendant de la fréquence à longue portée. Dans cette optique, cette thèse est divisée en trois parties.

Dans la première partie de cette thèse, les effets de la séparation de portée sont étudiés dans le cas indépendant du temps. Ceci est réalisé en suivant l'évolution des énergies des états excités d'un système en interaction partielle où seule la longue portée de l'interaction électronique a été introduite. La densité électronique est maintenue constante par optimisation du potentiel le long de la connexion adiabatique. Tout d'abord, un travail analytique est réalisé en étudiant les développements de Taylor des énergies au voisinage des deux cas limites où soit toute l'interaction est présente soit elle est complètement absente. Une étude numérique est également réalisée sur de petits systèmes. Dans ce cas, aucune approximation n'est utilisée à part la projection sur une base finie d'orbitales afin de pouvoir attribuer nos observations aux effets de la séparation de portée uniquement. Dans un deuxième temps, nous explorons différentes possibilités pour améliorer la description des énergies d'excitation du système physique à partir de celles du système en interaction partielle, soit par théorie de la perturbation soit par une technique d'extrapolation.

Dans la deuxième partie de cette thèse, nous appliquons la séparation de portée sur les noyaux d'échange et de corrélation TDDFT dans une approximation mono-déterminantale. Ceci définit l'extension dépendante du temps de la méthode «range-

separated hybrid» (RSH) utilisée pour des calculs sur l'état fondamental. Dans cette approximation, la partie de longue portée du noyau d'échange est traitée au niveau Hartree-Fock alors que le noyau de corrélation de longue portée est absent. Dans un deuxième temps, il sera alors possible d'ajouter de façon perturbative un noyau de corrélation de longue portée dépendant de la fréquence. En pratique, le noyau de longue portée doit être enlevé du noyau usuel, ce qui est réalisé dans l'approximation LDA dans le cas couches fermées. Cette méthode (TDRSH) est alors appliquée sur un ensemble de cinq petites molécules et sur un dimère à transfert de charge afin d'analyser l'impact du retrait de la longue portée du noyau de corrélation sur leurs premières énergies d'excitation.

Dans la dernière partie, nous proposons un noyau de corrélation de longue portée dépendant de la fréquence et l'ajoutons au noyau TDRSH obtenu précédemment. Pour ce faire, nous utilisons la théorie de la perturbation à plusieurs corps (MBPT) qui est basée non plus sur la densité électronique mais sur la fonction de Green à une particule. Cette méthode est largement utilisée en physique de la matière condensée mais reste marginale en chimie. Dans cette approche, les énergies d'excitation du système sont obtenues par résolution de l'équation de Bethe-Salpeter dont la forme est très proche des équations utilisées en TDDFT mais qui est cependant plus générale. Nous avons choisi d'utiliser ce formalisme plus complexe car dans ce cadre il est possible d'obtenir un noyau de corrélation dépendant de la fréquence et donc de contourner l'approximation adiabatique présente en TDDFT. Puisque nous considérons des systèmes moléculaires finis et non des solides infinis, les approximations habituelles utilisées par les physiciens ont besoin d'être remise en question dans ce cas. Dans cette partie, nous proposons un noyau de corrélation dynamique au deuxième ordre par rapport à l'interaction électronique. A chaque étape de sa construction, ce noyau est illustré sur le système modèle donné par la molécule de dihydrogène en base minimale. Cette construction est réalisée de façon algébrique et comporte de nombreuses étapes techniques qui sont essentiellement données en annexe. Seules les grandes lignes de cette construction et leur interprétation en diagrammes de Feynman sont détaillées dans le corps du texte pour plus de lisibilité. Ce noyau est enfin appliqué dans le cadre de la séparation de portée sur un ensemble de quatre petites molécules.

Partie I : Energies d'excitation en théorie de la fonctionnelle de la densité indépendante du temps

Chapitre 1 : Généralités sur la théorie de la fonctionnelle de la densité

Dans ce chapitre, le problème électronique à plusieurs corps est rappelé brièvement. Ce problème est rencontré à la fois par les chimistes et les physiciens que ce soit sur des systèmes finis ou sur des systèmes infinis et implique la résolution de l'équation de Schrödinger. Dans une approche non-relativiste indépendante du temps, plusieurs classes de méthodes sont disponibles pour traiter ce problème. Dans le cadre de cette thèse, nous nous concentrons essentiellement sur les méthodes basées sur la densité électronique. Par conséquent, ce chapitre rappelle la théorie de la fonctionnelle de la densité (DFT), avec tout d'abord ses fondements théoriques donnés par les théorèmes de Hohenberg et Kohn puis l'approche de Kohn et Sham ainsi que son extension par séparation de portée de l'interaction électronique. Les aspects pratiques et les approximations usuelles sont aussi discutés.

Chapitre 2 : Energies d'excitation le long de la connexion adiabatique à séparation de portée

Dans ce chapitre, nous étudions les variations des énergies des états excités et des énergies d'excitation le long d'une connexion adiabatique à séparation de portée. Cette connexion relie le système fictif de Kohn-Sham d'électrons non-interagissants au système physique d'électrons en interaction, en incluant progressivement l'interaction électronique tout en ajustant le potentiel effectif afin de maintenir la densité du fondamental constante. Dans ce travail, l'interaction est introduite en fonction de sa portée. Tout d'abord la longue portée de l'interaction est introduite majoritairement, jusqu'à ce que la totalité de l'interaction soit présente, au voisinage du système physique. Dans le cas de l'hélium, du béryllium et de la molécule de dihydrogène, des données de référence sont fournies. Elles ont été obtenues en calculant le potentiel effectif de courte portée par interaction de configuration complète en utilisant l'approche de la transformée de Legendre introduite par Lieb. Quand la portée de l'interaction augmente, les énergies d'excitation du système en interaction partielle le long de la connexion adiabatique décrivent de mieux en mieux les énergies exactes du système physique. De ce fait, les énergies d'excitation calculées à un point intermédiaire de la connexion adiabatique sont de bien meilleures approximations aux énergies exactes que ne l'étaient les énergies Kohn-Sham correspondantes. Ceci est particulièrement évident dans des situations impliquant des effets importants de corrélation statique ou des états ayant des caractères d'excitations multiples comme la molécule de dihydrogène à la dissociation. Ces résultats mettent en évidence l'utilité

de systèmes en interaction partielle de longue portée comme références pour le calcul des énergies d'excitation, et sont intéressants pour le développement et l'analyse des méthodes pratiques approchées basées sur la DFT à séparation de portée.

Chapitre 3 : Théorie de la perturbation le long d'une connexion adiabatique à séparation de portée

Dans ce chapitre, les effets d'une correction perturbative au premier ordre sont évalués le long de la connexion adiabatique à séparation de portée. Le point de départ est donné par les énergies d'excitation du système en interaction partielle défini au chapitre précédent. Une correction de premier ordre est alors définie avec deux variantes de la théorie de perturbation : la théorie de perturbation standard et une extension de la théorie de perturbation à la Görling-Levy qui a l'avantage de maintenir la densité du fondamental constante à chaque ordre de perturbation. Seule la première variante, plus simple, est testée sur les systèmes définis précédemment. Les énergies des états excités sont fortement améliorées par l'ajout de cette correction cependant les énergies d'excitation s'en trouvent détériorées par rapport à l'ordre zéro. Ceci peut s'expliquer par le fait que le potentiel d'ionisation n'est pas maintenu constant dans ce cas. La deuxième variante de la théorie de perturbation devrait améliorer ces résultats mais n'a pas été testée pour le moment.

Chapitre 4 : Extrapolation des énergies le long de la connexion adiabatique

Dans ce chapitre, nous proposons une méthode alternative pour améliorer l'estimation des énergies d'excitation du système physique à partir des énergies du système en interaction partielle où seule la partie de longue portée de l'interaction électronique est présente. Les énergies de ce système ont d'ores et déjà été étudiées dans les chapitres 2 et 3 à l'ordre zéro et à l'ordre zéro+un de la théorie de perturbation «standard». A partir de l'analyse de leur développements de Taylor au voisinage du système physique, les énergies du système physique peuvent être extrapolées à partir des énergies du système en interaction partielle et de leur dérivée première par rapport au paramètre de séparation de portée. Une méthode similaire est également étudiée dans le cadre d'une connexion adiabatique linéaire. Dans ce cas, cette technique est équivalente au premier ordre de la théorie de perturbation à la Görling-Levy étendue à un système en interaction partielle.

Cette extrapolation est ensuite appliquée sur les énergies d'ordre zéro de l'hélium, du béryllium et du dihydrogène. La convergence de ces énergies vers leur limite exacte est alors améliorée de façon significative, ce qui permet d'estimer les énergies du

système physique à la même précision que sans extrapolation mais avec un paramètre de séparation réduit de moitié. Lorsqu'on applique l'extrapolation sur les énergies de l'hélium obtenues à l'ordre zéro+un de perturbation, les résultats restent médiocres puisqu'une d'une part, le point de part est moins bon, et d'autre part, la correction est plus faible par construction que dans le cas de l'ordre zéro. Enfin, l'extrapolation est appliquée sur les énergies d'excitation de l'hélium le long d'une connexion adiabatique linéaire où l'interaction est multipliée par un factor d'atténuation allant de 0 à 1. L'extrapolation marche particulièrement bien dans ce cas puisque le point de départ a un comportement quasi-linéaire par rapport au paramètre et est donc plus facile à prévoir.

Partie II : Energies d'excitation en théorie de la fonctionnelle de la densité dépendante du temps

Chapitre 5 : Généralités sur la théorie de la fonctionnelle de la densité dépendante du temps

Dans ce chapitre, les grands principes de la théorie de la fonctionnelle de la densité dépendante du temps (TDDFT) sont rappelés en particulier dans le cadre de la théorie de la réponse linéaire. Cette méthode est utilisée pour décrire la réponse d'un système initialement dans son état fondamental à une petite perturbation dépendante du temps, typiquement une irradiation par un laser de faible intensité. Les fondements théoriques de la méthode sont rappelés brièvement ainsi que sa formulation dans l'approche de Kohn-Sham. Les approximations adiabatiques semi-locales usuelles sont présentées ainsi que leurs succès et leurs limitations. En particulier, elles ne décrivent pas correctement les excitations à transfert de charge ou présentant un caractère multiple. Enfin, l'extension de la séparation de portée au cas dépendant du temps est présentée dans sa variante la plus commune où la séparation n'est réalisée que sur le noyau d'échange.

Chapitre 6 : Energies d'excitation en théorie de la réponse linéaire pour la théorie de la fonctionnelle de la densité dépendante du temps à séparation de portée

Dans ce chapitre, nous étudions la TDDFT dans le cadre de la réponse linéaire, basée sur une méthode mono-déterminantale à séparation de portée (RSH), c'est-à-dire combinant un noyau d'échange HF de longue portée avec un noyau d'échange-corrélation DFT de courte portée, pour le calcul des énergies d'excitation électroniques de systèmes moléculaires. Cette méthode constitue une alternative à la méthode «long-range corrected» (LC) plus commune, qui combine un noyau d'échange HF de longue portée

avec un noyau d'échange DFT de courte portée et un noyau de corrélation DFT standard de portée totale. Nous étudions les effets de l'approximation locale (LDA) sur les noyaux de courte portée et évaluons la performance de cette méthode sur les premières énergies d'excitation vers des états de valence, ou de Rydberg, singulets ou triplets pour les molécules de N_2 , CO , H_2CO , C_2H_4 , et C_6H_6 et sur la première énergie d'excitation à transfert de charge du dimère $C_2H_4-C_2F_4$. Pour ces systèmes, la présence de la corrélation LDA de longue portée dans le calcul du fondamental et du noyau n'a quasiment pas d'impact sur les énergies d'excitation et les forces d'oscillateur. Les résultats en RSH sont donc très similaires à ceux obtenus en LC. De même qu'avec la méthode LC, l'introduction du noyau d'échange HF de longue portée corrige la sous-estimation des énergies d'excitation à transfert de charge et de Rydberg obtenue avec les approximations semi-locales habituelles. Cependant elle entraîne également la sous-estimation des énergies d'excitation vers les états de valence triplets. Ce problème est résolu dans le cadre de l'approximation Tamm-Dancoff qui permet une description relativement homogène de toutes les énergies d'excitation. Ce travail suggère que cette méthode est donc un point de départ raisonnable pour la description des énergies d'excitation, même avant l'ajout d'un noyau de corrélation de longue portée.

Partie III : Energies d'excitation en théorie de la perturbation à plusieurs corps

Chapitre 7 : Généralités sur les méthodes de type fonction de Green

La théorie de la perturbation à plusieurs corps constitue une approche alternative à la TDDFT pour le calcul des énergies d'excitation électroniques et est largement utilisée dans la communauté de la physique de la matière condensée. Un avantage important de cette approche est qu'elle est en principe capable de décrire les excitations doubles qui sont absentes en TDDFT dans l'approximation adiabatique. De plus, son formalisme est proche de celui de la TDDFT. Dans ce chapitre, nous étudions le transfert de cette méthode, des solides infinis vers des systèmes moléculaires finis où les équations sont projetées sur une base gaussienne de spin-orbitales, et où la validité des approximations utilisées sur les solides doit être remise en question. Nous introduisons ici les concepts de quasi-particule et de fonction de Green sur lesquels repose cette théorie. Nous rappelons ensuite les équations principales dans le cas à une particule (équation de Dyson) et à deux particules (équation de Bethe-Salpeter) et introduisons les concepts de self-énergie et de noyau de Bethe-Salpeter qui sont les quantités clés de cette approche. Toutes les équations sont exprimées dans un formalisme à quatre points afin de faciliter leur projection dans une base de spin-orbitales et la correspondance avec les diagrammes de

Feynman est également explicitée. Nous rappelons également les équations de Hedin qui procurent un ensemble de cinq équations couplées qui permettent en théorie de calculer la self-énergie.

Chapitre 8 : Noyau Bethe-Salpeter GW statique dans une base de spin-orbitales

L'approximation la plus utilisée dans le cadre de la méthode Bethe-Salpeter est l'approximation GW statique. Dans cette approximation, les corrections de vertex sont négligées dans l'expression de la self-énergie tant et si bien que celle-ci se réduit au produit d'une fonction de Green G et de l'interaction écrantée W . De plus, en général, le cycle de Hedin n'est pas résolu de façon auto-cohérente et une seule itération est réalisée.

Dans ce chapitre, la self-énergie est calculée au niveau GW et dans une variante GWx où l'échange est inclus dans la définition de la matrice diélectrique. Dans les deux cas, le noyau Bethe-Salpeter est obtenu dans son approximation statique en considérant l'interaction écrantée comme étant locale en temps. De plus, la réponse de l'interaction écrantée par rapport à la perturbation, c'est-à-dire la dérivée de W par rapport à G , est négligée comme habituellement fait en physique. Comme la self-énergie n'est pas obtenue de façon auto-cohérente, le choix de la fonction de Green de départ joue un rôle important. Nous comparons par conséquent la fonction de Green HF et la fonction de Green exacte. Dans chaque cas, les équations sont projetées dans une base de spin-orbitales et appliquées sur le système modèle donné par H_2 en base minimale.

Chapitre 9 : Noyau Bethe-Salpeter statique au deuxième ordre de perturbation

Dans ce chapitre, la self-énergie et le noyau de Bethe-Salpeter statique sont développés de façon perturbative au deuxième ordre par rapport à l'interaction électronique. Ce développement est d'abord fait dans l'espace réel en prenant compte ou non de l'inclusion de l'échange dans la self-énergie et de la dérivée de W par rapport à G dans le noyau. Les différentes expressions obtenues sont ensuite projetées sur une base de spin-orbitales. L'inclusion de l'échange dans la self-énergie de corrélation aboutit à une expression dans laquelle toutes les intégrales sont antisymétrisées. Cependant, cela ne suffit pas pour le noyau de corrélation de Bethe-Salpeter qui nécessite également l'inclusion de la dérivée de W par rapport à G afin d'avoir une forme totalement antisymétrisée satisfaisant alors les lois de conservations. Si une seule de ces deux contributions est prise en compte, alors seule une partie des intégrales est antisymétrique, ce qui confirme que ces deux termes doivent être traités simultanément pour des systèmes moléculaires finis pour lesquels cette antisymétrisation est importante. Le noyau obtenu est alors illustré sur le système

modèle donné par H_2 en base minimale où l'on montre que dans l'approximation statique une forme non physique est obtenue.

Chapitre 10 : Noyau Bethe-Salpeter dynamique de longue portée au deuxième ordre

Dans ce chapitre, nous développons un noyau dynamique effectif de corrélation Bethe-Salpeter dans l'espace réel et dans une base de spin-orbitales. Afin de satisfaire les lois de conservation dans le cadre de systèmes moléculaires finis, l'échange est inclus dans la matrice diélectrique et les effets de la perturbation sur l'interaction écrantée sont pris en compte dans la construction du noyau à partir de la self-énergie de corrélation. Quand l'équation de Bethe-Salpeter est résolue de façon dynamique, le noyau au deuxième ordre dépendant de la fréquence obtenu précédemment est convolué avec deux propagateurs dépendant de deux fréquences. Ce produit de convolution peut être reformulé comme le produit d'un noyau effectif et de deux fonctions de réponse ne dépendant que d'une seule fréquence. Ce noyau effectif ne dépend que d'une seule fréquence et est compatible avec la formulation TDDFT afin de calculer les pôles de la fonction de réponse. Si ce noyau est construit à partir d'une fonction de Green à séparation de portée et des intégrales de longue portée, ce noyau peut être utilisé dans le cadre de la TDDFT à séparation de portée comme un noyau effectif de corrélation de longue portée dépendant de la fréquence et être ajouté de façon perturbative au noyau TDRSH défini au chapitre 6. Dans les deux cas, l'inclusion d'un noyau dépendant de la fréquence complique la résolution numérique étant donné qu'un problème non-linéaire aux valeurs propres est alors obtenu. Nous adoptons par conséquent une approche perturbative dans l'approximation Tamm-Dancoff. Le comportement de ce noyau est illustré sur le système modèle donné par H_2 en base minimale. Dans ce cas, le caractère symétrique de ce système entraîne la disparition de la partie dépendante de la fréquence du noyau. Cependant, la comparaison du développement de Taylor au deuxième ordre des énergies d'excitation par rapport à l'interaction, et du développement des énergies exactes permet de mettre en évidence les limites de ce noyau. Il est ensuite appliqué au calcul des premières énergies d'excitation de N_2 , CO , H_2CO et C_2H_4 avec et sans séparation de portée. Pour ces systèmes, l'addition perturbative du noyau de corrélation dépendant en fréquence entraîne une augmentation systématique des énergies d'excitation. Sans séparation de portée, elle conduit à une détérioration importante des énergies d'excitation obtenues en Hartree-Fock. En revanche, lorsqu'elle est appliquée dans le cadre de la séparation de portée, elle améliore l'erreur moyenne et l'erreur maximale.

Conclusion générale et perspectives

Cette thèse contribue au traitement des énergies d'excitation électroniques dans des systèmes moléculaires finis par les méthodes à séparation de portée. En séparant l'interaction électronique en une partie de courte et de longue portée, ces méthodes permettent de combiner rigoureusement la théorie de la fonctionnelle de la densité (DFT) avec des méthodes basées sur la fonction d'onde ou les fonctions de Green. Elles ont été étudiées de façon intensive pour les calculs sur l'état fondamental mais sont toujours en cours de développement pour les états excités. Les calculs des énergies d'excitation par les méthodes DFT sont largement dominés par les calculs en théorie de la fonctionnelle de la densité dépendante du temps (TDDFT) dans la théorie de la réponse linéaire. Cependant cette méthode ne constitue pas la seule approche possible et de nombreuses méthodes indépendantes du temps sont également explorées. Dans cette thèse, la séparation de portée a été appliquée dans les cas dépendant et indépendant du temps mais dans des buts différents. Dans la multitude de méthodes disponibles, il est souvent difficile d'identifier la source d'un problème à cause du grand nombre d'approximations faites simultanément. La première partie de cette thèse avait donc pour but d'étudier les effets de la séparation de portée sur les énergies d'excitation en s'affranchissant de toute approximation. Les deuxième et troisième parties étaient en ce sens bien plus pragmatiques puisqu'elles visaient à améliorer le traitement des excitations multiples présent en TDDFT dans l'approximation adiabatique. Dans ce cas, l'approximation locale a été utilisée pour la fonctionnelle et une approximation mono-déterminantale pour la fonction d'onde.

Séparation de portée en DFT indépendante du temps

Les effets de l'approximation adiabatique sont difficiles à analyser et à corriger dans une approche dépendante du temps. De plus celle-ci n'est en principe pas nécessaire pour obtenir des énergies d'excitation. En effet, les théorèmes de Hohenberg-Kohn prouvent que la densité électronique du fondamental contient toute l'information du système et donc en particulier les énergies d'excitation. Nous nous sommes donc placés dans un premier temps dans une approche indépendante du temps où notre but n'était pas de concevoir une nouvelle méthode pragmatique pour calculer des énergies d'excitation avec la séparation de portée, tout du moins à court terme, mais plutôt de s'affranchir d'un maximum d'approximations et de réaliser une étude analytique et numérique poussée sur de très petits systèmes. Dans cette étude, la seule approximation réalisée concerne la base. Par conséquent, on peut espérer qu'avec une base suffisamment grande, les effets observés ne seront pas dus à la base mais uniquement à la séparation de portée. La première partie de cette thèse contient les résultats de cette étude dans laquelle nous avons suivi

les énergies d'excitation d'un système en interaction partielle le long d'une connexion adiabatique à séparation de portée reliant le système de Kohn-Sham et le système physique. Les développements de Taylor des énergies autour de ces deux limites nous a permis entre autres de proposer une technique d'extrapolation qui améliore la description des énergies d'excitation du système physique à partir d'un point intermédiaire de la connexion adiabatique où seule la partie de longue portée de l'interaction est présente. Cela nous a aussi permis de démontrer quelques conditions exactes que des énergies approchées devraient satisfaire autour des deux limites, et d'évaluer la proportion de l'interaction qui doit être incluse pour décrire correctement les énergies d'excitation du système physique. Nous sommes actuellement en train d'évaluer les effets de l'approximation LDA et de l'approximation mono-déterminantale utilisée dans la méthode RSH, sur les énergies d'excitation. Nous espérons que ce travail aidera au développement et à la compréhension des méthodes à séparation de portée pour le calcul des énergies d'excitation, que ce soit dans le cas indépendant ou dépendant du temps.

Séparation de portée et DFT dépendante du temps

La deuxième partie de cette thèse portait sur l'application de la séparation de portée à la TDDFT dans l'approximation locale adiabatique. Lorsqu'elle est appliquée sur la partie d'échange du noyau de Hartree-échange-corrélation (qui doit prendre en compte les effets venant de l'interaction électronique), la séparation de portée permet de d'améliorer significativement plusieurs points faibles de la TDDFT comme la description des excitations de Rydberg et à transfert de charge. Cependant jusqu'à récemment, le noyau de corrélation était uniquement traité en DFT et donc les excitations à caractère multiple ne pouvaient pas être décrites correctement. Dans l'approche RSH, du fait de l'approximation mono-déterminantale, le noyau de corrélation de longue portée disparaît. Nous avons par conséquent déterminé les noyaux singulet et triplet de courte portée LDA et les avons implémentés dans le logiciel de chimie quantique Molpro. L'effet du retrait de la corrélation de longue portée LDA a ensuite été étudié sur les énergies d'excitation de cinq petites molécules et d'un dimère à transfert de charge. Nous avons observé que ce retrait n'a quasiment pas d'effet sur les énergies d'excitation qui constituent par conséquent un bon point de départ pour l'addition perturbative d'un noyau de corrélation de longue portée dépendant de la fréquence capable de prendre en compte l'effet des excitations doubles. La construction d'un tel noyau fut l'objet de la dernière partie de cette thèse.

Noyau de corrélation Bethe-Salpeter au deuxième ordre de longue portée

Afin de concevoir un noyau de corrélation dépendant de la fréquence, nous nous sommes tournés vers l'approche Bethe-Salpeter utilisée en physique de la matière condensée qui

fournit un formalisme dépendant explicitement de la fréquence et très proche de celui utilisé en TDDFT. Dans la troisième partie de cette thèse, nous avons donc entrepris la construction d'un noyau de corrélation effectif au deuxième ordre dans cette approche.

La correspondance entre le formalisme de la physique de la matière condensée et celui de la chimie des systèmes moléculaires n'étant pas triviale, une première étape a consisté à transposer le formalisme des fonctions de Green dans une formulation en spin-orbitales et à vérifier la validité des approximations réalisées en physique dans le cas d'une molécule. Nous en avons conclu que pour un système moléculaire fini, il était préférable de considérer simultanément les contributions de Hartree et d'échange dans la matrice diélectrique et que l'effet de la perturbation sur l'interaction écrantée n'était pas négligeable. Un noyau de corrélation Bethe-Salpeter au deuxième ordre a alors été construit et testé dans un premier temps dans l'approximation statique. Dans ce cas une forme non physique fut obtenue ce qui confirma la nécessité d'un traitement dynamique. Ce noyau dynamique nécessita un effort supplémentaire afin d'obtenir un noyau de corrélation effectif compatible avec le formalisme TDDFT. Les étapes principales de sa construction furent illustrées sur le système modèle de H_2 en base minimale. En particulier, les effets du choix de la fonction de Green initiale, de l'inclusion de l'échange, de la troncation à l'ordre deux, et de l'approximation statique furent évalués sur ce modèle. Le noyau dynamique fut ensuite implémenté dans une approche perturbative dans l'approximation Tamm-Dancoff et testé sur quatre petites molécules avec et sans séparation de portée. Pour ces systèmes dans le cas à séparation de portée, les énergies d'excitation furent globalement améliorées par l'addition perturbative de ce noyau. Cependant, aucun de ces systèmes ne présentait des contributions doubles importantes pour les énergies étudiées alors que le noyau est censé jouer un rôle prédominant dans ce cas.

Perspectives

Il est difficile de mettre un point final à cette thèse où tant de choses restent à faire et à explorer. Je vais essayer ici de résumer les perspectives que ce travail a engendrées et qui restent sur ma "TO DO" liste.

Concernant la partie dépendante du temps, il faudrait réintroduire les approximations usuelles une par une afin d'évaluer leurs effets sur les énergies d'excitation et sur le potentiel d'ionisation. Nous avons observé dans le cas de la théorie de perturbation au premier ordre qu'une mauvaise description de ce potentiel pouvait avoir des conséquences importantes sur les énergies d'excitation. On peut s'attendre à une observation similaire dans le cas d'une approximation locale. Il faut également explorer les effets d'une approximation mono-déterminante ou de l'utilisation d'une interaction de configuration (IC) tronquée au lieu d'une IC complète. Cela permettrait d'apporter un éclairage nou-

veau sur la méthode TD-MC-srDFT qui a été proposée récemment et qui couple la TDDFT à courte portée avec une méthode multi-configurationnelle (MCSCF) à longue portée. Cela pourrait aussi amener au développement de nouvelles méthodes.

Concernant la deuxième partie de cette thèse, la construction et l'implémentation des noyaux de courte portée LDA n'a été réalisée que dans le cas couches fermées. Cependant, un code couches ouvertes et l'implémentation de noyaux de courte portée GGA seraient utiles pour de nombreuses applications.

La dernière partie de cette thèse reste probablement la plus frustrante pour moi puisque tant de choses restent à faire. Je vais donc essayer de faire une liste de ce que j'aurais voulu faire pendant une hypothétique quatrième année...

- Tout d'abord, le noyau effectif a besoin d'être testé de façon plus approfondie et sur des systèmes connus pour avoir des excitations doubles sans la partie basse de leur spectre d'absorption.
- Ensuite, je voudrais tester une résolution non-perturbative basée sur un «déplie» de Löwdin et sans l'approximation Tamm-Dancoff. De plus, le code a été conçu à des fins d'exploration et non d'efficacité, si le noyau s'avère réellement utile, ce module devrait être intégré dans un «vrai» code de chimie quantique.
- Enfin, la troncation au deuxième ordre a été faite par rapport à l'interaction électronique mais sans tenir compte des corrections de self-énergie qui pouvaient intervenir dans la fonction de réponse des quasi-particules sans interaction. Nous travaillons en ce moment sur cet aspect afin d'évaluer, tout d'abord dans le cas de H_2 puis dans le cas général, l'effet de ces corrections. Ceci serait particulièrement intéressant afin de mieux comprendre le lien entre cette méthode et les méthodes de propagateurs au deuxième ordre de type SOPPA.

Cette liste pourrait être bien plus longue et j'espère que certains de ces points seront résolus dans les prochains mois par mes collaborateurs ou moi-même. J'espère que ce travail sera d'une quelconque utilité pour le développement futur de projets similaires.

Range-separated density-functional theory for molecular excitation energies

Linear-response time-dependent density-functional theory (TDDFT) is nowadays a method of choice to compute molecular excitation energies. However, within the usual adiabatic semi-local approximations, it is not able to describe properly Rydberg, charge-transfer or multiple excitations. Range separation of the electronic interaction allows one to mix rigorously density-functional methods at short range and wave function or Green's function methods at long range. When applied to the exchange functional, it already corrects most of these deficiencies but multiple excitations remain absent as they need a frequency-dependent kernel. In this thesis, the effects of range separation are first assessed on the excitation energies of a partially-interacting system in an analytic and numerical study in order to provide guidelines for future developments of range-separated methods for excitation energy calculations. It is then applied on the exchange and correlation TDDFT kernels in a single-determinant approximation in which the long-range part of the correlation kernel vanishes. A long-range frequency-dependent second-order correlation kernel is then derived from the Bethe-Salpeter equation and added perturbatively to the range-separated TDDFT kernel in order to take into account the effects of double excitations.

Keywords: excitation energies, range separation, TDDFT, Bethe-Salpeter kernel, double excitation

Théorie de la fonctionnelle de la densité à séparation de portée pour les énergies d'excitation moléculaires

La théorie de la fonctionnelle de la densité dépendante du temps (TDDFT) est aujourd'hui une méthode de référence pour le calcul des énergies d'excitation électroniques. Cependant, dans les approximations usuelles, elle n'est pas capable de décrire correctement les excitations de Rydberg, à transfert de charge ou présentant un caractère multiple. La séparation de portée de l'interaction électronique permet de combiner rigoureusement les méthodes fonctionnelles pour décrire la courte portée de l'interaction et les méthodes fonctions d'onde ou fonctions de Green pour la longue portée. Dans cette thèse, les effets de cette séparation de portée sur les énergies d'un système en interaction partielle sont d'abord étudiés le long de la connexion adiabatique dans le cas indépendant du temps afin d'aider le développement des méthodes à séparation de portée pour les énergies d'excitation. La séparation de portée est ensuite appliquée dans le cadre de la TDDFT aux noyaux d'échange et de corrélation, où dans le cas d'une approximation monodéterminante, la longue portée du noyau de corrélation est absente. Afin de prendre en compte l'effet des doubles excitations, un noyau de corrélation de longue portée dépendant de la fréquence est développé en s'inspirant du noyau Bethe-Salpeter. Ce noyau est alors ajouté de façon perturbative au noyau TDDFT à séparation de portée afin de prendre en compte les effets des excitations doubles.

Mots-clés : énergies d'excitation, séparation de portée, TDDFT, noyau Bethe-Salpeter, excitation double